Geochemical Study of the Mesoproterozoic Belt-Purcell Supergroup, Western North America: Implications for Provenance, Weathering and Diagenesis

A Thesis Submitted to the College of
Graduate Studies and Research
in Partial Fulfillment of the Requirements
for the Degree of Doctor of Philosophy
in the Department of Earth Sciences
University of Saskatchewan
Saskatoon

By
Ignacio José González-Álvarez

Permission to use

In presenting this thesis in partial fulfillment of the requirements for a Postgraduate degree from the University of Saskatchewan, I agree that the Libraries of this University may make it freely available for inspection. I further agree that permission for copying of this thesis in any manner, in whole or in part, for scholarly purposes may be granted by the professor who supervised my thesis work or, in their absence, by the Head of the Department or the Dean of the College in which my thesis work was done. It is understood that any copying or publication or use of this thesis or parts there of for financial gain shall not be allowed without my written permission. It is also understood that due recognition shall be given to me and to the University of Saskatchewan in any scholarly use which may be made of any material in my thesis.

Requests for permission to copy or to make other use of material in this thesis in whole or part should be addressed to:

Head of the Department of Geological Sciences
University of Saskatchewan
Saskatoon, Saskatchewan S7N 5E2

Abstract

Provenance in the lower Belt-Purcell Supergroup is constrained based on geochemical systematics and chemical monazite ages of argillites and sandstones. Rare earth element (REE), Cr-Ni, and Th/Sc-Sc systematics is equivalent for both facies and consistent with a dominantly post-Archean source area. Detrital monazite chemical ages restrict major provenance for the Appekunny and Grinnell sandstones and argillites to Paleoproterozoic terranes at ~1800-1600 Ma, minor contributions at ~1600-1500 Ma, and marginal contributions from Archean terranes at ~2600, likely in Laurentia. Similar detrital age spectra for monazites of argillites and sandstones of the Appekunny Formation are consistent with a common provenance for the two facies.

The Belt-Purcell sequence records three major diagenetic stages displayed in argillites and sandstones: (1) K-addition and rare earth element post-Archean upper continental crust (PA-UCC)-like pattern; (2) a stage characterized by heavy REE enrichment relative to light REE and HFSE fractionation, and U and Ce mobility; and (3) local dolomitization with REE and high field strenght elements (HFSE) mobility. REE and HFSE mobility are interpreted as the result of oxidized alkaline brines developed by dissolution of evaporites. Monazites from the Appekunny and Grinnell formations differ compositionally and texturally in two groups. Rounded or inclusions with ages >~1400 Ma, interpreted as detrital, have higher Th_2O, Y_2O_3 and lower LREE/HREE contents than euhedral individual monazite grains with chemical ages <~1400 Ma that posses opposed compositional characteristics, and viewed as diagenetic. Monazites that span <~1400 to 300 Ma could be the result of basinal brine activity during stages (2) and (3).

Chemical index of alteration (CIA) for argillites and sandstones, corrected for a diagenetic K-addition average 73 and 66 respectively. These results, coupled with correlation of CIA with Eu/Eu, low K/Cs ratios, and low Sr, Ca, and Na relative to PA-UCC, could be interpreted as the result of an moderate weathered provenance in a hot, wet climate being drained by a large-scale river system. Presence of minor pristine feldspars lowers the CIA values, and may signify minor contributions from proximal source with short-river transport under the arid to semi-arid climate in the depositional setting. Moderate to intense weathering of the larger provenance may be associated with elevated levels of atmospheric CO_2 degassed from a mantle plume implicated in the rifting of the supercontinent Columbia at ~1500 Ma.*

Acknowledgements

I would like to thank specially Lara M. Shychosky for being a constant reason of enjoyment, challenge, unestimated help during the toughest field seasons, and for her motivation during the developement of this project.

To Eduardo J. González Álvarez, Felix González Álvarez, and Lidia Boscariol for their constant, solid, and unconditional support.

To Dayse Tavora Vieira, for being who she is, her critical views, patience, unestimated support, and saudades.

To my mentor Robert Kerrich, for his continuous professional and personal encouragement, guidance, advice, and scientific enlightenment. Without his outstanding supervision this work would have never been.

To my colleague and friend Arndt Peterhänsel for the million talks about the human and the divine on everything during the long winters; as well as to Tim Prokopiuk for his constant help.

To Reza Ahrabian, Mary England, Monika A. Kusiak, Robyn and Mike Pollock, Raul Mainar, Beatriz Berzal, Ulyses Ramírez, Tyler Birkham, Arthur Lieu, Antoine Zazzo, Elise Dufour, Chris Wuster and Sandor Sule for their friendship and support.

To Beverly Kerrich for her wise advice, Richard Cassidy, Jim Basinger, Kevin Ansdell, Luis Buatois, and Robin W. Renaut for their encouragement and professionalism; to Yuanming Pan and Steven Urquhart as my committee members; and to Robert Rainbird as my external for his incisive critique that greatly improved the current manuscript.

To K. McMullan, A. Vangool, B. Uzelman, and L. Skublicki; to the staff of Waterton-Glacier International Peace Park, especially to L. F. Marnell and C. Smith; to Q. Xie, J. Fan, T. Bonli, and B. Novokovski; to B. Britton, D. and T. Chapell; and to B. R. Pratt for introducing me to the field-area.

To my first mentor Salustiano Mateos Gomara who during my high school years endorsed me on free and critical thinking to stand up for what I believe in.

The Natural Sciences & Environment Research Council of Canada (NSERC), discovery grants to R. Kerrich and B. R. Pratt, the G. McLeod endowment to the Department of Geological Sciences, University of Saskatchewan, and a University of Saskatchewan graduate scholarship to I. González-Álvarez funded this study.

Dedication

To Angela,

Table of contents

List of tables

List of Figures

CHAPTER II

CHAPTER III

CHAPTER IV

CHAPTER V

CHAPTER VI

CHAPTER VII

Thesis work

In Chapter IV, Dr. Monika A. Kusiak from the Polish Academy of Sciences, Krákov, Poland, carried out 72 of the total 145 monazite chemical analyses presented in this study. The rest of the analyses were carried by the author who made most of the writing and interpretations helped by Dr. Robert Kerrich. Article based on Chapter IV has been favourably received and publication with minor revision is recommended in Chemical Geology since October 13th, 2005. Authors: González Álvarez, I., Kusiak, M.A., Kerrich, R.

Article based on Chapter V was submitted to G-cubed and it is in its second review round since September 21st, 2005. Authors: González Álvarez, I., Kerrich, R.

Manuscripts based on Chapters VI and VII are to be submitted. Authors: González Álvarez, I., Kerrich, R.

In Chapters I, II, III, IV, V, VI, VII, and VIII Dr. Robert Kerrich helped guide both scientific interpretations and editorial suggestions. The primary author did the majority of the writing and interpretation.

Global list of abbreviations and acronyms

PA-UCC	Post-Archean Upper Continental Crust
PAAS	Post-Archean Australian Shale
CIA	Chemical Index of Alteration
REE	Rare earth Elements
HREE	Heavy Rare Earth Elements (La-Lu)
LREE	Light Rare Earth Elements
HFSE	High Field Strength Elements (Nb, Ta, Zr, Hf)
ICP-MS	Inductively Coupled Plasma-Mass Spectrometry
App	Appekunny Formation
Gr	Grinnell Formation
Sd	Sandstones
Arg	Argillites
LKSD-1	Lake Sediments Canadian Shield
BCR-1	Basalt, reference material
BCR-2	Basalt, low trace element reference material
LOI	Loss On Ignition
EDS	Electron Dispersive Spectrometry
WDS	Wavelength Dispersive Spectrometry
SHRIMP	Sensitive High Resolution Ion Microprobe
XRFS	X-ray Fluorescense Spectrometry
EMPA	Electron Microprobe Analysis
Z	Atomic Number
rpm	Revolutions Per Minute
wt.%	Weight Percentage
ppm	Parts Per Million
ppb	Parts Per Billion

Note: due to limitations of the program used for the formatting of this thesis, Greek letters are spelled out in the text.

CHAPTER I

Introduction and scope

The Belt-Purcell Supergroup is a ~17 km thick Proterozoic sedimentary sequence of western North America (e.g., McMechan, 1981; Whipple et al., 1984; Winston, 1990; Lydon, 2000; Chandler, 2000; Ross and Villeneuve, 2003; Sears et al., 2004). This Supergroup is interpreted to be the result of the infilling of an intracratonic rift basin originated from the break up of the Mesoproterozoic supercontinent Columbia over ~1600-1400 Ma (e.g., Windley, 1995; Lydon, 2000; Price and Sears, 2000; Zhao et al., 2004). The preserved sedimentary sequence records up to 75 Ma of dominantly siliciclastic, and minor carbonate sedimentation, as well as sporadic magmatism (Anderson and Davies, 1995; Sears et al., 1998; Evans et al., 2000). The Belt-Purcell rocks display pristine preservation of some of the original features of the sediment, such as halite casts, representing an outstanding opportunity to address earth processes during a period of ~100 Ma at ~1500 Ma (e.g., Whipple et al., 1997).

This geochemical study of the Belt-Purcell Supergroup has been designed in three interrelated parts:

(1) Paleo-, Mesoproterozoic and Archean terranes of Laurentia to the east have been suggested as potential provenance areas. Alternatively, other terranes of the same age to the west or south, including Siberia or Australia, as well as some combination of sources, have been proposed based on a variety of lines of evidence (e.g., Frost and Winston, 1987; Ross et al., 1992; Windley, 1995; Link, 1997; Ross and Villeneuve, 2003; Sears et al., 2004). The diversity of potential catchment terrane(s) results from uncertainties in reconstruction of the Proterozoic continents at ~1500 Ma, and an apparent “magmatic gap” in Laurentia spanning ~1600-1500 Ma (Hoffman, 1988, 1989; Ross and Villeneuve, 2003). This study was designed originally to address the provenance of two formations: the Appekunny and Grinnell formations in the lower part of the stratigraphic Belt-Purcell Supergroup at Waterton-Glacier International Peace Park, western North America, using a geochemical approach based on trace elements and monazite chemical ages.

Rare earth elements (REE), Th, Y, Co and Sc are in many cases conserved when trans-

ferred from provenance areas into the sedimentary budget of many siliciclastic sequences, due to their retention on clay-sized particles, and short residence time in seawater. Consequently they can potentially preserve the geochemical signature of the source areas, and have been used in many geochemical studies to address provenance, specifically Archean versus post-Archean (e.g., Taylor and McLennan, 1985, 1995; Fralick and Kronberg, 1997; Fralick, 2003; McLennan et al., 2003). This study presents a high precision major and trace element data for the full stratigraphic extent of the Belt-Purcell Supergroup at three different locations. Accordingly, in the first part of this study new geochemical data of the Belt-Purcell rocks are reported as a proxy for provenance.

In addition, detrital monazites are used to address provenance age and can be dated using the chemical Th-U-total Pb method (e.g., Parrish, 1990; Suzuki and Adachi, 1994; Pyle et al., 2005; Dahl et al., 2005). Accordingly, to complement the whole-rock geochemistry, and due to the abundant occurrence of monazite in some samples from the Appekunny and Grinnell formations, and the availability of the technique, chemical ages of monazite grains have been measured to build on existing data from detrital zircons and monazites (cf. Ross et al., 1991, 1992; Ross and Villeneuve, 2003).

(2) From reconnaissance studies, some siliciclastic samples analyzed have rare earth and trace element patterns similar to post-Archean upper continental crust (PA-UCC; cf. Taylor and McLennan, 1995) with K-addition, whereas others recorded mobility of heavy REE (HREE), and elements such as Zr and Y that are generally isochemical. In addition, a significant number of calculated chemical secondary monazite ages post date deposition by up to ~1000 Ma. These two features are commensurate with mobilization and fractionation of trace elements during diagenesis (Kerrich and González-Álvarez, 2003; González-Álvarez et al., 2003).

Therefore, the second part of this study aims to evaluate the characteristics and scale of diagenetic element mobility throughout the Belt-Purcell sequence at three locations. Mass balance was applied assuming PA-UCC as the precursor rock. The characteristics of formation brines that fractionated trace elements during diagenesis are constrained by comparison to modern brines that have high aqueous solubility of heavy REE and high field strength elements (HFSE: Nb, Ta, Zr, Hf). That brine activity is linked to secondary monazite chemical ages that are younger than sedimentation.

Units rich in dolomite, with a variable siliciclastic component, occur at two main stratigaphic levels in the Belt-Purcell Supergroup, and adjacent siliciclastic rocks are locally dolomi-

tized. These dolomites have not been geochemically characterized, nor the cause of dolomitization identified. Dolomitization overprints samples that display K-addition and HREE mobility. A sample design was created to characterize geochemically progressive dolomitization of argillites and mass balance was used to feature geochemical changes during this diagenetic process.

(3) Proterozoic (2500-570 Ma) paleoclimates and interpretation of their driving forces are controversial. Inferred severe swings in climate during ~2000 Ma include at least two glacial periods, of uncertain latitudinal extent, and pronounced changes in atmospheric oxygen level (e.g., Hoffman, 1999; Ohmoto, 2004; Young, 2004). Unusually warm paleoclimate peaks are proposed at ~2700-2500 Ma, ~2100-1700 Ma, and ~800-600 Ma (Condie et al., 2001). Some of those peaks could record the breakup of supercontinents at ~2200-2000 and ~800-600 Ma, and the consequent increase in atmospheric CO_2 levels produced by associated mantle superplume events (Condie et al., 2000, 2001; Rogers and Santosh, 2004). Uncertainties in secular variations of weathering intensity need to be addressed by a more complete database on Proterozoic sedimentary sequences. Nesbitt and Young (1982) defined the chemical index of alteration (CIA) using a geochemical approach to address paleoclimate, an approach extended by Fedo et al. (1995) to account for diagenetic addition of K.

Consequently, the third part of this study builds on paleoclimate information using the ~1500 Ma siliciclastic rocks of the Belt-Purcell Supergroup at the time of the disaggregation of the Columbia supercontinent (Zhao et al., 2004) to test the plume-rifting hypothesis linking it to a potential increase in atmospheric CO_2 levels and therefore, increase in weathering intensity.

The database for Proterozoic siliclastic rocks is restricted, especially at ~1500 Ma, placing limitations on using CIA as a proxy of Proterozoic climate. This study addresses weathering intensity for the interval ~1500-1400 Ma for which there are few data, especially K-corrected values for CIA, restricted to the lower Belt sequence. Accordingly, the third part of this study contributes to unraveling of the original geochemical imprint of weathering in the catchment throughout the Belt-Purcell Supergroup sequence at three locations, taking into account diagenetic K-addition for corrected CIA (cf. Fedo et al., 1995). Results for corrected CIA are interpreted in the context of paleoclimate data during the Mesoproterozoic. Specifically, this study attempts to assess whether CIA values are in keeping with the intense silicate weathering expected from elevated atmospheric CO_2 concentrations, which could have arisen from mantle plumes and spreading systems in rifting of the Mesoproterozoic supercontinent Columbia (cf. Windley, 1995; Zhao et al., 2004).

In summary, the present geochemical study of the Belt-Purcell rocks comprises three interrelated contributions on provenance, diagenesis, and catchment weathering respectively. It embraces: (1) novel geochemical approaches to existing debates on provenance of the Belt-Purcell Supergroup, (2) wholly new diagenetic phenomena for the Belt-Purcell Supergroup, and (3) new weathering data. This study builds on the body of literature of the Proterozoic era, integrating global geodynamics with atmospheric conditions, weathering and protracted diagenetic fluid activity.

The geological setting of the Belt-Purcell Supergroup is summarized in Chapter II as background information for these studies. Chapter III sets out the analytical methodologies used, with their advantages and limitations, as well as how, where and why the sample set was collected and selected. In Chapter IV provenance is addressed using trace element geochemistry and monazite chemical ages. Chapters V and VI address diagenesis, and Chapter VII deals with weathering. In a synopsis Chapter VIII, the results are drawn together, and their significance presented.

1.1 References

Anderson, H.E., Davis, W.D., 1995. U-Pb geochronology of the Moyie sills, Purcell Supergroup, southeastern British Columbia: implications for the Mesoproterozoic geological history of the Purcell (Belt) Basin. Can. J. Earth Sci., 32, 1180-1193.

Chandler, F.W., 2000. The Belt-Purcell basin as a low-latitude passive rift: implications for the geological environment of Sullivan type deposits. In: Lydon, J.W., Höy, T., Slack, J.F., Knapp, M.E., (eds.), The Geological Environment of the Sullivan Deposit, British Columbia. Geol. Assoc. Can. Min. Dep. Div. Spec. Publ. 1, pp. 82-112.

Condie, K.C., Des Marais, D.J., Abbott, D., 2000. Geologic evidence for a mantle superplume event at 1.9 Ga. Geochm. Geophy. Geosys. 1, 2000GC000095.

Condie, K.C., Des Marais, D.J., Abbott, D., 2001. Precambrian superplumes and supercontinents: a record in black shales, carbon isotopes, and paleoclimates? Precambrian Res. 106, 239-260.

Dahl, P.S., Hamilton, M.A., Jercinovic, M.J., Terry, M.P., Williams, M.L., Frei, R., 2005. Comparative isotopic and chemical geochronometry of monazite, with implications for U-Th-Pb dating by electron microprobe: an example from metamorphic rocks of the eastern Wyoming Craton (U.S.A.). Am. Mineral. 90, 619-638.

Evans, K.V., Aleinikoff, J.N., Obradovich, J.D., Fanning, C.M., 2000. SHRIMP U-Pb geochronology of volcanic rocks, Belt Supergroup, western Montana: evidence for rapid deposition of sedimentary strata. Can. J. Earth Sci., 37, 1287-1300.

Fedo, C.M., Nesbitt, H.W., Young, G.M., 1995. Unraveling the effects of potassium metasomatism in sedi-

mentary rocks and paleosols, with implications for paleoweathering conditions and provenance. Geology 23, 921-924.

Fralick, P.W., 2003. Geochemistry of clastic sedimentary rocks: ratio techniques. In: Geochemistry of sediments and sedimentary rocks: evolutionary considerations to mineral-deposit forming environments. In: Lentz, D.R. (ed.), Geochemistry of Sediments and Sedimentary Rocks. Geol. Assoc. Can., pp. 85-103.

Fralick, P.W., Kronberg, B.I., 1997. Geochemical discrimination of clastic sedimentary rock sources. Sediment. Geol. 113, 111-124.

Frost, C.D., Winston, D., 1987. Nd isotope systematics of coarse- and fine-grained sediments: examples from the Middle Proterozoic Belt-Purcell Supergroup. J. Geol. 95, 309-327.

González-Álvarez, I.J., Kerrich, R., Pratt, B.R., 2003. Geochemistry of the Appekunny and the Grinnell formations: Mesoproterozoic siliciclastic rocks of the Belt-Purcell Supergroup, western USA and Canada. Int. Assoc. Sediment., 22nd International Meeting Sed., Abstracts book, 68.

Hoffman, P.F., 1988. United Plates of America, the birth of a craton: early Proterozoic assemble and growth of Laurentia. Ann. Rev. Earth Planet. Sci. 16, 543-603.

Hoffman, P.F., 1989. Speculations on Laurentia's first gigayear (2.0 to 1.0 Ga). Geology 17, 135-138.

Hoffman, P.F., 1999. "Snowball earth" theory still stands. Nature 400, 708.

Kerrich, R., González-Álvarez, I.J., 2003. Basinal fluid evolution in the Appekunny-Grinnell Formation, 1.4 Ga Belt Supergroup. Geol. Soc. Am., Annual Meeting, Abstracts with Programs, Abstract 243-3.

Link, P.K., 1997. The Grinnell, Empire and Helena formations along Baring Creek and at Siyeh Pass, Glacier National Park. In: Link, P. K., (ed.), Geologic Guidebook to the Belt-Purcell Supergroup, Glacier National Park and Vicinity, Montana and Adjacent Canada, Field Trip Guidebook for the Belt Symposium III, Belt Association, Pocatello, Idaho, pp. 113-124.

Lydon, J.W., 2000. A synopsis of the understanding of the geological environment of the Sullivan Deposit. In: Lydon, J.W., Höy, T., Slack, J.F., Knapp, M.E., (eds.), The Geological Environment of the Sullivan Deposit, British Columbia. Geol. Assoc. Can. Min. Dep. Div. Spec. Publ. 1, pp. 12-31.

McLennan, S.M., Bock, B., Hemming, R.S., Hurowitz, J.A., Lev, S.M., McDaniel, D.K., 2003. The roles of provenance and sedimentary processes in the geochemistry of sedimentary rocks. In: Lentz, D.R. (ed.), Geochemistry of Sediments and Sedimentary Rocks. Geol. Assoc. Can., pp. 7-38.

McMechan, M.E., 1981. The middle Proterozoic Purcell Supergroup in the southwestern Rocky and southeastern Purcell Mountains, British Columbia and the initiation of the Cordilleran miogeocline, southern Canada and adjacent United States. Bull. Can. Petrol. Geol. 29, 583-621.

Nesbitt, H.W., Young, G.M., 1982. Early Proterozoic climates and plate motions inferred from major element chemistry of lutites. Nature 299, 715-717.

Ohmoto, H., 2004. Archean atmosphere, hydrosphere and biosphere. In: Eriksson P.G., Alterman, W., Nel-

son, D.R., Mueller, W.U., Catuneanu, O., (eds.), The Precambrian Earth: Tempos and Events, Developments in Precambrian Geology, Condie, K.C., (series ed.), Elsevier, 12, pp.361-387.

Parrish, R.R., 1990. U-Pb dating of monazite and its applications to geological problems. Can. J. Earth Sci. 27, 1431-1450.

Price, R.A., Sears, J.W, 2000. A preliminary palinspastic map of the Mesoproterozoic Belt-Purcell Supergroup, Canada and USA: implications for the tectonic setting and structural evolution of the Purcell anticlinorium and the Sullivan deposit. In: Lydon, J.W., Höy, T., Slack, J.F., Knapp, M.E., (eds.), The Geological Environment of the Sullivan Deposit, British Columbia. Geol. Assoc. Can. Min. Dep. Div. Spec. Publ. 1, pp. 61-81.

Pyle, J.M., Spear, F.S., Wark, D.A., Daniel, C.G., Storm, L.C., 2005. Contributions to precision and accuracy of monazite microprobe ages. Am. Mineral. 90, 547-577.

Rogers, J.J.W., Santosh, M., 2004. Continents and supercontinents. Oxford Universy Press. New York, NY, U. S. A.

Ross, G.M., Parrish, R.R., Dudás, F.Ö., 1991. Provenance of the Bonner Formation (Belt Supergroup), Montana: insights from U-Pb and Sm-Nd analyses of detrital minerals. Geology 19, 340-343.

Ross, G.M., Parrish, R.R., Winston, D., 1992. Provenance and U-Pb geochronology of the Mesoproterozoic Belt Supergroup (northwestern United States): implications for age of deposition and pre-Panthalassa plate reconstructions. Earth Planet. Sci. Lett. 113, 57-76.

Ross, G.M., Villeneuve, M.E., 2003. Provenance of the Mesoproterozoic (1.45 Ga) Belt Basin (western North America): another piece in the pre-Rodinia paleogeographic puzzle. Geol. Soc. Am. 115, 1191-1217.

Sears, J.W., Price, R.A., Khudoley, A.K, 2004. Linking the Mesoproterozoic Belt-Purcell Supergroup and Udzha basin across the west Laurentia-Siberia connection. Precambrian Res. 129, 291-308.

Sears, J.W., Chamberlain, K.R., Buckley, S.N., 1998. Structural and U-Pb geochronological evidence for 1.47 Ga rifting in the Belt Basin, western Montana. Can. J. Earth Sci. 35, 467-475.

Suzuki, K., Adachi, M., 1994. Middle Precambrian detrital monazite and zircon of the Hide gneiss on Oki-Dogo island, Japan: their origin and implications for the correlation of basement gneiss of southwest Japan: constraints from CHIME monazite ages of gneisses and granitoids. J. Metamorph. Geol. 16, 23-37.

Taylor, S.R., McLennan, S.M., 1985. The continental crust: its composition and evolution. Blackwell, Oxford, U. K.

Taylor, S.R., McLennan, S.M., 1995. The geochemical evolution of the continental crust. Rev. Geophy. 33, 241-265.

Whipple, J.W., Binda, P.L., Winston, D., 1997. Geologic guide to Glacier National Park, Montana and areas adjacent to Waterton, Alberta. In: Link , P.K., (ed.), Belt Symposium III, Geologic Guidebook to the

Belt-Purcell Supergroup, Glacier National Park and Vicinity, Montana and adjacent Canada, Belt Association, Pocatello, Idaho, pp. 125-155.

Whiple, J. W., J. J. Connor, Raup O. B., McGrimsey R. G., 1984. Preliminary report on the stratigraphy of the Belt Supergroup, Glacier National Park and adjacent Whitefish Range, Montana, in northwest Montana and adjacent Canada. In: McBane, J.D., Garrison, P.B., (eds.), Guidebook, Field Conference and Symposium, Belt Association, Pocatello, Idaho, Montana Geol. Soc., pp. 33-50.

Windley, B.F., 1995. The evolving continents. Wiley and Sons, N.Y., New York, U.S.A.

Winston, D., 1990. Evidence for intracratonic, fluvial and lacustrine settings of Middle to late Proterozoic basins of western U.S.A. In: Gower, C. F., Rivers, T., Ryan, B., (eds.), Mid-Proterozoic Laurentia-Baltica. Geol. Assoc. Can. Spec. Paper 38, 535-564.

Young, G.M., 2004. Earth's two great Precambrian glaciations: aftermath of the "snowball earth" hypothesis. In: Eriksson P.G., Alterman, W., Nelson, D.R., Mueller, W.U., Catuneanu, O., (eds.), The Precambrian Earth: Tempos and Events, Developments in Precambrian Geology, Condie, K.C., (series ed.), Elsevier, 12, pp. 440-447.

Zhao, G., Sun, M., Wilde, S.A., Li, S., 2004. A Paleo-Mesoproterozoic supercontinent: assembly, growth and breakup. Earth Sci. Rev. 67, 91-123.

CHAPTER II

Geological setting

2.1 Introduction and tectonic setting

The preserved Mesoproterozoic Belt-Purcell Supergroup extends 500 km from southwestern Montana, where it is known as the Belt Supergroup, to southeastern British Columbia, where it is referred to as the Purcell Supergroup (Fig. 2.1). It outcrops in an antiformal structure of the Purcell Anticlinorium presenting an estimated sedimentary thickness of ~17 km that could reach up to ~22 km accounting for the buried sequence under the surface to the east of the anticlinorium (Harrison, 1972; Whipple et al., 1984; Yoos et al., 1991; Lydon, 2000). The Belt-Purcell sequence is an allochthonous wedge that has been displayed by thrust faults during the Jurassic-Paleocene (160 to 60 Ma) Laramide event of the North American Cordilleran orogen, eastward, being completely detached and unconformably emplaced over igneous and metamorphic basement rocks which are only locally exposed (Kleinkopf, 1997), as well as Cretaceous sedimentary rocks (Yin and Kelty, 1991; Price and Sears, 2000; Lydon, 2000).

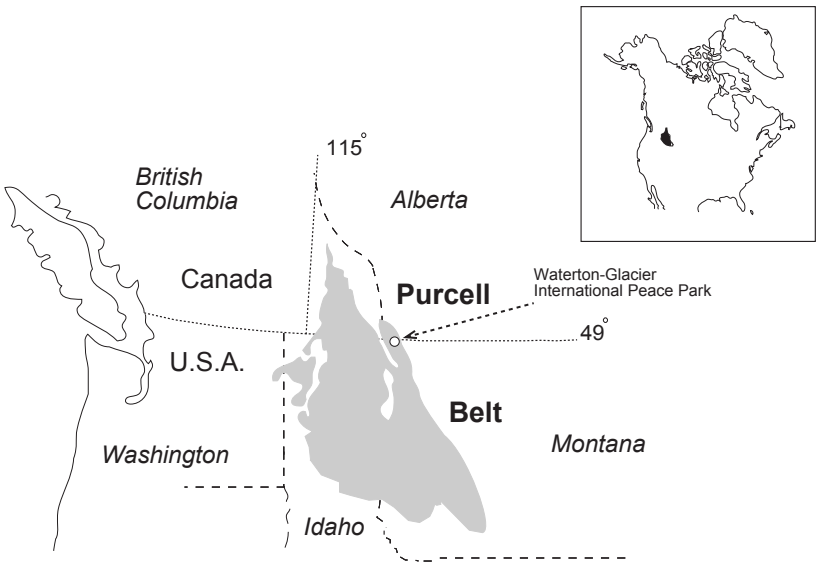

Fig. 2.1 Geographic extent of the Belt-Purcell Supergroup spanning the Canada-USA border.

The Belt-Purcell Basin is interpreted as an intracratonic basin that originated by rifting (e.g., Price and Sears, 2000; Poage et al., 2000; Lydon, 2000; Höy et al., 2000). Two main basin stages are identified: (1) at ~1470 Ma, and (2) at ~1445 Ma (Price and Sears, 2000); the first corresponding to extension and the second to thermal subsidence. Several lines of evidence support largely passive rifting: the absence of stratigraphic geometries associated with thermal doming from a mantle plume (e.g., Rainbird and Ernst, 2001); lack of pre-rift volcanism (Lydon, 2000); and intraplate tholeitiic Moyie sills intruding the lower Belt (e.g., Anderson and Davies, 1995; Höy et al, 2000). Specifically, based on trace element systematics of the Moyie sills Anderson and Goodfellow (2000) suggested that mafic magmatism associated with the passive intracontinental rift may have involved a weak plume that metasomatized extended lithosphere beneath the basin. Rift development may have been part of dispersal of the Mesoproterozoic supercontinent Columbia (Zhao et al., 2004).

Ross and Villeneuve (2003) showed evidence of an extensional basin active to the west based on predominant sediment input from the west, rapid rates of subsidence, coupled with large-scale facies pattern; from this evidence they compared the Belt-Purcell Basin with a Black Sea-type basin. A palinspastic map of the Belt-Purcell basin is presented by Price and Sears (2000).

2.2 The Belt-Purcell basement and associated structure

Rocks that underlie the Belt-Purcell Supergroup are mostly not exposed (Kleinkopf, 1997), but can be inferred from basement rock maps of western Laurentia to be the Wyoming Craton and the Archean Hearne Province (Fig. 2.2; Hoffman, 1988; Ross et al., 1990). The Wyoming Craton (~3100-2600 Ma; e.g., Price and Sears, 2000) is composed mainly of gneiss-migmatites, granitoid batholiths and minor greenstone, amphibolites and ultramafic rocks (Goodwin, 1991). The Hearne Province (3300-2600 Ma) includes the Medicine Hat Block (metaplutonic gneisses; 3270-2650 Ma), Vulcan Low (collisional suture; Hoffman, 1988), Matzhiwin High (magmatic belt) and the Loverna Domain (Ross et al., 1990; Price and Sears, 2000 and references therein). The whole Hearne Province is interpreted as a collage of Archean blocks (Ross et al, 1990).

Between the Wyoming Craton and the Hearne Province there is the Proterozoic suture zone of the Great Falls Tectonic Zone (~1900 Ma) that is represented by deformed calc-alkaline granitoids and gneisses at the little Belt Mountains (Mueller et al., 1993). This suture is interpreted as the result of the closure of an ocean basin between the Wyoming and the Medicine Hat Block at ~1900 Ma (Mueller et al., 1993). Western basement rocks to the Belt-Purcell Basin are the Mesoprotero-

zoic migmatitic gneisses of the Priest River Complex (~1570 Ma; Fig. 2.2). Other western terranes were rifted, probably by post-Belt fragmentation of Laurentia, and therefore are not present today (Fig. 2.2; e.g., Frost and Winston, 1987; Ross et al., 1991, 1992; Ross and Villeneuve, 2003).

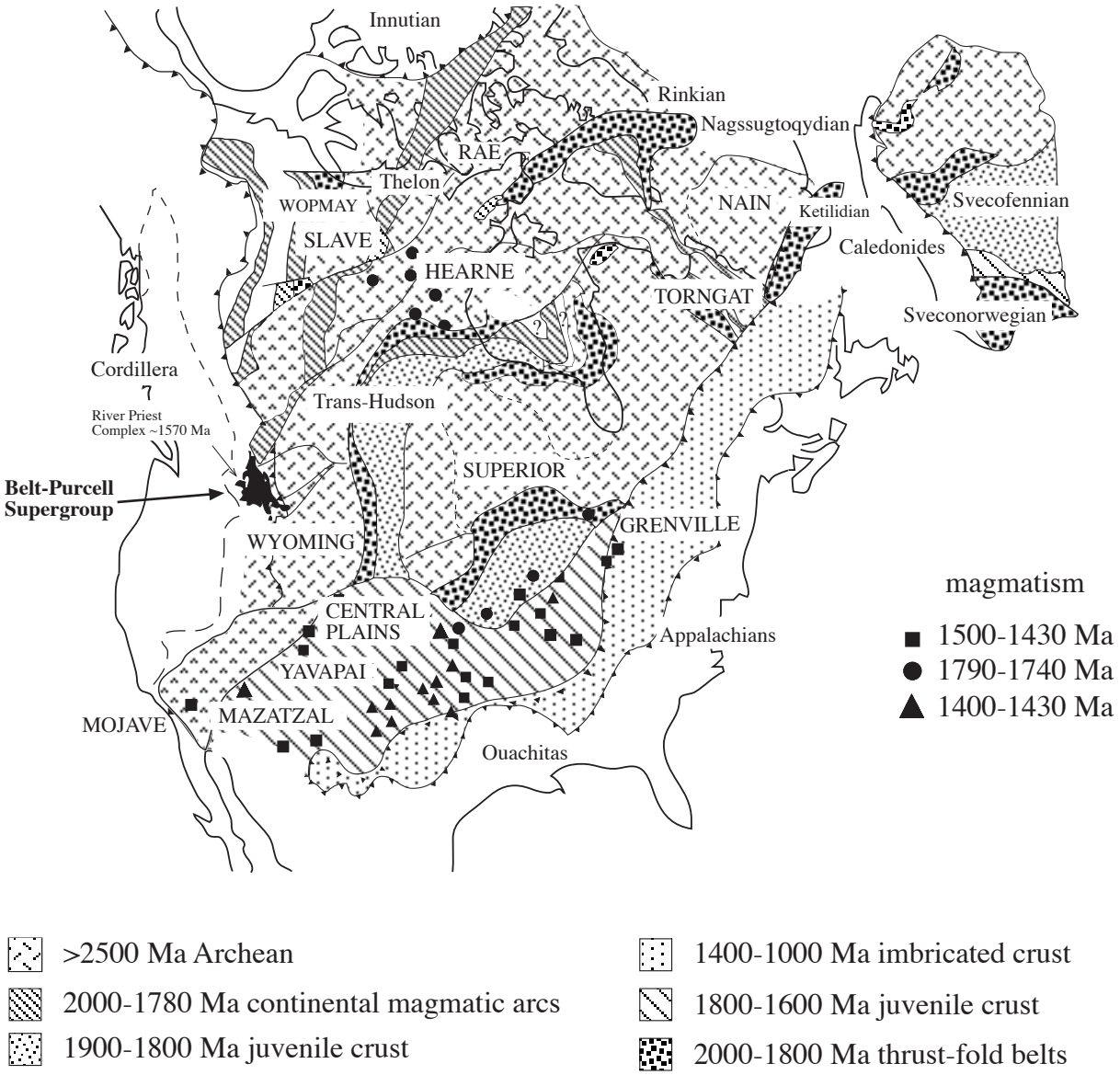

Fig. 2.2 Schematic map of the basement rocks of North America simplified from Ross and Villeneuve (2003) after Hoffman (1989) showing the main Proterozoic and Archean domains (tectono-stratigraphic terranes) and the Belt-Purcell Basin.

The main structural trend of the basement rocks is a northwest-trending Paleoproterozoic shear zone. This structure is cross-cut to the south by the northeastward trend of the Great Falls Tectonic Zone, and truncated to the north by the northeastward trends of the Vulcan Low. Ross et al. (1990) interpreted the former as due to a collisional suture. Structural trends of the Matzhiwin High are oriented northwestwards (Fig. 2.2; Price and Sears, 2000). The basement dips to the west due to thinning from ~35 km under the Cordilleran foreland belt to ~15 km under the Purcell Mountains (Yoos et al, 1991; Clowes et al., 1998). Basement structures determined the geometry of the Belt-Purcell Basin as the as the main northeast-southwest axes and the Helena Embayment that develops as an entrant to the east (e.g., Price and Sears, 2000).

2.3 Lithologies

The Belt-Purcell sequence is predominantly fine-grained silciclastic facies with subordinate units of medium and coarse-grained sandstones. The fine-grained facies has been termed argillite in the literature as a combination of siltite, mudstone, and very fine-grained sandstone (e.g., Harrison, 1972; McMechan, 1981; Whipple et al., 1984; Winston, 1990). The sandstone varies from quartzarenites, to subarkoses, and sublitharenites (terminology of Folk, 1968). Monazite, zircon, apatite, barite and pyrite are common in the siliciclastic facies as the heavy mineral fraction (Whipple et al., 1984; Winston, 1990; Lydon et al., 2000; Ross and Villeneuve, 2003; this study).

There is a characteristic interbedding of argillites with meter to decimeter thick units of mainly medium to coarse sandstone that is especially well developed in the Ravalli Group (e.g., Winston 1990, Whipple et al., 1997). Two main primary carbonate-rich units are present: one in the lower and the second in the middle part of the Belt-Purcell sequence. Siliciclastic-rich and carbonate-rich units in the Belt-Purcell sequence grade progressively into each other, such that the carbonate units include variable proportions of detrital silicates (e.g., Winston and Lyons, 1997; Chandler, 2000; Pratt, 2001). Euhedral dolomite crystals and lime mud comprise most of the carbonate fraction. Casts and moulds of halite, gypsum and other evaporitic minerals have been described in the sequence (e.g., Connors et al., 1984; Schieber, 1997; Lyons et al., 1997; Chandler, 2000 and references therein).

Mineralogically, argillites are an assemblage of quartz with minor plagioclase and microcline, in a matrix of smectite, chlorite, and/or illite-micas depending of their stratigraphic level (Maxwell and Hower, 1967; Harrison, 1972; Frost and Winston, 1987; Lydon et al., 2000). Sandstones have an assemblage of quartz, plagioclase, K-feldspar, monazite, muscovite, and chlorite,

and a matrix characterized by smectite for the upper stratigraphic units in the east, and/or illite-muscovite-chlorite for the rest of the sequence to the west (e.g., Ross, 1963; Maxwell and Hower, 1967; Harrison and Grimes, 1970; Harrison, 1972; Lydon et al., 2000).

Minor magmatic episodes are represented by tholeiitic gabbros and diorites, mafic lava flows as well as volcanic ash deposits present in the middle and upper part of the stratigraphic sequence (e.g., Whipple et al., 1984; Anderson and Davies, 1995; Evans et al., 2000; Lydon, 2000). The Belt-Purcell Supergroup hosts a number of orebodies. The largest is the Sullivan massive Pb-Zn-Ag sulfide deposit, in the lower Aldridge Formation, in southeast British Columbia formed close to the time of sedimentation (~1470 Ma; Fig. 2.3; Lydon, 2000; Schandl et al., 2000), and interpreted as the product of modified seawater interacting with a sill-sediment complex. Large bodies of hydrothermal tourmaline are present (Lydon, 2000, and references therein).

2.4 Stratigraphic divisions

The Belt-Purcell Supergroup has been classified into four main stratigraphic groups: (1) the lower Belt, (2) Ravalli Group, (3) middle Belt, and (4) Missoula Group (Figs. 2.3; Tables 2.1, and 2.3; e.g., Eargart et al., 1984; Whipple et al., 1984; Winston, 1989).

(1) The lower Belt is represented in the west by fine-grained deep marine turbiditic facies of the Aldridge and Prichard formations that grades westwards into deltaic facies, reaching a maximum thickness of ~12 km (e.g., Harrison, 1972; McMechan, 1981; Höy, 1993; Whipple et al., 1984; Lydon, 2000). Those two formations correlate to the east with shallow marine and peritidal carbonate units of the Waterton and Altyn formations, and to the south is represented by shallow marine carbonates of the Newland, Chamberlain and Greyson formations, as well as quartzites and conglomerates of the Fort Steele, Neihart and LaHood formations (Table 2.1; Figs. 2.5 and 2.6; e.g., McNannis, 1963; Schieber, 1989; Chandler, 2000 and references therein). Stratigraphically higher sections of the lower Belt record a shallowing sequence that grades into the overlying Ravalli Group (Fig. 2.4; Höy, 1982; Whipple et al., 1984, 1997; Chandler, 2000).

(2) The Ravalli Group includes siltite, argillite, and quartz arenite. It represents a major regressive cycle in the Belt-Purcell Basin, ending the turbiditic stratigraphic sequence and displaying shallow water deposits that are transitional to subaeral exposure conditions (Figs. 2.5 and 2.6; McMechan, 1981; Höy, 1982; Winston, 1986, 1990). The Creston Formation in the Purcell Mountains represents this group. South in Waterton-Glacier International Peace Park, the Creston Formation

is correlated with the Appekunny, Grinnell, and Empire formations, and to west by the Regis, Revett, and Burke formations (Fig. 2.5). There are two views of the depositional setting of the Ravalli Group: (1) the result of braided stream deposits, playa lakes and progradation of alluvial fans over mud-flats (Winston, 1986, 1990), whereas (2) other authors including McMechan (1981) proposed a tidally influenced setting (Table 2.2).

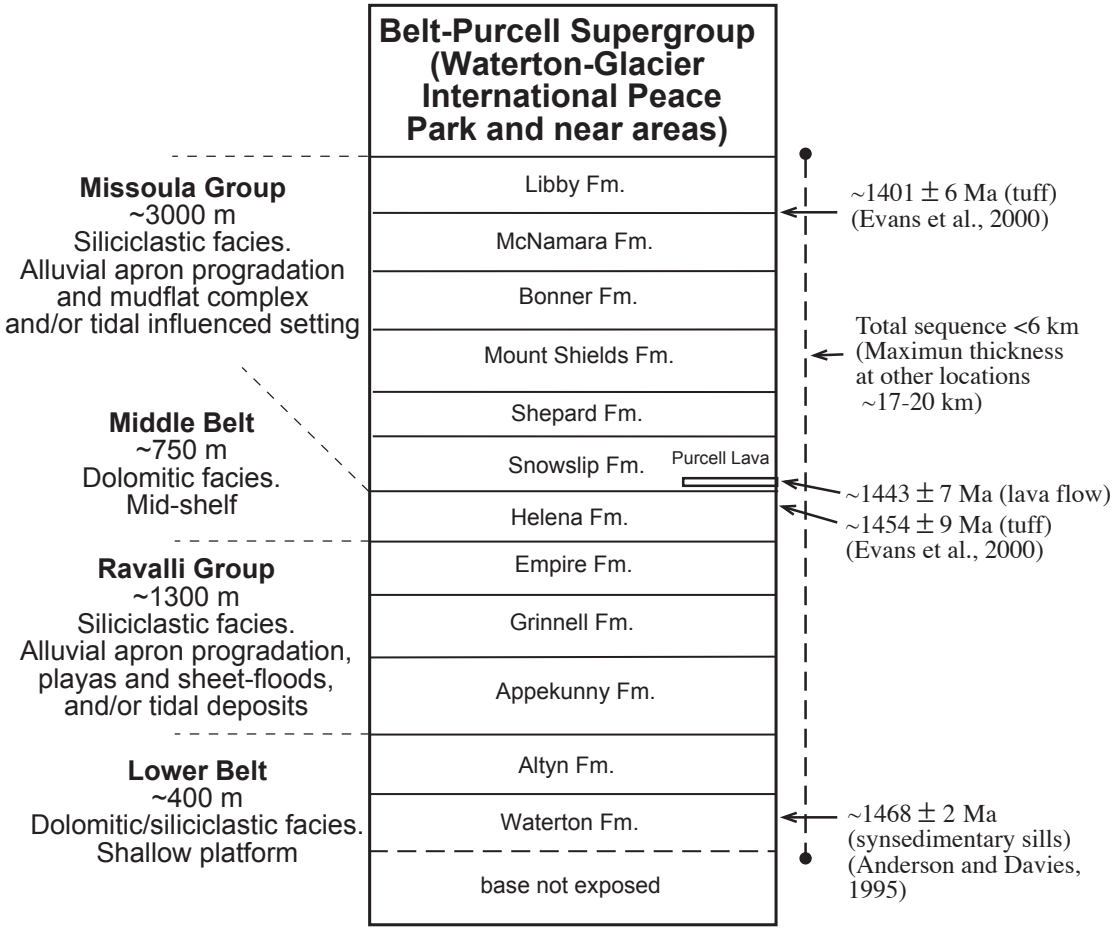

Fig. 2.3 Generalized stratigraphic section of the Belt-Purcell Supergroup at Waterton-Glacier International Peace Park (based on Whipple et al., 1984, 1997). Environmental settings from Winston (1986, 1990) and McMechan (1981), and U-Pb radiometric ages of various stratigraphic elements.

(3) In turn, the Ravalli Group grades into the middle Belt carbonate, represented by the Helena Formation at Waterton-Glacier International Peace Park. In the Purcell Mountains the Helena Formation is equivalent to the Kitchener Formation, and southeast to the Wallace Formation (Wallace et al., 1993; Figs. 2.5 and 2.6). The depositional setting has been interpreted as lacustrine

based on the presence of siliciclastic-carbonate cycles explained as the result of alternative wet and dry climates (Winston, 1986; Winston and Lyons, 1997). However, Wallace (1997) interpreted the argillite-limestone cycles of the Helena Formation as deposition in a subtidal environment in a carbonate shelf. Pratt (2001) interpreted the Helena Formation as a mid-shelf limestone. Mafic lava flows in the upper middle Belt are termed the Purcell Lavas (Table 2.3; Whipple et al., 1984).

(4) The stratigraphically highest Missoula Group comprises a wide variety of siliciclastic facies mainly argillites represented by the Snowslip and Shepard formations. Those formations have been laterally correlated with part of the Wallace Formation (Fig. 2.6; Whipple et al, 1984; Winston, 1986; Chandler, 2000), and the overlying Van Creek Formation. The Nicol Creek Formation includes tuff, massive, and amygdaloidal lava flows emplaced in shallow water non-marine flood plain setting (McMechan, 1981). These eruptives are correlative to the Purcell Lavas in the upper middle Belt and lower Snowslip Formation at Waterton-Glacier International Peace Park. The stratigraphically higher Mount Shields Formation is equivalent to the Gateway Formation and presents mud-cracks interpreted as the result of sedimentation in a lagoon in a hypersaline environment with periodic subaeral exposure (McMechan, 1981). The overlying Bonner Formation, and its correlative the Phillips Formation, display large-scale channels that to the southwest are interpreted as the result of an alluvial wedge associated with braided rivers (Winston, 1989), and to the southeast correlates with the McNamara Formation (Whipple et al., 1997). The highest Libby Formation, and its laterally equivalent the Rooseville Formation, have been interpreted as a whole as the result of northward progradational alluvial aprons and mud-flat complexes (e.g., Winston, 1986; Whipple et al., 1984, 1997), and/or tidal environments (e.g., McMechan, 1981; Table 2.4).

In summary, the Belt-Purcell rocks are variably interpreted as fluvial, alluvial, flood-plain, tidal, shallow water, shelf and deep turbiditic deposits. The general trend is that the sequence thickens westward, presenting more argillite content and less subaeral structures that suggest a deeper water environment. The lower Belt was a partially enclosed lake, or a restricted sea, that received most of the sediment as turbidites that represent the thickest part of the Belt-Purcell sequence. The Ravalli Group represents shallow water subaeral facies, whereas the middle Belt Supergroup comprises shallow-water shelf or lacustrine carbonates with fine-grained siliciclastic sediment. The Missoula Group is viewed as alluvial aprons deposited northward in a mud-flat environment (Fig. 2.4; e.g., Price, 1964; Harrison, 1972; Höy, 1982; Whipple et al., 1984, 1997; Winston 1986, 1990; McMechan, 1981).

There are drastic changes in formation thicknesses from the west to the east. For example,

the Prichard and Aldridge formations are up to ~12 km in the southwest, whereas their equivalents the Waterton and Altyn formations are only 2.5 km thick in the eastern Helena Embayment. Variations of stratigraphic thickness are related to syn-sedimentary faults; north-northwest basin parallel rift faults, and east north-east transfer faults (e.g., Lyons et al., 2000).

Fine clastic detritus of the Belt-Purcell Supergroup could represent the distal part of a large scale-river system (Price, 1964; McMechan, 1981; Rainbird et al., 1997; Chandler, 2000; Price and Sears, 2000; Ross and Villeneuve, 2003). The large volume of siliciclastic detritus represented by the Belt-Purcell sequence reflects fluvial transport from a low relief, continent scale catchment (Sears et al., 2004), and based on the palinspastically restored isopach map of the lower Belt presented by Price and Sears (2000), the fill entered the basin from the southwest forming a large delta. Lower units were deposited during active rifting, whereas the upper Belt is considered to represent basinal subsidence from thermal contraction of the lithosphere (Price and Sears, 2000; Lydon, 2000).

2.5 Controversy on the depositional setting

The depositional setting of the Belt-Purcell Supergroup is controversial. It has been interpreted variously as; (1) alluvial-lacustrine (e.g., Walcott, 1914; Winston, 1990; Lyons et al., 1997); (2) marine (e.g., Barrell, 1906; Fenton & Fenton, 1937; Ross, 1963; Frank et al., 1997; Schieber, 1997; Lydon, 2000); or (3) the result of a flood plain in a large subsiding delta (e.g., Price, 1964; Harrison, 1972). A detailed summary of the controversy on sedimentary setting of the Belt-Purcell Supergroup is presented in Winston et al. (1984) and Chandler (2000).

This controversy is based on the difficulty in interpretations of some of key data reported. Sedimentological observations such as polymodal cross-beds with bimodal orientation in the lower part of the Belt-Purcell sequence are viewed as evidence of marine tidal deposition (e.g., McMechan, 1981), whereas Winston (1990) interpreted the cross beds as the result of flows traveling back up tributaries and depressions adjacent to the main flood-plains. Reticulate patterns of cracks have been interpreted as desiccation cracks produced by subaerial exposure (e.g., Winston, 1990), or alternatively as syneresis produced by subaqueous shrinkage of clay by the loss of pore water (Pratt, 1998). Syneresis cracks form in sediments of saline lakes, but are not restricted to them, and can be found in seawater environments (Chandler, 2000 and references therein).

Several geochemical studies have produced non-conclusive results. Strontium concentrations in the carbonates of the Newland Formation are consistent with marine water

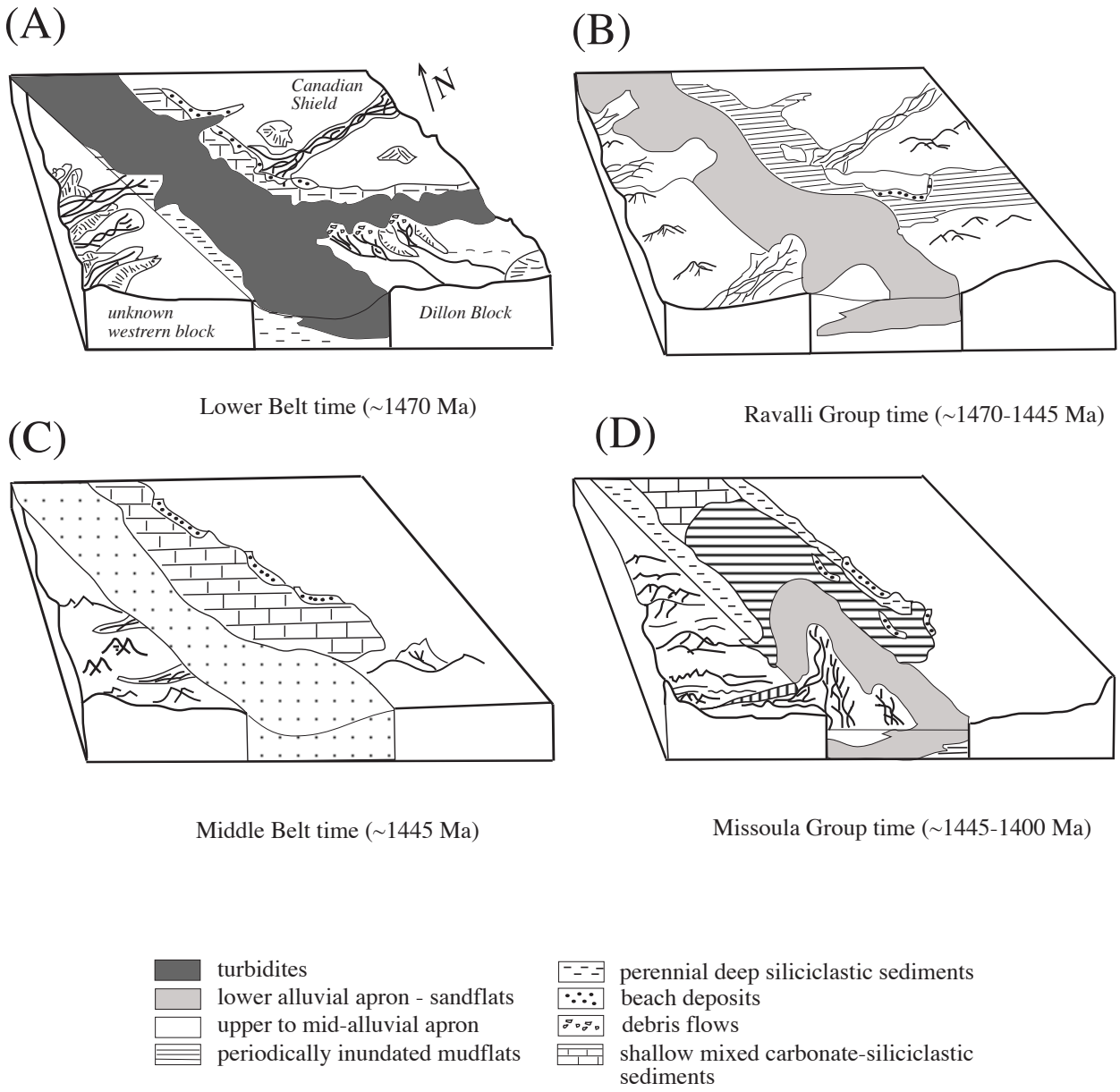

Fig. 2.4 Block diagrams showing inferred evolution of the Belt-Purcell Basin setting through time: (A) the lower Belt, (B) middle Belt, (C) middle Belt, and (D) Missoula Group. Modified by Chandler (2000) from Winston and Link (1997).

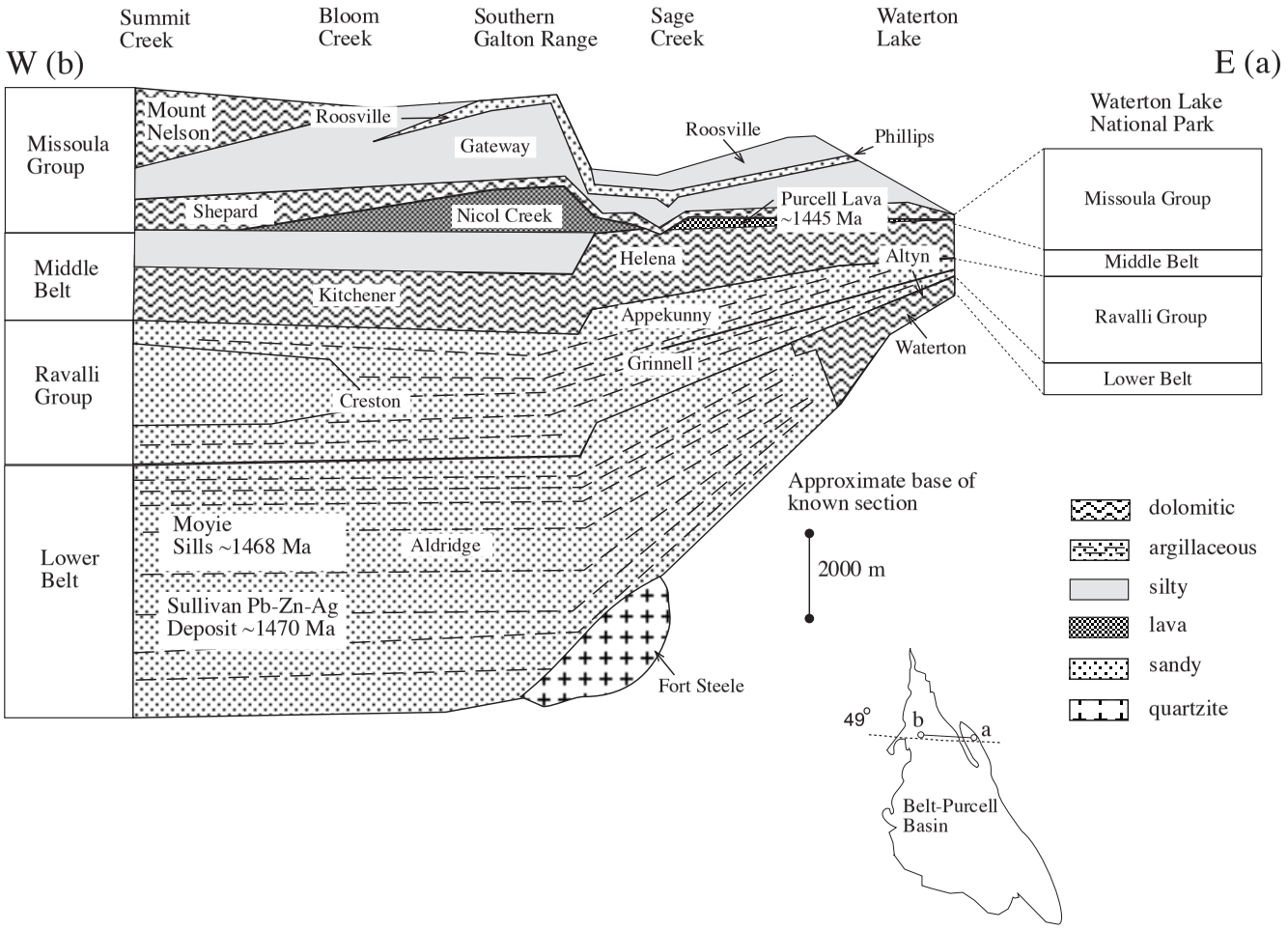

Fig. 2.5 Stratigraphic correlation of the Belt-Purcell Supergroup from McMechan (1981) displaying the main lithologies for locations close to the 49th parallel in Alberta and British Columbia. Dates from Evans et al. (2000) and Chandler (2000), and the addition of Fort Steele Formation (Ross and Villeneuve, 2003).

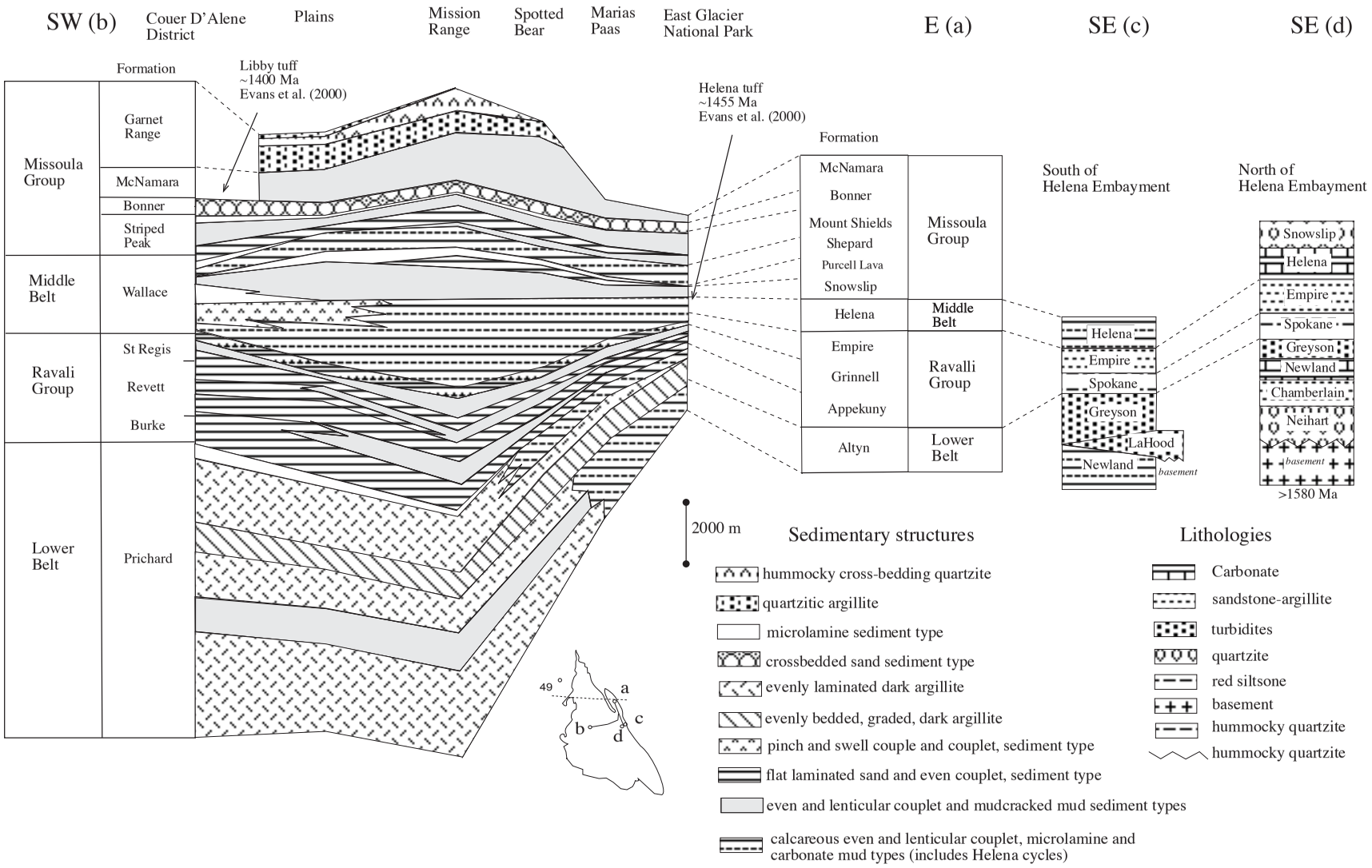

Fig. 2.6 (A) Stratigraphic correlation of the Belt-Purcell Supergroup from Winston (1990) for northwestern Montana. (B) Part of a simplified compilation from Chandler (2000), and dating insets from Evans et al. (2000).

Table 2.1 Principal stratigraphic features of the Belt-Purcell Supergroup at Waterton-Glacier International Peace Park and nearby areas.

Formation	Thickness (m)	Lithology	Sedimentary structures	Lateral correlation	Depositional environment	References
Libby	~950	Arenaceous, siltite argillite	Even-parallel lamination, mud-chip breccias, subaqueous shrinkage cracks	Garnet Formation to the southwest and Roosville Formation to the northwest	Shoreline and subaereal or alluvial aprons	Whipple et al. (1984; 1997)
McNamara	~60	Calcareous siltite, arenite, and quartz arenite	Mud-chip breccias, oolites	Phillips Formation to the northwest	Drawing of alluvial aprons	Whipple et al. (1984; 1997) Winston (1989)
Bonner	~250	Quartzite, minor siltite	Ripple cross-lamination, large-scale channels	Phillips Formation to the northwest	Alluvial wedge from braided rivers	Whipple et al. (1984; 1997) Link (1997)
Mount Shields	~800	Siltite-argillite, very fine-grained arenite, dolomites	Oolites, stromatolites, evaporitic casts, ripple cross-lamination, thin laminated	Striped Peak Formation southwest and Gateway Formation to the northwest	Floods in alluvial fan or playas	Slover and Winston (1986) Winston (1986)
Shepard	~470	Dolomite, siltite and argillite, with stromatolitic limestone	Wavy and non-parallel lamination, ripple marks, mud-chip breccias	Wallace Formation to the southwest and Nicol Creek Formation to the northwest	Mud-flats or shallow water	Whipple et al. (1984) Winston (1986) Chandler (2000)
Snowslip	~300	Calcareous siltite, argillite, and oolitic arenite. Intruded by the Purcell Lava, lava flows.	Laminated, wave ripples, mud-chip intraclasts	Wallace Formation to the southwest and Nicol Creek Formation to the northwest	Intertidal or subaereal	Whipple et al. (1984) Winston (1986) Chandler (2000)
Helena	~750	Lime mudstone, ooidal grainstones and with argillite, siltite and sandy dolomite. Halite and gypsum casts	Molar tooth structures, horizontally laminated, and stromatolites	Wallace Formation to the west and Kitchener Formation to the northwest	Mid-shelf or lacustrine.	Winston and Lyons (1997) Whipple et al. (1984) Grozinger (1986) Pratt (2001)
Empire	~360	Argillite, siltite, quartz arenite, becoming richer in carbonate content to the top	Herringbone cross-bedding, lamination, ripple, syneresis crack	Creston Formation to the north	Subtidal conditions	Whipple et al. (1984) Connor et al. (1984) Link (1997) Chandler (2000)
Grinnell	~800	Mainly red argillite with interbedding of white quartz arenite mainly at the top of the sequence	Parallel and non-parallel lamination, mud-breccias, fluid escape structures, subaqueous shrinkage cracks, cross laminated	St Regis-Revett-Burke formations to the southwest and Creston Formation to the north	Alluvial aprons, playas and sheet-floods or intertidal-subtidal	McMechan (1981) Höy (1982) Whipple et al. (1984) Winston (1990) Link (1997)
Appekunny	~700	Predominant green argillite, with sparse layers of quartz arenite	Parallel and non-parallel lamination, low angle cross-laminae, mud-breccias, fluid escape structures, subaqueous shrinkage cracks and fining- upward couplets	Prichard Formation to the southwest and Creston Formation to the north	Alluvial aprons, playas and sheet-floods or intertidal- subtidal	McMechan (1981) Höy (1982) Whipple et al. (1984) Winston (1990) Link (1997)
Altyn	~375	Arenaceous dolomite, dolomitic limestone and stromatolites. Argillite and quarzt arenite in the upper sequence. Anhydrite and gypsum	Herringbone cross-bedding, wave ripples, bimodal cross-lamination.	Prichard Formation to the west, Aldridge Formation to the north, and Newland-LaHood-Greyson-Neihart formations to the southeast in the Helena Embayment	Tidally influenced or lacustrine	McMannis (1963) Whipple et al. (1984; 1997) Winston (1989) Schieber (1989) Chandler (2000)
Waterton	~160	Algal dolomite with gypsum casts	Hummocky cross-bedding, wavy and lenticular bedding, lamination, mudcracks	Prichard Formation to the west and Aldridge Formation to the north	Shallow-subtidal to supratidal	Fermor and Price (1983) Chandler (2000)

Dashed lines delimit the four main stratigraphic divisions.

Table 2.2 Principal stratigraphic features of the Belt-Purcell Supergroup in the Purcell Mountains.

Formation	Thickness (m)	Lithology	Sedimentary structures	Lateral correlation	Depositional environment	References
Roosville	~1300	Argillite, dolomitic argillite, siltstone, sandstone	Lamination, stromatolites	Libby, McNamara and Garnet Range formations to the south	Mud-flat, tidal-flat shallow water	Price (1964) McMechan (1981) Chandler (2000)
Phillips	~150	Argillite, micaceous argillite, siltite, very fine to medium-grained quartzite	Ripple, mudcracks, lamination	Bonner Formation to the south	Sheet-flood, subaereal	McMechan (1981) Chandler (2000)
Gateway	~1350	Siltite, dolomitic siltite	Lamination, graded, symmetric and asymmetric ripples, salt casts, mudcracks	Mount Shields Formation to the south	Lagoon, hipersaline	McMechan (1981) Chandler (2000)
Shepard	~115	Dolomite, very fine-grained quartz arenite, dolomitic siltite, and argillite	Mudcracks, salt casts, stromatolites, cross bedding, ooilites, bioherms	Shepard Formation to the south	intertidal	McMechan (1981) Chandler (2000)
Nicol Creek	~750	Dolomitic siltite and argillite, tuff, volcanic sandstone; lava flows from basaltic to andesitic composition	Mudcracks, lamination, climbing ripples	Lower Shepard Formation to the south	Flood-plain or tidal-flat	McMechan (1981) Chandler (2000)
Van Creek	~420	Argillite and siltite, dolomitic siltite-argillite	Bipolar ripple cross-lamination, climbing ripples, mudcracks, syneresis cracks	Upper Helena Formation or lower Snowslip Formation south	Intertidal to mud-flat	McMechan (1981) Chandler (2000)
Kitchener	~1500	Calcareous dolomitic siltite and argillite, silty dolomite, argillite, siltite, minor quartzite	Climbing ripples, mudcracks, lenticular bedding, lamination, couplets argillite-siltite, graded bedding	Wallace Formation to the southwest and Helena Formation to the southeast	Carbonate shelf	McMechan (1981) Wallace et al. (1993)
Creston	~2200	Siltite and argillite with minor quartz arenites	Very fine laminated, cross-bedding, mudcracks, herringbone	Appekunny-Grinnell-Empire formations to the southeast and Prichard-St. Regis-Revett-Burke formations to the southwest	Shallow-subtidal	McMechan (1981) Chandler (2000)
Aldridge/ Fort Steele	~4200	Argillaceous quartzite and siltite, quartzites	Cross-bedding, turbiditic sequences, mudcracks	Prichar Formation to the southwest and Altyn and Waterton formations to the southeast.	Shallow to tidal and fluvial facies in the Fort Steele Formation	McMechan (1981) Lyons et al. (2000) Chandler (2000)

Dashed lines delimit the four main stratigraphic divisions. Wider space dashed lines signify that the limit of the stratigraphic group is approximated.

Table 2.3 Principal stratigraphic features of the Belt-Purcell Supergroup at Whitefish Range.

Formation	Thickness (m)	Lithology	Sedimentary and other structures	Lateral correlation	Depositional environment	Reference
Libby	~950	Arenaceous, siltite argillite	Even-parallel lamination, mud-chip breccias, subaqueous shrinkage cracks	Garnet Formation to the southwest and Roosville Formation to the northwest	Shoreline and subaereal or alluvial aprons	Whipple et al. (1984; 1997)
McNamara	~1200	Calcareous lithic arenite, dolomitic siltite, arenite, and quartz arenite	Mud-chip breccias, oolites, graded lamination	Phillips Formation to the northwest	Drawing of alluvial aprons	Whipple et al. (1984; 1997) Winston (1989)
Bonner	~250	Quartzite, minor siltite	Ripple cross-lamination, large-scale channels	Phillips Formation to the northwest	Alluvial wedge from braided rivers	Whipple et al. (1984; 1997) Link (1997)
Mount Shields	~800	Siltite-argillite, very fine-grained arenite, dolomites	Oolites, stromatolites, evaporitic casts, ripple cross-lamination, thin laminated.	Striped Peak Formation southwest and Gateway Formation to the northwest	Floods in alluvial fan or playas	Slover and Winston (1986) Winston 1986
Shepard	~220	Very fine-grained feldespatic arenite, calcareous arenite, siltite and argillite	Bioherms of stromatolites, oolites, oncolites, ripple marks, mud-chip breccias, molar-tooth structures	Wallace Formation to the southwest and Nicol Creek Formation to the northwest	Mud-flats or shallow water	Whipple et al. (1984) Winston (1986)
Snowslip (Purcell lava)	~600	Argillite, siltite, arenite, limestone. Lava flows.	Lamination, wavy and non-parallel, ripple marks, mud-chip breccias	Wallace Formation to the southwest and Nicol Creek Formation to the northwest	Mud-flats or shallow water	Whipple et al. (1984) Winston (1986)
Wallace	~350	Lime mudstone, dolomitic argillite, siltite and sandy dolomite	Stromatolites, oolites, lamination, erosional sufaces	Helena Formation to the southwest, Kitchener Formation to the north	Peritidal to subtidal, mid-shelf or lacustrine	Whipple et al. (1984) Grozinger (1986) Wallace et al. (1993) Winston and Lyons (1997) Pratt (2001)
Helena	~400	Lime mudstone, ooidal grainstones and with argillite, siltite and sandy dolomite. Halite and gypsum casts. Diorite intrusion	Molar tooth structures, horizontally laminated, stromatolites	Wallace Formation to the west and Kitchener Formation to the northwest	Peritidal to subtidal, mid-shelf or lacustrine	Whipple et al. (1984) Grozinger (1986) Wallace et al. (1993) Winston and Lyons (1997) Pratt (2001)
Empire	~300	Argillite, siltite, quartz arenite, becoming richer in carbonate content to the top	Herringbone cross-bedding, lamination, ripple, syneresis crack, mud-chip breccias	Creston Formation to the north	Subtidal conditions	Whipple et al. (1984) Connor et al. (1984) Chandler (2000)
Spokane	~1100	Mainly red argillite with interbedding of white quartz arenite	Parallel and non-parallel lamination, mud-breccias, shrinkage cracks, cross laminated	Creston Formation to the north, Grinnell Formation to the northwest	Alluvial aprons, playas, sheet-floods, lacustrine	Whipple et al. (1984) Connor et al. (1984) Winston (1990) Link (1997) Chandler (2000)
Burke	~300	Argillite, siltite, sparse layers of quartz arenite	Parallel and non-parallel lamination, low angle crosslaminae,	Grinnell Formation to the northeast, Creston Formation to the north	Alluvial aprons, playas and sheet-floods or intertidal- subtidal	Whipple et al. (1984) Winston (1990) Chandler (2000)
Prichard	~1500	Argillite, siltite, and minor quartzie	Lamination, tubiditic facies.	Aldridge Formation to the north, Altyn and Waterton formations to the northeast, and Newland-LaHood-Greyson-Neihart formations to the southeast in the Helena Embayment	Deep-basinal and upper sequence shallow water	Whipple et al. (1984; 1997) Winston (1989) Godward (1997) Chandler (2000)

Dashed lines delimit the four main stratigraphic divisions. Wider space dashed lines signify that the limit of the stratigraphic group is approximated.

(Schieber, 1993). Lyons et al. (1997) found C-O isotopic ratios similar to meteoric water in the middle Belt suggesting lacustrine or highly restricted conditions during deposition. However, carbonates are readily reset compositionally and isotopically by recent groundwater (O'Neill, 1987). Alteration in wall rocks of the Sullivan deposit, and massive tourmaline, are in keeping with hot, modified seawater (Leitch et al., 2000). Argillites of the Ravalli Group present glauconite, S content and sulfur isotope data coupled with major element contents that are interpreted by Schieber (1997) as the signature of marine waters. In addition, Chandler and Grégorie (2000) using delta^{34}S from evaporitic nodules in the Altyn Formation to interpret the Belt-Purcell rocks as marine with limited access to the ocean.

Regardless of the controversy about the marine, freshwater, or fluctuating environmental setting of the Belt-Purcell sedimentary rock, a general agreed view is that the lower Belt was deposited in deep waters with marginal shoreline facies that evolved into the shallow and subaeral facies (Ravalli Group). Water depth deepened during deposition of carbonates of the middle Belt, and evolved into very shallow to subaerally exposed deposits (Fig. 2.4). Diversity of evaporitic minerals found locally in the Belt-Purcell sequence, coupled with the presence of syneresis cracks, are interpreted as indicative of saline waters in the Belt-Purcell Basin (e.g., McMechan, 1981; Connor et al., 1984; Schieber, 1993, 1997; Chandler, 2000 and references therein).

2.6 Paleoclimate

Most paleomagnetic, paleoclimatic and sedimentary data suggest that the Belt-Purcell Supergroup sediments were deposited at latitudes between 10^{o} and 35^{o} (Chandler, 2000). Weathering-alteration studies, coupled with petrographic observations of feldspars, hematitic clasts, and presence of evaporites in the Belt-Purcell rocks, as well as geochemical studies based on major and trace elements, have interpreted the Belt-Purcell depositional setting as under arid to semi-arid climate with intermittent wetter intervals (e.g., Harrison, 1972; White and Winston, 1982; Schieber, 1992; Slack and Höy, 2000; Lydon, 2000; Chandler, 2000 and references therein). However, calcretes or sea-sands typically associated with modern arid environments have not been described (Chandler, 2000).

2.7 Age of sedimentation

The Purcell Lava is up to 15 m of tholeiitic basalts, and locally pillow lavas indicative of subaqueous environment constituting an excellent index marker in the Belt-Purcell sequence (e.g.,

Whipple et al., 1984; Anderson and Goodfellow, 2000). The Purcell Lava intrudes the lower part of Snowslip Formation in the Missoula Group, or the upper Helena Formation at Waterton-Glacier International Peace Park (e.g., Whipple et al., 1984).

The duration of sedimentation for the Belt-Purcell Supergroup was ≤75 Ma. A minimum age of sedimentation is estimated at 1468 ± 2 Ma and 1469 ± 3 Ma by U-Pb from zircons in the tholeiitic basalt Moyie sills located in the Aldridge Formation near the base of the Belt-Purcell sequence (Anderson and Davis, 1995; Sears et al., 1998). This age excludes hidden strata below the Aldridge Formation and above the basement (Lydon, 2000). The Moyie sills intruded the sediment when it was still soft, constraining early sedimentation of lower Belt-Purcell strata. The lower-middle Belt spans ≤25 Ma; a minimum age of 1454 ± 9 Ma is determined from zircons in a tuff horizon at the upper part of the middle Belt (Fig. 2.3; Evans et al., 2000). A maximum age of 1401 ± 6 Ma was obtained from U-Pb dating of zircons extracted from a tuff horizon in the Bonner and Libby formations, of the upper Missoula Group (Fig. 2.3; Evans et al., 2000). These dates, coupled with stratigraphic thicknesses of the Belt-Purcell sequence, show that two thirds of the sedimentation took place between ~1470 Ma and ~1445 Ma of lava flows in the middle Belt (Fig. 2.3).

2.8 Thermal history

Lydon (2000) presented three main tectono-thermal events recorded in the Belt-Purcell Supergroup: (1) intracontinental rift system at ~1500 Ma accompanied by heat flow during thinning of lithosphere; (2) extensional events during the breakup of Rodinia at ~850 Ma; and (3) the Jurassic-Paleocene (160 to 60 Ma) Laramide event of the North American Cordillera.

Metamorphic grade spans from subgreenschist at upper stratigraphic levels in the east, through greenschist facies at the lowest stratigraphic levels, to amphibolite facies in the west proximal to major plutons (Maxwell and Hower, 1967; Harrison, 1972). According to Maxwell and Hower (1967), the illite 1Md transforms in the Belt-Purcell sequence at depth into 2M polymorph in dioctaedral mica (muscovite-like mica polymorph). 1Md illite is more abundant in the upper sequence reacting at depth to 2M that becomes more predominant. The 2M polymorph is stable to ~350^{o} C (Rosenberg, 2002). Metamorphic grade is lower greenschist facies at the three localities sampled for this study.

2.9 Provenance from geochemistry and detrital mineral ages

Ross and Villeneuve (2003) reported an extensive summary of data to constrain potential

source terranes for the four stratigraphic groups of the Belt-Purcel Supergroup. They compiled: over 400 detrital zircons dated by spatial high resolution ion microprobe (SHRIMP), complemented by Ar-Ar ages of detrital muscovite throughout the Belt-Purcell sequence; paleocurrent, stratigraphic and sedimentological data; as well as in Sm-Nd isotopic and trace element data. (e.g., Price 1964; Harrison, 1972, McMechan, 1981; Whipple et al., 1984; Höy, 1993; Winston, 1986, 1989; 1990; Ross et al., 1991, 1992; Frost and Winston, 1987; Slack and Höy, 2000). They argued that lower Belt, Ravalli Group and middle Belt have age signatures corresponding to an eastern Laurentian source with Proterozoic (older than 1750 Ma) and Archean ages from the eastern Canadian Shield. In addition, a southern source was inferred with mainly Archean and minor Proterozoic ages (1800-1750 Ma) that could be from the Dillon Block; and an unknown western source invoked due to the presence of paleocurrents from the west combined with 1610-1490 Ma detrital zircons ("magmatic gap"; ages are not present in Laurentia), that drifted away (Fig. 2.4a). The Missoula Group could have been fed from the Mojave and/or Yavapai Provinces (Fig. 2.2). Ross and Villeneuve (2003) suggested as a potential western source some terranes in Australia. The eastern source, contributing mainly sandstones in the Belt-Purcell sequence, interfingers stratigraphically to the west with argillites derived from the western source (e.g., Frost and Winston, 1987; Winston, 1990).

2.10 References

Anderson, H.E., Davis, W.D., 1995. U-Pb geochronology of the Moyie sills, Purcell Supergroup, southeastern British Columbia: implications for the Mesoproterozoic geological history of the Purcell (Belt) basin. Can. J. Earth Sci., 32, 1180-1193.

Anderson, H.E., Goodfellow, W.D., 2000. Geochemistry and isotope chemistry of the Moyie sills: implications for the early tectonic setting of the Mesoproterozoic Purcell basin. In: Lydon, J.W., Höy, T., Slack, J.F., Knapp, M.E., (eds.), The Geological Environment of the Sullivan Deposit, British Columbia. Geol. Assoc. Can. Min. Dep. Div. Spec. Publ. 1, pp. 302-321.

Barrell, J., 1906. Relative geological importance of continental, littoral, and marine sedimentation, part II. J. Geol., 14, 430-457.

Chandler, F.W., 2000. The Belt-Purcell basin as a low-latitude passive rift: implications for the geological environment of Sullivan type deposits. In: Lydon, J.W., et al., Höy, T., Slack, J.F., Knapp, M.E., (eds.), The Geological Environment of the Sullivan Deposit, British Columbia. Geol. Assoc. Can. Min. Dep. Div. Spec. Publ. 1, pp. 82-112.

Chandler, F.W., Grégoire, D.C., 2000. Sulphur, strontium, and boron isotopes from replaced sulphate evaporite nodules in the Altyn Formation, lower Belt Supergroup, Montana: clues to the sedimentary environment of the Sullivan deposit. In: Lydon, J.W., Höy, T., Slack, J.F., Knapp, M.E., (eds.), The

Geological Environment of the Sullivan Deposit, British Columbia. Geol. Assoc. Can. Min. Dep. Div. Spec. Publ. 1, pp. 251-258.

Clowes, R.M., Cook, F.A., Ludden, J.N., 1998. Lithopobe leads to new perspectives on continental evolution. Geol. Soc. Am. Today 8, 2-7.

Connor, J.J., Reynolds, M.W., Whipple, J.W., 1984. Stratigraphy of the Ravalli Group, Belt basin, Montana and Idaho. In: Hobbs, S.W., (ed.), The Belt Abstracts with Summaries, Belt Symposium II, Montana Bur. Min. Geol., Spec. Publ. 90, pp. 13-15.

Earhart, R.L., Mudge, M.R., Connor, J.J., 1984. Belt Supergroup lithofacies in the northern disturbed Belt, northwest Montana. The Belt Series, Montana Geol. Soc., Field Conf., pp. 51-66.

Evans, K.V., Aleinikoff, J.N., Obradovich, J.D., Fanning, C.M., 2000. SHRIMP U-Pb geochronology of volcanic rocks, Belt Supergroup, western Montana: evidence for rapid deposition of sedimentary strata. Can. J. Earth Sci., 37, 1287-1300.

Fenton, C.L., Fenton, M.A., 1937. Belt Series of the north: stratigraphy, sedimentation, paleontology. Geol. Soc. Am. Bull. 48,1873-1970.

Fermor, P.R., Price, R.A., 1983. Stratigraphy of the lower part of the Belt-Purcell Supergroup (middle Proterozoic) in the Lewis Thrust sheet of southern Alberta and British Columbia. Bull. Can. Petrol. Geol. 31, 164-194.

Folk, R.L., 1968. Petrology of sedimentary rocks. Hemphill's, Austin, U.S.A.

Frank, T.D., Lyons, T.W., Lohmann, K., 1997. Isotopic evidence for the environmental evolution of the Mesoproterozoic Helena Formation, Belt Supergroup, Montana, USA. Geochim. Cosmochim. Acta 61, 5023-5041.

Frost, C.D., Winston, D., 1987. Nd isotope systematics of coarse- and fine-grained sediments: examples from the middle Proterozoic Belt-Purcell Supergroup. J. Geol. 95, 309-327.

Godard, E.N.J., 1997. Sediment dispersal pathways in quartzite units of the lower Prichard Formation Pine Creek drainage, Idaho. In: Link, P. K., (ed.), Geologic Guidebook to the Belt-Purcell Supergroup, Glacier National Park and Vicinity, Montana and Adjacent Canada, Field Trip Guidebook for the Belt Symposium III, Belt Association, Pocatello, Idaho, pp. 44-55.

Goodwin, A.M., 1991. Precambrian geology: the dynamic evolution of the continental crust. Academic Press, San Diego, U.S.A., 666 pp.

Grotzinger, J.P., 1986. Shallowing-upward cycles of the Wallace Formation, Belt Supergroup, northwestern Montana and northern Idaho. In: Roberts, S.M., (ed.), Belt Supergroup, a Guide to Proterozoic Rocks of Western Montana and Adjacent Areas, Montana Bur. Min. Geol., Spec. Publ. 94, 143-160.

Harrison, J.E., 1972. Precambrian Belt basin of northwestern United States: its geometry, sedimentation, and copper occurrences. Geol. Soc. Am. Bull. 83, 1215-1240.

Harrison, J.E., Grimes, D.J., 1970. Mineralogy and geochemistry of some Belt rocks, Montana and Idaho,

U.S. Geol. Survey Bull. 1312-O, 49 pp.

Hoffman, P. F., 1988. United plates of America, the birth of a craton: early Proterozoic assembly and growth of Laurentia, Ann. Rev. Earth Planet. Sci. 16, 543-603.

Hoffman, P. F., 1991. Did the breakout of Laurentia turn Gondwanaland inside-out? Science 252, 1409-1412.

Höy, T., 1982. The Purcell Supergroup in southeastern British Columbia: sedimentation, tectonics and stratiform lead-zinc deposits. In: Hutchinson, R.W., Spence, C.D., Franklin, J.M., (eds.), Precambrian Sulphide Deposits, H.S. Robinson Memorial vol., Geol. Assoc. Can. Spec. Paper 25, 127-147.

Höy, T., 1993. Geology of the Purcell Supergroup in the Fernie west-half map-area, southeastern British Columbia. British Columbia Ministry of Energy, Min. Petrol. Resour. Bull. 84, 157.

Höy, T., Anderson, D., Turner, R.J.W., Leitch, C.H.B., 2000. Tectonic, magmatic, and metallogenic history of the early synrift phase of the Purcell basin, southeastern British Columbia. In: Lydon, J.W., Höy, T., Slack, J.F., Knapp, M.E., (eds.), The Geological Environment of the Sullivan Deposit, British Columbia. Geol. Assoc. Can. Min. Dep. Div. Spec. Publ. 1, pp. 32-60.

Kleinkopf, M.D., 1997. Interpretation of regional aeromagnetic and gravity anomalies in the Belt-Purcell terrane and adjacent areas, northern Rocky Mountains, United States and Canada. In: Berg, R.B., (ed.), Belt Symposium III. Montana Bur. Min. Geol. Spec. Publ. 112, 210-221.

Leitch, C.H.B., Turner, R.J.W. Ross, K.V., Shaw, D.R., 2000. Wallrock alteration at the Sullivan deposit and surrounding area, In: Lydon, J.W., Höy, T., Slack, J.F., Knapp, M.E., (eds.), The Geological Environment of the Sullivan Deposit, British Columbia. Geol. Assoc. Can. Min. Dep. Div. Spec. Publ. 1, pp. 618-632

Link, P.K., 1997. The Grinnell, Empire and Helena formations along Baring Creek and at Siyeh Pass, Glacier National Park. In: Link, P. K., (ed.), Geologic Guidebook to the Belt-Purcell Supergroup, Glacier National Park and Vicinity, Montana and Adjacent Canada, Field Trip Guidebook for the Belt Symposium III, Belt Association, Pocatello, Idaho, pp. 113-124.

Lydon, J.W., 2000. A synopsis of the understanding of the geological environment of the Sullivan Deposit, In: Lydon, J.W., Höy, T., Slack, J.F., Knapp, M.E., (eds.), The Geological Environment of the Sullivan Deposit, British Columbia. Geol. Assoc. Can. Min. Dep. Div. Spec. Publ. 1, pp. 12-31.

Lydon, J.W., Walker, R., Anderson, H.E., 2000. Lithogeochemistry of the Aldridge Formation and the chemical effects of burial diagenesis. In: Lydon, J.W., Höy, T., Slack, J.F., Knapp, M.E., (eds.), The Geological Environment of the Sullivan Deposit, British Columbia. Geol. Assoc. Can. Min. Dep. Div. Spec. Publ. 1, pp. 137-179.

Lyons, T.W., Luepke, J.J., Schreiber, M.E., Zieg, G.A., 2000. Sulfur geochemical constraints on Mesoproterozoic restricted marine deposition: lower Belt Supergroup, northwestern United States, Geochim. Cosmochim. Acta 64, 427-437.

Lyons, T.W., Frank, T.D., Schreiber, M.E., Winston, D., Lohmann, K.C., 1997. Geochemical constraints on paleoenvironments within the Belt Supergroup (Middle Proterozoic), Montana, In: Berg, R.B., (ed.), Belt Symposium III. Montana Bur. Min. Geol., Spec. Publ. 112, 190-201.

Maxwell, D.T., Hower, J., 1967. High-grade diagenesis and low-grade metamorphism of illite in the Precambrian Belt series. Am. Mineral. 52, 843-857.

McMannis, W.J., 1963. LaHood Formation – A coarse facies of the Belt series in southwestern Montana, Geo. Soc. Am. Bull. 74, 407-436.

McMechan, M.E., 1981. The middle Proterozoic Purcell Supergroup in the southwestern Rocky and southeastern Purcell Mountains, British Columbia and the initiation of the Cordilleran miogeocline, southern Canada and adjacent United States. Bull. Can. Petrol. Geol. 29, 583-621.

Mueller, P.A., Shuster, R.D., Wooden, J.L., Erslev, E.A., Bowes, D.R., 1993. Age and composition of Archean crystalline rocks from the southern Madison Range, Montana: implications for crustal evolution in the Wyoming Craton. Geo. Soc. Am. Bull. 105, 437-446.

O'Neil, J.R., 1987. Preservation of H, C, and O isotopic ratios in the low temperature environment. In: Kyser, T.K. (ed.), Short Course in Stable Isotope Geochemistry of Low Temperature Fluids. Mineral. Assoc. Can. 13, pp. 85-128.

Poage, M.A., Hyndman, D.W., Sears, J.W., 2000. Petrology, geochemistry, and diabase-granophyre relations of a thick basaltic sill emplaced into wet sediments, western Montana. Can. J. Earth Sci. 37, 1109-1119.

Pratt, B.R., 1998. Syneresis cracks: subaqueous shrinkage in argillaceous sediments caused by earthquake-induced dewatering. Sed. Geol. 117, 1-10.

Pratt, B.R., 2001. Oceanography, bathymetry and syndepositional tectonics of a Precambrian intracratonic basin: integrating sediment, storms, earthquakes and tsunamis in the Belt Supergroup (Helena Formation, ca. 1.45 Ga), western North America. Sed. Geol. 141, 371-394.

Price, R.A., 1964. The Precambrian Purcell System in the Rocky Mountains of southern Alberta and British Columbia. Bull. Can. Petrol. Geol., Spec. Publ. 12, 399-426.

Price, R.A., Sears, J.W, 2000. A preliminary palinspastic map of the Mesoproterozoic Belt-Purcell Supergroup, Canada and USA: implications for the tectonic setting and structural evolution of the Purcell anticlinorium and the Sullivan deposit. In: Lydon, J.W., Höy, T., Slack, J.F., Knapp, M.E., (eds.), The Geological Environment of the Sullivan Deposit, British Columbia. Geol. Assoc. Can. Min. Dep. Div. Spec. Publ. 1, pp. 61-81.

Rainbird, R.H., Ernst, R.E., 2001. The sedimentary record of mantle-plume uplift. In: Ernst, R.E., Buchan, K.L., (eds.), Mantle Plumes: Their Identification Through Time. Geol. Soc. Am. Spec. Paper 352, pp. 227-246.

Rainbird, R.H., McNicoll, V.J., Theriault, R.J., Heaman, L.M., Abbott, J.G., 1997. Pan-continental river

system draining Grenville Orogen recorded by U-Pb and Sm-Nd geochronology of Neoproterozoic quartzarenites and mudrocks, northwestern Canada. J. Geol. 105, 1-17.

Rosenberg, P.E., 2002. The nature, formation, and stability of end-member illite: a hypothesis. Am. Mineral. 87, 103-107.

Ross, C.P, 1963. The Belt series in Montana. U. S. Geol. Survey Prof. Paper 346, 1-122.

Ross, G.M., Villeneuve, M.E., 2003. Provenance of the Mesoproterozoic (1.45 Ga) Belt basin (western North America): another piece in the pre-Rodinia paleogeographic puzzle. Geol. Soc. Am. 115, 1191-1217.

Ross, G.M., Parrish, R.R., Dudás, F.Ö., 1991. Provenance of the Bonner Formation (Belt Supergroup), Montana: insights from U-Pb and Sm-Nd analyses of detrital minerals. Geology 19, 340-343.

Ross, G.M., Parrish, R.R., Winston, D., 1992. Provenance and U-Pb geochronology of the Mesoproterozoic Belt Supergroup (northwestern United States): implications for age of deposition and pre-Panthalassa plate reconstructions. Earth Planet. Sci. Lett. 113, 57-76.

Ross, C.P., Parrish, R.R., Villenueve, M.E., Bowring, S.A., 1990. Geophysics and geochronology of the crystalline basement of the Alberta basin, western Canada. Can. J. Earth Sc. 28, 512-522.

Schandl, E. S., Gorton M. P., Lydon J. W., 2000, Trace and rare earth element study of sediments associated with the Sullivan sedex deposit, British Columbia: implications for element mobility and tectonic environment. In: Lydon, J.W., Höy, T., Slack, J.F., Knapp, M.E., (eds.), The Geological Environment of the Sullivan Deposit, British Columbia. Geol. Assoc. Can. Min. Dep. Div. Spec. Publ. 1, pp. 202-217

Schieber, J., 1989. The origin of the Neihart quartzite, a basal deposit of the Mid-Proterozoic Belt Supergroup, Montana, U.S.A. Geol. Mag. 126, 271-281.

Schieber, J., 1992. A combined petrographical-geochemical provenance study of the Newland Formation, mid-Proterozoic of Montana. Geol. Mag. 129, 223-237.

Schieber, J., 1993. Sedimentological, geochemical, and mineralogical features of the Belt Supergroup and their bearing on the lacustrine versus marine debate. In: Berg, R.G., (ed.), Belt Symposium III. Montana Bur. Min. Geol. Spec. Publ. 112, pp. 177-189.

Schieber, J., 1997. Sedimentological, geochemical, and mineralogical features of the Belt Supergroup and their bearing on the lacustrine versus marine debate. In: Link, P. K., (ed.), Belt Symposium III, Geologic Guidebook to the Belt-Purcell Supergroup, Glacier National Park and Vicinity, Montana and Adjacent Canada, Belt Association, Pocatello, Idaho, pp. 177-189.

Sears, J.W., Chamberlain, K.R., Buckley, S.N., 1998. Structural and U-Pb geochronological evidence for 1.47 Ga rifting in the Belt Basin, western Montana. Can. J. Earth Sci. 35, 467-475.

Sears, J.W., Price, R.A., Khudoley, A.K, 2004. Linking the Mesoproterozoic Belt-Purcell Supergroup and Udzha Basin across the west Laurentia-Siberia connection. Precambrian Res. 129, 291-308.

Slack, J.F., Höy, T., 2000. Geochemistry and provenance of clastic metasedimentary rocks of the Aldridge and Fort Steele formations, Purcell Supergroup, southeastern British Columbia. In: Lydon, J.W., Höy, T., Slack, J.F., Knapp, M.E., (eds.), The Geological Environment of the Sullivan Deposit, British Columbia. Geol. Assoc. Can. Min. Dep. Div. Spec. Publ. 1, pp. 180-201.

Slover, S.M., Winston, D., 1986. Fining-upward sequences in Mount Shields Formation members 1, and 2, central Belt basin, Montana. In: Roberts, S.M., (ed.), Belt Supergroup, a Guide to Proterozoic Rocks of Western Montana and Adjacent Areas. Montana Bur. Min. Geol. Spec. Publ. 94, 169-181.

Walcott, C.D., 1914. Precambrian Algonkian algal flora, in Cambrian geology and paleontology III. Smithsonian Miscell. Collec. 64 , 77-156.

Wallace, C.A., 1997. Paleotransport directions and basin configuration, middle part of the Missoula Group (Belt Supergroup, middle Proterozoic) western Montana. Belt Symposium III, Montana Bur. Min. Geol. Spec. Publ., 112, 88-103.

Wallace, C.A., Harrison, J.E., Lidke, D.J., 1993. Lithofacies of the Helena and Wallace Formations (Belt Supergroup, middle Proterozoic), Montana and Idaho. Belt Symposium III, Informal program and abstracts, Montana, pp. 3.

Whiple, J. W., J. J. Connor, Raup O. B., McGrimsey R. G., 1984. Preliminary report on the stratigraphy of the Belt Supergroup, Glacier National Park and adjacent Whitefish Range, Montana, in northwest Montana and adjacent Canada. In: McBane, J.D., Garrison, P.B., (eds.), Guidebook, Field Conference and Symposium, Belt Association, Pocatello, Idaho, Montana Geol. Soc., pp. 33-50.

Whipple, J.W., Binda, P.L., Winston, D., 1997. Geologic guide to Glacier National Park, Montana and areas adjacent to Waterton, Alberta. In: Link , P.K., (ed.), Belt Symposium III, Geologic Guidebook to the Belt-Purcell Supergroup, Glacier National Park and Vicinity, Montana and adjacent Canada, Belt Association, Pocatello, Idaho, pp. 125-155.

White, B.G., Winston, D., 1982. The Revett-St. Regis “transition zone” near the Bunker Hill mine, Coeur d’Alene District, Idaho. In: Reid, R.R., Williams, G.A., (eds.), Society of Economic Geologists Coeur d’Alene Field Conference. Idaho Bur. Min. Geol. Bull. 24, pp.16-17.

Winston, D., 1986. Sedimentology of the Ravalli Group, middle Belt carbonate and Missoula Group, middle Proterozoic Belt Supergroup, Montana, Idaho and Washington. In: Roberts, S.M., (ed.), A Guide to Proterozoic Rocks of Western Montana and Adjacent Areas. Montana Bur. Min. Geol. Spec. Publ. 94, pp. 85-124.

Winston, D., 1989. A sedimentary and tectonic interpretation of the Belt. In: Hanshaw, P.M., (ed.), Middle Proterozoic Belt Supergroup, Western Montana, 28th International Geological Congress, Field Trip Guidebook T334. Am. Geophysical Union, pp. 437-469.

Winston, D., 1990. Evidence for intracratonic, fluvial and lacustrine settings of Middle to late Proterozoic basins of western U.S.A. In: Gower, C.F., Rivers, T., Ryan, B., (eds.), Mid-Proterozoic Laurentia-

Baltica. Geol. Assoc. Can. Spec. Paper 38, 535-564.

Winston, D., Link, P.K., 1993. Middle Proterozoic rocks of Montana, Idaho ans eastern Washington: the Belt Supergroup. In: Reed, J.C., Bickford, M.E., Houston, R.S., Link, P.K., Rankin, D.W., Sims, P.K., Van Schmus, W.R., Precambrian Conterminous U.S., The Geology of North America. Geol. Assoc. Am., C-2, pp. 487-517.

Winston, D., Lyons, T., 1997. Sedimentary cycles in the St. Regis, Empire and Helena formations of the middle Proterozoic Belt Supergroup, northwestern Montana. In: Link, P.K., (ed.), Geological Guidebook to the Belt-Purcell Supergroup, Glacier National Park and Vicinity, Montana and Adjacent Canada, Belt Symposium III, Field Trip guidebook, Belt association, Spokane, pp. 21-51.

Winston, D., Woods, M., Byer, G.B., 1984. The case for an intracratonic Belt-Purcell basin: tectonic, stratigraphic and stable isotopic considerations. Montana Geol. Soc., Field Conf., Northwestern Montana, pp. 103-118.

Yin, A., Kelty, T.K., 1991. Structural evolution of the Lewis plate in Glacier National Park, Montana: implications for regional tectonic development. Geol. Soc. Am. Bull. 103, 1073-1089.

Yoos, T.R., Potter, C.J., Thigpen, J.L., Brown, L.D., 1991. The Cordilleran foreland thrust belt in northwestern Montana and northern Idaho from COCORP and industry seismic reflection data. Am. Assoc. Petrol. Geol. Bull. 75, 1089-1106.

Zhao, G., Sun, M., Wilde, S.A., Li, S., 2004. A Paleo-Mesoproterozoic supercontinent: assembly, growth and breakup. Earth Sci. Rev. 67, 91-123.

CHAPTER III

Analytical Methods

The present geochemical study on sedimentary rocks of the Belt-Purcell Supergroup describes major and trace element systematics in order to address three main issues: (1) provenance; (2) diagenesis; and (3) weathering. To accomplish these goals, three analytical techniques were applied to quantify elemental composition of the sedimentary rocks of the Belt-Purcell sequence: (1) X-Ray fluorescence spectrometry (XRFS) for major elements (>90 wt.% oxide to 0.01 wt.% oxide) and clay mineralogical identification; (2) inductively coupled plasma mass spectrometry (ICP-MS) for trace elements (100s ppm to 0.001 ppm); and (3) chemical Th-U-total Pb method based on electron microprobe analyses using wavelength dispersive spectrometry (WDS) to determine monazite ages. This chapter aims to describe the basis and reasons for use of the mentioned techniques, as well as setting out the protocols for sample preparation.

3.1 Sample design

Three field seasons were conducted to collect a total of 217 representative samples of the Belt-Purcell Supergroup sequence at three locations: (1) Waterton-Glacier International Peace Park and areas close by in Alberta and Montana; (2) the Purcell Mountains, British Columbia; and (3) Whitefish Range, Montana (Fig. 3.1). These three locations were selected for two interrelated reasons: (1) near complete stratigraphic sections could be sampled, and (2) distances of around 100 km between the locations confers greater confidence in stratigraphic, and therefore geochemical testing correlations.

Various studies have established that REE in sedimentary rocks are concentrated mainly in the clay-size and silt-size (<20 μm) fractions, but are not associated with any particular clay mineral species, such that fine-grained sedimentary rocks best preserve the geochemical characteristics of the source area (e.g., Cullers et al., 1979; Chaudhuri and Cullers, 1979; Taylor and McLennan, 1985, 1995; Condie, 1991; Gao and Wedepohl, 1995; Nesbitt et al., 1996; Faupl et al., 1998). Sandstone facies may display geochemical effects due to heavy mineral sorting as a significant fraction of their trace element budget may reside in heavy minerals (e.g., Roaldset, 1979; Taylor

and McLennan, 1985; Condie, 1991; Roser, 1996).

Accordingly, samples were collected from exposed outcrops to cover the full extent of the stratigraphic Belt-Purcell stratigraphic sequence at the three locations mentioned, including, argillite and sandstone facies, to address potential geochemical differences based on sorting effects and/or different source areas. A subset of 126 samples, representative of the dominant facies, was processed for this study based on uniformity of facies and stratigraphic coverage of the total sequence at the three locations sampled (Figs. 3.2, 3.3, 3.4, and 3.5). The remainder of the samples were archived for future research. Sample geographic coordinates, rock description, and major and trace element dataset are compiled in Appendices I, II, and III respectively.

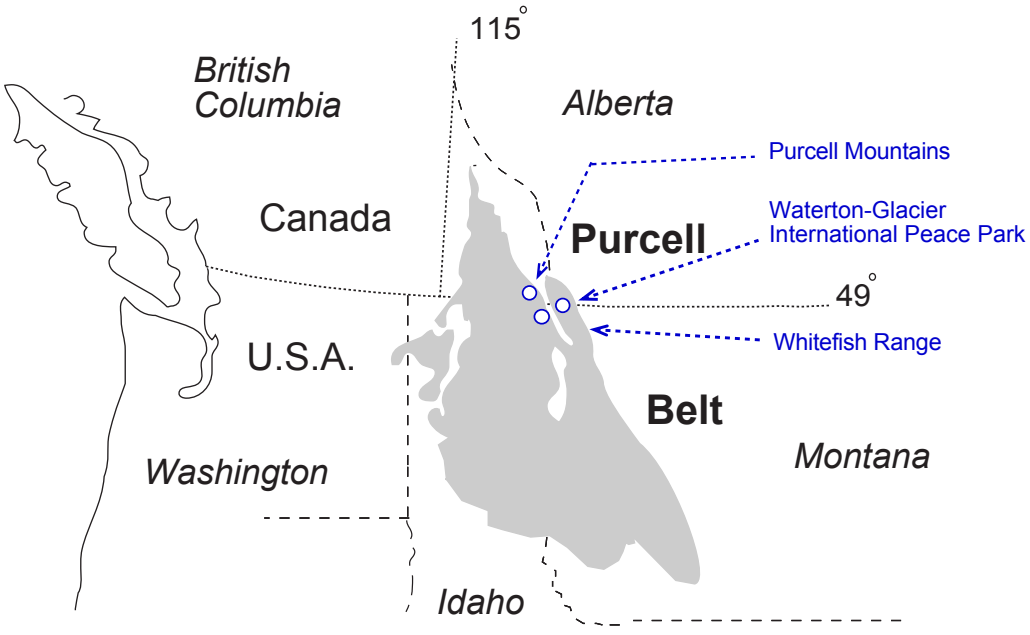

Fig. 3.1 Geographic location of the three areas sampled for this study in relation to the Belt-Purcell Supergroup outcrop area.

Based on grain size and SiO_2 content two facies were defined: (1) sandstones (>75 wt.% SiO_2), and (2) argillites (<75 wt.% SiO_2). Argillites and sandstones were subdivided in four populations based on SiO_2 and loss-on-ignition (LOI; volatile content as structural water and/or CO_2 contents) relationship: (1) sandstones (<10 wt.% LOI); (2) argillites (<10 wt.% LOI); (3) dolomitizied argillites (<20-10 wt.% LOI); and (4) dolomites (>20 wt.% LOI). Different sample populations were used for each chapter based on the scope of the study. Carbon dioxide content of selected samples was calculated following Tiessen et al. (1983).

Waterton-Glacier International Peace Park and near areas

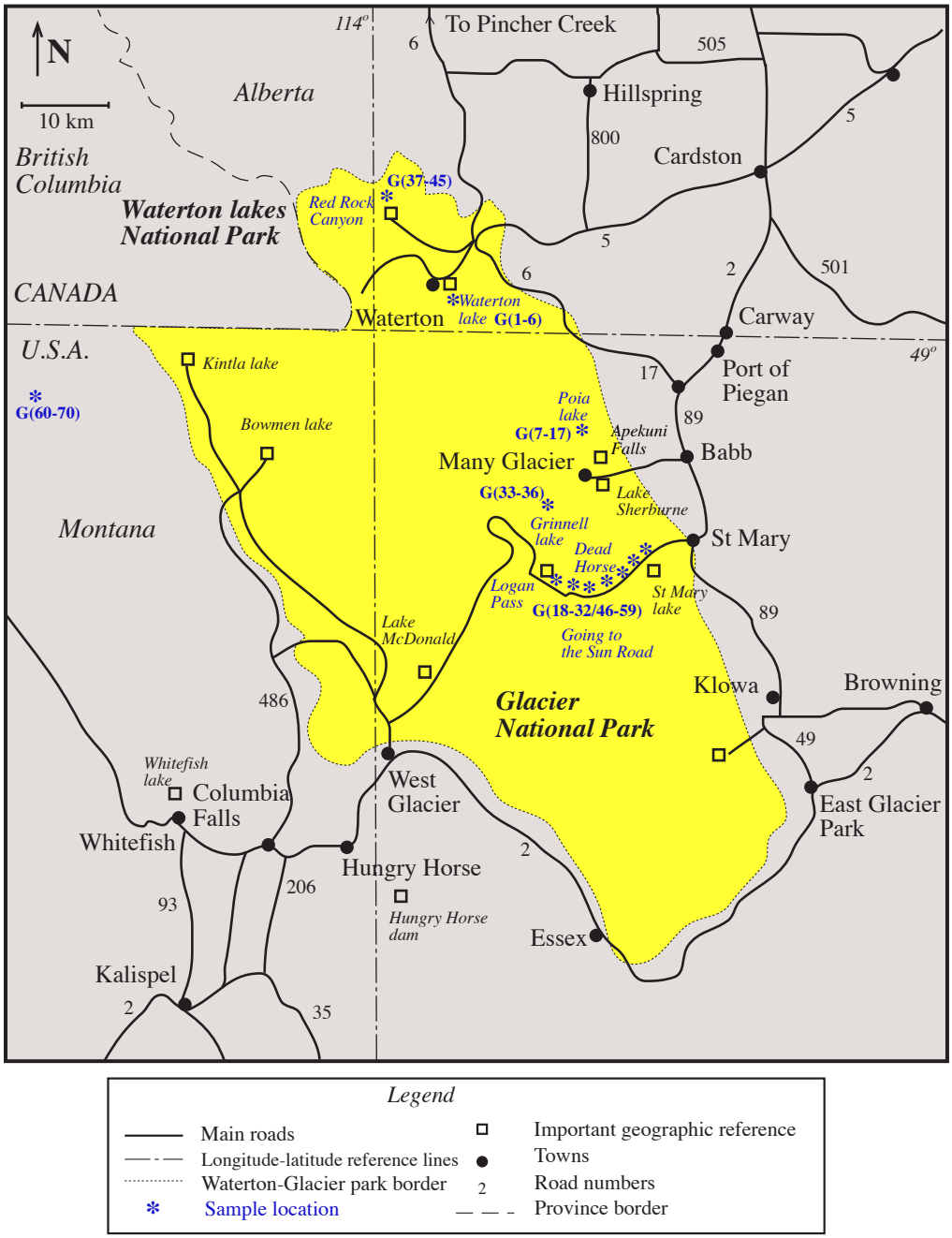

Fig. 3.2 Waterton-Glacier International Peace Park and near areas displaying the locations where samples were collected for this study. Labels on the map are cross-referenced with Fig. 3.5 for stratigraphic position and with Appendices Ia, IIa, and IIIa for geographic coordinates, rock sample description, and trace element composition respectively. Road numbers indicated. Sample labels outside the geographic limits of the Park correspond to two formations which outcrops were not reachable within the Park limits.

Purcell Mountains

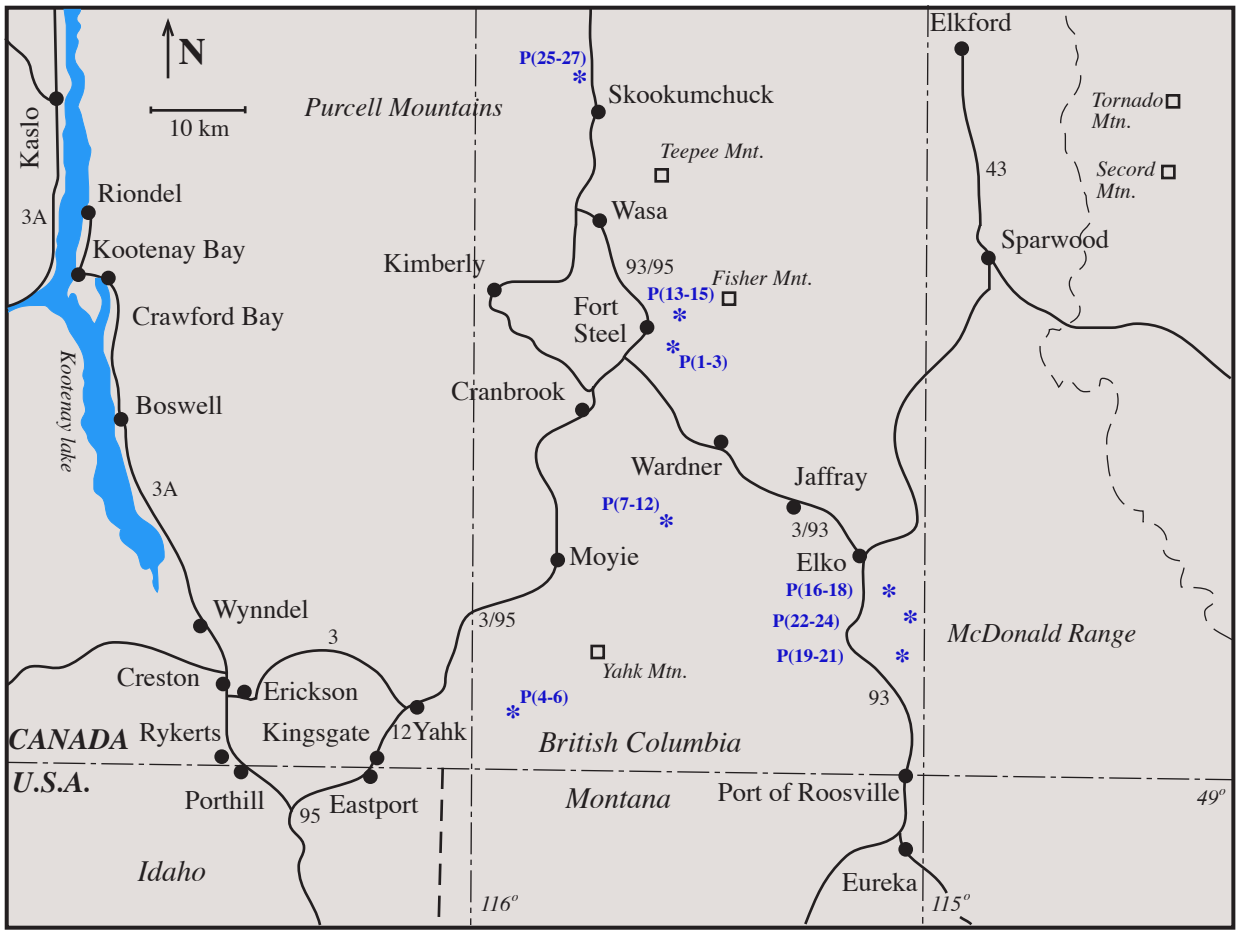

Legend

Main roads	Important geographic reference
Longitude-latitude reference lines	Towns
Waterton-Glacier park border	Road numbers
Sample location	Province border

Fig. 3.3 The Purcell Mountains area displaying the locations where samples were collected. Labels on the map are cross-referenced with Fig. 3.5 for stratigraphic position and with Appendices Ib, IIb, and IIIb for geographic coordinates, rock sample description, and trace element composition respectively. Road numbers are indicated.

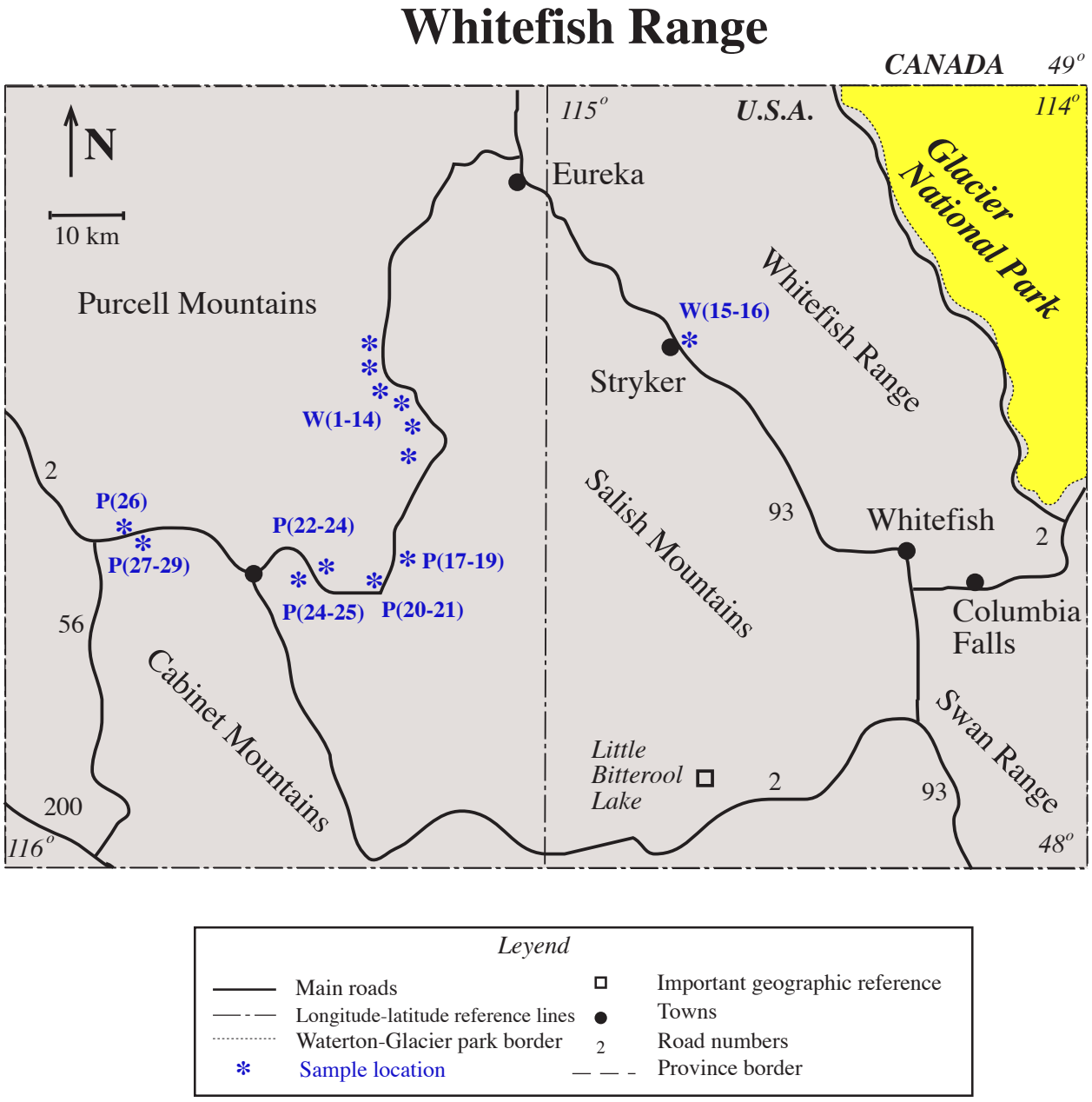

Fig. 3.4 Whitefish Range area displaying the locations where samples were collected. Labels on the map are cross-referenced with Fig. 3.5 for stratigraphic position and with Appendices Ic, IIc, and IIIc for geographic coordinates, rock sample description, and trace element composition respectively. Road numbers are indicated.

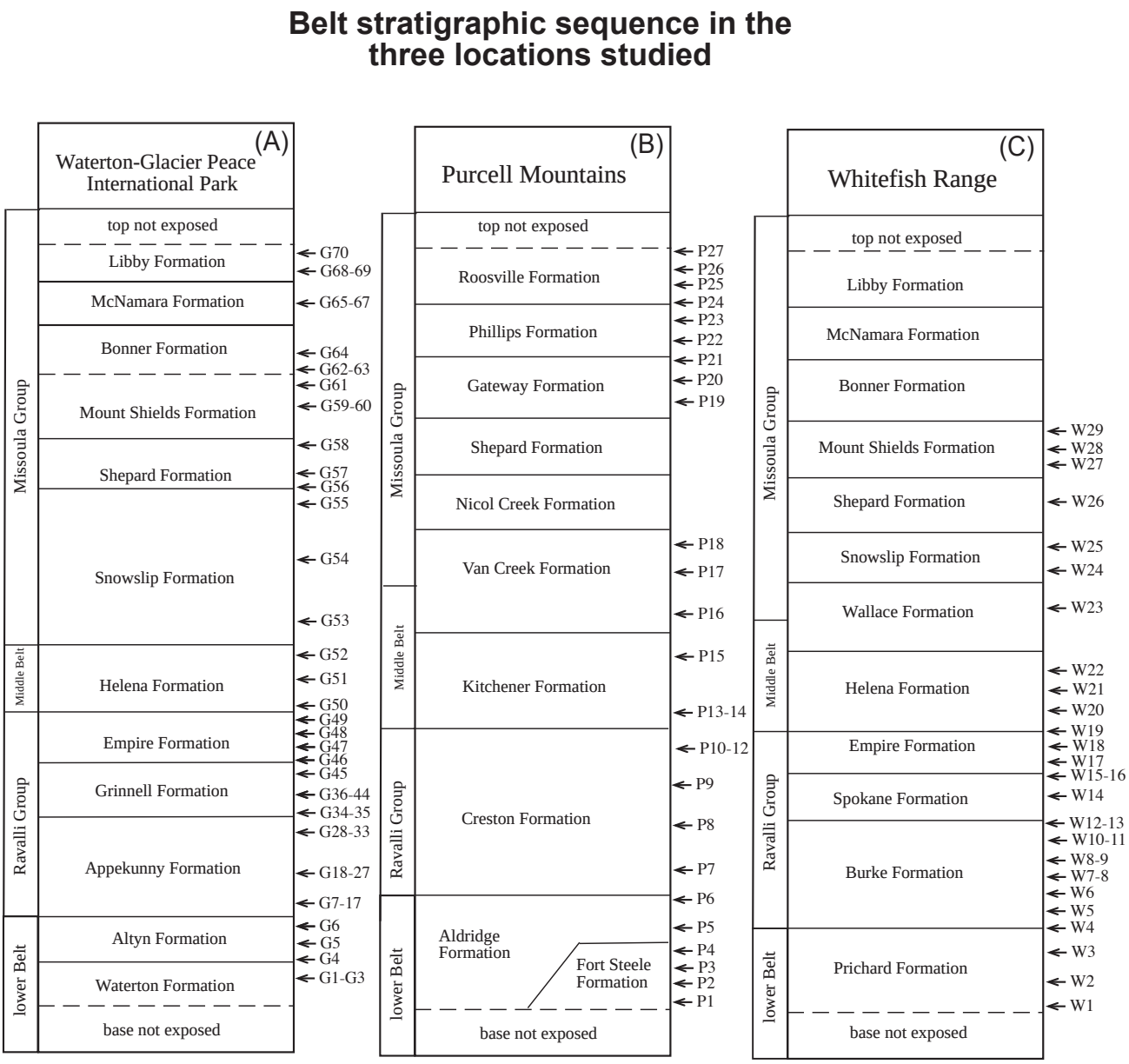

Fig. 3.5 Approximate stratigraphic positions of the samples analyzed in this study.

3.2 X-Ray fluorescence spectrometry

XRFS is an analytical technique established in the 1960's. The XRFS technique is reliable for most elements in concentrations that range from 1 ppm to 100%, depending on the element (Fitton, 1997). This method was used in this study to determine major elemental concentration such as Si, Mg, Mn, Na, K, Ca, Al, and P, present from 0.01 to >90 wt.% in rocks with a precision of ±0.01 wt.% based on its accuracy, availability and low-cost. By convention, major elements are expressed as oxides in wt.%.

XRFS is based on the principle that when matter is irradiated with high-energy incident X-rays, electrons are ejected from inner shells, mainly from shells K and L, to a higher level of energy producing an excited ion. This state is unstable, and when electrons decay back to their original energy level, they emit X-ray photons characterized by the energy difference between the two shell levels. This radiation has a wavelength between 10^{-3} to 10 nm. Since each element has a unique distribution of energy levels, a specific X-ray pattern is characteristic of each chemical element. Therefore this technique enables precise determination of the chemical composition of certain elements in rock samples.

Rock sample analysis using X-ray is based on the interpretation of the X-ray spectra emitted from the rock sample when bombarded by an X-ray beam. The incident X-ray beam is produced in an X-ray tube with two main parts: (1) a tungsten filament, and (2) a metal anode in a vacuum. When the filament is heated, it emits electrons that are accelerated due to a high negative potential voltage. The X-ray tube has a beryllium "window" from where the X-ray beam exits towards the sample. Beryllium is used due to its transparency to X-rays. This high-energy electron beam bombards the anode, which due to a rapid deceleration in their interaction with the anode atoms excites electrons from the inner shells of the anode and produces an emission of primary X-rays that are directed to the sample. Tungsten, Cr and Rh are the most used anode materials for geological purposes. Tungsten is used to analyze heavy elements with short-wavelength peaks, whereas Cr is used for the analysis of lighter elements (Gill, 1997).

Interaction between the primary incident X-rays produced from the anode and the sample glass disc produces secondary (fluorescent) X-rays (Fig. 3.1). Fluorescent X-rays have specific wavelengths characteristic of the elements present, and a smooth continuous background resulting from deceleration of the primary X-ray bombardment on the sample, but not the quantized energy of the inner electrons. Based on the wavelength and each emitted X-ray intensity chemical com

positions are calculated (e.g., Vandecasteele and Block, 1993). Out of the total energy produced to emit X-rays, only 1% emerges as quantized radiation from the inner shells.

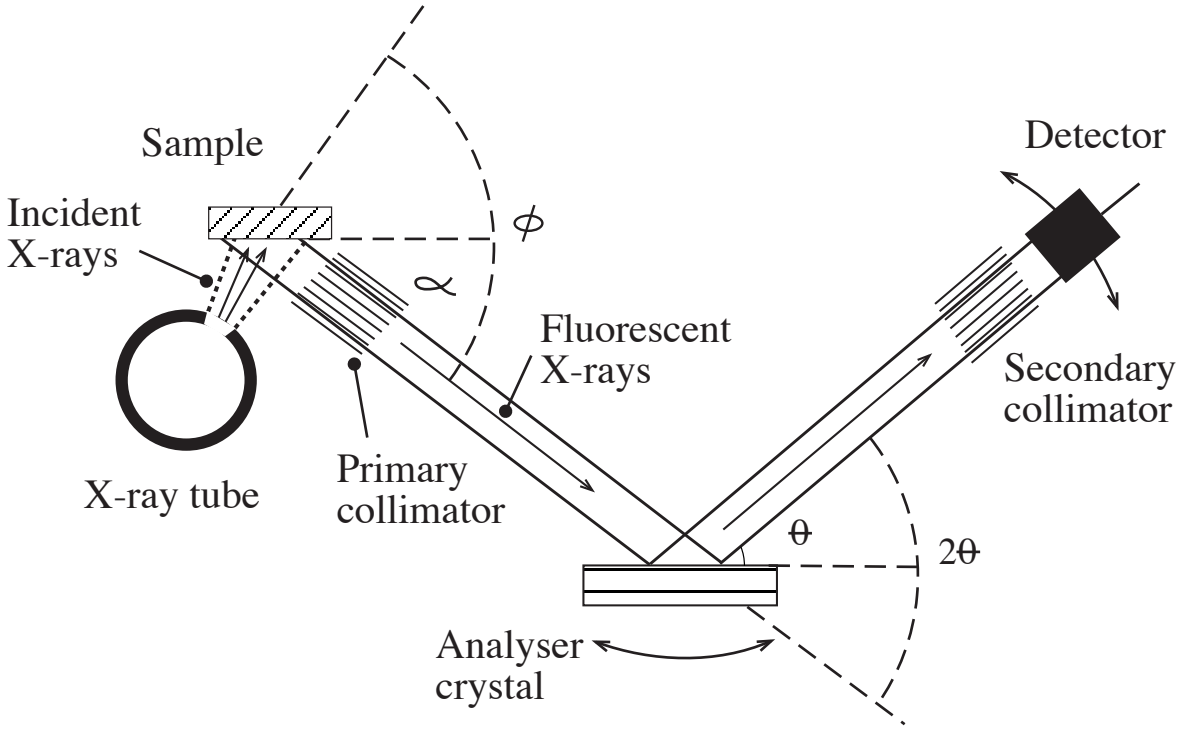

Fig. 3.6 Scheme of an X-ray fluorescence spectrometer (Fitton, 1997). Theta is the diffraction angle that disperses the secondary radiation in a spectrum. Alpha is the take-off angle. Phi is the scattering angle. The former two are fixed, whereas Theta varies.

3.2.1 Sample analysis and preparation

Major element compositions were determined using X-ray fluorescence spectrometry (XRFS) at the Société Générale de Surveillance (SGS) Laboratories (XRAL Laboratories, 1885 Leslie St., Don Mills, Ontario M3B 3J4, Canada).

All Samples were crushed to a fine powder in order to generate a compositionally homogeneous medium for analysis. Rocks were first reduced to cm-size fragments in a rock crusher with iron jaws, then comminuted to a powder of <100 μm grain size in a tema mill having stainless steel rings. Tungsten carbide rings were not used due to possible Co, Nb, and W contamination. In order

to further ensure homogeneity of the rock sample powders were mixed with a lithium metaborate flux and fused into a glass disc. Contamination was validated by the analysis of reference materials.

Rock reference materials are used for calibration and matched to the sample unknowns. Three sample replicates were submitted with each batch; reproducibility was <0.02 wt.%.

3.3 Inductively coupled plasma-mass spectrometry (ICP-MS)

ICP-MS was used for this study due to the advantages of its 60 element capability, detection limits of 0.001 ppb to wt.% levels, dynamic range of 8 orders of magnitude, and availability. By comparison, XRF has detection limits in the ppm range, and for instrumental neutron activation several key elements including Ta, Hf, and some REE cannot be determined.

ICP-MS is based on the determination of elements using the mass spectrometry of ions. It combines an Ar plasma ion source with either a quadrupole mass spectrometer (mass analyzer) or magnetic sector mass spectrometer. The quadrupole ICP-MS can determine many chemical elements from sub-ppb (parts per billion) to wt.% levels, whereas sector ICP-MS is used for high-precision isotope ratio analyses of a few elements with more than one isotope. This study employed a Perkin Elmer Elan 5000 quadrupole ICP-MS. All rock samples were analyzed for a total of 42 elements.

The quadrupole mass spectrometer is also coaxial with the aperture and lenses in the Perkin Elmer Elan 5000. The ion beam enters the quadrupole, where each combination of potentials applied to opposing pairs of rods permits one mass at the time to travel coaxially to the detector. The mass spectrum is scanned in a few milliseconds and integrated counts are generated for each mass by repeated scans. Ion detection is by an electron multiplier.

The quadrupole ICP-MS has 7 main parts: (1) a sample introduction system (a sample tray, automated sampler); (2) spray chamber; (3) Ar plasma; (4) interface; (5) electrostatic lenses; (6) mass spectrometer, also termed a mass filter; and (7) detector (Fig. 3.7).

Samples that are placed in the automated sampler, with quartz glass tip, are drawn from the tubes in sequence, through tygon tubing, into the spray chamber driven by a peristaltic pump. The spray chamber generates an aerosol of the analyte. The aerosol is entrained in a stream of Ar

gas and passed down a quartz glass tube surrounded by a Cu coil powered to couple with the Ar, generating an Ar-plasma. The analyte is first desolvated and then ionized in the plasma. Given a temperature of ~7000 K, ionization is efficient. Ions are accelerated towards the interface by an accelerating voltage. The interface consists of two Ni cones, each with a small central aperture. The purpose of the interface is to permit a drop in pressure from nearly atmospheric in the Ar plasma to the 10^{-4} Pa required for operation of the quadrupole mass analyzer. Electrostatic lenses, behind and coaxial with the apertures, focus the ion beam. Ions are injected into the quadrupole mass filter. Mass separation is achieved changing the intensity of the electric field on the quadrupole. Only ions with a precise mass/charge ratio for a specific electric field can pass through the mass filter, reaching the ion detector and the counting system.

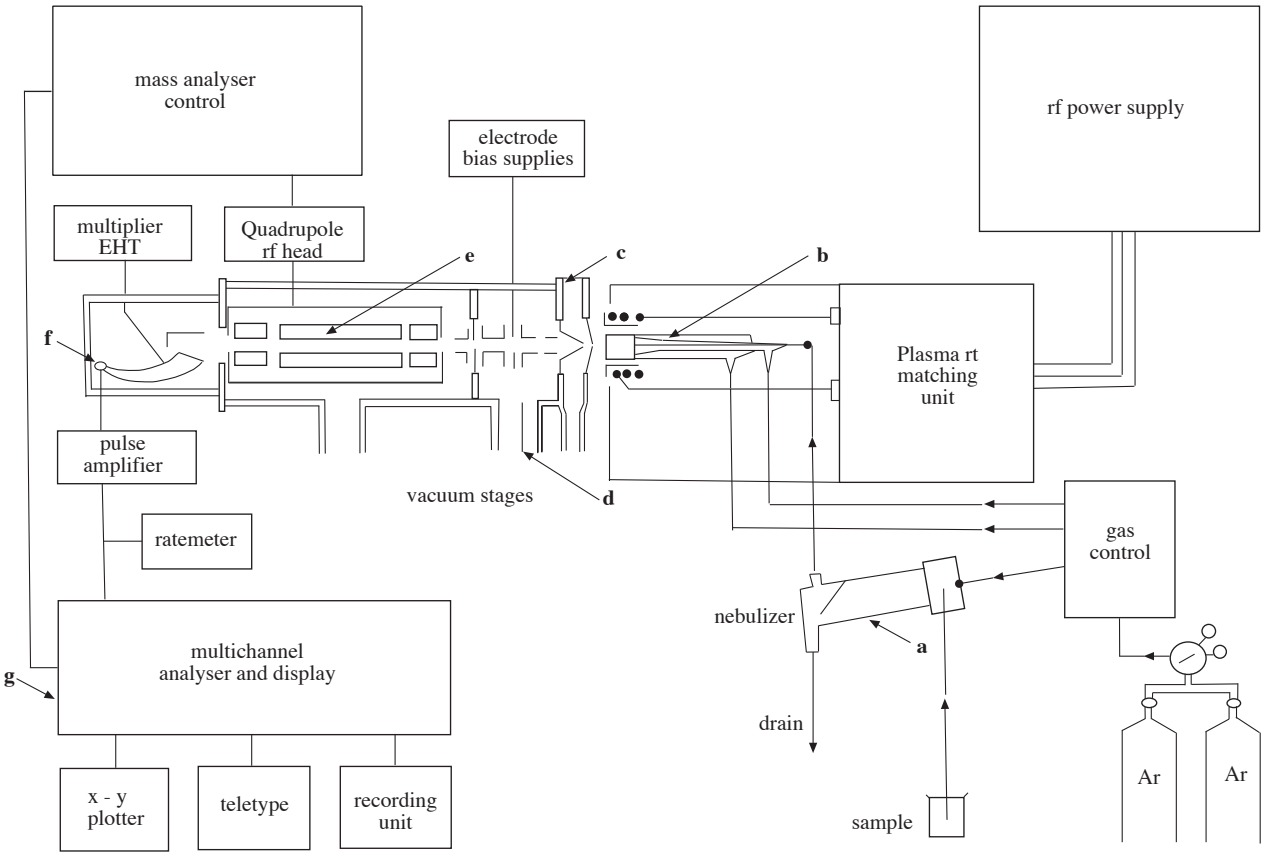

Fig. 3.7 Schematic diagram of an inductively coupled plasma-mass spectrometry instrument (ICP-MS). (a) nebulizer; (b) torch; (c) intermediate vacuum; (d) second intermediate vacuum; (e) quadrupole mass filter; (f) multiplier ion detector; (g) instrumental control (Date and Gray, 1981).

3.3.1 Sample analysis and preparation

Rocks may contain minerals that are difficult to dissolve in a mixture of HF and HNO_3, such as zircon ($ZrSiO_4$) and fluorite (CaF_2) that contain rare earth elements and high field strength elements (HFSE: large valence/small ionic radius). Accordingly, aqueous analytes of rock powders were prepared using two protocols. The first, using a sodium peroxide sinter, breaks down refractory minerals and was used for determination of REE, Th, Nb, Ta, Zr, Sc and Hf. In the second, an HF-HNO_3 solution was used to dissolve the sample for the determination of Li, Rb, Sr, Cs, Ba, Y, U, V, Mo, Cr, Ni, Cu, Zn, Sn, W, Pb, Cd, Tl, Ga, As, Ag and Sb.

Samples were prepared following the standard procedure of Longerich et al. (1990) described below:

1) Na_2O_2-Sinter. 200 mg of rock powder was mixed with 800 mg of ground Na_2O_2 into a clean nickel crucible, and covered. After 90 minutes in the oven at 500°-450° C, the mixture was cooled, and deionized water was added. The resulting slurry was centrifuged at 3000 rpm for 10 minutes three times following rinse and decanting steps. After this, 2.5 ml of 8N HNO_3 was added to the tubes and sonicated until the solid material was completely dissolved. The final solution was transferred to a 125 ml bottle, and the tube rinsed with distilled deionized water (DDIW) to ensure complete sample transfer. The 125 ml bottle was filled gravimetrically to 100 g and shaken.

2) HF-HNO_3 dissolution. 100 mg of sample powder was put into a teflon beaker. One ml concentrated HNO_3 was added, swirled and 1.5 ml concentrated HF were added and mixed. The beaker was capped and placed on a hot plate for three days at 100° C until the sample was completely dissolved. The beaker was then uncovered and the solution left to dry. Two ml of 8N HNO_3 was then added and heated for 0.5 days, following which the sample was dried again. 2.5 ml 8N HNO_3 was then added, capped, and heated for 6 hours. The sample in solution was cooled and transferred to a 125 ml bottle. The beaker was rinsed to complete the sample transfer. The solution was then taken to 80 g with deionized water.

Aqueous samples, spiked counterparts, blanks, reference materials, standards, pure element standards in aqueous solution and deionized water wash were placed in polyethelyne tubes in the sample tray.

During the process several aspects have to be monitored:

a) Matrix effects: one of the advantages of the ICP-MS is that sample and reference materials have similar matrices, since both are diluted in acids dominated by H_2O. Matrices are controlled by the major cations Si, Ti, Al, Fe, Mn, Mg, Ca, Na, K, O, and P, which constitute >99% of most rocks. However, references and unknown matrices cannot be perfectly matched, especially for varied samples, including sandstones, argillites, and dolomites of this study. To address this question of matrix effects, the strategy of Longerich et al. (1990) using "standard additions" was adopted. In this strategy each sample is run unspiked and spiked with known concentrations of selected trace elements, allowing evaluation of matrix effects.

b) Reference materials: international rock and sediment reference materials have published "preferred" concentrations of many chemical elements. Preferred concentrations are not necessarily accurate; for example, Xie et al. (1994), using the University of Saskatchewan ICP-MS laboratory, demonstrated errors of 15-40% for Zr and Hf in the basalt reference material BIR-1 as published by Jochum et al. (1990). Therefore, reference materials are used so that the reference and unknowns undergo identical digestion procedures under the same conditions, to monitor any problems with sample preparation, and to monitor long term reproducibility of the references. A problem rarely encountered is a bad batch of sodium peroxide.

c) Pure elemental standards: pure elemental Zr (99.99999%) and other elements of interest are taken into solution in HF-HNO_3 and diluted gravimetrically, as well as unknowns. This strategy is used given the uncertainties in element concentrations of some reference materials. Two sets of standards were prepared, A and B, so that there were no isobaric interferences in either standard (Jenner et al., 1990).

d) Instrumental drift: drift is monitored from ion counts on elements in standards A and B that cover the mass spectrum.

e) Mass bias: heavy ions are more efficiently transmitted through the interface and electrostatic lenses than light ions. To address this issue, "internal standards" are used to cover the mass spectrum: the elements Rb, Cs and Ta were selected because they are of significance in geochemical studies.

f) Memory effect: elements may be deposited on the sampler, skimmer cones, and then ablated into the ion beam during a subsequent sample analysis. Two strategies are used to deal with memory effects. Zirconium concentrations are obtained with major element oxides in XRFS analy-

ses of the rocks. Zirconium content is a proxy for contents of many elements, including Th, U, Nb, Ta, and light rare earth elements. Samples are then run in a sequence of increasing Zr content. In addition, a two minutes wash with distilled de-ionized water is used between unknowns, standards and reference materials.

g) Isobaric interferences: a few elements cannot be determined by ICP-MS due to isobaric interferences, such as ^{40}Ar on ^{40}K, or where polyatomic species form as in ^{16}O + ^{40}Ar on ^{56}Fe.

h) Precision, accuracy: long term precision and accuracy for the low-level trace element reference basalt BIR-1 in the University of Saskatchewan ICP-MS laboratory is given in Xie et al. (1994). Most incompatible (those that enter the liquid not the residue during partial melting of a rock) trace elements such as Th, Nb, Ce and Hf are present in rocks of this study at more than three times the concentration in BIR-1; therefore, detection limits were not an issue.

Detection limits (in ppm) defined as 3Sigma of the calibration blank for some critical elements are as follows: Nb (0.016), Hf (0.042), Zr (0.103), La (0.018), Ce (0.014), Nd (0.086), and Sm (0.065). Wet chemistry operations were conducted under clean laboratory conditions. Long-term reproducibility in this lab for the low-level reference material basalt (BCR-1) is given in the Table 3.1

Table 3.1 ICP-MS multi-element analysis of international reference material basalt BCR-1 for selected trace elements by the University of Saskatchewan ICP-MS laboratory (excerpted from Xie et al., 1994).

Elements	x	1σ	C%	CV
Zr	201	12	6	190
Nb	14.6	0.7	4.8	14
La	26	0.8	3.1	24.9
Pr	6.95	0.33	4.7	6.8
Eu	1.95	0.11	5.6	1.95
Ho	1.26	0.05	4	1.26
Tm	0.54	0.02	3.7	0.56
Lu	0.502	0.02	4	0.51
Hf	5.87	1.49	8.3	4.95
Ta	1.03	0.16	15.5	0.81
Th	6.7	0.52	7.8	5.98
U	1.75	0.1	5.7	1.75

(x) Average; (1σ) standard deviation; (C%) relative standard deviation; (CV) compiled values from Potts et al. (1992).

3.4 Chemical Th-U total Pb age method using electron microprobe

Monazite grains [Ce, La, Th $(PO)_4$] were dated using the chemical Th-U-total Pb age method described by Suzuki and Adachi (1991, 1994). This method is based on the premise that during growth of monazite crystals which contain Th and U, the initial Pb content is negligible, and the mineral remains closed, such that measured U/Pb and Th/Pb ratios are due only to radioactive decay (Faure, 1986; Montel et at., 1996, Harrison et al., 2002). The common (initial) lead in monazite does not exceed 1 ppm (Parrish, 1990), and monazite does not incorporate appreciable external lead during its crystallization (Scherrer et al., 2000). In addition, monazite generally behaves as a geochemically closed system without loss of parent or daughter nuclides below ~725°C (Copeland et al., 1988).

Chemical Th-U-total Pb age method provides a quick, low-cost, and non-destructive way of determining the chemical age of monazites. Suitable monazite grains are first selected by optical microscopy on polished thin sections. Analyses are performed using an electron microprobe on the same thin sections (Montel et al., 1996). Generally chemical Th-U-total Pb age method offers no information on discordance in the Th-U-Pb system, and consequently whether Pb loss occurred, as is possible with isotopic dating methods. Pb loss can only be estimated using chemical age if many measurements can be taken in the same grain (Suzuki and Adachi, 1991). However, in case of mainly single grain analysis, chemical Th-U-total Pb dating combined with petrographic information of individual grains, local and regional geology, and/or with other dating techniques, has been successfully used in many studies, specifically of metamorphic events and provenance (e.g., Parrish, 1990; Suzuki and Adachi, 1991, 1994; Dahl et al., 2005).

Chemical dating using an electron microprobe was selected as the preferred method due to the small size of most of the monazite grains ~5 μm, only possible to be analyzed with the high spatial resolution of this method, low-cost of the analyses, and availability of the electron microprobe. Samples for monazite chemical dating were selected based on their high rare earth element content for the two facies studied: argillites and sandstones, to address possible differences in provenance.

Electron microprobe analysis (EMPA) is a non-destructive method for determining chemical compositions of materials. The electron microprobe can quantitatively analyze elements from atomic numbers from 9 to 92 at concentrations of >1-20 ppm depending on the elements. The electron microprobe analysis is based on the bombardment of incident electrons to generate secondary

X-rays from the sample. X-rays from each element have a distinctive wavelength. X-rays emitted by the sample in the electron microprobe allows quantification of element concentrations in the sample.

The electron microprobe has four main components: (1) electron gun, a heated tungsten filament emits electrons to generate an electron beam; (2) vacuum system, to avoid oxidation of the tungsten filament and scattering of electrons; (3) the beam column, magnetic and objective lenses used to focus the beam on the sample; and (4) X-ray spectrometers to measure X-rays emitted from the sample (Fig 3.8).

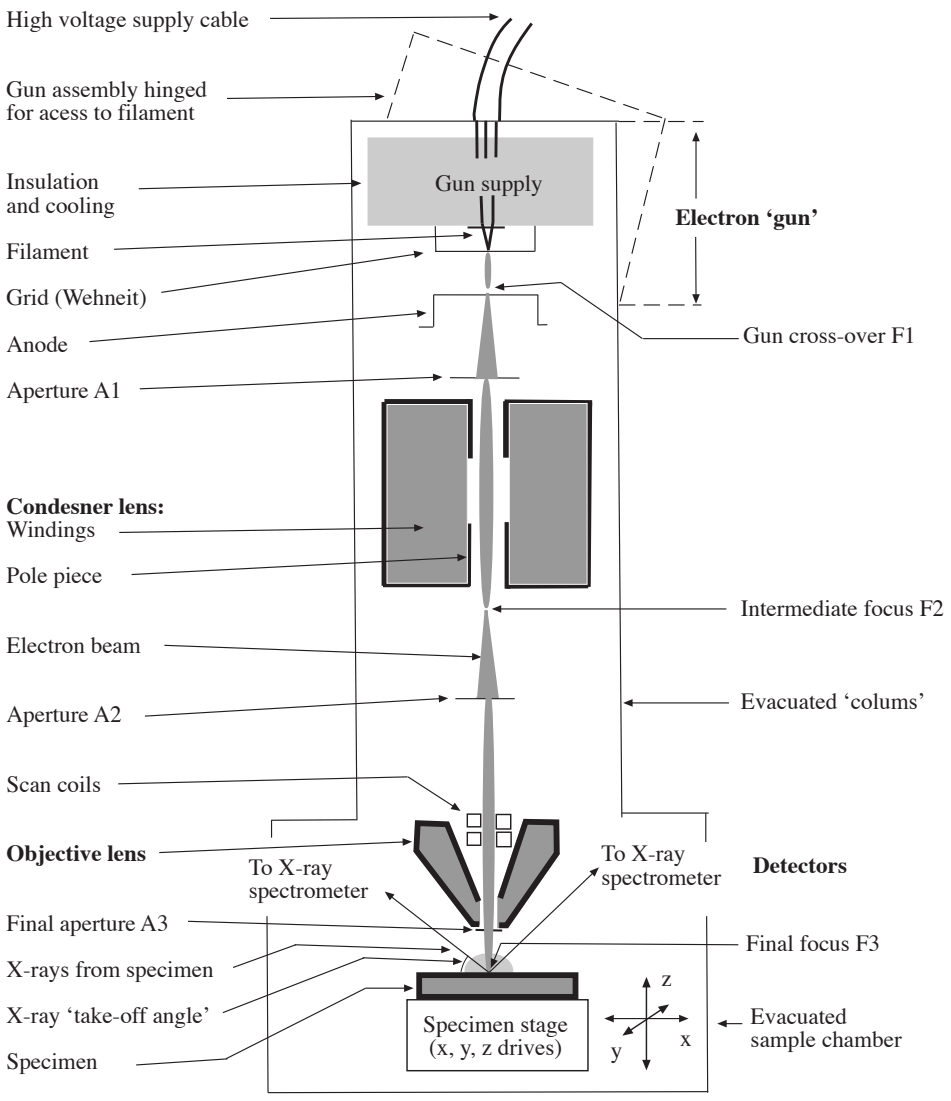

Fig. 3.8 Schematic diagram of an electron microprobe main column (Gill, 1997).

Analyses for REE, Th, U, Pb, and Y elements were conducted on a Cameca SX-100 electron microprobe, with three wavelength-dispersive spectrometers (WDS), at the Warsaw University Faculty of Geology, Poland. The accelerating voltage was 20 kV, probe current 50 nA, and beam diameter 3 μm. Pentaerythritol (PET) crystals were used to analyze Th, U, Pb and thallium acid phtalate (TAP) for Y, and lithium fluoride (LIF). Standards were synthesized glasses doped with Th and U from P&H Developments Ltd., Derbyshire, UK; $PbCrO_4$ for Pb; and Y-Al garnet for Y.

Additional analyses for Th, U, Pb, and Y in monazites were conducted on a Jeol JXA-8600 Superprobe electron microprobe, with three wavelength-dispersive spectrometers (WDS), at the University of Saskatchewan, Canada. The accelerating voltage was 15 kV, probe current 200 nA, and beam diameter 3 μm. Pentaerythritol (PET) crystals were used to analyze Th, U, Pb and thallium acid phtalate (TAP) for Y. Standards were structure probe ink (SPI) Smithsonian synthetic phosphates doped with Th and U; and SPI Y-Al garnet for Y.

Table 3.2 Standard X-ray lines, crystals used for X-Ray diffraction for WDS, counting times, and calibration standards used for monazite analyses.

Element	X-ray line	Crystal	Counting time (sec.)	Calibration standard
Si	K	TAP	60	Diopside
Ca	K	PET	30	Diopside
P	K	PET	20	AptBB2
La	L	LIF	90	LaP_5O_{14}
Ce	L	LIF	90	CeP_5O_{14}
Pr	L	LIF	50	PrP_5O_{14}
Nd	L	LIF	90	NdP_5O_{14}
Sm	L	LIF	50	SmP_5O_{14}
Gd	L	LIF	50	GdP_5O_{14}
Dy	L	LIF	50	DyP_5O_{14}
Ir	L	LIF	50	IrP_5O_{14}
Yb	L	LIF	50	YbP_5O_{14}
Lu	L	LIF	50	LuP_5O_{14}
Y	L	TAP	100/200	Y-A1Garnet SPI Y-A1Garnet
Th	M	PET	100/200	Th P&H glass SPI metal
U	M	PET	200/200	U P&H glass SPI metal
Pb	M	PET	300/200	$PbCrO_4$ SPI crocoite

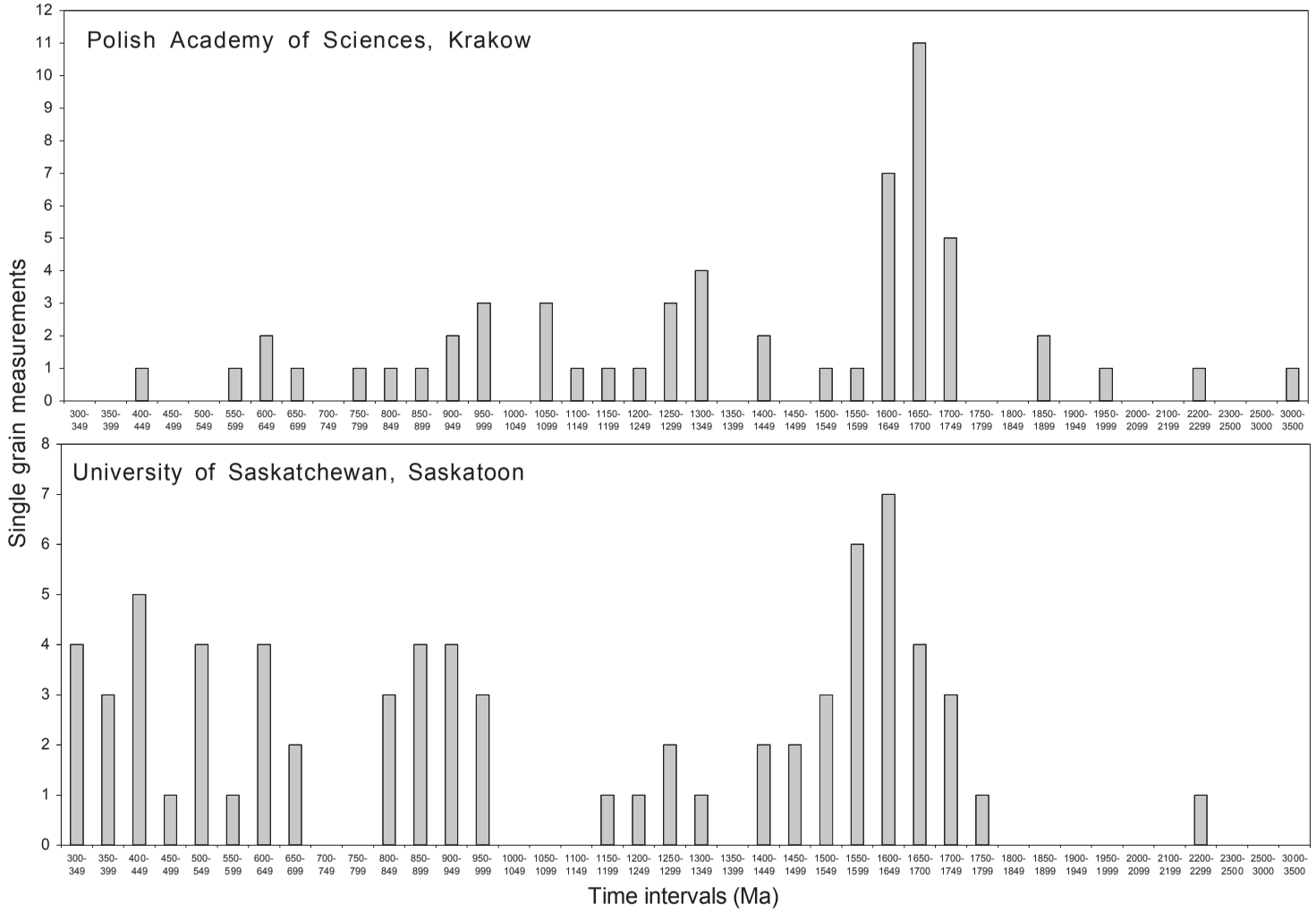

Fig. 3.9 Complementary histograms of individual monazite grains calculated from analyses preformed for U, Th, Pb, and Y in the the Polish Academy of Sciences, Krákov, and the University of Saskatchewan, Canada, for the Appekunny Formation. Both graphs display the same range of ages. Analyses preformed in The Polish Academy of Sciences display more measurements on grains at ~1700-1600 Ma than the analyses from the University of Saskatchewan in which a more abundant population at ~1600-1500 Ma is displayed. Both datasets show a wide range of post-depositional ages.

Both sets of data from Poland and Canada are compared in Fig. 3.9. Analyses were selected based on total oxide wt.% (~97-~102) and cation relationships (Si+P=1; Th+U=Ca+Si).

Monazites were analyzed using wavelength dispersive spectrometry (WDS). This method identifies the elements by their specific X-ray wavelength, provides good spatial resolution, and offers lower detection limits of >1-20 ppm than energy dispersive spectrometry (EDS; Vandecasteele and Block, 1993). However, WDS is slower than EDS, since one element is analyzed at a time, and is more expensive.

This technique was developed based on Bragg's law that describes how an X-ray beam is diffracted as:

$$n\lambda = 2d\sin\alpha \quad (3.1)$$

Where n is any natural number, *Lambda* is the wavelength of the incident beam X-ray, *d* is the spacing between the crystal planes, and *Alpha* is the angle between the crystal plane and the diffracted beam. Using WDS, the X-rays resulting from the electron microprobe electron-beam interaction with the sample are diffracted by crystals selected to match the X-ray wavelength (PET, TAP, and LIF), and the intensity of different wavelengths. Chemical composition is determined by comparing the intensity of X-rays of unknowns with those from standards using an X-ray detector. Standards are selected to match unknowns (monazite standard for a monazite unknown composition), to correct for effects of X-ray absorption and fluorescence in the sample.

Maximum background error for each element measured on each side of their peak was ~1% of the concentration, which is close to or less than the uncertainty in the X-ray counting. The detection limit for PbO at 2Sigma was 0.007%, and relative error for PbO ~6% for 0.1 wt.% concentrations. Relative errors for ThO_2 and UO_2 were ~2-3% at 0.5 wt.% concentrations and <2% for higher concentrations. The standard X-ray lines and counting time are presented in Table 3.2. Analytical corrections due to X-ray line interference between Th for U and Pb, and Y for Pb, were addressed following Pyle et al., (2005):

$$C_{Pb^*s} = C_{Pb,\,s} - [(CF_{Th\text{-}Pb} * C_{Th,s}) + (C_{Y\text{-}Pb} * C_{Y,s})] \quad (3.2)$$

$$C_{U^*s} = C_{U,\,s} - (CF_{Th\text{-}U} * C_{Th,\,s}) \quad (3.3)$$

Where *C* is concentration, *CF* the correction factor, and *s* sample.

After X-ray peak interference corrections chemical age was calculated solving the equation:

$$\frac{PbO}{W_{Pb}} = \frac{ThO_2}{W_{Th}}\{\exp(\lambda_{232}t) - 1\} + \frac{UO_2}{W_U}\left\{\frac{\exp(\lambda_{235}t) + 137.88\exp(\lambda_{238}t)}{138.88} - 1\right\} \quad (3.4)$$

Where *W* is the gram-molecular weight of each oxide (W_{Pb}=224 , W_{Th}=264 and W_U=270 for monazite); $Lambda_{232}$, $Lambda_{235}$, and $Lambda_{238}$ the radioactive constant decay of ^{232}Th, ^{235}U, and ^{238}U respectively.

For Th rich minerals, thorium and uranium variations in time on total Pb were corrected by converting the sum of ThO_2 and UO_2 into ThO_2* for all the monazites analyzed for an expected *t* value (e.g., Suzuky and Adachi, 1994):

$$ThO_2^* = ThO_2 + \frac{UO_2 W_{Th}}{W_U\{\exp(\lambda_{232}t) - 1\}}\left\{\frac{\exp(\lambda_{235}t) + 137.88\exp(\lambda_{238}t)}{138.88} - 1\right\} \quad (3.5)$$

Lead versus ThO_2* relation should satisfy the following equation obtaining m:

$$PbO = m\ ThO_2^* + b \quad (3.6)$$

Using the equation from York (1966), and replacing m for the value obtained in the equation 3.6:

$$T=1/Lambda_{232}\{\ln[1=m(W_{Th}/ W_{Pb})]\} \quad (3.7)$$

T should be the same as the *t* expected in equation 3.4. Changing back and forth the expected *t*, and recalculating *m*, the match between *T* and *t* is obtained when the expected *t* is correct for each analysis. Best-fit regressions can be calculated from multiple spot analyses on a grain (Suzuki and Adachi, 1991); however, the small size of monazites allowed only single-spot analysis.

3.4.1 Sample analysis and preparation

Monazite grains were analyzed *in situ* (directly on the polished rockslide). Samples for the

electron microprobe were prepared by polishing rockslides to an even surface with disks of 1 μm abrasion. The surface of the slide is carbon-coated to make it highly conductive in order to drain the incident electron beam. This process was done with a JEOL Jee-4x vacuum evaporator. After sample preparation, the rockslide was placed on the x-y-z stage of the electron microprobe. The rockslide was scanned in the backscatter image mode to recognize high-concentration of heavy elements (high Z) content in grains. Monazite grains were first identified using EDS, and if large enough were then analyzed in WDS mode for chemical Th-U total Pb age dating.

3.5 Clay mineral identification

Energy dispersive spectrometry (EDS) has been described in the section above as well as its principles in *section 3.2*. Energy dispersive spectrometry was used in this study to identify clay minerals directly in the rockslides using the electron microprobe (*section 3.2*). In order to identify potential presence of smectites, samples were prepared for X-ray diffraction using a Rigaku R200 X-ray diffractometer with rotating Cu anode (Fig. 3.6).

3.5.1 Sample analysis and preparation

Samples were crushed by hand in a mortar to <0.0625 mm size. 300 ml of Calgon was used for an ultrasonic bath at 30^{o} C for 15 minutes to deflocculate the samples. The fluid was centrifuged at 750 rpm for ~3 minutes at 50 ml fractions. A second centrifuging was done for 15 ml fractions at 2500 rpm for 15 minutes. Methanol was added to the resulting sediment fraction and placed on glass slides to dry. Samples were mounted for X-ray diffraction and analyzed. Afterwards, samples were submerged in ethylene glycol at 50 cm depth for 48 hours and reanalyzed a second time. Clay minerals were identified following Moore and Reynolds (1997) X-ray spectra.

3.6 References

Chaudhuri, S., Cullers, R.L., 1979. Distribution of rare-earth elements in deeply buried Gulf coast sediments. Chem. Geol. 24, 327-338.

Condie, K.C., 1991. Another look at rare earth elements in shales. Geochim. Cosmochim. Acta 55, 2527-2531.

Copeland, P., Parrish, R.R., Harrison, T.M., 1988. Identification of inheritated radiogenic Pb in monazite and its implication for U-Pb systematics. Nature 333, 760-763.

Cullers, R.L., Chaudhuri, S., Kilbane, N., Koch, R., 1979. Rare-earths in size fractions and sedimentary-rocks of Pennsylvanian-Permian age from the mid-continent of the USA. Geochim, Cosmochim.

Acta 43, 1285-1301.

Date, A. R., Gray, A. L., 1981. Plasma source mass spectrometry using an inductively coupled plasma and a high resolution quadrupole mass filter. Analyst 106, 1255-1267.

Dahl, P.S., Hamilton, M.A., Jercinovic, M.J., Terry, M.P., Williams, M.L., Frei, R., 2005. Comparative isotopic and chemical geochronometry of monazite, with implications for U-Th-Pb dating by electron microprobe: an example from metamorphic rocks of the eastern Wyoming Craton (U.S.A.). Am. Mineral. 90, 619-638.

Faupl, P., Pavlopoulos, A., Migiros, G., 1998. On the provenance of flysch deposits in the external Hellenides of mainland Greece: results from heavy mineral studies. Geol. Magaz. 135, 421-442.

Faure, G., 1986. Principles of Isotope Geology. Wiley and Sons, New York, NY, U.S.A.

Fitton, G., 1997. X-ray fluorescence spectrometry. In: Gill, R., (ed.), Modern Analytical Geochemistry: an Introduction to Quantitative Chemical Analysis for Earth, Environmental and Materials Scientists. Wesley Longman, England, U.K., pp. 87-115.

Gao, S., Wedepohl, K.H., 1995. The negative Eu anomaly in Archean sedimentary rocks: implications for decomposition, age and importance of their granitic sources. Earth Planet. Sci. Lett. 133, 81-94.

Gill, R., 1997. Electron beam methods. In: R. Gill (ed.), Modern Analytical Geochemistry: an Introduction to Quantitative Chemical Analysis for Earth, Environmental and Materials Scientists. Wesley Longman, England, U.K., pp. 215-234.

Harrison, T.M., Catlos, E.J., Montel, J.M., 2002. U-Th-Pb dating of phosphate minerals. In: Kohn, M.J. et al. (eds.), Phosphates: Geochemical, Geobiological, and Materials Importance. Rev. Mineral. Geochem. 48, 523-558.

Jenner, G.A, Longerich, H.P., Jackson, S.E., Fryer, B.J., 1990. ICP-MS a powerful tool for high precision trace-element analyses in earth sciences: evidence from analyses of selected USGS reference samples. Chem. Geol. 83, 133-148.

Jochum, K.P., Seufert, H.M., Thirlwall, M.F., 1990. Multi-element analysis of 15 international standard rocks by isotope-dilution spark source mass spectrometry. Geostandards Newsletter 14, 469-473

Longerich, H.P., Jenner, G.A., Fryer, B.J., Jackson, S.E., 1990. Inductively coupled plasma-mass spectrometric analysis of geological samples: a critical evaluation based on case studies. Chem. Geol. 83, 105-118.

Moore, D.M., Reynolds, R.C., 1997. X-ray diffraction and the identification and analysis of clay minerals. Oxford University Press, New York, NY, U.S.A.

Montel, J.M., Foret, S., Veschambre, M., Nicollet, Ch., Provost, A., 1996. Electron microprobe dating of monazite. Chem. Geol. 131, 37-53.

Nesbitt, H.W., Young, G.M., McLennan, S.M., Keays, R.R., 1996. Effects of chemical weathering and sorting on the petrogenesis of siliciclastic sediments, with implications for provenance studies. J. Geol.

104, 525-542.

Parrish, R.R., 1990. U-Pb dating of monazite and its application to geological problems. Can. J. Earth Sci. 27, 1431-1450.

Potts, P.J., Tindle, A.G., Webb, P.C., 1992. Geochemical reference material compositions. In: Whittles, F.L., (ed.), Rocks, Minerals, Sediment, Soils, Carbonates, Refractories and Ores Used in Research and Industry. CRC Press, Boca Raton, Latheronwheel, Caithness, U.K., pp. 220-221.

Pyle, J.M., Spear, F.S., Wark, D.A., Daniel, C.G., Storm, L.C., 2005. Contributions to precision and accuracy of monazite microprobe ages. Am. Mineral. 90, 547-577.

Roaldset, E., 1979. Rare earth elements in different size fractions of marine quick clay from Ullensaker, and a till from upper Numedal, Norway. Clay Miner. 14, 229-239.

Roser, B., 1996. Sandstone geochemistry, provenance, and tectonic setting: application of the Al203/SiO2-basicity index diagram to New Zealand sedimentary suites. Earth Sci. 50, 138-147.

Scherrer, N.C., Engi, M., Gnos, E., Jakob, V., Liechti, A., 2000. Monazite analysis; from sample preparation to microprobe age dating and REE quantification. Schweiz. Mineral. Petrogr. Mitt. 80, 93-105.

Suzuki, K., Adachi, M., 1991. The chemical Th-U-total Pb isochron ages of zircon and monazite from the Gray Granite of the Hida Terrane, Japan. J. Earth Planet. Sci. 38, 11-37.

Suzuki, K., Adachi, M., 1994. Middle Precambrian detrital monazite and zircon the Hide gneiss on Oki-Dogo Island, Japan: their origin and implications for the correlation of basement gneiss of Southwest Japan and Korea. Tectonophysics 235, 277-292.

Taylor, S.R., McLennan, S.M., 1985. The continental crust: its composition and evolution. Blackwell, Oxford, U.K.

Taylor, S.R., McLennan, S.M., 1995. The geochemical evolution of the continental crust. Rev. Geophy. 33, 241-265.

Tiessen, H., Roberts, T.L., Stewart, J.W.B., 1983. Carbonate analysis in soils and minerals by accid digestion and two-endpoint titration. Comm. Soil Sci. Plant An. 14, 161-164.

Vandecasteele, C., Block, C.B., 1993. Modern methods for trace element determination. Wiley and Sons, New York, NY, U.S.A.

Xie, Q., Jain, J., Sun, M., Kerrich, R., Fan, J., 1994. ICP-MS analyses of basalt BIR-1 for trace elements. Geostandards Newsletters 18, 53-63.

York, D., 1966. Least-square fitting of straight line. Can. J. Phys. 44, 1079-1088.

CHAPTER IV

A Trace Element and Chemical Th-U total Pb Dating Study in the Lower Belt-Purcell Supergroup, Western North America: Provenance and Diagenetic Implications

Abstract

Comprehensive geochemical and monazite chemical age data on the Mesoproterozoic Belt-Purcell Supergroup reveals information on provenance age(s), and the sources of interbedded argillites and sandstones. Compliance of rare earth element (REE) and multi-element patterns of argillites to post-Archean upper continental crust (PA-UCC), Cr-Ni, and Th/Sc-Sc systematics are consistent with a dominantly post-Archean source area. Sandstones have the same geochemical signature as argillite for the Appekunny and Grinnell formations in the lower Belt-Purcell Supergroup sequence, albeit variably depleted by detrital quartz. Sandstone developed in a separate high-energy environment, and argillite and sandstone became interbedded during storms, accounting for the sharp interbedding of the two facies.

New data from the Appekunny Formation argillites show that chemical monazite ages are the same as for their sandstone counterparts. Both facies display the same age peak at ~1700 Ma which is commensurate with a common provenance.

Detrital monazite chemical Th-U total Pb ages from the Grinnell and Appekunny sandstones, and argillites of the former, cluster at ~1700 Ma. Paleocurrents and chemical ages support a major Laurentian Paleoproterozoic provenance, likely the Penokean, Yavapai, Mazatzal, and Central Plains provinces. Other potential sources could have been terranes at ~1875-1750 Ma that cooled through the blocking temperature of monazite ~1700 Ma such as sectors of the Wyoming Province. Minor age peaks at ~1550 Ma in the Appekunny Formation are not known from Laurentian terranes, and stem from sparse contribution from a western source. Rare >2500 Ma monazite ages in argillite and sandstone stem for minor contributions from Archean terrane(s), likely in Laurentia.

Diagenetic overprint in the Belt-Purcell rocks is widespread and displayed geochemically as heavy REE enrichment relative to light REE, normalized to PA-UCC. There are two populations of monazites: the first has detrital textures, ages >1400 Ma, and lower LREE/HREE, and higher ThO_2 and Y contents; whereas the second has euhedral texture, ages up to ~1000 Ma post-deposition, and lower ThO_2 and Y, but higher LREE/HREE contents than their counterparts. The second population is interpreted as the product of protracted migration of basinal brines that mobilized HREE, as documented in several Proterozoic sedimentary basins.

4.1 Introduction

The Belt-Purcell Supergroup is a Mesoproterozoic, dominantly siliciclastic, sedimentary sequence ~17 km thick, located in northwestern Montana and southern Alberta and British Columbia (Fig. 4.1). This Supergroup was deposited at ~1470-1400 Ma as part of a series of intracontinental rifts (e.g., Höy, 1989; Poage et al., 2000; Lydon, 2000; Chandler, 2000) that developed as the Mesoproterozoic supercontinent Columbia dispersed (Pesonen et al., 2003; Zhao et al., 2004; Rogers and Santosh, 2004). The provenance of the Belt-Purcell Supergroup has been controversial, and addressed both from sedimentological and stratigraphic criteria, as well as geochronological data on detrital zircon and monazites (e.g., Harrison, 1972; Frost and Winston, 1987; Winston, 1990; Ross et al., 1992; Whipple et al., 1997; Ross and Villeneuve, 2003). Paleocurrents and geographic variations in the stratigraphic thickness of several formations are consistent with an eastern source in Laurentia, and in other formations a separate western provenance.

Specifically, in the lower Belt-Purcell sequence, sandstones were interpreted to have a provenance in Laurentia to the southeast, whereas argillites (fine-grained sedimentary rock that includes shale, mudstone, siltstone, and claystone; usage of e.g., Harrison, 1972; McMechan, 1981; Winston, 1986; Whipple et al., 1984) were transported from a western catchment (Winston, 1990; Link, 1997; Whipple et al., 1997) that, depending on paleoreconstructions of Columbia, could be Paleo- or Mesoproterozoic terranes of Australia or East Antarctica that match the age of detrital minerals in the lower Belt-Purcell sequence (1920-1460 Ma and less abundant Archean ages; Ross et al., 1992; Ross and Villenueve, 2003).

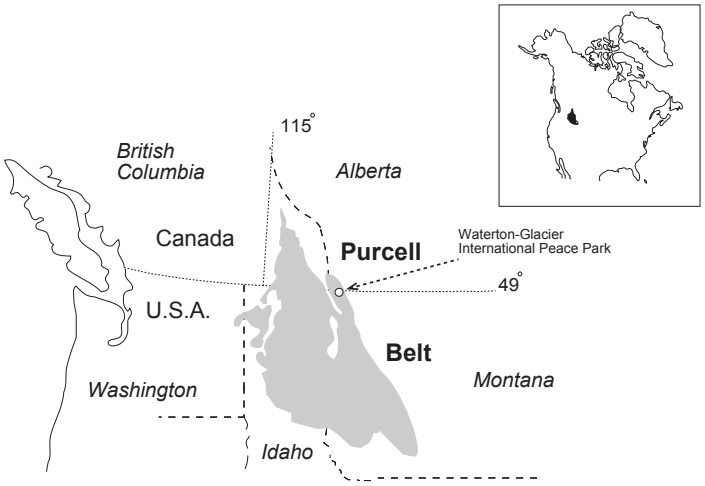

Fig. 4.1 Generalized geographic location of the Belt-Purcell Supergroup outcrops spanning the Canada-USA border.

The rare earth elements (REE), Th, Y, Co, and Sc are in many cases preserved when transferred from provenance areas into the sedimentary budget of many siliciclastic sequences. Consequently they can preserve the geochemical fingerprint of the source areas, and have been used in many geochemical studies to address provenance (e.g., Taylor and McLennan, 1995; Fralick and Kronberg, 1997; Fralick, 2003; McLennan et al., 2003). Accordingly, this Chapter builds on the existing sedimentological and stratigraphic literature on the Belt-Purcell Supergroup, and geochronological studies of detrital minerals.

New high-precision geochemical analyses of extensive argillites and sandstones are reported from the Appekunny and Grinnell formations (Ravalli Group) at Waterton-Glacier International Peace Park, as one proxy of their provenance, inasmuch as there are few modern high precision analyses of this part of the Belt-Purcell sedimentary sequence. The Appekunny and Grinnell formations were selected as they are characterized by well-developed interbedding of sandstones and argillites. To complement the whole rock geochemistry, chemical Th-U total Pb ages of monazite grains from both facies of the same stratigraphic levels have been measured, to build on previous studies of detrital zircons and monazites of sandstones of the Belt-Purcell Supergroup (cf. Ross et al., 1991, 1992; Ross and Villenueve, 2003).

4.2 Geologic setting

The preserved Belt-Purcell sedimentary sequence extends 500 km from southwestern Montana, where it is known as the Belt Supergroup, to southeastern British Columbia where it is referred to as the Purcell Supergroup (Fig. 4.1). It outcrops in an anticlinal structure of the Purcell Anticlinorium (Yoos et al., 1991). This succession overlies igneous and metamorphic basement rocks of Archean, Wyoming to Paleoproterozoic, Hearne age, which are only locally exposed (Kleinkopf, 1997), it was trusted over Cretaceous sedimentary rocks during the Laramide event (Yin and Kelty, 1991).

4.2.1 Stratigraphic divisions and sedimentary environment

The Belt-Purcell Supergroup has been divided into four main stratigraphic divisions: the lower Belt, Ravalli Group, middle Belt, and Missoula Group (Fig. 4.2a; e.g., Whipple et al., 1984; Earhart et al., 1984; Winston, 1986). The lower Belt is interpreted as platform carbonate and subtidal turbidites (McMechan, 1981; Whipple et al., 1984). These rocks grade upwards into the Ravalli Group, which includes the Appekunny, Grinnell, and Empire formations, composed dominantly of argillites with interbedded crossbedded medium-coarse sandstone viewed as subaeral and shal-

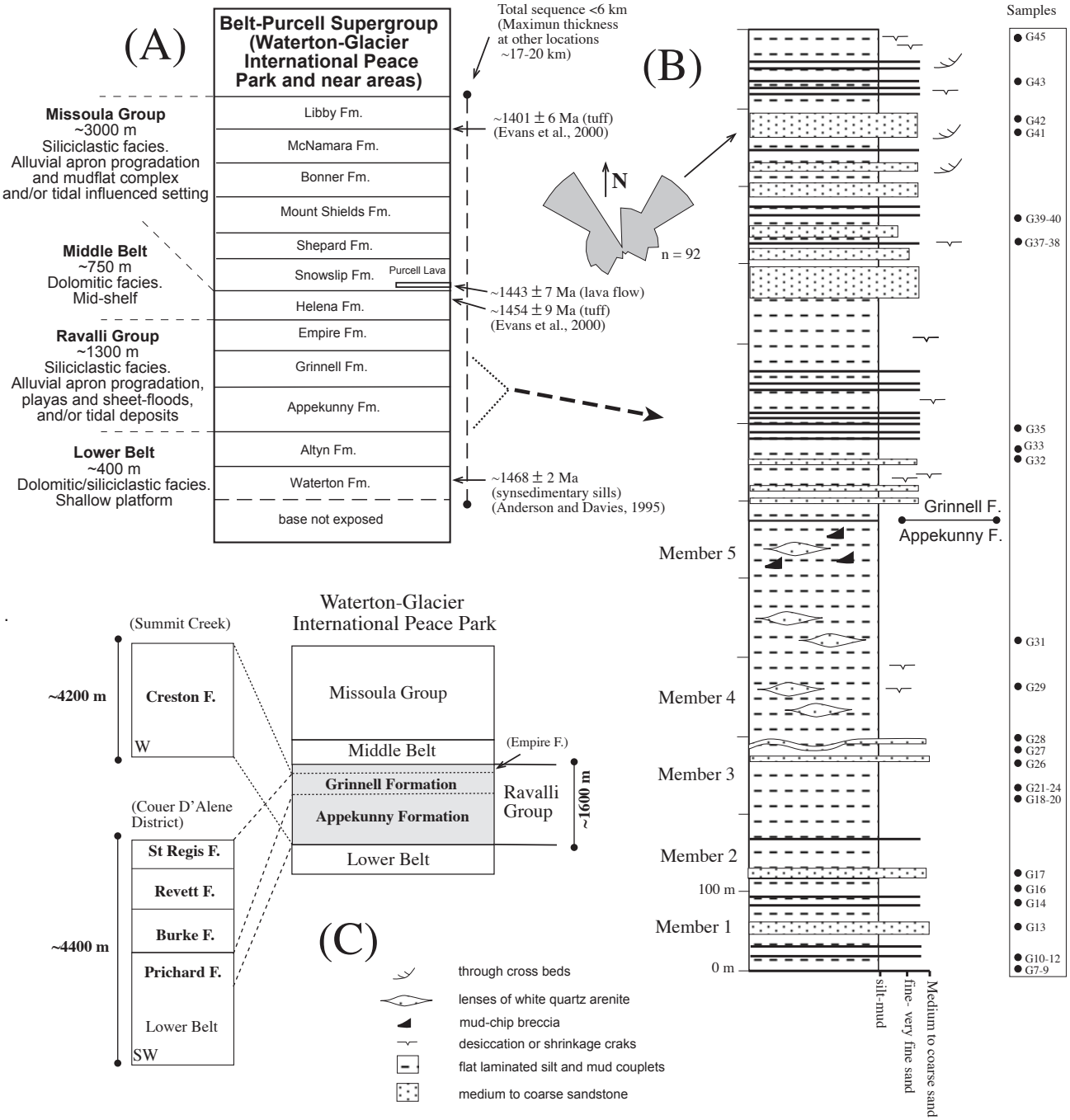

Fig. 4.2 (A) General stratigraphic sequence of the Belt-Purcell Supergroup at Waterton-Glacier International Peace Park (based on Whipple et al., 1997). (B) Sample stratigraphic positions and sample number illustrated (Whipple et al., 1984; Link, 1997). (C) Lateral correlation of the Appekunny and Grinnell formations according to McMechan (1981), Whipple et al. (1984), and Winston (1990).

low water facies (McMechan, 1981; Winston, 1990; Whipple et al., 1997). In turn, the Ravalli Group grades into the middle Belt carbonate, the Helena Formation, interpreted as mid-shelf limestones (Pratt, 2001), or shallow lacustrine carbonate deposits (Winston and Lyons, 1997). The stratigraphically highest Missoula Group comprises a wide variety of siliciclastic facies that have been interpreted as the result of progradational alluvial aprons and mud-flat complex (e.g., Winston, 1984; Whipple et al., 1997).

Accordingly, the Belt-Purcell sediments were deposited in deep water with marginal shoreline facies that evolved into the shallow and subaeral exposure facies (Ravalli Group), that deepen during deposition of carbonates of the middle Belt, and evolved into very shallow to subaeral exposed deposits. Diversity of evaporitic minerals found throughout the Belt-Purcell sequence coupled with the presence of syneresis cracks are interpreted as the result of saline waters (e.g., McMechan, 1981; Connor et al., 1984; Schieber, 1993, 1997; Chandler, 2000 and references therein).

4.2.2 The Appekunny and Grinnell formations

This study focused in the Appekunny and the Grinnell formations (Ravalli Group; Fig. 4.2). These two formations are dominantly argillites with white sandstones, where interbedding is more developed at the top of the upper Grinnell Formation. Sandstones include quartzarenites, subarkoses, and sublitharenites (terminology of Folk, 1968; Fig. 4.2b; e.g., Whipple et al., 1984, 1997; Winston, 1990).

The Appekunny Formation presents internal key marker layers of sandstones in the lower part that thin towards the north (Whipple et al., 1984, 1997). Sedimentary structures include parallel, even curvy, wavy and nonparallel laminations as well as small-scale, low-angle hummocky cross-stratification, syneresis cracks, load structures, and mud-chip breccia; fluid-escape and dolomite filled subaqueous shrinkage structures are more abundant in the middle and upper part of the formation (Table 4.1; Whipple et al., 1984, 1997).

The Grinnell Formation conformably overlies the Appekunny Formation, and has been divided into two main divisions in which interbedding of white sandstones and red argillites are more developed to the top of the sequence. Red and green argillites are present. The former is predominant, with differentiated dominant facies types such as argillites, and white and red sandstones. The most common sedimentary structures include syneresis cracks, ripple marks, mud-chip breccias, parallel, wavy, and non parallel laminations (Table 4.1; Whipple et al., 1984, 1997). Within the

Grinnell Formation at the upper part of the sequence, braided fluvial sandstones units thicken to the east and southeast, and present two main paleocurrent directions to the northeast and northwest (Fig. 4.2b and c; Winston, 1990; Link, 1997 and references therein).

Winston (1989, 1990) interpreted the Appekunny and Grinnell formations as the result of prograding of playas, alluvial aprons and sheet-floods in a lacustrine setting, whereas McMechan (1981) viewed the laterally equivalent Creston Formation to the northwest as subtidal to tidal deposits (Fig. 4.3a; Table 4.1).

4.2.3 Constraints on sedimentation

Previous studies constrained the duration of sedimentation for the Belt-Purcell Supergroup to be ≤75 Ma. The lower-middle Belt spans ≤25 Ma, with a minimum age of sedimentation constrained at 1468 ± 2 Ma and 1469 ± 3 Ma by U-Pb dating of zircons in synsedimentary sills situated near the base of the Supergroup (Anderson and Davies, 1995; Sears et al., 1998). A maximum age of 1454 ± 9 Ma is determined from zircons in a tuff horizon at the upper part of the middle Belt carbonate (Fig. 4.2a; Evans et al., 2000).

There are several key characteristics of the Belt-Purcell Supergroup: (1) an enormous amount of subsidence over 75 Ma; (2) large volumes of detrital input; (3) and a consistency of sediment contribution for almost 75 Ma of indicating long semi-continuous deposition interrupted by hiatuses but not major unconformities (Harrison, 1972).

4.2.4 Tectonic setting and metamorphism

From trace element systematics of tholeiitic gabbros and diorites of the Moyie sills intruded into the lower Belt, Anderson and Goodfellow (2000) suggested their origin as the result of intraplate magmatism. Ross and Villeneuve (2003) documented predominant sediment input from the west, rapid rates of subsidence, and large-scale facies distributions, which they interpreted as evidence for an extensional basin to the west, comparable to a Black Sea-type setting. Sears et al. (2004) interpreted the large volume of siliciclastic detritus to reflect fluvial transport from a low relief, continent-scale catchment discharging to the Belt-Purcell Basin from the southwest. Lower units were deposited during active rifting, whereas the upper Belt is considered to represent basinal subsidence from thermal contraction of the lithosphere (Sears and Price, 2000; Lydon, 2000).

Table 4.1 Principal stratigraphic features of the Appekunny and Grinnell formations.

Formation	Thickness (west-east)	Lithology	Sedimentary structures	Paleocurrents	Lateral correlation	Depositional environment	References
Grinnell	~800 m	Mainly red argillite with interbedding of white quartzarenite mainly at the top of the sequence.	Parallel and non-parallel lamination, mud-breccias, fluid escape structures, subaqueous shrinkage cracks, cross-laminated	Northeast and northwest trends (quartzarenite)	St Regis-Revett-Burke to the southwest in Mission Range, Montana, and Creston to the north in Alberta and B.C.	Alluvial aprons, playas and sheet-floods or intertidal-subtidal.	(1) McMechan (1981) (2) Höy (1993) (3) Whipple et al. (1984) (4) Winston (1990) (5) Link (1997)
Appekunny	~700-100 m	Predominant green argillite, with sparse layers of quartzarenite.	Parallel and non-parallel lamination, low angle crosslamination, mud-breccias, fluid escape structures, subaqueous shrinkage cracks and fining- upward couplets	----------	Prichard to the southwest in Mission Range, Montana and Creston to the north in Alberta and B.C.	Alluvial aprons, playas and sheet-floods or intertidal- subtidal.	(1) McMechan (1981) (2) Höy (1993) (3) Whipple et al. (1984) (4) Winston (1990)

The Belt-Purcell Supergroup records a range of metamorphism from subgreenschist in the upper sequence, through greenschist facies in the northeast, to amphibolite facies in the southwest (Maxwell and Hower, 1967; Harrison, 1972). Samples of this study were metamorphosed to lower greenschist facies. In the Jurassic-Paleocene (160 to 60 Ma), during the Laramide event of the North American Cordillera, the Belt-Purcell Supergroup was displaced eastward by thrusting, being completely detached and emplaced onto the basement and Cretaceous strata (O'Neill, 1997; Lydon, 2000).

4.2.5 The Belt-Purcell basement rocks

The basement where the Belt-Purcell Supergroup is overlying is mostly not exposed (Kleinkopf, 1997). Inferred from basement maps of the western Laurentia, the Wyoming Craton and the Archean Hearne Province could be located underneath (Fig. 4.3; Hoffman, 1988; Ross et al., 1990). The Wyoming Craton (~3100-2600 Ma; e.g., Price and Sears, 2000) is composed mainly of gneiss-migmatites, granitoid batholiths and minor greenstone, amphibolites and ultramafic rocks (Goodwin, 1991). The Hearne Province (3300-2600 Ma) includes the Medicine Hat Block (metaplutonic gneisses; 3270-2650 Ma), Vulcan Low (collisional suture; Hoffman, 1988), Matzhiwin High (magmatic belt) and the Loverna Domain (Ross et al., 1990; Price and Sears, 2000 and references therein). The whole Hearne Province is interpreted as a collage of Archean blocks (Ross et al., 1990).

Between the Wyoming Craton and the Hearne Province there is the Proterozoic suture zone of the Great Falls Tectonic Zone (~1900 Ma) that is represented by deformed calc-alkaline granitoids and gneisses at the little Belt Mountains. This suture is interpreted as the result of closure of an ocean basin between the Wyoming and the Medicine Hat Block at ~1900 Ma (Mueller et al., 1993). Western basement rocks to the Belt-Purcell Basin are the Mesoproterozoic migmatitic gneisses of the Priest River Complex (~1570 Ma; Doughty et al., 1997; Fig. 4.3). Other western terranes were rifted, probably by post-Belt fragmentation, and therefore are not present today (Fig. 4.3; e.g., Frost and Winston, 1987; Ross et al., 1991, 1992; Ross and Villeneuve, 2003).

4.2.6 Other Paleo-Mesoproterozoic terranes/provinces

Paleo-Mesoproterozoic basement terranes to the north of the Belt-Purcell Basin are the Rimbey magmatic rocks (1850-1790 Ma), Thorsby (2300-1900 Ma) and the Wabamun (2320 Ma) as part of the northern Alberta, which are a collage of terranes accreted during the Proterozoic to

Laurentia (Fig. 4.2; Ross et al., 1990; Price and Sears, 2000 and references therein). Further north Paleo/Mesoproterozoic basement rocks are the continental magmatic arcs of Talston (2000-1800 Ma), Wompay (2300-2100 Ma), and the Slave Craton; to the south-southeast the Yavapai, Mazatzal Provinces and the Central Plains (1800-1600 Ma), Mojave juvenile crust (1900-1800 Ma), Trans-Hudson Orogenic Belt (1900-1800 Ma), Penokean Province (1900-1800 Ma), arc magmatism related to accretionary events (1500-1400/1790-1740 Ma), and the Grenville imbricated crust (1400-1000 Ma; Fig. 4.2; Hoffman 1988, 1991; Ross et al., 1990; Ross and Villenueve, 2003; Zhao et al., 2004).

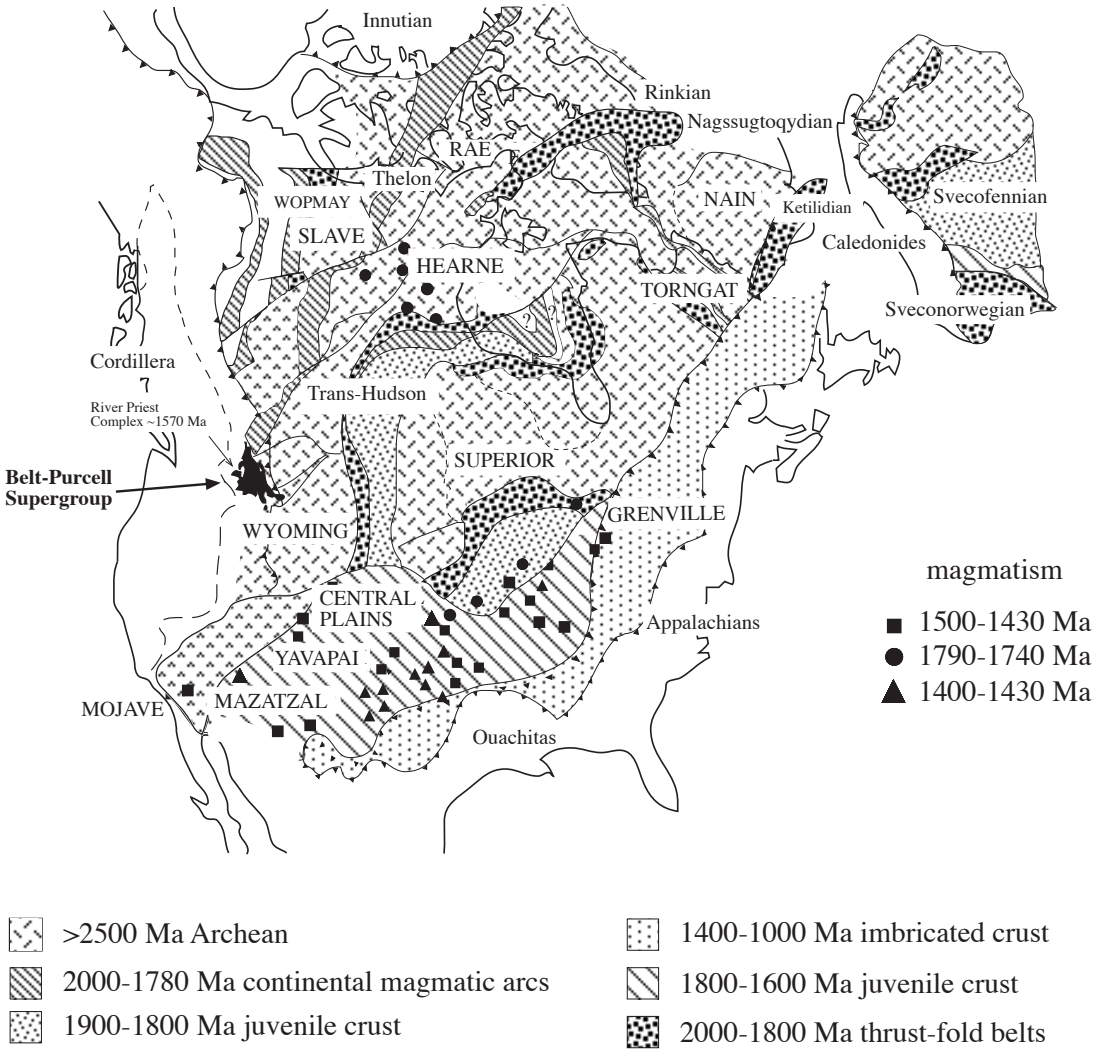

Fig. 4.3 Basement rocks of Laurentia showing potential sources for the lower Belt-Purcell Supergroup sequence (based on Ross and Villeneuve, 2003).

4.3 Sample design

The Appekunny and Grinnell formations were selected for this study given that they are mainly argillites interbedded with sandstones (Whipple et al., 1984; 1997; Winston, 1986). Both formations are thick and are well exposed throughout the Belt-Purcell Basin. These formations are differentiated based on colour and abundance of sandstone-argillite interbedding (Whipple et al., 1984).

The presence of interbedded argillites and sandstones in these two formations allows testing of hypotheses for distinct or common provenance of these two facies for the lower Belt-Purcell sequence, both by whole rock compositions and monazite chemical age populations.

Mineralogically, argillites have an assemblage of quartz with minor plagioclase and microcline, in a matrix of chlorite and illite-micas (Maxwell and Hower, 1967; Harrison, 1972; Frost and Winston, 1987; Lydon, 2000). Sandstones have an assemblage of quartz, plagioclase, with <5 modal percent K-feldspar, muscovite, monazite, and chlorite (quartzarenites, subarkoses, and sublitharenites; terminology of Folk, 1968). Most monazite grains in argillites are <5 μm, whereas counterparts in sandstones are typically <10 μm. Rarely monazites have diameters of >15 μm. Monazites occur in three textural varieties in both facies: (1) as separate elements of a detrital skeleton; (2) as crystals within rock fragments or inclusions; or (3) as euhedral individual grains. Based on texture, the former two are interpreted as detrital whereas the third is diagenetic. Many of the detrital grains that were not included in rock fragments display overgrowths.

Various studies have established that REE in sedimentary rocks are concentrated mainly in the clay-size and silt-size (<20 μm) fractions, but are not associated with any particular clay mineral species, such that fine-grained sedimentary rocks best preserve the geochemical characteristics of the source area (Cullers et al., 1979; Chaudhuri and Cullers, 1979; Taylor and McLennan, 1985; Condie, 1991; Gao and Wedepohl, 1995; Nesbitt et al., 1996; Faupl et al., 1998). Sandstone facies may display geochemical effects due to heavy mineral sorting as a significant fraction of their trace element budget may reside in heavy minerals (e.g., Roaldset, 1979; Taylor and McLennan, 1985; Condie, 1991; Roser, 1996).

Accordingly, taking into account these geochemical effects the Appekunny and Grinnell formations from Waterton-Glacier International Peace Park, northern Montana, and southwestern Alberta were comprehensively sampled (Figs. 4.1 and 4.2). A subset of 33 samples, selected to be

representative of argillites and sandstones over the stratigraphic extent of the two formations, were analyzed for major and trace elements (Fig. 4.2b).

Monazite is a common detrital mineral in siliciclastic deposits, and in this study has been identified as relatively abundant in some units in the Appekunny and Grinnell formations. Monazite contains a high concentration of rare earth elements (e.g., Ni et al., 1995; Cressey et al., 1999; Pyle et al., 2005 and references therein). Accordingly, six samples of argillites and five of sandstones with high total REE abundances were selected for monazite chemical Th-U total Pb dating.

4.4 Analytical methods

4.4.1 Elemental compositions

Major elements were determined using X-ray fluorescence spectrometry (XRF) at the Société Générale de Surveillance (SGS) Laboratories, Ontario, Canada. Precision is ±0.01 wt.%. Trace elements, including the REE and high field strength elements (HFSE), were analyzed using inductively coupled plasma mass spectrometry (ICP-MS; model Perkin Elmer Elan 5000) at the University of Saskatchewan. To address potential problems stemming from incomplete dissolution of refractory minerals, the procedure of Jenner et al. (1990) was followed, whereby a sodium peroxide sinter was used for Th, Nb, Ta, Zr, Hf, Y, Sc and REE, and an HF-HNO_3 digestion on a separate aliquot was used for the remaining trace elements. Detailed analytical methodology is presented in Fan and Kerrich (1997). The protocol includes standard additions, pure elemental standards for external calibration, and reference materials. Modern Canadian Shield lake sediment (LKSD-1) was used as a reference material, inasmuch as the REE and HFSE contents are comparable to those in the argillite analyzed, and reference material basalt (BCR-2). Long-term reproducibility in this lab for the low-level reference material basalt (BCR-1) is given in Table 4.2.

Detection limits (in ppm) defined as 3Sigma of the calibration blank for some critical elements are as follows: Nb (0.016), Hf (0.042), Zr (0.103), La (0.018), Ce (0.014), Nd (0.086) and Sm (0.065). Wet chemistry operations were conducted under clean laboratory conditions. Analyses of acids, distilled deionized water and procedural blanks give levels of <1 ppb for REE, Nb, Zr, and Hf, relative to their concentration in the rocks (Xie et al., 1994).

Values of Ce/Ce* and Eu/Eu* were calculated relative to the post-Archean upper continental crust (PA-UCC) average of Taylor and McLennan (1995), following Taylor and McLennan

(1985).

Table 4.2 ICP-MS multi-element analyses of international reference material basalt BCR-1 for selected trace elements by the University of Saskatchewan ICP-MS laboratory (excerpted from Xie et al., 1994).

Elements	x	1σ	C%	CV
Zr	201	12	6	190
Nb	14.6	0.7	4.8	14
La	26	0.8	3.1	24.9
Pr	6.95	0.33	4.7	6.8
Eu	1.95	0.11	5.6	1.95
Ho	1.26	0.05	4	1.26
Tm	0.54	0.02	3.7	0.56
Lu	0.502	0.02	4	0.51
Hf	5.87	1.49	8.3	4.95
Ta	1.03	0.16	15.5	0.81
Th	6.7	0.52	7.8	5.98
U	1.75	0.1	5.7	1.75

(x) Average; (1σ) standard deviation; (C%) relative standard deviation; (CV) compiled values from Potts et al. (1992).

4.4.2 Monazite chemical Th-U total Pb dating

The chemical Th-U total Pb method has been developed on the basis of precise electron probe microanalyses (Suzuki and Adachi, 1991, 1994) and has been widely used with monazite for geochronology (e.g., Suzuki and Adachi, 1994; Rhede et al., 1996; Mougeot et al., 1997; Finger and Helmy, 1998). Monazite does not become metamict from radiation (Nasdala et al., 1999) and behaves as a geochemically closed system without loss of parent or daughter nuclides below ~725°C (Copeland et al., 1988). Belt-Purcell rocks did not exceed ~400°C in the study area during metamorphism (e.g., Harrison, 1972).

The chemical Th-U total Pb dating method is based on the premise that initial lead in monazite does not exceed 1 ppm (Parrish, 1990), and monazite does not incorporate appreciable external lead during its crystallization (Scherrer et al., 2000). Standard assumptions are that monazites remained as a closed system, such that measured U/Pb and Th/Pb ratios are due only to radioac-

tive decay (e.g., Faure, 1986; Montel et al., 1996; Harrison et al., 2002; Hodges, 2004; Dahl et al., 2005). These appear to be robust assumptions, and the monazite chemical dating method has been used in numerous studies of metamorphism and detrital age populations (e.g., Suzuki and Adachi, 1991; Ayers et al., 1999; Montel et al., 2000; Rasmussen et al., 2001).

The Th-U total lead chemical dating method is a relatively quick and low-cost method to obtain ages for detrital monazites using the electron microbe that allows high spatial resolution in small sized grains, but is less accurate than isotopes methods (e.g., Pyle et al., 2005; Cocherie et al., 2005). In this study, all monazite grains of ~5 μm or larger were analyzed *in situ* on polished thin sections. Monazites in Appekunny argillites were large enough to be analyzed, but not in Grinnell counterparts. Due to the generally small grain sizes (5-10 μm) most monazites were analyzed for one spot. Larger monazite grains did not generate enough valid analyses to permit construction of an isochron from multiple spot analyses to determine possible Pb loss (Suzuki and Adachi, 1991), and therefore the provenance data in this study have to be put in the regional geologic context for interpretation.

In the chemical Th-U total Pb dating method age (t) is calculated by solving the following equation (e.g., Suzuki and Adachi, 1991,1994):

$$\frac{PbO}{W_{Pb}} = \frac{ThO_2}{W_{Th}} \{\exp(\lambda_{232} t) - 1\} + \frac{UO_2}{W_U} \left\{ \frac{\exp(\lambda_{235} t) + 137.88 \exp(\lambda_{238} t)}{138.88} - 1 \right\} \quad (4.1)$$

Where *W* is the gram-molecular weight of each oxide (W_{Pb}=224, W_{Th}=264 and W_U=270 for monazite), and $Lambda_{232}$, $Lambda_{235}$, and $Lambda_{238}$ are the radioactive decay constants for ^{232}Th, ^{235}U and ^{238}U respectively.

Analyses for Th, U, Pb, Y, and REE were conducted on a Cameca SX-100 electron microprobe equipped with three wavelength-dispersive spectrometers (WDS) at the Warsaw University, Faculty of Geology, Poland. The accelerating voltage was 20 kV, probe current 50 nA, and beam diameter 3 μm. Standards were synthesized glasses of Th and U from P&H Developments Ltd., Derbyshire, UK; and $PbCrO_4$ for Pb; a Y-Al garnet standard was used to measure the Y content of monazite. Complementary analyses for Th, U, Pb, and Y were conducted on a Jeol JXA-8600 Superprobe electron microprobe with three wavelength-dispersive spectrometers (WDS) attached at the University of Saskatchewan, Canada following the protocol of Pyle et al. (2005). The accelerating voltage was 15 kV, probe current 200 nA, and beam diameter 3 μm. Standards were Smithsonian synthetic phosphates doped with Th and U; and SPI Y-Al garnet for Y. In both pro-

tocols Pentaerythritol (PET) crystals were used to analyze Th_{MAlpha}, U_{MBeta}, Pb_{MBeta}, thallium acid phtalate (TAP) for Y_{LAlpha}. Spectral interferences of Y_{LGamma} and Th_{MAlpha} on Pb_{MAlpha} and Th_{MGamma} on U_{MBeta} were corrected following Pyle et al. (2005). Only monazites with total wt.% oxides between ~97 and ~102 are reported. Chemical ages were plotted using Isoplot (Ludwig, 1999). Errors were calculated based on counting uncertainties of the electron microprobe.

4.5 Analytical results

From sample grain-size characteristics, petrographic observations, and SiO_2-loss on ignition (LOI) relationships, there are two distinct facies of rocks: 15 sandstones and 18 argillites (Figs. 4.2b and 4.4).

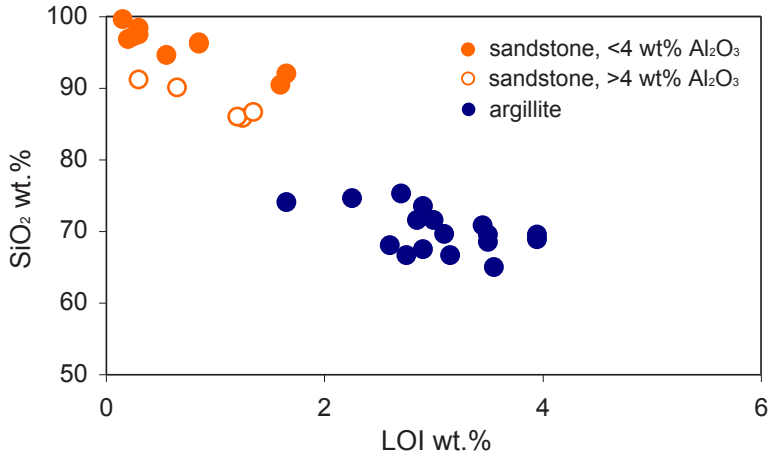

Fig. 4.4 Sample groupings based on SiO_2-LOI (loss-on-ignition) relationship. Two main facies are delineated: sandstones (>75 wt.% SiO_2-<2 wt.% LOI and argillites <75-60 wt.% SiO_2 - <5 wt.% LOI).

4.5.1 Geochemistry of argillites

Argillites comprise a compositionally uniform population. They possess contents of most major elements close to post-Archean upper continental crust (PA-UCC) of Taylor and McLennan (1995), but with systematically greater abundances of MgO and K_2O, and pronounced depletions of MnO, CaO, and Na_2O (Fig. 4.5c; see Appendix 4.1). Potassium is correlated with Al_2O_3, potentially indicative of primary smectite, and is also highly correlated with Rb, Cs, and Tl. Na_2O covaries with Al_2O_3. From major element composition the primary mineralogy is estimated to be quartz-feldspar-smectite clays. This inferred primary mineralogy is in keeping with the conclusions of Lydon et al. (2000) for compositionally similar argillites of the lower Belt in southern British Columbia; based on major element compositions they compared that mineral assemblage

to counterparts in the Gulf Basin, southeastern U.S.A. Thorium, light rare earth elements (LREE), total REE (∑REE), Sc, V and Co also correlate with Al_2O_3 (r^2 >0.64).

Two types of REE patterns are evident in the Appekunny and Grinnell formations. (1) Type 1, PA-UCC-like REE pattern, having similar REE and multi-element patterns as PA-UCC, albeit at 1.3 to 1.5 times PA-UCC due to less/more quartz. Normalized HFSE and transition metals broadly follow REE. Light REE and middle REE covary with Al_2O_3. (2) Type 2 pattern characterized by flat LREE relative to PA-UCC at 1 to 1.5 times PA-UCC, in conjunction with more abundant HREE than LREE relative to PA-UCC (Fig. 4.5a and b).

4.5.2 Geochemistry of sandstones

Two compositional groups of sandstones cluster at values ≥4 wt.% Al_2O_3 and <4 wt.% Al_2O_3 (Fig. 4.4). Both groups are present in the Appekunny and Grinnell formations. There is no correlation between Al_2O_3 and Eu/Eu*, interpreted as an insignificant contribution from plagioclase to the whole-rock Al budget. Consequently, the Al budget is controlled by the clay sized fraction. The former population shows covariation of Th, U, Nb, K_2O, Zr, La, Yb, ∑REE, V, and Sc with Al_2O_3, as in the argillite. The latter population has similar covariant trends for Th, Zr, K_2O, V, and Sc, whereas Nb, REE and U are scattered. From these relationships, combined with petrographic observations, to a first approximation sandstones compositionally are argillites highly diluted by detrital quartz.

Rare earth element abundances are controlled by quartz content. There are two REE patterns referenced to PA-UCC, as for argillites: type 1 is flat at 0.1 to 0.9 relative to PA-UCC, whereas type 2 features flat LREE at 0.1 to 0.9 PA-UCC and more abundant HREE than LREE. In some samples there are variably negative Ce anomalies and variable upturns at Yb-Lu. Positive peaks at Eu in a few type 2 samples likely reflect detrital plagioclase (Fig. 4.5f). On PA-UCC normalized diagram peaks at K could be explained by secondary illite (cf. Lydon et al., 2000).

4.5.3 Monazite chemical Th-U total Pb ages

One hundred and forty-five chemical Th-U total Pb ages were calculated, yielding 77 ages for sandstones and 68 for argillites covering the three textural varieties (Appendices 4.2 and 4.3). Twenty-six grains in the Appekunny Formation argillites were considered detrital and 37 diagenetic based on the combination of textures, ages and composition, whereas in the sandstones 29 were detrital and 31 diagenetic. For the Grinnell Formation sandstones, 11 grains were considered

detrital and 6 diagenetic. Seventy-three were analyzed for REE contents. Representative analyses of interpreted detrital and diagenetic monazites are reported in Tables 4.3 and 4.4.

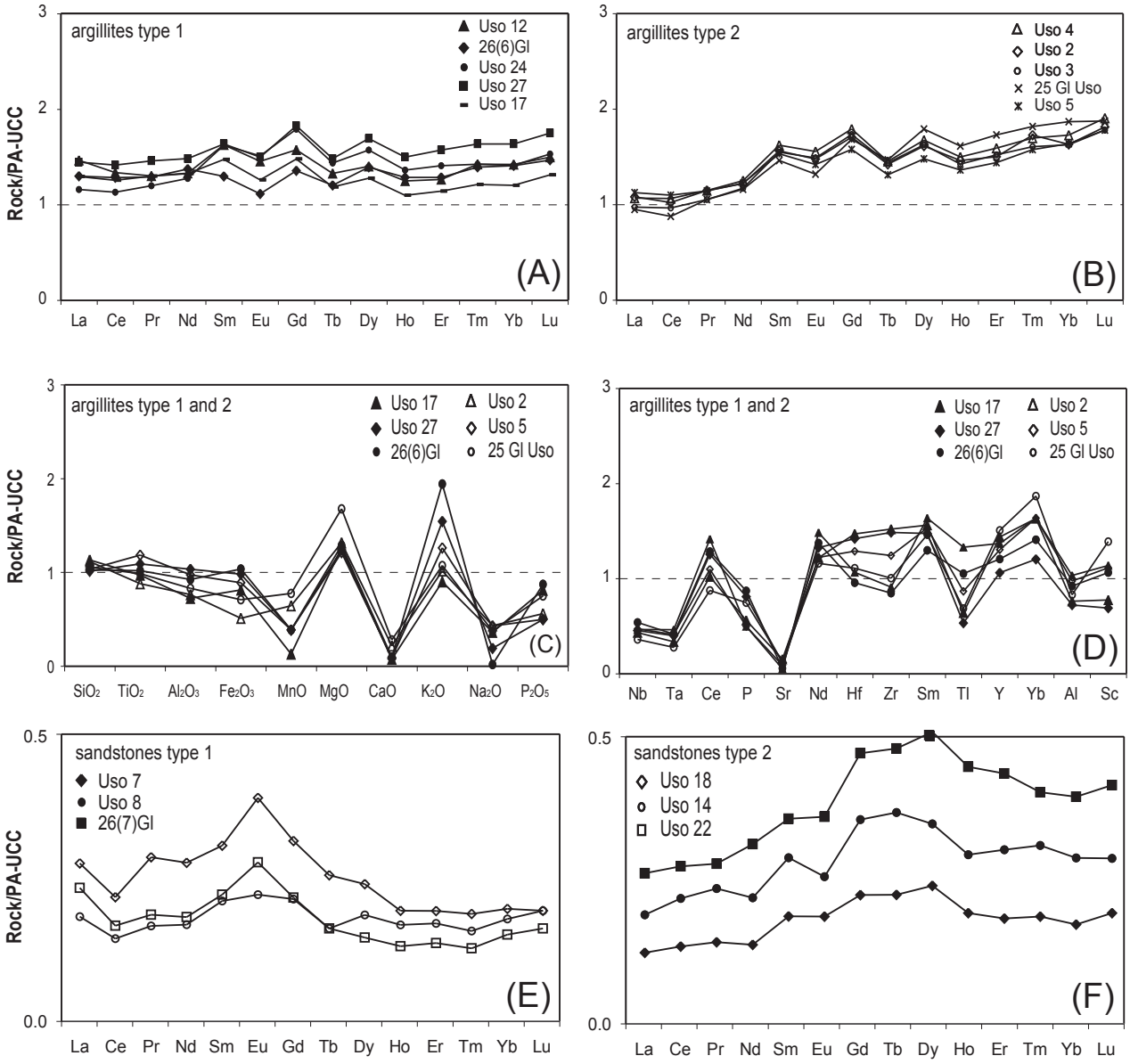

Fig. 4.5 Plots for argillites and sandstones: (A) rare earth elements (REE) for argillites type 1, displaying flat REE patterns on linear scales and values are normalized to post-Archean upper continental crust (values from Taylor and McLennan, 1995); (B) REE for argillites type 2, representing an enrichment of HREE relative to LREE; (C) variation diagram of major elements for each of the argillite types; (D) multi-element plot for argillite types 1 and 2; (E) REE pattern for sandstones with Al_2O_3 content lower than 4 wt.%; (F) REE plot for sandstones with Al_2O_3 >4 wt.%.

Table 4.3 Selected monazite analyses of argillites from the Appekunny Formation presenting main detrital and post-depositional ages.

Sample	Detrital USO3(2)	Detrital USO1(26)	Detrital USO1(30)	Detrital USO1(18)	Detrital USO13(6)	Detrital USO13(4)	Detrital USO13(5)	Diagenetic USO3(3)	Diagenetic USO3(12)	Diagenetic USO1(22)
La_2O_3(wt%)	13.43	14.57	13.48	14.81	14.58	14.24	13.9	16.61	14.17	17.69
Ce_2O_3	26.84	28.23	27.57	28.79	28.06	27.91	27.95	31.21	30.44	30.00
Pr_2O_3	3.10	3.08	3.06	3.00	3.11	2.98	3.18	3.20	3.54	3.17
Nd_2O_3	11.75	10.74	12.06	10.39	11.91	11.67	11.78	11.79	14.10	12.05
Sm_2O_3	2.09	1.73	2.12	1.89	2.13	2.06	2.12	1.46	2.6	2.05
Gd_2O_3	1.72	1.08	1.49	1.24	1.51	1.58	1.68	0.65	1.32	1.19
Tb_2O_3	0.27	0.10	0.15	0.19	0.19	0.20	0.11	0.09	0.09	0.01
Dy_2O_3	0.80	0.26	0.48	0.39	0.52	0.56	0.61	0.08	0.10	0.18
Ho_2O_3	0.04	0.06	0.02	0.08	0.06	0.11	0.07	0.11	u.d.	0.00
Er_2O_3	0.17	0.11	0.10	0.09	0.04	0.15	0.20	0.01	0.06	u.d.
Yb_2O_3	0.02	u.d.	u.d.	u.d.	u.d.	u.d.	u.d.	u.d.	u.d.	u.d.
P_2O_5	30.32	30.03	29.92	29.36	29.51	29.69	29.23	29.34	29.55	30.55
PbO	0.44	0.52	0.44	0.50	0.33	0.43	0.44	0.20	0.03	0.06
UO_2	0.60	0.24	0.45	0.13	0.16	0.80	0.83	0.07	0.02	0.02
ThO_2	3.18	6.48	4.47	6.03	4.05	2.91	2.71	3.31	0.76	1.10
CaO	0.91	1.10	1.15	0.78	0.77	0.90	0.88	0.43	0.28	0.31
Y_2O_3	3.19	1.44	1.59	1.33	1.02	2.37	2.49	0.23	0.19	0.26
SiO_2	0.75	0.61	0.42	0.78	0.43	0.11	0.09	0.61	0.56	0.44
Total	99.69	100.45	99.04	99.84	98.46	98.76	98.35	99.47	97.88	99.14
Age (Ma)	1859±9	1614±18	1663±21	1743±29	1641±37	1704±32	1747±17	1307±32	852±26	1200±39

(u.d.) Under detection limit; (App) Appekunny Formation.

Monazites in argillite of the Appekunny Formation display a main peak at ~1680, with minor peaks at ~1860, ~1740, and ~1580 Ma, with one date at ~3080 Ma. Sandstones have main peaks at ~1690, ~1650, and ~1550 Ma, minor peaks at ~1890 and ~1780, and a single point date at ~2290 Ma; both facies display a wide range of ages from~1400 Ma to ~300 Ma, with a main peak at ~900 Ma. Sandstones from the Grinnell Formation show peaks at ~1880, ~1790, and ~1720 Ma, one date at ~2660 Ma, as well as a few scattered ages <~1400 Ma (Tables 4.4 and 4.5; Fig. 4.6).

Monazite grains and their counterparts older than ~1400 Ma show more rounded features and some grains display syntaxial cement (texture 1) coupled with other euhedral grains as inclusions in quartz and feldspars (texture 2), whereas grains younger than ~1400 Ma are more euhedral (texture 3; Figs. 4.7 and 4.8). Compositional differences between monazites >~1400 Ma and <~1400 Ma are plotted in Fig. 4.9. All chemical analyses not listed in Tables 4.4 and 4.5 are in the Appendices 4.2 and 4.3.

The chemical monazite ages presented in this study cannot be checked for possible resetting. Their small grain size or the lack of enough multiple analyses on the same grain did not allow to apply the chemical isochron method of Suzuki and Adachi (1991) to test for Pb loss. However, all monazite age peaks found in the Grinnell and the Appekunny formations are consistent with previous studies based on isotopic analyses of detrital zircons and monazites of the same or laterally equivalent formations, detrital ages are consistent with the geochemical systematics, and can be accounted for based on the regional geology and paleotectonic reconstructions.

Table 4.4 Selected monazite analyses of sandstones in the Appekunny and Grinnell formations, displaying selected examples of detrital and post-depositional ages.

	Detrital	Detrital	Detrital	Detrital	Detrital	Detrital	Diagenetic	Diagenetic	Diagenetic	Diagenetic	Diagenetic	Diagenetic
Sample	3AP(19)	2AP(6)	2AP(3)	2AP(4)	1AP(3)	MGR6(11)	MGR6(10)	2AP(16)	2AP(11)	3AP(20)	2AP(8)	2AP(5)
La_2O_3 (wt%)	23.71	13.80	14.49	14.58	16.69	12.05	14.13	15.82	28.31	18.20	16.16	14.42
Ce_2O_3	27.62	27.40	27.71	27.97	30.10	27.40	29.18	27.42	28.07	29.77	27.44	28.10
Pr_2O_3	3.08	2.95	2.97	2.96	3.05	3.12	3.12	3.74	2.29	3.61	3.85	2.89
Nd_2O_3	9.66	10.25	10.32	10.401	10.47	12.45	12.37	14.95	6.94	13.26	14.13	10.41
Sm_2O_3	1.42	1.90	1.70	1.66	1.20	2.22	2.26	2.60	0.98	1.86	2.51	1.93
Gd_2O_3	0.68	1.43	1.32	1.40	0.53	1.82	1.57	1.41	0.53	0.69	1.25	1.32
Tb_2O_3	0.03	0.13	0.16	0.07	0.01	0.19	0.21	0.12	0.10	u.d.	0.14	0.23
Dy_2O_3	0.11	0.58	0.44	0.42	0.05	0.73	0.47	0.11	0.06	u.d.	0.04	0.46
Ho_2O_3	u.d.	0.05	0.05	0.02	0.01	0.23	0.14	0.03	u.d.	u.d.	u.d.	0.12
Er_2O_3	u.d.	0.15	0.11	0.12	0.01	0.28	0.12	0.01	u.d.	0.02	0.03	0.11
Yb_2O_3	u.d.	0.02	0.02	0.04	0.04	u.d.	0.01	u.d.	u.d.	u.d.	u.d.	u.d.
P_2O_5	29.70	29.05	28.18	28.51	30.30	29.38	30.57	30.73	30.39	29.47	29.59	28.95
PbO	0.04	0.61	0.58	0.58	0.42	0.29	0.18	0.07	0.03	0.01	0.04	0.42
UO_2	0.01	0.39	0.34	0.37	0.23	0.18	0.15	0.01	0.02	0.01	0.01	0.32
ThO_2	0.55	7.04	6.72	6.60	5.42	2.96	3.49	1.86	0.68	0.45	1.21	6.18
CaO	0.37	0.84	0.65	0.66	0.76	0.34	0.72	0.20	0.31	0.25	0.18	0.75
Y_2O_3	0.17	2.45	1.97	2.05	0.56	3.98	1.11	0.26	0.18	0.07	0.26	2.11
SiO_2	0.54	1.08	1.20	1.15	0.86	2.22	0.41	0.49	0.09	0.35	0.83	1.00
Total	97.78	100.22	99.01	99.62	100.77	99.83	100.25	99.90	99.04	98.08	97.73	99.80
Age (Ma)	1585±46	1648±18	1668±22	1682±29	1546±37	1833±32	1059±37	870±38	941±44	492±28	753±18	1334±32

(u.d.) Under detection limit; (App) Appekunny Formation; (Gr) Grinnell Formation.

4.6 Discussion

4.6.1 Provenance

Taylor and McLennan (1985) considered that REE profiles from Proterozoic shales are distinct from Archean counterparts. This compositional transition is due to a major period of growth

and differentiation of continental crust at the end of the Archean. Archean UCC is characterized by high $(La/Yb)_{cn}$, with no Eu anomalies, combined with low Y, Th/Sc, and LREE/HREE, whereas PA-UCC has opposite geochemical features including systematic negative Eu anomalies. This general compositional switch was interpreted to reflect a transition from first-cycle detritus shed off juvenile terranes dominated by bimodal basalt and dacite/tonalite arcs, to a period of growth and differentiation of continents caused by intracrustal melting that gave rise to K-rich granites. K-rich granites are rare in Archean supracrustal terranes, with sparse exceptions (Feng and Kerrich, 1992; Vearncombe and Kerrich, 1999). In shales, the Th/Sc ratio is an indicator of crustal differentiation, given that it is an index of felsic versus mafic lithologies. Thorium is enriched in felsic rocks whereas Sc is depleted, and the inverse is true for mafic lithologies (Taylor and McLennan, 1985; Young, 1999).

Argillites of the Appekunny and Grinnell formation REE patterns plot subparallel and close to 1 when normalize to PA-UCC, consistent with a dominantly post-Archean source area for the sediments. The same samples, normalized to Archean upper continental crust values, display a pronounced Eu depletion (Fig. 4.5a and b). Similarly, Th/Sc ratios, Cr–Ni contents, and Eu/Eu* versus $(Gd/Yb)_{cn}$, plot in the post-Archean field (Fig. 4.10a, c, and d). These results are in keeping with dominantly Paleoproterozoic ages of detrital zircons and monazites for the Ravalli Group at Waterton-Glacier International Peace Park area (Ross et al., 1992; Ross and Villeneuve, 2003; this study: see below).

Total LREE versus total HREE plot mostly across the Archean field (Fig. 4.10b). This last, apparently contradictory, feature is interpreted as a diagenetic overprint of secondary HREE enrichment in some samples (type 2 REE pattern), as discussed in *section 4.6.5*.

Slack and Höy (2000) suggested four distinct source terranes for the Aldridge and the Fort Steele formations of the equivalent lower Belt in southeastern British Columbia, determined largely on the basis of argillite REE-Th-Sc systematics. They equate these with the following lithologies: (1) dominant in all stratigraphic units are sediments derived from a fractionated calc-alkaline igneous and (or) meta-igneous terrane; (2) an unfractionated counterpart; (3) a terrane dominated by fractionated granites and (or) rhyolites, including alkalic granites; and (4) a terrane comparable to the third example, but with contributions from Fe-rich chemical sediments (see also Schandl et al., 2000). They suggested the possibility of the Mazatzal and Yavapai Provinces as possible minor sources for the Aldridge Formation in the lower Belt (Fig. 4.3). Argillites (type 1) of the stratigraphically higher Appekunny and Grinnell formations are geochemically more uniform than Aldridge and Fort Steele counterparts, presenting similar REE, Th/Sc, and $(La/Yb)_{cn}$ values.

Table 4.5 Summary of monazite chemical age data.

Stratigraphic position (Fig. 4.2b)	Sample	Formation	Location at Waterton-Glacier International Peace Park	Single grain analyses (total 145)	Age range (Ma) a) Archean source b) Proterozoic source c) post-Belt deposition	Errors (±Ma)	Facies
G7	USO 13	Appekunny	Poia Lake/Apekuni Mountain	5	--- 1747-1641 1347-907	 7-37 8-32	Green laminated arg
G18	USO 1	Appekunny	Dead Horse	45	--- 1743-1431 1074-301	 7-39 12-60	Green laminated arg
G20	USO 3	Appekunny	Dead Horse	11	--- 1859-1551 1339-628	 9-20 17-35	Green laminated arg
G29	USO 12	Appekunny	Dead Horse	7	3074 1874-1663 1298-1057	19 17-26 21-27	Green laminated arg
G13	App1	Appekunny	Poia Lake/Apekuni Mountain	43	--- 1790-1479 (2296) 1274-301	 7-37 18-67	Medium to coarse –g white sandstone
G14	2App	Appekunny	Poia Lake/Apekuni Mountain	14	 1950-1648 (2285) 1334-602	 9-29 18-44	Medium to coarse –g white sandstone
G17	3App	Appekunny	Poia Lake/Apekuni Mountain	3	--- 1723 906-870	 46 26-28	Medium to coarse –g white sandstone
G37	MGR	Grinnell	Red Rock Canyon	14	2654 1877-1699 1069-264	12 17-32 37-47	Medium to coarse –g white sandstone
G41	UGR	Grinnell	Red Rock Canyon	3	--- --- 1344-845	 14-35	Medium to coarse –g white sandstone

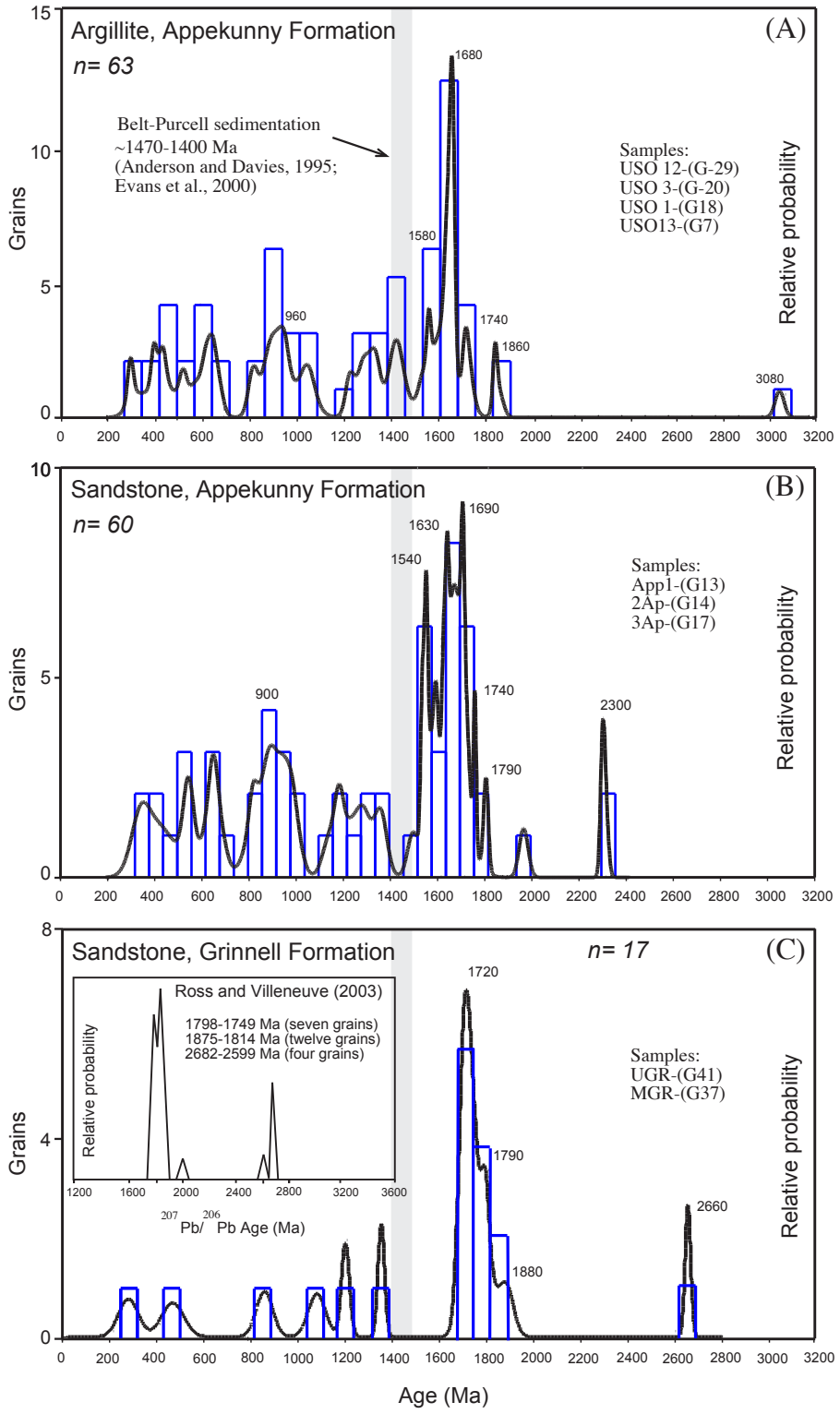

Fig. 4.6 Probability plots of monazite chemical ages from this study for the Grinnell Formation. (A) Argillites from the Appekunny Formation display a main peak at ~1700 Ma; (B) medium-coarse grained sandstones of the same formation peak at ~1550, ~1650, and ~1700 Ma and display post-Belt-Purcell deposition population; (C) medium-coarse grained sandstones from the Grinnell Formation present peaks at ~1880 Ma, ~1780 Ma, and ~1720 Ma. The inset from data of Ross and Villeneuve (2003) shows main peaks at 2680-2600 Ma, ~1875-1815 Ma, and ~1800-1750 Ma for sandstones from the Grinnell Formation.

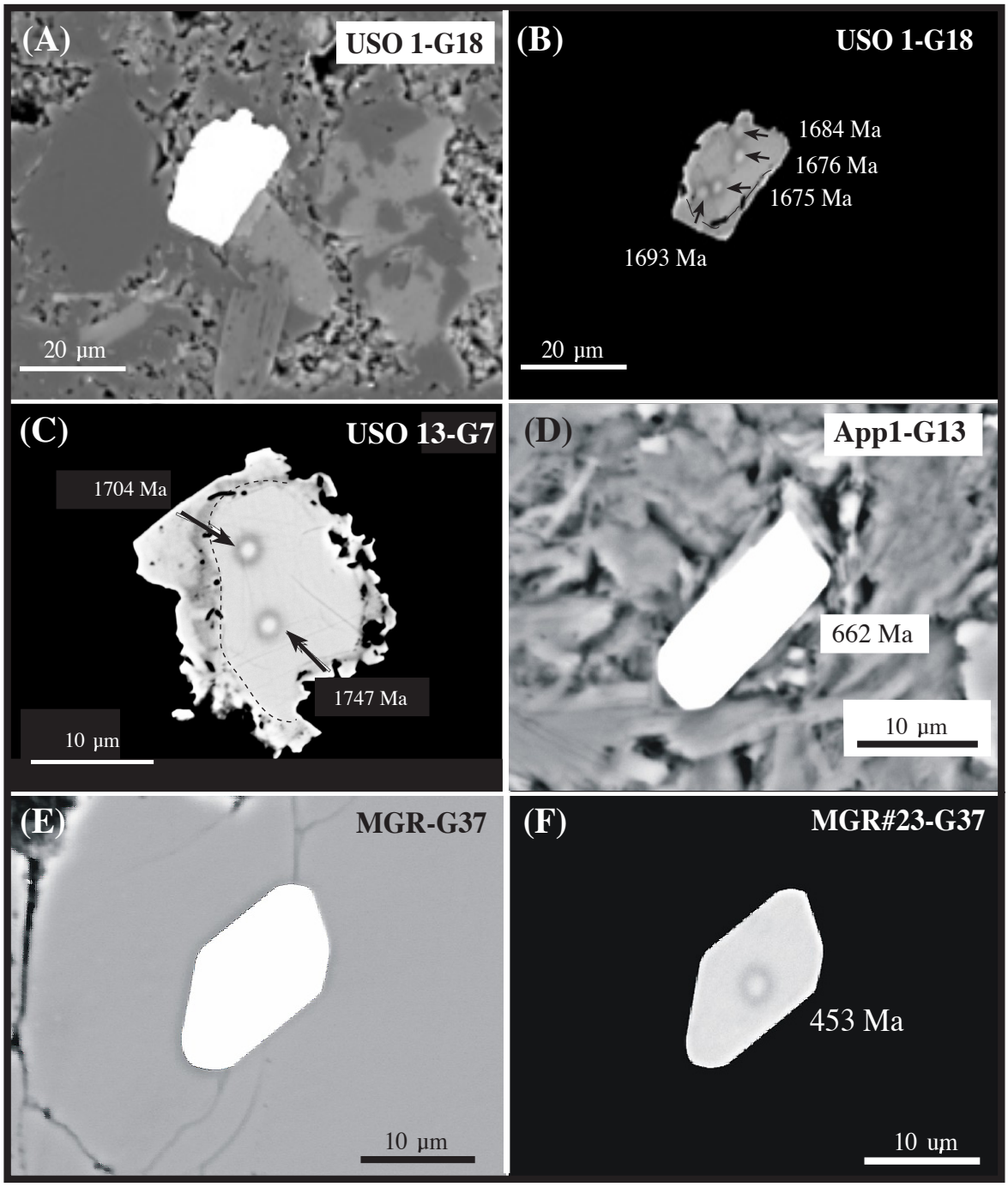

Fig. 4.7 Backscattered electron images of monazite grains. (A), (B) and (C) argillite samples USO 1 and USO 13 from the Appekunny Formation displaying detrital grains presenting syntaxial cement surrounding part of the core with ages ~1700 Ma; and euhedral monazite grains from medium-coarse grained sandstone (D) in the Appekunny Formation with ~650 Ma age. (E) And (F) morphology of monazite from the Grinnell Formation with post-Belt-Purcell deposition age of ~450 Ma.

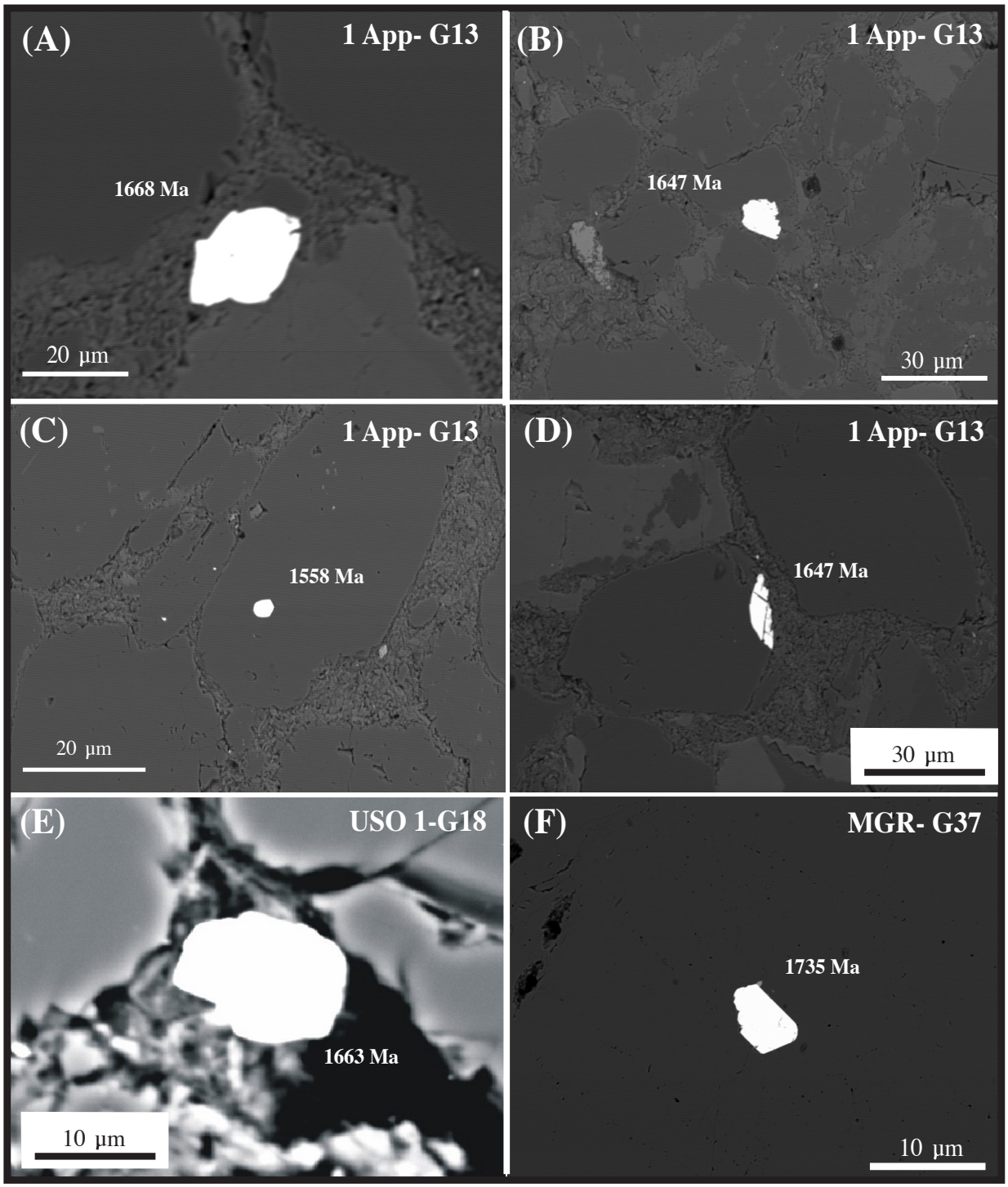

Fig. 4.8 Backscattered electron images of monazite grains showing pre-Belt depositional chemical ages associated with individual rounded grains (A), (B), and (E); inclusions as rock fragments (D) and in rounded quartz grains (C) and (F).

Compositional uniformity could be interpreted as reflecting as the result of progressive growth of the river-catchment system as the Belt-Purcell Basin was filled and mixing. The compositional uniformity of argillites is in keeping with uniform Nd-isotope systematics (Frost and Winston, 1987). Type 2 REE patterns are discussed in *section 4.6.5*.

4.6.2 Chemical Th-U total Pb dates

Ross and Villenueve (2003) conducted an extensive study of SHRIMP U-Pb ages on zircons collected from sandstones of the Belt-Purcell Supergroup. Their results for the Ravalli Group (Fig. 4.3c) are summarized in Table 4.6. They interpreted the data in terms of the Grinnell Formation having a main Paleoproterozoic provenance from the Canadian Shield, but with an Archean source in Laurentia for the Creston Formation. The Revett Formation and the turbiditic facies of the Prichard Formation in the west of the Belt-Purcell Basin were interpreted as mainly fed from a western terrane. Two lines of evidence were used to argue for a western catchment: (1) paleocurrents, and (2) detrital zircon ages of 1620 to 1505 Ma are within the so-called "magmatic gap" (1610-1490 Ma; usage from Ross and Villeneuve, 2003) when there are no known magmatic provinces in Laurentia (Fig. 4.3; Ross and Villeneuve, 2003). In addition, Ross et al. (1992) suggested that at least part of the Revett Formation sediment could have been contributed from the ~1570 Ma Priest River Complex in the west (Fig. 4.3).

Table 4.6 Principal zircon age clusters of the Ravalli Group and lower Belt from Ross and Villeneuve (2003). See Fig. 4.3b for stratigraphic correlations.

Revett F.	Grinnell F.	Prichard F.	Creston F.
1590-1505	1798-1749 (7)	1452 (1)	discordant array at 1900
1682	1875-1814 (12)	1489 (1)	2678-2502 (14)
1893-1793	2682-2599 (4)	1611-1540 (16)	
		1818-1740 (6)	
		2551-2509 (2)	

Age is in Ma and number of grains in brackets.

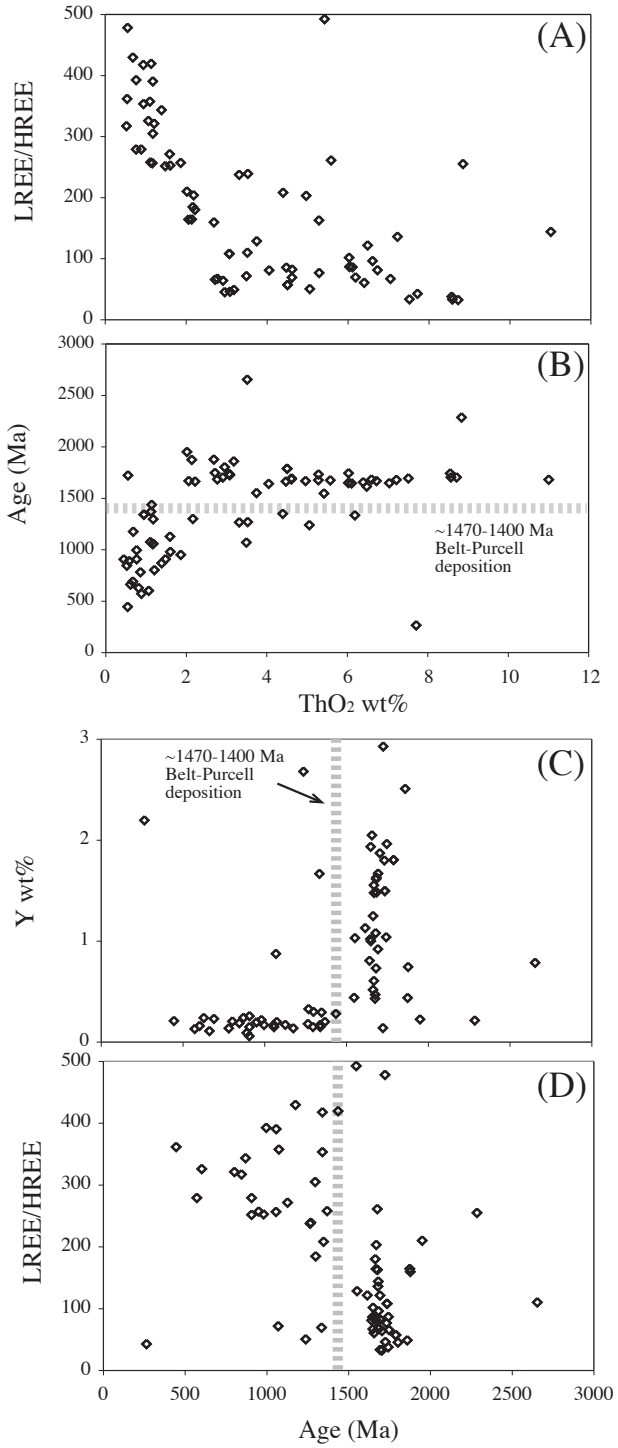

Fig. 4.9 Plots of monazite compositions and ages: variation of light rare earth elements/heavy rare earth elements ratios (LREE/HREE) (A) and age (B) versus ThO_2 content. (C) and (D), Y and LREE/HREE content versus age. There is a systematic trend in composition which indicates two monazite populations: detrital >~1400 Ma and diagenetic <~1400 Ma. The dashed bar in (B), (C), and (D) indicates time of deposition of the Belt-Purcell Supergroup (Anderson and Davies, 1995; Evans et al., 2000).

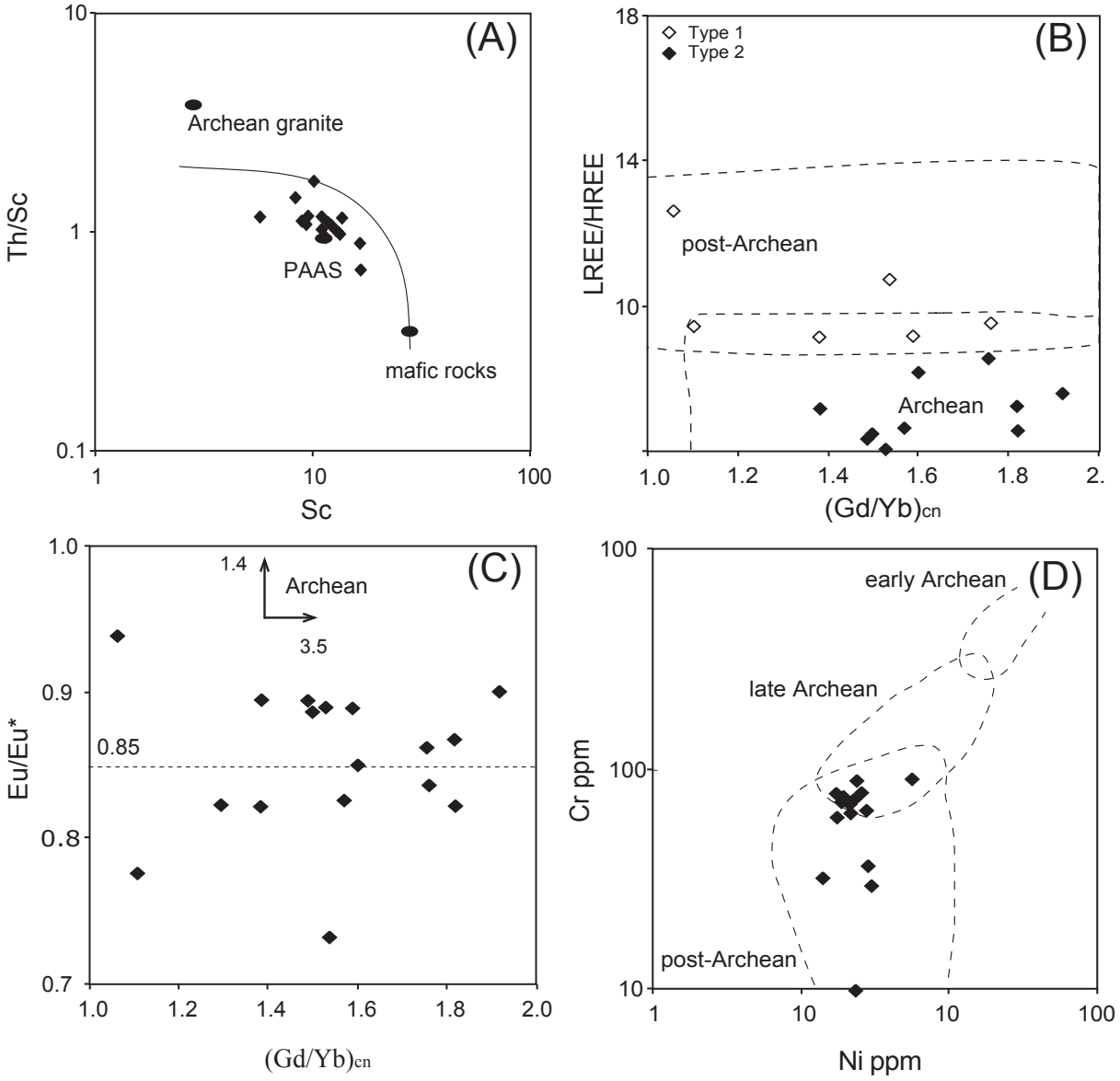

Fig. 4.10 (A) Plots of Th/Sc versus Sc; (B) LREE/HREE versus $(Gd/Yb)_{cn}$; (C) Eu/Eu versus $(Gd/Yb)_{cn}$; (D) Cr versus Ni. In (A) Archean granite and the mixing line from Archean granite to mafic rocks are from Bhat and Ghosh (2001). Post-Archean fields in (B) and (C) are from Taylor and McLennan (1985), and McLennan et al. (1990) respectively. The dashed field in (D) is from Wronkiewicz and Condie (1989, Fig. 4). Argillites from the Appekunny and Grinnell formations plot in post-Archean fields except for (B) which is interpreted as a probable effect of HREE mobility during diagenesis. See Discussion.*

For the Grinnell sandstones, three older peaks of this study are in agreement with the results of Ross and Villeneuve (2003), consistent with Paleoproterozoic and Archean terranes of Laurentia. However, the main peak at ~1700 Ma and the <~1400 Ma ages are not recorded in their zircon study. The distribution of monazite ages in sandstones of the Appekunny Formation is similar, with a younger peak at ~1700 Ma for sandstones.

For the Grinnell Formation, paleocurrents from the southeast and southwest (Fig. 4.2b; Link, 1997 and references therein), coupled with general thinning of sandstones to the west, and thickening of the argillites to the southwest for the Appekunny and Grinnell formations, collectively could be consistent with a main source terrane(s) in Laurentia. The southern Wyoming Province of the mid continent region (Frost and Winston, 1987) could be a possible source for the upper range of the monazite ages found in the Grinnell sandstones.

Detrital monazites having ages in the range ~1800-1600 Ma could be sourced in Laurentia. Included are the Penokean, Yavapai, Mazatzal Provinces and the Central Plains of the southwest USA and Mexico (~1800-1600 Ma; e.g., Hoffman, 1988; Clowes et al., 1998; Fig. 4.2), which fits the paleocurrent data. The Yavapai Province has been previously suggested as a potential source that could have fed at least in part the lower Belt and Missoula Group (Windley, 1995; Slack and Höy, 2000; Ross and Villeneuve, 2003). The absence of a ~1700 Ma peak in the zircon dataset for the Grinnell Formation of Ross and Villeneuve (2003) could be due to an artifact of sampling. According to Vermeesch (2004), datasets of less than 117 grains do not have a 95% probability of reflecting the complete age spectrum of a sediments provenance, with the caveat that smaller datasets are not necessarily invalid: “It is not the purpose of this paper to suggest that studies reporting fewer than 117 single-grains measurements would be scientifically wrong”. Alternatively, the absence of that peak could stem from igneous zircons but metamorphic monazites (see *section 4.6.3*). Similar difference between monazite and zircon ages is reported by Ross et al. (1991) in the Bonner Formation (upper Belt) where U-Pb analysis of eight and five detrital zircons and monazites cluster at 1860-1700 Ma and 1790-1640 Ma respectively, displaying a ~70 Ma range difference.

Archean monazite chemical ages are present sparsely in the Appekunny Formation argillite and the Grinnell Formation sandstone: peaks are at 3080 Ma and 2660 Ma respectively (Fig. 4.6). Proximal Archean terranes are present in the Hearne, Sask and Wyoming cratons, and the Black Hills of South Dakota in Western Laurentia. More distal are the Paleoproterozoic Huronian Supergroup sourced in the Superior Province, the former contiguous with the Paleoproterozoic Snowy Pass Supergroup, Wyoming (Frost and Winston, 1987; Bekker and Ericksson, 2003).

The Prichard Formation in the west displays turbiditites that contain ~1600-1500 Ma ages and is stratigraphically equivalent to the Appekunny Formation in the southwest (Ross and Villeneuve, 2003). Turbiditic deposits of the former could have interfingered distally with sediments in the east, and during storms be admixed, and brought by currents to the shorelines of the east part of the basin to be deposited as part of the shallow to subaeral facies of the playa lakes and mudflats, or tidal influenced deposits of the Appekunny Formation (McMechan, 1981; Winston, 1986, 1990).

The primary interpretation of the new argillite data is that they are characterized by the same detrital age spectrum as sandstones, and therefore likely had common provenance. That interpretation is in keeping with the geochemical results that sandstones are compositionally argillites diluted with quartz, but the trace element data is not a robust argument for a common provenance given that the REE budget of sandstones is dominated by admixed argillites. Similarly, Frost and Winston (1987) reported comparable Sm-Nd isotopic data for argillites and sandstones, but in light of the geochemical data of this study common Nd- isotope compositions of the two facies could be viewed as also reflecting the mixing characteristic.

In summary, with the data available, the Grinnell Formation in the lower Belt-Purcell sequence is interpreted as fed from Laurentian sources inasmuch as both Archean and Paleoproteroic terranes, or metamorphic belts, of requisite age are present. Paleocurrents from the southeast support this interpretation, whereas the Appekunny Formation could be the result of mixing of a major Laurentian source with subordinate contribution from a terrane that contained ages ~1600-1500 Ma or within the "magmatic gap" (usage from Ross and Villeneuve, 2003). These ages could be met by distal minor contribution of the Priest River Complex (Ross et al., 1992) or by an unknown western terrane (Ross and Villeneuve, 2003). They interpreted that western source to be Australia, given the presence of ~1600-1500 Ma terranes, and this is consistent with the recent reconstruction of the Mesoproterozoic supercontinent Columbia (Fig. 4.11; Zhao et al., 2004).

4.6.3 Thermochronology

There are two possible explanations for the younger monazite peaks at ~1700 Ma. One is that the dataset of this study records another Paleoproterozoic terrane ~200 to ~30 Ma younger than the Laurentian terrane recorded in other studies (Ross et al., 1991; Ross and Villeneuve, 2003). Paleoproterozoic terranes of this age in Laurentia are presented in Fig. 4.2.

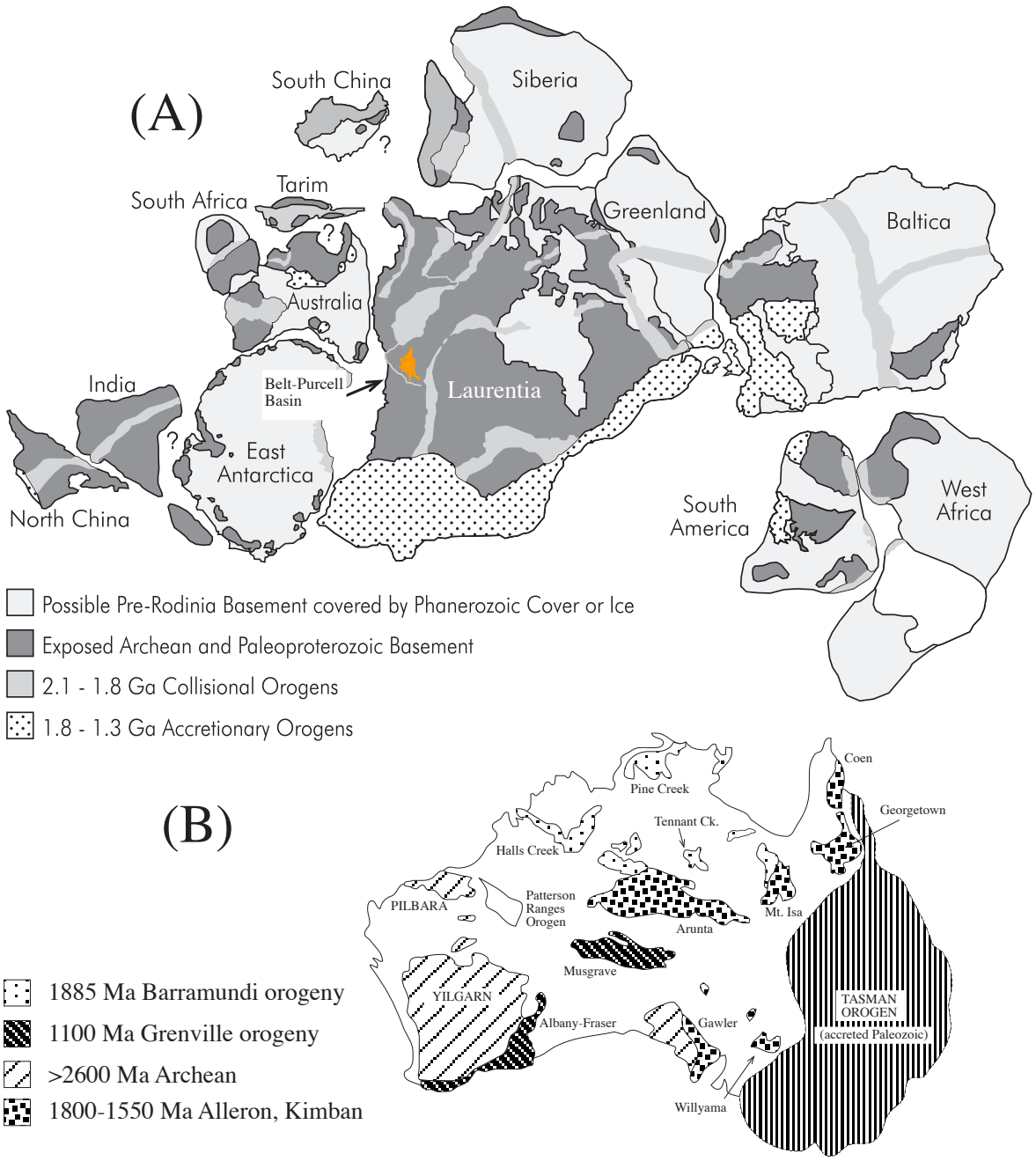

Fig. 4.11 (A) Reconstruction of the Mesoproterozoic supercontinent Columbia based on Zhao et al. (2004) showing collisional and accretionary orogens, and the relative position of the Belt-Purcell Basin; (B) basement terranes of Australia (Ross et al., 1992).

Given that all monazites >~1400 Ma are detrital, an alternative explanation may lie in a two stage process. The common older peaks for both zircons and monazites are magmatic ages. In con-

trast the younger ~1700 Ma ages reflect cooling of metamorphic monazites through the blocking temperature of 725° ± 25° C (Copeland et al., 1988), or as low as 530° ± 25° C according to Black et al. (1984), following monazite growth during regional metamorphism and unroofing. Zircon behaves as a closed system at temperatures up to 900° C (Cherniak et al., 2004). Studies of the thermochronology of deeply buried metamorphic rocks in orogenic belts constrains the duration from magmatism, through burial and peak metamorphism, to cooling through ~700° C from ~100 to 30 Ma (Eglington and Armstrong 2004; Hodges, 2004 and references therein). A metamorphic origin for the younger monazites could concurrently explain the lack of zircon ages of this range (~1700 Ma) in the dataset of Ross and Villeneuve (2003). The Wyoming province has metamorphic monazites of ~1800-1600 Ma explained as due to sequential episodes of compression of Paleoproterozoic crustal terranes as the accretion of the Yavapai Province (Fig. 4.2 of Laurentian terranes; Dahl et al., 2002, 2005).

4.6.4 One or more cratonic provenance catchments?

The provenance of the Belt-Purcell Supergroup is controversial. Western sources in Australia, Siberia, and/or catchments in Laurentia have variously been suggested, or combinations. Frost and Winston (1987) reported Nd-isotope data for argillites of the Belt-Purcell Supergroup. Crustal residence ages range from 2100 to 1600 Ma, averaging 2000 Ma. They concluded that argillites could have been derived from a variety of provinces in Laurentia, but on sedimentologic grounds preferred a western terrane; Siberia or Australia. Sandstones have similar Nd-isotopic compositions as argillites, exepting one sample from the LaHood Formation (lower Belt) with a 3800-2900 Ma crustal residence age that they ascribed to a proximal catchment in the Wyoming Province (Frost and Winston, 1987). As discussed above, the Sm-Nd isotope data fron Frost and Winston (1987), could be interpreted as inconclusive as to common or different sources.

Ross et al. (1992) and Ross and Villeneuve (2003) determined U-Pb detrital zircon ages from quartzarenites of the lower Belt-Purcell sequence collected from the western part of the basin, which gave concordant ages of 1600-1590 Ma, and a discordant age of 1780 Ma. The 1600-1590 Ma age range has no possible source known in North America (so called “magmatic gap” by Ross and Villeneuve, 2003; Fig. 4.2). Based on this and coupled with paleocurrent data, they concluded that this was the age of the source terrane from the west. Given detrital zircon ages of the Revett Formation at ~1600-1500 Ma, and ~1875-1750 Ma for the Grinnell Formation, Ross and Villeneuve (2003) concluded that the former sandstones were fed from the Laurentian craton whereas the latter formation was derived from a western source, likely Australia.

Sears et al. (2004) place Siberia to the west of Laurentia at the time of the Belt-Purcell sedimentation. They interpreted the sediment being channeled from a cratonic source through the Siberian Udzha Rift. Pesonen et al. (2003) based on paleomagnetic data placed Siberia to the west of Laurentia separated by part of the ocean reconstructing the Columbia supercontinent. The Siberian craton presents Proterozoic ages at ~2000 Ma and ~1850 Ma (Poller et al., 2004) that could match some of the Grinnell detrital zircons (cf. Ross and Villeneuve, 2003). A large-draining system could bypass the Siberian Craton and bring sediments from a further source with the main geochemical signature of the headwaters province as the modern Amazon River (McLennan et al., 2003 and references therein). However, only paleocurrent directions from the southwest for some of the sandstone units at the Grinnell formation would be consistent with a western provenance, whereas the southeast paleocurrents of other sandstones units are not consistent with a western provenance (Winston, 1990; Link, 1997 and references therein).

The most recent reconstruction of the supercontinent Columbia places Australia adjacent to western Laurentia in the Mesporoterozoic (Fig. 4.11a; Zhao et al., 2004). This reconstruction is in keeping with the conclusions of Ross and Villeneuve (2003) based on Proterozoic terrane ages in Australia. If the Appekunny and Grinnell formations, in whole or in part, have a catchment in Australia the following terranes are possible source areas: Arunta (~1700 Ma), Gawler (~2000-1600 Ma); Willyama (~1800-1600 Ma); Mt. Isa (~1800-1600 Ma); Georgetown (~1700-1600 Ma) and Musgrave (1900-1700 Ma) (Fig. 4.10b; cf. Ross et al., 1992 and references therein; Kyser et al., 2000).

There has also been the more specific controversy as to whether sandstones and argillites were derived from common or different provenances. Sandstones tend to thin to the west and argillites thicken to the southwest (Table 4.1; Winston, 1990; Link, 1997 and references therein). Rounded grains in the Grinnell and Appekunny formations are common. In sandstones, the presence of hummocky cross-stratification, current-ripples, normal grading, and sharp contacts are evidence for high-energy depositional environment events (e.g., Whipple et al., 1984, 1997). Pronounced sorting of heavy mineral titanite and zircon occurred which is reflected in deep troughs at Nb-Ta, Ti, and variable Zr-Hf (Fig. 4.5d).

Given that the REE, Th, Sc, and Co budget of the quartzite is dominated by the admixed clay fraction, these data are inconclusive as to a common or separate source. However, the most straightforward explanation of the common monazite age populations of the Appekunny and Grinnell sandstones and the Appekunny argillite is a common provenance, and the presence of similar

older and younger peaks in the Appekunny sandstones and argillites is consistent with the same source too. However, there is a subordinate age population between ~1600-1500 Ma that is consistent with the ages of the Prichard Formation further west in the Belt-Purcell Basin (Fig. 4.3b; Ross and Villeneuve, 2003). These ages could be interpreted as the result of a subordinate input of a "western source".

From these considerations, sandstones and argillites of the Appekunny and Grinnell formations are interpreted as having a common major provenance in Laurentia, likely to the southeast; the two facies had geographically separate high- and low-energy depositional environments respectively, and became interbedded during storms, with a minor western contribution for the Appekunny Formation.

4.6.5 Diagenetic effects

Monazite chemical ages in argillite and sandstone display an age range <~1400 Ma, up to ~1000 Ma post-Belt-Purcell deposition (Fig. 4.6). Grains that present theses ages are euhedral, and are compositionally distinct, supporting their interpretation as secondary (see Figs. 4.7 and 4.9). Various studies show that REE can be redistributed locally in sedimentary environments, and that growth of diagenetic monazite may play a part in this process (e.g., Milodowski and Zalasiewicz, 1991; McDaniel et al., 1994; Lev et al., 1999; Evans et al., 2002). Several studies describe secondary monazite formation in shales (e.g., Milodowski and Zalasiewicz, 1991; Evans and Zalasiewicz, 1996; Rasmussen et al., 2001). Studies by Burnotte et al. (1989), and Schandl and Gorton (2004) interpreted low ThO_2 contents of ~<0.1 wt.% could be used as a criterion for identifying hydrothermal monazite, whereas igneous monazites typically have 2-12 wt.% ThO_2. Low ThO_2 content of hydrothermal monazites is attributed to a slow growth and low mobility of Th in the environment of crystallization (Fig 4.9; Milodowski and Zalasiewicz, 1991; Schandl and Gorton, 2004).

Monazites of the Appekunny and Grinnell formations that are <~1400 Ma have high values of LREE/HREE, <2 wt.% ThO_2, and lower Y contents different than their counterparts at >~1400 Ma (Fig. 4.9). Based on the combination of chemical ages, compositional features, and textural characteristics such as the euhedral of individual grains, and chemical ages, the former are interpreted as diagenetic, whereas the latter are detrital.

Normalized enrichment of HREE over LREE relative to PA-UCC in some samples of sandstones and argillites could be a provenance signature, or result from weathering, sorting or diagen-

esis. Boninites and low-Ti tholeiites are the only igneous, or meta-igneous, rock types known to have primary normalized HREE>LREE. However, these igneous rocks are rare, and possess high contents of Cr, Co, and Ni, unlike Belt-Purcell sediments (e.g., Brown and Jenner, 1989). The compositional and Nd-isotopic homogeneity also rule out such singular rock types (Frost and Winston, 1987; Table 4.7).

*Table 4.7 Crustal residence ages (T_{cr}) and ϵ_{Nd}** of fine- and coarse-grained facies of the Belt-Purcell Supergroup rocks from Frost and Winston (1987).*

	Fine-grained facies	Coarse-grained facies*	Appekunny Formation	Grinnell Formation
T_{cr}	2100-1600 Ma	2240-1980 Ma	1950 Ma	2240-2060 Ma
ϵ_{Nd}	-8.1 - (-20.0)	-6.6 – (-20.2)	-15.6	-6.61 – (-15.8)

(*) LaHood Formation results are not included.

(**) €Nd = {[(143Nd/144Nd) sample/(143Nd/144Nd) bulk earth] – 1} 104

Studies of soil-protolith profiles have identified fractionation of REE in regolith relative to the parent rock (e.g., Nesbitt, 1979). Overall, saprolite is generally enriched in total REE (Duddy, 1980). In detail, there is enrichment of LREE but depletion in HREE due to preferential removal of HREE by complexation reactions (e.g., Braun et al., 1993). The top horizon of the saprolite develops a positive Ce anomaly due to crystallization of cerianite (Braun et al., 1990; Marsh, 1991). Such effects are not present in the argillites or sandstones of this study, nor in the North American Shale Composite (NASC), or post-Archean Australian Shale (PAAS) composite that "integrate" compositional signatures from varied protoliths and weathering regimes (e.g., Taylor and McLennan, 1985).

Sedimentary sorting with accumulation of minerals enriched in HREE could generate the observed patterns: (1) PA-UCC-like REE pattern and (2) HREE enriched relative to LREE pattern Zircon is the most likely candidate. However, sandstones and argillites with type 1 REE patterns have variably negative normalized troughs at Zr-Hf relative to MREE, and there is no covariation of the magnitude of the anomaly with $(Gd/Yb)_{cn}$. The low abundance of zircon in argillites and sandstones with more abundant monazite and HREE enriched patterns suggests that sedimentary sorting processes are an unlikely cause of the observed HREE fractionations.

Normalized enrichments of HREE over LREE have been documented in alkaline brines discharging into lakes of the East African Rift where Magadi-type cherts, which have similar REE patterns, are precipitating (Kerrich et al., 2002). High contents of Y have been documented in diagenetic U deposits of the Paleoproterzoic Athabasca sliciclastic sequence Saskatchewan (Fayek and Kyser, 1997). Accordingly, the <~1400 Ma monazite ages, restricted to euhedral lower-ThO_2 monazites, and the HREE-enriched patterns relative to LREE when normalized to PA-UCC, is interpreted as due to protracted flow of basinal brines, preferentially through permeable units, of the Appekunny and Grinnell formations. Protracted, episodic, flow of diagenetic brines has been recorded in several Proterozoic siliciclastic sequences (Kyser et al., 2000). These flows could have been driven by changes in hydrological gradients due to regional tectonic events. Therefore, the <~1400 Ma monazites found in this study could be viewed as possible distal effects of regional tectonism: for example the assemblage of Rodinia from ~1300 Ma to ~900 Ma (Condie, 2002); Rodinia's break up, which produced the rifting of Australia-Laurentia, Laurentia-South China and Siberia-North China during ~900-700 Ma; and their local deformation and intrusive rocks that are part of the evolution of the Belt-Purcell Supergroup (cf. Raemakers and Catuneanu, 2004; Raemakers et al., 2005).

4.7 Conclusions

(1) Coarse-grained sandstones have the same geochemical signature as argillite for both the Appekunny and Grinnell Formations of the lower Belt-Purcell Supergroup sequence. Sandstone developed in a separate high-energy environment, generating efficient transport winnowing of fine from coarse-grained quartz and feldspar. Argillite and sandstone become interbedded during storms. Geochemical data are consistent with a dominantly Paleoproterozoic source area for the lower Belt sediments: specifically, compliance of rare earth element and multi-element patterns to PA-UCC, Cr–Ni, and Th/Sc-Sc systematics.

(2) Argillites of the Appekunny Formation display monazite chemical Th-U total Pb age data that mimics the age spectrum of their sandstone counterparts, presenting a main age peak at ~1700 Ma. This is commensurate with a common provenance for both facies.

(3) The Appekunny argillites and sandstones present the same monazite chemical age spectra as well as the same geochemical signature. This is because the REE budget of sandstones is dominated by admixed argillites. Therefore, the trace element signature of sandstones could be an inconclusive approach testing for provenance.

(4) Detrital monazite chemical Th-U total Pb ages from the Appekunny and Grinnell sandstones, and argillites supports a main Paleoproterozoic provenance source. This could represent a Laurentian source at ~1700 Ma or at ~1875-1750 Ma source that cooled through the blocking temperature of monazite at ~1700 Ma. The Penokean orogen (1900-1800~Ma) to the east, Yavapai (~1800-1700 Ma), and the Mazatzal-Central Plains orogens (~1700-1600 Ma) to the south are potential sources. Minor peaks at ~1550 Ma in the argillites and sandstones of the Appekunny Formation implies a subordinate non-Laurentian source. Rare >2500 Ma monazite ages in argillite and sandstone represent minor contributions from Archean terrane(s) from the southeast and southwest of the Belt-Purcell Basin possibly in Laurentia.

(5) Diagenetic alteration of the Appekunny and Grinnell formations is displayed as HREE enrichment relative to LREE normalized to PA-UCC. Two distinct groups of monazites are present; Those with chemical ages of >~1400 Ma possess higher Th and Y, but lower LREE/HREE ratios than those having chemical ages <~1400 Ma to ~300 Ma. The former are interpreted as detrital, whereas the latter may could be interpreted as the result of protracted flow of oxidized basinal brines intermittently over ~1000 Ma in response to regional or local tectonic events that changed hydraulic gradients

4.8 Acknowledgements

The staff of Waterton-Glacier International Peace Parks are thanked for enduring support, most especially L. F. Marnell and C. Smith; as well as Q. Xie and J. Fan who assisted with ICP-MS analyses. Thanks are also given to: P. Dzierzanowski, L. Jezak, and Tom Bonli for their assistance in EMPA analyses; to L. M. Shychosky, A. Vangool, M. England, R. Ahrabian, A. Peterhänsel and L. Skublicki for their dedicated help during fieldwork; to J. Srodon, T. Prokopiuk, M. R. Stauffer, L. Buatois, R. Renaut, K. Ansdell, and M. Paszkowski for their comments on the earlier versions of this Chapter. The journal reviewers D. K. McDaniel and K. Suzuki, whose incisive critique of an earlier version greatly improved the current Chapter are acknowledged with gratitude. Natural Sciences & Environment Research Council of Canada (NSERC), discovery grants to R. Kerrich and B. R. Pratt, and a University of Saskatchewan graduate scholarship to I. González-Álvarez, funded this study. R. K. acknowledges NSERC MFA support of the ICP-MS facility, and the George McLeod endowment to the Department of Geological Sciences, University of Saskatchewan.

4.9 Appendices

Appendix 4.1 Major and trace element concentration of the Belt-Purcell Supergroup at Waterton-Glacier International Peace Park.

Formation	Grinnell	Grinnell	Grinnell	Grinnell	Grinnell	Grinnell	Grinnell	Grinnell	Grinnell	Grinnell	Grinnell	App.	App.	App.
Sample	26(14)Gl	26(10)G1	26(9)G1	26(7)G1	26(6)G1	26(5)G1	26(4)G1	26(3)G1	USO 27	USO 24	USO 23	26 Gl Uso	USO 12	USO 8
SiO_2	70.82	74.08	99.64	94.62	67.54	97.24	58.63	96.82	66.70	65.00	91.20	96.40	68.50	92.00
TiO_2	0.49	0.46	0.04	0.07	0.51	0.04	0.62	0.03	0.55	0.61	0.06	0.09	0.52	0.04
Al_2O_3	12.24	12.36	0.21	2.45	14.02	1.22	19.19	1.17	15.70	13.70	4.65	1.12	13.60	2.14
Fe_2O_3	2.57	3.02	0.20	0.70	5.18	0.24	6.12	0.21	4.91	7.23	0.16	0.34	4.73	1.34
MnO	0.02	0.01	0.00	0.01	0.03	0.00	0.04	0.00	0.52	0.08	0.03	0.02	0.03	0.05
MgO	4.48	1.43	0.11	0.40	2.84	0.20	3.44	0.32	2.74	4.02	0.13	0.43	2.74	1.46
CaO	0.61	0.09	0.00	0.07	0.39	0.03	0.15	0.15	0.33	0.73	0.12	0.27	1.15	0.80
K_2O	4.58	6.73	0.16	1.20	6.55	0.77	7.89	0.57	5.21	3.80	1.36	0.22	4.53	0.34
Na_2O	0.79	0.14	0.00	0.00	0.07	0.01	0.28	0.03	0.74	1.13	1.73	0.29	0.65	0.25
P_2O_5	0.10	0.06	0.00	0.04	0.14	0.00	0.10	0.02	0.08	0.19	0.02	0.02	0.12	0.05
LOI	3.45	1.65	0.15	0.55	2.90	0.25	3.70	0.20	3.15	3.55	0.30	0.85	3.50	1.65
Sum	100.1	100.0	100.5	100.1	100.1	100.0	100.1	99.5	100.6	100.0	99.7	100.0	100.0	100.1
Li (ppm)	100	40	9	25	74	17	81	18	50	77	5	13	50	24
Rb	124	158	3	31	166	14	243	17	200	140	24	7	198	13
Sr	25	17	2	6	20	5	13	114	19	48	88	10	53	34
Cs	6	10	0	2	11	1	16	1	12	9	1	1	10	0
Ba	416	358	37	85	380	105	393	6525	492	465	4661	243	1273	691
Y	19.7	20.1	4.4	9.5	26.5	6.7	32.9	18.8	30.1	27.7	6.5	4.5	26.8	7.1
Zr	141	120	10	37	161	27	188	17	173	202	39	14	182	43
Hf	4.3	4.7	0.2	1.1	5.6	0.7	6.2	0.7	6.2	6.6	1.0	0.4	5.5	1.0
Nb	12.38	16.12	0.68	1.58	13.47	0.94	16.89	0.58	11.63	12.69	0.87	0.47	11.85	0.74
Ta	0.84	1.28	0.03	0.10	0.92	0.07	1.06	0.04	1.02	1.05	0.06	0.04	0.89	0.06
Th	10.17	15.68	1.56	2.05	11.79	1.63	13.97	1.43	14.35	11.85	1.11	0.83	11.83	1.71
U	3.55	3.64	0.38	0.67	3.22	0.41	4.67	0.39	3.90	4.58	0.48	0.45	2.90	0.63
La	37.77	31.30	3.47	7.67	38.98	5.84	46.65	11.92	43.39	34.83	5.73	3.06	43.96	5.54
Ce	73.91	63.88	8.32	17.12	82.16	11.60	100.22	20.89	90.56	72.41	6.70	5.61	85.54	13.61
Pr	8.25	7.56	1.01	1.93	9.17	1.35	11.37	2.64	10.36	8.51	0.98	0.84	9.25	1.63
Nd	32.65	27.68	3.95	7.94	35.72	5.13	41.56	11.13	38.58	33.17	3.54	3.42	34.59	5.56
Sm	5.79	4.68	0.82	1.57	5.84	1.18	7.27	3.00	7.36	7.31	0.76	0.87	7.33	1.27
Eu	0.81	0.69	0.14	0.31	0.98	0.22	1.29	0.62	1.32	1.33	0.21	0.18	1.28	0.22
Gd	4.48	3.58	0.78	1.75	5.16	1.34	6.81	3.75	6.94	6.81	1.07	0.99	5.99	1.32
Tb	0.61	0.58	0.14	0.30	0.77	0.21	0.97	0.59	0.95	0.92	0.17	0.14	0.85	0.23
Dy	3.52	3.56	0.77	1.74	4.88	1.29	6.31	3.27	5.93	5.51	1.10	0.84	4.91	1.19
Ho	0.76	0.75	0.16	0.35	1.03	0.24	1.29	0.60	1.20	1.09	0.21	0.16	1.00	0.23
Er	2.28	2.40	0.40	0.98	2.96	0.65	3.84	1.48	3.62	3.24	0.54	0.43	2.91	0.68
Tm	0.36	0.38	0.06	0.13	0.46	0.09	0.60	0.20	0.54	0.47	0.08	0.06	0.47	0.10
Yb	2.42	2.69	0.33	0.85	3.10	0.59	4.16	1.15	3.60	3.11	0.51	0.37	3.13	0.62
Lu	0.35	0.40	0.06	0.13	0.47	0.07	0.61	0.15	0.56	0.49	0.07	0.05	0.48	0.09
Sc	8.7	9.3	0.2	1.8	11.7	0.7	17.5	0.7	12.5	11.1	0.7	1.8	12.0	1.3
V	49.1	41.9	1.5	9.1	55.0	3.5	72.5	3.4	72.7	69.6	3.0	5.7	61.4	10.1
Mo	0.3	0.3	0.1	0.1	0.3	0.1	0.6	0.6	0.5	0.4	0.1	6.5	0.2	0.1
Cr	6.5	6.2	0.7	1.4	10.1	0.8	11.7	0.5	75.9	30.0	10.8	12.9	89.6	14.2
Co	7.1	6.0	0.6	1.8	11.5	0.7	12.3	1.4	6.9	11.0	5.5	1.4	11.6	6.2
Ni	13.7	11.7	1.3	4.0	21.5	1.9	21.2	2.3	17.8	27.4	2.8	45.3	21.9	6.3
Cu	3.1	2.1	3.5	12.9	2.3	1.6	14.0	3.4	1.8	3.8	2.6	33.2	2.7	1.8
Zn	36.8	34.7	4.4	11.6	67.3	6.0	70.4	13.2	50.1	93.4	11.9	23.4	58.3	24.0
Sn	3.7	6.3	3.7	3.9	6.5	1.2	7.5	1.2	2.4	2.5	1.5	2.0	3.5	2.8
W	1.6	1.8	0.1	0.1	1.9	0.1	2.0	0.0	2.8	1.7	11.2	0.2	4.9	11.6
Pb	7.7	11.3	2.6	2.9	17.1	2.6	19.6	4.5	15.2	14.2	2.9	4.8	3.4	1.3
Cd	0.0	0.0	0.0	0.0	0.0	0.0	0.1	0.0	0.0	0.1	0.0	0.0	0.0	0.0
Tl	0.6	0.7	0.0	0.1	0.8	0.1	1.1	0.1	1.0	0.7	0.1	0.0	0.8	0.0
Ga	14.7	13.3	0.3	3.0	17.8	1.0	26.4	0.0	12.1	16.5	5.6	0.2	12.7	0.0
As	2.5	6.7	1.2	2.8	7.7	3.0	10.2	4.6	3.5	4.2	0.9	6.2	1.5	0.7
Ag	0.0	0.0	0.0	0.0	0.0	0.0	0.0	0.0	0.4	0.4	0.1	0.1	0.4	0.1
Sb	1.0	1.4	0.1	0.3	2.2	0.2	2.2	0.1	0.7	1.0	0.2	1.6	1.0	0.1
$(La/Sm)_{cn}$	4.08	4.18	2.65	3.06	4.18	3.10	4.01	2.49	3.69	2.98	4.72	2.21	3.75	2.73
$(Gd/Yb)_{cn}$	1.53	1.10	1.96	1.70	1.38	1.88	1.35	2.70	1.60	1.81	1.74	2.23	1.58	1.76
$(La/Yb)_{cn}$	11	8	7	6	9	7	8	7	8	8	8	6	10	6
∑REE	182	157	21	45	200	31	0.99	64	225	187	23	18	210	34
Ce/Ce*	0.95	0.95	1.01	1.01	0.99	0.94	0.84	0.85	0.97	0.96	0.64	0.80	0.97	1.03
Eu/Eu*	0.73	0.77	0.80	0.86	0.82	0.80	244	0.85	0.85	0.87	1.07	0.91	0.89	0.78
Zr/Hf	33	26	40	35	29	38	31	24	28	31	40	36	33	44
Th/Sc	1.17	1.69	7.09	1.13	1.01	2.30	0.80	2.01	1.15	1.06	1.63	0.47	0.98	1.35
Th/U	2.86	4.31	4.11	3.06	3.66	3.98	2.99	3.67	3.68	2.59	2.31	1.85	4.08	2.71
Y/Ho	26	27	28	27	26	28	26	31	25	25	31	29	27	31
V/Sc	5.64	4.52	6.82	5.04	4.70	4.97	4.15	4.80	5.81	6.26	4.34	3.21	5.11	7.96
Facies	Arg.	Arg.	Sd.	Sd.	Arg.	Sd.	Arg.	Sd.	Arg.	Arg.	Sd.	Sd.	Arg.	Sd.
Map-label	G45	G43	G42	G41	G40	G39	G38	G37	G35	G33	G32	G31	G29	G28

Appendix 4.1 (continued).

Formation Sample	App. 25 Gl Uso	App. USO 9	App. USO 7	App. USO 6	App. USO 5	App. USO 4	App. USO 3	App. USO 2	App. USO 1	App. USO 19	App. USO 20	App. USO 22	App. USO 18	App. USO 17
SiO_2	69.50	90.50	97.50	66.70	68.10	69.50	68.90	73.50	71.60	96.20	75.30	85.80	90.10	74.60
TiO_2	0.49	0.04	0.02	0.62	0.59	0.47	0.45	0.44	0.39	0.02	0.29	0.06	0.03	0.49
Al_2O_3	12.60	3.29	0.92	16.30	14.80	13.00	12.60	11.60	11.50	1.31	9.57	6.88	5.34	11.00
Fe_2O_3	3.54	1.38	0.37	4.37	4.45	3.72	3.62	2.55	3.41	0.27	4.14	0.72	0.42	4.07
MnO	0.07	0.06	0.18	0.02	0.06	0.06	0.11	0.04	0.12	0.02	0.04	0.02	0.01	0.02
MgO	3.70	1.53	0.09	2.77	2.67	3.94	3.87	2.90	2.17	0.41	4.23	1.27	0.92	2.78
CaO	1.17	0.55	0.18	0.26	0.38	0.92	1.47	0.90	2.68	0.40	0.72	0.53	0.13	0.31
K_2O	3.62	0.69	0.20	4.92	4.25	3.56	3.51	3.43	2.14	0.63	1.26	1.48	1.65	3.03
Na_2O	1.44	0.53	0.26	1.25	1.65	1.47	1.55	1.66	3.07	0.00	1.91	2.19	1.06	1.40
P_2O_5	0.12	0.08	0.06	0.09	0.08	0.10	0.09	0.09	0.10	0.03	0.08	0.03	0.05	0.13
LOI	3.95	1.60	0.30	2.75	2.60	3.50	3.95	2.90	3.00	0.85	2.70	1.25	0.65	2.25
Sum	100.2	100.2	100.0	100.0	99.6	100.2	100.1	100.0	100.1	100.1	100.2	100.2	100.3	100.0
Li (ppm)	44	27	6	54	48	56	56	45	33	9	93	21	19	44
Rb	118	23	6	191	162	133	126	120	73	14	39	38	38	106
Sr	44	10	7	27	32	37	59	53	57	21	32	28	10	40
Cs	7	1	0	10	7	7	7	6	3	0	1	1	1	4
Ba	721	183	170	595	562	544	964	1142	293	754	205	331	146	838
Y	33.2	9.0	4.1	36.7	28.7	32.6	31.5	31.6	26.5	2.5	17.6	2.6	4.9	23.4
Zr	191	37	22	203	236	255	220	289	248	12	163	43	23	282
Hf	6.4	0.9	0.7	6.6	7.5	7.7	6.5	8.5	7.3	0.3	4.4	1.1	0.5	8.2
Nb	9.02	0.70	0.25	13.58	11.78	10.95	9.29	10.79	9.81	0.30	6.66	0.85	0.31	11.34
Ta	0.61	0.07	0.03	1.05	0.91	0.80	0.66	0.74	0.71	0.03	0.49	0.07	0.04	0.88
Th	10.13	1.79	1.25	13.31	11.83	9.84	10.23	9.15	9.04	1.07	6.04	1.40	1.26	10.81
U	2.98	0.56	0.42	3.37	3.35	2.74	3.16	2.68	2.39	0.35	1.63	0.35	0.51	2.17
La	28.46	14.08	3.60	46.13	33.78	32.04	29.20	32.45	28.41	4.63	18.67	6.83	8.13	38.84
Ce	56.10	30.76	8.37	100.39	70.32	68.07	61.74	65.36	60.20	5.34	38.48	10.31	13.53	80.41
Pr	7.47	3.74	0.98	11.45	8.11	8.15	7.47	8.14	7.38	0.83	4.82	1.28	2.00	9.23
Nd	30.15	14.40	3.47	44.97	31.83	32.51	30.48	31.69	29.19	3.10	18.96	4.58	7.07	34.50
Sm	6.58	2.87	0.82	9.52	6.89	7.30	6.97	7.03	7.05	0.69	4.12	0.97	1.36	6.64
Eu	1.16	0.51	0.16	1.81	1.25	1.37	1.31	1.30	1.21	0.13	0.71	0.24	0.34	1.11
Gd	6.40	2.43	0.83	8.99	6.00	6.81	6.59	6.48	6.51	0.65	3.80	0.80	1.18	5.62
Tb	0.94	0.30	0.14	1.19	0.84	0.93	0.92	0.91	0.87	0.10	0.55	0.10	0.16	0.76
Dy	6.27	1.61	0.82	7.34	5.18	5.86	5.69	5.65	5.02	0.49	3.26	0.49	0.82	4.47
Ho	1.29	0.30	0.15	1.41	1.09	1.20	1.14	1.17	1.01	0.09	0.67	0.10	0.15	0.88
Er	3.98	0.78	0.41	4.04	3.31	3.66	3.50	3.45	2.91	0.28	1.95	0.30	0.43	2.63
Tm	0.60	0.11	0.06	0.60	0.52	0.56	0.53	0.57	0.45	0.04	0.29	0.04	0.06	0.40
Yb	4.11	0.70	0.37	3.89	3.60	3.80	3.58	3.59	2.97	0.30	2.01	0.32	0.42	2.65
Lu	0.60	0.11	0.06	0.60	0.57	0.61	0.57	0.58	0.47	0.04	0.32	0.05	0.06	0.42
Sc	15.3	1.4	0.6	15.2	12.3	10.5	10.1	8.5	8.1	0.8	5.2	1.7	0.7	7.6
V	32.4	13.2	2.9	72.4	56.0	41.5	36.6	36.3	31.7	2.1	28.6	9.4	3.8	36.5
Mo	1.6	0.2	0.2	0.3	0.3	1.3	0.3	0.5	0.4	0.2	0.3	0.2	0.2	0.4
Cr	36.9	19.2	14.0	91.1	63.8	61.2	70.2	78.4	65.7	4.7	32.5	7.5	3.6	73.5
Co	5.3	5.4	3.2	11.4	7.3	8.9	10.0	11.3	13.6	3.3	4.4	3.5	3.2	11.7
Ni	26.0	7.3	7.7	51.3	19.9	16.1	19.6	15.9	25.4	3.8	12.9	22.7	2.1	21.0
Cu	8.8	1.3	6.8	29.2	7.2	38.9	10.7	5.8	20.3	1.8	7.1	4.1	6.1	2.7
Zn	58.6	28.0	7.2	58.5	50.4	65.2	72.8	91.0	84.9	6.2	55.1	43.6	4.2	33.9
Sn	3.1	0.8	2.9	3.0	2.8	2.5	3.1	3.4	2.2	3.8	2.4	3.2	0.5	2.2
W	1.0	0.3	0.2	4.3	1.0	3.6	1.4	5.1	4.2	8.3	0.7	0.2	0.3	7.0
Pb	3.0	1.3	2.3	3.6	4.7	15.3	4.0	8.5	12.7	1.0	10.8	3.2	1.9	4.8
Cd	0.0	0.0	0.0	0.1	0.0	0.0	0.0	0.1	0.0	0.0	0.0	0.0	0.0	0.1
Tl	0.5	0.1	0.0	0.9	0.7	0.5	0.5	0.5	0.3	0.1	0.2	0.1	0.2	0.4
Ga	17.1	4.3	1.3	19.4	11.0	13.8	12.7	19.8	13.7	1.7	10.4	0.0	2.6	11.0
As	1.0	0.6	1.5	2.1	3.9	0.9	1.4	1.9	4.8	1.7	1.5	1.1	0.6	2.8
Ag		0.1	0.1	0.6	0.6	0.6	0.7	0.5	0.5	0.0	0.3	0.1	0.0	0.4
Sb	0.6	0.2	0.4	1.0	0.7	0.7	0.7	0.6	0.6	0.2	0.5	0.4	0.1	1.4
$(La/Sm)_{cn}$	2.71	3.07	2.75	3.03	3.07	2.75	2.62	2.89	2.52	4.20	2.83	4.40	3.74	3.66
$(Gd/Yb)_{cn}$	1.29	2.87	1.86	1.91	1.38	1.48	1.52	1.49	1.81	1.79	1.56	2.07	2.32	1.75
$(La/Yb)_{cn}$	5	14	7	8	7	6	6	6	7	11	6	15	13	10
∑REE	161	76	21	253	181	180	167	176	161	18	103	28	38	197
Ce/Ce*	0.88	0.97	1.02	1.00	0.97	0.96	0.95	0.92	0.95	0.62	0.93	0.80	0.77	0.97
Eu/Eu*	0.82	0.89	0.89	0.90	0.89	0.89	0.89	0.88	0.82	0.89	0.82	1.25	1.23	0.83
Zr/Hf	30	40	34	31	32	33	34	34	34	36	37	38	43	34
Th/Sc	0.66	1.29	1.95	0.88	0.97	0.93	1.02	1.07	1.11	1.37	1.16	0.81	1.88	1.42
Th/U	3.40	3.20	2.98	3.95	3.53	3.59	3.24	3.41	3.78	3.06	3.71	4.00	2.47	4.98
Y/Ho	26	30	27	26	26	27	28	27	26	28	26	26	32	27
V/Sc	2.12	9.47	4.59	4.78	4.57	3.94	3.64	4.25	3.89	2.69	5.50	5.42	5.64	4.80
F acies	Arg.	Sd.	Sd.	Arg.	Arg.	Arg.	Arg.	Arg.	Arg.	Sd.	Arg.	Sd.	Sd.	Arg.
Map-label	G27	G26	G24	G23	G22	G21	G20	G19	G18	G17	G16	G14	G13	G12

Appendix 4.1 (continued).

Formation	App.	App.	App.	App.	App.
Sample	USO 16	USO 21	USO 15	USO 14	USO 13
SiO_2	86.00	98.40	71.60	86.70	69.60
TiO_2	0.07	0.02	0.57	0.07	0.49
Al_2O_3	7.03	0.55	13.50	5.75	13.40
Fe_2O_3	0.87	0.25	2.02	0.64	4.75
MnO	0.02	0.02	0.01	0.02	0.07
MgO	1.50	0.28	3.16	1.23	2.59
CaO	0.11	0.11	0.30	0.80	0.59
K_2O	2.54	0.17	5.61	2.32	4.63
Na_2O	0.90	0.00	0.47	1.18	0.57
P_2O_5	0.02	0.03	0.10	0.03	0.11
LOI	1.20	0.30	2.85	1.35	3.10
Sum	100.2	100.1	100.1	100.0	99.9
Li (ppm)	23	11	102	29	48
Rb	62	4	163	44	193
Sr	19	3	28	28	47
Cs	1	0	12	1	9
Ba	365	37	1551	607	1167
Y	5.7	4.2	12.7	3.9	30.4
Zr	52	15	208	37	156
Hf	1.0	0.4	6.1	0.8	5.1
Nb	1.04	0.17	11.14	1.57	11.90
Ta	0.09	0.01	0.87	0.12	1.00
Th	1.50	0.78	11.70	1.43	11.76
U	0.54	0.31	2.51	0.44	2.80
La	5.84	2.40	32.69	5.31	45.10
Ce	8.69	3.80	55.55	8.84	90.93
Pr	1.43	0.64	5.78	1.14	10.60
Nd	4.87	2.59	19.79	4.23	41.58
Sm	0.91	0.69	3.03	0.92	7.97
Eu	0.30	0.16	0.55	0.19	1.42
Gd	1.02	0.87	2.40	0.79	7.21
Tb	0.18	0.15	0.32	0.10	0.98
Dy	0.97	0.72	2.07	0.63	5.71
Ho	0.19	0.15	0.46	0.13	1.12
Er	0.54	0.38	1.56	0.38	3.47
Tm	0.08	0.05	0.27	0.05	0.55
Yb	0.54	0.30	1.88	0.38	3.41
Lu	0.09	0.05	0.31	0.06	0.53
Sc	1.4	0.4	10.1	1.7	10.7
V	8.3	1.6	49.4	6.6	61.4
Mo	0.1	0.2	0.5	0.1	0.4
Cr	12.6	4.2	71.6	8.3	79.1
Co	3.3	5.6	7.1	4.3	13.8
Ni	2.8	1.1	17.2	12.6	23.5
Cu	9.5	3.1	13.0	12.4	2.4
Zn	14.7	5.2	23.2	6.2	48.3
Sn	1.1	0.4	3.0	0.4	2.9
W	0.4	15.6	33.2	8.6	1.5
Pb	4.3	1.2	16.8	9.0	3.2
Cd	0.0	0.0	0.0	0.0	0.0
Tl	0.2	0.0	0.6	0.2	0.8
Ga	7.6	0.6	7.9	0.0	11.3
As	0.6	0.8	3.6	5.7	1.5
Ag	0.1	0.0	0.5	0.1	0.4
Sb	0.3	0.1	1.5	0.2	1.0
$(La/Sm)_{cn}$	4.01	2.18	6.75	3.61	3.54
$(Gd/Yb)_{cn}$	1.56	2.40	1.06	1.72	1.75
$(La/Yb)_{cn}$	8	6	12	10	9
∑REE	27	14	132	24	231
Ce/Ce*	0.69	0.70	0.92	0.82	0.95
Eu/Eu*	1.43	0.95	0.94	1.02	0.86
Zr/Hf	52	43	34	49	30
Th/Sc	1.07	2.11	1.16	0.86	1.10
Th/U	2.78	2.52	4.66	3.25	4.20
Y/Ho	30	28	28	30	27
V/Sc	5.95	4.35	4.90	3.93	5.72
Facies	Sd.	Sd.	Arg.	Sd.	Arg.
Map-label	G11	G10	G9	G8	G7

Sample order is from the upper sequence (left) to the lower sequence (right); (App.) Appekunny; (Gr.) Grinnell; (Arg.) argillite; and (Sd.) sandstone.

Appendix 4.2a Monazite analyses, with selected REE contents, and chemical ages >~1400 Ma.

Label Fig. 4.3b	G7	G7	G7	G7	G18	G18	G18	G18	G18	G18	G18	G18	G18	G18
sample	USO13	USO13	USO13	USO13	USO1	USO1	USO1	USO1	USO1	USO1	USO1	USO1	USO1	USO1
spot number	#1	#4	#5	#6	#13	#14	#15	#16	#17	#18	#19	#24	#25	#26
La_2O_3 (wt%)	13.64	14.24	13.91	14.58	13.93	13.36	13.59	14.16	14.71	14.81	14.93	12.72	13.41	14.58
Ce_2O_3	28.87	27.92	27.96	28.07	27.40	27.97	28.21	27.52	28.62	28.79	28.55	27.06	26.53	28.23
Pr_2O_3	3.21	2.99	3.19	3.12	3.07	3.20	3.14	3.01	3.02	3.00	2.95	3.12	3.01	3.08
Nd_2O_3	11.73	11.68	11.78	11.91	11.12	11.83	11.64	10.87	10.52	10.40	10.37	10.87	10.37	10.74
Sm_2O_3	1.87	2.07	2.13	2.14	1.95	2.24	2.08	1.90	1.95	1.89	1.85	1.94	1.89	1.74
Gd_2O_3	1.38	1.59	1.68	1.52	1.39	1.61	1.56	1.49	1.14	1.24	1.16	1.40	1.34	1.08
Tb_2O_3	0.09	0.21	0.12	0.20	0.16	0.04	0.11	0.17	0.13	0.19	0.13	0.18	0.10	0.10
Dy_2O_3	0.37	0.57	0.62	0.52	0.49	0.19	0.27	0.54	0.46	0.40	0.47	0.53	0.58	0.26
Ho_2O_3	0.06	0.12	0.08	0.07	0.05	0.02	u.d.	0.02	u.d.	0.08	0.11	u.d.	0.16	0.06
Er_2O_3	0.13	0.16	0.20	0.05	0.08	0.01	0.03	0.21	0.06	0.10	0.07	0.12	0.16	0.11
Yb_2O_3	0.01	u.d.	u.d.	u.d.	u.d.	u.d.	u.d.	u.d.	u.d.	u.d.	u.d.	u.d.	0.03	u.d.
P_2O_5	29.93	29.69	29.23	29.51	30.55	30.34	30.47	30.87	29.14	29.37	29.55	30.35	30.79	30.04
PbO	0.47	0.44	0.44	0.33	0.56	0.60	0.60	0.56	0.47	0.51	0.47	0.54	0.65	0.52
UO_2	0.42	0.80	0.83	0.17	0.77	0.70	0.78	0.79	0.13	0.13	0.14	0.51	0.67	0.25
ThO_2	4.97	2.91	2.72	4.05	4.62	5.58	5.28	4.61	6.03	6.04	6.11	5.29	6.40	6.49
CaO	1.10	0.91	0.88	0.77	1.27	1.34	1.31	1.26	0.81	0.79	0.82	1.59	1.58	1.11
Y_2O_3	1.88	2.38	2.49	1.03	2.12	0.55	0.60	2.08	1.28	1.33	1.30	2.29	2.61	1.45
SiO_2	1.23	0.11	0.10	0.43	0.18	0.38	0.31	0.22	0.81	0.78	0.79	0.20	0.28	0.62
Total wt%	101.35	98.76	98.35	98.46	99.71	99.93	99.98	100.28	99.27	99.84	99.76	98.69	100.56	100.45
Age (Ma)	1669±8	1704±32	1747±17	1641±37	1693±14	1675±7	1676±9	1684±7	1649±15	1743±29	1646±17	1732±12	1656±11	1614±18
Facies	Arg.	Arg.	Arg.	Arg.	Arg.	Arg.	Arg.	Arg.	Arg.	Arg.	Arg.	Arg.	Arg.	Arg.

Appendix 4.2a (continued).

Label Fig. 4.3b	G18	G20	G20	G20	G29	G29	G29	G29	G29	G13	G13	G17	G17	G17
sample	USO1	USO3	USO3	USO3	USO12	USO12	USO12	USO12	USO12	APP1	APP1	2AP	2AP	2AP
spot number	#30	#2	#1	#8	#1	#2	#3	#8	#2	#2	#3	#3	#4	#6
La_2O_3	13.48	13.43	14.73	15.26	13.72	16.33	13.87	14.24	16.33	10.12	16.70	14.49	14.59	13.81
Ce_2O_3	27.58	26.84	29.11	28.39	28.38	32.25	29.71	29.69	32.25	20.17	30.10	27.72	27.97	27.41
Pr_2O_3	3.07	3.11	3.00	3.04	3.13	3.15	3.40	3.18	3.15	2.46	3.05	2.97	2.96	2.96
Nd_2O_3	12.06	11.75	10.23	11.05	11.92	9.79	13.04	12.13	9.79	8.87	10.47	10.33	10.40	10.26
Sm_2O_3	2.12	2.10	1.48	1.89	2.22	1.48	2.34	2.15	1.48	1.86	1.20	1.71	1.67	1.91
Gd_2O_3	1.50	1.72	0.92	1.29	1.20	0.93	1.20	1.18	0.93	1.22	0.54	1.32	1.40	1.43
Tb_2O_3	0.16	0.27	u.d.	0.05	0.08	0.07	0.09	0.14	0.07	0.07	0.01	0.16	0.07	0.14
Dy_2O_3	0.49	0.81	0.31	0.37	0.18	0.05	0.25	0.25	0.05	0.30	0.06	0.45	0.42	0.59
Ho_2O_3	0.03	0.04	0.08	0.01	u.d.	u.d.	0.06	u.d.	u.d.	u.d.	0.01	0.05	0.02	0.05
Er_2O_3	0.10	0.18	0.09	0.09	0.07	0.05	0.03	u.d.	0.05	0.03	0.01	0.12	0.12	0.16
Yb_2O_3	u.d.	0.02	u.d.	u.d.	u.d.	u.d.	u.d.	u.d.	u.d.	u.d.	0.05	0.02	0.05	0.02
P_2O_5	29.92	30.33	29.93	30.33	31.38	29.65	30.36	29.82	29.65	24.12	30.30	28.19	28.51	29.05
PbO	0.44	0.45	0.62	0.38	0.43	0.08	0.29	0.24	0.08	1.74	0.43	0.58	0.59	0.61
UO_2	0.45	0.60	0.32	0.52	0.20	0.03	0.39	0.30	0.03	0.80	0.23	0.34	0.38	0.39
ThO_2	4.48	3.18	7.22	3.75	2.19	1.14	2.14	2.22	1.14	20.58	5.42	6.73	6.61	7.05
CaO	1.15	0.91	1.20	1.06	0.73	0.62	0.90	0.88	0.62	1.35	0.77	0.66	0.66	0.85
Y_2O_3	1.59	3.19	1.38	1.31	2.30	0.35	0.56	0.66	0.35	1.17	0.56	1.97	2.05	2.46
SiO_2	0.43	0.76	0.78	0.22	0.34	1.12	0.27	1.04	1.12	4.29	0.87	1.20	1.16	1.09
Total wt%	99.04	99.69	101.41	99.03	98.46	97.09	98.87	98.11	97.09	99.16	100.78	99.01	99.62	100.22
Age (Ma)	1663±21	1859±9	1679±12	1551±20	3074±19	1435±26	1874±19	1663±17	1435±26	1692±7	1546±37	1668±22	1682±29	1648±18
Facies	Arg.	Arg.	Arg.	Arg.	Arg.	Arg.	Arg.	Arg.	Arg.	Sd.	Sd.	Sd.	Sd.	Sd.

Appendix 4.2a (continued).

Label Fig. 4.3b	G14	G14	G14	G17	G37	G37	G37	G37	G37	G37	G37	G37	G37
sample	2AP	2AP	2AP	3AP	MGR11	MGR11	MGR8	MGR8	MGR1	MGR1	MGR6	MGR6	MGR4
spot number	#10	#13	#17	#19	#1	#4	#3	#4	#2	#3	#9	#11	#12
La_2O_3	10.31	17.31	14.71	23.71	13.87	14.04	11.90	10.20	15.21	14.81	12.43	12.05	10.58
Ce_2O_3	24.62	29.36	30.15	27.63	28.00	28.38	25.70	24.11	28.50	29.48	27.89	27.40	24.28
Pr_2O_3	3.08	2.60	3.21	3.08	2.92	3.03	2.82	2.73	2.97	3.30	3.32	3.12	2.78
Nd_2O_3	12.16	7.76	12.57	9.67	10.85	11.72	10.64	10.66	11.11	12.19	12.41	12.45	10.07
Sm_2O_3	2.10	0.68	2.26	1.43	1.91	2.11	2.11	2.52	1.75	1.98	2.27	2.22	2.11
Gd_2O_3	0.98	0.30	1.36	0.69	1.24	1.41	1.47	2.04	1.12	1.35	1.93	1.82	1.95
Tb_2O_3	0.11	u.d.	0.12	0.04	0.17	u.d.	0.25	0.25	0.16	0.05	0.14	0.19	0.15
Dy_2O_3	0.24	0.17	0.19	0.12	0.66	0.51	0.69	0.97	0.32	0.24	0.85	0.73	0.97
Ho_2O_3	0.01	0.05	0.01	u.d.	0.14	0.04	0.09	0.18	0.02	0.09	0.12	0.23	0.25
Er_2O_3	0.05	0.04	0.02	u.d.	0.16	0.07	0.18	0.25	0.11	0.06	0.25	0.28	0.28
Yb_2O_3	u.d.	u.d.	u.d.	u.d.	u.d.	u.d.	0.07	0.05	u.d.	u.d.	0.08	u.d.	0.05
P_2O_5	29.90	26.18	29.12	29.71	3u.d.	29.41	29.71	29.04	29.30	29.04	29.70	29.38	28.71
PbO	0.90	0.97	0.19	0.05	0.53	0.35	0.67	0.76	0.77	0.28	0.27	0.29	0.78
UO_2	0.35	0.18	0.04	0.01	0.63	0.40	0.52	0.75	0.72	0.17	0.14	0.18	0.52
ThO_2	11.01	8.84	2.02	0.55	4.51	3.07	7.14	7.52	3.52	2.69	3.08	2.96	8.58
CaO	2.17	0.96	0.75	0.38	1.14	0.68	1.43	1.31	1.09	0.64	0.33	0.34	1.43
Y_2O_3	0.93	0.27	0.29	0.18	2.29	1.90	2.72	4.59	1.00	0.95	3.72	3.98	4.70
SiO_2	0.67	2.58	0.26	0.55	0.41	0.66	1.24	1.31	0.32	0.50	0.72	2.22	0.93
Total wt%	99.60	98.26	97.27	97.78	99.44	97.77	99.34	99.24	97.99	97.82	99.65	99.83	99.11
Age (Ma)	1681±16	2285±9	1950±19	1585±46	1788±17	1735±30	1699±28	1693±21	2654±12	1877±31	1725±31	1833±32	1704±25
Facies	Sd.	Sd.	Sd.	Sd.	Sd.	Sd.	Sd.	Sd.	Sd.	Sd.	Sd.	Sd.	Sd.

Appendix 4.2a (continued).

Label Fig. 4.3b	G37	G37
sample	MGR4	MGR4
spot number	#13	#14
La_2O_3	10.31	10.45
Ce_2O_3	24.29	24.56
Pr_2O_3	2.74	2.88
Nd_2O_3	10.11	10.27
Sm_2O_3	2.13	2.10
Gd_2O_3	1.88	1.90
Tb_2O_3	0.17	0.21
Dy_2O_3	1.09	0.96
Ho_2O_3	0.15	0.12
Er_2O_3	0.28	0.22
Yb_2O_3	0.04	u.d.
P_2O_5	29.10	29.23
PbO	0.79	0.79
UO_2	0.53	0.50
ThO_2	8.72	8.56
CaO	1.44	1.39
Y_2O_3	4.83	4.49
SiO_2	0.92	1.01
Total wt%	99.53	99.62
Age (Ma)	1703±23	1742±24
Facies	Sd.	Sd.

(u.d.) Under detection limits; (Arg.) argillites; (Sd.) sandstones.

Appendix 4.2b Monazite analyses for the complete rare earth elements and chemical ages <~1400 Ma population

Label Fig. 4.3b	G7	G18	G18	G18	G18	G20	G20	G20	G20	G20	G20	G20	G20	G29
sample	USO13	USO1	USO1	USO1	USO1	USO3	USO3	USO3	USO3	USO3	USO3	USO3	USO3	USO12
spot number	#2	#11	#22	#27	#29	#3	#4	#5	#6	#7	#9	#10	#12	#5
La_2O_3 (wt%)	18.58	12.65	17.69	12.96	13.63	16.62	13.99	14.77	19.60	12.54	13.30	13.34	14.18	17.55
Ce_2O_3	32.34	30.72	30.01	31.57	31.01	31.21	30.52	30.45	29.92	27.17	3u.d.	29.99	30.45	32.07
Pr_2O_3	2.87	3.68	3.18	3.82	3.56	3.20	3.72	3.52	3.10	3.08	3.66	3.63	3.55	3.15
Nd_2O_3	8.69	14.85	12.05	14.69	14.00	11.79	14.54	14.11	11.40	11.85	14.87	14.77	14.10	10.95
Sm_2O_3	0.82	2.67	2.06	2.41	2.54	1.46	2.83	2.57	2.10	2.31	2.87	2.78	2.60	1.56
Gd_2O_3	0.36	1.31	1.20	1.23	1.18	0.66	1.54	1.52	1.22	1.73	1.55	1.42	1.33	0.72
Tb_2O_3	0.02	0.18	0.01	0.11	0.07	0.09	0.10	0.11	0.05	0.21	0.11	0.03	0.09	0.06
Dy_2O_3	0.20	u.d.	0.19	0.08	0.07	0.08	0.07	0.06	0.01	0.76	0.05	0.08	0.10	0.04
Ho_2O_3	0.06	0.02	0.01	0.02	0.03	0.12	u.d.	0.01	u.d.	0.11	0.10	0.08	u.d.	0.05
Er_2O_3	u.d.	u.d.	u.d.	u.d.	0.01	0.02	0.02	0.03	0.02	0.19	0.02	0.05	0.07	0.04
Yb_2O_3	0.07	u.d.	u.d.	0.06	u.d.	u.d.	u.d.	u.d.	u.d.	u.d.	u.d.	u.d.	u.d.	u.d.
P_2O_5	27.92	30.71	30.55	30.12	30.93	29.35	29.77	30.35	30.14	29.10	30.35	29.71	29.55	30.05
PbO	0.31	0.02	0.06	0.02	0.06	0.20	0.04	0.06	0.03	0.32	0.06	0.07	0.04	0.06
UO_2	0.24	0.02	0.03	0.01	0.01	0.08	u.d.	u.d.	u.d.	0.23	0.02	0.01	0.02	0.03
ThO_2	4.40	0.54	1.11	0.89	0.95	3.31	0.77	0.95	0.82	5.06	1.17	1.18	0.77	1.18
CaO	0.09	0.21	0.31	0.18	0.22	0.43	0.27	0.32	0.32	0.96	0.27	0.24	0.28	0.44
Y_2O_3	0.37	0.27	0.26	0.17	0.22	0.24	0.23	0.20	0.31	3.40	0.22	0.20	0.20	0.19
SiO_2	1.62	0.80	0.45	0.34	1.19	0.61	0.40	0.20	0.19	0.52	0.28	0.38	0.56	0.34
Total wt%	98.94	98.64	99.15	98.67	99.68	99.47	98.79	99.22	99.22	99.55	98.89	97.95	97.89	98.47
Age (Ma)	1347±19	445±61	1200±39	572±37	1339±31	1307±32	996±31	1339±29	628±37	1237±17	1056±27	1295±35	852±26	1057±27
Facies	Arg.	Arg.	Arg.	Arg.	Arg.	Arg.	Arg.	Arg.	Arg.	Arg.	Arg.	Arg.	Arg.	Arg.

Appendix 4.2b (continued).

Label Fig. 4.3b	G29	G13	G14	G14	G14	G14	G14	G14	G14	G14	G17	G17	G37	G37
sample	USO12	APP1	2AP	2AP	2AP	2AP	2AP	2AP	2AP	2AP	3AP	3AP	MGR10	MGR6
spot number	#9	#1	#5	#7	#8	#11	#12	#14	#15	#16	#20	#21	#1	#10
La_2O_3	14.12	19.28	14.42	17.00	16.16	28.31	14.96	18.18	15.67	15.83	18.20	19.39	10.70	14.14
Ce_2O_3	30.76	27.86	28.10	27.78	27.45	28.07	27.54	27.51	27.47	27.42	29.78	29.49	24.19	29.19
Pr_2O_3	3.50	3.62	2.89	3.70	3.85	2.30	4.02	3.61	3.84	3.74	3.62	3.18	2.62	3.12
Nd_2O_3	12.84	13.00	10.42	14.41	14.14	6.95	15.60	13.73	14.90	14.96	13.26	9.29	10.33	12.38
Sm_2O_3	2.16	2.36	1.94	2.40	2.51	0.98	2.69	2.36	2.70	2.60	1.86	1.59	2.78	2.26
Gd_2O_3	1.15	1.18	1.33	1.22	1.25	0.53	1.33	1.03	1.42	1.42	0.70	0.93	2.40	1.57
Tb_2O_3	0.15	0.14	0.24	0.10	0.15	0.11	0.11	0.03	0.09	0.12	u.d.	0.13	0.29	0.22
Dy_2O_3	0.13	0.06	0.47	0.11	0.05	0.07	0.10	u.d.	0.10	0.12	u.d.	0.06	0.80	0.47
Ho_2O_3	0.06	u.d.	0.13	u.d.	u.d.	u.d.	u.d.	u.d.	0.07	0.03	u.d.	0.02	0.11	0.14
Er_2O_3	0.04	u.d.	0.11	0.01	0.03	u.d.	0.05	u.d.	0.03	0.01	0.03	u.d.	0.14	0.12
Yb_2O_3	u.d.	u.d.	u.d.	u.d.	u.d.	u.d.	u.d.	u.d.	u.d.	u.d.	u.d.	u.d.	u.d.	0.01
P_2O_5	29.90	29.82	28.96	29.57	29.59	30.40	30.02	29.87	29.98	30.73	29.47	30.26	29.19	30.58
PbO	0.13	0.03	0.42	0.03	0.04	0.04	0.08	0.03	0.07	0.08	0.02	0.06	0.14	0.18
UO_2	0.05	0.05	0.33	0.02	0.02	0.02	0.02	0.01	0.02	0.02	0.02	0.03	1.50	0.15
ThO_2	2.17	0.62	6.19	1.07	1.21	0.68	1.60	0.86	1.61	1.87	0.45	1.39	7.72	3.49
CaO	0.77	0.15	0.75	0.28	0.18	0.32	0.26	0.24	0.23	0.21	0.25	0.58	1.84	0.73
Y_2O_3	0.38	0.15	2.12	0.20	0.26	0.19	0.22	0.17	0.28	0.26	0.07	0.31	2.79	1.11
SiO_2	0.35	0.23	1.00	0.68	0.84	0.09	0.39	0.49	0.44	0.49	0.36	0.43	0.27	0.41
Total wt%	98.64	98.48	99.80	98.60	97.74	99.05	98.99	98.13	98.90	99.90	98.09	97.12	97.79	100.26
Age (Ma)	1298±21	662±31	1334±34	602±28	753±18	1174±44	1126±29	781±32	980±29	870±38	492±28	870±26	264±42	1059±37
Facies	Arg.	Sd.	Sd.	Sd.	Sd.	Sd.	Sd.	Sd.	Sd.	Sd.	Sd.	Sd.	Sd.	Sd.

Appendix 4.2B (continued).

Label Fig. 4.3b	G37	G41
sample	MGR6	UGR
spot number	#23	#2
La_2O_3	4.05	14.94
Ce_2O_3	18.03	26.79
Pr_2O_3	5.05	4.06
Nd_2O_3	31.28	15.31
Sm_2O_3	6.70	2.84
Gd_2O_3	1.92	1.46
Tb_2O_3	0.04	0.06
Dy_2O_3	0.04	0.08
Ho_2O_3	0.02	0.07
Er_2O_3	0.01	0.02
Yb_2O_3	u.d.	u.d.
P_2O_5	28.90	27.64
PbO	0.01	0.03
UO_2	0.01	0.05
ThO_2	0.30	0.53
CaO	0.82	0.26
Y_2O_3	0.44	0.24
SiO_2	0.36	0.41
Total wt%	98.13	98.78
Age (Ma)	453±47	845±35
Facies	Sd.	Sd.

(u.d.) Under detection limits; (Sd..) sandstone; (Arg.) argillite.

Appendix 4.3a Monazite analyses for ThO_2, PbO, UO_2, and Y_2O_3, and chemical ages >~1400 Ma.

Label Fig. 4.3b	G13	G13	G13	G13	G13	G13	G13	G13	G13	G13	G13	G13	G13	G13
sample	1App	1App	1App	1App	1App	1App	1App	1App	1App	1App	1App	1App	1App	1App
spot number	#2	#9	#10	#11	#12	#13	#18	#20	#21	#27	#29	#30	#31	#32
PbO	0.24	0.12	0.45	0.43	0.44	0.43	0.45	0.15	0.45	0.46	0.53	0.55	0.53	0.58
UO_2	0.28	0.16	0.83	0.84	0.73	0.80	0.37	0.06	0.35	0.26	0.25	0.29	0.26	0.30
ThO_2	2.58	1.27	3.44	3.49	3.47	3.34	5.42	2.00	5.53	5.72	6.42	6.78	6.51	7.14
Yb_2O_3	0.76	1.57	6.27	2.46	2.85	2.47	2.50	0.59	2.56	0.09	1.78	1.93	1.78	2.07
Age (Ma)	1559±16	1479±23	1611±8	1533±9	1647±31	1579±10	1537±7	1558±19	1519±7	1599±17	1651±18	1626±7	1630±18	1637±22
Facies	Sd.	Sd.	Sd.	Sd.	Sd.	Sd.	Sd.	Sd.	Sd.	Sd.	Sd.	Sd.	Sd.	Sd.

Label Fig. 4.3b	G13	G13	G13	G13	G13	G13	G18	G18	G18	G18	G18	G18	G18
sample	1App	1App	1App	1App	1App	1App	1USO	1USO	1USO	1USO	1USO	1USO	1USO
spot number	#33	#34	#36	#37	#38	#39	#9	#10	#11	#12	#13	#14	#15
PbO	0.58	0.49	1.23	1.08	1.43	0.81	0.45	0.41	0.41	0.70	0.43	0.41	0.60
UO_2	0.27	0.35	0.78	0.71	1.47	1.76	0.45	0.21	0.22	1.23	0.80	0.56	0.86
ThO_2	7.02	5.40	12.91	11.62	8.35	4.43	4.91	5.92	5.75	5.75	3.89	4.00	5.44
Yb_2O_3	1.64	3.59	0.77	0.36	2.25	2.31	1.31	3.44	3.51	1.88	0.00	1.30	2.55
Age (Ma)	1668±22	1699±17	1790±10	1743±6	2296±12	1708±18	1576±9	1431±36	1431±36	1593±25	1460±35	1554±39	1609±30
Facies	Sd.	Sd.	Sd.	Sd.	Sd.	Sd.	Arg.	Arg.	Arg.	Arg.	Arg.	Arg.	Arg.

Appendix 4.3b Monazite analyses for ThO_2, PbO, UO_2, and Y_2O_3, and chemical ages <~1400 Ma.

Label Fig. 4.3b	G13	G13	G13	G13	G13	G13	G13	G13	G13	G13	G13	G13	G13	G13
sample	1App	1App	1App	1App	1App	1App	1App	1App	1App	1App	1App	1App	1App	1App
spot number	#1	#3	#4	#5	#6	#6	#7	#8	#14	#15	#16	#17	#19	#22
PbO	0.02	0.01	0.03	0.02	0.06	0.08	0.10	0.12	0.04	0.03	0.02	0.14	0.07	0.04
UO_2	0.10	0.01	0.12	0.18	0.05	0.15	0.21	0.16	0.06	0.12	0.16	0.18	0.04	0.02
ThO_2	0.93	0.72	0.79	0.66	1.27	0.96	1.19	1.45	1.01	1.13	0.57	2.22	1.74	1.25
Yb_2O_3	3.52	0.24	0.24	0.17	0.39	1.65	1.88	1.42	0.19	0.20	0.11	0.83	0.17	0.16
Age (Ma)	362±50	325±34	640±27	310±42	960±22	1213±29	1265±27	1345±24	840±24	525±22	491±67	1167±18	884±24	632±18
Facies	Sd.	Sd.	Sd.	Sd.	Sd.	Sd.	Sd.	Sd.	Sd.	Sd.	Sd.	Sd.	Sd.	Sd.

Label Fig. 4.3b	G13	G13	G13	G13	G13	G13	G41	G41	G18	G18	G18	G18	G18	G18
sample	1App	1App	1App	1App	1App	1App	UGR	UGR	1USO	1USO	1USO	1USO	1USO	1USO
spot number	#23	#24	#25	#26	#28	#35	#1	#2	#1	#2	#3	#4	#5	#6
PbO	0.05	0.03	0.02	0.02	0.06	0.08	0.34	0.83	0.06	0.03	0.11	0.03	0.01	0.06
UO_2	0.00	0.09	0.10	0.10	0.03	0.09	0.19	0.46	0.03	0.06	0.04	0.07	0.01	0.11
ThO_2	0.82	1.08	1.12	0.76	1.50	2.03	5.99	12.78	1.72	2.49	2.53	0.79	0.51	1.92
Yb_2O_3	2.55	0.25	0.23	0.18	0.20	2.55	3.91	0.77	0.20	6.87	0.22	0.39	0.20	0.17
Age (Ma)	1274±35	530±22	396±54	425±58	926±21	856±34	1191±17	1344±14	826±19	301±12	960±18	637±26	439±46	652±15
Facies	Sd.	Sd.	Sd.	Sd.	Sd.	Sd.	Sd.	Sd.	Arg.	Arg.	Arg.	Arg.	Arg.	Arg.

Appendix 4.3b (continued).

Label Fig. 4.3b	G18	G18	G18	G18	G18	G18	G18	G18	G18	G18	G18	G18	G18	G18
sample	1USO	1USO	1USO	1USO	1USO	1USO	1USO	1USO	1USO	1USO	1USO	1USO	1USO	1USO
spot number	#7	#8	#9	#16	#17	#18	#19	#20	#21	#22	#23	#24	#25	#26
PbO	0.02	0.05	0.05	0.05	0.02	0.05	0.11	0.03	0.04	0.02	0.03	0.02	0.05	0.01
UO_2	0.03	0.07	0.06	0.01	0.07	0.06	0.10	0.24	0.02	0.01	0.05	0.02	0.02	0.03
ThO_2	1.00	1.48	1.14	1.32	0.72	1.59	2.29	0.00	1.03	1.09	1.12	0.63	1.32	0.99
Yb_2O_3	0.26	0.14	0.18	0.31	0.51	0.26	0.20	0.17	0.22	0.00	0.14	0.25	0.26	0.13
Age (Ma)	438±60	677±19	825±23	929±26	438±14	624±17	948±24	977±40	879±25	379±52	576±24	540±74	922±26	316±33
Facies	Arg.	Arg.	Arg.	Arg.	Arg.	Arg.	Arg.	Arg.	Arg.	Arg.	Arg.	Arg.	Arg.	Arg.

Label Fig. 4.3b	G18	G18	G18
sample	1USO	1USO	1USO
spot number	#27	#28	#29
PbO	0.04	0.02	0.02
UO_2	0.07	0.01	0.07
ThO_2	0.85	0.79	0.78
Yb_2O_3	0.26	0.28	0.62
Age (Ma)	887±25	526±16	402±12
Facies	Arg.	Arg.	Arg.

(Arg.) argillites; (Sd.) sandstones.

4.10 References

Anderson, H.E., Davis, W.D., 1995. U-Pb geochronology of the Moyie sills, Purcell Supergroup, southeastern British Columbia: implications for the Mesoproterozoic geological history of the Purcell (Belt) Basin. Can. J. Earth Sci. 32, 1180-1193.

Anderson, H.E., Goodfellow, W.D., 2000. Geochemistry and isotope chemistry of the Moyie sills: implications for the early tectonic setting of the Mesoproterozoic Purcell Basin. In: Lydon, J.W., Höy, T., Slack, J.F., Knapp, M.E., (eds.), The Geological Environment of the Sullivan Deposit, British Columbia. Geol. Assoc. Can. Min. Dep. Div. Spec. Publ. 1, pp. 302-321.

Ayers, J.C., Miller, C., Gorisch, B., Milleman, J., 1999. Textural development of monazite during high-grade metamorphism: hydrothermal growth kinetics, with implications of U, Th-Pb geochronology. Am. Mineral. 84, 1766-1780.

Bekker, A., Ericksson, K., 2003. A Paleoproterozoic drowned carbonate platform on the southeastern margin of the Wyoming Craton: a record of the Kenorland breakup. Precambrian Res. 120, 327-364.

Bhat, M.I., Ghosh, S.K., 2001. Geochemistry of the 2.51 Ga old Rampur Group pelites, western Himalayas: implications for their provenance and weathering. Precambrian Res. 108, 1-16.

Braun, J. J., Pagel, M., Herbillion, A., Rosin, C., 1993. Mobilization and redistribution of REEs and thorium in a syenitic lateritic profile: a mass balance study. Geochim. Cosmochim. Acta 57, 4419-4434.

Braun, J. J., Pagel, M., Muller, J.P., Bilong, P., Michard, A., Guillet, B., 1990. Cerium anomalies in lateritic profiles. Geochim. Cosmochim. Acta 54, 781-795.

Brown, A.V., Jenner, G.A., 1989. Geological setting, petrology and chemistry of Cambrian boninite and low-Ti tholeiite lavas in western Tasmania. In: Crawford, A.J., (ed.), Boninites and related rocks, Unwin Hyman, London, U. K., pp. 232-263.

Burnotte, E., Pirard, E., Michel, G., 1989. Genesis of gray monazites: evidence from the Paleozoic of Belgium. Econ. Geol. 84, 1417-1429.

Chandler, F.W., 2000. The Belt-Purcell Basin as a low-latitude passive rift: implications for the geological environment of Sullivan type deposits. In: Lydon, J.W., Höy, T., Slack, J.F., Knapp, M.E., (eds.), The Geological Environment of the Sullivan Deposit, British Columbia. Geol. Assoc. Can. Min. Dep. Div. Spec. Publ. 1, pp. 82-112.

Chaudhuri, S., Cullers, R.L., 1979. Distribution of rare-earth elements in deeply buried Gulf coast sediments. Chem. Geol. 24, 327-338.

Cherniak, D.J., Watson, E.B., Grove, M., Harrison, T.M., 2004. Pb diffusion in monazite: a combined RBS/SIMS study. Geochim. Cosmochim. Acta 68, 829-840.

Clowes, R.M., Cook, F.A., Ludden, J.N., 1998. Lithopobe leads to new perspectives on continental evolution. Geol. Soc. Am. Today 8, 2-7.

Cocherie, A., Mezeme, E.B., Legendre, O., Fanning, C.M., Faure, M., Rossi, P., 2005. Electron-microprobe dating as a tool determining the closure of Th-U-Pb systems in migmatitic monazites. Am. Mineral. 90, 607-618.

Condie, K.C., 1991. Another look at rare earth elements in shales. Geochim. Cosmochim. Acta 55, 2527-2531.

Condie, K.C., 2002. The supercontinent cycle: are there two patterns of cyclicity? J. African Earth Sci. 35, 179-183.

Connor, J.J., Reynolds, M.W., Whipple, J.W., 1984. Stratigraphy of the Ravalli Group, Belt Basin, Montana and Idaho. In: Hobbs, S.W., (ed.), The Belt Abstracts with Summaries, Belt Symposium II, Montana Bur. Min. Geol., Spec. Publ. 90, pp. 13-15.

Copeland, P., Parrish, R.R., Harrison, T.M., 1988. Identification of inheritated radiogenic Pb in monazite and its implication for U-Pb systematics. Nature 333, 760-763.

Cressey, G., Wall, F., Cressey, A., 1999. Differential REE uptake by sector growth of monazite. Mineral. Magaz. 63, 813-828.

Cullers, R.L., Chaudhuri, S., Kilbane, N., Koch, R., 1979. Rare-earths in size fractions and sedimentary-rocks of Pennsylvanian-Permian age from the mid-continent of the USA. Geochim. Cosmochim. Acta 43, 1285-1301.

Dahl, P. S., Jercinovic, M.J, Williamns, M. L., 2002. Chemical dating of monazite in the Black Hills, South Dakota, with implications for proterozoic thermotectonism in the eastern Wyoming Province. Geol. Assoc. Am. Annual Meeting, Abstracts 25-9.

Dahl, P.S., Hamilton, M.A., Jercinovic, M.J., Terry, M.P., Williams, M.L., Frei, R., 2005. Comparative isotopic and chemical geochronometry of monazite, with implications for U-Th-Pb dating by electron microprobe: an example from metamorphic rocks of the eastern Wyoming Craton (U.S.A.). Am. Mineral. 90, 619-638.

Doughty, P.T., Price, R.A., Parrish, R.R., 1997. Geology and U-Pb geochronology of Archean basement and Proterozoic cover in the Priest River complex, northwestern United States, and their implications for Cordilleran structure and Precambrian continent reconstructions. Can. J. Earth Sci. 35, 39-54.

Duddy, I. R., 1980. Redistribution and fractionation of rare-earth and other elements in a weathering profile. Chem. Geol. 30, 363-381.

Earhart, R.L., Mudge, M.R., Connor, J.J., 1984. Belt Supergroup lithofacies in the northern disturbed Belt, northwest Montana. In: McBane, J.D., Garrison, P.B., (eds.), Montana Geol. Soc. Guidebook, Field Conference and Symposium, pp. 51-66.

Eglington, B.M., Armstrong, R.A., 2004. The Kaapvaal Craton and adjacent orogens, southern Africa: a geochronological database and overview of the geological development of the craton. Geol. Soc. South Africa 107, 13-32.

and copper occurrences. Geol. Soc. Am. Bull. 83, 1215-1240.

Harrison, T.M., Catlos, E.J., Montel, J.M., 2002. U-Th-Pb dating of phosphate minerals. In: Kohn, M.J., Todd, S.P., Haughton, P.D.W., (eds.), Phosphates: Geochemical, Geobiological, and Materials Importance. Rev. Mineral. Geochem. 48, pp. 523-558.

Hodges, K.V., 2004. Geochronology and thermochronology in orogenic systems. In: Rudnick, R.L., (ed.), The Crust, Treatise on Geochimistry, Holland, H.D., Turekian, K.K., (eds.), Elsevier, Oxford, New York, 3, pp. 263-292.

Hoffman, P.F., 1988. United Plates of America, the birth of a craton: early Proterozoic assemble and growth of Laurentia. Ann. Rev. Earth Planet. Sci. 16, 543-603.

Hoffman, P.F., 1991. Did the breakout of Laurentia turn Gondwana inside out? Science 252, 1409-1412.

Höy, T., 1989. The age, chemistry, and tectonic setting of the middle Proterozoic Moyie sills, Purcell Supergroup. Southeastern British Columbia. Can. J. Earth Sci. 26, 2305-2317.

Höy, T., 1993. Geology of the Purcell Supergroup in the Fernie west-half map-area, southeastern British Columbia. British Columbia Ministry of Energy, Min. Petrol. Resour. Bull. 84, 157.

Jenner, G.A, Longerich, H.P., Jackson, S.E., Fryer, B.J., 1990. ICP-MS a powerful tool for high precision trace-element analysis in earth sciences: evidence from analysis of selected USGS reference samples. Chem. Geol. 83, 133-148.

Kerrich, R., Renaut, R.W., Bonli, T., 2002. Trace-element composition of cherts from alkaline lakes in the east African rift: a probe for ancient counterparts. In: Renaut, R.W., Ashley, G.M. (eds.), Sedimentation in Continental Rifts, Boulder, Colorado, Soc. Sed. Geol. Spec. Publ. 73, pp. 277-298.

Kleinkopf, M.D., 1997. Interpretation of regional aeromagnetic and gravity anomalies in the Belt-Purcell terrane and adjacent areas, northern Rocky Mountains United States and Canada. In: Berg, R.B., (ed.), Belt Symposium III, Montana Bureau Min. Geol. Spec. Publ. 112, pp. 210-221.

Kyser, K., Hiatt, E., Renac, C., Durocher, K., Holk, G., Deckart, K., 2000. Diagenetic fluids in Paleo- and Mesoproterozoic sedimentary basins and their implications for long protected fluid histories. In: Kyser, K., (ed.), Fluids and Basin Evolution, Min. Assoc. Can., Short Course Series, Kingston, Ontario, 28, pp. 225-262.

Lev, S.M., McLennan, S.M., Hanson, G.N., 1999. Mineralogic controls on REE mobility during black-shale diagenesis, J. Sed. Res. 69, 1071-1082.

Link, P.K., 1997. The Grinnell, Empire and Helena formations along Baring Creek and at Siyeh Pass, Glacier National Park. In: Link, P.K., (ed.), Geologic Guidebook to the Belt-Purcell Supergroup, Glacier National Park and Vicinity, Montana and Adjacent Canada, Field Trip Guidebook for the Belt Symposium III, Belt Association, Pocatello, Idaho, U.S.A., pp. 113-124.

Ludwig, K. R., 1999. Users manual for Isoplot/Ex, version 2.34, a geochronological toolkit for Microsoft excel. Berkeley Geochronology Center, U.S.A.

Evans, K.V., Aleinikoff, J.N., Obradovich, J.D., Fanning, C.M., 2000. SHRIMP U-Pb geochronology of volcanic rocks, Belt Supergroup, western Montana: evidence for rapid deposition of sedimentary strata. Can. J. Earth Sci. 37, 1287-1300.

Evans, J.A., Zalasiewicz, J.A., 1996. U-Pb, Pb-Pb and Sm-Nd dating of authigenic monazite: implications for the diagenetic evolution of the Wels Basin. Earth Planet. Sc. Lett. 144, 421-433.

Evans, J.A., Zalasiewicz, J.A., Fletcher, I., Rasmussen, B., Pearce, N.J.G., 2002. Dating diagenetic monazite in mudrocks: constraining the oil window? Geol. Soc. London 159, 619-622.

Fan, J., Kerrich, R., 1997. Geochemical characteristics of aluminum depleted and undepleted komatiites and HREE-enriched low-Ti tholeiites, western Abitibi greenstone belt: a heterogeneous mantle plume-convergent margin environment. Geochim. Cosmochim. Acta 61, 4723-4744.

Faupl, P., Pavlopoulos, A., Migiros, G., 1998. On the provenance of flysch deposits in the external Hellenides of mainland Greece: results from heavy mineral studies. Geol. Magaz. 135, 421-442.

Faure, G., 1986. Principles of Isotope Geology. Wiley and Sons, New York, NY, U.S.A.

Fayek, M, Kyser, T.K., 1997. Characterization of multiple fluid-flow events and rare-earth element mobility associated with formation of unconformity-type uranium deposits in the Athabasca Basin, Can. Min. 35, 627-658.

Feng, R., Kerrich, R., 1992. Geochemical evolution of granitoids from the Archean Abitibi southern volcanic zone and the Pontiac Subprovince, Superior Province, Canada: Implications for tectonic history and source regions. Chem. Geol. 98, 23–70.

Finger, F., Helmy, H.M., 1998. Composition and total-Pb model ages of monazite from high-grade paragneisses in the Abu Swayel area, southern eastern desert, Egypt. Miner. Petrol. 62, 269-289.

Folk, R.L., 1968. Petrology of sedimentary rocks. Hemphill's, Austin, U.S.A.

Fralick, P.W., 2003. Geochemistry of clastic sedimentary rocks: ratio techniques. In: Geochemistry of Sediments and Sedimentary Rocks: Evolutionary Considerations to Mineral-deposit Forming Environments. In: Lentz, D.R., (ed.), Geol. Assoc. Can., St. John's, Newfoundland, Canada, Geo Text 4, pp. 85-103.

Fralick, P.W., Kronberg, B.I., 1997. Geochemical discrimination of clastic sedimentary rock sources. Sediment. Geol. 113, 111-124.

Frost, C.D., Winston, D., 1987. Nd isotope systematics of coarse-and fine-grained sediments: examples from the Middle Proterozoic Belt-Purcell Supergroup. J. Geol. 95, 309-327.

Gao, S., Wedepohl, K.H., 1995. The negative Eu anomaly in Archean sedimentary rocks: implications for decomposition, age and importance of their granitic sources. Earth Planet. Sci. Lett. 133, 81-94.

Goodwin, A.M., 1991. Precambrian geology: the dynamic evolution of the continental crust. Academic Press, San Diego, U.S.A.

Harrison, J.E., 1972. Precambrian Belt Basin of northwestern United States: its geometry, sedimentation,

Lydon, J.W., 2000. A synopsis of the understanding of the geological environment of the Sullivan Deposit. In: Lydon, J.W., Höy, T., Slack, J.F., Knapp, M.E., (eds.), The Geological Environment of the Sullivan Deposit, British Columbia. Geol. Assoc. Can. Min. Dep. Div. Spec. Publ. 1, pp. 12-31.

Lydon, J.W., Walker, R., Anderson, H.E., 2000. Lithogeochemistry of the Aldridge Formation and the chemical effects of burial diagenesis. In: Lydon, J.W., Höy, T., Slack, J.F., Knapp, M.E., (eds.), The Geological Environment of the Sullivan Deposit, British Columbia. Geol. Assoc. Can. Min. Dep. Div. Spec. Publ. 1, pp. 137-179.

Marsh, J., 1991. REE fractionation and Ce anomalies in weathered Karoo dolerite, Chem. Geol. 90, 189-194.

Maxwell, D.T., Hower, J., 1967. High-grade diagenesis and low-grade metamorphism of illite in the Precambrian Belt Series. Am. Mineral. 52, 843-857.

McDaniel, D.K., Hemming, S.R., McLennan, S.M., Hanson, G.N., 1994. Resetting of neodymium isotopes and redistribution of REEs during sedimentary processes: the early Proterozoic Chelmsford Formation, Sudbury Basin, Ontario, Canada. Geochim. Cosmochim. Acta 58, 931-941.

McLennan, S.M., Taylor, S.R., McCulloch, M.T., Maynard, J.B., Geochemical and Nd-Sr isotopic composition of deep-sea turbidites: crustal evolution and plate tectonic associations. Geochim. Cosmochim. Acta 54, 2015-2050.

McLennan, S.M., Bock, B., Hemming, R.S., Hurowitz, J.A., Lev, S.M., McDaniel, D.K., 2003. The roles of provenance and sedimentary processes in the geochemistry of sedimentary rocks. In: Lentz, D.R. (ed.), Geochemistry of Sediments and Sedimentary Rocks: Evolutionary Considerations to Mineral-Deposit Forming Environments. St. John's, Newfoundland, Canada, Geol. Assoc. Can. Geo Text 4, pp. 7-38.

McMechan, M.E., 1981. The middle Proterozoic Purcell Supergroup in the southwestern Rocky and southeastern Purcell Mountains, British Columbia and the initiation of the Cordilleran miogeocline, southern Canada and adjacent United States. Bull. Can. Petrol. Geol. 29, 583-621.

Milodowski, A.E., Zalasiewicz, J.A., 1991. Redistribution of rare earth elements during diagenesis of turbidite/hemipelagite mudrock sequences of Llandovery age from central Wales. In: Morton, A.C., (ed.), Developments in Sedimentary Provenance Studies. Geol. Soc. Am. Spec. Publ. 57, 101-124.

Montel, J.M., Foret, S., Veschambre, M., Nicollet, C., Provost, A., 1996. Electron microprobe dating of monazite. Chem. Geol. 131, 37-53.

Montel, J.M., Kornprobst, J., Vielzeuf, D., 2000. Preservation of old U-Th-Pb ages in shielded monazite: example from the Beni Bousera Hercynian kinzigites (Morocco). J. Metamorphic Geol. 18, 335-342.

Mougeot, R., Respaut, J.P., Ledru, P., Marignac, Ch., 1997. U-Pb chronology on accessory minerals of the Velay anatectic dome (French Massif Central). Eur. J. Mineral. 9, 141-156.

Mueller, P.A., Shuster, R.D., Wooden, J.L., Erslev, E.A., Bowes, D.R., 1993. Age and composition of Ar-

chean crystalline rocks from the southern Madison Range, Montana: implications for crustal evolution in the Wyoming Craton. Geo. Soc. Am. Bull. 105, 437-446.

Nasdala, L., Finger, F., Kinny, P., 1999. Can monazite be metamict? Eur. J. Mineral. 11, 165.

Nesbitt, H.W., 1979. Mobility and fractionation of rare earth elements during weathering of a granodiorite. Nature 279, 206-210.

Nesbitt, H.W., Young, G.M., McLennan, S.M., Keays, R.R., 1996. Effects of chemical weathering and sorting on the petrogenesis of siliciclastic sediments, with implications for provenance studies. J. Geol. 104, 525-542.

Ni. Y., Hughes, M., Mariano, A.N., 1995. Crystal chemistry of the monazite and xenotime structures. Am. Mineral. 80, 21-26.

O'Neill, J.M., 1997. Stratigraphic character and structural setting of the Belt Supergroup in the Highland Mountains southwestern Montana. In: Berg, R.B., (ed.), Belt Symposium III, Montana Bureau Min. Geol. Spec. Publ. 117,12-16.

Parrish, R.R., 1990. U-Pb dating of monazite and its applications to geological problems. Can. J. Earth Sci., 27, 1431-1450.

Pesonen, L.J., Elming, Elming, S.-A., Mertanen, S., Pisarevsky, S., D'Agrella-Filho, M.S., Meert, J.G., Schmidt, P.W., Abrahamsen, N., Bylund, G., 2003. Paleomagnetic configuration of continents during the Proterozoic. Tectonophysics 375, 289-324.

Poage, M.A., Hyndman, D.W., Sears, J.W., 2000. Petrology, geochemistry, and diabase-granophyre relations of a thick basaltic sill emplaced into wet sediments, western Montana. Can. J. Earth Sci. 37, 1109-1119.

Poller, U., Gladkochub, D. Donskaya, T., Mazukabzov, A., Sklyarov, E., Todt, W., 2004. New Archean to Proterozoic SHRIMP ages on granulites from the Siberian Craton. Geochim. Cosmochim. Acta 68, A664-A664.

Potts, P.J., Tindle, A.G., Webb, P.C., 1992. Geochemical reference material compositions. In: Whittles, F.L., (ed.), Rocks, Minerals, Sediment, Soils, Carbonates, Refractories and Ores Used in Research and Industry. CRC Press, Boca Raton, Latheronwheel, Caithness, U.K., pp. 220-221.

Pratt, B.R., 2001. Oceanography, bathymetry and syndepositional tectonics of a Precambrian intracratonic basin: integrating sediment, storms, earthquakes and tsunamis in the Belt Supergroup (Helena Formation, ca. 1.45 Ga), western North America. Sediment. Geol. 141, 371-394.

Price, R.A., Sears, J.W, 2000. A preliminary palinspastic map of the Mesoproterozoic Belt-Purcell Supergroup, Canada and USA: implications for the tectonic setting and structural evolution of the Purcell anticlinorium and the Sullivan deposit. In: Lydon, J.W., Höy, T., Slack, J.F., Knapp, M.E., (eds.), The Geological Environment of the Sullivan Deposit, British Columbia. Geol. Assoc. Can. Min. Dep. Div. Spec. Publ. 1, pp. 61-81.

Pyle, J.M., Spear, F.S., Wark, D.A., Daniel, C.G., Storm, L.C., 2005. Contributions to precision and accu-

racy of monazite microprobe ages. Am. Mineral. 90, 547-577.

Ramaekers, P., Catuneanu, O., 2004. Development and sequences of the Athabasca Basin, early Proterozoic, Saskatchewan and Alberta, Canada. In: Eriksson, P.G., Altermann, W., Nelson, D.R., Mueller, W.U., Catuneanu, O., (eds.), The Precambrian: Tempos and Events, Developments in Precambrian Geology 12, Elsevier, Amsterdam, pp. 705-723.

Ramaekers, P., Yeo, G., Catuneanu, O., Jefferson, C.W., Rainbird, R., 2005. Proterozoic to Mesozoic basin development, uranium deposits and heavy oil accumulations, Athabasca region, western Canada. Extech 4.

Rasmussen, B., Fletcher, I.R., McNaughton, N.J., 2001. Dating low-grade metamorphic events by SHRIMP U-Pb analysis of monazite in shales. Geol. Soc. Am., 29, 963-966.

Rhede, D., Wendt, I., Förster, H.J., 1996. A three-dimensional method for calculating independent chemical U/Pb- and Th/Pb-ages of accessory minerals. Chem. Geol. 130, 247-253.

Roaldset, E., 1979. Rare earth elements in different size fractions of marine quick clay from Ullensaker, and a till from upper Numedal, Norway. Clay Miner. 14, 229-239.

Rogers, J.J.W., Santosh, M., 2004. Continents and Supercontinents. Oxford Universy Press, New York, NY, U. S. A.

Roser, B., 1996. Sandstone geochemistry, provenance, and tectonic setting: application of the Al203/SiO2-basicity index diagram to New Zealand sedimentary suites. Earth Sci. 50, 138-147.

Ross, G.M., Villenueve, M.E., 2003. Provenance of the Mesoproterozoic (1.45 Ga) Belt Basin (western North America): another piece in the pre-Rodinia paleogeographic puzzle. Geol. Soc. Am. 115, 1191-1217.

Ross, G.M., Parrish, R.R., Dudás, F.Ö., 1991. Provenance of the Bonner Formation (Belt Supergroup), Montana: insights from U-Pb and Sm-Nd analyses of detrital minerals. Geology 19, 340-343.

Ross, G.M., Parrish, R.R., Winston, D., 1992. Provenance and U-Pb geochronology of the Mesoproterozoic Belt Supergroup (northwestern United States): implications for age of deposition and pre-Panthalassa plate reconstructions. Earth Planet. Sci. Lett. 113, 57-76.

Ross, C.P., Parrish, R.R., Villenueve, M.E., Bowring, S.A., 1990. Geophysics and geochronology of the crystalline basement of the Alberta basin, western Canada. Can. J. Earth Sc. 28, 512-522.

Schandl, E.S., Gorton, M.P., Lydon, J.W., 2000. Trace and rare earth element study of sediments associated with the Sullivan sedex deposit, British Columbia: implications for element mobility and tectonic environment. In: Lydon, J.W., Höy, T., Slack, J.F., Knapp, M.E., (eds.), The Geological Environment of the Sullivan Deposit, British Columbia. Geol. Assoc. Can. Min. Dep. Div. Spec. Publ. 1, pp. 202-217.

Schandl, E.S., Gorton, M.P., 2004. A textural and geochemical guide to the identification of hydrothermal monazite: criteria for selection of samples for dating epigenetic hydrothermal ore deposits. Econ. Geol. 99, 1027-1035.

Scherrer, N.C., Gnos, E., Chopin, Ch., 2000. Retrograde monazite-forming reaction in bearthite-bearing high-pressure rocks. Schweiz. Miner. Petrog. Mitt. 81, 369-378.

Schieber, J., 1993. Sedimentological, geochemical, and mineralogical features of the Belt Supergroup and their bearing on the lacustrine versus marine debate. In: Berg, R.G., (ed.), Belt Symposium III. Montana Bur. Min. Geol. Spec. Publ. 112, pp. 177-189.

Schieber, J., 1997. Sedimentological, geochemical, and mineralogical features of the Belt Supergroup and their bearing on the lacustrine versus marine debate. In: Link, P. K., (ed.), Belt Symposium III, Geologic Guidebook to the Belt-Purcell Supergroup, Glacier National Park and Vicinity, Montana and Adjacent Canada, Belt Association, Pocatello, Idaho, pp. 177-189.

Sears, J.W., Price, R.A., 2000. New look at the Siberian connection: no SWEAT. Geology 28, 423-426.

Sears, J.W., Chamberlain, K.R., Buckley, S.N., 1998. Structural and U-Pb geochronological evidence for 1.47 Ga rifting in the Belt basin, western Montana. Can. J. Earth Sci. 35, 467-475.

Sears, J.W., Price, R.A., Khudoley, A.K, 2004. Linking the Mesoproterozoic Belt-Purcell Supergroup and Udzha Basin across the west Laurentia-Siberia connection. Precambrian Res. 129, 291-308.

Slack, J.F., Höy, T., 2000. Geochemistry and provenance of clastic metasedimentary rocks of the Aldridge and Fort Steele formations, Purcell Supergroup, southeastern British Columbia. In: Lydon, J.W., Höy, T., Slack, J.F., Knapp, M.E., (eds.), The Geological Environment of the Sullivan Deposit, British Columbia. Geol. Assoc. Can. Min. Dep. Div. Spec. Publ. 1, pp. 180-201.

Suzuki, K., Adachi, M., 1991. The chemical Th-U-total Pb isochron ages of zircon and monazite from the Gray Granite of the Hida Terrane, Japan. J. Earth Planet. Sci. 38, 11-37.

Suzuki, K., Adachi, M., 1994. Middle Precambrian detrital monazite and zircon the Hide gneiss on Oki-Dogo island, Japan: their origin and implications for the correlation of basement gneiss of southwest Japan: constraints from CHIME monazite ages of gneisses and granitoids. J. Metamorph. Geol. 16, 23-37.

Taylor, S.R., McLennan, S.M., 1985. The continental crust: its composition and evolution. Blackwell, Oxford, U. K.

Taylor, S.R., McLennan, S.M., 1995. The geochemical evolution of the continental crust. Rev. Geophys. 33, 241-265.

Vearncombe, S., Kerrich, R., 1999. Geochemistry and Geodynamic setting of volcanic and plutonic rocks associated with early Archaean volcanogenic massive sulphide mineralisation, Pilbara Craton. Precambrian Res. 94, 243-270.

Vermeesch, P., 2004. How many grains are needed for a provenance study? Earth Planet. Sci. Lett. 224, 441-451.

Whiple, J.W., Connor, J.J., Raup, O.B., McGrimsey, R.G., 1984. Preliminary report on the stratigraphy of the Belt Supergroup, Glacier National Park and adjacent Whitefish Range, Montana. In: McBane, J.D., Garrison, P.B., (eds.), Northwest Montana and Adjacent Canada, Montana Geol. Soc. Guide-

book, 1984 Field Conference and Symposium, pp. 33-50.

Whipple, J.W., Binda, P.L., Winston, D., 1997. Geologic guide to Glacier National Park, Montana and areas adjacent to Waterton, Alberta. Belt Symposium III. In: Link, P.K., (ed.), Geologic Guidebook to the Belt-Purcell Supergroup, Glacier National Park and vicinity, Montana and Adjacent Canada, Field Trip Guidebook for the Belt Symposium III. Belt Association, Pocatello, Idaho, pp. 125-155.

Windley, B.F., 1995. The evolving continents. Wiley and Sons, New York, NY, U.S.A.

Winston, D., 1984. Sedimentology and stratigraphy of the Missoula Group. In: S. Warren Hobbs, (ed.), The Belt: Abstracts with Summaries, Belt Syposium II, Montana Bur. Min. Geol. Spec. Publ. 90, 30-32.

Winston, D., 1986. Sedimentology of the Ravalli Group, middle Belt carbonate and Missoula Group, Middle Proterozoic Belt Supergroup, Montana, Idaho and Washington. In: Roberts, S.M., (ed.). Belt Supergroup: A Guide to Proterozoic Rocks of Western Montana and Adjacent Areas. Montana Bur. Min. Geol., Spec. Publ. 94, 85-124.

Winston, D., 1989. A sedimentary and tectonic interpretation of the Belt. In: Hanshaw, P.M., (ed.), Middle Proterozoic Belt Supergroup, Western Montana, 28th International Geological Congress, Field Trip Guidebook T334. Am. Geophysical Union, pp. 437-469.

Winston, D., 1990. Evidence for intracratonic, fluvial and lacustrine settings of middle to late Proterozoic basins of Western U.S.A. In: Gower, C.F., Rivers, T., and Ryan, B., (eds.), Mid-Proterozoic Laurentia-Baltica. Geol. Assoc. Can., Spec. Paper 38, 535-564.

Winston, D., Lyons, T., 1997. Sedimentary cycles in the St. Regis, Empire and Helena formations of the middle Proterozoic Belt Supergroup, northwestern Montana. In: Link, P.K., (ed.), Geological Guidebook to the Belt-Purcell Supergroup, Glacier National Park and Vicinity, Montana and Adjacent Canada, Belt Symposium III, Field Trip guidebook, Belt association, Spokane, pp. 21-51.

Wronkiewicz, D.J., Condie, K.C., 1989. Geochemistry and provenance of sediments from the Pongola Supergroup, South Africa: evidence for a 3.0-Ga-old continental craton, Geochim. Cosmochim. Acta 53, 1537-1549.

Xie, Q., Jain, J., Sun, M., Kerrich, R., Fan, J., 1994. ICP-MS analysis of basalt BIR-1 for trace elements. Geostandars Newsletters 18, 53-63.

Yin, A., f, T.K., 1991. Development of normal faults during emplacement of a thrust sheet: An example from the Lewis allochthon, Glacier National Park, Montana: J. Struct. Geol. 13, 37-47.

Yoos, T.R., Potter, C.J., Thigpen, J.L., Brown, L.D., 1991. The Cordilleran foreland thrust belt in northwestern Montana and northern Idaho from COCORP and industry seismic reflection data. Am. Assoc. Petrol. Geol. Bull. 75, 1089-1106.

Young, G.M., 1999. Some aspects of the geochemistry, provenance and palaeoclimatology of the Torridonian of NW Scotland. J. Geol. Soc., 156, 1097-1111.

Zhao, G., Sun, M., Wilde, S.A., Li, S., 2004. A Paleo-Mesoproterozoic supercontinent: assembly, growth and breakup. Earth Sci. Rev. 67, 91-123.

Connecting paragraph from Chapter IV to Chapter V

The geochemical and geochronological study of the Appekunny and Grinnell formations in the Belt-Purcell Supergroup in Chapter IV identified two main features: (1) two rare earth element (REE) patterns, type 1, post-Archean upper continental crust (PA-UCC)-like REE pattern with K enrichment, and type 2, heavy REE enriched relative to light REE when normalized to PA-UCC; and (2) two groups of monazites based on chemical ages and composition. Geochemical features identified were the subject of a wider stratigraphic study in Chapter V.

CHAPTER V

Mobility of REE and HFSE in Basinal Brines of the Mesoproterozoic Belt-Purcell Supergroup, Western North America

Abstract

Trace element analysis and mass balance calculations of the Belt-Purcell Supergroup argillites and sandstones display two systematic rare earth element (REE) patterns throughout the stratigraphic sequence at the three locations studied: type 1 and type 2. Type 1 features K_2O enrichment, having similar REE and multi-element patterns as PA-UCC, variable Th/U and Ce/Ce fractionations, systematic negative anomalies for Nb and Ta, and variable anomalies for Zr and Hf; whereas (2) type 2, is characterized as having relative enrichment of HREE relative to LREE when normalized to PA-UCC, high field strength elements (HFSE; Zr, Nb, Ta, Nb), and HFSE/REE fractionations, coupled with enrichments of U, Ag, Mo, and/or Sb. Both type 1 and 2 display convex-up pattern for MREE. Negative Eu anomalies, and pronounced depletion of Sr, CaO, and Na_2O, are interpreted as due to intense provenance weathering. A caveat is that there may be a continuum between type 1 and 2 patterns, but they are treated separately for purposes of mass balance. Low SiO_2 contents and negative anomalies of Zr-Hf in type 1 argillites could be linked to airborne removal.*

Post-depositional potassic addition has been described previously as a widespread feature in many Precambrian siliciclastic sedimentary sequences, but not HREE enrichment or HFSE fractionations. Provenance, weathering, and sorting signatures do not explain the latter.

Presence of halite and gysum casts, and other evidence of evaporites in the Belt-Purcell sequence are commensurate with dissolution of evaporitic units generating oxidized-alkaline diagenetic basinal brines that advected through the Belt-Purcell rocks. Episodic migration of basinal brines through other Paleoproterozoic sedimentary sequences has been described where local enrichments of HREE and HFSE fractionations are present. Accordingly, type 1 and 2 REE patterns argillites and sandstones in the Belt-Purcell Supergroup are interpreted as due to diagenetic processes. Cerium anomalies coupled to Th/U variability is consistent with oxidizing fluids. During these diagenetic processes Al_2O_3, Th, W, and Ga seem to have behaved isochemically.

Illite alteration is interpreted as the product of potassium metasomatism of type 1 argillites and sandstones, whereas diagenetic monazites are interpreted as reflecting redistribution of REE and HFSE by basinal brines that caused type 2 REE pattern.

5.1 Introduction

Rare earth elements (REE), Th, Y, Co, and Sc are in many cases conserved when transferred from provenance areas into many siliciclastic sedimentary sequences, and accordingly have been used broadly to address provenance of sediments (e.g., Taylor and McLennan, 1985, 1995). However, some studies describe processes that influence the fractionation of trace elements during transfer into the sedimentary budget: weathering, sedimentary sorting, and locally during diagenesis (McDaniel et al., 1994; Nesbitt, 2003; Fralick, 2003; McLennan et al., 2003; Rudnick and Gao, 2004).

Kyser and coworkers have shown that a protracted history of episodic basinal brine migration occurred in the Paleoproterozoic Athabasca and McArthur River basins, over hundreds of million years, and that U, Y, and REE may have been mobilized by these brines (Fayek and Kyser, 1997; Kyser et al., 2000). A recent reconnaissance geochemical study of argillites of the Mesoproterozic Belt-Purcell Supergroup revealed a population of samples with REE patterns comparable to post-Archean upper continental crust (PA-UCC; cf. Taylor and McLennan, 1995), whereas other samples are characterized by a pronounced enrichment of HREE relative to PA-UCC and fractionation of high field strength elements (HFSE; González-Álvarez et al., 2003).

This Chapter reports an extensive database of major and trace elements for siliciclastic rocks at three locations in the Belt-Purcell Supergroup to further evaluate the characteristics and scale of element mobility during diagenesis. It builds on the previous reconnaissance study, Chapter IV, that addresses the provenance of the Belt-Purcell Supergroup from geochemical data on argillites (a combination of siltite, mudstone, and very fine-grained sandstone) and sandstones (mainly quartzarenites, subarkoses, and sublitharenites; terminology of Folk, 1968), and detrital and secondary monazite chemical ages (Chapter IV; González-Álvarez et al., *in press*). The nature of the formation brines is addressed by comparison to modern brines with high aqueous solubility of REE and HFSE, and in conjunction linking brine activity to post-depositional secondary monazite chemical ages.

5.2 Geologic setting

This Mesoproterozoic sedimentary sequence has been named the Belt Supergroup in the United States, whereas its Canadian counterpart is referred to as the Purcell Supergroup (Fig. 5.1). The preserved Belt-Purcell Supergroup is a remnant of an extensive intracontinental rift system

that developed by extensional faulting at ~1500 Ma (Hoffman, 1991; Ross et al., 1991; Chandler, 2000; Price and Sears, 2000).

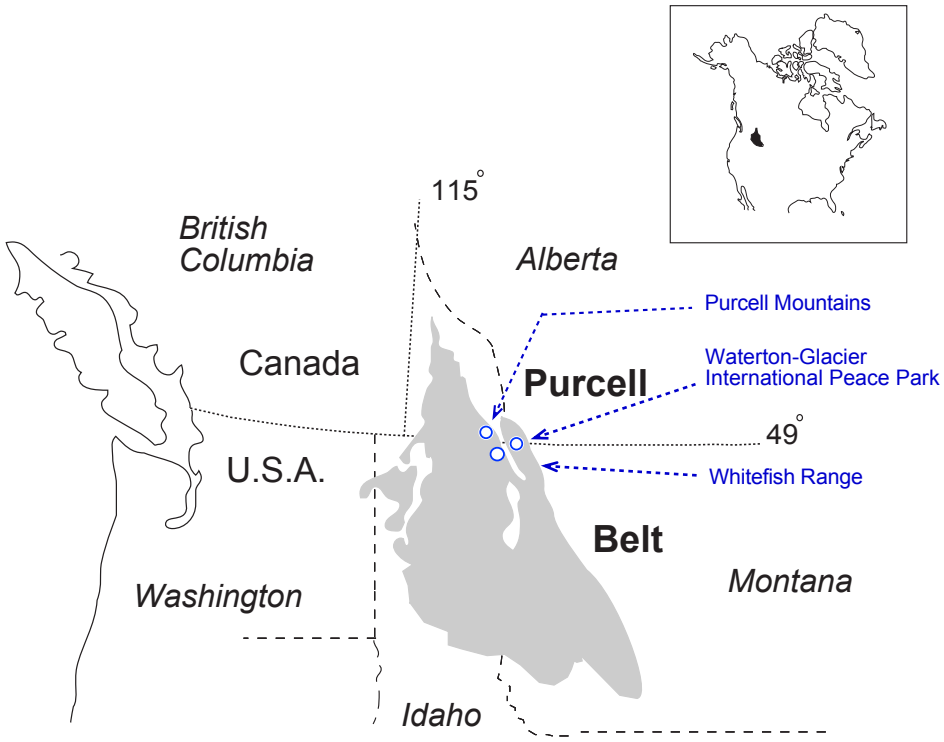

Fig. 5.1 Geographic extent of the Belt-Purcell Supergroup spanning the Canada-USA border and locations of the three areas sampled in the present study.

The Belt-Purcell Supergroup has been divided into four major stratigraphic divisions (Fig. 5.2). (1) The lower Belt-Purcell, mainly fluvial to deltaic and fine-grained marine turbiditic facies, deposited in the northwest of the basin, and up to ~12 km thick (e.g., McMechan, 1981; Cook and Van Der Velden, 1995; Lydon et al., 2000). (2) The lower Belt grades upwards into the Ravalli Group, composed dominantly of fine-grained siliciclastic facies, shales and argillites, with interbedded medium to coarse sandstone more developed in the upper part of the sequence. The depositional setting of the Ravalli Group has been interpreted by Winston (1986, 1990) as prograding alluvial aprons, playas and sheet-floods, whereas for the northwest of the basin McMechan (1981) describes the setting as subtidal to intertidal. (3) In turn, the Ravalli Group grades upwards into the middle Belt-Purcell carbonate, represented by mid-shelf limestones (Pratt, 2001). (4) The stratigraphically highest Missoula Group of the upper Belt-Purcell sequence comprises siliciclastic facies that have been interpreted as mainly alluvial (e.g., Whipple et al., 1984, 1997).

Sears et al. (2004) viewed the large volume of siliciclastic detritus as reflecting fluvial transport from a low relief, continent-scale catchment. Lower units were deposited during active rifting, whereas the upper Belt-Purcell is considered to record basinal subsidence from thermal contraction of the lithosphere (Sears and Price, 2000; Lydon, 2000). Stratigraphically, the Belt-Purcell Supergroup thickens to the west and southwest reaching a maximun of ~17 km (Fig. 5.2; e.g., Harrison, 1972; Whipple et al., 1984). Four main source areas are considered to have contributed sediment; from the Trans-Hudson orogen to the east, south from the Dillon Block (Wyoming Craton and the Great Falls Tectonic Zone), from the Mojave or/and Yavapai Province for the Missoula Group, and from an unknown craton to the west, possibly Siberia or Australia (e.g., Ross and Villeneuve, 2003; Sears et al., 2004). The eastern source, contributing mainly sandstones in the Belt-Purcell sequence, interfingers stratigraphically to the west with argillites derived from the western source (e.g., Frost and Winston, 1987; Winston, 1990).

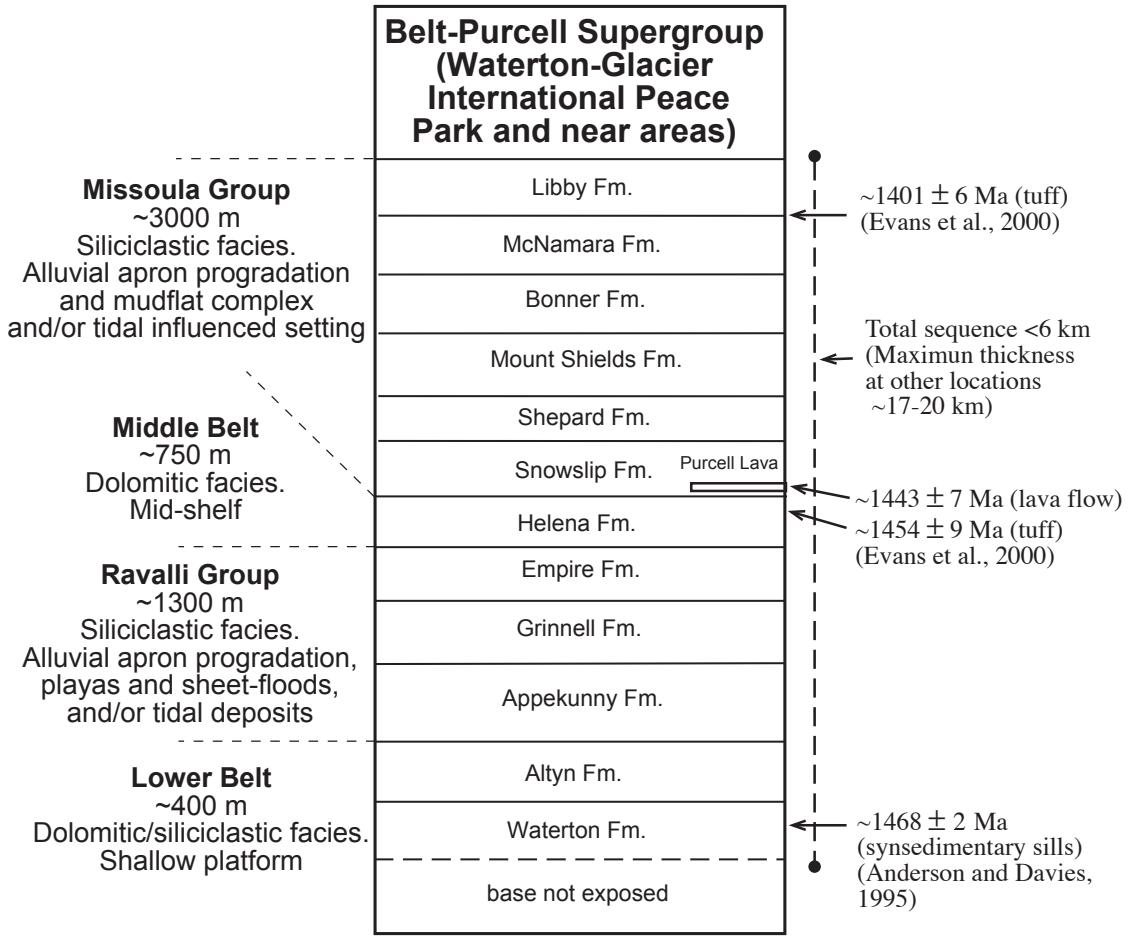

Fig. 5.2 Generalized stratigraphic section of the Belt-Purcell Supergroup at Waterton-Glacier International Peace Park (based on Whipple et al., 1984, 1997).

The duration of sedimentation for the Belt-Purcell Supergroup was ≤75 Ma. A minimum age of sedimentation is estimated at 1468 ± 2 Ma and 1469 ± 3 Ma by U-Pb from zircons in sills located near the base of the Belt-Purcell sequence. This age excludes hidden strata below the Aldridge Formation and above the basement (Lydon, 2000). This sill intruded the sediment when it was still soft, constraining early sedimentation of lower Belt-Purcell strata (Fig. 5.2; Anderson and Davis, 1995; Sears et al. 1998). A maximum age of 1401 ± 6 Ma was obtained from U-Pb dating of zircons extracted from a tuff horizon in the Bonner and Libby formations, of the upper Missoula Group (Fig. 5.2; Evans et al., 2000).

The Belt-Purcell Supergroup records a range of metamorphic conditions from sub-greenschist facies in the northeast, where sampling was conducted, to amphibolite facies in the southwest (Maxwell and Hower, 1967; Harrison, 1972). According to Lydon (2000) three tectonic-thermal events are recorded in the Supergroup: (1) intracontinental rift systems at ~1500 Ma accompanied by heat flow during thinning of lithosphere; (2) extensional events during the breakup of Rodinia at 900 Ma; and (3) the Jurassic-Paleocene (160 to 60 Ma) Laramide event of the North American Cordillera when the Belt-Purcell Supergroup was displaced eastward by thrusting. Rifting at ~1500 Ma may be associated with dispersal of the postulated Mesoproterozoic supercontinent Columbia (e.g., Zhao et al., 2004).

Petrographically, the argillites are fine-grained quartz, plagioclase, and K-feldspar in a matrix of smectite, illite-micas, and/or chlorite depending of the startigraphic level (Maxwell and Hower, 1967; Harrison, 1972; Frost and Winston, 1987; Lydon, 2000; Lydon et al., 2000). Sandstones have the same matrix assemblage as argillites, variably diluted by coarse-grained quartz (~50%), plagioclase (~7%), and K-feldspar (~1%).

5.3 Sampling and analytical techniques

A total of ninety-three siliciclastic rock samples, representative of all formations of the Belt-Purcell Supergroup, were collected from outcrops at three locations: Waterton-Glacier International Peace Park (n=37), the Whitefish Range (n=29), and the Purcell Mountains (n=27), in northern Montana, southwestern Alberta, and southeastern British Columbia respectively (Fig. 5.1). This sample suite includes areal extent and stratigraphic coverage of all Belt-Purcell formations (Fig. 5.3). Samples were collected to represent argillite and sandstone facies to address potential geochemical differences based on sorting effects and/or different source areas. Subsets of 25, 24, and 27 were selected from the three localities for this study based on low values of LOI.

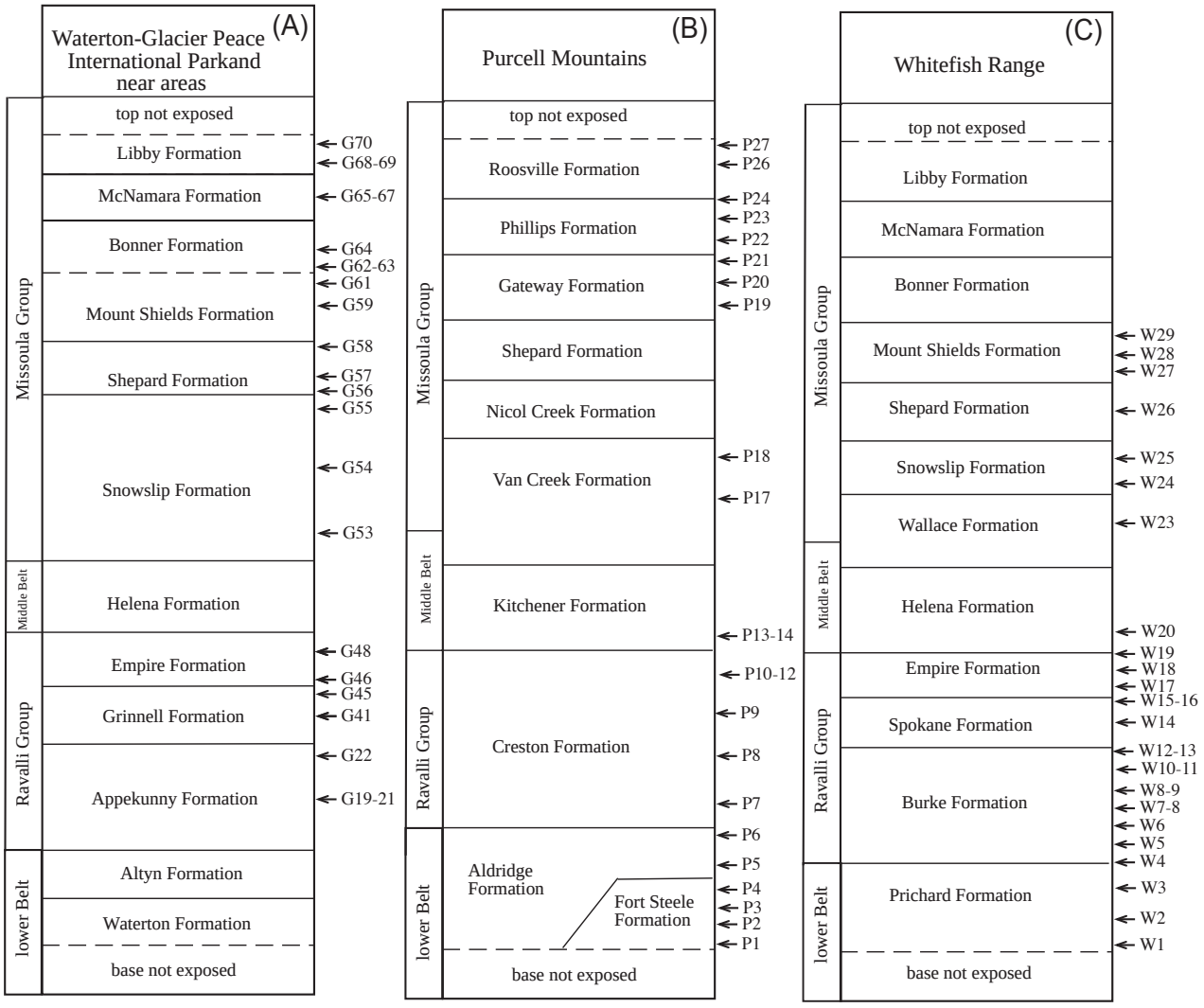

Fig. 5.3 Stratigraphic position of samples taken for this study at the three locations cross-referenced to Appendix 5.1a, b, and c.

Major elements were determined using X-ray fluorescence spectrometry (XRFS) at the Société Générale de Surveillance (SGS) Laboratories (XRAL Laboratories, 1885 Leslie St., Don Mills, Ontario M2B 3J4, Canada). Precision is ±0.01 wt.%. Trace elements, including REE and HFSE, were analyzed using inductively coupled plasma-mass spectrometry (model Perkin Elmer Elan 5000) at the University of Saskatchewan. To address potential problems stemming from incomplete dissolution of refractory minerals, the procedure of Jenner et al. (1990) was followed, whereby a sodium peroxide sinter was used for analyses of Th, Nb, Ta, Zr, Hf, Y, Sc, and REE, and an HF-HNO_3 digestion on a separate aliquot was used for the remaining trace elements. Detailed

analytical methodology is presented in Fan and Kerrich (1997). Included are standard additions, pure elemental standards for external calibration, and data for modern lake sediment samples representative of various locations within the Canadian Shield (LKSD-1), and basalt (BCR-2) as reference materials. LKSD-1 was used as a reference material, inasmuch as the REE and HFSE contents are comparable to those in the argillites analyzed. Long-term reproducibility in this lab for the low-level reference material basalt (BCR-1) is given in Table 5.1, excerpted from Xie et al. (1994).

Table 5.1 ICP-MS multi-element analysis of international reference material basalt BCR-1 for selected trace elements by the University of Saskatchewan ICP-MS laboratory (excerpted from Xie et al., 1994).

Elements	x	1σ	C%	CV
Zr	201	12	6	190
Nb	14.6	0.7	4.8	14
La	26	0.8	3.1	24.9
Pr	6.95	0.33	4.7	6.8
Eu	1.95	0.11	5.6	1.95
Ho	1.26	0.05	4	1.26
Tm	0.54	0.02	3.7	0.56
Lu	0.502	0.02	4	0.51
Hf	5.87	1.49	8.3	4.95
Ta	1.03	0.16	15.5	0.81
Th	6.7	0.52	7.8	5.98
U	1.75	0.1	5.7	1.75

(x) Average; (1σ) standard deviation; (C%) relative standard deviation; (CV) compiled values from Potts et al. (1992).

Detection limits (in ppm) defined as 3Sigma of the calibration blank for some critical elements are as follows: Nb (0.016), Hf (0.042), Zr (0.103), La (0.018), Ce (0.014), Nd (0.086), and Sm (0.065). Wet chemistry operations were conducted under clean laboratory conditions. Analyses of acids, distilled deionized water and procedural blanks give levels of <1 ppb for REE, Nb, Zr, and Hf, relative to their concentration in the rocks (Xie et al., 1994).

Values of Ce/Ce* and Eu/Eu* were calculated relative to values for average post-Archean upper continental crust of Taylor and McLennan (1995), following Taylor and McLennan (1985).

5.4 Analytical results

Based on petrographic observations and SiO_2-loss on ignition (LOI) relationships, for this study of diagenetic trace element mobility, two facies were differentiated (argillites and sandstones) from which only samples with <10 wt.% LOI were used to avoid dilution effects (see Chapter III, *section 3.1*): (1) sandstones, (>75 wt.% SiO_2, <10 wt.% LOI), and (2) argillites (<75 - 50 wt.% SiO_2, <10 wt.% LOI (Fig. 5.4a; Appendices 5.1a, b, and c).

From inspection of diagrams of REE normalized to PA-UCC, argillites were divided into three different patterns: type 1, PA-UCC-like REE pattern, having similar REE and multi-element patterns as PA-UCC, albeit at 0.8 to 1.5 times PA-UCC due to less/more quartz and pronounced depletions of Ca and Na, and average type 1 which has more REE than PA-UCC; type 2, variably heavy REE (HREE) enriched relative to light REE (LREE) normalized to PA-UCC; and type 3, displaying erratic REE patterns combined with variable anomalies at Zr-Hf normalized to PA-UCC (Figs. 5.5 and 5.6). Type 3 is only briefly considered due to its lack of systematic pattern. Types 1 and 2 share negative Eu anomalies. The same three types of pattern characterize sandstones; pattern 2 is prevalent in both facies. A convex-up pattern for MREE with a negative Tb anomaly occurs in most of the samples that is not due to monazite content; these features are not present in PA-UCC, post-Archean Australian average shale (PAAS), or North American Shale Composite (NASC; Taylor and McLennan, 1995), and are the subject of an ongoing study (Figs. 5.5c and 5.6c).

5.4.1 Argillites

The two REE patterns are present in the argillites, consistently from each of the three locations sampled, and throughout their stratigraphic sequences. Type 1 is flat at 0.8 to 1.5 times PA-UCC, with abundances related to modal quartz. Multi-element normalized diagrams show: (1) addition of K_2O; (2) pronounced depletion of Sr, CaO, and Na_2O; (3) variable Th-U (1.3 to 6.2), and Ce/Ce* (0.95 to 0.99) fractionations; (4) systematic negative anomalies for Nb and Ta; and (5) variable anomalies for Zr and Hf. (Fig. 5.5b; Appendices 5.1a, b, and c). In a correlation matrix the main features are that Al_2O_3 correlates weakly with LREE and MREE (r^2 = ~0.45), and Sc, V, Cr, and Ga (r^2 = >0.80). The Al-REE relationship is consistent with earlier studies showing that the REE budget of fine-grained siliciclastic rocks is associated with the clay fraction (Cullers et al., 1979; Taylor and McLennan, 1985). Nb-Ta and Zr-Hf are unfractionated, correlating strongly as element pairs (r^2 >0.90), with crustal ratios of 11 and 34, respectively (cf. Rudnick and Gao, 2004).

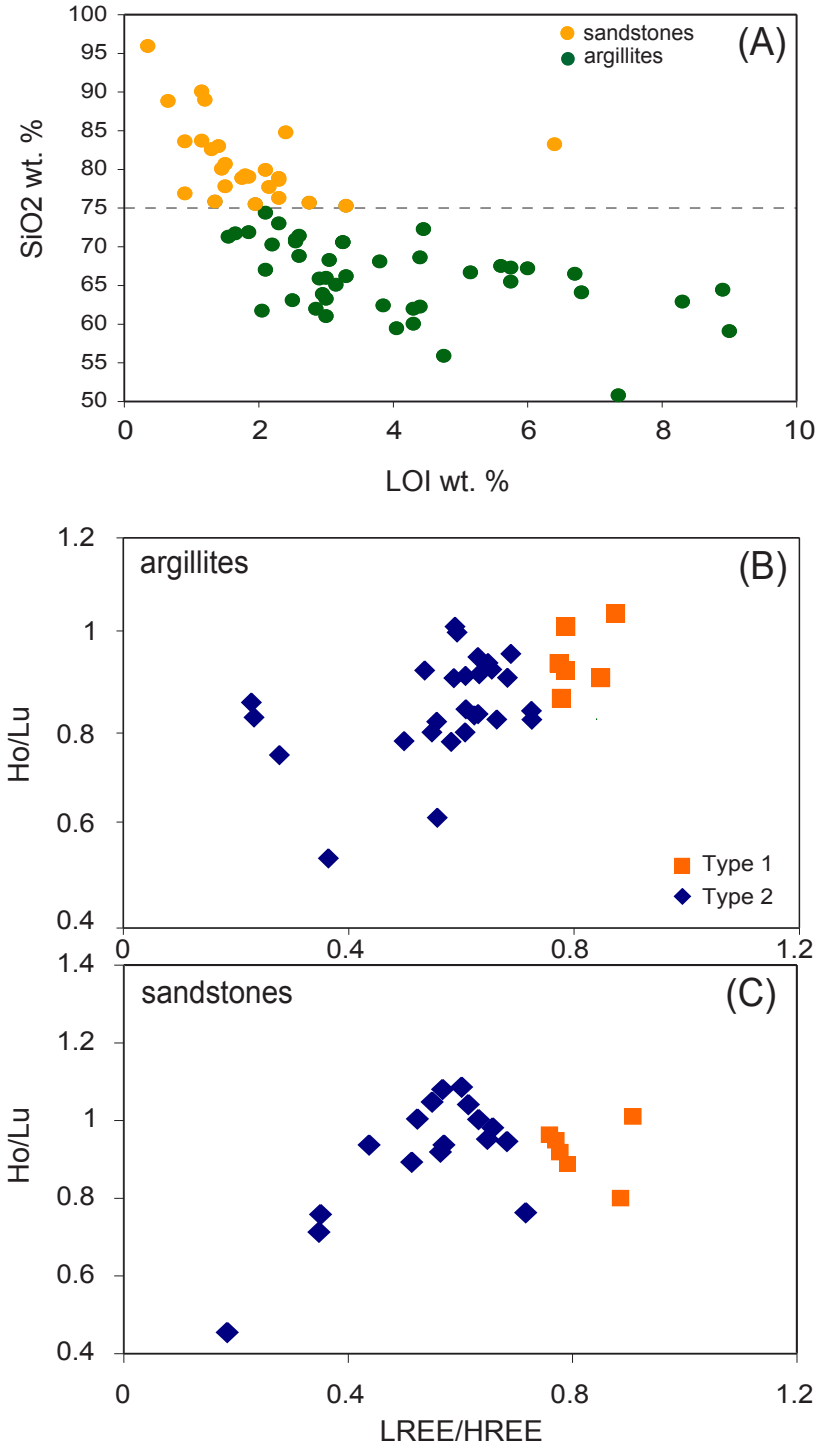

Fig. 5.4 (A) Plot of SiO_2 versus LOI (loss-on-ignition) separating two different facies: (1) sandstones, and (2) argillites; (B) and (C) ∑LREE/∑HREE versus Ho/Lu normalized to post-Archean upper continental crust (PA-UCC; from Taylor and McLennan, 1995).

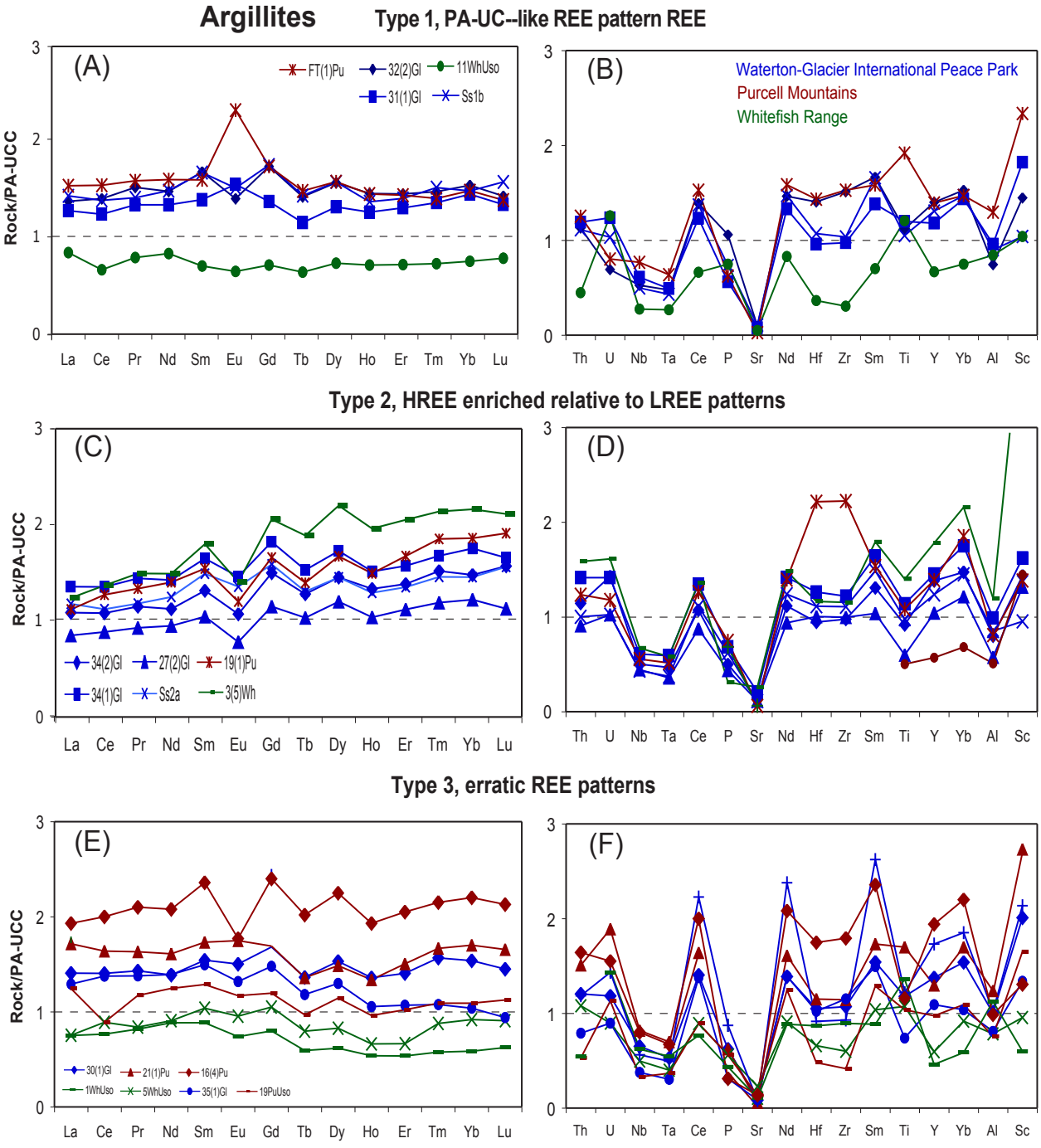

Fig. 5.5 (A), (C), and (E) REE plots and multi-element diagrams (B), (D), and (F) for argillites at Waterton-Glacier International Peace Park, Purcell Mountains and Whitefish Range showing Type 1, PA-UCC-like REE patterns, type 2, HREE enrichment relative to LREE, and type 3, erratic REE patterns. All graphs are linear and normalized to PA-UCC (Taylor and McLennan, 1995).

Type 2 argillites are enriched in HREE relative to LREE and present the same major and trace element features as type 1, with the exception of variable enrichment of HREE relative to LREE, and REE have a higher correlation coefficient with alumina that increases from LREE (r^2 = ~0.5) to HREE (r^2 = ~0.6). Only V and Ga correlate to Al_2O_3, and As and Sb are highly correlated (r^2 = 0.9).

Low contents of Ca, Na, and Sr relative to PA-UCC are a common feature of modern large-river systems draining intensely weathered areas (Gaillardet et al., 1999), and are indicative of intense weathering of the source terrane of the Belt-Purcell Supergroup (see Chapter VII; González-Álvarez and Kerrich, *submitted*).

5.4.2 Sandstones

From petrographic observations, sandstones are variable dilution of a clay-size fraction by dominantly quartz, plus minor plagioclase and K-feldspar (<10%). That dilution effect is also broadly present for Th and REE. Sandstones having type 1 patterns share many of the major and trace element patterns of type 1 argillites, albeit at lower absolute abundance due to addition of quartz. Common type 1 patterns in sandstones and argillites endorses the result of the previous more limited study of the Appekunny and Grinnell formations at Waterton-Glacier International Peace Park, that compositionally sandstones are argillites diluted by quartz, such that neither sorting or heavy minerals control the REE budget (Chapter IV; González-Álvarez et al., *in press*; Fig. 5.6).

Alumina correlates strongly with REE (r^2 >0.80 and >0.74), as well as with Ti and Sc (r^2 >0.85 and r^2 >0.61), for types 2 and 1 respectively. Type 1 sandstones show a strong correlation of REE with Sb, Pb, Th, and Y (r^2 >0.80), whereas type 2 does not.

5.5 Discussion

A recent study of the Appekunny and Grinnell formations in Waterton-Glacier International Peace Park evaluated Archean versus Proterozoic provenance (Ravalli Group; Fig. 5.2). Argillites characterized by REE patterns close to PA-UCC also have Cr-Ni and Th/Sc-Sc systematics plotting in the post-Archean field of Taylor and McLennan (1985, 1995), and detrital monazite ages are ~1800-1600 Ma (González-Álvarez et al., *in press*). Other studies describe multiple sources for the Belt-Purcell sequence as mostly Paleoroterozoic sources, with minor Archean contributions for the stratigraphic location of this study (e.g., Frost and Winston, 1987; Slack and Höy, 2000; Ross and

Villeneuve, 2003). The geochemical characteristics of type 1 argillites, endorses a predominantly Proterozoic catchment for the Belt-Purcell Supergroup at the three locations sampled.

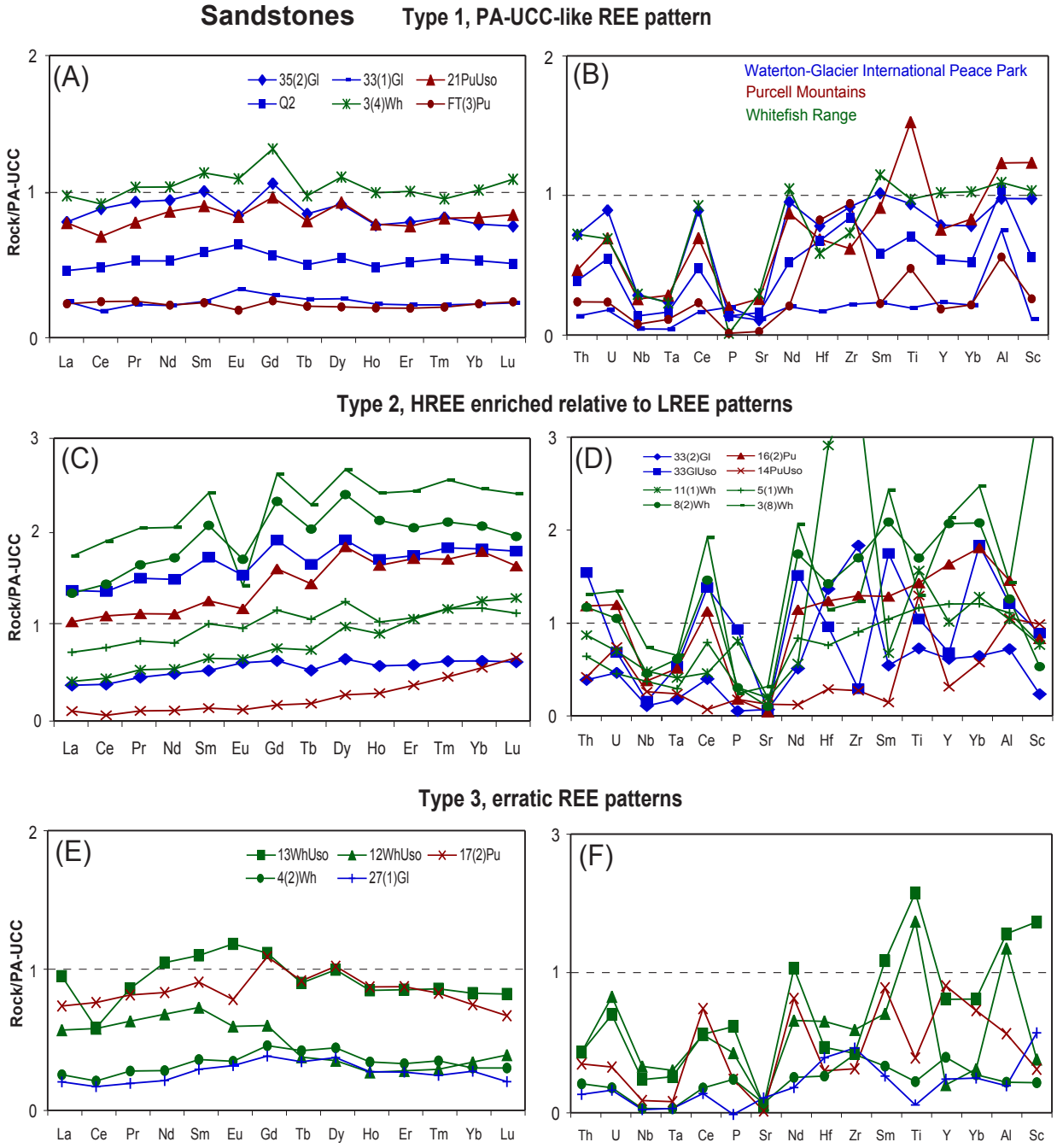

Fig. 5.6 (A), (C), and (E) REE plots and multi-element diagrams (B), (D), and (F) for sandstones at Waterton-Glacier International Peace Park, Purcell Mountains and Whitefish Range, displaying types 1, 2 and 3 REE patterns. All graphs are linear and normalized to PA-UCC (Taylor and McLennan, 1995).

Type 1 and 2 patterns could be considered as a continuum of REE compositions in argillites and sandstones (Figs. 5.5 and 5.6). However, in order to simplify the discussion and mass balance calculations they are considered as two different populations for each facies. Enrichment of HREE relative to LREE of type 2 patterns could result from a number of possible processes including provenance characteristics, weathering, sedimentary sorting, or diagenesis.

5.5.1 Provenance

In terms of provenance, there are two rock types that feature systematic normalized enrichment of HREE relative to LREE: boninites and low-Ti tholeiites. Boninites were initially identified in recent oceanic arcs, such as the Izu-Bonin-Mariana arc of the southwest Pacific, but have now been documented from Proterozoic and Archean greenstone terranes (Crawford et al., 1989; Kerrich et al., 1998; Wyman, 1999; Polat et al., 2002; Smithies et al., 2003). Boninites are characterized by U-shaped REE patterns that are thought to arise from a two-stage melt history. Stage one involves high degree melt extraction leaving a residue more depleted than mid oceanic ridge basalts (MORB), and chondrite normalized LREE<MREE<HREE. Stage two involves hydrous fluxing of the residue by LREE, and incompatible element- enriched fluids in a convergent margin. Boninites are enriched in Cr, Co, Ni, and LREE, compositional features not found in the Belt sedimentary rocks. Low-Ti tholeiites, like boninites, also have a two-stage history, but in which the second stage is anhydrous, such that these basalts are depleted in the order chondrite normalized LREE<MREE<HREE (Brown and Jenner, 1989). Low-Ti tholeiites share the high contents of Cr, Co, Ni with boninites. Boninites and low-Ti tholeiites are rare, and accordingly an unlikely cause of HREE enriched argillites that possess Cr, Co, and Ni abundances comparable to PA-UCC.

5.5.2 Weathering

Studies of soil-protolith profiles have identified fractionation of REE in regoliths relative to the parent rock. Overall, saprolite is generally enriched in total REE (Duddy, 1980), in which the REEs are fixed in secondary phosphate and clay minerals (Braun et al., 1993). In detail, there is enrichment of LREE but depletion in HREE due to preferential removal of HREE by complexation reactions involving inorganic and/or organic ligands (e.g, Braun et al., 1993). The top horizon of the saprolite develops a positive Ce anomaly due to crystallization of cerianite (Braun et al., 1990; Marsh, 1991). Such effects are not present in PA-UCC, Post-Archean Australian shale (PAAS) or North American shale composite (NASC), which integrate all weathering-transport-diagenetic effects over many catchment-basin systems (Taylor and McLennan, 1985; 1995; Rudnick and Gao,

2004), nor are such fractionations present in argillites of this study (Figs. 5.4 and 5.5).

There are no correlations of REE, REE fractionations, or REE/HFSE fractionations with the chemical index of alteration (CIA; Nesbitt and Young, 1982) corrected for K-addition (Fedo et al., 1995), which ranges from 57 to 81 (Kerrich and González-Álvarez, 2004; González-Álvarez and Kerrich, *submitted*; see Chapter VII).

5.5.3 Sedimentary sorting

Potentially, sedimentary accumulation of minerals enriched in HREE could generate the observed type 2 patterns. Zircon is the most likely candidate, having normalized HREE>MREE>LREE. The Zr budget of type 1 argillites is likely determined by zircon, given a correlation coefficient of 0.85 for Zr and Yb. However, the absolute content of Zr in type 1 and 2 argillites is comparable, but the Zr-Yb correlation is lower at 0.6 for the latter, ruling out zircon accumulation as the cause of HREE enrichment. Rare positive Zr-Hf peaks are discussed below (Fig. 5b, d, and f). The presence of xenotime (YPO_4) in sufficient amount could be the responsible of type 2 REE pattern due to xenotime HREE content. However, xenotime was less than one in one hundred heavy minerals identified in the electron backscatter surveys, and HREE and phosphate content in type 2 REE pattern display no correlation ($r^2<0.20$). Collectively, these observations suggest that xenotime does not control type 2 REE pattern. The presence of types 1 and 2 patterns in both argillites and sandstones further eliminates sorting as a cause of HREE enrichment. Systematic negative anomalies at Nb-Ta, that are larger in sandstones than argillites, are interpreted as reflecting hydraulic sorting of heavy minerals, commensurate with the higher energy depositional environment of the former (Figs. 5.5, 5.6b, d and f).

Type 1 argillites display lower SiO_2 values and some samples with negative anomalies of Zr-Hf. Rudnick and Gao (2004) linked these two features observing that quartz and zircon grains are preferentially transported into loess. Based on this, type 1 argillites could in part be due to airborne removal of fines. Positive Eu anomalies in a few sandstones are interpreted as local accumulations of detrital plagioclase feldspar (Appendices 5.1a, b and c). There is no correlation between Al_2O_3 and Eu/Eu*, therefore plagioclase does not contribute significantly to the alumina budget which from petrographic observations is dominantly in illite-micas and chlorite.

In summary, notwithstanding multiple potential source areas, and varied intensities of weathering (Chapter VII; González-Álvarez and Kerrich, *submitted*), types 1 and 2 REE patterns are consistently present throughout all the Belt-Purcell sequence in both argillites and sandstones.

Based on the lines of evidence presented above, types 1 and 2 REE pattern are an intrinsic feature of the provenance and diagenetic histories of the Belt-Purcell Supergroup. Type 2 has not been reported before in any Proterozoic siliciclastic sequence. Different provenance (e.g., Ross and Villeneuve, 2003; Slack and Höy, 2000) or lithologiies, variable weathering intensities, or local diagenetic REE mobility, can all be ruled out as the cause type 2 patterns. Therefore, type 2 argillites and sandstones, characterized by HREE enrichment relative to LREE, stem from diagenetic mobility of REE as discussed below.

5.5.4 Diagenetic mobility of REE and HFSE

Taylor and McLennan (1985, 1995) have shown that for many siliciclastic sequences REE, Th, Sc, and Co are quantitatively transferred from the catchment into the sedimentary budget given low aqueous solubility of these elements. In general, Al, Ti, LREE, HFSE, Y, and Sc behave isochemically during hydrothermal activity and metamorphism (Fryer et al., 1979; Humphries, 1984; Terakado and Fujitani, 1998). These elements may fractionate in sedimentary systems under certain local conditions: (1) during diagenesis at the sediment-water interface; (2) by detrital/biogenic dissolution; or (3) during the breakdown of unstable detrital facies like volcanic debris (McDaniel et al., 1994; McLennan et al., 2003).

In type 2 argillites and sandstones, at low REE-HFSE concentrations Nb, Ta/MREE and Zr, Hf/MREE anomalies are coherent, and Nb/Ta and Zr/Hf ratios maintain PA-UCC ratios of 11 and 34, respectively (Taylor and McLennan, 1995; Rudnick and Gao, 2004). At higher HREE abundances, however, Th/U, Nb/Ta, Zr/Hf, Ti/Sm, and HREE/Al ratios are all erratic. Relative to PA-UCC ratios, Th/U ratios are mostly <5 consistent with the addition of U given probable low Th solubility (Fig. 5.7b; cf. Pearce and Peate, 1995). Ratios of Nb/Ta are >11, whereas Zr/Hf ratios scatter about the PA-UCC value of 34 (Fig. 5.7a; Appendices 5.1a, b, and c). As argued above, correlation of Zr with $(Gd/Yb)_{cn}$, and Zr/Hf ratios averaging 34, in type 1, argillites is consistent with zircon dominating the Zr budget. Magmatic zircons have a narrow range of Zr/Hf ratios from ~37 to 68 (e.g., Murali et al., 1983), whereas erratic Zr/Hf ratios have been reported for hydrothermal and authigenic zircons (Kerrich and King, 1993; *section 5.7*). Consequently, erratic Zr/Hf ratios in types 2 and 3 likely result from differential behaviour of Zr and Hf during diagenesis.

Yttrium and Ho, like Zr-Hf, behave coherently during most geological processes. The primitive mantle, PAAS, and PA-UCC all have a Y/Ho value of 27 (Sun and McDonough, 1989; Taylor and McLennan, 1995; Rudnick and Gao, 2004). Argillites with type 1 REE patterns show Y/Ho close to 27. In contrast, for samples characterized by HREE enrichment relative to LREE, Y/Ho ra-

tios vary from ~23 to ~32 (Fig. 5.7b). Modern seawater has a range of Y/Ho ratios from 44-74 due to differential adsorption of Ho onto Fe-Mn oxyhydroxides (Nozakui et al., 1997). However, Fe_2O_3 does not correlate with Y/Ho or Eu/Eu* (cf. Kamber and Webb, 2001). Accordingly, scattered Y/Ho ratios and Zr-Hf fractionations in HREE enriched samples are all interpreted as stemming from their mobility due to processes that involved basinal brines.

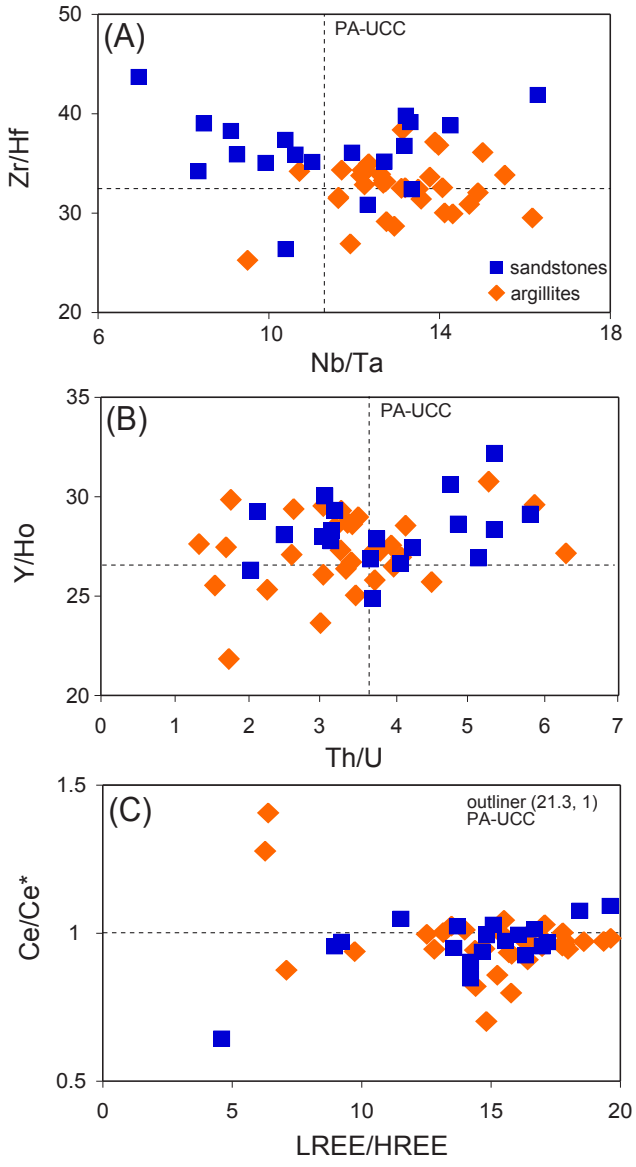

Fig. 5.7 Plots for HREE enriched argillites and sandstones. (A) Zr/Hf versus Y/Ho displaying higher values for both ratios than PA-UCC mostly seen in the sandstone population. (B) Nb/Ta versus Th/U. (C) LREE/HREE versus Ce/Ce presenting mainly negative Ce anomalies and lower LREE/HREE ratios than PA-UCC.*

5.5.5 Ce anomalies

Cerium and Eu are sensitive to redox conditions (e.g., Humphries, 1984; De Baar et al., 1985). Cerium anomalies are not present in either chondrite normalized PA-UCC or PAAS (Taylor and McLennan, 1985), but negative anomalies may occur in some pelagic sediment (Plank and Langmuir, 1998). Variable Ce anomalies are present in many Belt-Purcell argillites with type 2 HREE enrichment (Ce/Ce*= ~1.1-0.8, with two outliners at 1.2 and 1.4; Fig. 5.7c), and some sandstones (Ce/Ce*= ~1.1-0.9). These anomalies could be due to oxidized diagenetic brines, but there is no correlation of Ce/Ce* with LREE/HREE or U.

Weathering may generate positive or negative Ce anomalies, depending on the Ce-phase (e.g., Braun et al., 1990; Marsh, 1991; Mongelli, 1993; Morey and Setterholm, 1997). Slack and Höy (2000) studied 110 sedimentary rocks of the Aldridge and Fort Steele Formations, and found negative Ce anomalies in only four outcrop samples all of which were moderately weathered; none of their 41 unweathered sedimentary samples collected from drill cores have negative Ce anomalies (Fig. 5.7c). They did not describe type 2 patterns of this study with variable HREE enrichment and REE/HFSE fractionations or enrichment of U. Samples for this study were selected to be unweathered; where a weathered surface was present on a specimen it was sawed off prior to analysis. Cerium is mobile in oxidizing fluids, as is U (Humphries, 1984). Consequently, the variably negative Ce anomalies and U variability reflected as scattered Th/U ratios from ~1 to ~10 compared to 3.8 PA-UCC, are consistent with oxidized diagenetic fluids.

5.5.6 Mass balance

It is useful to evaluate the relative gains or losses of elements during the formation of types 1 and 2 patterns. Gresens (1967) developed a set of equations that allows calculation of gains and losses of chemical analyses following open-system alteration of a precursor lithology. For bulk rock the mass balance is calculated using the expression:

$$100[f_v(g_b/g_a)c_{nb}-c_{na}]=x_n \quad (5.1)$$

Where f_v is the volume factor, or the amount by which the volume on the left part of the equation has to be multiplied in order to obtain the volume on the right side; g_b/g_a is the relation between the specific gravities of the product *(b)* and precursor *(a)* lithologies; cnb and cna are the amounts of a specified chemical element in *(a)* and *(b)*; and x_n is the total amount of element *n* lost

or gained in the process. The amounts are represented as g/100g of the precursor. From mineralogical considerations it is assumed that g_a/g_b was close to 1. Gresens (1967) showed that in any chemical transformation the ratios of isochemical elements in the precursor and product are uniform.

The principle of these equations has been widely used to describe metasomatic alteration in sedimentary and hydrothermal systems (e.g., Kerrich, 1983; Grant, 1986; Braun et al., 1993; Mori et al., 2003). Hence, chemical mass balance calculations have been used to quantify mass transfer across the alteration of different possible diagenetic stages displayed by different trace element patterns in the Belt-Purcell rocks.

Given that the average of type 1 argillites plots parallel and close to 1 referenced to PA-UCC, that reference composition was used for mass balance to type 1, argillites. A second mass balance was conducted of type 1 average to the average composition of argillites having type 2 REE patterns.

Ratios of Al, Th, W, and Ga relative to their PA-UCC values (Taylor and McLennan, 1995) are similar for argillites within each of the averages of the two types considered, but differ among them, consistent with isochemical behavior of these elements throughout the basin history. For sandstones Ti, Al, Th, V, W, and Ga have uniform ratios for each transformation. These elements have been shown to behave as immobile elements in many different metasomatic processes (e.g., Kerrich et al., 1980; Adachi et al., 1999). Based on averages of those ratios, values of the volume factor, fv, were calculated (Table 5.2). Results in Tables 3 and 4 are given in g/100 g relative to the precursor rock, as percentage changes, as well as changes in mass percentage referenced to a mass of 1 for the precursor rock, PA-UCC of Taylor and McLennan (1995).

The average of argillites having type 1 pattern displays net mass gains for REE and K_2O from ~30% to ~35% relative to PA-UCC; Cs, Sc, Co, As, and Ag from ~50% to ~100%; and for Li, Cr, and Sb from ~160% to ~420%; but losses of Na_2O, MnO, CaO, Sr, Mo, Cu, Sn, Pb, and Cd from ~40% to ~95%. Apparent losses of Nb-Ta, and Zr-Hf resulted from heavy mineral sorting given average crustal ratios of ~11 and ~32 for those element pairs. These changes are mostly mirrored for the average composition of argillites having type 2 pattern, but with a continuous change in mass from –20% for La up to ~16% for Lu (Figs. 5.8a and b, and 5.9). Type 2 argillites display mass gains of ~10% U and mass losses for Nb, Ta, Zr, Hf and Ti. Pronounced depletions of Sr, CaO, and Na_2O stem from weathering, and of Nb-Ta from sedimentary sorting as discussed above, the remaining changes being diagenetic.

Table 5.2 Inter-element ratios for argillites and sandstones with PA-UCC-like REE pattern, type 1 (T1), and HREE enriched relative to LREE, type 2 (T2).

Argillites	T1/PA-UCC	T2/T1
Al_2O_3	0.957	0.922
Th	1.057	0.905
W	0.968	1.169
Ga	0.997	0.930
Average fv*	0.994	0.982

Sandstones	T1/PA-UCC	T2/T1
TiO_2	1.052	1.459
Al_2O_3	1.092	1.135
Th	0.958	1.814
V	0.905	1.248
W	1.441	1.322
Ga	1.015	1.162
Average fv*	1.077	1.357

**fv. Volume factor*

Type 1 sandstones display net mass gains for U of ~25 %; LREE and HREE of ~40%, MREE ~55%; Li, Ba, Cr, and Co from ~110% to 220%; As and Sb of ~490% and ~430% respectively; as well as mass losses of Mo from 50% to 75%. Type 2 display mass gains of ~90 % U, and all other elements with the only exception of loss of 45% for As. Rare earth elements present mass gain from 90% for La to 175% for Lu (Figs. 5.8c and d, and 5.10). Larger percentage gains of REE in type 2 sandstones relative to argillite counterparts are attributed to greater permeability (Fig. 5.7).

Type 3 patterns in both facies feature more extreme fractionations of REE, of Zr-Hf, and Y from neighbouring REE and Al, and of Nb-Ta and Zr-Hf than in type 2 counterparts, and are considered an end member of diagenetic processes involved in type 2 patterns (Figs. 5.5 and 5.6). Zirconium, Hf, and HREE are mobile in oxidized alkaline brines (Section 5.5.7).

Table 5.3 Mass balance of the average type 1 and 2 argillite populations referenced to post-Archean upper continental crust (Taylor and McLennan, 1995).

	PA-UCC	Av. T1.	Av. T2.	T1/PA-UCC	T2/T1	T1 g/100g	M %	T2 g/100 g	M %
SiO_2	66	63	67	0.96	1.06	-2.8	-4	2.3	4
TiO_2	0.50	0.64	0.54	1.28	0.84	0.1	27	-0.1	-18
Al_2O_3	15.2	14.5	13.4	0.96	0.92	-0.7	-5	-1.4	-9
Fe_2O_3	5.00	5.44	4.06	1.09	0.75	0.4	8	-1.5	-27
MnO	0.08	0.04	0.07	0.54	1.62	0.0	-46	0.0	59
MgO	2.20	4.29	3.40	1.95	0.79	2.1	94	-0.9	-22
CaO	4.20	1.44	2.36	0.34	1.64	-2.8	-66	0.9	61
K_2O	3.37	4.55	3.68	1.35	0.81	1.2	34	-0.9	-21
Na2O	3.86	0.76	1.56	0.20	2.06	-3.1	-80	0.8	103
P_2O_5	0.16	0.12	0.08	0.73	0.70	0.0	-28	0.0	-31
Li	20	53	51	2.64	0.97	32.6	163	-2.3	-4
Rb	112	149	139	1.33	0.94	35.9	32	-12.2	-8
Sr	350	26	66	0.07	2.55	-324.4	-93	38.8	150
Cs	3.70	6.10	7.57	1.65	1.24	2.4	64	1.3	22
Ba	550	588	706	1.07	1.20	34.5	6	105.2	18
Y	22	27	27	1.22	1.00	4.7	21	-0.4	-1
Zr	190	203	200	1.07	0.99	12.2	6	-6.6	-3
Hf	5.80	6.07	6.19	1.05	1.02	0.2	4	0.0	0
Nb	25	14	12	0.55	0.88	-11.2	-45	-1.8	-13
Ta	2.20	1.04	0.95	0.47	0.91	-1.2	-53	-0.1	-10
Th	10.7	11.3	10.2	1.06	0.91	0.5	5	-1.3	-11
U	2.80	2.90	3.23	1.03	1.11	0.1	3	0.3	9
La	30	39	31	1.30	0.80	8.9	30	-8.5	-22
Ce	64	81	65	1.26	0.80	16.5	26	-17.0	-21
Pr	7.10	9.50	7.81	1.34	0.82	2.3	33	-1.8	-19
Nd	26	35	30	1.34	0.85	8.8	34	-5.9	-17
Sm	4.50	6.40	5.80	1.42	0.91	1.9	41	-0.7	-11
Eu	0.88	1.30	1.00	1.48	0.77	0.4	47	-0.3	-25
Gd	3.80	5.66	5.44	1.49	0.96	1.8	48	-0.3	-6
Tb	0.64	0.79	0.79	1.24	1.00	0.1	23	0.0	-2
Dy	3.50	4.81	5.14	1.37	1.07	1.3	37	0.2	5
Ho	0.80	1.01	1.07	1.26	1.06	0.2	25	0.0	4
Er	2.30	2.94	3.25	1.28	1.11	0.6	27	0.3	9
Tm	0.33	0.44	0.50	1.33	1.12	0.1	33	0.0	10
Yb	2.20	3.01	3.36	1.37	1.12	0.8	36	0.3	10
Lu	0.32	0.42	0.50	1.32	1.18	0.1	31	0.1	16
Sc	11.0	17.8	18.8	1.62	1.06	6.7	61	0.7	4
V	60	77	55	1.28	0.71	16.5	28	-23.1	-30
Mo	1.50	0.34	1.10	0.23	3.19	-1.2	-77	0.7	213
Cr	35	107	82	3.05	0.77	71.1	203	-25.9	-24
Co	10	15	11	1.51	0.76	5.1	51	-3.9	-26
Ni	20	27	16	1.36	0.60	7.1	36	-11.1	-41
Cu	25.0	4.1	19.5	0.16	4.75	-20.9	-84	15.1	367
Zn	71	52	61	0.73	1.18	-19.7	-28	8.1	16
Sn	5.50	3.00	3.26	0.54	1.09	-2.5	-46	0.2	7
W	2.00	1.94	2.26	0.97	1.17	-0.1	-4	0.3	15
Pb	20.0	8.8	13.7	0.44	1.55	-11.2	-56	4.6	52
Cd	0.10	0.04	0.09	0.42	2.20	-0.1	-58	0.0	116
Tl	0.75	0.63	0.73	0.84	1.16	-0.1	-16	0.1	14
Ga	17	17	16	1.00	0.93	-0.2	-1	-1.5	-9
As	1.50	3.02	4.29	2.01	1.42	1.5	100	1.2	40
Ag	0.05	0.08	0.07	1.65	0.80	0.0	64	0.0	-22
Sb	0.20	1.04	0.96	5.22	0.92	0.8	419	-0.1	-10

(PA-UCC) Post-Archean upper continental crust; type 1 (T1), PA-UCC-like REE pattern; type 2, (T2) HREE enriched relative to LREE; (Av.) average; and (M) mass.

Table 5.4 Mass balance of the average sandstone population types 1 and 2 referenced to post-Archean upper continental crust (Taylor and McLennan, 1995).

	PA-UCC	Av. T1.	T1(r)	Av. T2	T1/PA-UCC	T2/T1	T1 g/100g	M %	T2 g/100 g	M %
SiO_2	66	84	85	81	1.29	0.97	26	40	26	32
TiO_2	0.50	0.24	0.53	0.35	1.05	1.46	0.07	14	0.24	98
Al_2O_3	15.2	7.5	16.6	8.5	1.09	1.13	2.7	18	4	54
Fe_2O_3	5.00	2.4	5.3	2.6	1.05	1.10	0.67	13	1.2	50
MnO	0.08	0.02	0.04	0.04	0.45	2.29	-0.04	-51	0.03	211
MgO	2.20	1.1	2.5	1.5	1.14	1.29	0.50	23	0.86	75
CaO	4.20	0.5	1.0	0.7	0.24	1.61	-3.12	-74	0.54	119
K_2O	3.37	1.7	3.7	2.1	1.09	1.27	0.61	18	1.21	72
Na_2O	3.86	1.5	3.3	1.2	0.85	0.81	-0.31	-8	0.16	11
P_2O_5	0.16	0.02	0.04	0.06	0.23	3.29	-0.12	-75	0.06	348
Li	20	34	76	26	3.80	0.76	62	310	0.97	3
Rb	112	57	126	84	1.13	1.47	24	22	57	100
Sr	350	52	115	53	0.33	1.02	-226	-65	20	38
Cs	3.7	2.4	5.2	4.2	1.41	1.80	2.0	52	3.4	144
Ba	550	543	1198	724	2.18	1.33	743	135	441	81
Y	22	13	28	24	1.28	1.85	8.1	38	19	152
Zr	190	134	295	221	1.55	1.66	128	67	167	125
Hf	5.8	3.5	7.8	6.2	1.35	1.74	2.6	46	4.8	136
Nb	25.0	4.3	9.4	8.0	0.38	1.88	-15	-59	6.6	155
Ta	2.2	0.4	0.8	0.7	0.37	2.04	-1.33	-60	0.65	178
Th	10.7	4.7	10.3	8.4	0.96	1.81	0.37	3	6.8	147
U	2.8	1.5	3.3	2.1	1.17	1.39	0.74	26	1.31	89
La	30	17	38	24	1.26	1.39	10	36	15	89
Ce	64	36	78	53	1.22	1.49	20	32	36	102
Pr	7	4	10	6	1.36	1.43	3.3	47	4.1	95
Nd	26	16	36	23	1.38	1.42	12.7	49	15	94
Sm	4.5	3.1	6.7	4.7	1.49	1.53	2.71	61	3.3	108
Eu	0.88	0.57	1.25	0.82	1.42	1.44	0.47	53	0.544	96
Gd	3.8	2.8	6.1	4.5	1.61	1.63	2.83	74	3.38	121
Tb	0.6	0.4	0.8	0.7	1.30	1.82	0.26	40	0.56	147
Dy	3.5	2.3	5.0	4.5	1.44	1.95	1.94	55	3.78	165
Ho	0.80	0.45	1.00	0.91	1.25	2.02	0.28	35	0.79	175
Er	2.3	1.3	2.9	2.7	1.26	2.07	0.84	36	2.4	181
Tm	0.33	0.19	0.43	0.41	1.29	2.11	0.13	39	0.36	186
Yb	2.2	1.3	2.9	2.7	1.30	2.11	0.89	40	2.43	188
Lu	0.32	0.19	0.43	0.39	1.33	2.02	0.14	44	0.34	174
Sc	11.0	7.6	16.7	11.7	1.52	1.55	7	64	8	110
V	60	25	54	31	0.90	1.25	-1.38	-2	17	70
Mo	1.5	0.2	0.4	0.5	0.29	2.40	-1.03	-69	0.45	227
Cr	35	47	103	55	2.95	1.17	76	219	27	59
Co	10	9	19	8	1.93	0.87	10	108	1.67	19
Ni	20	14	31	11	1.57	0.79	13	69	1.0	7
Cu	25	10	22	10	0.89	0.95	-1.03	-4	3.0	29
Zn	71	26	58	32	0.82	1.21	-8	-12	16	64
Sn	5.5	1.4	3.1	2.0	0.57	1.42	-2.14	-39	1.32	94
W	2.0	1.3	2.9	1.7	1.44	1.32	1.11	56	1.04	80
Pb	20	7	14	16	0.72	2.48	-4.4	-22	15	237
Cd	0.10	0.07	0.15	0.07	1.45	1.07	0.06	57	0.03	46
Tl	0.8	0.3	0.6	0.5	0.84	1.60	-0.07	-9	0.34	118
Ga	17	8	17	9	1.02	1.16	1.64	10	4.6	58
As	1.5	3.7	8.2	1.5	5.50	0.41	7.4	493	-1.67	-44
Ag	0.05	0.01	0.03	0.04	0.62	2.74	-0.016	-33	0.04	272
Sb	0.2	0.4	1.0	0.9	4.92	1.95	0.862	431	0.74	166

(PA-UCC) Post-Archean upper continental crust; type 1 (T1), PA-UCC-like REE pattern; type 1 recalculated, [T1(r)]; type 2, (T2) HREE enriched relative to LREE; (Av.) average; and (M) mass.

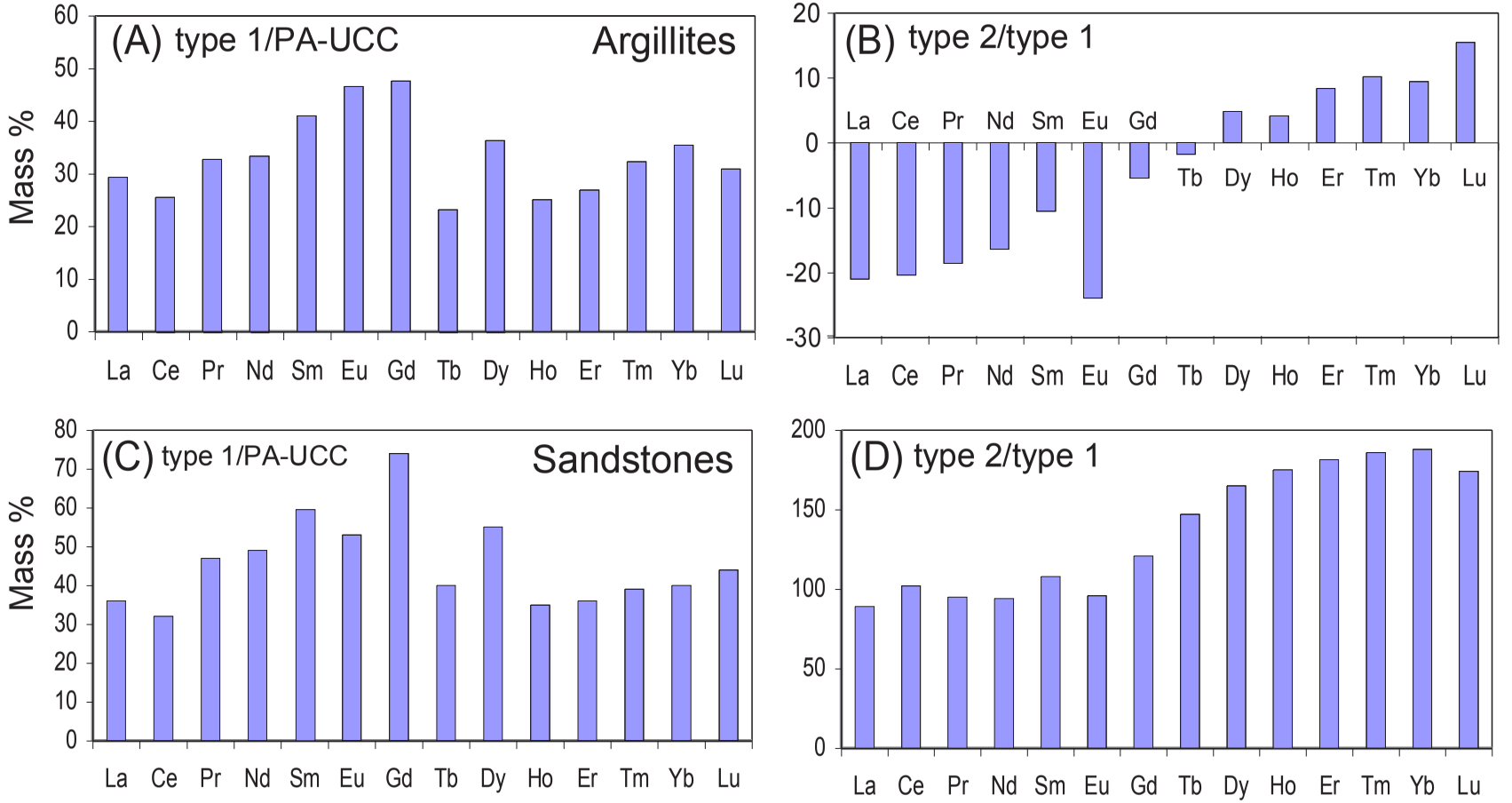

Fig. 5.8 Mass balance histograms for argillites and sandstones. (A) A percentage mass gain of REE relative to PA-UCC for argillites with type 1 patterns, whereas (B) shows a continuous mass change from LREE loss to HREE gain for type 2 referenced to type 1 argillites. (C) And (D), calculated percentage mass changes for sandstones.

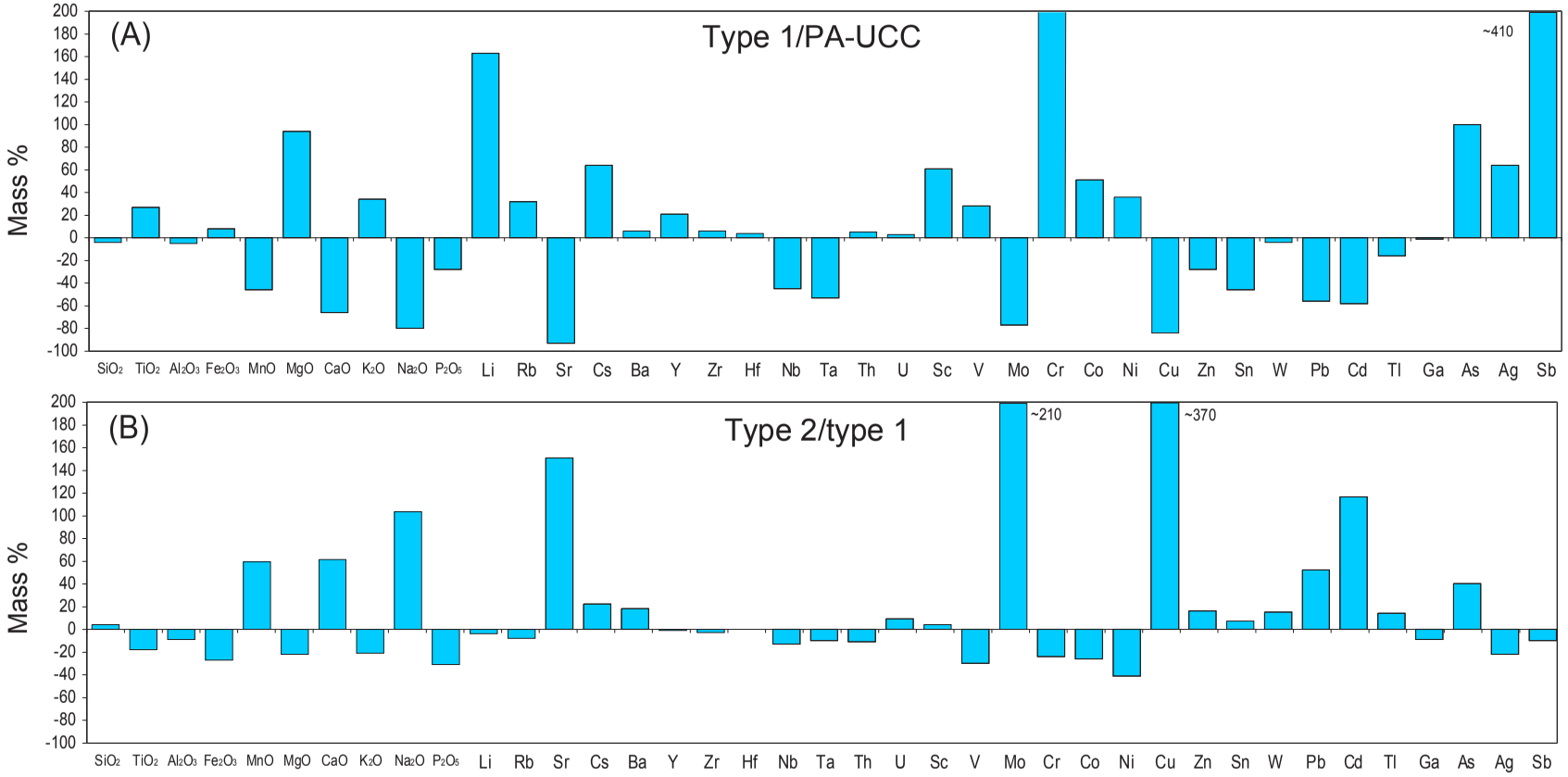

Fig. 5.9 Mass balance in mass % for argillites from the precursor rock PA-UCC to type 1 and from type 1 to type 2 REE patterns for specified major and trace elements. Main changes in (A) are mirrored in (B).

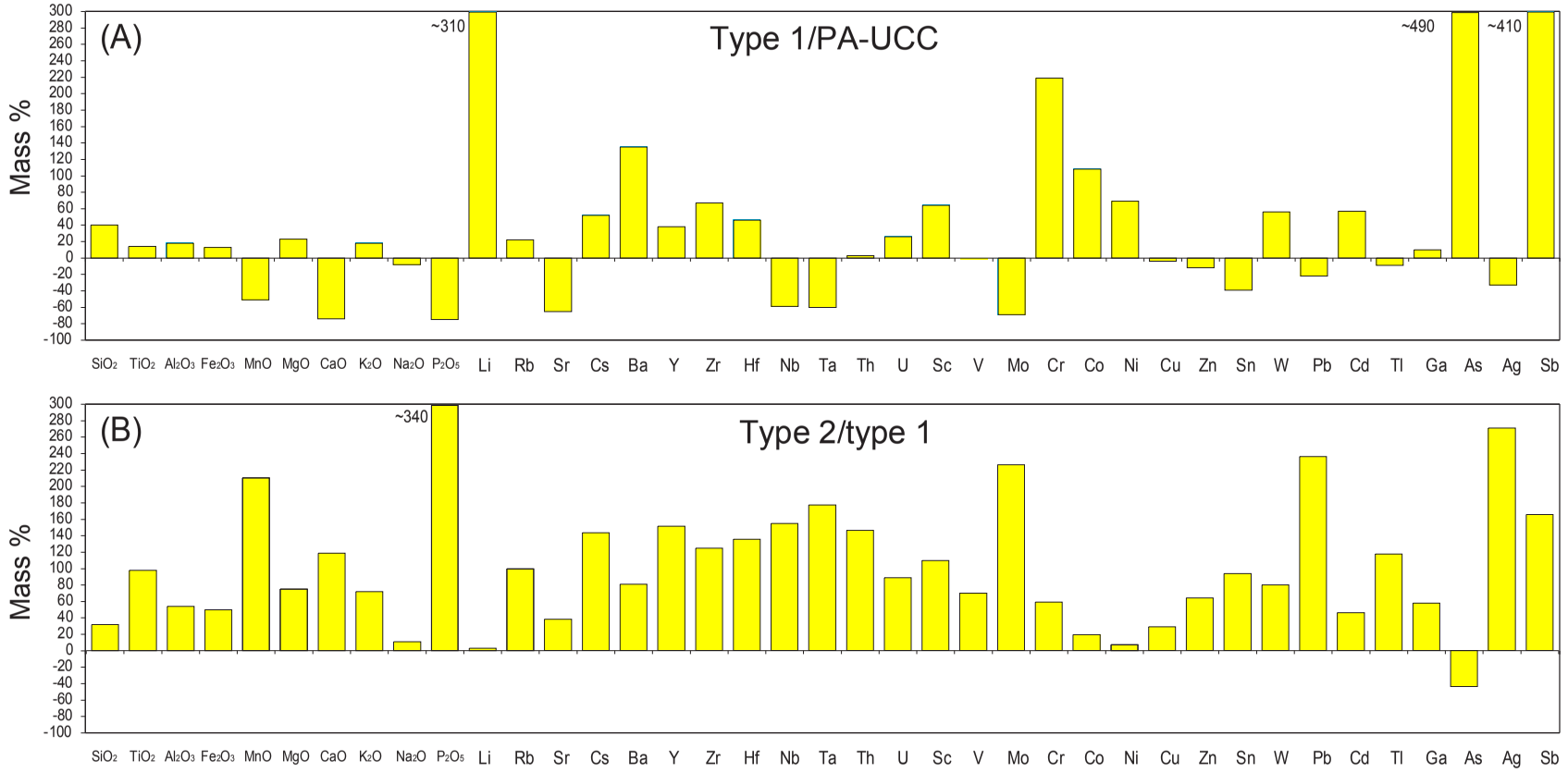

Fig. 5.10 Mass balance in mass % for sandstones from the precursor rock PA-UCC to type 1 and from type 1 to type 2 REE patterns for specified major and trace elements. (A) Changes in Fig. 5.9a are mimic, whereas (B) presents a general positive trend. The former is interpreted as due to a higher permeability of sandstones, higher average value of SiO_2 for the sandstones type 2 related to type 1 and higher presence of clay size fraction.

5.5.7 K-addition

Post-depositional potassic alteration has been described previously as a widespread feature in many Precambrian siliciclastic sedimentary sequences and saproliths (Wronkiewicz and Condie, 1989; Rainbird et al., 1990; Maas and McCulloch, 1991; Condie, 1993; Fedo et al., 1995; McLennan et al., 2000; Bhat and Ghost, 2001; Cullers and Podkovyrov, 2002). Diagenetic potassic addition is supported by the illite-rich matrix in argillites, and was also reported by Lydon et al. (2000) for the Aldridge Formation (lower Belt; Figs. 5.2 and 5.3) in the Purcell Mountains of southern British Columbia; he interpreted addition of K as due to formation waters and heat flow associated with rifting that transformed semectite to illite. Values up to ~140% K_2O PA-CC in type 1 argillites and sandstones (Tables 5.3 and 5.4) stem for the result of diagenetic metasomatism of the Belt-Purcell rocks. With the available data it is not possible to constrain whether K-addition predated, or was part of the development of, type 1 patterns.

5.5.8 Source of the brines

The Sullivan Pb-Zn-Ag deposit in the lower Belt-Purcell Supergroup of southeastern British Columbia formed close to the time of sedimentation. Hydrothermal ore fluids are considered to have been seawater that was modified and reduced by subsurface convection through a thick sill-sediment complex (Lydon, 2000; Schandl et al., 2000). Alteration proximal to the deposit involved net gains of Fe, Pb, and Zn, with losses of Na, K, Ca, and Mg (Leitch et al., 2000). Diagenetic basinal fluids that generated types 1 and 2 patterns are unlike those involved in the Sullivan deposit, inasmuch as different elements were mobile.

Alkaline oxidizing fluids lie in the upper right hand sector of the limits to the Eh and pH of natural waters (Krauskopf, 1985). A number of possible processes may have contributed to alkalinity: (1) enrichment of K as recorded by mass balance and the presence of illite; (2) silicate weathering of mafic igneous units in the sequence (cf. Gíslason and Eugster, 1987; Anderson and Evans, 2000), potentially raising the pH to 10-12 (Krauskopf, 1985); and (3) buffering by sedimentary carbonate units in the Belt Supergroup . For example, Berner (1971) report ranges of pH from 8.2 to 10.2 for dolomitization in a variety of sedimentary basins, commensurate with conditions of high pH and Mg activity for dolomitization Morse (2004) in the Belt-Purcell Supergroup.

An oxidizing diagenetic brine is signified by mobility of U and Ce. At pH 4.5-14 and Eh >0, U has a high aqueous mobility as the complex UO_2 [CO_3^0; $(CO_3)_2^{-2}$; $(CO_3)_3^{-4}$] (Brookins, 1988; cf.

Fayek and Kyser, 1997), Heavy REE have relatively greater solubility than LREE with dicarbonate complexes (Johanneson and Lyons, 1995), such that U-mobility and type 2 HREE-enriched pattern are both consistent with high Eh fluids. Oxidizing conditions were likely promoted by sedimentary Fe^{3+} oxides and oxyhydroxides developed during weathering (cf. Holland, 1978). Oxidizing conditions may also have stemmed initially in part from discharge of mantle CO_2 during rifting of the lithosphere, from CO_2-^3He sysyematics of hot springs in the Pannonian Basin in the Pannonian Basin (Mattews et al., 1987). CO_2 is also generated within sedimentary basins by reactions between clays and carbonate (Hutcheon, 1989).

Several Mesoproterozoic sedimentary sequences have direct or indirect evidence for evaporites (see Table 5.5 for examples). Accordingly, continental land-masses may have been at low latitudes, or alternatively a warm climate prevailed globally. The presence of halite casts as well as large amounts of scapolite, and other evidence of evaporites, in the Belt-Purcell sequence has been documented (e.g., McMechan, 1981; Horodyski, 1993; Schieber, 1997 and references therein;

Table 5.5 Same examples of Proterozoic sedimentary sequences with direct or indirect evidence of evaporites.

Sequence	Location	Age (Ma)	Reference
Yanshan Group	P. R. China	1730-850	Li et al. (2003)
Aravalli Supergroup	India	2150	Golani et al. (2002)
Vindhyan Supergroup	India	1600-700	Ray et al. (2003)
Ui Group	Russia	1600-650	Cullers and Podkovyrov (2002)
Wollaston Group	Canada	2100-1860	Tran et al. (2003)
Dhanjori Group	India	2100	Mazumder and Sarkar (2004)
Baker Lake Group	Canada	1800	Aspler et al. (2004)
Calcsilicate Suite	Australia	1700	Cook and Ashley (1992)
Liaohe Group	China	2400	Peng and Palmer (1995)
Chameis Group	Namibia	600	Frimmel and Jiang (2001)
Belt Supergroup	Canada and U.S.A.	1500-1400	Schieber (1997)
Shaler Supergroup	Canada	1000-750	Rainbird et al. (1996)
Bylot Supergroup	Canada	1200-1000	Jackson and Iannelli (1981)

Chandler, 2000 and references therein); these likely record the source of inferred high aqueous dissolved content of the diagenetic brines. Accordingly, alkaline oxidizing brines are believed to have transported REE, HFSE, U and Ce in the Belt-Purcell siliciclastic samples.

Mobility of Zr has been documented under conditions such as intense weathering of volca-

nic soils, or hydrothermal metasomatism involving the precipitation of tourmaline (Rubin et al., 1989; Gieré, 1989; Kerrich and King, 1993; Kurt et al., 2000). Aqueous transport of Zr, and by inference all HFSE, is enhanced by F- in the fluids (Alderton et al., 1980). Aqueous transport of REE and HFSE has been identified in low-temperature alkaline oxidizing fluids. High concentrations of Zr and REE were reported in saline ground-waters with pH 12 (Kraynov et al., 1969). Magadi-type cherts from the East African Rift are precipitating from low-temperature alkaline oxidizing brines having LREE at ~0.01 and HREE ~0.6 times PA-UCC. Magadi-type cherts are characterized by the conjunction of: (1) normalized HREE enrichment relative to MREE; (2) anomalies of Nb and Zr relative to neighbouring REE; (3) extreme Nb/Ta up to 120, and Zr/Hf up to 1300 fractionations compared to PA-UCC ratios of 11 and 34, respectively; (4) Th/U fractionation; and (5) U, Mo, Ag, and Sb enrichments (Kerrich et al., 2002). Several of these geochemical features are present in both Belt-Purcell facies having type 2 and 3 patterns (Figs. 5.5 and 5.6). Similar anomalous trace element features have been documented for sediments in saline alkaline lakes of the Pamirs in central Asia (Volkova, 1998).

Experimental data of Johannesson and Lyons (1995) show that in fluids at high pH, REE (preferentially HREE) are associated with dicarbonate complexes. These results are consistent with the empirical study by Kraynov et al. (1969), who described how alkaline ground waters (pH 12), concentrated by evaporation with high fluorine, silica and sodium contents, have elevated REE, Zr and other trace element concentrations, commensurate with the geochemistry of Magadi-type chert.

Secondary monazites in the Belt-Purcell sedimentary rocks have post-depositional chemical ages ~1400 Ma to ~600 Ma, are euhedral, and display different Y, ThO_2 and LREE/HREE contents than their detrital counterparts (Chapter IV; González-Álvarez et al., *in press*). These monazites have been described in argillite and sandstone samples with types 1 and 2 REE patterns. Therefore, Post-Belt deposition ages have been interpreted as reflecting basinal brine events that redistributed REE and HFSE. The implication of protracted basinal fluid migration is long-term preservation of hydraulic conductivity. Similarly, Kyser et al. (2000, and references therein) reported episodic migration of basinal brines through some Paleoproterozoic sedimentary sequences including the Athabasca sequence, Canada, and siliciclastic rocks of the McArthur Basin, Australia, over ~600 Ma post deposition where local enrichments of HREE and Y are present. Rénac et al. (2002) reported ages of fluid migration in the Thelon Basin, Canada, and relate them to regional tectonic events.

5.6 Conclusions

(1) Regardless of potentially different provenance and weathering, two systematic REE patterns are consistently present for sandstones and argillites throughout the Belt-Purcell stratigraphic sequence at three different locations: (1) type 1, with a PA-UCC-like REE pattern, and K enrichment, and similar multi-element patterns as PA-UCC, variable Th/U, and Ce/Ce* fractionations, systematic negative anomalies for Nb and Ta, and variable anomalies for Zr and Hf; whereas (2) type 2, features relative enrichment of HREE relative to LREE when normalized to PA-UCC, HFSE fractionation, and enrichments of U, Mo, Ag, and/or Sb.

(2) Both type 1 and 2 display convex-up pattern for MREE, negative Tb and Eu anomalies; and pronounced depletion of Sr, Ca, and Na. The latter is interpreted as intense chemical weathering in the source area.

(3) Low SiO_2 contents and negative anomalies of Zr-Hf in type 1 argillites is commensurate with airborne removal of quartz.

(4) In the Belt-Purcell Basin, brine compositions likely reflect the dissolution of evaporite units within the sequence, which produced oxidized-alkaline basinal brines that advected through the Belt-Purcell Supergroup rocks, preferentially in permeable sandstones, over hundreds of million of years. The brines are suggested to be responsible for mobility of HREE and HFSE.

(5) Variably negative Ce anomalies and enrichments of U in argillites and sandstones with type 2 patterns are consistent with oxidized diagenetic fluids.

(6) Al_2O_3, Th, W, and Ga behaved isochemically during the diagenetic processes.

(7) The presence of illite reported in this and other studies of siliciclastic sequences reflects the enrichment in potassium that characterizes type 1 argillites and sandstones.

(8) Whereas secondary monazites with post-Belt-Purcell depositional chemical ages reported in recent studies are interpreted as reflecting basinal brine events that redistributed REE and HFSE.

5.7 Acknowledgements

Staff of Waterton-Glacier International Peace Park are thanked for support, especially L. F. Marnell and C. Smith; as well as Q. Xie and J. Fan who assisted with ICP-MS analyses; to L. M. Shychosky, M. England, A. Vangool, R. Ahrabian, A. Peterhänsel, and L. Skublicki for help during fieldwork; and to T. Prokopiuk, M. J. Hendry, M. Reid, and M. A. Kusiak for comments on early versions of these Chapter. Incisive reviews by two journal reviewers, R. Cullers and J. F. Slack have significantly improved this Chapter based on their comments on the *submitted* manuscript. Natural Sciences & Environment Research Council of Canada (NSERC) discovery grants to R. Kerrich and B. R. Pratt, and a University of Saskatchewan graduate scholarship to I. González-Álvarez funded this study. R. K. acknowledges NSERC MFA support of the ICP-MS facility, and the G. McLeod endowment to the Department of Geological Sciences, University of Saskatchewan.

5.8 Appendices

Appendix 5.1a Major and trace element concentration of the Belt-Purcell Supergroup at Waterton-Glacier International Peace Park.

Formation	Libby	Libby	Libby	McNamara	McNamara	McNamara	Bonner	Bonner	Bonner	Mount Sh.	Mount Sh.	Shepard	Shepard	Shepard
Levels Fig. 3	G70	G69	G68	G67	G66	G65	G64	G63	G62	G61	G59	G58	G57	G56
Sample	35(2)G1	35(1)G1	35G1USO	34(2)G1	34(1)G1	34G1USO	33(2)G1	33(1)G1	33G1USO	32(2)G1	32G1USO	31G1USO	31(2)G1	31(1)G1
SiO_2 (wt%)	78.7	70.7	62.0	65.5	66.0	70.6	88.9	82.6	80.7	59.1	66.7	76.3	60.1	62.4
TiO_2	0.28	0.37	0.72	0.46	0.57	0.50	0.22	0.21	0.31	0.56	0.57	0.47	0.61	0.60
Al_2O_3	7.82	12.29	19.00	12.12	15.01	13.00	5.83	8.35	9.73	11.30	12.10	9.68	15.50	14.57
Fe_2O_3	5.81	8.42	6.70	3.14	5.33	2.81	0.69	1.88	1.79	3.66	3.42	4.11	8.95	8.70
MnO	0.05	0.05	0.06	0.08	0.04	0.03	0.00	0.00	0.00	0.08	0.03	0.02	0.03	0.03
MgO	1.41	2.06	2.03	3.50	3.77	2.91	0.70	1.25	1.26	5.71	4.38	2.57	5.47	5.37
CaO	1.23	0.12	0.20	4.75	0.43	1.38	0.12	0.13	0.32	5.50	2.36	0.58	0.23	0.19
K_2O	1.35	2.24	4.57	2.60	4.07	3.88	1.70	2.19	2.98	3.41	3.94	2.83	3.75	3.33
Na_2O	1.17	1.21	1.48	2.08	1.71	1.61	1.22	1.47	1.36	1.62	1.39	1.21	0.98	1.02
P_2O_5	0.02	0.05	0.05	0.08	0.11	0.09	0.01	0.02	0.15	0.17	0.14	0.09	0.14	0.09
LOI	2.30	2.55	2.85	5.75	3.00	3.25	0.65	1.30	1.50	9.00	5.15	2.30	4.30	3.85
Sum	100.2	100.1	99.7	100.1	100.2	100.3	100.1	99.6	100.2	100.2	100.4	100.2	100.1	100.3
Li (ppm)	77	73	60	46	95	59	16	27	18	59	79	40	79	64
Rb	71	92	227	107	176	132	55	82	102	95	134	94	140	128
Sr	33	30	83	47	73	39	27	52	25	34	37	34	27	27
Cs	1.96	2.95	14.86	3.85	6.91	5.47	2.17	3.68	4.03	4.13	5.43	3.99	6.61	4.72
Ba	383	390	849	326	1509	753	419	930	371	318	458	482	638	519
Y	17.2	24.0	5.3	30.4	32.0	26.9	13.7	11.7	15.1	30.8	5.1	14.0	38.1	25.9
Zr	173	219	243	186	232	129	348	158	57	287	240	89	177	185
Hf	4.48	5.92	7.07	5.49	7.33	5.13	7.94	3.87	5.59	8.15	7.23	3.37	5.31	5.56
Nb	6.85	9.43	11.23	12.54	15.21	9.77	2.93	3.11	4.16	13.18	11.65	6.91	14.08	15.30
Ta	0.50	0.67	0.91	1.02	1.30	1.02	0.42	0.34	1.19	1.05	0.91	0.66	1.09	1.08
Th	7.58	8.45	1.58	12.23	15.15	6.98	4.24	4.06	16.52	12.08	2.18	4.85	12.69	12.75
U	2.48	2.51	3.41	3.99	3.96	3.88	1.32	1.50	1.93	1.94	2.28	2.31	4.01	3.46
La	23.72	38.79	41.94	32.30	40.50	42.56	11.87	13.29	41.94	40.92	2.21	13.92	66.58	38.00
Ce	56.70	88.11	88.75	68.61	86.19	93.80	25.97	29.92	88.75	88.92	8.06	26.73	142.57	78.86
Pr	6.64	9.78	10.84	8.11	10.20	11.51	3.41	3.63	10.84	10.70	0.77	3.32	16.77	9.42
Nd	24.61	36.19	39.37	29.00	36.87	43.51	13.48	13.34	39.37	38.07	3.56	13.53	61.85	34.55
Sm	4.55	6.73	7.87	5.89	7.39	8.60	2.48	2.58	7.87	7.50	0.88	2.76	11.81	6.22
Eu	0.738	1.161	1.368	0.934	1.279	1.376	0.557	0.555	1.370	1.224	0.220	0.460	2.606	1.353
Gd	4.05	5.62	7.33	5.67	6.91	7.90	2.49	2.10	7.33	6.54	1.03	2.77	9.51	5.18
Tb	0.544	0.756	1.069	0.814	0.975	1.038	0.354	0.311	1.070	0.902	0.190	0.440	1.221	0.733
Dy	3.21	4.55	6.76	5.06	6.03	6.29	2.36	1.86	6.76	5.44	1.31	2.74	7.28	4.58
Ho	0.615	0.844	1.376	1.061	1.206	1.266	0.480	0.375	1.380	1.155	0.270	0.550	1.398	1.003
Er	1.82	2.46	4.06	3.17	3.60	3.83	1.40	1.16	4.06	3.31	0.86	1.52	4.08	2.98
Tm	0.272	0.356	0.614	0.499	0.552	0.596	0.215	0.175	0.610	0.483	0.130	0.230	0.617	0.445
Yb	1.71	2.28	4.04	3.24	3.85	4.02	1.44	1.13	4.04	3.36	0.90	1.54	4.08	3.16
Lu	0.244	0.301	0.584	0.501	0.529	0.592	0.205	0.158	0.580	0.454	0.130	0.210	0.568	0.426
Sc	11	15	2	16	18	14	3	6	10	16	4	10	24	20
V	46	70	85	41	64	37	13	25	30	36	60	58	120	114
Mo	0.64	0.54	0.82	0.53	0.37	0.45	0.31	0.00	0.00	0.68	0.15	0.22	0.54	0.17
Cr	115	109	124	62	88	53	20	35	32	54	100	75	137	133
Co	22	21	15	8	12	2	3	8	5	13	7	10	33	22
Ni	34	40	24	13	15	11	8	15	9	16	18	12	37	27
Cu	37	51	35	3	3	4	3	2	2	9	0	1	8	4
Zn	54	54	108	95	124	58	11	20	15	34	29	58	132	143
Sn	2.19	2.26	4.78	2.82	3.96	3.99	0.95	0.91	1.17	1.60	2.71	2.13	3.79	3.59
W	2.08	0.94	3.17	1.65	3.20	2.35	0.12	0.47	0.75	0.96	1.37	1.84	1.17	1.26
Pb	8.62	6.47	24.51	5.85	6.02	4.98	4.71	6.39	24.06	19.23	12.11	4.73	7.93	10.81
Cd	0.00	0.00	0.14	0.00	0.14	0.00	0.18	0.00	0.00	0.00	0.00	0.00	0.13	0.00
Tl	0.33	0.47	1.01	0.68	1.10	0.65	0.34	0.50	1.07	0.42	0.60	0.47	0.54	0.61
Ga	13.60	15.10	24.99	15.84	18.59	16.67	5.18	7.89	12.00	7.81	14.15	11.85	25.28	22.64
As	11.20	10.53	0.00	0.46	1.11	0.00	0.84	0.62	0.76	4.30	0.70	0.69	16.70	6.53
Ag	0.00	0.00	0.05	0.00	0.00	0.00	0.00	0.00	0.00	0.15	0.00	0.00	0.04	0.00
Sb	0.66	0.44	0.54	0.73	0.99	0.80	0.22	0.42	0.54	0.68	0.50	0.48	0.73	0.82
$(La/Sm)_{cn}$	3.3	3.6	3.3	3.4	3.4	3.1	3.0	3.2	3.3	3.4	1.6	3.2	3.5	3.8
$(Gd/Yb)_{cn}$	2.0	2.0	1.5	1.4	1.5	1.6	1.4	1.5	1.5	1.6	0.9	1.5	1.9	1.4
$(La/Yb)_{cn}$	9.6	11.8	7.2	6.9	7.3	7.4	5.7	8.2	7.2	8.4	1.7	6.3	11.3	8.3
Ce/Ce*	1.0	1.0	0.9	1.0	1.0	1.0	0.9	1.0	0.9	1.0	1.4	0.9	1.0	1.0
Eu/Eu*	0.8	0.9	0.8	0.7	0.8	0.8	1.0	1.1	0.8	0.8	1.1	0.8	1.1	1.1
∑REE	129	198	216	165	206	227	67	71	216	209	21	71	331	187
Ti/V	36	32	51	66	53	81	100	50	64	94	58	48	30	32
Zr/Hf	39	37	34	34	32	25	44	41	10	35	33	26	33	33
Th/Ce	0.1	0.1	0.0	0.2	0.2	0.1	0.2	0.1	0.2	0.1	0.3	0.2	0.1	0.2
La/Sc	2.2	2.6	17.3	2.0	2.3	3.0	4.4	2.2	4.3	2.6	0.5	1.3	2.8	1.9
Th/Sc	0.7	0.6	0.7	0.8	0.8	0.5	1.6	0.7	1.7	0.8	0.5	0.5	0.5	0.6
Co/Th	2.9	2.5	9.6	0.6	0.8	0.3	0.7	2.1	0.3	1.1	3.2	2.0	2.6	1.7
Th/U	3.1	3.4	0.5	3.1	3.8	1.8	3.2	2.7	8.6	6.2	1.0	2.1	3.2	3.7
Ni/Co	1.6	1.9	1.6	1.6	1.2	4.6	2.6	1.8	1.7	1.2	2.5	1.3	1.1	1.2
Y/Ho	27.9	28.5	3.9	28.6	26.5	21.3	28.5	31.1	10.9	26.7	18.7	25.5	27.3	25.9
V/Sc	4.4	4.7	34.9	2.6	3.6	2.6	4.9	4.1	3.0	2.2	13.5	5.6	5.1	5.7
Facies	Sd.	Arg.	Arg.	Arg.	Arg.	Arg.	Sd.	Sd.	Sd.	Arg.	Arg.	Sd.	Arg.	Arg.

Appendix 5.1a (continued).

Formation	Snowslip	Snowslip	Snowslip	Empire	Empire	Appekunny-Grinnell	Appekunny-Grinnell	Appekunny-Grinnell	Appekunny-Grinnell	Appekunny-Grinnell	Appekunny-Grinnell
Levels Fig. 3	G55	G54	G53	G48	G46	G45	G41	G22	G21	G19	G18
Sample	30G1USO	30(2)G1	30(1)G1	27(2)G1	27(1)G1	Sd.1	Sd.2	Slt1a	Slt1b	Slt2a	Slt2b
SiO_2 (wt%)	66.5	79.0	62.3	64.4	83.3	95.9	88.3	68.9	69.4	70.4	69.4
TiO_2	0.46	0.41	0.59	0.30	0.02	0.04	0.05	0.53	0.53	0.49	0.49
Al_2O_3	10.30	8.96	15.22	8.74	1.64	1.44	5.98	13.36	13.66	12.96	12.83
Fe_2O_3	3.88	3.94	5.45	2.41	0.18	0.53	0.54	5.14	4.62	3.78	4.07
MnO	0.17	0.02	0.08	0.05	0.03	0.04	0.02	0.02	0.03	0.04	0.08
MgO	3.37	2.26	3.51	6.15	2.69	0.52	0.96	2.76	2.74	3.20	3.32
CaO	3.75	0.13	1.37	5.16	4.53	0.26	0.22	0.40	0.54	0.84	1.18
K_2O	3.45	1.81	5.70	3.38	1.13	0.50	1.76	5.69	4.73	3.88	3.47
Na_2O	1.04	1.50	0.77	0.50	0.09	0.14	1.47	0.45	0.79	1.33	1.71
P_2O_5	0.11	0.04	0.10	0.07	0.00	0.03	0.03	0.13	0.12	0.10	0.11
LOI	6.70	1.85	4.40	8.90	6.40	0.67	0.85	2.70	2.90	3.12	3.35
Sum	99.9	100.1	99.6	100.2	100.3	100.1	100.2	100.1	100.1	100.1	100.1
Li (ppm)	32	49	74	88	9	16	17	63	54	59	51
Rb	135	60	238	97	20	13	41	154	171	139	125
Sr	63	27	30	40	41	21	36	28	37	39	47
Cs	5.76	2.54	11.23	4.56	0.45	0.55	0.70	10.13	9.00	7.31	6.61
Ba	1002	279	797	544	3223	883	1376	401	851	769	670
Y	21.5	23.1	30.3	23.0	5.5	7.1	4.9	24.8	28.8	27.2	30.2
Zr	86	343	203	190	89	23	39	161	197	211	235
Hf	3.07	9.50	6.09	5.82	2.33	0.63	0.91	5.62	6.21	6.46	7.23
Nb	6.22	9.48	16.28	11.12	0.85	0.64	0.77	14.09	12.43	10.87	10.62
Ta	0.40	0.79	1.16	0.79	0.09	0.05	0.07	1.08	0.95	0.82	0.78
Th	4.79	9.59	12.88	9.72	1.53	1.41	1.32	13.11	11.90	10.73	10.30
U	2.64	2.59	3.31	2.87	0.48	0.46	0.47	3.81	2.89	2.87	3.13
La	22.16	23.94	42.19	25.22	5.48	6.22	6.63	35.04	42.60	35.06	31.31
Ce	46.14	47.46	89.84	56.00	9.49	12.54	9.81	72.82	87.89	71.25	64.89
Pr	5.43	5.49	10.16	6.52	1.21	1.56	1.42	8.41	9.94	8.32	7.89
Nd	21.69	19.43	36.08	24.42	4.96	6.07	5.02	32.19	38.27	32.25	31.29
Sm	4.44	3.79	6.94	4.67	1.23	1.38	1.00	5.94	7.46	6.68	7.02
Eu	0.810	0.626	1.321	0.679	0.263	0.265	0.273	1.000	1.320	1.186	1.276
Gd	4.36	3.82	6.39	4.34	1.40	1.47	1.02	5.18	6.59	6.02	6.51
Tb	0.620	0.615	0.872	0.656	0.209	0.230	0.153	0.757	0.910	0.830	0.904
Dy	4.09	4.17	5.36	4.17	1.25	1.27	0.85	4.65	5.46	5.06	5.60
Ho	0.840	0.886	1.087	0.824	0.204	0.243	0.163	0.957	1.088	1.029	1.141
Er	2.43	2.71	3.23	2.56	0.58	0.65	0.45	2.87	3.20	3.09	3.44
Tm	0.340	0.396	0.517	0.391	0.075	0.090	0.065	0.437	0.496	0.479	0.529
Yb	2.27	2.72	3.39	2.67	0.57	0.56	0.45	2.97	3.24	3.19	3.54
Lu	0.330	0.397	0.464	0.358	0.059	0.081	0.068	0.453	0.500	0.498	0.556
Sc	12	9	22	14	6	1	1	11	11	10	11
V	41	37	69	28	2	5	6	56	57	48	43
Mo	0.43	0.58	0.40	0.82	0.00	0.82	0.17	0.34	0.31	0.52	0.69
Cr	64	71	102	44	3	7	9	15	69	64	58
Co	10	8	13	9	1	3	4	10	12	9	10
Ni	20	17	23	11	2	8	8	20	28	22	21
Cu	3	6	2	16	2	7	6	3	8	11	14
Zn	35	54	60	28	2	13	19	65	53	56	74
Sn	2.19	1.36	3.52	2.15	0.61	2.27	1.59	5.10	3.63	2.88	2.80
W	1.74	1.22	1.94	0.93	0.00	3.66	3.02	1.81	3.92	5.17	2.58
Pb	4.93	4.97	9.81	8.85	1.79	2.45	3.07	14.19	6.41	8.12	8.91
Cd	0.00	0.14	0.20	0.00	0.00	0.00	0.01	0.05	0.05	0.03	0.04
Tl	0.59	0.29	1.12	0.63	0.13	0.05	0.16	0.70	0.73	0.59	0.52
Ga	13.46	8.73	18.66	11.06	3.56	1.23	3.94	15.88	14.43	13.39	14.93
As	0.00	1.39	2.04	3.62	0.00	2.32	0.80	6.19	3.11	2.35	2.59
Ag	0.00	0.00	0.00	0.00	0.00	0.04	0.08	0.13	0.34	0.44	0.46
Sb	0.86	0.40	1.54	0.73	0.08	0.33	0.25	1.50	1.30	0.85	0.68
$(La/Sm)_{cn}$	3.1	3.9	3.8	3.4	2.8	2.8	4.1	3.7	3.6	3.3	2.8
$(Gd/Yb)_{cn}$	1.6	1.2	1.6	1.3	2.0	2.2	1.9	1.4	1.7	1.6	1.5
$(La/Yb)_{cn}$	6.8	6.1	8.6	6.6	6.7	7.7	10.3	8.2	9.1	7.6	6.1
Ce/Ce*	1.0	0.9	1.0	1.0	0.8	0.9	0.7	1.0	1.0	1.0	0.9
Eu/Eu*	0.8	0.8	0.9	0.7	0.9	0.9	1.2	0.8	0.9	0.9	0.9
∑REE	116	116	208	133	27	33	27	174	209	175	166
Ti/V	67	66	52	64	51	47	54	57	55	62	68
Zr/Hf	28	36	33	33	38	37	43	29	32	33	32
Th/Ce	0.1	0.2	0.1	0.2	0.2	0.1	0.1	0.2	0.1	0.2	0.2
La/Sc	1.9	2.7	1.9	1.7	0.9	6.4	5.9	3.3	3.7	3.3	2.9
Th/Sc	0.4	1.1	0.6	0.7	0.2	1.5	1.2	1.2	1.0	1.0	0.9
Co/Th	2.2	0.8	1.0	0.9	0.4	2.1	2.9	0.7	1.0	0.9	0.9
Th/U	1.8	3.7	3.9	3.4	3.2	3.1	2.8	3.4	4.1	3.7	3.3
Ni/Co	1.9	2.1	1.7	1.2	2.5	2.7	2.0	2.1	2.3	2.3	2.2
Y/Ho	25.6	26.1	27.9	27.9	27.0	29.2	30.3	25.9	26.4	26.5	26.5
V/Sc	3.5	4.1	3.1	1.9	0.4	5.5	5.5	5.2	5.0	4.5	4.0
Facies	Arg.	Sd.	Arg.	Arg.	Sd.	Sd.	Sd.	Arg.	Arg.	Arg.	Arg.

Sample order is from the upper sequence (left) to the lower sequence (right). (Arg.) Argillite; and (Sd.) sandstone.

Appendix 5.1b Major and trace element concentration of the Belt-Purcell Supergroup at the Purcell Mountains.

Formation	Roosville	Roosville	Phillips	Phillips	Phillips	Gateway	Gateway	Gateway	Van Cr.	Van Cr.	Kitchener	Kitchener	Creston	Creston
Levels Fig. 3	P27	P26	P24	P23	P22	P21	P20	P19	P18	P17	P14	P13	P12	P11
Sample	22(1)Pu	22(2)PU	21(2)PU	21(1)Pu	21PuUSO	19(2)PU	19(1)Pu	19PuUSO	18PuUSO	18(1)Pu	17(2)PU	17PuUSO	16(5)PU	16(4)PU
SiO_2 (wt%)	68.6	66.2	71.9	61.0	78.9	71.4	67.5	62.9	68.8	83.0	89.0	50.8	75.5	70.9
TiO_2	0.47	0.63	0.40	0.85	0.46	0.58	0.54	0.52	0.72	0.34	0.12	0.25	0.47	0.58
Al_2O_3	13.55	18.27	11.91	18.82	9.88	16.17	12.30	11.50	15.30	7.81	4.60	7.74	12.39	14.98
Fe_2O_3	2.92	3.77	2.98	6.79	2.95	1.59	4.08	2.90	4.62	2.75	1.88	3.84	2.78	4.13
MnO	0.06	0.00	0.01	0.01	0.00	0.00	0.30	0.05	0.01	0.09	0.02	0.11	0.02	0.04
MgO	3.32	1.84	1.34	2.01	1.18	1.69	4.45	5.23	2.06	1.04	1.50	9.70	1.85	1.49
CaO	1.71	0.13	2.70	0.16	0.44	0.19	1.86	4.39	0.22	0.17	0.27	14.60	0.19	0.22
K_2O	3.60	5.34	3.52	6.08	2.51	5.45	3.29	4.05	4.48	2.15	1.44	4.40	2.85	3.89
Na_2O	1.43	0.45	1.66	1.18	2.04	0.27	0.06	0.38	1.23	1.23	0.10	1.16	1.89	1.10
P_2O_5	0.10	0.06	1.83	0.10	0.03	0.09	0.12	0.09	0.08	0.06	0.04	0.07	0.12	0.05
LOI	4.40	3.30	1.85	3.00	1.75	2.60	5.60	8.30	2.60	1.40	1.20	7.35	1.95	2.55
Sum	100.3	100.1	100.2	100.2	100.2	100.2	100.3	100.3	100.2	100.1	100.2	100.2	100.1	100.2
Li (ppm)	50	35	34	30	65	30	63	57	69	40	13	0	8	22
Rb	134	199	139	254	72	186	111	131	128	61	62	50	124	187
Sr	21	7	50	21	87	28	21	46	25	21	9	65	12	48
Cs	2.97	8.81	5.82	7.86	4.29	5.04	3.35	3.10	8.71	3.38	2.44	0.28	3.53	7.56
Ba	442	392	371	1044	169	513	255	392	575	316	324	1579	349	966
Y	27.1	24.7	34.3	28.5	16.5	30.4	30.6	21.4	28.0	22.3	20.1	12.6	35.2	42.7
Zr	285	189	280	217	116	279	423	79	168	187	62	66	212	341
Hf	8.41	6.36	8.15	6.67	3.93	8.87	12.86	2.79	5.62	5.21	1.80	1.96	6.06	10.14
Nb	13.06	13.37	9.81	20.45	6.18	15.44	13.91	8.25	10.78	5.32	2.46	6.08	11.79	19.99
Ta	1.03	1.24	0.80	1.54	0.60	1.32	1.13	0.81	0.75	0.57	0.20	0.39	0.89	1.48
Th	11.98	15.34	8.88	16.15	4.89	15.10	13.21	5.66	8.65	6.63	3.83	4.40	11.77	17.58
U	3.56	3.05	6.35	5.29	1.92	4.69	3.30	3.17	3.74	2.17	0.94	1.65	2.55	4.34
La	33.29	48.79	19.75	51.45	23.55	32.04	33.31	37.29	34.11	16.61	21.77	13.94	69.99	57.80
Ce	66.09	104.41	48.79	104.95	44.00	61.01	80.88	57.00	62.00	38.52	48.09	28.52	152.68	128.03
Pr	7.77	12.32	6.37	11.58	5.60	6.83	9.44	8.33	8.09	4.26	5.72	3.56	17.96	14.88
Nd	27.52	45.62	30.82	41.87	22.52	23.82	36.25	32.43	30.63	16.44	21.41	12.98	66.27	54.12
Sm	5.40	8.35	11.26	7.79	4.08	4.50	6.92	5.79	5.68	3.28	4.04	2.46	12.67	10.61
Eu	0.840	1.340	2.960	1.540	0.730	0.730	1.050	1.030	1.090	0.700	0.680	0.390	2.060	1.560
Gd	4.90	6.35	14.44	6.43	3.68	4.43	6.28	4.55	5.24	3.84	4.10	2.20	8.35	9.11
Tb	0.740	0.790	1.750	0.870	0.510	0.680	0.890	0.620	0.770	0.650	0.580	0.320	1.020	1.290
Dy	4.66	4.46	8.19	5.20	3.26	5.03	5.83	4.00	5.34	4.14	3.54	2.05	6.31	7.88
Ho	1.060	0.960	1.280	1.070	0.620	1.100	1.190	0.770	1.140	0.820	0.690	0.440	1.300	1.540
Er	3.39	3.08	3.27	3.46	1.75	3.58	3.84	2.35	3.33	2.50	1.99	1.37	3.75	4.72
Tm	0.540	0.510	0.450	0.550	0.270	0.540	0.610	0.360	0.520	0.360	0.270	0.210	0.560	0.710
Yb	3.86	3.57	3.03	3.74	1.81	3.88	4.08	2.40	3.37	2.56	1.62	1.50	3.73	4.84
Lu	0.530	0.520	0.430	0.530	0.270	0.570	0.610	0.360	0.500	0.350	0.210	0.220	0.510	0.680
Sc	15	21	13	30	14	14	15	18	21	7	4	16	10	14
V	52	59	50	100	27	60	46	66	85	31	14	37	46	37
Mo	0.78	0.74	0.44	0.68	0.12	1.74	4.77	0.61	0.37	2.11	2.04	0.34	0.29	0.85
Cr	78	79	71	171	49	57	93	78	120	56	34	55	67	67
Co	7	10	15	13	5	13	59	10	14	16	6	8	11	12
Ni	11	11	18	18	11	14	43	15	20	20	8	12	14	13
Cu	0	4	1	0	3	25	210	6	11	22	4	2	2	12
Zn	11	36	18	0	32	11	16	11	47	7	36	73	33	44
Sn	3.79	4.95	1.96	4.01	1.64	5.28	2.88	3.38	3.39	1.71	1.10	1.46	2.42	3.29
W	1.97	2.04	1.14	2.66	1.17	2.57	4.78	1.06	2.47	1.66	1.14	0.25	1.74	2.47
Pb	3.70	2.55	8.98	6.43	4.41	27.06	12.11	7.05	7.35	12.56	2.78	8.92	3.81	5.60
Cd	0.15	0.00	0.00	0.00	0.38	0.00	0.00	0.00	0.32	0.00	0.00	0.00	0.00	0.00
Tl	0.55	0.74	0.70	1.15	0.30	0.83	1.64	0.44	0.51	0.70	0.39	0.20	0.61	0.89
Ga	14.94	22.98	14.72	24.78	8.33	21.14	14.18	14.29	18.18	8.65	6.32	3.61	15.14	18.13
As	2.65	6.27	3.57	0.85	8.14	47.82	6.11	1.70	1.07	5.82	0.84	0.00	1.08	2.33
Ag	0.00	0.00	0.00	0.00	0.00	0.12	0.00	0.00	0.08	0.08	0.00	0.00	0.04	0.00
Sb	0.78	1.05	0.77	1.25	0.30	5.12	2.47	0.82	0.55	1.02	0.26	0.81	0.49	0.84
$(La/Sm)_{cn}$	3.9	3.7	1.1	4.1	3.6	4.5	3.0	4.0	3.8	3.2	3.4	3.5	3.5	3.4
$(Gd/Yb)_{cn}$	1.1	1.5	3.9	1.4	1.7	0.9	1.3	1.6	1.3	1.2	2.1	1.2	1.9	1.6
$(La/Yb)_{cn}$	6.0	9.5	4.5	9.5	9.0	5.7	5.7	10.8	7.0	4.5	9.3	6.4	13.0	8.3
Ce/Ce*	0.9	1.0	1.0	1.0	0.9	0.9	1.0	0.7	0.9	1.0	1.0	0.9	1.0	1.0
Eu/Eu*	0.8	0.8	1.1	1.0	0.9	0.8	0.8	0.9	0.9	0.9	0.8	0.8	0.9	0.7
∑REE	161	241	153	241	113	149	161	157	162	95	115	70	347	298
Ti/V	190	184	189	170	202	248	190	171	205	279	204	95	295	242
Zr/Hf	34	30	34	33	29	31	34	28	30	36	34	34	35	34
Th/Ce	0.2	0.1	0.2	0.2	0.1	0.2	0.2	0.1	0.1	0.2	0.1	0.2	0.1	0.1
La/Sc	2.2	2.4	1.6	1.7	1.7	2.3	2.2	2.1	1.6	2.3	6.2	0.9	7.3	4.0
Th/Sc	0.8	0.7	0.7	0.5	0.4	1.1	0.8	0.3	0.4	0.9	1.1	0.3	1.2	1.2
Co/Th	0.6	0.6	1.6	0.8	1.0	0.9	0.6	1.8	1.6	2.4	1.6	1.9	0.9	0.7
Th/U	3.4	5.0	1.4	3.1	2.5	3.2	3.4	1.8	2.3	3.1	4.1	2.7	4.6	4.1
Ni/Co	1.4	1.2	1.3	1.3	2.3	1.1	1.4	1.4	1.4	1.3	1.4	1.5	1.3	1.1
Y/Ho	25.6	25.8	26.8	26.6	26.6	27.6	25.6	27.8	24.6	27.2	29.1	28.5	27.1	27.7
V/Sc	3.5	2.9	4.0	3.3	2.0	4.3	3.5	3.6	4.1	4.3	3.9	2.4	4.8	2.5
Facies	Arg.	Arg.	Arg.	Arg.	Sd.	Arg.	Arg.	Arg.	Arg.	Sd.	Sd.	Arg.	Sd.	Arg.

Appendix 5.1b (continued).

Formation	Creston	Creston	Creston	Creston	Aldridge	Aldridge	Aldridge	Fort Steele	Fort Steele	Fort Steele
Levels Fig. 3	P10	P9	P8	P7	P6	P5	P4	P3	P2	P1
Sample	16(3)PU	16(2)PU	16(1)PU	16PuUSO	14(1)Pu	14PuUSO	14(2)Pu	FT(3)PU	FT(2)Pu	FT(1)Pu
SiO_2 (wt%)	73.0	77.7	75.7	62.0	65.1	83.7	79.2	90.1	55.9	59.5
TiO_2	0.50	0.43	0.40	0.49	0.57	0.39	0.44	0.14	0.40	0.96
Al_2O_3	13.32	11.72	10.78	12.80	15.43	8.48	9.68	4.42	10.11	19.69
Fe_2O_3	4.23	3.12	4.46	4.34	8.71	2.13	3.26	1.65	3.46	5.85
MnO	0.05	0.01	0.00	0.10	0.06	0.02	0.04	0.00	0.07	0.02
MgO	1.21	0.67	3.33	7.73	2.23	0.78	1.08	1.66	7.54	4.32
CaO	0.39	0.02	0.07	2.67	0.18	0.14	0.68	0.05	10.87	0.12
K_2O	2.47	3.39	2.59	1.12	3.40	1.98	2.39	0.96	3.71	5.12
Na_2O	2.44	0.76	0.10	3.63	1.08	1.21	1.26	0.07	3.14	0.24
P_2O_5	0.04	0.03	0.04	0.09	0.12	0.03	0.04	0.00	0.08	0.10
LOI	2.30	2.15	2.75	4.30	3.15	1.15	1.80	1.15	4.75	4.05
Sum	100.1	100.1	100.3	99.3	100.2	100.1	100.0	100.2	100.2	100.1
Li (ppm)	20	22	16	40	68	12	29	10	0	19
Rb	120	149	112	58	173	94	122	21	46	116
Sr	116	17	9	91	69	47	110	4	73	9
Cs	6.53	3.39	4.07	4.18	20.77	5.72	8.45	0.29	0.19	1.30
Ba	562	544	289	174	648	351	379	108	923	704
Y	65.7	36.0	41.6	22.6	29.3	7.1	23.8	3.8	23.9	30.7
Zr	394	247	239	92	216	53	337	178	120	290
Hf	11.82	7.20	6.81	3.16	6.30	1.72	9.58	4.74	3.74	8.32
Nb	15.82	9.61	7.90	8.59	12.19	6.69	11.42	1.65	11.22	19.19
Ta	1.24	1.14	0.79	0.67	1.13	0.54	1.03	0.22	0.75	1.40
Th	15.61	12.70	10.86	7.26	12.81	4.56	13.26	2.42	8.97	13.42
U	3.75	3.36	2.03	2.75	3.12	2.09	2.58	0.63	2.60	2.25
La	52.33	32.00	41.60	26.37	10.72	3.69	16.41	6.13	28.18	45.70
Ce	117.25	72.24	92.20	50.00	32.09	5.00	36.54	14.12	58.62	97.75
Pr	13.73	8.18	10.85	6.03	3.06	0.88	4.54	1.59	6.77	11.17
Nd	50.32	29.85	39.21	24.50	11.86	3.35	16.01	5.10	25.43	41.20
Sm	10.20	5.80	7.88	4.48	2.67	0.69	3.22	0.96	4.91	7.12
Eu	1.530	1.060	1.540	0.790	0.560	0.120	0.690	0.140	1.000	2.020
Gd	10.64	6.18	7.59	4.45	3.75	0.71	2.98	0.86	4.67	6.54
Tb	1.710	0.940	1.130	0.630	0.700	0.130	0.510	0.120	0.680	0.940
Dy	11.30	6.51	7.23	4.31	5.06	1.03	3.79	0.64	4.11	5.47
Ho	2.370	1.330	1.510	0.860	1.120	0.250	0.910	0.140	0.860	1.150
Er	7.01	3.99	4.54	2.50	3.52	0.91	2.91	0.40	2.65	3.28
Tm	0.980	0.570	0.650	0.360	0.500	0.160	0.460	0.060	0.390	0.460
Yb	6.49	3.98	4.18	2.44	3.57	1.28	3.22	0.45	2.70	3.24
Lu	0.940	0.530	0.580	0.360	0.520	0.220	0.480	0.070	0.370	0.440
Sc	14	9	10	15	23	11	13	3	16	26
V	45	38	37	61	74	29	39	20	52	121
Mo	0.71	0.83	0.34	8.90	0.68	0.66	0.42	0.00	0.41	0.51
Cr	77	58	67	81	162	47	85	39	71	190
Co	11	10	9	14	26	4	11	7	8	22
Ni	12	13	19	19	38	5	8	11	12	42
Cu	9	7	16	9	70	9	25	2	2	0
Zn	85	41	37	109	112	26	26	8	41	0
Sn	3.38	4.08	2.29	3.14	2.98	2.46	1.97	0.51	1.95	2.53
W	2.12	2.05	2.04	1.74	1.71	1.29	1.15	0.15	0.42	1.22
Pb	17.73	12.62	2.76	9.40	28.12	10.94	14.13	5.55	2.03	1.56
Cd	0.00	0.00	0.00	0.00	0.38	0.00	0.00	0.00	0.24	0.00
Tl	0.54	0.79	0.46	0.50	1.13	0.46	0.64	0.06	0.11	0.36
Ga	17.06	14.83	14.03	17.02	18.83	9.55	9.65	5.65	6.23	22.16
As	9.86	2.62	1.73	0.54	20.59	0.00	0.87	0.66	0.97	0.97
Ag	0.00	0.00	0.00	0.09	0.00	0.00	0.10	0.00	0.00	0.00
Sb	0.75	1.64	0.57	0.40	1.91	0.17	0.24	0.05	0.61	0.10
$(La/Sm)_{cn}$	3.2	3.5	3.3	3.7	2.5	3.3	3.2	4.0	3.6	4.0
$(Gd/Yb)_{cn}$	1.4	1.3	1.5	1.5	0.9	0.5	0.8	1.6	1.4	1.7
$(La/Yb)_{cn}$	5.6	5.6	6.9	7.5	2.1	2.0	3.5	9.4	7.2	9.8
Ce/Ce*	1.0	1.0	1.0	0.9	1.3	0.6	1.0	1.0	1.0	1.0
Eu/Eu*	0.7	0.8	0.9	0.8	0.8	0.8	1.0	0.7	1.0	1.4
∑REE	287	173	221	128	80	18	93	31	141	226
Ti/V	214	280	235	192	152	214	211	307	152	224
Zr/Hf	33	34	35	30	34	31	35	37	32	35
Th/Ce	0.1	0.2	0.1	0.1	0.4	0.9	0.4	0.2	0.2	0.1
La/Sc	3.7	3.5	4.1	1.7	0.5	0.3	1.3	2.2	1.8	1.8
Th/Sc	1.1	1.4	1.1	0.5	0.6	0.4	1.1	0.9	0.6	0.5
Co/Th	0.7	0.8	0.9	2.0	2.1	0.8	0.9	2.9	0.9	1.6
Th/U	4.2	3.8	5.3	2.6	4.1	2.2	5.1	3.8	3.5	6.0
Ni/Co	1.1	1.4	2.0	1.3	1.4	1.3	0.7	1.5	1.6	2.0
Y/Ho	27.7	27.1	27.5	26.3	26.2	28.4	26.1	27.4	27.8	26.7
V/Sc	3.2	4.1	3.7	4.0	3.3	2.6	3.1	7.4	3.3	4.7
Facies	Arg.	Sd.	Sd.	Arg.	Arg.	Sd.	Sd.	Sd.	Arg.	Arg.

Sample order is from the upper sequence (left) to the lower sequence (right). (Arg.) Argillite; and (Sd.) sandstone.

Appendix 5.1c Major and trace element concentration of the Belt-Purcell Supergroup at Whitefish Range.

Formation	Mount Sh.	Mount Sh.	Mount Sh.	Shepard	Snowslip	Snowslip	Wallace	Helena	Empire	Empire	Empire	Spokane	Spokane	Spokane	Burke
Levels Fig. 3	W29	W28	W27	W26	W25	W24	W23	W20	W19	W18	W17	W16	W15	W14	W13
Sample	11(2)Wh	11WhUSO	11(1)Wh	10WhUSO	8(2)Wh	8 Wh USO	7 Wh USO	6(1)Wh	5(2)Wh	5 Wh USO	5(1)Wh	4(2)Wh	4(1)Wh	4WhUSO	3(8)Wh
SiO_2 (wt%)	72.3	68.1	78.9	75.3	80.1	74.4	68.3	67.3	67.2	64.1	79.9	95.9	63.3	84.8	77.8
TiO_2	0.52	0.60	0.47	0.41	0.51	0.67	0.58	0.34	0.43	0.54	0.35	0.07	0.64	0.22	0.39
Al_2O_3	10.18	12.80	8.35	7.27	10.15	12.60	13.80	10.06	9.98	11.90	8.95	1.84	17.68	5.58	11.56
Fe_2O_3	3.11	4.37	3.19	4.66	2.62	3.79	3.93	2.53	2.97	2.86	2.09	0.65	6.01	2.01	2.49
MnO	0.02	0.00	0.01	0.01	0.02	0.03	0.01	0.04	0.09	0.10	0.03	0.01	0.03	0.17	0.07
MgO	3.78	4.09	2.77	3.94	1.11	1.76	4.32	4.21	3.67	4.67	0.84	0.38	2.64	1.52	0.93
CaO	1.76	0.93	0.60	2.01	0.18	0.09	0.86	5.37	5.81	3.66	1.77	0.09	0.21	1.24	0.86
K_2O	3.95	5.00	3.02	3.06	1.86	2.58	3.65	3.11	1.60	2.35	1.85	0.39	5.23	1.43	2.99
Na_2O	0.08	0.11	0.03	0.07	2.22	1.99	1.45	1.22	2.22	2.55	2.11	0.30	1.06	0.59	1.37
P_2O_5	0.08	0.12	0.13	0.11	0.05	0.04	0.07	0.10	0.09	0.09	0.05	0.04	0.14	0.05	0.04
LOI	4.45	3.80	2.30	3.30	1.45	2.10	3.05	5.75	6.00	6.80	2.10	0.35	3.00	2.40	1.50
Sum	100.3	100.1	100.2	100.3	100.4	100.2	100.2	100.2	100.2	99.8	100.2	100.1	100.1	100.1	100.2
Li (ppm)	32	47	29	43	49	31	105	78	44	46	19	20	46	22	28
Rb	109	145	86	48	78	107	151	133	67	96	72	27	235	67	140
Sr	19	17	70	22	39	36	25	46	153	80	71	28	37	27	113
Cs	4.09	6.21	5.41	1.87	3.69	5.55	5.58	8.54	4.48	5.56	3.78	1.46	16.95	5.14	8.08
Ba	331	338	3213	353	226	364	710	682	854	715	531	92	934	353	670
Y	26.4	14.7	22.3	15.9	45.5	28.2	24.3	22.1	27.7	13.1	26.6	8.9	30.0	14.7	46.9
Zr	267	58	662	151	324	99	186	169	220	114	173	81	240	59	234
Hf	6.94	2.11	16.86	4.06	8.27	3.34	6.93	4.83	6.41	3.82	4.44	1.58	6.74	1.82	6.65
Nb	13.65	6.85	12.22	6.28	11.64	10.78	15.93	7.71	9.25	12.40	9.46	1.07	15.53	3.22	18.50
Ta	1.03	0.59	0.91	0.45	1.36	0.76	1.33	0.62	0.79	0.88	0.66	0.09	1.07	0.24	1.45
Th	11.78	4.80	9.37	4.15	12.55	6.11	10.41	9.02	9.65	11.55	6.93	2.32	14.67	3.14	14.03
U	2.97	3.53	1.97	2.27	2.95	3.79	3.44	2.73	1.64	2.51	1.29	0.53	4.06	1.24	3.77
La	29.70	25.22	13.07	14.78	41.05	37.84	35.53	19.48	25.49	22.60	22.36	7.01	53.77	13.08	52.82
Ce	66.07	42.49	30.01	32.12	93.68	49.42	63.00	45.03	57.46	57.00	50.84	12.00	115.12	29.63	122.70
Pr	8.37	5.61	3.97	4.21	11.85	7.48	8.80	5.20	6.88	5.97	6.13	1.84	13.24	3.33	14.60
Nd	31.23	21.59	14.82	16.27	45.32	33.32	36.19	19.18	25.14	23.60	21.89	6.82	48.05	12.85	53.67
Sm	5.68	3.16	3.06	2.60	9.39	5.98	6.85	4.03	5.19	4.67	4.70	1.54	8.59	2.68	10.93
Eu	1.036	0.570	0.592	0.510	1.520	1.030	1.060	0.553	0.910	0.840	0.878	0.290	1.429	0.480	1.274
Gd	5.23	2.71	2.99	2.39	8.89	5.67	5.60	3.86	4.87	3.99	4.52	1.68	6.84	2.71	9.98
Tb	0.766	0.410	0.492	0.380	1.310	0.840	0.760	0.590	0.793	0.510	0.699	0.260	0.901	0.410	1.475
Dy	4.67	2.56	3.56	2.53	8.44	5.39	4.97	3.81	4.89	2.90	4.48	1.49	5.43	2.71	9.36
Ho	0.986	0.570	0.751	0.550	1.710	1.130	1.060	0.778	0.964	0.530	0.851	0.260	1.119	0.540	1.942
Er	2.88	1.65	2.52	1.58	4.74	3.36	3.51	2.43	2.83	1.53	2.55	0.72	3.57	1.53	5.63
Tm	0.438	0.240	0.397	0.250	0.700	0.490	0.580	0.401	0.427	0.290	0.398	0.110	0.571	0.220	0.846
Yb	2.88	1.65	2.83	1.68	4.57	3.15	4.15	2.60	2.84	2.02	2.66	0.62	3.87	1.42	5.44
Lu	0.410	0.250	0.422	0.240	0.630	0.490	0.680	0.398	0.383	0.290	0.370	0.090	0.604	0.200	0.775
Sc	12	11	8	8	6	18	25	13	12	11	9	2	37	8	37
V	46	65	31	23	38	56	49	36	34	50	28	11	78	24	34
Mo	0.18	0.00	0.20	0.41	1.19	4.30	0.34	0.41	0.29	0.42	0.00	0.00	0.37	0.33	0.34
Cr	88	92	97	90	63	87	73	56	71	61	51	15	113	39	58
Co	8	9	14	14	7	3	5	4	8	8	3	3	15	7	6
Ni	17	28	19	15	9	7	9	9	13	13	0	5	27	12	6
Cu	0	3	0	2	9	6	4	8	19	3	5	4	3	2	1
Zn	1	20	23	14	49	39	47	51	54	54	18	15	88	41	40
Sn	2.30	3.12	1.38	1.06	2.21	2.79	3.37	2.30	2.07	2.67	1.90	1.25	4.34	1.26	3.76
W	1.63	2.32	6.15	1.47	2.11	3.02	1.66	1.17	1.58	1.80	1.60	0.33	2.74	0.46	1.93
Pb	5.19	5.13	5.06	4.32	133.53	22.22	7.51	12.20	8.82	4.40	6.27	4.56	27.03	9.78	22.18
Cd	0.00	0.00	0.30	0.26	0.42	0.00	0.00	0.18	0.00	0.00	0.10	0.00	0.15	0.00	0.00
Tl	0.36	0.54	0.35	0.16	0.37	0.46	0.64	0.85	0.39	0.48	0.34	0.08	1.26	0.24	0.67
Ga	10.83	15.96	0.00	6.78	12.46	13.73	16.28	10.95	12.47	12.65	7.90	2.00	21.60	5.69	14.31
As	1.35	1.19	1.09	1.95	7.02	6.74	1.02	9.54	0.77	0.00	1.17	0.99	1.72	1.17	0.64
Ag	0.00	0.00	0.14	0.00	0.03	0.00	0.00	0.00	0.04	0.00	0.00	0.00	0.00	0.00	0.26
Sb	1.16	1.84	6.86	0.57	0.58	0.72	0.52	0.45	0.63	1.19	0.73	0.22	1.90	0.83	0.70
$(La/Sm)_{cn}$	3.3	5.0	2.7	3.6	2.7	4.0	3.2	3.0	3.1	3.0	3.0	2.8	3.9	3.1	3.0
$(Gd/Yb)_{cn}$	1.5	1.4	0.9	1.2	1.6	1.5	1.1	1.2	1.4	1.6	1.4	2.2	1.5	1.6	1.5
$(La/Yb)_{cn}$	7.1	10.6	3.2	6.1	6.2	8.3	5.9	5.2	6.2	7.8	5.8	7.8	9.6	6.4	6.7
Ce/Ce*	1.0	0.8	0.9	0.9	1.0	0.7	0.8	1.0	1.0	1.1	1.0	0.8	1.0	1.0	1.0
Eu/Eu*	0.9	0.9	0.9	0.9	0.8	0.8	0.8	0.6	0.8	0.9	0.9	0.8	0.9	0.8	0.6
∑REE	201	140	100	99	284	199	217	136	172	161	150	44	331	87	355
Ti/V	9393	6252	15222	19772	12512	7963	8287	11168	11913	7657	17049	54384	4833	20914	13804
Zr/Hf	38	27	39	37	39	30	27	35	34	30	39	51	36	32	35
Th/Ce	0.2	0.1	0.3	0.1	0.1	0.1	0.2	0.2	0.2	0.2	0.1	0.2	0.1	0.1	0.1
La/Sc	2.5	2.2	1.5	1.8	6.9	2.1	1.4	1.5	2.1	2.2	2.6	2.8	1.5	1.6	1.4
Th/Sc	1.0	0.4	1.1	0.5	2.1	0.3	0.4	0.7	0.8	1.1	0.8	0.9	0.4	0.4	0.4
Co/Th	0.6	1.4	1.2	2.2	0.6	0.3	0.3	0.6	0.9	0.7	0.4	3.1	0.9	2.2	0.3
Th/U	4.0	1.4	4.8	1.8	4.3	1.6	3.0	3.3	5.9	4.6	5.4	4.4	3.6	2.5	3.7
Ni/Co	2.1	3.0	1.3	1.1	1.3	2.1	1.9	2.1	1.7	1.6	0.0	1.5	1.8	1.7	1.1
Y/Ho	26.7	25.8	29.7	29.0	26.6	25.0	22.9	28.4	28.7	24.7	31.2	34.2	26.8	27.3	24.1
V/Sc	3.9	5.7	3.7	2.7	6.5	3.0	2.0	2.8	2.7	4.8	3.3	4.3	2.1	2.9	0.9
Facies	Arg.	Arg.	Sd.	Sd.	Sd.	Arg.	Arg.	Arg.	Arg.	Arg.	Sd.	Sd.	Arg.	Sd.	Sd.

Appendix 5.1c (continued).

Formation	Burke	Burke	Burke	Burke	Burke	Burke	Burke	Burke	Pric.-Burke	Prichard	Prichard	Prichard
Levels Fig. 3	W12	W11	W10	W9	W8	W7	W6	W5	W4	W3	W2	W1
Sample	3(7)Wh	3(6)Wh	3(5)Wh	3(4)Wh	3(3)Wh	3(2)Wh	3(1)Wh	3WhUSO	2WhUSO	1(2)Wh	1(1)Wh	1WhUSO
SiO_2 (wt%)	76.9	71.7	63.9	83.6	75.8	63.1	67.0	71.3	70.6	61.8	70.3	65.9
TiO_2	0.40	0.65	0.70	0.29	0.41	0.82	0.56	0.62	0.50	0.64	0.59	0.68
Al_2O_3	11.43	14.75	18.17	8.74	12.17	18.99	15.77	14.20	13.10	18.55	14.98	17.10
Fe_2O_3	3.72	3.84	4.80	1.47	3.41	4.98	4.97	4.36	2.76	5.28	5.07	5.52
MnO	0.08	0.05	0.16	0.03	0.05	0.07	0.07	0.06	0.03	0.07	0.05	0.03
MgO	1.17	0.96	2.35	0.36	0.84	1.12	3.47	1.49	2.89	2.14	1.53	1.76
CaO	1.06	1.00	0.57	0.66	0.99	0.86	1.03	0.78	1.27	1.41	0.24	0.22
K_2O	1.80	3.28	5.12	1.26	2.90	5.31	3.57	3.49	3.89	3.66	3.55	4.30
Na_2O	2.62	1.95	1.25	2.73	1.97	2.14	1.48	2.13	1.62	3.31	1.41	1.49
P_2O_5	0.01	0.07	0.05	0.00	0.10	0.02	0.11	0.03	0.09	0.05	0.06	0.07
LOI	0.90	1.65	2.95	0.90	1.35	2.50	2.10	1.55	3.25	2.05	2.20	2.90
Sum	100.2	100.1	100.2	100.2	100.2	100.1	100.3	100.2	100.2	99.1	100.1	100.1
Li (ppm)	31	34	61	10	29	42	57	38	53	53	52	47
Rb	95	127	242	58	138	232	152	171	134	236	174	171
Sr	125	99	90	100	160	132	103	125	39	218	50	36
Cs	6.33	7.84	14.44	3.26	8.51	12.05	10.83	10.22	5.53	20.75	12.63	6.28
Ba	311	882	1173	293	709	1283	886	716	771	544	620	1098
Y	19.4	25.3	39.2	22.3	37.5	39.5	30.5	27.6	25.6	31.5	21.5	10.2
Zr	130	179	219	137	205	274	222	97	143	185	222	170
Hf	3.08	5.42	6.75	3.35	5.13	8.89	6.13	3.29	4.55	5.49	6.02	5.03
Nb	10.95	12.24	16.80	7.05	13.34	19.41	16.08	9.09	10.09	17.11	17.62	15.52
Ta	0.67	0.96	1.28	0.48	1.00	1.31	1.07	0.56	0.74	1.24	1.26	1.20
Th	8.46	11.22	16.95	7.64	10.44	18.22	9.04	8.90	6.88	13.15	10.14	5.80
U	1.74	3.21	4.52	1.91	3.29	4.04	2.56	3.87	3.91	2.08	1.92	4.00
La	25.29	34.36	36.91	29.36	42.52	46.15	16.15	36.03	31.46	43.07	18.00	22.54
Ce	61.34	78.35	87.12	58.88	101.28	107.40	31.54	69.60	53.24	91.60	36.27	49.05
Pr	6.52	9.26	10.56	7.38	10.91	12.38	4.25	8.00	7.51	10.59	4.37	5.81
Nd	23.62	32.78	38.59	27.10	40.67	44.23	16.21	34.25	30.65	37.98	15.73	23.03
Sm	4.43	6.74	8.07	5.14	8.08	8.59	3.98	6.33	6.00	6.92	2.91	3.98
Eu	0.801	1.259	1.229	0.968	1.359	1.772	0.679	1.090	0.950	1.450	0.502	0.650
Gd	4.03	5.53	7.80	4.99	7.56	7.85	4.11	5.47	5.66	6.36	2.80	3.04
Tb	0.534	0.751	1.206	0.626	1.097	1.167	0.677	0.720	0.740	0.886	0.416	0.380
Dy	3.38	4.85	7.69	3.89	6.79	7.62	4.77	5.25	4.79	5.64	3.07	2.16
Ho	0.698	1.036	1.565	0.801	1.365	1.582	1.084	1.090	0.960	1.196	0.719	0.430
Er	2.14	3.25	4.71	2.32	4.05	4.63	3.49	3.19	2.92	3.45	2.60	1.23
Tm	0.335	0.522	0.705	0.316	0.606	0.698	0.560	0.460	0.440	0.525	0.445	0.190
Yb	2.43	3.41	4.75	2.24	4.02	4.66	3.91	3.07	3.02	3.60	3.36	1.29
Lu	0.366	0.484	0.675	0.351	0.577	0.756	0.576	0.450	0.460	0.579	0.533	0.200
Sc	30	31	44	11	28	47	37	18	18	49	33	7
V	32	56	87	23	52	71	75	58	36	90	65	99
Mo	0.23	0.33	0.57	0.26	0.21	0.50	2.01	0.27	0.56	1.87	0.66	0.71
Cr	69	89	124	35	61	130	120	78	60	120	107	123
Co	10	10	19	7	8	13	15	11	2	11	7	15
Ni	16	8	32	7	14	18	28	16	8	13	6	27
Cu	19	10	68	10	5	0	0	13	4	29	17	8
Zn	74	45	99	26	53	58	83	76	57	105	74	44
Sn	2.73	3.37	4.20	1.63	2.75	4.66	2.92	3.68	3.89	3.50	3.36	3.87
W	1.28	2.65	2.70	0.96	1.94	3.36	1.96	2.25	2.21	2.87	3.07	2.27
Pb	17.36	11.89	22.42	11.39	15.20	19.86	27.71	19.71	4.76	59.80	15.47	8.11
Cd	0.20	0.32	0.00	0.00	0.00	0.14	0.00	0.00	0.32	0.27	0.11	0.53
Tl	0.53	0.59	1.22	0.36	0.67	1.08	0.82	0.95	0.72	1.41	0.81	0.80
Ga	12.07	15.66	26.79	7.57	13.94	20.54	20.11	16.33	14.73	21.73	18.40	17.49
As	0.35	1.58	0.00	1.02	0.55	1.36	1.85	0.63	1.06	0.54	1.93	6.97
Ag	0.00	0.00	0.36	0.00	0.04	0.00	0.08	0.05	0.00	0.17	0.03	0.00
Sb	0.47	0.65	0.55	1.00	0.19	0.58	0.17	1.19	0.69	0.33	0.64	0.86
$(La/Sm)_{cn}$	3.6	3.2	2.9	3.6	3.3	3.4	2.5	3.6	3.3	3.9	3.9	3.5
$(Gd/Yb)_{cn}$	1.4	1.3	1.4	1.8	1.6	1.4	0.9	1.5	1.6	1.5	0.7	1.9
$(La/Yb)_{cn}$	7.2	7.0	5.4	9.1	7.3	6.9	2.9	8.1	7.2	8.3	3.7	12.1
Ce/Ce*	1.1	1.0	1.0	0.9	1.1	1.0	0.9	0.9	0.8	1.0	0.9	1.0
Eu/Eu*	0.9	0.9	0.7	0.9	0.8	1.0	0.8	0.9	0.7	1.0	0.8	0.9
∑REE	168	227	264	180	282	312	115	220	187	267	117	145
Ti/V	14299	7669	4418	21880	8793	5334	5362	7334	11758	4095	6451	4004
Zr/Hf	42.0	33.0	32.5	41.1	39.9	30.9	36.2	29.6	31.4	33.7	36.9	33.8
Th/Ce	0.1	0.1	0.2	0.1	0.1	0.2	0.3	0.1	0.1	0.1	0.3	0.1
La/Sc	0.8	1.1	0.8	2.6	1.5	1.0	0.4	2.0	1.7	0.9	0.5	3.4
Th/Sc	0.3	0.4	0.4	0.7	0.4	0.4	0.2	0.5	0.4	0.3	0.3	0.9
Co/Th	0.9	0.8	1.1	0.9	0.6	0.7	0.9	1.2	0.2	0.7	0.4	1.0
Th/U	4.9	3.5	3.8	4.0	3.2	4.5	3.5	2.3	1.8	6.3	5.3	1.4
Ni/Co	1.6	0.8	1.7	1.1	1.8	1.4	1.9	1.4	3.3	1.1	0.8	1.9
Y/Ho	27.8	24.4	25.0	27.9	27.5	24.9	28.1	25.3	26.7	26.4	29.9	23.6
V/Sc	1.1	1.8	2.0	2.0	1.9	1.5	2.0	3.3	1.9	1.8	2.0	15.0
Facies	Sd.	Arg..	Arg.	Sd.	Sd.	Arg.	Arg.	Arg.	Arg.	Arg.	Arg.	Arg.

Sample order is from the upper sequence (left) to the lower sequence (right). (Arg.) Argillite; and (Sd.) sandstone.

5.9 References

Adachi, M.N., Aktai, K.M.T., Edach, Y.N., 1999. Geochemistry of paleosols formed under oxic and anoxic conditions in Babeldaob Island, Palau. South Pacific Study 20, 39-59.

Alderton, D.H. Pearce, M., J.A., Potts, P.J., 1980. Rare earth element mobility during granite alteration: evidence from southwestern England. Earth Planet. Sci. Lett. 49, 149-165.

Anderson, H.E., Davis, D.W., 1995. U-Pb geochronology of the Moyie sills, Purcell Supergroup, southeastern British Columbia: implications for the Mesoproterozoic geological history of the Purcell Belt Basin. Can. J. Earth Sci. 32, 1180-1193.

Aspler, L.B., Chiarenzelli, J.R., Cousens, B.L., 2004. Fluvial, lacustrine and volcanic sedimentation in the Angikuni sub-basin, and initiation of ~1.84-1.79 Ga Baker Lake basin, western Churchill Province, Nunavut, Canada. Precambrian Res. 129, 225-250.

Berner, R.A., 1971. Principles of chemical sedimentology. McGraw-Hill, New York, N.Y., U.S.A.

Bhat, M.I., Ghosh, S.K., 2001. Geochemistry of the 2.51 Ga old Rampur group pelites, western Himalayas: implications for their provenance and weathering. Precambrian Res. 108, 1-16.

Braun, J.J., Pagel, M., Herbillion, A., Rosin, C., 1993. Mobilization and redistribution of REEs and thorium in a syenitic lateritic profile: a mass balance study. Geochim. Cosmochim. Acta 57, 4419-4434.

Braun, J.J., Pagel, M., Muller, J.P., Bilong, P., Michard, A., Guillet, B., 1990. Cerium anomalies in lateritic profiles. Geochim. Cosmochim. Acta 54, 781-795.

Brown, A.V., Jenner, G.A., 1989. Geological setting, petrology and chemistry of Cambrian boninite and low-Ti tholeiite lavas of western Tasmania. In: Crawford, A.J., (ed.), Boninites and Related Rocks, Unwin-Hyman, London. pp. 232–263.

Brookins, D.G., 1988. Eh-pH diagrams for geochemistry. Springer-Verlag, Albuquerque, N.M., U.S.A.

Chandler, F.W., 2000. The Belt-Purcell Basin as a low-latitude passive rift: implications for the geological environment of Sullivan type deposits. In: Lydon, J.W., Höy, T., Slack, J.F., Knapp, M.E., (eds.), The Geological Environment of the Sullivan Deposit, British Columbia. Geol. Assoc. Can. Min. Dep. Div. Spec. Publ. 1, pp. 82-112.

Condie, K.C. 1993. Chemical composition and evolution of the upper continental crust: contrasting results from surface samples and shales. Chem. Geol. 104, 1-37.

Cook, N.D.J., Ashley, P. M., 1992. Metaeveporite sequence, exhalative chemical sediments and associate rocks in the Proterozoic Willyama Supergroup, south Australia: implications for metallogenesis. Precambrian Res. 56, 211-226.

Cook, F.A., Van Der Velden, A.J., 1995. Three-dimensional crustal structure of the Purcell anticlinorium in the Cordillera of southwestern Canada. Geol. Soc. Am. Bull. 107, 642-664.

Crawford, A.J., T.J., Falloon, D. H., Green, 1989. Classification, petrogenesis, and tectonic setting of bo-

ninites. In: Boninites and Related Rocks, Crawford, A.J., (ed.), Unwin-Hyman, London. pp. 1-49.

Cullers, R.L., Podkovyrov, V.N., 2002. The source and origin of terrigenous sedimentary rocks in the Mesoproterozoic Ui group, southeastern Russia. Precambrian Res. 117, 157-183.

Cullers, R.L., Chaudhuri, S., Kilbane, N., Koch, R., 1979. Rare-earths in size fractions and sedimentary-rocks of Pennsylvanian-Permian age from the mid-continent of the USA. Geochim. Cosmochim. Acta 43, 1285-1301.

De Baar, H.J.W., Bacon, M.P., Brewer, P.G., 1985. Rare earth elements in the Pacific and Atlantic Oceans. Geochim. Cosmochim. Acta 49, 1943-1959.

Duddy, I. R., 1980. Redistribution and fractionation of rare-earth and other elements in a weathering profile. Chem. Geol. 30, 363-381.

Evans, K.V., Aleinikoff, J.N., Obradovich, J.D., Fanning, C.M., 2000. SHRIMP U-Pb geochronology of volcanic rocks, Belt Supergroup, western Montana: evidence for rapid deposition of sedimentary strata. Can. J. Earth Sci. 37, 1287-1300.

Fan, J., Kerrich, R., 1997. Geochimical characteristics of aluminum depleted and undepleted komatiites and HREE-enriched low-Ti tholeiites, western Abitibi greenstone belt: a heterogeneous mantle plume-convergent margin environment. Geochim. Cosmochim. Acta 61, 4723-4744.

Fayek, M, Kyser, T.K., 1997. Characterization of multiple fluid-flow events and rare-earth element mobility associated with formation of unconformity-type uranium deposits in the Athabasca Basin, Can. Min. 35, 627-658.

Fedo, C.M., Nesbitt, H.W., Young, G.M., 1995. Unraveling the effects of potassium metasomatism in sedimentary rocks and paleosols, with implications for paleoweathering conditions and provenance. Geology 23, 921-924.

Folk, R.L., 1968. Petrology of sedimentary rocks. Hemphill's, Austin, U.S.A.

Fralick, P.W., 2003. Geochemistry of clastic sedimentary rocks: ratio techniques. In: Geochemistry of Sediments and Sedimentary Rocks: Evolutionary Considerations to Mineral-deposit Forming Environments. In: Lentz, D.R. (ed.), Geol. Assoc. Can., St. John's, Newfoundland, Canada, Geo Text 4. pp. 85-103.

Frimmel, H.E., Jian, S.Y., 2001. Marine evaporites from an oceanic island in the Neoproterozoic Adamastor Ocean. Precambrian Res. 105, 57-71.

Frost, C.D., Winston, D., 1987. Nd isotope systematics of coarse-and fine-grained sediments: examples from the Middle Proterozoic Belt-Purcell Supergroup. J. Geol. 95, 309-327.

Fryer, B.J., Kerrich, R., Hutchinson, R.W., Pierce, M.G., Rogers, D.S., 1979. Archean precious-metal hydrothermal systems, Dome mine, Abitibi greenstone-belt. Patterns of alteration and metal distribution. Can. J. Earth Sci. 16, 421-439.

Gaillardet, J., Dupré, B., Allègre, C.J, 1999. Geochemistry of large river suspended sediments: silicate

weathering or recycling tracer? Geochim. Cosmochim. 63, 4037-4051.

Gíslason, S.R., Eugster, H.P., 1987. Meteoric water-basalt interactions: I. A laboratory study. Geochim. Cosmochim. Acta 51, 2827-2840.

Gieré, R. 1989. Hydrothermal mobility of Ti, Zr and REE: examples from the Bergell and Adamello contact aureoles Italy. Terra Nova 2, 60-67.

Golani, P.R., Pandit, M.K., Sial, A.N., Fallick, A.E., Ferreira, V.P., Roy, A.B., 2002. B-Na rich Palaeoproterozoic Aravalli metasediments of evaporitic association, NW India: a new repository of gold mineralization. Precambrian Res. 116, 183-198.

González-Álvarez, I., Kerrich, R., *submitted*. Weathering intensity on Laurentia in the Mesoproterozoic: evidence from the Belt-Purcell Supergroup, Western North America.

González-Álvarez, I.J., Kerrich, R., Pratt, B.R., 2003. Geochimistry of the Appekunny and the Grinnell formations: Mesoproterozoic siliciclastic rocks of the Belt-Purcell Supergroup, western USA and Canada. IAS 22nd International Meeting of Sedimentologists, Abstract book, 68.

González-Álvarez, I.J., Kusiak, M.A., Kerrich, R., *in press*. A trace element and chemical Th-U total Pb dating study in the lower Belt-Purcell Supergroup, western North America: provenance and diagenetic implications. Chem. Geol.

Grant, J.A., 1986. The isocon diagram-a simple solution to Gressens' equation for metasomatic alteration. Econ. Geol. 81, 1976-1982.

Gresens, R.L., 1967. Composition-volume relationships of metasomatism. Chem. Geol. 2, 47-65.

Harrison, J.E., 1972. Precambrian Belt Basin of northwestern United States: its geometry, sedimentation, and copper occurrences. Geol. Soc. Am. Bull. 83, 1215-1240.

Hoffman, P.F., 1991. Did the breakout of Laurentia turn Gondwana inside out? Science 252, 1409-1412.

Holland, H.D., 1978. The chemistry of the atmosphere and oceans. Wiley & Sons, N.Y., U.S.A.

Horodyski, R.J., 1993. Paleontology of Proterozoic shales and mudstones: examples from the Belt Supergroup, Chuar group and Pahrump Group, western U.S.A. Precambrian Res. 61, 241-278.

Hutcheon, I., 1989. Application of chemical and isotopic analyses of fluids to problems in sandstone diagenesis. In: Hutcheon, I.E. (ed.), Burial Diagenesis. Geol. Assoc. Canada 15, pp. 279-310.

Humphries, S.E., 1984. The mobility of the rare earth elements in the crust. In: Henderson, P. (ed.), Rare Earth Element Geochimistry, Elsevier, Oxford, New York, pp. 317-342.

Jackson, G.D., Iannelli, T.R. 1981. Rift-related cyclic sedimentation in the Neohelikian Borden Basin, northern Baffin Island. In: Campbell, F.H.A. (ed.), Proterozoic Basins of Canada. Geol. Surv. Canada, Paper 81-10, pp. 269–302.

Jenner, G.A, Longerich, H.P., Jackson, S.E., Fryer, B.J., 1990. ICP-MS a powerful tool for high precision trace-element analysis in earth sciences: evidence from analysis of selected USGS reference samples. Chem. Geol. 83, 133-148.

Johannesson, K.H., Lyons, W.B., 1995. Rare-earth element Geochimistry of Colour Lake and acidic freshwater lake on Axel Heiberg Island, Northwest Territories, Canada. Chem. Geol. 119, 209-223.

Kamber, B.S., Webb, G.E., 2001. The Geochimistry of late Archaean microbial carbonate: implications for ocean chemistry and continental erosion history. Geochim. Cosmochim. Acta 65, 2509-2525.

Kerrich, R., 1983. Geochemistry of gold deposits in the Abitibi Greenstone Belt, Geochemical Exploration, Archean lode Au, Canada. Can. Inst. Min. Metal. Petrol. Spec. Publ. 27, pp. 75.

Kerrich, R., González-Álvarez, I.J., 2004. Weathering intensity on Laurentia in the Mesoproterozoic: evidence from CIA of the lower Belt Supergroup. Eos Trans. American Geophysicist Union, 8517, Jt. Assem. Suppl., Abstract V43A-01.

Kerrich, R., King, R., 1993. Hydrothermal zircon and baddeleyite in Val-d'Or Archean mesothermal gold deposits: characteristics, compositions, and fluid-inclusion properties, with implications for timing of primary gold mineralization. Can. J. Earth Sci., 30, 2334-2351.

Kerrich, R., Renaut, R.W., Bonli, T., 2002. Trace-element composition of cherts from alkaline lakes in the east African rift: a probe for ancient counterparts. In: Renaut, R.W., Ashley, G.M. (eds.), Sedimentation in Continental Rifts, Soc. Sed. Geol., Boulder, Colorado, Spec. Publ. 73, pp. 277-298.

Kerrich, R., Wyman, D., Fan, J., Bleeker, W., 1998. Boninite–low Ti–tholeiite associations from the 2.7 Ga Abitibi greenstone belt. Earth Planet. Sci. Lett. 164, 303–316.

Kerrich, R., Allison, I., Barnett, R.L., Moss, S., Starkey, J., 1980. Microstructural and chemical transformations accompanying deformation of granite in a shear zone at Miéville, Switzerland; with implications for stress corrosion and superplastic flow. Contrib. Mineral. Petrol. 73, 221–242.

Krauskopf, K.B., 1985. Introduction to geochemistry. McGraw-Hill, Singapore.

Kraynov, S.R., Mer'kov, A.N., Petrova, N.G., Baturinskaya, I.V., Zharikova, V.M., 1969. Highly alkaline pH 12 flurosilicate waters in the deeper zones of the Lovozero massif. Geokhimiya 7, 791-796.

Kurt, A.C., Derry, L.A., Chadwick, O.A., Alfano, M.J., 2000. Refractory element mobility in volcanic soils. Geology 28, 683-686.

Kyser, K., Hiatt, E., Renac, C., Durocher, K., Holk, G., Deckart, K., 2000. Diagenetic fluids in Paleo- and Mesoproterozoic sedimentary basins and their implications for long protected fluid histories. In: Kyser, K. (ed.), Fluids and Basin Evolution, Min. Assoc. Can., Short Course Series, vol. 28, Kingston, Ontario, pp. 225-262.

Leitch, C. H. B., R. J. W. Turner, K. V. Ross, and D. R. Shaw 2000, Wallrock alteration at the Sullivan deposit and surrounding area. In: Lydon, J.W., Höy, T., Slack, J.F., Knapp, M.E., (eds.), The Geological Environment of the Sullivan Deposit, British Columbia. Geol. Assoc. Can. Min. Dep. Div. Spec. Publ. 1, pp. 618-632.

Li, C., Peng, P., Sheng, G., Fu, J., Yan, Y., 2003. A molecular an isotopic study of Meso- to Neoproterozoic 1.73-0.85 Ga sediments from the Jixian section, Yanshan Basin, North China. Precambrian Res. 125,

337-356.

Lydon, J.W., 2000. A synopsis of the understanding of the geological environment of the Sullivan Deposit. In: Lydon, J.W., Höy, T., Slack, J.F., Knapp, M.E., (eds.), The Geological Environment of the Sullivan Deposit, British Columbia. Geol. Assoc. Can. Min. Dep. Div. Spec. Publ. 1, pp. 12-31.

Lydon, J.W., Walker, R., Anderson, H.E., 2000. Lithogeochemistry of the Aldridge Formation and the chemical effects of burial diagenesis. In: Lydon, J.W., Höy, T., Slack, J.F., Knapp, M.E., (eds.), The Geological Environment of the Sullivan Deposit, British Columbia. Geol. Assoc. Can. Min. Dep. Div. Spec. Publ. 1, pp. 137-179.

Maas, R., McCulloch, M.T., 1991. The provenance of Archean clastic metasediments in the Narryer gneiss complex, western Australia: trace element geochemistry, Nd isotopes, and U-Pb ages for detrital zircons. Geochim. Cosmochim. Acta 55, 1915-1932.

Marsh, J., 1991. REE fractionation and Ce anomalies in weathered Karoo dolerite, Chem. Geol. 90, 189-194.

Matthews, A., Fouillac, C., Hill, R., O'Nions, R.K., Oxburgh, E.R., (1987). Mantle-derived volatiles in continental crust: the Massif Central of France. Earth Planet. Sci. Lett. 85, 117–128.

Maxwell, D.T., Hower, J., 1967. High-grade diagenesis and low-grade metamorphism of illite in the Precambrian Belt Series. Am. Mineral. 52, 843-857.

Mazumder R., Sarkar, S., 2004. Sedimentation history of the Palaeoproterozoic Dhanjori Formation, Singhbhum, eastern India. Precambrian Res. 130, 267-287.

McDaniel, D.K., Hemming, S.R., McLennan, S.M., Hanson, G.N., 1994. Resetting of neodymium isotopes and redistribution of REEs during sedimentary processes: the early Proterozoic Chelmsford Formation, Sudbury Basin, Ontario, Canada. Geochim. Cosmochim. Acta 58, 931-941.

McLennan, S.M., Simonetti, A., Goldstein, S.L., 2000. Nd and Pb isotopic evidence for provenance and post-depositional alteration of the Paleoproterozoic Huronian Supergroup, Canada. Precambrian Res. 102, 263-278.

McLennan, S.M., Bock, B., Hemming, R.S., Hurowitz, J.A., Lev, S.M., McDaniel, D.K., 2003. The roles of provenance and sedimentary processes in the geochemistry of sedimentary rocks. In: Lentz, D.R. (ed.), Geochemistry of Sediments and Sedimentary Rocks: Evolutionary Considerations to Mineral-Deposit Forming Environments. Geol. Assoc. Can., St. John's, Newfoundland, Canada, Geo Text 4, pp. 7-38.

McMechan, M.E., 1981. The middle Proterozoic Purcell Supergroup in the southwestern Rocky and southeastern Purcell Mountains, British Columbia and the initiation of the Cordilleran miogeocline, southern Canada and adjacent United States. Bull. Can. Petrol. Geol. 29, 583-621.

Mongelli, G., 1993. REE and other trace elements in a granitic weathering profile from "Serre", southern Italy. Chem. Geol. 103, 17-25.

Morey, G.B., Setterholm, D.R., 1997. Rare earth element in weathering profiles and sediments of Minnesota: implications for provenance studies. J. Sed. Res. 67, 105-115.

Mori, Y., Nishiyama, T., Yanagi, T., 2003. Mass transfer and reaction paths in alteration zones around carbonate veins in the Nishisonogi metamorphic rocks, southwest Japan. Am. Mineral. 88, 611–623.

Morse, J.W., 2004. Formation and diagenesis of carbonate sediments. In: MacKenzie, F.T., (ed.), Sediments, Diagenesis, and Sedimentary Rocks, Treatise on Geochimistry, Holland, H.D., Turekian, K.K., (eds.), Elsevier, Oxford, New York, 7, pp. 67-86.

Murali, A.V., Parthasarathy, R., Mahadevan, T.M., Sankar Das, M., 1983. Trace element chracteristics, REE patterns and partition coefficients of zircons from different geological environments-A case study on Indian zircons. Geochim. Cosmochim. Acta 47, 2047-2052.

Nesbitt, H.W., 2003. Petrogenesis of siliciclastic sediments and sedimentary rocks. In: Lentz, D.R. (ed.), Geochimistry of Sediments and Sedimentary Rocks: Evolutionary Considerations to Mineral-Deposit Forming Environments, Geo Text 4, Geol. Assoc. Can., St. John's, Newfoundland, Canada, pp. 39-103.

Nesbitt, H.W., Young, G.M., 1982. Early Proterozoic climates and plate motions inferred from major element chemistry of lutites. Nature 299, 715-717.

Nozaki, Y., Zhang, J., Amakawa, H., 1997. The fractionation between Y and Ho in the marine environment, Earth Planet. Sci. Lett. 148, 329-340.

Pearce, J.A., Peate, D.W., 1995. Tectonic implications of the composition of volcanic arc magmas. Ann. Rev. Earth Planet. Sc. 23, 251-285.

Peng, Q.M., Palmer, M.R., 1995. The Palaeoproterozoic boron deposits in eastern Liaoning, China: a metamorphosed evaporite. Precambrian Res. 27, 185-197.

Plank, T., Langmuir, C.H., 1998. The chemical composition of subducting sediment and its consequences for the crust and mantle. Chem. Geol. 145, 325-394.

Polat, A., Hofmann, A.W., Rosing, M.T., 2002. Boninite-like volcanic rocks in the 3.7–3.8 Ga Isua greenstone belt, West Greenland: Geochemical evidence for intraoceanic subduction zone processes in the early Earth. Chem. Geol. 184, 231–254.

Potts, P.J., Tindle, A.G., Webb, P.C., 1992. Geochemical reference material compositions. In: Whittles, F. L. (ed.), Rocks, Minerals, Sediment, Soils, Carbonates, Refractories and Ores Used in Research and Industry. CRC Press, Boca Raton, Latheronwheel, Caithness, U.K., pp. 220-221.

Pratt, B.R., 2001. Oceanography, bathymetry and syndepositional tectonics of a Precambrian intracratonic basin: integrating sediment, storms, earthquakes and tsunamis in the Belt Supergroup (Helena Formation, ca. 1.45 Ga), western North America. Sediment. Geol. 141, 371-394.

Price, R.A., Sears, J.W, 2000. A preliminary palinspastic map of the Mesoproterozoic Belt-Purcell Supergroup, Canada and USA: implications for the tectonic setting and structural evolution of the Purcell

anticlinorium and the Sullivan deposit. In: Lydon, J.W., Höy, T., Slack, J.F., Knapp, M.E., (eds.), The Geological Environment of the Sullivan Deposit, British Columbia. Geol. Assoc. Can. Min. Dep. Div. Spec. Publ. 1, pp. 61-81.

Rainbird, R.H., Nesbitt, H.W., Donalson, J.A., 1990. Formation and diagenesis of a sub-huronian saprolith: comparison with a modern weathering profile. J. Geol. 98, 801-822.

Rainbird, R.H., Jefferson, C.W., Young, C.M., 1996. The early Neoproterozoic sedimentary Succession B of northwestern Laurentia: correlations and paleogeograpic significance. Geol. Soc. Am. Bull. 108, 454-470.

Ray, J.S., Veizer, J., Davis, W.J., 2003. C, O, Sr and Pb isotope systematics of carbonate sequences of the Vindhyan Supergroup, India: age, diagenesis, correlations and implications for global events. Precambrian Res. 121, 103-140.

Renac, C., Kyser, T.K., Durocher, K., Dreaver, G., O'Connor, T., 2002. Comparison of diagenetic fluids in the Proterozoic Thelon and Athabasca basins, Canada: implications for long protracted fluid histories in stable intracratonic basins. Can. J. Earth Sci. 39, 113– 132.

Ross, G.M., Villenueve, M.E., 2003. Provenance of the Mesoproterozoic (1.45 Ga) Belt Basin (western North America): another piece in the pre-Rodinia paleogeographic puzzle. Geol. Soc. Am. 115, 1191-1217.

Ross, G.M., Parrish, R.R., Dudás, F.Ö., 1991. Provenance of the Bonner Formation (Belt Supergroup), Montana: insights from U-Pb and Sm-Nd analyses of detrital minerals. Geology 19, 340-343.

Rubin, J.N., Henry, C.D., Price, J.G., 1989. Hydrothermal zircons and zircon overgrowths, Sierra Blanca Peaks, Texas. Am. Mineral. 74, 865-869.

Rudnick, R.L., S., Gao, 2004. The composition of the continental crust. In: Rudnick, R.L. (ed.), The Crust-Treatise on Geochimistry, Holland, H.D., Turekian, K.K., (eds.), Elsevier, Oxford, New York, 3, pp. 1-64.

Schandl, E.S., Gorton, M.P., Lydon, J.W., 2000. Trace and rare earth element study of sediments associated with the Sullivan sedex deposit, British Columbia: implications for element mobility and tectonic environment. In: Lydon, J.W., Höy, T., Slack, J.F., Knapp, M.E., (eds.), The Geological Environment of the Sullivan Deposit, British Columbia. Geol. Assoc. Can. Min. Dep. Div. Spec. Publ. 1, pp. 202-217.

Schieber, J., 1997. Sedimentological, geochemical, and mineralogical features of the Belt Supergroup and their bearing on the lacustrine versus marine debate. In: Link, P. K., (ed.), Belt Symposium III, Geologic Guidebook to the Belt-Purcell Supergroup, Glacier National Park and Vicinity, Montana and Adjacent Canada, Belt Association, Pocatello, Idaho, pp. 177-189.

Sears, J.W., Price, R.A., 2000. New look at the Siberian connection: no SWEAT. Geology 28, 423-426.

Sears, J.W., Chamberlain, K.R., Buckley, S.N., 1998. Structural and U-Pb geochronological evidence for

1.47 Ga rifting in the Belt basin, western Montana. Can. J. Earth Sci. 35, 467-475.

Sears, J.W., Price, R.A., Khudoley, A.K, 2004. Linking the Mesoproterozoic Belt-Purcell Supergroup and Udzha Basin across the west Laurentia-Siberia connection. Precambrian Res. 129, 291-308.

Slack, J.F., Höy, T., 2000. Geochemistry and provenance of clastic metasedimentary rocks of the Aldridge and Fort Steele formations, Purcell Supergroup, southeastern British Columbia. In: Lydon, J.W., Höy, T., Slack, J.F., Knapp, M.E., (eds.), The Geological Environment of the Sullivan Deposit, British Columbia. Geol. Assoc. Can. Min. Dep. Div. Spec. Publ. 1, pp. 180-201.

Smithies, H.R., Champion, D.C., Cassidy, K.F., 2003. Formation of Earth's early Archaean continental crust. Precambrian Res. 127, 89–101.

Sun, S.S., McDonough, W.F., 1989. Chemical and isotopic systematics of ocean basalts: implications or mantle composition and processes. In: Magmatism in the Ocean Basins, Saunders, A.D., Norry, M.J. (eds.), Geol. Soc. London, Spec. Publ. 42, pp. 313-346.

Taylor, S.R., McLennan, S.M., 1985. The continental crust: its composition and evolution. Blackwell, Oxford, U. K.

Taylor, S.R., McLennan, S.M., 1995. The geochemical evolution of the continental crust. Rev. Geophys. 33, 241-265.

Terakado, Y., Fujitani, T., 1998. Behavior of the rare earth elements and other trace elements during interactions between acidic hydrothermal solutions and silicic volcanic rocks, southwestern Japan. Geochim. Cosmochim. Acta 62, 1903-1917.

Tran, H.T., Ansdell, K., Bethune, K., Watters, B., Ashton, K., 2003. Nd isotope and geochemical constraints on the depositional setting of Paleoproterozoic metasedimentary rocks along the margin of the Archean Hearne craton. Precambrian Res. 123, 1-28.

Volkova, N.I., 1998. Geochimistry of rare elements in waters and sediments of alkaline lakes in the Sasykkul depression, east Pamirs. Chem. Geol. 147, 265-277.

Whiple, J.W., Connor, J.J., Raup, O.B., McGrimsey, R.G., 1984. Preliminary report on the stratigraphy of the Belt Supergroup, Glacier National Park and adjacent Whitefish Range, Montana. In: McBane, J.D., Garrison, P.B., (eds.), Northwest Montana and Adjacent Canada, Montana Geol. Soc. Guidebook, 1984 Field Conference and Symposium, pp. 33-50.

Whipple, J.W., Binda, P.L., Winston, D., 1997. Geologic guide to Glacier National Park, Montana and areas adjacent to Waterton, Alberta. Belt Symposium III. In: Link, P.K., (ed.), Geologic Guidebook to the Belt-Purcell Supergroup, Glacier National Park and vicinity, Montana and Adjacent Canada, Field Trip Guidebook for the Belt Symposium III. Belt Association, Pocatello, Idaho, pp. 125-155.

Winston, D., 1986. Sedimentology of the Ravalli Group, middle Belt carbonate and Missoula Group, Middle Proterozoic Belt Supergroup, Montana, Idaho and Washington. In: Roberts, S.M., (ed.). Belt Supergroup: A Guide to Proterozoic Rocks of Western Montana and Adjacent Areas. Montana Bur. Min.

Geol., Spec. Publ. 94, 85-124.

Winston, D., 1990. Evidence for intracratonic, fluvial and lacustrine settings of middle to late Proterozoic basins of Western U.S.A. In: Gower, C.F., Rivers, T., and Ryan, B., (eds.), Mid-Proterozoic Laurentia-Baltica. Geol. Assoc. Can., Spec. Paper 38, 535-564.

Wronkiewicz, D.J., Condie, K.C., 1989. Geochemistry and provenance of sediments from the Pongola Supergroup, South Africa: evidence for a 3.0-Ga-old continental craton, Geochim. Cosmochim. Acta 53, 1537-1549.

Wyman, D.A., 1999. Paleoproterozoic boninites in an ophiolite-like setting, Trans-Hudson orogen, Canada. Geology 27, 455–458.

Xie, Q., Jain, J., Sun, M., Kerrich, R., Fan, J., 1994. ICP-MS analysis of basalt BIR-1 for trace elements. Geostandars Newsletters 18, 53-63.

Zhao, G., Sun, M., Wilde, S.A., Li, S., 2004. A Paleo-Mesoproterozoic supercontinent: assembly, growth and breakup. Earth Sci. Rev. 67, 91-123.

Connecting paragraph from Chapter V to Chapter VI

To understand rare earth element patterns, trace element systematics, and post-depositional monazite ages, a set of samples representative of the Belt-Purcell stratigraphic sequence was collected and classified in four distinct facies: sandstones, argillites, dolomitized argillites and dolomites. Primary depositional characteristics and two diagenetic stages were identified in argillites and sandstones. Dolomitized argillites and dolomites were the subject of a subsequent study in Chapter VI.

CHAPTER VI

Mobility of REE and HFSE During Dolomitization in the Mesoproterozoic Belt-Purcell Supergroup

Abstract

Carbonate-rich stratigraphic units of the Mesoproteozoic Belt-Purcell Supergroup grade continuously into fine-grained siliciclastic units devoid of carbonate. Primary carbonate was pervasively dolomitized during diagenesis. This diagenetic stage caused major gains of Ca, Mg, and Sr, as well as additions of heavy rare earth element (REE) and Y mobility coupled with fractionation of Nb-Ta and Zr-Hf.

Dolomitization is considered a major diagenetic stage that overprinted diagenesis featuring K-addition and high field strength elements (HFSE) fractionation, and/or absolute additions of heavy REE commensurable with alkaline, oxidized brines. Gains of elements such as Cs, Sb, Co, Cr, V, Mo, Cu, and W during diagenesis that produced K enrichment and REE mobilization are losses during dolomitization, and similarly losses of Cd, Pb, W, Zn, Cu, Mo, and V during K-addition, and/or absolute additions of heavy REE enrichment are gains during dolomitization. These complementary relationships are consistent with evolution of basinal fluids that caused heavy REE enrichment to lower pH during dolomitization where its pH was buffered by limestones. There is no evidence that the diagenetic stages recognized in the Belt-Purcell sequence were associated in time or space with the syn-sedimentary Sullivan ore deposit.

Changes in hydraulic gradients could have generated episodic fluid events over ~1000 Ma due to regional tectonic events such as the dispersal of the supercontinent Columbia at ~1400 Ma, the Grenville Orogen at ~1300-900 and break up of Rodinia at ~900-700 Ma. Other Proterozoic basins record the effect of large-scale advective flows of basinal brines 100s Ma after deposition. The Belt-Purcell Supergroup could reflect similar episodes.

6.1 Introduction

Conventionally, dolomitization involves secondary replacement of primary sedimentary calcite or aragonite, $CaCO_3$, with dolomite, $MgCa(CO_3)_2$. This process can take place during diagenesis by basinal fluids having relatively high Mg-activity (Zenger, 1981 and references therein; Morse, 2004; Sageman and Lyons, 2004). Siliciclastic rocks may also become dolomitized during diagenesis by introduction of secondary carbonate or carbonation of silicates or oxides (LaTour et al., 1984). This process can affect the distribution of trace elements in the sediment/rock (e.g., Pingitore, 1982; Milodowski and Zalasiewicz, 1991; Canaveras et al., 1998; Lev et al., 1998; Billon et al., 2002). Fractionation of trace elements during diagenesis in general has been described

in many studies over the past decade (e.g., McDaniel et al., 1994; Fayek and Kyser, 1997; Kyser et al., 2000; Lev et al., 1998; McLennan et al., 2003).

Siliciclastic units of the Belt-Purcell Supergroup record two diagenetic stages (Chapters IV and V; González-Álvarez et al., in press; González-Álvarez and Kerrich, submitted), as well as a third stage characterized mineralogically by dolomitization of primary carbonate units and mixed carbonate-siliciclastic units. This study reports high precision trace element data on rocks selected to represent a spectrum of intensities of dolomite development of mixed units in the Belt-Purcell sequence. Geochemical changes accompanying progressive dolomitization relative to precursors are addressed applying the mass balance procedure of Gresens (1967). The present study builds on the existing submitted paper (Chapter V) that addresses mobility of rare earth elements (REE) and high field strength elements (HFSE) by oxidized-alkaline basinal brines in the Belt-Purcell sequence in siliciclastic rocks devoid of dolomite during diagenesis.

6.2 Geologic setting

The Belt-Purcell Supergroup is a Mesoproterozoic, dominantly siliciclastic, sedimentary sequence that unconformably overlies igneous and metamorphic Paleoproterozoic basement and Cretaceous rocks (Link, 1997; O'Neill, 1997). This sequence outcrops from southwestern Montana, United States, to southeastern British Columbia, Canada (Fig. 6.1).

The ~17 km thick Belt-Purcell Supergroup has been interpreted to be deposited by a large-river system in an intracontinental rift basin at ~1500 Ma (e.g., Price, 1964; Harrison, 1972; Ross et al., 1991; Price and Sears, 2000; Chandler, 2000 and references therein; Sears et al., 2004). That rift may be part of the dispersal of the Mesoproterozoic supercontinent Columbia (e.g., Windley, 1995; Zhao et al., 2004). The stratigraphic sequence spans ~70 Ma and is divided into four principal divisions: (1) the lower Belt, mainly deltaic, fine-grained turbiditic facies, and carbonate-rich shallow water deposits (e.g., McMechan, 1981; Whipple et al., 1997); (2) the Ravalli Group, shallow to subaeral deposits (McMechan, 1981; Winston, 1986, 1990); (3) the middle Belt, carbonate-rich shallow water deposits (Winston, 1990; Pratt, 2001); and (4) the Missoula Group, alluvial deposits (e.g., Whipple et al., 1984, 1997; Winston, 1990; Fig. 6.2).

This large volume of siliciclastic detritus is divided mainly in two main lithologies: (1) argillites (a combination of siltite, mudstone, and very fine-grained sandstone; e.g., Harrison, 1972; McMechan, 1981; Whipple et al., 1984; Winston, 1990), and (2) sandstones (mainly quartzaren-

ites, subarkoses, and sublitharenites; terminology of Folk, 1968; e.g., Harrison, 1972; this study). Although most of the Belt-Purcell Supergroup is predominantly siliciclastic, there are two main carbonate-rich units: (1) the lower Belt, comprising the Waterton and Altyn formations, and (2) the middle Belt, represented by the Helena Formation at Waterton-Glacier International Peace Park (Fig. 6.2).

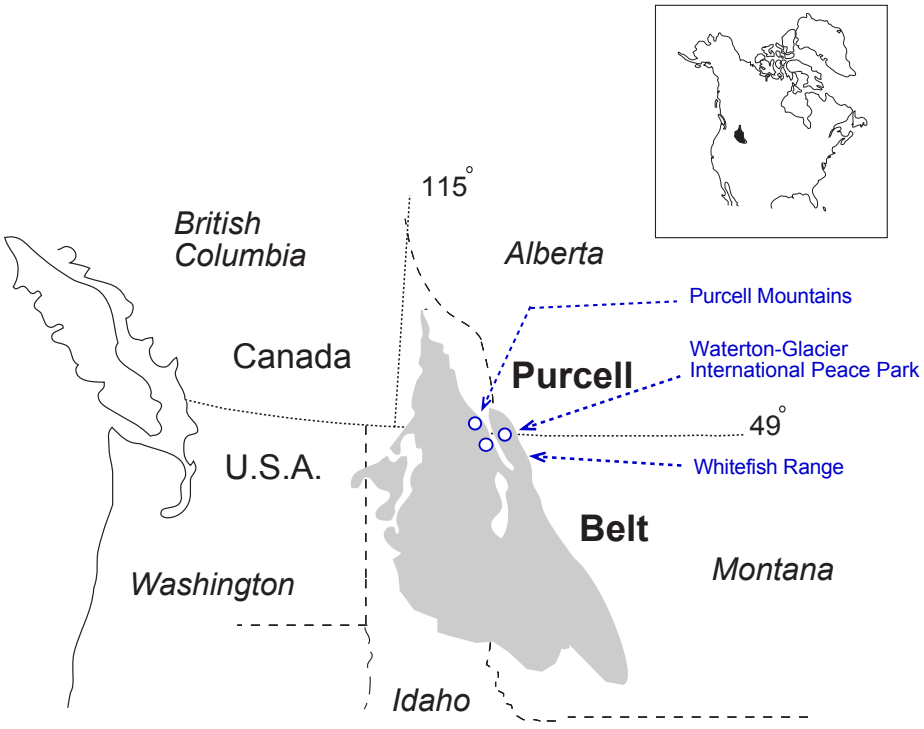

Fig. 6.1 Generalized geographic location of the Belt-Purcell Supergroup outcrops spanning the Canada-USA border, and the location of the three areas sampled in the present study.

Siliciclastic and carbonate-rich units in the Belt-Purcell sequence grade progressively into each other, such that the carbonate units include variable proportions of detrital siliciclastics. Euhedral dolomite crystals and dolomite lime mud comprise most of the carbonate fraction. The main geological features of the lower and middle Belt, with their primary carbonate structures where secondary dolomite occurs, are described below.

The lower Belt is represented at Waterton-Glacier International Peace Park by the Waterton and Altyn formations that reach maximums of ~160 and ~370 m thickness respectively. They are constituted of dolomitic, areanceous, and algal limestone with stromatolites. The Waterton and Altyn formations present hummocky cross-bedding, wavy and lenticular bedding, lamination,

mud-cracks, and gypsum and halite casts. These sedimentary features have been interpreted as the result of deposition in a shallow-subtidal to supratidal, or shallow lacustrine, setting that possibly underwent sabkha stages (McMannis, 1963; Fermor and Price, 1983; Whipple et al., 1984, 1997; Winston, 1989; Schieber, 1989; Chandler, 2000). The former formations correlate to the north and west with the deep turbiditic facies of the Aldridge and Prichard formations, and to the southeast, at the Helena Embayment, to the shallow water deposits of the Newland, LaHood, Greyson, and Neihart formations.

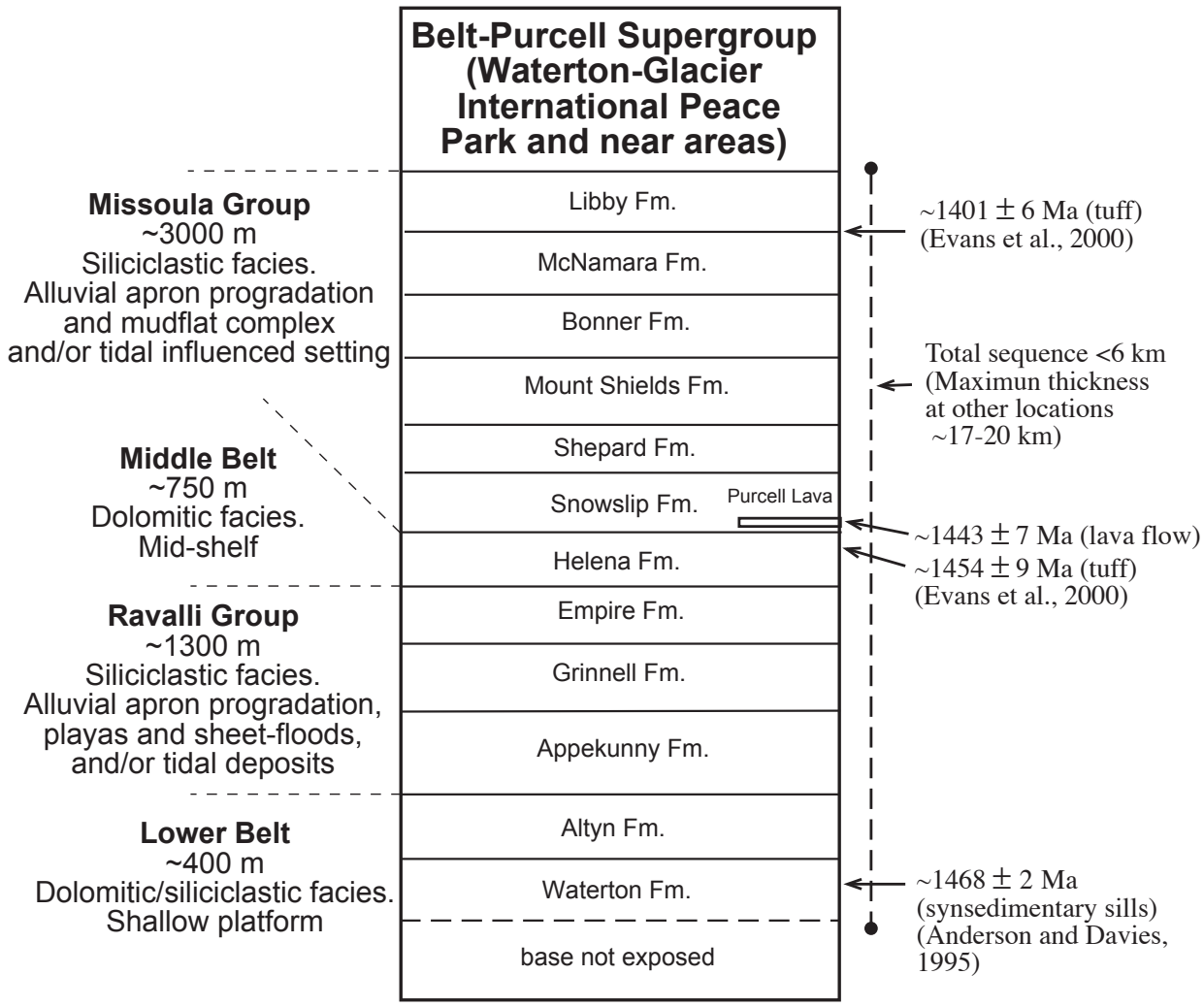

Fig. 6.2 Generalized stratigraphic sequence of the Belt-Purcell Supergroup at Waterton-Glacier International Peace Park (based on Whipple et al., 1984, 1997).

Higher in the startigraphic sequence (Fig. 6.2), the middle Belt is represented by the Helena Formation in the east of the Belt-Purcell Basin. The Helena Formation reaches up to ~750 m thickness, and is prevalently lime mudstone, ooidal grainstones, stromatolites with argillite, siltite, and sandy dolomite. Sedimentary features include evaporitic casts and moulds of halite and gypsum, as well as molar tooth structures (Fig. 6.2; Winston and Lyons, 1997; Lyons et al., 1997; Chandler, 2000 and references therein; Pratt, 2001). The Helena Formation has been interpreted as lacustrine based on the presence of siliciclastic-carbonate cycles explained as the result of alternative wet and dry climates in a lacustrine setting (Winston, 1986; Winston and Lyons, 1997). However, Wallace (1997) interpreted the argillite-carbonate cycles of the Helena Formation as deposition in a subtidal environment in a carbonate shelf. Pratt (2001) interpreted the Helena Formation as a mid-shelf limestone.

In the Purcell Mountains the Helena Formation is equivalent to the Kitchener Formation that is divided into a lower dolomitic-siltite part of the sequence and an upper siltite dolomite and dolomite sequence. The latter formation presents abundant climbing ripples and mud cracks, suggesting an intertidal zone in a carbonate shelf when the supply of siliciclastics was restricted (McMechan, 1981). The Wallace Formation is correlative to the Helena Formation in the southeast of the Belt-Purcell Basin (Wallace et al., 1993). The former presents shallowing cyclicity of siliciclastic to carbonate of argillite, siltstone and carbonate facies viewed as deposits from a shallow water, mud-flat, or shallow shelf depositional setting. Alternatively, Grozinger (1986) suggested that the Wallace Formation could be the result of a lacustrine environment due to lack of tidal structures.

In summary, primary carbonates in the Belt-Purcell Supergroup are viewed as the result of precipitation in a shallow-marine environment reflecting periodic changes of water salinity (Chandler, 2000 and references therein), or partially lacustrine. Casts and moulds of halite, gypsum, and other evaporitic minerals have been interpreted as indicative of periodic sabkha conditions in the Belt-Purcell Basin (Chandler, 2000 and references therein).

Extensive dolomitization is present in the mentioned two main carbonate units in the Belt stratigraphic sequence, and to a lesser extenst in other units such as the upper part of the Empire Formation in the Ravalli Group (Fig. 6.2), and the Sheppard, Snowslip, and Mount Shields formations in the Missoula Group (Fig. 6.2; e.g., McMechan, 1981; Whipple et al., 1984, 1997). The primary carbonate, of unknown mineralogy, probably of calcitic, aragonitic and protodolomitic mud (Chandler, 2000 and references therein), has been replaced by dolomite (e.g., Winston and Lyons, 1997). Dolomitization is also sporadically present in siliciclastic-rich units adjacent to the carbon-

ate-rich units, as irregular, meter scale, domains that overprint sedimentary fabrics. Euhedral dolomite is interstitial and overgrows, detrital silicates, and overprints primary sedimentary structures such as lamination, consistent with replacement of primary carbonates by secondary dolomite in the carbonate-rich units (Fig. 6.3). The secondary dolomitic domains cross-cutt argillites and sandstones having types 1 and 2 REE patterns as described in Chapter V (González-Álvarez and Kerrich, *submitted*), so they are coeval to later than 1400-300 Ma diagenetic monazites discussed in Chapter IV (González-Álvarez et al., *in press*).

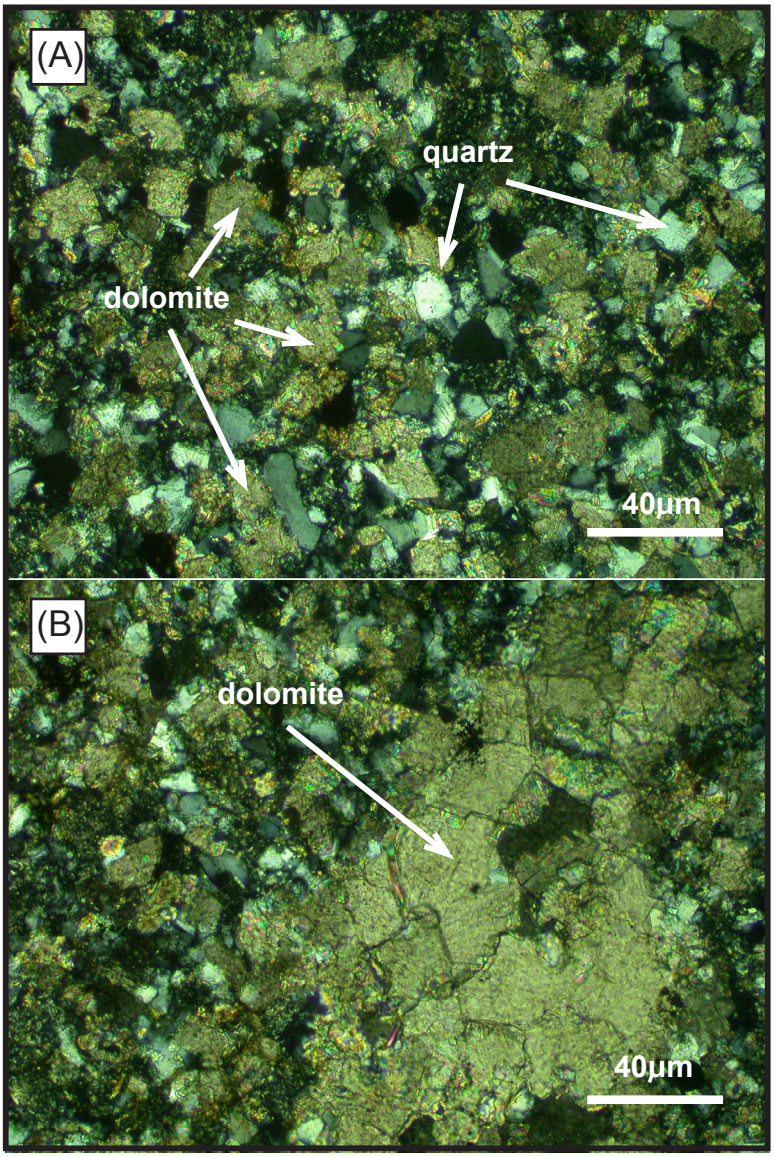

Fig. 6.3 Photomicrographs of dolomitized argillite from the Appekunny Formation. Crossed-nichols.

Metamorphic grade in the Belt Purcell rocks spans from subgreenschist at upper stratigraphic levels in the east, through greenschist facies at the lowest stratigraphic levels, to amphibolite facies in the west proximal to major plutons (Maxwell and Hower, 1967; Harrison, 1972). Maxwell and Hower (1967) reported that illite 1Md transforms in the Belt-Purcell sequence at depth into 2M polymorph in dioctaedral mica (muscovite-like mica polymorph). 1Md illite is more abundant in the upper sequence reacting at depth to 2M. The 2M polymorph is stable to ~350^{o} C (Rosenberg, 2002). Metamorphic grade is lower greenschist facies at the three localities sampled for this study.

6.3 Sampling and analytical techniques

A total of 112 rock samples were collected from the Belt-Purcell Supergroup for a trace element geochemical study at three locations; Waterton-Glacier International Peace Park, Whitefish Range and the Purcell Mountains. A subset of nineteen was selected for the present study mainly from the Waterton-Glacier International Peace Park area as explained in *section 6.4* (Figs. 6.1 and 6.4; Appendix 6.1).

Major elements were determined using X-ray fluorescence spectrometry (XRFS) at the Société Générale de Surveillance (SGS) Laboratories, Ontario, Canada. Precision is ±0.01 wt.%. Trace elements, including REE and HFSE, were analyzed using inductively coupled plasma-mass spectrometry (model Perkin Elmer Elan 5000) at the University of Saskatchewan. To address potential problems stemming from incomplete dissolution of refractory minerals, the procedure of Jenner et al. (1990) was followed, whereby a sodium peroxide sinter was used for analyses of Th, Nb, Ta, Zr, Hf, Y, Sc, and REE, and an HF-HNO_3 digestion on a separate aliquot was used for the remaining trace elements. Detailed analytical methodology is presented in Fan and Kerrich (1997). Included are standard additions, pure elemental standards for external calibration, and data for modern lake sediment samples representative of various locations within the Canadian Shield (LKSD-1), and basalt (BCR-2) as reference materials. LKSD-1 was used as a reference material, inasmuch as the REE and HFSE contents are comparable to those in the argillites analyzed. Long-term reproducibility in this lab for the low-level reference material basalt (BCR-1) is given in Table 6.1, excerpted from Xie et al. (1994).

Detection limits (in ppm) defined as 3Sigma of the calibration blank for some critical elements are as follows: Nb (0.016), Hf (0.042), Zr (0.103), La (0.018), Ce (0.014), Nd (0.086), and Sm (0.065). Wet chemistry operations were conducted under clean laboratory conditions. Analyses

of acids, distilled deionized water and procedural blanks give levels of <1 ppb for REE, Nb, Zr, and Hf, relative to their concentration in the rocks (Xie et al., 1994).

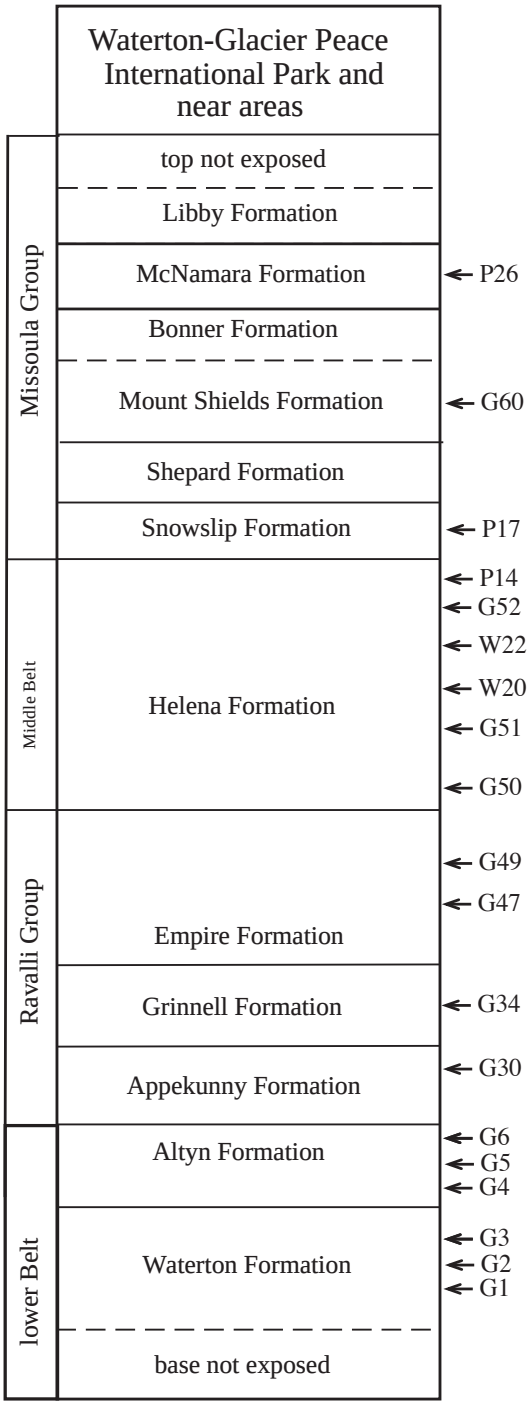

Fig. 6.4 Stratigraphic position of samples collected for this study cross-referenced to Appendix 6.1.

Table 6.1 ICP-MS multi-element analysis of international reference material basalt BCR-1 for selected trace elements by the University of Saskatchewan ICP-MS laboratory (excerpted from Xie et al., 1994).

Elements	x	1σ	C%	CV
Zr	201	12	6	190
Nb	14.6	0.7	4.8	14
La	26	0.8	3.1	24.9
Pr	6.95	0.33	4.7	6.8
Eu	1.95	0.11	5.6	1.95
Ho	1.26	0.05	4	1.26
Tm	0.54	0.02	3.7	0.56
Lu	0.502	0.02	4	0.51
Hf	5.87	1.49	8.3	4.95
Ta	1.03	0.16	15.5	0.81
Th	6.7	0.52	7.8	5.98
U	1.75	0.1	5.7	1.75

(x) Average; (1σ) standard deviation; (C%) relative standard deviation; (CV) compiled values from Potts et al. (1992).

6.4 Analytical results

Petrographic observations and Al_2O_3-, SiO_2-loss on ignition (LOI) relationships reveal the gradation of siliciclastic and carbonate units into each other in the two carbonate-rich units (Fig. 6.5a). Based on that relationship, nineteen samples were selected for this study from the three locations sampled. All are variably dolomitized argillites characterized by <75 wt.% SiO_2 and 45-10 wt.% LOI (Fig. 6.5a).

Major element trends display SiO_2, TiO_2, Al_2O_3, Fe_2O_3, K_2O, Na_2O, and P_2O_5 down to 0.1 post-Archean upper continental crust (PA-UCC) values (Taylor and McLennan, 1995); variable MnO anomalies; as well as systematically enriched CaO and MgO up to 8 times PA-UCC (Fig 6.6e and f).

From inspection of REE patterns, dolomitized argillites were divided into two different types using a plot of total light REE/total heavy REE (∑LREE/∑HREE) versus Ho/Lu normalized

to PA-UCC (Fig. 6.5b). Two systematic REE patterns occur: type 1, a PA-UCC-like REE pattern, and type 2, heavy REE enriched relative to light REE when normalized to PA-UCC (Fig. 6.6a and b). A third REE type is erratic without consistent trends and therefore is not further considered here. Type 1 and type 2 REE patterns were already described as diagenetic effects in both argillites and sandstones of the Belt-Purcell siliciclastic sequence by González-Álvarez et al. (*in press*) and González-Álvarez and Kerrich (*submitted*; Chapters IV and V); those two patterns are inherited by the dolomitization stage of diagenesis.

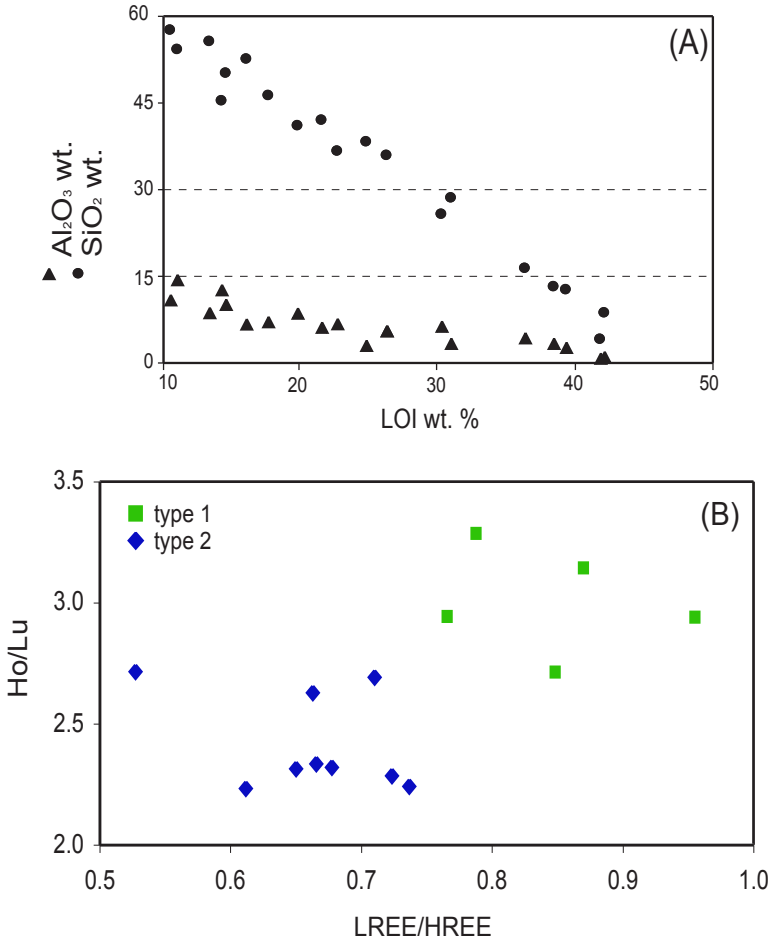

Fig. 6.5 (A) Plot of SiO_2 and Al_2O_3 wt.% content versus LOI (loss-on-ignition; volatile content; e.g., H_2O, CO_2) wt.% showing continuous trends consistent with progressive addition of secondary dolomite to dominantly siliciclastic rocks. For reference, argillites from González-Álvarez and Kerrich, (submitted); (B) Plot of LREE/HREE versus Ho/Lu, displaying two sample groups; type 1 carbonate-rich facies with PA-UCC-like REE pattern, and type 2 carbonate-rich facies with HREE enrichment relative to LREE when normalized to PA-UCC (of Taylor and McLennan, 1995).

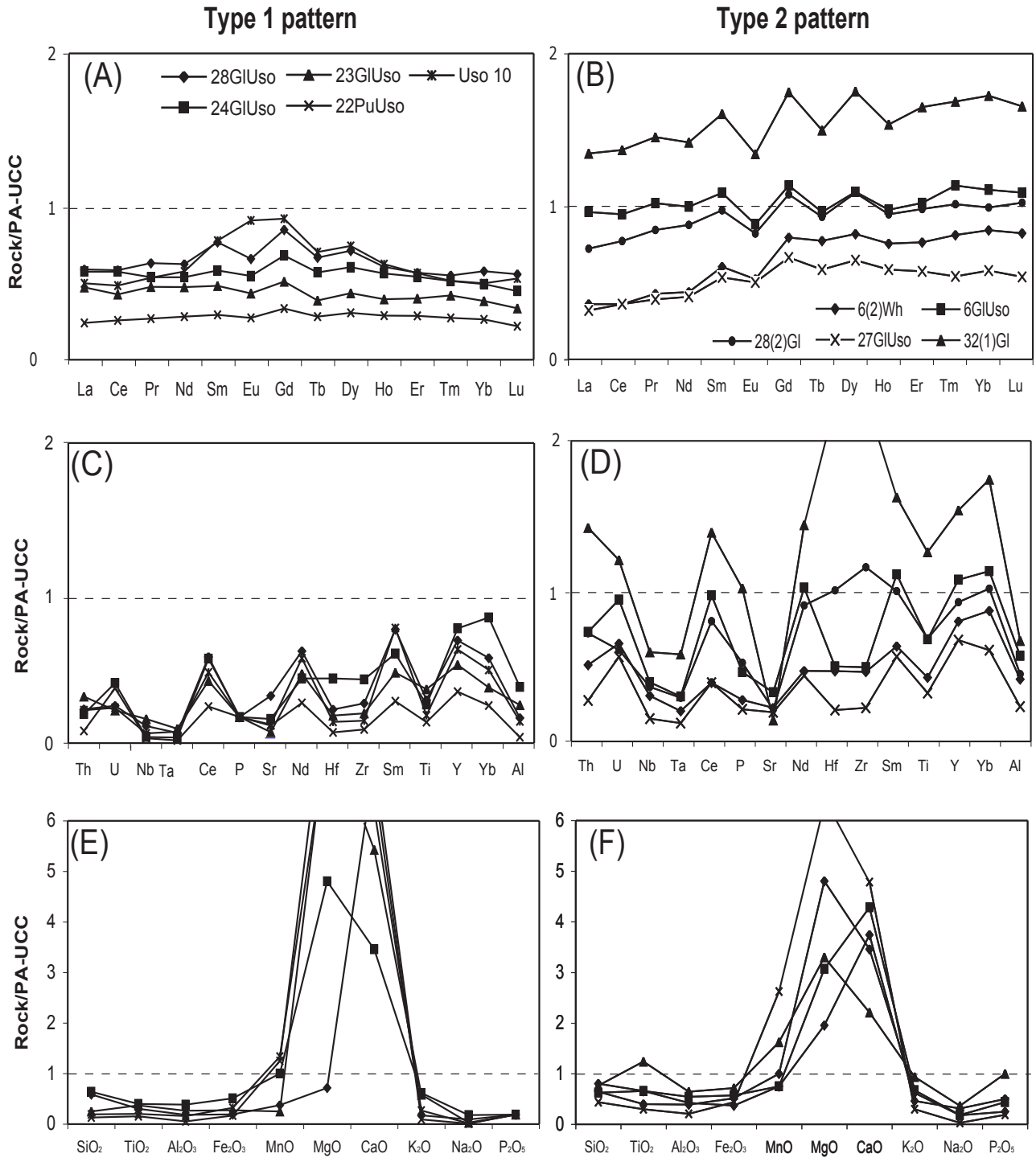

Fig. 6.6 Plots of dolomitized argillites, normalized to PA-UCC: rare-earth elements (A and B), multi-element (C and D), and major elements (E and F) for types 1 and 2 REE patterns.

In more detail, type 1 features near flat normalized patterns at ~0.25 to ~0.60 PA-UCC, and MREE become irregular at greater REE abundance (Fig. 6.6a). On multi-element plots: (1) U is variably enriched over Th; (2) Nb-Ta and Zr-Hf are unfractionated and systematically depleted relative to neighbouring REE; (3) HREE are enriched over Ti and Al; and (4) Y-Yb fractionation increases with HREE. Average values of Al_2O_3 and SiO_2 are 2.6 wt.% and 18 wt.%, respectively, compared to values of 15 and 66 in PA-UCC (Fig. 6.6c), whereas average ∑REE is ~100 ppm relative to 150 ppm. In a correlation matrix, the only relationship is antivariance of Sb with HFSE (r^2=~ -0.85).

Type 2 patterns display negative slopes from La to Lu, and more irregular MREE at greater REE abundance than type 1 (Fig 6.6b). On multi-element diagrams fractionations are similar to those in type 1, albeit more pronounced, excepting fractionations of both Zr-Hf and Nb-Ta from neighboring REE (Fig. 6.6d). Al_2O_3 covaries with REE, HFSE, TiO_2, P_2O_5, Sb, Cr, and Co (r^2=0.61-0.95).

6.5 Discussion

Primary calcite or aragonite sediments may be transformed to dolomite during diagenesis (Moore, 1989; Morse, 2004). During burial, evaporite minerals such as gypsum convert to anhydrite releasing large amounts of water, and at ~2000 m and ~60° C smectite reacts to illite, releasing Mg (e.g., Bozkaya and Yalcin, 2004). Formation fluids having high Mg-activities are the agent of dolomitization (e.g., Lonnee and Al-Aasm, 2000; Gareth et al., 2002). It has been described in other Proterozoic basins that diagenetic fluids may have residence times of 100's Ma, reacting with rocks during major tectonic events (Kyser et al., 2000). In addition, González-Álvarez and Kerrich (*submitted;* Chapter V), based on chemical Th-U total Pb monazite ages, determined that basinal fluids mobilized REE intermittently over ~1300-300 Ma. Mass balance calculations in this study (see 6.5.2 discussion) show REE mobilization during dolomitization.

6.5.1 Diagenetic stages

Two diagenetic stages have previously been identified in the Belt-Purcell sequence based on petrographic observations, cross-cutting relationships and chemical composition: (1) a stage characterized mainly by addition of up to ~35% of K in argillites and sandstones; and (2) a second stage basinal fluid event during which HREE were enriched relative to LREE when normalized to PA-UCC. Both display U mobility developed over the full stratigraphic extent of the Belt-Purcell

sequence (Kerrich and González-Álvarez, 2003; González-Álvarez and Kerrich, *submitted*; Chapter V). Diagenesis with K-addition is common in Precambrian sedimentary sequences, but not HREE enrichment (Rainbird et al., 1990; Maas and McCulloch, 1991; Fedo et al., 1995; Bhat and Ghosh, 2001; Cullers and Podkovyrov, 2002).

Based on the presence of type 1 and 2 REE patterns in argillites and dolomitized units, and cross-cutting relationships, dolomitization is interpreted as a third major diagenetic stage in the Belt-Purcell sequence, confined mostly to primary carbonate-rich units. Therefore, dolomitized argillites are compared to their non-dolomitized counterparts using mass balance to determine how dolomitization affected the geochemistry of the rock.

6.5.2 Mass Balance

Mass balance equations defined by Gresens (1967) were applied to quantify metasomatic gains or losses of different elements during dolomitization of the Belt-Purcell argillites. Calculations were made relative to a precursor rock(s), which in the present study are averages of types 1 and 2 of non-dolomitized argillite previous diagenetic stages. For a bulk rock, the mass balance is calculated using the expression:

$$100[f_v(g_b/g_a)\, c_{nb}\text{-}c_{na}]=x_n \qquad (6.1)$$

Where f_v is the volume factor, the amount by which the volume on the left part of the equation has to be multiplied in order to obtain the volume on the right side; g_b/g_a is the relation between the specific gravities of the product *(b)* and precursor (a) lithologies; c_{nb} and cna are the amounts of a specified chemical element in *(a)* and *(b)*; and x_n is the total amount of element *n* lost or gained in the process. The amounts are represented as g/100g relative to the precursor. From mineralogical considerations it is assumed that g_b/g_a is close to 1.

Gresens (1967) showed that in any chemical transformation the ratios of isochemical elements in the precursor and product would be identical. Accordingly, ratios of several elements likely to be immobile were inspected in the previous study of chemical diagenetic changes from PA-UCC to type 1 diagenesis with K-addition and REE addition, and from type 2 interpreted as stage two diagenesis; Al, Th, and Ga were found to be isochemical (Chapter V; González-Álvarez and Kerrich, *submitted*). Similarly, Al, Th, and Ga have comparable ratios for each of types 1 and 2 argillites to types 1 and 2 dolomitized equivalents, but differ between them, consistent with iso-

chemical behavior throughout the basin history. Based on averages of these ratios, values of f_v were calculated (Table 6.2).

Table 6.2 Inter-element ratios for recalculated dolomitized argillite with PA-UCC like REE pattern, type 1 [DolT1(c)] and non-dolomitized type 1 (T1), and HREE enriched relative to LREE REE pattern, type 2 [DolT2(c)], and non-dolomitized type 2 (T2) patterns for specified elements.

	DolT1(c)/T1	DolT2(c)/T2
TiO_2	0.946	1.013
Al_2O_3	0.841	0.923
Th	0.969	1.237
Ga	1.017	0.913
fv.*	0.943	1.022

**fv. Volume factor*

Chemical mass balance of selected elements for types 1 and 2 diagenesis is compiled and compared to mass balance calculations for dolomitizied argillites in Fig. 6.7a and b from Chapter V (González-Álvarez and Kerrich, *submitted*). Results are given in g/100g and also as mass percentage changes relative to the precursor rock. Relative to PA-UCC stage one features average gains of ~25% K. In the second diagenetic stage, type 1 argillites reveal average gains of ~35% LREE and HREE; ~45% MREE; enrichments of Ag and Sb up to 430%; Mo losses of 77%; as well as other features displayed in Table 6.3 and Fig. 6.7a. Argillites, type 2 display a continuous change from -20% La to +16% Lu (Table 6.3; Fig. 6.7b).

In this study, mass balance calculations were conducted to compare type 1 and 2 dolomitized argillites to their non-dolomitized counterparts. Given common dilution of the immobile elements Al, Th, and Ga by replacement or addition of carbonate, average volume factors of 4.7 and 1.9 were estimated for types 1 and 2 argillites respectively (Tables 6.2 and 6.3).

Dolomitized argillites for both types 1 and 2 differ from their precursor non-dolomitized counterparts in having large additions of MnO, CaO, MgO, and Sr from ~70% to ~8000%, as expected for the dolomitization process (Fig. 6.7). Dolomitized type 1 has gains of Pb, Cd, W, Cu, and Zn up to ~1500%; additions of Sc, Li, Pb, Cd, U, Y, and As; but losses of Cr and Sb (Table 6.3; Fig. 6.7a).

Table 6.3 Mass balance of the average of the dolomitized argillite population referenced to post-Archean upper continental crust (Taylor and McLennan, 1995).

	Av. T1 (p)	Av. DolT1	Av. DolT1 (c)	Av. T2 (p)	Av. Dol T2	Av. Dol T2(c)	Dol T1(c)/T1	DolT2(c)/T2	DolT1 g/100g	M %	DolT2 g/100g	M %
SiO2	63	17.89	83.36	67	41.71	77.59	1.314	1.159	15.147	24	12.335	18
TiO2	0.64	0.13	0.60	0.54	0.29	0.54	0.946	1.013	-0.069	-11	0.019	4
Al2O3	14.5	2.62	12.23	13.4	6.65	12.37	0.841	0.923	-3.010	-21	-0.756	-6
Fe2O3	5.44	1.20	5.57	4.06	2.25	4.19	1.024	1.032	-0.186	-3	0.224	6
MnO	0.04	0.06	0.28	0.07	0.08	0.14	6.821	2.177	0.220	543	0.081	123
MgO	4.29	14.58	67.92	3.40	8.87	16.50	15.831	4.847	59.762	1393	13.462	395
CaO	1.44	26.42	123.12	2.36	16.36	30.42	85.399	12.889	114.658	7953	28.729	1217
K2O	4.55	0.95	4.42	3.68	2.34	4.35	0.971	1.184	-0.383	-8	0.771	21
Na2O	0.76	0.17	0.81	1.56	0.56	1.04	1.070	0.666	0.007	1	-0.500	-32
P2O5	0.12	0.03	0.14	0.08	0.07	0.12	1.202	1.482	0.015	13	0.042	51
Li	53	41.30	192.46	51	69.36	129.02	3.640	2.507	128.618	243	80.386	156
Rb	149	28.87	134.53	139	67.62	125.76	0.904	0.904	-21.982	-15	-10.657	-8
Sr	26	60.03	279.76	66	60.69	112.88	10.846	1.717	238.021	923	49.624	75
Cs	6.10	1.25	5.84	7.57	3.24	6.03	0.958	0.797	-0.587	-10	-1.407	-19
Ba	588	81.72	380.81	706	483.45	899.21	0.648	1.274	-228.885	-39	213.088	30
Y	27	12.77	59.50	27	19.35	35.99	2.216	1.336	29.251	109	9.845	37
Zr	203	34.82	162.28	200	136.44	253.78	0.798	1.266	-50.370	-25	58.908	29
Hf	6.07	0.95	4.44	6.19	3.84	7.14	0.731	1.153	-1.885	-31	1.105	18
Nb	14	2.42	11.30	12	7.45	13.86	0.815	1.130	-3.216	-23	1.905	16
Ta	1.04	0.16	0.75	0.95	0.51	0.95	0.725	1.009	-0.328	-32	0.029	3
Th	11.3	2.35	10.96	10.2	6.80	12.66	0.969	1.237	-0.974	-9	2.702	26
U	2.90	0.86	4.01	3.23	2.09	3.88	1.383	1.201	0.880	30	0.736	23
La	39	14.26	66.46	31	20.37	37.89	1.700	1.215	23.570	60	7.538	24
Ce	81	29.80	138.86	65	43.76	81.40	1.715	1.251	49.989	62	18.106	28
Pr	9.50	3.48	16.20	7.81	5.21	9.69	1.706	1.241	5.781	61	2.093	27
Nd	35	12.98	60.48	30	19.06	35.45	1.730	1.199	22.068	63	6.659	23
Sm	6.40	2.61	12.18	5.80	3.80	7.06	1.904	1.217	5.087	80	1.415	24
Eu	1.30	0.50	2.31	1.00	0.63	1.17	1.777	1.175	0.879	68	0.201	20
Gd	5.66	2.50	11.67	5.44	3.58	6.66	2.063	1.225	5.348	95	1.368	25
Tb	0.79	0.33	1.56	0.79	0.52	0.98	1.958	1.230	0.672	85	0.204	26
Dy	4.81	1.96	9.14	5.14	3.26	6.06	1.899	1.178	3.804	79	1.051	20
Ho	1.01	0.40	1.85	1.07	0.67	1.24	1.831	1.158	0.733	73	0.196	18
Er	2.94	1.09	5.06	3.25	2.00	3.73	1.721	1.146	1.832	62	0.556	17
Tm	0.44	0.15	0.70	0.50	0.30	0.56	1.588	1.130	0.219	50	0.077	16
Yb	3.01	0.98	4.55	3.36	2.01	3.74	1.514	1.113	1.287	43	0.462	14
Lu	0.42	0.13	0.62	0.50	0.28	0.52	1.479	1.054	0.167	39	0.038	8
Sc	17.8	13.32	62.09	18.8	15.50	28.83	3.492	1.534	40.772	229	10.675	57
V	77	13.38	62.33	55	29.20	54.31	0.810	0.990	-18.188	-24	0.648	1
Mo	0.34	0.08	0.38	1.10	0.43	0.81	1.089	0.735	0.009	3	-0.273	-25
Cr	107	16.96	79.05	82	41.98	78.08	0.741	0.949	-32.172	-30	-2.487	-3
Co	15	2.86	13.33	11	5.58	10.39	0.880	0.904	-2.570	-17	-0.873	-8
Ni	27	8.05	37.52	16	12.58	23.40	1.375	1.421	8.093	30	7.447	45
Cu	4.1	9.24	43.04	19.5	9.44	17.56	10.469	0.898	36.477	887	-1.598	-8
Zn	52	26.22	122.17	61	34.00	63.24	2.369	1.041	63.623	123	3.874	6
Sn	3.00	0.69	3.20	3.26	1.49	2.77	1.068	0.850	0.023	1	-0.430	-13
W	1.94	7.21	33.62	2.26	0.85	1.58	17.367	0.700	29.766	1538	-0.645	-28
Pb	8.8	8.21	38.26	13.7	8.81	16.39	4.335	1.196	27.253	309	3.051	22
Cd	0.04	0.07	0.33	0.09	0.13	0.24	7.866	2.592	0.266	642	0.150	165
Tl	0.63	0.10	0.45	0.73	0.33	0.62	0.707	0.848	-0.210	-33	-0.097	-13
Ga	17	3.70	17.22	16	7.74	14.39	1.017	0.913	-0.699	-4	-1.053	-7
As	3.02	1.39	6.49	4.29	3.55	6.60	2.148	1.537	3.099	103	2.449	57
Ag	0.08	0.02	0.11	0.07	0.04	0.07	1.372	0.996	0.024	29	0.001	2
Sb	1.04	0.19	0.88	0.96	0.44	0.83	0.843	0.863	-0.214	-20	-0.113	-12

(Av.) Average; (T1) argillites type 1; (T2) argillites type 2; (DolT1) dolomitized argillites type 1, PA-UCC-like REE pattern; [DolT1(c)] recalculated dolomitized argillite type 1; (DolT2) dolomitized argillite type 2, HREE enriched relative to LREE; [DolT2(c)] recalculated dolomitized argillite type 2; (M) mass; and (p) precursor.

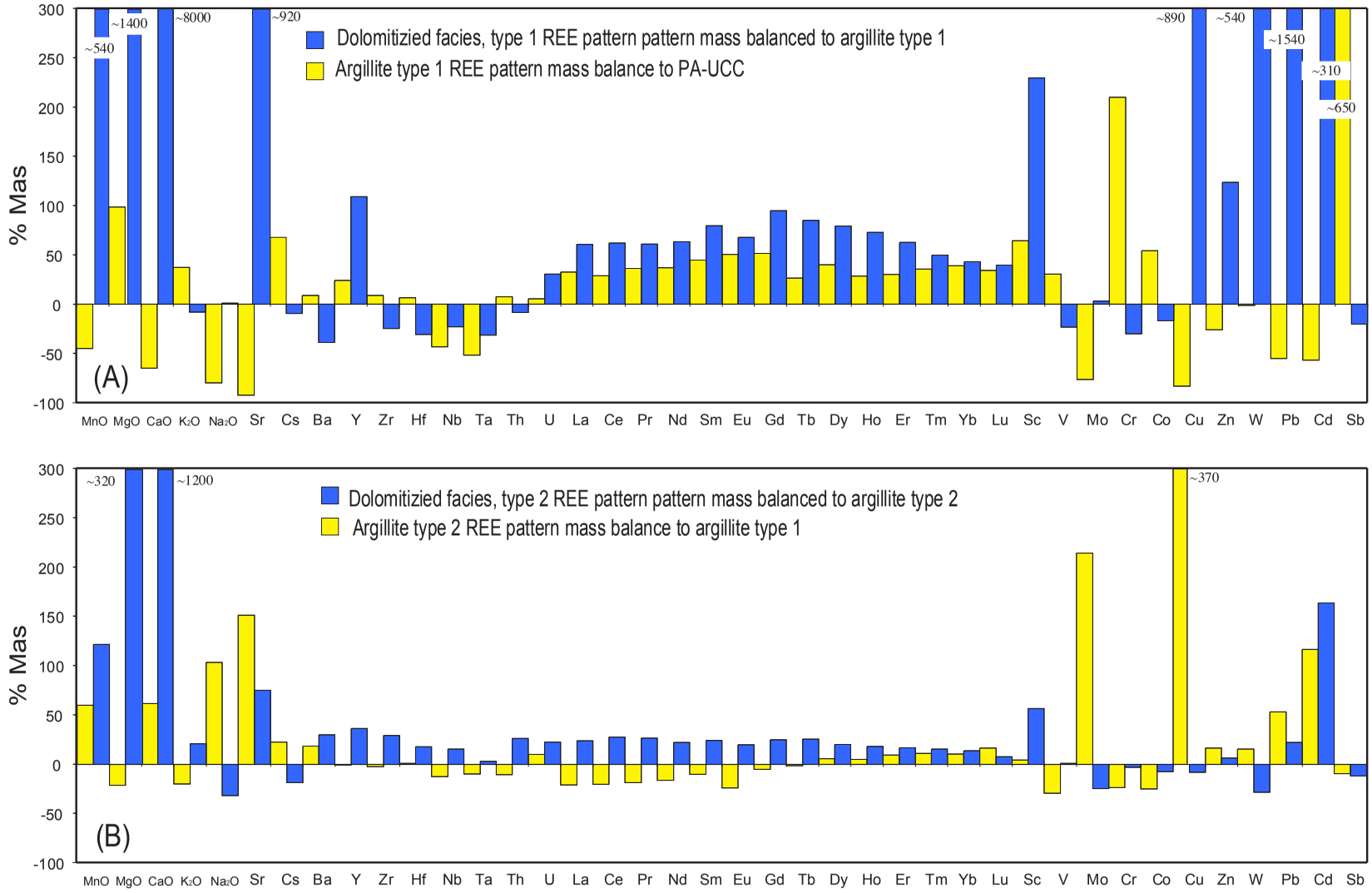

Fig. 6.7 Mass balance histograms presenting % mass changes of (A) argillites type 1 and (B) type 2 argillites with their dolomitized counterparts. Type 1 and 2 argillite mass balance data are from González-Álvarez and Kerrich (submitted; Chapter V). The histogram display major gains of Ca, Mg, and Sr, as well as additions of Y and gain-losses of Nb-Ta and Zr-Hf.

Chemical transformations for dolomitized argillite type 2 show three main differences compared to type 1: (1) HFSE are gained; (2) REE present a continuous trend of loss from La (24%) to Lu (8%); and (3) losses of W and Cu. Therefore, many element-patterns of gains or losses of previous diagenetic stages are reciprocal during dolomitization (Fig. 6.7b).

6.5.3 Basinal fluids

Generally, Al, Ti, REE, HFSE, Y, and Sc behave isochemically during hydrothermal activity and metamorphism (Fryer et al., 1979; Humphries, 1984; Terakado and Fujitani, 1998). However, under special conditions REE and HFSE appear to be both mobile and fractionated. Fayek and Kyser (1997) reported enrichments of U, Y, and HREE proximal to unconformity U deposits in the Mesoproterozoic Athabasca Basin. Magadi-type cherts from the East African Rift are precipitating from low-temperature alkaline oxidizing brines having LREE at ~0.01 and HREE ~0.6 times PA-UCC. In addition, Magadi-type cherts have the following features: (1) HREE enrichment relative to MREE; (2) anomalies of Nb and Zr relative to neighbouring REE; (3) extreme fractionations of Nb/Ta up to 120, and Zr/Hf up to 1300, compared to PA-UCC values of 11 and 34 respectively; (4) Th/U fractionation; and (5) U, Mo, Ag, and Sb enrichments (Kerrich et al., 2002). Similar anomalous trace element features were documented for sediments in saline alkaline lakes of the Pamirs in central Asia (Volkova, 1998). According to experimental data of Johannesson and Lyons (1995), preferential aqueous solubility of HREE occurs with bicarbonate complexes. Schieber (1988) reported REE redistribution during diagenesis of carbonate rocks in the Newland Formation, lower Belt, featured by positive Eu anomalies and relative enrichments of LREE.

Argillites, type 1, influenced by basinal fluids during diagenetic possesses added absolute enrichment of REE compared to PA-UCC. Samples having type 2 REE patterns have enrichment of HREE relative to LREE when normalized to PA-UCC, in conjunction with enrichments of Y and U.

Based on empirical evidence from other Mesoproterozoic siliciclastic sequences, Magadi saline lakes, and experimental data, González-Álvarez and Kerrich (*submitted*) interpreted their mobility as due to alkaline oxidizing brines. In the Belt-Purcell Basin, such brine compositions likely stem from dissolution of evaporite units. This is supported by the presence of halite and gypsum casts, and domains of scapolite in some of the Belt-Purcell formations as evidence of evaporitic domains (Schieber, 1997, and references therein; Chandler, 2000).

Additions of MnO, MgO, and CaO, coupled with REE and HFSE redistribution, these results are characteristic of dolomitization in the Belt-Purcell argillites. Enrichment of Ag, Mo, and Sb typical of types 1 and/or 2 in argillites and sandstones is not present. These results may be interpreted as dolomitization involving evolution of the oxidized-alkaline basinal brines of stage two by a shift of pH by reaction with the primary sedimentary carbonates, comparable to the Pamir alkaline lakes with a pH of 9 to 10 where basinal fluids are in equilibrium with dolomite. This is supported by the fact gains of elements such as Cs, Sb, Co, Cr, V, Mo, Cu, and W during diagenesis that produced K enrichment and/or HFSE and REE fractionations are losses during dolomitization, and similarly losses of Cd, Pb, W, Zn, Cu, Mo, and V during K-addition, and/or HFSE and REE fractionations are gains during dolomitization, presenting complementary trends at both stages (Fig. 6.7; Table 6.3).

No evidence link the basinal fluids associated with the three diagenetic stages of the Belt-Purcell Supergroup and the Sullivan deposit. This strataform Pb-Zn sulfide deposit is interpreted to have formed at ~1470-1475 Ma close to the time of sedimentation of the host Aldridge Formation, lower Belt, by seawater that was modified and reduced by convection through a sill-sediment complex (Lydon, 2000; Schandl et al., 2000). Proximal sediments hosting the Sullivan deposit are characterized by positive Eu anomalies, and LREE depletions or enrichments (Schandl et al., 2000).

Types 1 and 2 diagenetic stages have been constrained at ~1400-300 Ma from chemical ages of secondary monazites (Chapter IV; González-Álvarez et al., *in press*). Given the complementary geochemical relationships described above, dolomitization is interpreted to have closely followed the diagenetic stage that produced type 2 REE patterns, when alkaline oxidizing brines encountered limestone units that buffered the pH to where fluids were in equilibrium with dolomite.

6.5.4 Fluids in Proterozoic basins

Basinal fluids are driven by changes in hydraulic gradients that, in many cases, have a tectonic origin (Bethke and Marshak, 1990). Oliver (1986) interpreted how the distribution of mineral deposits and hydrocarbon resources of the U.S. mid-continent to tectonic pumping of formation brines by the advancing Appalachian Orogen. Long-distance influence on formation brines by tilting of sedimentary basins has been described by Bethke and Marshak (1990). The thermal and diagenetic fluid histories of the Athabasca Basin have been established from successive diagenetic mineral assemblages (Kyser, 2000; Kyser et al., 2000; Ross, 2000).

Table 6.4 Main geological features of the Athabasca, Thelon, Kombolgie and Belt-Purcell sequences (Kyser et al., 2000 and references therein).

Basin/ sequence	Basin age (Ma)	Strat-Sed.	Paleoenvironment	Thickness (km)	Ore deposit type	Mineral paragenesis	Diagenesis
Athabasca	~1700-1500	flat flying	fluvial-shallow marine	~2-5	unconformity U	2Millite+dictite+Q+chl+hem+U	<240^{o} C
Thelon	<1700	flat lying	fluvial-shallow marine	~2	- - - - - - - - - - - -	Q+2Mllite+chl+K-felds+dol	<200^{o} C
Kombolgie	~1900-1700	flat lying	near shore-shallow marine	~5-15	unconformity U Pb-Zn-Ag	Q+2Millite+hem+chl+U	<450^{o} C
Belt-Purcell	~1400	flat lying	near shore-shallow marine	~17	Pb-Zn-Ag	Q+2Mllite+chl+K-felds+dol	<340^{o} C

Regardless of many differences to other Proterozioc basins in Laurentia, such as the Athabasca and Thelon basins, and counterparts in Australia including the Kombolgie Basin north of the McArthur Basin, the Belt-Purcell Basin could have some similarities in terms of large-scale basinal fluids events with the former. Common general characteristics of their stratigraphic sequences are: (1) shallow lacustrine to marine paleoenvironments settings; (2) evolved brines from their own evaporitic units; and (3) a long residence time of diagenetic fluid activity (up to ~600 Ma, mainly from ~1600-1000 Ma) compared to the lifespan of Phanerozoic basins (cf. Woodcock, 2004); (4) major ore deposits such as the world-class uncomformity U deposits contained in the Athabasca and Kombolgie sequences; as well as major Pb-Zn-Ag deposits in the Belt-Purcell, the McArthur and Mt Isa basins; and (5) in the Thelon and Athabasca basins, late basinal fluids resulted in precipitation of carbonates from fluids having low relative salinities and temperatures (Table 6.4; Kyser et al., 2000).

The Athabasca (~1700 Ma) and Kombolgie basins (~1800 Ma) were developed during the assembled of the supercontinent Columbia (e.g., Pesonen, 2003; Zhao et al., 2004). Kyser et al. (2000) described differences of the Athabasca and Kombolgic basin fill during basinal fluid-flow events at several stages of their history. They related ~1000 Ma diagenetic events in the Athabasca Basin to the distal effects to the Grenvillian orogeny. Major tectonic events during Proterozoic times such as the assemblage of Rodinia from ~1300 Ma to ~900 Ma (Condie, 2002), and Rodinia's break up, which produced the rifting of Australia-Laurentia, Laurentia-S. China and Siberia-N. China during ~900-700 Ma, may have driven the migration and evolution of basinal fluids in Laurentia (Kyser et al., 2000) with essential implications, such as redistribution of REE and HFSE elements for the Belt-Purcell Supergroup, and for the fluid-diagenetic histories of other Proterozoic basins.

Secondary monazites of ~1300 to 300 Ma in the Belt-Purcell Supergroup were interpreted by González Álvarez et al. (*in press*) initially as a result of large basinal fluids events in the Belt-Purcell sequence (Chapters IV).

6.6 Conclusions

(1) The Belt-Purcell Supergroup has two main stratigraphic units of primary carbonate, with variable proportions of fine-grained siliciclastics, affected by secondary dolomitization. That was accompanied by major gains of Ca, Mg, and Sr, as well as REE and Y mobility coupled with fractionation of Nb-Ta and Zr-Hf.

(2) Secondary dolomitization was constrained from <~1400 to ~300 Ma in the Belt-Purcell

Supergroup.

(3) Dolomitization is considered as a post-diagenetic stage that followed K-addition and enrichment of HREE relative to LREE by alkaline, oxidized brines.

(4) Gains of elements including Cs, Sb, Co, Cr, V, Mo, Cu, and W during diagenesis that produced K enrichment and/or REE and HFSE fractionations are losses during dolomitization. Similarly, losses of Cd, Pb, W, Zn, Cu, Mo, and V during K-addition, and/or REE and HFSE fractionations, are gains during dolomitization. These complementary relationships are consistent with evolution of the basinal fluids to lower pH during dolomitization where its pH was buffered by sedimentary carbonates.

(5) From data of this study, there is no evidence linking the three diagenetic stages recognized in the Belt-Purcell sequence, in time or space, with the syn-sedimentary Pb-Zn-Ag Sullivan ore deposit that displays different geochemical signatures in proximal altered sedimentary rocks. Dolomitization post-dates stage 2 addition of HREE that is constrained to ~1400-300 Ma from chemical ages of diagenetic monazites, or is broadly coeval based on complementary geochemical relationships.

(6) Fluid events in other Proterozoic basins in Laurentia and Australia could be linked and correlated as the result of large-scale advective flow of basinal brines 100s Ma after deposition. Changes of hydraulic gradient could be connected to distal tectonic effects of the assembly and dispersal of the supercontinent Columbia at ~1500 Ma, the Grenville Orogen at ~1300-900 Ma, and break up of Rodinia at ~900-700 Ma.

6.7 Acknowledgements

Staff of Waterton-Glacier International Peace Park are thanked for support, especially L. F. Marnell and C. Smith; as well as Q. Xie and J. Fan who assisted with ICP-MS analyses; to L. M. Shychosky, M. England, A. Vangool, R. Ahrabian, A. Peterhänsel, and L. Skublicki for help during fieldwork; and T. Prokopiuk, A. Zazzo, L. Buatois and R. Renaut for their input on the Chapter. Natural Sciences & Environment Research Council of Canada (NSERC) discovery grants to R. Kerrich and B. R. Pratt, and a University of Saskatchewan graduate scholarship to I. González-Álvarez funded this study. R. Kerrich acknowledges NSERC MFA support of the ICP-MS facility, and the George McLeod endowment to the Department of Geological Sciences, University of Saskatchewan.

6.8 Appendix

Appendix 6.1 Major and trace element concentration of the Belt-Purcell Supergroup carbonate-rich units.

Formation	Mount Shields	Helena	Helena	Helena	Empire	Empire	Grinnell	Appekunny	Altyn	Altyn	Altyn	Waterton	Waterton	Waterton
Sample	32(1)G1	28(2)G1	28G1USO	28(1)G1	27(3)G1	27G1USO	USO 25	USO 10	24G1USO	24(2)G1	24(1)G1	23G1USO	23(2)G1	23(1)G1
SiO_2 (wt%)	50.50	52.90	38.50	36.90	56.00	28.70	58.00	12.70	13.20	36.10	4.10	16.40	25.90	45.60
TiO_2	0.62	0.33	0.15	0.24	0.29	0.15	0.31	0.10	0.14	0.17	0.04	0.19	0.30	0.34
Al_2O_3	9.81	6.43	2.75	6.49	8.40	3.12	10.60	2.41	3.11	5.27	0.56	4.05	6.03	12.32
Fe_2O_3	3.59	1.85	0.97	2.51	2.62	2.18	4.61	1.60	1.19	0.60	0.41	1.37	1.19	1.19
MnO	0.13	0.06	0.03	0.03	0.07	0.21	0.04	0.11	0.04	0.01	0.12	0.02	0.02	u.d.
MgO	7.26	4.30	1.58	4.34	7.55	14.00	5.90	17.40	17.80	12.02	0.96	17.10	13.53	8.92
CaO	9.29	15.71	29.80	25.22	8.10	20.10	6.29	25.70	25.40	16.86	51.93	22.80	19.22	8.51
K_2O	3.19	1.57	0.59	1.62	3.48	1.02	1.99	0.92	0.94	2.68	0.08	1.98	4.02	9.33
Na_2O	1.41	1.20	0.35	0.43	0.44	0.12	1.81	0.06	0.32	0.45	0.05	0.11	0.10	0.10
P_2O_5	0.16	0.08	0.03	0.04	0.07	0.03	0.10	0.03	0.03	0.06	0.06	0.03	0.03	0.03
LOI	14.2	15.7	24.5	22.4	13.0	30.7	10.2	39.1	38.2	26.0	41.6	36.1	30.0	14.0
Sum	100.3	100.3	99.2	100.2	100.2	100.4	99.9	100.1	100.4	100.4	99.9	100.1	100.3	100.4
Li (ppm)	58	51	46	105	75	76	64	17	39	74	4	85	43	152
Rb	99	47	27	61	88	35	73	29	31	46	3	40	67	138
Sr	39	65	115	72	40	58	50	48	61	46	347	30	28	20
Cs	4	2	1	4	4	1	4	1	2	3	0	1	2	3
Ba	346	322	88	256	1436	210	295	76	87	870	330	108	207	234
Y	33	20	15	14	21	14	26	14	15	14	4	12	13	24
Zr	430	216	53	71	116	37	117	31	30	134	6	40	61	238
Hf	12.70	5.70	1.38	1.91	3.25	1.05	3.80	0.90	0.84	3.26	0.15	1.14	1.63	7.47
Nb	14.3	8.4	3.2	5.1	8.5	3.1	7.0	2.0	1.4	1.7	0.8	4.4	8.6	17.7
Ta	1.2	0.6	0.2	0.3	0.6	0.2	0.6	0.2	0.1	0.1	0.0	0.2	0.5	1.2
Th	15.0	7.4	2.6	4.2	7.5	2.6	8.5	2.5	2.2	4.3	0.2	3.5	6.0	16.9
U	3.3	1.6	0.7	1.0	3.2	1.5	1.9	0.7	1.2	1.8	1.2	0.6	2.1	4.0
La	40	22	18	15	23	10	51	15	17	14	2	14	13	56
Ce	88	50	37	33	47	23	99	31	37	28	3	27	26	100
Pr	10	6	4	4	6	3	11	4	4	3	0	3	3	11
Nd	37	23	16	15	20	11	44	15	14	11	2	12	11	35
Sm	7.23	4.40	3.46	2.84	4.23	2.43	9.30	3.50	2.62	2.27	0.24	2.17	2.04	4.34
Eu	1.18	0.73	0.58	0.54	0.64	0.45	1.80	0.80	0.48	0.41	0.06	0.38	0.35	0.52
Gd	6.65	4.11	3.23	2.71	3.92	2.54	8.50	3.50	2.59	2.03	0.26	1.94	1.86	3.32
Tb	0.96	0.60	0.43	0.40	0.58	0.38	1.06	0.45	0.36	0.29	0.04	0.25	0.26	0.52
Dy	6.14	3.82	2.49	2.31	3.63	2.28	5.60	2.60	2.12	1.97	0.27	1.52	1.62	3.77
Ho	1.23	0.76	0.49	0.48	0.75	0.47	1.00	0.50	0.45	0.39	0.06	0.32	0.35	0.89
Er	3.80	2.27	1.31	1.44	2.21	1.33	2.80	1.30	1.25	1.27	0.20	0.92	1.10	2.86
Tm	0.56	0.34	0.18	0.19	0.35	0.18	0.38	0.17	0.17	0.20	0.03	0.14	0.17	0.46
Yb	3.80	2.19	1.27	1.43	2.21	1.28	2.60	1.10	1.09	1.12	0.18	0.84	1.07	3.24
Lu	0.53	0.33	0.18	0.18	0.34	0.17	0.39	0.17	0.14	0.15	0.01	0.11	0.15	0.44
Sc	16.02	12.99	21.67	21.81	12.51	17.32	9.00	7.00	12.71	14.58	6.51	14.49	16.10	12.70
V	50.83	20.65	13.26	36.24	33.09	16.07	39.00	15.00	14.84	21.15	6.98	14.47	26.49	20.90
Mo	0.78	0.48	0.20	0.30	0.65	0.00	0.70	0.20	0.00	0.37	0.54	0.00	0.25	0.24
Cr	89	36	14	36	44	25	103	23	16	22	5	22	31	21
Co	18	5	2	5	7	2	15	5	3	2	1	3	4	4
Ni	21	9	9	25	12	6	17	7	9	6	10	10	9	9
Cu	14	5	4	9	9	2	3	3	4	13	2	33	9	3
Zn	37	40	12	76	27	19	63	6	16	13	8	14	18	15
Sn	2.5	1.0	0.8	1.3	1.7	0.8	3.4	0.8	0.6	1.1	0.2	0.9	1.0	3.2
W	1.4	0.9	0.2	0.7	1.1	0.5	3.4	35.6	0.0	0.5	0.0	0.3	0.4	0.6
Pb	27.8	6.9	4.5	5.1	7.8	2.7	17.0	2.0	4.8	4.5	2.3	2.6	15.0	13.3
Cd	0.19	0.25	0.00	0.22	0.00	0.00	u.d.	u.d.	0.00	0.00	0.00	0.00	0.00	0.13
Tl	0.55	0.24	0.09	0.25	0.50	0.10	0.32	0.08	0.17	0.27	0.10	0.14	0.25	0.33
Ga	10.24	6.80	3.85	9.98	9.91	4.36	21.00	3.00	4.81	4.08	2.52	5.72	7.39	14.29
As	7.10	2.21	0.63	2.06	9.57	1.66	7.40	1.60	2.63	0.00	0.50	0.88	0.61	2.01
Ag	0.25	0.00	0.00	0.00	0.00	0.00	0.29	0.09	0.03	0.06	0.00	0.00	0.00	0.00
Sb	1.07	0.34	0.00	0.38	0.57	0.37	1.19	0.23	0.28	0.34	0.13	0.00	0.10	0.30
Label Fig. 6.3	G60	G52	G51	G50	G49	G47	G34	G30	G6	G5	G4	G3	G2	G1

Appendix 6.1 (continued).

Formation	Roosville	Van Creek	Kitchener	Helena	Helena
Sample	22PuUSO	18(2)PU	17(1)Pu	6(2)Wh	6 Wh USO
SiO_2 (wt%)	8.60	54.60	46.60	42.30	41.30
TiO_2	0.08	0.58	0.30	0.20	0.33
Al_2O_3	0.80	14.02	6.82	5.88	8.28
Fe_2O_3	0.85	1.83	2.57	2.56	2.87
MnO	0.10	0.01	0.10	0.08	0.06
MgO	19.00	6.31	8.41	10.57	6.75
CaO	28.40	6.11	16.53	14.52	18.00
K_2O	0.31	5.15	1.44	2.10	2.29
Na_2O	0.03	0.67	0.05	0.69	0.71
P_2O_5	0.03	0.11	0.07	0.04	0.07
LOI	41.9	10.7	17.3	21.2	19.5
Sum	100.1	100.3	100.3	100.2	100.2
Li (ppm)	19	259	65	59	88
Rb	18	206	72	84	77
Sr	46	30	87	69	105
Cs	0	18	4	5	4
Ba	50	675	169	420	599
Y	8	31	24	17	23
Zr	20	294	127	83	89
Hf	0.50	9.17	3.58	2.57	2.74
Nb	1.2	18.8	8.7	6.9	9.2
Ta	0.1	1.4	0.6	0.4	0.6
Th	1.0	19.3	8.3	5.2	7.5
U	1.1	6.2	1.9	1.8	2.6
La	7	47	27	11	29
Ce	16	102	59	23	61
Pr	2	12	7	3	7
Nd	7	41	26	12	26
Sm	1.32	7.00	4.88	2.74	4.91
Eu	0.24	0.88	0.76	0.46	0.78
Gd	1.27	5.57	4.60	3.04	4.33
Tb	0.18	0.74	0.67	0.50	0.62
Dy	1.07	5.25	4.07	2.88	3.84
Ho	0.23	1.17	0.84	0.61	0.78
Er	0.66	3.79	2.50	1.77	2.36
Tm	0.09	0.62	0.38	0.27	0.38
Yb	0.58	4.39	2.69	1.86	2.45
Lu	0.07	0.60	0.36	0.26	0.35
Sc	10.75	15.58	14.35	13.77	15.54
V	9.31	46.49	27.03	21.49	38.91
Mo	0.00	1.37	0.12	0.34	1.04
Cr	10	50	49	37	51
Co	1	10	5	3	7
Ni	6	15	11	8	19
Cu	2	26	3	2	29
Zn	83	15	32	26	52
Sn	0.3	3.4	1.6	1.6	2.1
W	0.0	2.2	1.2	0.6	1.4
Pb	27.2	33.1	4.4	6.6	7.4
Cd	0.28	0.00	0.38	0.00	0.24
Tl	0.00	1.22	0.30	0.48	0.38
Ga	1.10	16.70	8.33	6.58	9.71
As	1.22	23.67	8.14	2.63	1.49
Ag	0.00	0.00	0.00	0.04	0.00
Sb	0.43	3.57	0.30	0.31	0.67
Label Fig. 6.3	P26	P17	P14	W22	W20

(u.d.) Under detection limits.

6.9 References

Anderson, H.E., Davis, W.D., 1995. U-Pb geochronology of the Moyie sills, Purcell Supergroup, southeastern British Columbia: implications for the Mesoproterozoic geological history of the Purcell (Belt) Basin. Can. J. Earth Sci. 32, 1180-1193.

Bethke, C. M., Marshak, S., 1990. Brine migrations across North America - the plate tectonics groundwater. Ann. Rev. Earth Plan. Sci. 18, 387-316.

Bhat, M.I., Ghosh, S.K., 2001. Geochemistry of the 2.51 Ga old Rampur Group pelites, western Himalayas: implications for their provenance and weathering. Precam. Res. 108, 1-16.

Billon, G., Ouddane, B., Recourt, P., Boughriet, A., 2002. A depth variability and some geochemical characteristics of Fe, Mn, Ca, Mg, Sr, S, P, Cd, and Zn in anoxic sediments from Authie Bay (northern France). Estuarine Coastal Shelf Sci. 55, 167-181.

Bozkaya, O., Yalcin, H., 2004. Diagenetic to low-grade metamorphic evolution of clay mineral assemblages in Palaeozoic to early Mesozoic rocks of the Eastern Taurides, Turkey. Clay Mineral. 39, 481-500.

Canaveras, J.C., Sánchez-Moral, S., Sanz-Rubio, E., Hoyos, M., 1998. Meteoric calcitization of magnesite in Miocene lacustrine deposits (Calatayud Basin, NE Spain). Sed. Geol. 119, 183-194.

Chandler, F.W., 2000. The Belt-Purcell basin as a low-latitude passive rift: implications for the geological environment of Sullivan type deposits. In: Lydon, J.W., et al., Höy, T., Slack, J.F., Knapp, M.E., (eds.), The Geological Environment of the Sullivan Deposit, British Columbia. Geol. Assoc. Can. Min. Dep. Div. Spec. Publ. 1, pp. 82-112.

Condie, K.C., 2002. The supercontinent cycle: are there two patterns of cyclicity? J. African Earth Sci. 35, 179-183.

Cullers, R.L., Podkovyrov, V.N., 2002. The source and origin of terrigenous sedimentary rocks in the Mesoproterozoic Ui group, southeastern Russia. Precam. Res. 117, 157-183.

Evans, K.V., Aleinikoff, J.N., Obradovich, J.D., Fanning, C.M., 2000. SHRIMP U-Pb geochronology of volcanic rocks, Belt Supergroup, western Montana: evidence for rapid deposition of sedimentary strata. Can. J. Earth Sci. 37, 1287-1300.

Fan, J., Kerrich, R., 1997. Geochemical characteristics of aluminum depleted and undepleted komatiites and HREE-enriched low-Ti tholeiites, western Abitibi greenstone belt: a heterogeneous mantle plume-convergent margin environment. Geochim. Cosmochim. Acta 61, 4723-4744.

Fayek, M, Kyser, T.K., 1997. Characterization of multiple fluid-flow events and rare earth element mobility associated with formation of unconformity-type uranium deposits in the Athabasca basin. Can. Mineral. 35, 627-658.

Fedo, C.M., Nesbitt, H.W., Young, G.M., 1995. Unraveling the effects of potassium metasomatism in sedimentary rocks and paleosols, with implications for paleoweathering conditions and provenance. Ge-

ology 23, 921-924.

Fermor, P.R., Price, R.A., 1983. Stratigraphy of the lower part of the Belt-Purcell Supergroup (middle Proterozoic) in the Lewis Thrust sheet of southern Alberta and British Columbia. Bull. Can. Petrol. Geol. 31, 164-194.

Folk, R.L., 1968. Petrology of sedimentary rocks. Hemphill's, Austin, U.S.A.

Fryer, B.J., Kerrich, R., Hutchinson, R.W., Pierce, M.G., Rogers, D.S., 1979. Archean precious-metal hydrothermal systems, Dome Mine, Abitibi greenstone-belt. Patterns of alteration and metal distribution. Can. J. Earth Sci. 16, 421-439.

Gareth, D.J., Fiona, F., Whitaker, P.L., Smart, W. E., 2002. Fate of reflux brines in carbonate platforms. Geology 30, 371-374.

González-Álvarez, I., Kerrich R., *submitted*. Mobility of REE and HFSE in Basinal Brines of the Mesoproterozoic Belt-Purcell Supergroup, Western North America. G-cubed.

González-Álvarez, I., Kusiak, M.A., Kerrich, R., *in press*. A trace element and chemical Th-U total Pb dating study in the lower Belt-Purcell Supergroup, western North America: provenance and diagenetic implications. Chem. Geol.

Gresens, R.L., 1967. Composition-volume relationships of metasomatism. Chem. Geol. 2, 47-65.

Grotzinger, J.P., 1986. Shallowing-upward cycles of the Wallace Formation, Belt Supergroup, northwestern Montana and northern Idaho. In: Roberts, S.M., (ed.), Belt Supergroup, a Guide to Proterozoic Rocks of Western Montana and Adjacent Areas, Montana Bur. Min. Geol. Spec. Publ. 94, 143-160.

Harrison, J.E., 1972. Precambrian Belt basin of northwestern United States: its geometry, sedimentation, and copper occurrences. Geol. Soc. Am. Bull. 83, 1215-1240.

Humphries, S.E., 1984. The mobility of the rare earth elements in the crust. In: Henderson, P. (ed.), Rare Earth Element Geochemistry, Elsevier, Oxford, pp. 317-342.

Jenner, G.A, Longerich, H.P., Jackson, S.E., Fryer, B.J., 1990. ICP-MS a powerful tool for high precision trace-element analyses in earth sciences: evidence from analyses of selected USGS reference samples. Chem. Geol. 83, 133-148.

Johannesson, K.H., Lyons, W.B., 1995. Rare earth elements geochemistry of Colour Lake and acidic freshwater lake on Axel Heiberg island, Northwest Territories. Canada, Chem. Geol. 119, 209-223.

Kerrich, R., González-Álvarez, I., 2003. Basinal fluid evolution in the Appekunny-Grinnell Formation, 1.4 Ga Belt Supergroup. Geol. Soc. Am. Annual Meeting, Seattle, Abstract 243-3.

Kerrich, R., Renaut, R.W., Bonli, T., 2002. Trace-element composition of cherts from alkaline lakes in the east African rift: a probe for ancient counterparts. In: Renaut, R.W., Ashley, G.M. (eds.), Sedimentation in Continental Rifts, Soc. Sed. Geol., Boulder, Colorado, Spec. Publ. 73, pp. 277-298.

Kyser, K., 2000. Controls on fluids and basins. In: Kyser, K. (ed.), Fluids and Basin Evolution, Min. Assoc. Can., Short Course Series, vol. 28, Kingston, Ontario, pp. 1-18.

Kyser, K., Hiatt, E., Renac, C., Durocher, K., Holk, G., Deckart, K., 2000. Diagenetic fluids in Paleo- and Mesoproterozoic sedimentary basins and their implications for long protected fluid histories. In: Kyser, K. (ed.), Fluids and Basin Evolution, Min. Assoc. Can., Short Course Series, vol. 28, Kingston, Ontario, pp. 225-262.

LaTour, T.E., Kerrich, R., Barnett, R.L., 1984. Hydrothermal alteration and dynamic recrystalization of feldspar in an Archean iron formation. Can. Mineral. 22, 621-630.

Lev, S.M., McLennan, S.M., Meyers, W.J., Hanson, G.N., 1998. A petrographic approach for evaluating trace-element mobility in a black shale. J. Sed. Res. 68, 970–980.

Link, P.K., 1997. The Grinnell, Empire and Helena formations along Baring Creek and at Siyeh Pass, Glacier National Park, In: Link, P. K., (ed.), Geologic Guidebook to the Belt-Purcell Supergroup, Glacier National Park and Vicinity, Montana and Adjacent Canada, Field Trip Guidebook for the Belt Symposium III, Belt Association, Pocatello, Idaho, pp. 113-124.

Lonnee, J., Al Aasm, I. S., 2000. Dolomitization and fluid evolution in the middle Devonian sulphur Point Formation, Rainbow South Field, Alberta: Petrographic and geochemical evidence. Bull. Can. Petr. Geol. 48, 262-283.

Lydon, J.W., 2000. A synopsis of the understanding of the geological environment of the Sullivan Deposit, In: Lydon, J.W., Höy, T., Slack, J.F., Knapp, M.E., (eds.), The Geological Environment of the Sullivan Deposit, British Columbia. Geol. Assoc. Can. Min. Dep. Div. Spec. Publ. 1, pp. 12-31.

Lyons, T.W., Frank, T.D., Schreiber, M.E., Winston, D., Lohmann, K.C., 1997. Geochemical constraints on paleoenvironments within the Belt Supergroup (Middle Proterozoic), Montana, In: Berg, R.B., (ed.), Belt Symposium III. Montana Bur. Min. Geol., Spec. Publ. 112, 190-201.

Maas, R., McCulloch, M.T., 1991. The provenance of Archean clastic metasediments in the Narryer gneiss complex, western Australia: trace element geochemistry, Nd isotopes, and U-Pb ages for detrital zircons. Geochim. Cosmochim. Acta 55, 1915-1932.

Maxwell, D.T., Hower, J., 1967. High-grade diagenesis and low-grade metamorphism of illite in the Precambrian Belt Series. Am. Mineral. 52, 843-857.

McDaniel, D.K., Hemming, S.R., McLennan, S.M., Hanson, G.N., 1994. Resetting of neodymium isotopes and redistribution of REEs during sedimentary processes: the early Proterozoic Chelmsford Formation, Sudbury Basin, Ontario, Canada. Geochim. Cosmochim. Acta 58, 931-941.

McLennan, S.M., Bock, B., Hemming, R.S., Hurowitz, J.A., Lev, S.M., McDaniel, D.K., 2003. The roles of provenance and sedimentary processes in the geochemistry of sedimentary rocks. In: Lentz, D.R. (ed.), Geochemistry of Sediments and Sedimentary Rocks: Evolutionary Considerations to Mineral-Deposit Forming Environments. Geol. Assoc. Can., St. John's, Newfoundland, Canada, Geo Text 4, pp. 7-38.

McMannis, W.J., 1963. LaHood Formation–A coarse facies of the Belt series in southwestern Montana,

Geo. Soc. Am. Bull. 74, 407-436.

McMechan, M.E., 1981. The middle Proterozoic Purcell Supergroup in the southwestern Rocky and southeastern Purcell Mountains, British Columbia and the initiation of the Cordilleran miogeocline, southern Canada and adjacent United States. Bull. Can. Petrol. Geol. 29, 583-621.

Milodowski, A.E., Zalasiewicz, J.A., 1991. Redistribution of rare earth elements during diagenesis of turbidite/hemipelagite mudrock sequences of Llandovery age from central Wales. In: Morton, A.C., et al., (eds.), Developments in Sedimentary Provenance Studies. Geol. Soc. London Spec. Publ. 57, p. 101–124.

Moores, C.H., 1989. Carbonate diagenesis and porosity. Elsevier, Amsterdam, The Netherlands.

Morse, J.W., 2004. Formation and diagenesis of carbonate sediments. In: MacKenzie, F.T., (ed.), Sediments, Diagenesis, and Sedimentary Rocks, Treatise on Geochimistry, Holland, H.D., Turekian, K.K., (eds.), Elsevier, Oxford, New York, 7, pp. 67-86.

Oliver, J., 1986. Fluids expelled tectonically from orogenic belts: their role in hydrocarbon migration and other phenomena. Geology 74, 1234-1253.

O'Neill, J.M., 1997. Stratigraphic character and structural setting of the Belt Supergroup in the Highland Mountains southwestern Montana. In: Berg, R.B., (ed.), Belt Symposium III, Montana Bureau Min. Geol. Spec. Publ. 117,12-16.

Pingitore, N. E., 1982. The role of diffusion during carbonate diagenesis. J. Sed. Res. 52, 27-40.

Potts, P.J., Tindle, A.G., Webb, P.C., 1992. Geochemical reference material compositions. In: Whittles, F. L. (ed.), Rocks, Minerals, Sediment, Soils, Carbonates, Refractories and Ores Used in Research and Industry. CRC Press, Boca Raton, Latheronwheel, Caithness, U.K., pp. 220-221.

Pratt, B.R., 2001. Oceanography, bathymetry and syndepositional tectonics of a Precambrian intracratonic basin: integrating sediment, storms, earthquakes and tsunamis in the Belt Supergroup (Helena Formation, ca. 1.45 Ga), western North America. Sediment. Geol. 141, 371-394.

Price, R.A., 1964. The Precambrian Purcell System in the Rocky Mountains of southern Alberta and British Columbia. Bull. Can. Petrol. Geol. Spec. Publ. 12, 399-426.

Price, R.A., Sears, J.W, 2000. A preliminary palinspastic map of the Mesoproterozoic Belt-Purcell Supergroup, Canada and USA: implications for the tectonic setting and structural evolution of the Purcell anticlinorium and the Sullivan deposit. In: Lydon, J.W., Höy, T., Slack, J.F., Knapp, M.E., (eds.), The Geological Environment of the Sullivan Deposit, British Columbia. Geol. Assoc. Can. Min. Dep. Div. Spec. Publ. 1, pp. 61-81.

Rainbird, R.H., Nesbitt, H.W., Donalson, J.A., 1990. Formation and diagenesis of a sub-Huronian saprolith: comparison with a modern weathering profile. J. Geol. 98, 801-822.

Rosenberg, P.E., 2002. The nature, formation, and stability of end-member illite: a hypothesis. Am. Mineral. 87, 103-107.

Ross, M. G., 2000. Tectonics of sedimentary basins: a prelude to fluid evolution. In: K. Kyser (ed.), Fluids and Basin Evolution, Short Course Series, Kingston, Ontario, Min. Assoc. Can., 28, pp. 39-62.

Ross, G.M., Parrish, R.R., Dudás, F.Ö., 1991. Provenance of the Bonner Formation (Belt Supergroup), Montana: insights from U-Pb and Sm-Nd analyses of detrital minerals. Geology 19, 340-343.

Sageman, B.B., Lyons, T.W., 2004. Geochemistry of fine-grained sediments and sedimentary rocks. In: MacKenzie, F.T.,(ed.), Sediments, Diagenesis, and Sedimentary Rocks, Treatise on Geochimistry, Holland, H.D., Turekian, K.K., (eds.), Elsevier, Oxford, New York, 7, pp. 115-158.

Schandl, E. S., Gorton M. P., Lydon J. W., 2000, Trace and rare earth element study of sediments associated with the Sullivan sedex deposit, British Columbia: implications for element mobility and tectonic environment. In: Lydon, J.W., Höy, T., Slack, J.F., Knapp, M.E., (eds.), The Geological Environment of the Sullivan Deposit, British Columbia. Geol. Assoc. Can. Min. Dep. Div. Spec. Publ. 1, pp. 202-217.

Schieber, J.A., 1988. Redistribution of rare earth elements during diagenesis of carbonate rocks from the mid-Proterozoic Newland Formation, Montana, U.S.A. Chem. Geol. 69, 111-126.

Schieber, J., 1989. The origin of the Neihart quartzite, a basal deposit of the Mid-Proterozoic Belt Supergroup, Montana, U.S.A. Geol. Mag. 126, 271-281.

Schieber, J.A., 1997. Sedimentological, geochemical, and mineralogical features of the Belt Supergroup and their bearing on the lacustrine versus marine debate. In: Berg, R.B., (ed.), Belt Symposium III. Montana Bur. Min. Geol., Spec. Publ. 112, pp. 177-189.

Sears, J.W., Price, R.A., Khudoley A.K., 2004. Linking the Mesoproterozoic Belt-Purcell Supergroup and Udzha Basin across the west Laurentia-Siberia connection. Precambrian Res. 129, 291-308.

Taylor, S.R., McLennan, S.M., 1995. The geochemical evolution of the continental crust. Rev. Geophys. 33, 241-265.

Terakado, Y., Fujitani, T., 1998. Behavior of the rare earth elements and other trace elements during interactions between acidic hydrothermal solutions and silicic volcanic rocks, southwestern Japan. Geochim. Cosmochim. Acta 62, 1903-1917.

Volkova, N.I., 1998. Geochemistry of rare elements in waters and sediments of alkaline lakes in the Sasykkul depression, east Pamirs. Chem. Geol. 147, 265-277.

Wallace, C.A., 1997. Paleotransport directions and basin configuration, middle part of the Missoula Group (Belt Supergroup, middle Proterozoic) western Montana. Belt Symposium III, Montana Bur. Min. Geol. Spec. Publ., 112, 88-103.

Wallace, C.A., Harrison, J.E., Lidke, D.J., 1993. Lithofacies of the Helena and Wallace Formations (Belt Supergroup, middle Proterozoic), Montana and Idaho. Belt Symposium III, Informal program and abstracts, Montana, pp. 3.

Whiple, J. W., J. J. Connor, Raup O. B., McGrimsey R. G., 1984. Preliminary report on the stratigraphy

of the Belt Supergroup, Glacier National Park and adjacent Whitefish Range, Montana, in northwest Montana and adjacent Canada. In: McBane, J.D., Garrison, P.B., (eds.), Guidebook, Field Conference and Symposium, Belt Association, Pocatello, Idaho, Montana Geol. Soc., pp. 33-50.

Whipple, J.W., Binda, P.L., Winston, D., 1997. Geologic guide to Glacier National Park, Montana and areas adjacent to Waterton, Alberta. In: Link, P.K., (ed.), Belt Symposium III, Geologic Guidebook to the Belt-Purcell Supergroup, Glacier National Park and Vicinity, Montana and adjacent Canada, Belt Association, Pocatello, Idaho, pp. 125-155.

Windley, B.F., 1995. The evolving continents. Wiley and Sons, New York, NY, U.S.A.

Winston, D., 1986. Sedimentology of the Ravalli Group, middle Belt carbonate and Missoula Group, middle Proterozoic Belt Supergroup, Montana, Idaho and Washington. In: Roberts, S.M., (ed.), A Guide to Proterozoic Rocks of Western Montana and Adjacent Areas. Montana Bur. Min. Geol. Spec. Publ. 94, pp. 85-124.

Winston, D., 1989. A sedimentary and tectonic interpretation of the Belt. In: Hanshaw, P.M., (ed.), Middle Proterozoic Belt Supergroup, Western Montana, 28th International Geological Congress, Field Trip Guidebook T334. Am. Geophysical Union, pp. 437-469.

Winston, D., 1990. Evidence for intracratonic, fluvial and lacustrine settings of Middle to late Proterozoic basins of western U.S.A. In: Gower, C.F., Rivers, T., Ryan, B., (eds.), Mid-Proterozoic Laurentia-Baltica. Geol. Assoc. Can., Spec. Paper 38, 535-564.

Winston, D., Lyons, T., 1997. Sedimentary cycles in the St. Regis, Empire and Helena formations of the middle Proterozoic Belt Supergroup, northwestern Montana. In: Link, P.K., (ed.), Geological Guidebook to the Belt-Purcell Supergroup, Glacier National Park and Vicinity, Montana and Adjacent Canada, Belt Symposium III, Field Trip guidebook, Belt association, Spokane, pp. 21-51.

Woodcock, N.H., 2004. Life span and fate of basins. Geology, 32, 685-688.

Xie, Q., Jain, J., Sun, M., Kerrich, R., Fan, J., 1994. ICP-MS analysis of basalt BIR-1 for trace elements. Geostandards Newsletters 18, 53-63.

Zenger D.H., 1981. On the formation and occurrence of saddle dolomite discussion. J. Sed. Petrol. 51, 1350-1352.

Zhao, G., Sun, M., Wilde, S.A., Li, S., 2004. A Paleo-Mesoproterozoic supercontinent: assembly, growth and break up. Earth Sci. Rev. 67, 91-123.

Connecting paragraph from Chapter VI to Chapter VII

The Belt-Purcell Basin may be part of a system of intracontinental rifts that developed as the Mesoproterozoic supercontinent Columbia dispersed at ~1500 Ma, possibly due to plume impingement. Intense weathering, inferred from geochemical CIA values, of the provenance may be associated with elevated levels of atmospheric CO_2 degassed from volcanic activity generated as a consequence of the mantle plume and new ocean spreading centres. The following study addresses geochemical signature of weathering corrected for the diagenetic effects described in previous chapters and aims to describe the weathering in the source area of the Belt-Purcell Supergroup.

CHAPTER VII

Weathering Intensity on Laurentia in the Mesoproterozoic: Evidence from the Belt-Purcell Supergroup, Western North America

Abstract

Argillites and sandstones of the Belt-Purcell Supergroup spanning over ~17 km of stratigraphic section, and sampled at three localities, display systematic negative anomalies of Eu/Eu relative to post-Archean upper continental crust. The chemical index of alteration (CIA), corrected for diagenetic K-addition, spans 55 to 85 relative to post-Archean Australian average shale (PAAS) of 70. Argillites, average at 73, and sandstones at 66. These results, in conjunction with low absolute contents of Sr, Ca, and Na, together with high Rb/Sr and K/Cs ratios, and covariations of CIA-Eu/Eu* collectively could be viewed as a combination of moderate to intense chemical weathering and a recycled sedimentary component in the provenance. Such geochemical relationships are in keeping with large, modern, river system, as the Ganges, Mekong, or Amazon rivers that drain moderately to intensely weathered source regions.*

The presence of minor pristine detrital feldspars could be explained by a local source proximal to the Belt-Purcell Basin with short-river transport, under local arid to semi-arid climate. Stratigraphic variation of CIA values through the sequence is not correlated with the presence of preserved evaporites that are a proxy of arid to semi-arid conditions in the depositional setting. Sporadically low CIA values, throughout the Belt-Purcell sequence, are interpreted as due to a mixture of a distally weathered terranes, and feldspar content from a proximal juvenile source area.

The Belt-Purcell Basin was part of an intracontinental rift system, and developing spreading centres, that developed as the Mesoproterozoic supercontinent Columbia dispersed at ~1500 Ma, possibly due to plume impingement. Moderate to intense weathering in the source region may be associated with elevated levels of atmospheric CO_2 degassed from the mantle plume and new spreading centres.

7.1 Introduction

Proterozoic paleoclimates and their driving forces are controversial. Severe swings in climate during ~2000 Ma brought at least two low-latitude glacial periods, at ~2400-2200 and ~800-600 Ma (e.g., Hoffman, 1999; Ohmoto, 2004; Young, 2004).

Siliciclastic sediments may record chemical signatures of weathering intensity in the source area, which in turn reflect paleoclimate. Climate may influence the weathering intensity in the

source area of sediments (e.g., Holland, 1978; Duddy, 1980; Nesbit and Young, 1982; Sawyer, 1986; Marsh, 1991; Young, 1999; Young, 2004; Nesbitt and Young, 2004). Feldspar and quartz constitute ~80% of the modal mineralogical composition of the upper crust (Taylor and McLennan, 1985 and references therein). Hydrolysis of feldspars and ferromagnesian minerals, accompanied by the depletion of mainly alkali and alkaline-earth metals in the residual bedrock, are the most common features of the weathering process (Krauskopf, 1982). Based on these principles, the Chemical Index of Alteration (CIA) was formulated by Nesbitt and Young (1982) using a geochemical approach to address paleoclimate. The formula defining CIA is as follows:

$$CIA=[Al_2O_3/(Al_2O_3+CaO^*+Na_2O+K_2O)]*100 \quad (7.1)$$

Where CaO* is associated with the silicate fraction of the rock. The CIA varies from 100 in severely weathered residual clays to ~50 in unweathered rocks. Values of CIA in PA-UCC and post-Archean Australian Shale (PAAS) are ~50 and 70 respectively (Taylor and McLennan, 1985). Warm paleoclimate peaks are proposed at ranges of ~2700-2500 Ma and ~2000-1700 Ma based on CIA peaks and black shale ratios in sedimentary sequences (Condie et al., 2001). Some of those peaks could record the breakup of supercontinents at ~2200-2000 and ~800-600 Ma, and the consequent increase in atmospheric CO_2 levels produced by associated mantle superplume events (Condie et al., 2000, 2001; Rogers and Santosh, 2004). This study addresses weathering intensity for the interval ~1500-1400 Ma for which there are few data, especially K-corrected values for CIA.

The main factors in the alteration of the chemical composition of sediments are weathering, hydraulic sorting, and diagenesis. Based on these factors, this study attempts to ascertain the original geochemical signature of weathering in the catchment of the Belt-Purcell Supergroup in order to assess paleoclimate during part of the Mesoproterozoic, between the two main glacial periods in the Proterozoic. It also aims to test if high CIA values are in keeping with plume and spreading centre systems in rifting of the Mesoproterozoic supercontinent Columbia (cf. Windley, 1995; Pesonen et al., 2003; Zhao et al., 2004).

7.2 Geologic setting

The Belt-Purcell Supergroup is a remnant of an extensive, ~17 km thick, dominantly siliciclastic sequence (e.g., Harrison, 1972; McMechan, 1981; Whipple et al., 1984; Link, 1997). It outcrops over 500 km, from southwestern Montana, where it is known as the Belt Supergroup, to southeastern British Columbia, where it is referred to as the Purcell Supergroup (Fig. 7.1). This

sedimentary sequence unconformably overlies igneous, metamorphic basement, and Cretaceous rocks which are only locally exposed (e.g., Kleinkopf, 1997; O'Neill, 1997).

This large volume of siliciclastic detritus is divided mainly in two main lithologies: (1) argillites (a combination of siltite, mudstone, and very fine-grained sandstone; e.g., Harrison, 1972; McMechan, 1981; Whipple et al., 1984; Winston, 1990), and (2) sandstones (mainly quartzarenites, subarkoses, and sublitharenites; terminology of Folk, 1968; e.g., Harrison, 1972; this study). The formers are interpreted as a result of fluvial transport from a low relief, continent scale catchment (Sears et al., 2004).

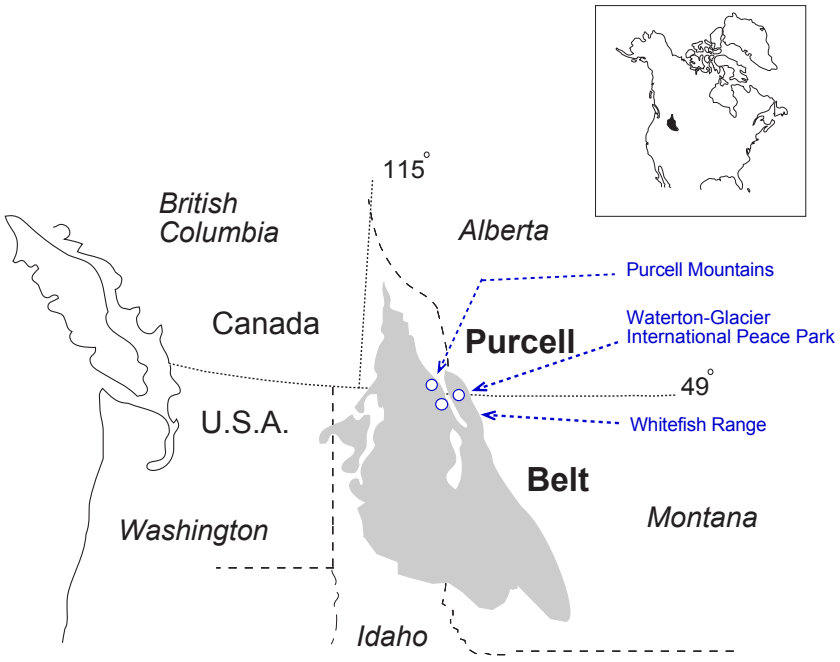

Fig. 7.1 Generalized geographic location of the Belt-Purcell Supergroup outcrops spanning the Canada-USA border, illustrating the three sampling locations.

The Belt-Purcell Supergroup comprises four stratigraphic divisions: the lower Belt; the Ravalli Group; the middle Belt; and the Missoula Group (Fig. 7.2; e.g., Whipple et al., 1984; Winston, 1986; Link, 1997).

(1) The lower Belt is the thickest part of the Belt-Purcell stratigraphic sequence reaching ~12 km thickness (Lydon, 2000). The lower Belt is represented by deep-sea fine-grained turbiditic facies of the Prichard Formation at Whitefish Range, with a northwest trendi parallel to the main

axes of the Belt-Purcell Basin (e.g., Godard, 1997). The lower Belt exhibits shallower depositional settings to the north and east. In Waterton-Glacier International Peace Park the lower Belt comprises the dolomitic Altyn and Waterton formations interpreted as the result of shallow-water to tidally influenced deposition (Figs. 7.2 and 7.3; e.g., Whipple et al., 1984, 1997). Laterally to the northwest in Canada, the stratigraphic equivalent units of the Fort Steele Formation presents fluvial deposits (Chandler, 2000), and southeast in the Helena Embayment, the LaHood Formation is explained as fan delta-complex deposits (Chandler, 2000 and references therein). (2) The lower Belt turns into the overlying Ravalli Group that represents in general a shallowing stage of the Belt-Purcell sedimentation. Red and green argillite, siltite, and less abundant white quartz arenite in a sharp interlayering represent the Appekunny, Grinnell and Empire formations (Figs. 7.2 and 7.3). The formers are interpreted as progradation of alluvial aprons in a flood-plain in Montana (Winston, 1986, 1989, 1990), whereas their lateral equivalent in British Columbia, the Creston Formation, is viewed as the result of a tidal influenced setting (McMechan, 1981). The Empire Formation is more calcareous to the top, representing the transitional stage into the deeper and richer carbonate middle Belt (Connor et al., 1984). (3) The carbonate-rich units of the middle Belt is featured by the Helena Formation in the east, and its equivalents the Wallace Formation to the west, and the Kitchener Formation in British Columbia (Figs. 7.2 and 7.3). They are viewed as lacustrine (Winston, 1986; 1990), subtidal-tidal (Wallace et al., 1993), or mid-shelf deposits (Pratt, 2001). (4) The stratigraphically highest Missoula Group overlies the middle Belt (Fig. 7.2). It represents later stages of filling of the Belt-Purcell Basin by mainly fine-grained siliciclastic sediment deposited in alluvial aprons, flood-plain, and shallow-water marine depositional environments (Snowslip, Shepard, Mount Shields, Bonner, McNamara and Libby formations) at the Waterton-Glacier International Peace Park and near areas (Figs. 7.2 and 7.3; e.g., Winston, 1986; Whipple et al., 1984, 1997; Link, 1997).

The tectonic setting for the Belt-Purcell Basin is interpreted to be part of an intracontinental rift system that formed at ~1500 Ma (e.g., Chandler, 2000; Price and Sears, 2000), associated with dispersal of the supercontinent Columbia (Zhao et al., 2004). Sedimentation spanned ≤75 Ma, with a minimum age of sedimentation constrained at 1468 ± 2 Ma and 1469 ± 3 Ma by U-Pb dating of zircons in synsedimentary sills situated near the base of the Supergroup (Anderson and Davies, 1995; Sears et al., 1998), to a maximum age estimated at 1401 ± 6 Ma from a tuff horizon in the upper Missoula Group, located amidst the Bonner and Libby formations (Fig. 2; Evans et al., 2000). Metamorphic grade trends are from subgreenschist facies in the northeast to amphibolite facies in the lowest part of the sequence southwest due to the burial and higher heat flow produced by local plutons (Maxwell and Hower, 1967; Harrison, 1972). Metamorphic grade is lower greenschist facies at the three localities sampled for this study.

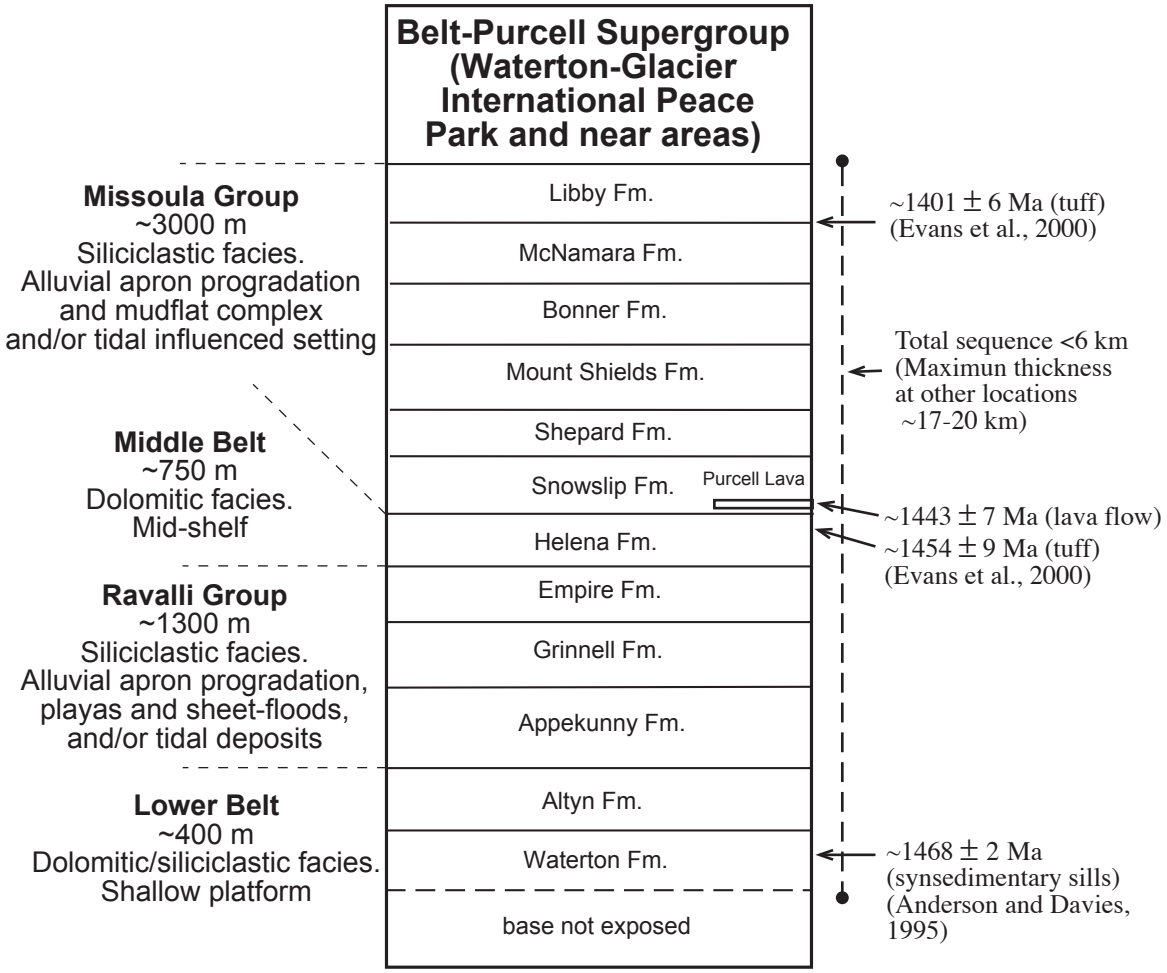

Fig. 7.2 Generalized stratigraphic section of the Belt-Purcell Supergroup at Waterton-Glacier International Peace Park (based on Whipple et al., 1984; 1997).

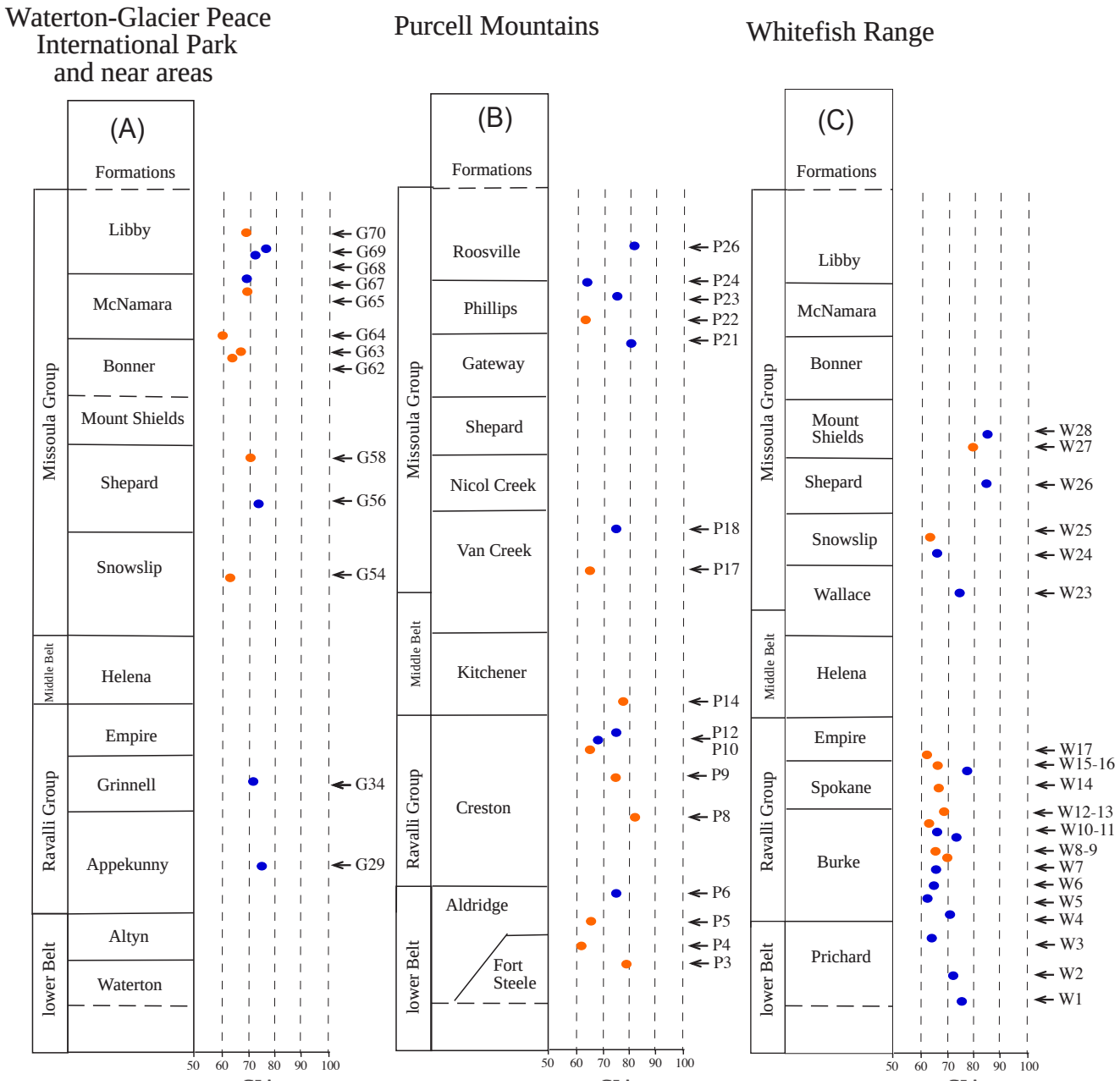

Fig. 7.3. Stratigraphic situation of samples taken for this study at the three locations cross-referenced to Appendix 7.1A, B, and C, and values of corrected chemical index of alteration (cf. Fedo et al., 1995) throughout the stratigraphic sequence at the three locations studied (see discussion). Orange coloured dots represent sandstones and blue coloured dots argillites.

7.3 Sampling and analytical techniques

A total of ninety-three siliciclastic rock samples, representative of all formations of the Belt-Purcell Supergroup, were collected from three locations: (1) Waterton-Glacier International Peace Park, Whitefish Range, and the Purcell Mountains, in northern Montana, southwestern Alberta, and southeastern British Columbia, respectively (Figs. 7.1 and 7.3). This sample suite includes areal extent and stratigraphic coverage of the formations. Due to the influence of loss-on-ignition (LOI) in the CIA calculations, only a subset of 54 argillites and sandstones with <4 wt.% LOI were considered for this study (Appendices 7.1a, b, and c). A similar dataset was used in a previous Chapter V to address trace element mobility during diagenesis (González-Álvarez and Kerrich, *submitted*). Only those elements used for evaluation of CIA and other criteria of weathering such as rare earth elements (REE), Sr, Rb, and Cs that pertain to Chapter V are reproduced in the Appendix 7.1a, b and c.

Major elements were determined using X-ray fluorescence spectrometry (XRF) at the Société Générale de Surveillance (SGS) Laboratories, Ontario, Canada. Precision is ±0.01 wt.%. Carbon dioxide content of selected samples was calculated following Tiessen et al. (1983). Trace elements, including rare earth elements (REE) and high field strength elements (HFSE), were analyzed using inductively coupled plasma-mass spectrometry (model Perkin Elmer Elan 5000) at the University of Saskatchewan. To address potential problems stemming from incomplete dissolution of refractory minerals, the procedure of Jenner et al. (1990) was followed, whereby a sodium peroxide sinter was used for analyses of Th, Nb, Ta, Zr, Hf, Y, Sc, and REE, and an HF-HNO_3 digestion on a separate aliquot was used for the remaining trace elements. Detailed analytical methodology is presented in Fan and Kerrich (1997). Included are standard additions, pure elemental standards for external calibration, and data for modern lake sediment samples representative of various locations within the Canadian Shield (LKSD-1), and basalt (BCR-2) as reference materials. LKSD-1 was used as a reference material, inasmuch as the REE and HFSE contents are comparable to those in the argillites analyzed. Long-term reproducibility in this lab for the low-level reference material basalt (BCR-1) is given in Table 5.1, abstracted from Xie et al. (1994).

Detection limits (in ppm) defined as 3Sigma of the calibration blank for some critical elements are as follows: Nb (0.016), Hf (0.042), Zr (0.103), La (0.018), Ce (0.014), Nd (0.086), and Sm (0.065). Wet chemistry operations were conducted under clean laboratory conditions. Analyses of acids, distilled deionized water and procedural blanks give levels of <1 ppb for REE, Nb, Zr, and Hf, relative to their concentration in the rocks (Xie et al., 1994).

Values of Ce/Ce* and Eu/Eu* were calculated relative to values for average post-Archean upper continental crust (PA-UCC) of Taylor and McLennan (1995), following Taylor and McLennan (1985).

Table 7.1 ICP-MS multi-element analysis of international reference material basalt BCR-1 for selected trace elements by the University of Saskatchewan ICP-MS laboratory (excerpted from Xie et al., 1994).

Elements	x	1σ	C%	CV
Zr	201	12	6	190
Nb	14.6	0.7	4.8	14
La	26	0.8	3.1	24.9
Pr	6.95	0.33	4.7	6.8
Eu	1.95	0.11	5.6	1.95
Ho	1.26	0.05	4	1.26
Tm	0.54	0.02	3.7	0.56
Lu	0.502	0.02	4	0.51
Hf	5.87	1.49	8.3	4.95
Ta	1.03	0.16	15.5	0.81
Th	6.7	0.52	7.8	5.98
U	1.75	0.1	5.7	1.75

(x) Average; (1σ) standard deviation; (C%) relative standard deviation; (CV) compiled values from Potts et al. (1992).

Electron microprobe energy dispersive spectrometry (EDS), and X-ray diffraction were used in this study to identify clay minerals. Analyses were conducted on a Jeol JXA-8600 Superprobe electron microprobe with three wavelength-dispersive spectrometers (WDS) at the University of Saskatchewan, Canada, to identify potential presence of smectites. Samples were also prepared for X-ray diffraction using a Rigaku R200 X-ray diffractometer with rotating Cu anode. Clay minerals were identified following Moore and Reynolds (1997) X-ray spectra. Details are given in Chapter III.

7.4 Analytical results

From field observations, petrographic analyses, and SiO2-LOI relationships, two facies are differentiated: sandstones (>75 wt.% SiO_2, <4 wt.% LOI); argillites (>75-50 wt.% SiO_2, <4 wt.% LOI; see *section 7.3*).

Argillites have an assemblage of smectite, illite-muscovite and/or chlorite, with quartz, plagioclase, and K-feldspar. Feldspars are pristine in many samples (Fig. 7d). Chlorite and illite are the most abundant matrix minerals (Fig. 7.4e and f).

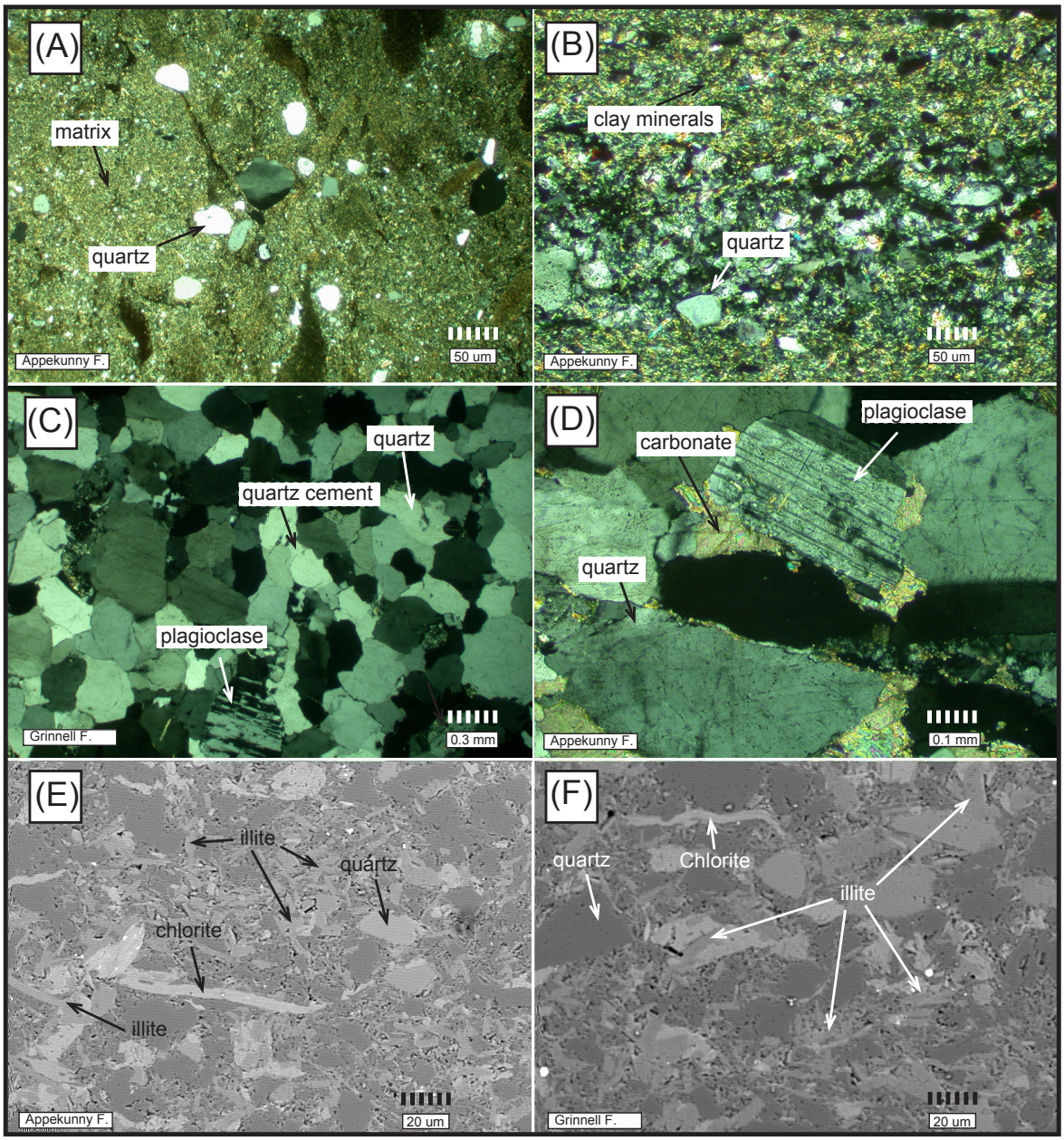

Fig. 7.4 Photomicrographs (crossed nichols and backscattered electron images) of argillites and sandstones. (A) and (B) are argillites displaying quartz grains and clay minerals as matrix; (C) sandstone showing angular and rounded quartz grains and feldspars; (D) Pristine plagioclase in sandstone; (E) and (F) backscattered images of argillites from the Appekunny and Grinnell formations illustrating illite and chlorite as the main clay mineral components of the matrix .

Normalized to PA-UCC (Taylor and McLennan, 1995), argillites are characterized by: (1) positive anomalies of Ce, Rb, K, Ti, and Cs; (2) average values for Al; and (3) deep negative Sr, Ca, and Na anomalies (Fig. 7.5a). The chemical index of alteration for argillites, corrected for the apatite and carbonate effects (Fedo et al., 1995), nominally ranges between 63 and 85 (Fig. 7.6a). Average Eu/Eu* is 0.88, and K/Cs ratios are <7600 (Fig. 7.7a and c).

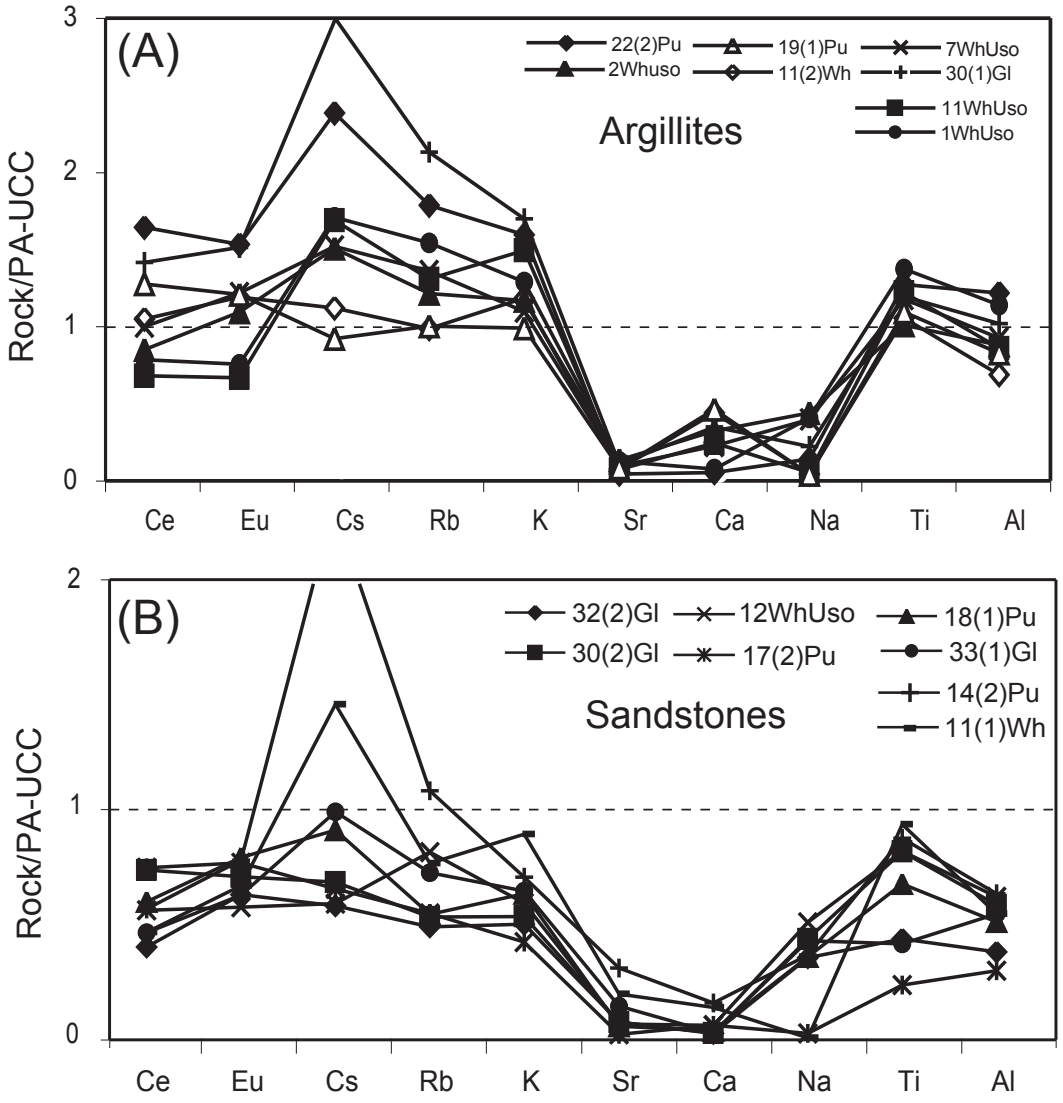

Fig. 7.5 Multi-element plots for representative argillites (A) and sandstones (B). Both reveal pronounced depletions in Ca, Na, and Sr. Both graphs are plotted on linear scales and normalized to post-Archean upper continental crust (PA-UCC) values from Taylor and McLennan (1995).

Sandstones consist of quartz, plagioclase, microcline, and chert fragments (Fig. 7.4c and d). Multi-element plots mimic argillite patterns with lower average normalized values, consistent with a dilution effect due to quartz (Figs. 7.5b and 7.7c). Chemical index of alteration, corrected for the CaO apatite effect and the CO_2 content due to carbonate, nominally ranges between 55 and 80 (Fig. 7.6b). Average Eu/Eu* normalized to PA-UCC is 0.89 (Fig. 6.7a). Pristine feldspars are found in sandstones and argillites (Fig. 7.4d).

7.5 Basinal brines

Any evaluation of weathering intensity based on CIA, REE, and other trace elements must first evaluate secondary mobility of these elements during diagenesis (cf. McDaniel et al., 1994). In the ca. 1700 Ma Athabasca Group of Saskatchewan and Alberta, Kyser and coworkers determined a ~600 Ma history of intermittent brine flow, involving mobility of U, heavy REE and Y (Fayek and Kyser, 1997; Kyser et al., 2000 and references therein). Therefore, trace element mobility during diagenesis can affect to the original signature of geochemical proxies used to approach weathering.

The Belt-Purcell Supergroup has experienced multiple stages of diagenesis (González-Álvarez et al., 2003; Kerrich and González-Álvarez, 2003). Many samples have REE and multi-element patterns comparable to PA-UCC, consistent with Paleoproterozoic source terranes, supported by detrital monazite chemical ages of ~1800-1600 Ma (González-Álvarez et al., *in press*; Chapter IV). Negative anomalies at Ca, Na, and Sr, normalized to PA-UCC, are coherent, consistent with a signature of weathering, and K normalized to PA-UCC is positive as in many other Precambrian siliciclastic sequences (e.g., Fedo et al., 1995) from diagenetic addition (Figs. 7.5a and 7.7c; see below).

Two populations of REE patterns are present in argillites and sandstones of the Belt-Purcell Supergroup when normalized to PA-UCC: the first, type 1, is a PA-UCC-like REE pattern at 0.2 to 1.5 PA-UCC depending on quartz (SiO_2) content, and the second, type 2, is enriched in heavy REE relative to light REE when normalized to PA-UCC. The first population is interpreted as a first approximation of the provenance geochemical signature. The second population is interpreted to record diagenetic brines that mobilized REE, U, Zr, Hf, and Y (González-Álvarez and Kerrich, *submitted*; Chapter V). Argillites and sandstones do not show correlations of Eu/Eu* and CIA with total light REE (∑LREE) or total heavy REE (∑HREE) contents for either population; accordingly it is concluded that brine activity did not influence Eu/Eu* neither CIA (Fig. 7.8).

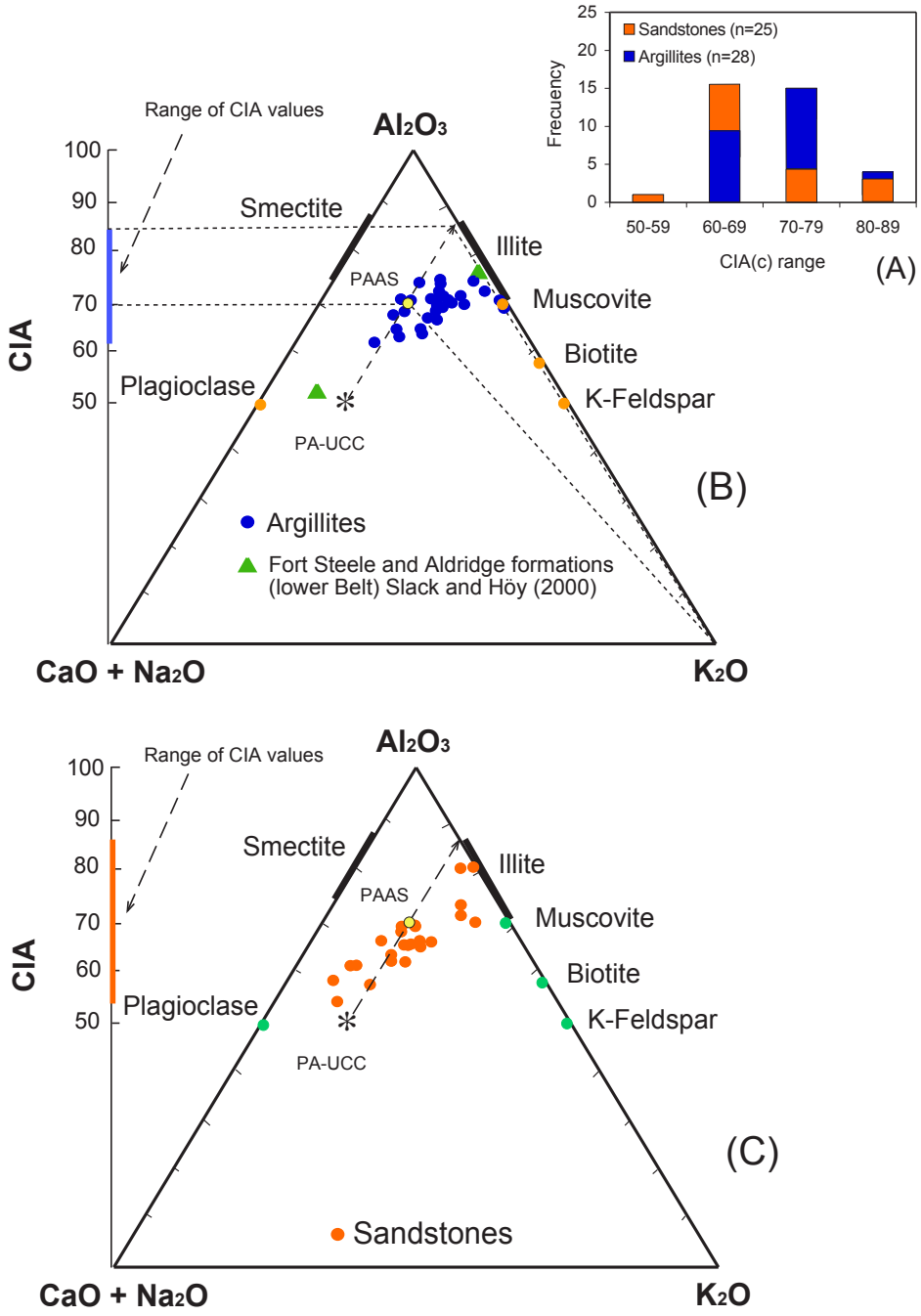

Fig. 7.6 (A) Histogram of CIA corrected values for argillites and sandstones showing a higher CIA value for the argillites group; (B) and (C) are triangular plots of the molecular proportions of Al_2O_3-CaO+Na_2O-K_2O for argillites and sandstones respectively. The data array lies to the right of the theoretical weathering line dashed from post-Archean upper continental crust (PA-UCC) parallel to the Al_2O_3-CaO+Na_2O join. One example of a corrected CIA is illustrated, projected from the K_2O apex and read off the CIA y-axis as explained in Fedo at al. (1995). Bold line on the y-axis shows range of CIA values. Locus or range of selected minerals from Lydon et al. (2000). In (B) maximum and minimum CIA values from Slack and Höy (2000) recalculated for K-addition.

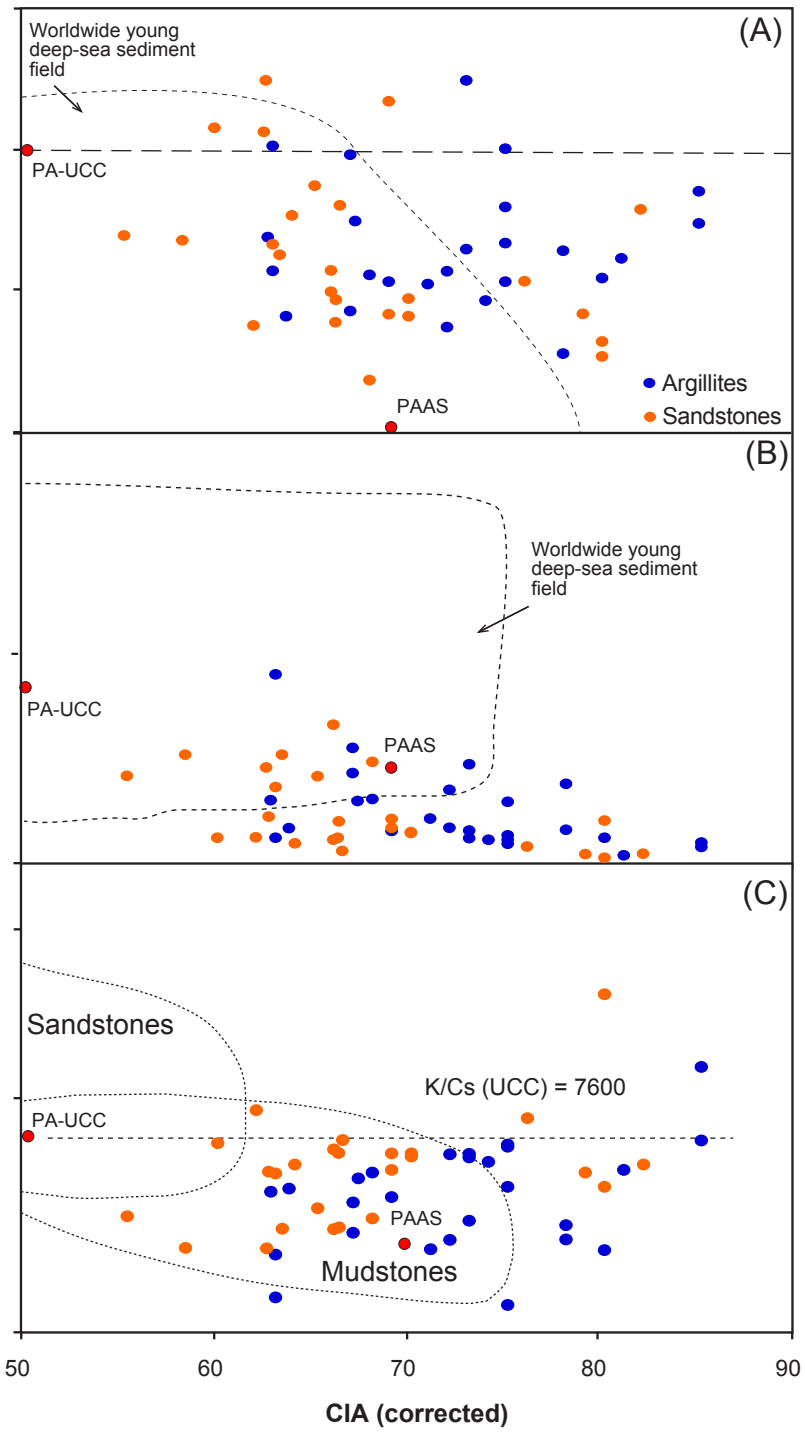

Fig. 7.7 Plots of Eu/Eu (A), Sr (B), and K/Cs (C) versus corrected CIA. In (A) and (B) the fields are for modern deep-sea sediments from Gao and Wedepohl (1995). In (C), the fields for sandstones and mudstones are from McLennan et al. (1990). The K/Cs reference line value of 7600 is for the post-Archean upper continental crust (Taylor and McLennan, 1995). Post-Archean American shale (PAAS) values from Tylor and McLennan (1985).*

7.6 Intensity of weathering in the source area

7.6.1 K-addition

An important factor to take into account when calculating CIA values is possible diagenetic addition of K into the rock/sediment. Post-depositional potassic alteration has been described previously as a widespread feature in many Precambrian siliciclastic sedimentary sequences and saprolith (Wronkiewicz and Condie, 1989; Rainbird et al., 1990; Maas and McCulloch, 1991; Condie, 1993; Fedo et al., 1995; McLennan et al., 2000; Bhat and Ghosh, 2001; Cullers and Podkovyrov, 2002). This diagenetic addition of K has been factored by Fedo et al. (1995) into a corrected CIA. In Al_2O_3-CaO+Na_2O-K_2O (A-CN-K) coordinate-space, unweathered rocks plot at CIA 50 on the plagioclase-K-feldspar join. Chemical weathering generates a trend from a point representing unweathered PA-UCC, parallel to the CN-A axis. Corrected CIA values are calculated by projecting from the K apex (100%) through data points to the weathering trend, then read off the CIA y-axis (Fig. 7.6; Fedo et al., 1995).

Content of K_2O for argillites is enriched by a factor of 1.12 on average, but up to 35% addition relative to PA-UCC (Fig. 7.5a; Appendix 7.1). Diagenetic potassic addition is supported by the illite-rich matrix in argillites. Secondary digenetic addition of K was also reported by Lydon et al. (2000) for the Aldridge Formation (lower Belt) in the Purcell Mountains of southern British Columbia, and interpreted as the result of the convection of formational water flow linked to heat flow associated with rifting. When CIA corrected values are plotted in the stratigraphic sequence, variations are more pronounced in the lower Belt and Ravalli Group at Whitefish Range and the Purcell Mountains. Carbonate-rich content of the lower Belt at Waterton-Glacier International Peace Park do not give reliable CIA values due to the interference between CaO content from feldspar and carbonate. The Missoula Group displays scattered CIA values; and the middle Belt, due to carbonate content cannot have viable calculated CIA (Fig. 7.3).

Given K enrichment due to diagenetic addition by basinal fluids, corrected values using the procedure of Fedo et al. (1995) range from 63 to 85, and 55 to 80 for argillites and sandstones respectively (Fig. 7.6). Most of the argillites CIA values are >67, with an average of 73, and for sandstones >65, with an average of 68. Minor pristine feldspars mixed with large amounts of clay size fraction could be accounted for by variable contributions from a proximal, relatively unweathered area (Fig. 7.4d). The addition of fresh feldspar would have the effect of reducing CIA values.

For comparison, PA-UCC and post-Archean Australian average shale (PAAS) have CIA values of 50 and 70, respectively. For the Aldridge and Fort Steele formations of the lower Belt, Slack and Höy (2000) reported low CIA values of 50 to 76 for 87 samples, concluding that weathering in the source areas was not intense. However, their CIA values were not corrected for diagenetic addition of K; their minimum and maximum values plotted in Figure 7.6b and corrected for K addition are calculated by the authors to 50 and 82 respectively (Fig. 7.6b).

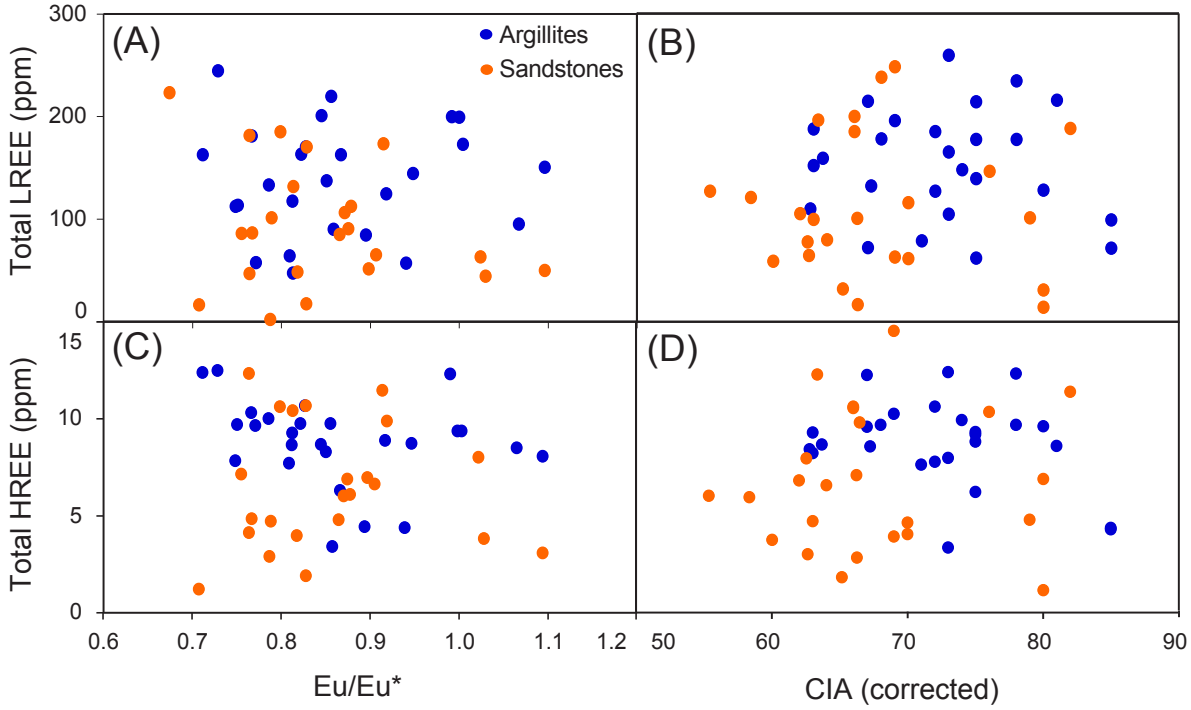

Fig. 7.8 Total LREE and total HREE plot versus CIA corrected and Eu/Eu. There is no correlation shown for diagenetic REE mobility.*

7.6.2 Eu/Eu and CIA correlation*

Negative correlations between CIA and Eu/Eu*, and Sr and Eu/Eu* are recorded worldwide in different tectonic settings associated with modern deep-sea sediments (Fig. 7.7a and b). Gao and Wedephol (1995) interpreted this feature to be the result of progressive weathering, involving transitions from plagioclase and (or) K-feldspar to mica and (or) kaolinite, and ferromagnesian silicates such as amphibole to chlorite and (or) smectite. They explained the covariation of decreasing Eu/E* with increasing CIA values as due to decreasing contributions of juvenile terranes but larger siliciclastic input from older recycled sediments from broader provenance. That Eu/Eu*-CIA co-

variation is exemplified by accretionary sediments of the Izu-Bonin arc through the Sea of Japan to the South Atlantic Ocean. This is based on the premise that juvenile crustal terranes from local sources are only weakly weathered due to short transport, whereas long transport or broad catchment areas with an important recycling component develop more Eu anomalies and hydrolysis of feldspar and ferromagnesian silicates.

7.6.3 Other trace and major element proxies

The Belt-Purcell argillites and sandstones with <4 wt.% LOI values display pronounced negative CaO, Na_2O, and Sr anomalies, as low as 0.1, relative to PA-UCC values, consistent with intense chemical weathering of the source terrane(s) (e.g., Maas and McCulloch, 1991; Bhat and Ghosh, 2001), but high Rb/Sr ratios relative to PA-UCC. These geochemical features have been reported in several Archean and Proterozoic metasedimentary sequences (e.g., Wronkiewiz and Condie, 1989; Maas and McCulloch, 1991; Bhat and Ghosh, 2001). The data are consistent with deeply weathered cratonic rocks, where Sr is lost in the weathered regolith, whereas Rb is retained in the clay fraction (Nesbitt et al., 1980; McLennan et al., 1983). Elevated Rb/Sr may also result from diagenetic addition of Rb with K.

Ratios of K/Cs in this database are mostly lower than the PA-UCC average value of 7600, consistent with an intensely weathered source where Cs is preferentially retained over K in the weathering profile (Fig. 7.7c; see McLennan et al., 1990). Fractionation of K/Cs may also stem from diagenetic introduction of K. There is no robust test for weathering versus diagenetic influence for the measured K/Cs values, or some combination; however, the simplest interpretation given the combination of covariant CIA versus Eu/Eu*, Sr, and K/Cs is in terms of weathering intensity. Like CIA values, K/Cs could be viewed as some combination of contemporaneous weathering intensity in the catchment and any proportion of recycled sedimentary rocks in the provenance from a previous weathering-sedimentation cycle. According to Veizer and Jansen (1979), post-Archean sediments are ~90 % cannibalistic (Veizer and McKenzie, 2004).

In summary: corrected CIA values; the conjunction of low absolute contents of Sr, Ca, and Na; high Rb/Sr, and K/Cs ratios, as well as covariations of CIA-Eu/Eu*, Sr-Eu/Eu*, and K/Cs-CIA, collectively suggest a dominantly intensely weathered provenance under hot, wet climate for argillites and sandstones of the Belt-Purcell Supergroup (Figs. 7.5 and 7.7).

The coexistence of clays from an intensely weathered source with pristine detrital feldspar

could be interpreted as the result of provenance areas with respectively high and low intensities of weathering lowering the total CIA average. This could be explained with the mixture of an extensive distal catchment characterized by intense weathering under wet tropical climate, and a small source proximal to the Belt-Purcell Basin with short-river transport under arid to semi-arid climate.

7.7 The drainage system

Other studies suggested that continental-scale river systems were developed in western Laurentia during the Proterozoic (Rainbird, 1992; Rainbird et al., 1992; Rainbird et al., 1997; Ross et al., 2001). For example, based on detrital zircons, the ca. ~1700 Ma Athabasca Basin initially received detritus from the proximal source ~1850 Ma Trans-Hudson Orogen to the east, but the upper two of four sequences had a catchment in the Yavapai, Mazatzal, and Central Plains provinces of the SW USA as distal sources (Rainbird et al., 2003). From detrital zicons ages Ross and Villenueve (2003) suggest that provenance areas for the Belt-Purcell Supergroup may have included Archean and Paleoproterozoic Laurentian sources to the east and south, and a western terrane for ages of ~1600-1500 Ma.

The sediment in the Belt-Purcell Basin could be transported by a large scale-river system draining mainly fine-grained sediment (Price, 1964; McMechan, 1981; Rainbird et al., 1997; Chandler 2000; Price and Sears, 2000; Ross and Villeneuve, 2003). The large volume of siliciclastic detritus of the Belt-Purcell sequence reflects fluvial transport from a low relief, continent scale catchment (Sears et al., 2004), and based on the palinspastic restored isopach map of the lower Belt presented by Price and Sears (2000), the fill entered the basin from the southwest forming a large delta.

Modern large-river systems, classified as tropical-wet rivers, that drain areas with intense weathering include the Mekong, Congo, Orinoco, Amazon, and Xijiang rivers. The geochemistry of their suspended sediment features large negative anomalies in Ca, Na, and Sr relative to PAUCC (Gaillardet et al., 1999). In addition, Maynard et al. (1991) in a study comparing the geochemistry of sand from modern rivers and the Archean Witwatersrand siliciclastic rocks, presents the CIA values of sands of tropical rivers including the Orinoco (75), Ganges (68), Mekong (56), and Amazon (55). These values are comparable with the range and average CIA of 73 and 66 for argillites and sandstones of the Belt-Purcell Supergroup respectively.

Accordingly, negative correlations between CIA and Eu/Eu*, Sr and Eu/Eu*, and pronounced depletions in Sr, Ca, and Na in the Belt-Purcell rocks could be interpreted as consistent with the results from previous studies that envision a major river system that drained a large catchment area, supplying a substantial amount of weathered sediments to the Belt-Purcell Basin (see *section 7.6*).

7.8 Proterozoic climate and geodynamics

Condie and coworkers have shown common time series for mantle plumes, CIA, black shales, percentage of shale to total sediments, and iron formations from ~2500 to 1700 Ma. (see Appendix in Condie et al., 2001; Condie, 2004). Condie et al. (2000) proposed that mantle plumes release large quantities of CO_2 through volcanic gases that intensified silicate weathering on the continents. Values of CIA span 67-88 in black shales at ~1900 Ma, albeit uncorrected for diagenetic K-addition (cf. Fedo et al., 1995) which correspond to possible superplume events (Isley and Abbott, 1999; Condie et al., 2001). Major perturbations in the atmosphere-hydrosphere-biosphere have also been linked by Kerr (1998) and Jahren (2002) to the Cretaceous superplume.

Windley (1995) argued that a Mesoproterozoic supercontinent assembled at ~1900-1800 Ma and then dispersed by ~1500 Ma due to plume impingement (Ernst and Buchan, 2002; Zhao et al., 2004). The Belt-Purcell Basin was part of a system of intracontinental rifts that developed ~1500 Ma associated with that dispersal, and the basal sections have tholeiitic gabbro sills compositionally consistent with intra-plate magmatism (Anderson and Goodfellow, 2000). New spreading systems developed as the continents separated, and together with possible mantle plumes involved of the break up of Columbia at~1500 Ma, may have raised sea-level by up to 450 m and increased levels of atmospheric CO_2 (cf. Eriksson et al., 2004).

Weathering intensity of the Belt-Purcell Supergroup catchment provides a test for perturbation of atmospheric CO_2 associated with the inferred ~1500 Ma coupled plume-rifting of the Mesoproterozoic supercontinent. Condie et al. (2001; Fig. 7.9) show a minor peak of CIA at ~1500 Ma. The average CIA of argillites is 73, extending to 85, compared to ~75 for shales associated with the ~1900 Ma superplume and 70 for PAAS. These results are consistent with moderate to intense chemical weathering for the catchment of the intracratonic rift Belt-Purcell Basin.

There are complexities in evaluating CIA values of Precambrian sedimentary rocks. Given the absence of land biota, Ramaekers and Catuneanu (2004) attributed the lack of fine-grained

shale facies in the ~1750-1500 Ma Athabasca Group to aeolian removal of fines from the provenance area. Argillites are the prevalent siliciclastic facies in the Belt-Purcell Supergroup, with interbedded sandstone units, rare shales, and two limestone units (e.g., Whipple et al., 1997) in the Belt-Purcell Supergroup. As proposed for the Athabasca Group, fines may have been removed as airborne dust, consequently influencing calculated CIA due to fines would include residual clays. Additionally, the time series of Condie and coworkers did not use CIA corrected for diagenetic K-addition (Condie et al., 2001).

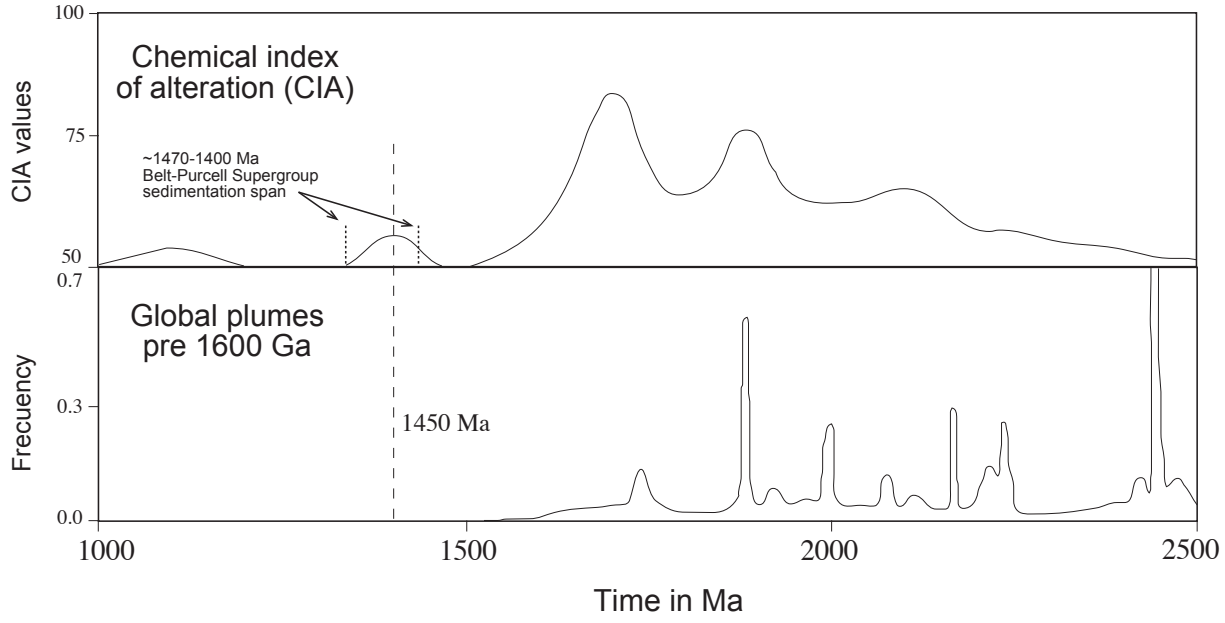

Fig. 7.9 Correlation graph of global plumes and CIA indexes versus time displaying the Belt-Purcell Supergroup span sedimentation and CIA index (Condie et al., 2000).

Condie et al. (1991) linked the total percentage of shale in the sedimentary sequences with plume activity. Release of gases due to magmatic activity enhanced by plumes would intensify chemical weathering by silicate hydrolysis and be commensurately responsible for larger shale volumes in the sedimentary record. The plume-shale time series peaks at ~1900 Ma, and has time correlating values of CIA that extend to 88, and shales as a percentage of total sedimentary sequences of ~36% (see Appendix in Condie et al., 2001). In the Belt-Purcell sequence at ~1470-1400 Ma, CIA extends to ~80 (this study), and total-shale thickness percentage is 40% (Condie et al., 2001 and references therein), suggesting that the Belt-Purcell Supergroup could be associated to the same weathering-plume relationship. However, this potential link between total shale and weathering can be affected by the type of basin; the percentage shale of distal passive margins would be greater than for intracontinental basins. Most paleomagnetic, paleoclimatic and sedimen-

tary data are consistent with deposition of the Belt-Purcell Supergroup sediments at low latitudes between 10° and 35° (Chandler, 2000). Alternatively, weathering alteration studies, coupled with petrographic observations of feldspars, hematitic clasts, and evaporites in the Belt-Purcell rocks, as well as geochemical studies, have been interpreted as a semi-arid to arid climate with intermittent wetter intervals (e.g., Harrison, 1972; White and Winston, 1982; Schieber, 1992; Slack and Höy, 2000; Lydon, 2000; Chandler, 2000 and references therein).

Values of Eu/Eu* from this study are consistent with REE data of Schieber (1990) who suggested that negative Eu anomalies in the Newland Formation, lower Belt, were related to changes in weathering intensity and tectonic activity in the catchment. Schieber (1992) combined petrographic and geochemical features and determined a CIA average value of 72 (not corrected for possible K-addtition) for the shales that was interpreted to indicate modest amounts of weathering and the sandstones in semi-arid conditions. In addition, data for the argillites of the Aldridge and the Fort Steele formations of southeastern British Columbia show depletions of CaO, Na_2O, and Sr relative to PA-UCC, in conjunction with K enrichment and calculated CIA of 50 to 76 (Slack and Höy, 2000). After K-addition correction calculated by the author for their maximum and minimum values, their CIA varies from 50 to 82 (Fig. 7.6b).

Other independent potential evidence for hot climate during deposition of the Belt-Purcell Supergroup is in halite casts, and abundant scapolite $\{(Na,Ca)_4[Al_3Si_9O_{24}]Cl\}$ (Schieber, 1997 and references therein). Evaporites are a potential sources of the inferred hypersaline basinal brines. Evaporites are present in many Proterozoic siliciclastc sequences spanning ~2100 to ~700 Ma (Table 7.2). However, there is no evidence of bedded evaporites in the Belt-Purcell sequence (Chandler, 2000). Halite casts are common in the carbonate–rich shallow water deposits of the Waterton and Altyn formations, lower Belt, and they are present as well in the Helena Formation, middle Belt, mainly in the east (McMechan, 1981; Chandler, 2000 and references therein; Pratt, 2001). In the Missoula Group, the Shepard and Gateway formations present traces of evaporites (McMechan, 1981). These evaporites, coupled with the presence of oolites and pristine feldspars preserved in the sediment, are indicative of arid to semi-arid climate. However, there is no evidence in the sedimentary record of the Belt-Purcell Supergroup of hot arid climate such as calcretes or eolian sand-seas (Chandler, 2000), nor correlation between evaporite proxies and low CIA values (this study, see Fig. 7.3). For example, the Mount Shields Formation at Whitefish Range presents salt casts and oolites (Whipple et al., 1984), and its lateral equivalent in the Purcell Mountains the Gateway Formation, interpreted as a lagoonal setting, preserves salt casts (McMechan, 1981), and their CIA corrected values are ~85 and ~80 respectively (Fig. 7.3).

There is lack for extensive evidence of continuous arid climate in the Belt-Purcell sequence. Based on that and the presence of mud-chip breccias with evidence of plasticity of the mud intraclasts, paucity of mud-cracks, and evidence of alluvial aprons and flood-plain deposits produced by abundant stream flow and sheet-flows (e.g., Winston, 1986, 1989, 1990), Chandler (2000) suggested that the climate was possibly arid with wetter intervals. Climatic fluctuations during the Belt-Purcell Supergroup deposition were interpreted as well by Winston (1986) and Winston and Lyons (1997) to explain terrigenous-to carbonate cycles in the middle Belt.

Table 7.2 Selected examples of Proterozoic sedimentary sequences with direct or indirect evidence of evaporites.

Sequence	Location	Age (Ma)	Reference
Yanshan Group	P. R. China	1730-850	Li et al. (2003)
Aravalli Supergroup	India	2150	Golani et al. (2002)
Vindhyan Supergroup	India	1600-700	Ray et al. (2003)
Ui Group	Russia	1600-650	Cullers and Podkovyrov (2002)
Wollaston Group	Canada	2100-1860	Tran et al. (2003)
Dhanjori Group	India	2100	Mazumder and Sarkar (2004)
Baker Lake Group	Canada	1800	Aspler et al. (2004)
Calcsilicate Suite	Australia	1700	Cook and Ashley (1992)
Liaohe Group	China	2400	Peng and Palmer (1995)
Chameis Group	Namibia	600	Frimmel and Jiang (2001)
Belt Supergroup	Canada and U.S.A.	1500-1400	Schieber (1997)
Shaler Supergroup	Canada	1000-750	Rainbird et al. (1996)
Bylot Supergroup	Canada	1200-1000	Jackson and Iannelli (1981)

Collectively, CIA values measured for the argillites and sandstones in the Belt-Purcell Supergroup are commensurable with moderate to intense weathered provenance whereas the depositional setting was arid. The latter conclusion is consistent with minor pristine feldspar, interpreted as low weathering intensity, in a juvenile source proximal to the depositional basin.

7.9 Conclusions

(1) Calculated CIA values in the Belt-Purcell Supergroup, corrected for diagenetic K-addition, span 55 to 85, with average values of 73 and 66 for argillites and sandstones respectively.

(2) CIA values in argillites are 63 to 85, averaging 73, *versus* 50 and 70 for PA-UCC and PAAS respectively. These data, in conjunction with low absolute contents of Sr, Ca, and Na, together with high Rb/Sr and K/Cs ratios, and covariations of CIA-Eu/Eu*, Sr-Eu/Eu*, and K/Cs-CIA collectively are commensurate with a moderate to intensely weathered provenance. Such geochemical relationships and CIA values are in keeping with large, modern, river systems including the Ganges, Mekong or Amazon rivers.

(3) Argillites and sandstones from Waterton-Glacier International Peace Park, the Purcell Mountains, and Whitefish Range display Eu/Eu*-CIA relationships consistent with a major river system that drained a large-scale catchment area, as previously suggested by other studies, and can be interpreted as indicative of a long distance transport and/or significant recycled sedimentary component in the provenance.

(4) The presence of pristine feldspars is likely from a small, juvenile, source proximal to the Belt-Purcell Basin with low weathering and short-river transport; that proximal contribution lowers the average CIA. Geological evidence for evaporites in the Belt sequence confers independent evidence for an arid depositional setting.

(5) Moderate to intense weathering of the provenance may be associated with elevated levels of atmospheric CO_2 degassed from volcanoes associated with the mantle plume implicated in rifting of the supercontinent Columbia, and oceanic spreading centres as intracontinental rifts, including the Belt-Purcell Basin, evolved into ocean basins.

7.10 Acknowledgements

The staff of Waterton-Glacier International Peace Park is thanked for their enduring support, most especially L. F. Marnell and C. Smith; as well as Q. Xie and J. Fan who assisted with ICP-MS analyses; L. M. Shychosky, A. Vangool, M. England, R. Ahrabian, A. Peterhänsel and L. Skublicki for their dedicated help during fieldwork; T. Prokopiuk, R. Renaut, L. Batuois, and M. A. Kusiak for their incisive comments on the Chapter; and Paul Ramaekers for many insights on Proterozoic sedimentation. Natural Sciences & Environment Research Council of Canada (NSERC) discovery grants to R. Kerrich and B. R. Pratt, and a University of Saskatchewan graduate scholarship to I. González-Álvarez, funded this study. R. Kerrich acknowledges NSERC MFA support of the ICP-MS facility, and the George McLeod endowment to the Department of Geological Sciences, University of Saskatchewan.

7.11 Appendix

Appendix 7.1a Major and trace element concentration of the Belt-Purcell Supergroup at Waterton-Glacier International Peace Park.

Formation	Libby	Libby	Libby	McNamara	McNamara	Bonner	Bonner	Bonner	Shepard	Shepard	Snowslip	Grinnell
Sample	35(2)G1	35(1)G1	35G1USO	34(1)G1	34G1USO	33(2)G1	33(1)G1	33G1USO	31G1USO	31(1)G1	30(2)G1	USO 24
SiO_2 (wt%)	78.7	70.7	62.0	66.0	70.6	88.9	82.6	80.7	76.3	62.4	79.0	65.00
TiO_2	0.28	0.37	0.72	0.57	0.50	0.22	0.21	0.31	0.47	0.60	0.41	0.609
Al_2O_3	7.82	12.29	19.00	15.01	13.00	5.83	8.35	9.73	9.68	14.57	8.96	13.70
Fe_2O_3	5.81	8.42	6.70	5.33	2.81	0.69	1.88	1.79	4.11	8.70	3.94	7.23
MnO	0.05	0.05	0.06	0.04	0.03	0.00	0.00	0.00	0.02	0.03	0.02	0.04
MgO	1.41	2.06	2.03	3.77	2.91	0.70	1.25	1.26	2.57	5.37	2.26	4.02
CaO	1.23	0.12	0.20	0.43	1.38	0.12	0.13	0.32	0.58	0.19	0.13	0.73
K_2O	1.35	2.24	4.57	4.07	3.88	1.70	2.19	2.98	2.83	3.33	1.81	3.80
Na_2O	1.17	1.21	1.48	1.71	1.61	1.22	1.47	1.36	1.21	1.02	1.50	1.13
P_2O_5	0.02	0.05	0.05	0.11	0.09	0.01	0.02	0.15	0.09	0.09	0.04	0.19
LOI (CO_2)	2.30 (1.02)	2.55 (u.d.)	2.85 (u.d.)	3.00 (u.d.)	3.25 (1.01)	0.65 (u.d.)	1.30 (u.d.)	1.50 (u.d.)	2.30 (0.84)	3.85 (u.d.)	1.85 (u.d.)	3.55 (1.36)
Sum	100.2	100.1	99.7	100.2	100.3	100.1	99.6	100.2	100.2	100.3	100.1	100.00
Rb (ppm)	71	92	227	176	132	55	82	102	94	128	60	140
Sr	33	30	83	73	39	27	52	25	34	27	27	48
Cs	1.96	2.95	14.86	6.91	5.47	2.17	3.68	4.03	3.99	4.72	2.54	9.5
Ce	56.70	88.11	88.75	86.19	93.80	25.97	29.92	88.75	26.73	78.86	47.46	72.41
Sm	4.55	6.73	7.87	7.39	8.60	2.48	2.58	7.87	2.76	6.22	3.79	7.31
Eu	0.738	1.161	1.368	1.279	1.376	0.557	0.555	1.370	0.460	1.353	0.626	1.33
Gd	4.05	5.62	7.33	6.91	7.90	2.49	2.10	7.33	2.77	5.18	3.82	6.810
Eu/Eu*	0.8	0.9	0.8	0.8	0.8	1.0	1.1	0.8	0.8	1.1	0.8	0.87
CIA	70	73	71	66	65	59	62	63	66	73	66	69
CIA (c)	70	75	72	68	69	60	63	66	70	73	66	72
Facies	Sd.	Arg.	Arg.	Arg.	Sd.	Sd.	Sd.	Sd.	Sd.	Arg.	Sd.	Arg.
Labels Fig. 7.3	G70	G69	G68	G67	G65	G64	G63	G62	G58	G56	G54	G34

Sample order is from the upper sequence (left) to the lower sequence (right). (Arg.) Argillite; and (Sd.) sa
[CIA(c)] Corrected CIA, (u.d.) Under detection limit.

Appendix 7.1b Major and trace element concentration of the Belt-Purcell Supergroup at the Purcell Mountains.

Formation	Roosville	Phillips	Phillips	Phillips	Gateway	Van Cr.	Van Cr.	Kitchener	Creston	Creston	Creston	Creston	Creston	Aldridge	Aldridge	Aldridge	Fort Steel
Sample	22(2)PU	21(2)PU	21(1)Pu	21PuUSO	19(2)PU	18PuUSO	18(2)Pu	17(1)Pu	16(5)PU	16(4)PU	16(3)PU	16(2)PU	16(1)PU	14(1)Pu	14PuUSO	14(2)Pu	FT(3)PU
SiO_2 (wt%)	66.2	71.9	61.0	78.9	71.4	68.8	83.0	89.0	75.5	70.9	73.0	77.7	75.7	65.1	83.7	79.2	90.1
TiO_2	0.63	0.40	0.85	0.46	0.58	0.72	0.34	0.12	0.47	0.58	0.50	0.43	0.40	0.57	0.39	0.44	0.14
Al_2O_3	18.27	11.91	18.82	9.88	16.17	15.30	7.81	4.60	12.39	14.98	13.32	11.72	10.78	15.43	8.48	9.68	4.42
Fe_2O_3	3.77	2.98	6.79	2.95	1.59	4.62	2.75	1.88	2.78	4.13	4.23	3.12	4.46	8.71	2.13	3.26	1.65
MnO	0.00	0.01	0.01	0.00	0.00	0.01	0.09	0.02	0.02	0.04	0.05	0.01	0.00	0.06	0.02	0.04	0.00
MgO	1.84	1.34	2.01	1.18	1.69	2.06	1.04	1.50	1.85	1.49	1.21	0.67	3.33	2.23	0.78	1.08	1.66
CaO	0.13	2.70	0.16	0.44	0.19	0.22	0.17	0.27	0.19	0.22	0.39	0.02	0.07	0.18	0.14	0.68	0.05
K_2O	5.34	3.52	6.08	2.51	5.45	4.48	2.15	1.44	2.85	3.89	2.47	3.39	2.59	3.40	1.98	2.39	0.96
Na_2O	0.45	1.66	1.18	2.04	0.27	1.23	1.23	0.10	1.89	1.10	2.44	0.76	0.10	1.08	1.21	1.26	0.07
P_2O_5	0.06	1.83	0.10	0.03	0.09	0.08	0.06	0.04	0.12	0.05	0.04	0.03	0.04	0.12	0.03	0.04	0.00
LOI	3.30	1.85	3.00	1.75	2.60	2.60	1.40	1.20	1.95	2.55	2.30	2.15	2.75	3.15	1.15	1.80	1.15
(CO_2)	(u.d.)	(u.d.)	(u.d.)	(0.72)	(u.d.)	(0.44)	(u.d.)	(0.88)	(u.d.)	(u.d.)	(0.64)	(u.d.)	(u.d.)	(u.d.)	(u.d.)	(u.d.)	(u.d.)
Sum	100.1	100.2	100.2	100.2	100.2	100.2	100.1	100.2	100.1	100.2	100.1	100.1	100.3	100.2	100.1	100.0	100.2
Rb (ppm)	199	139	254	72	186	128	61	62	124	187	120	149	112	173	94	122	21
Sr	7	50	21	87	28	25	21	9	12	48	116	17	9	69	47	110	4
Cs	8.81	5.82	7.86	4.29	5.04	8.71	3.38	2.44	3.53	7.56	6.53	3.39	4.07	20.77	5.72	8.45	0.29
Ce	104.41	48.79	104.95	44.00	61.01	62.00	38.52	48.09	152.68	128.03	117.25	72.24	92.20	32.09	5.00	36.54	14.12
Sm	8.35	11.26	7.79	4.08	4.50	5.68	3.28	4.04	12.67	10.61	10.20	5.80	7.88	2.67	0.69	3.22	0.96
Eu	1.340	2.960	1.540	0.730	0.730	1.090	0.700	0.680	2.060	1.560	1.530	1.060	1.540	0.560	0.120	0.690	0.140
Gd	6.35	14.44	6.43	3.68	4.43	5.24	3.84	4.10	8.35	9.11	10.64	6.18	7.59	3.75	0.71	2.98	0.86
Eu/Eu*	0.8	1.1	1.0	0.9	0.8	0.9	0.9	0.8	0.9	0.7	0.7	0.8	0.9	0.8	0.8	1.0	0.7
CIA	73	63	60	62	71	69	63	73	66	70	67	70	78	74	66	62	78
CIA (c)	81	63	75	63	80	74	64	79	66	73	68	76	82	75	66	62	80
Facies	Arg.	Arg.	Arg.	Sd.	Arg.	Arg.	Sd.	Sd.	Sd.	Arg.	Arg.	Sd.	Sd.	Arg.	Sd.	Sd.	Sd.
Labels Fig. 7.3	P26	P24	P23	P22	P21	P18	P17	P14	P10	P11	P12	P9	P8	P6	P5	P4	P3

Sample order is from the upper sequence (left) to the lower sequence (right). (Arg.) Argillite; and (Sd.) sandstone. [CIA(c)] Corrected CIA. (u.d.) Under detection limit.

Appendix 7.1c Major and trace element concentration of the Belt-Purcell Supergroup at Whitefish Range.

Formation	Mount Sh.	Mount Sh.	Shepard	Snowslip	Snowslip	Wallace	Empire	Spokane	Spokane	Spokane	Burke	Burke	Burke	Burke	Burke	Burke	Burke	Burke	Burke	Pric.-Burke	Prichard	Prichard	Prichard
Sample	11WhUSO	11(1)Wh	10WhUSO	8(2)Wh	8 Wh USO	7 Wh USO	5(1)Wh	4(2)Wh	4(1)Wh	4WhUSO	3(8)Wh	3(7)Wh	3(6)Wh	3(5)Wh	3(4)Wh	3(3)Wh	3(2)Wh	3(1)Wh	3WhUSO	2WhUSO	1(2)Wh	1(1)Wh	1WhUSO
SiO_2 (wt%)	68.1	78.9	75.3	80.1	74.4	68.3	79.9	95.9	63.3	84.8	77.8	76.9	71.7	63.9	83.6	75.8	63.1	67.0	71.3	70.6	61.8	70.3	65.9
TiO_2	0.60	0.47	0.41	0.51	0.67	0.58	0.35	0.07	0.64	0.22	0.39	0.40	0.65	0.70	0.29	0.41	0.82	0.56	0.62	0.50	0.64	0.59	0.68
Al_2O_3	12.80	8.35	7.27	10.15	12.60	13.80	8.95	1.84	17.68	5.58	11.56	11.43	14.75	18.17	8.74	12.17	18.99	15.77	14.20	13.10	18.55	14.98	17.10
Fe_2O_3	4.37	3.19	4.66	2.62	3.79	3.93	2.09	0.65	6.01	2.01	2.49	3.72	3.84	4.80	1.47	3.41	4.98	4.97	4.36	2.76	5.28	5.07	5.52
MnO	0.00	0.01	0.01	0.02	0.03	0.01	0.03	0.01	0.03	0.17	0.07	0.08	0.05	0.16	0.03	0.05	0.07	0.07	0.06	0.03	0.07	0.05	0.03
MgO	4.09	2.77	3.94	1.11	1.76	4.32	0.84	0.38	2.64	1.52	0.93	1.17	0.96	2.35	0.36	0.84	1.12	3.47	1.49	2.89	2.14	1.53	1.76
CaO	0.93	0.60	2.01	0.18	0.09	0.86	1.77	0.09	0.21	1.24	0.86	1.06	1.00	0.57	0.66	0.99	0.86	1.03	0.78	1.27	1.41	0.24	0.22
K_2O	5.00	3.02	3.06	1.86	2.58	3.65	1.85	0.39	5.23	1.43	2.99	1.80	3.28	5.12	1.26	2.90	5.31	3.57	3.49	3.89	3.66	3.55	4.30
Na_2O	0.11	0.03	0.07	2.22	1.99	1.45	2.11	0.30	1.06	0.59	1.37	2.62	1.95	1.25	2.73	1.97	2.14	1.48	2.13	1.62	3.31	1.41	1.49
P_2O_5	0.12	0.13	0.11	0.05	0.04	0.07	0.05	0.04	0.14	0.05	0.04	0.01	0.07	0.05	0.00	0.10	0.02	0.11	0.03	0.09	0.05	0.06	0.07
LOI (CO_2)	3.80 (1.12)	2.30 (0.44)	3.30 (1.76)	1.45 (u.d.)	2.10 (u.d.)	3.05 (0.64)	2.10 (1.28)	0.35 (u.d.)	3.00 (u.d.)	2.40 (1.24)	1.50 (0.52)	0.90 (u.d.)	1.65 (u.d.)	2.95 (u.d.)	0.90 (u.d.)	1.35 (0.96)	2.50 (u.d.)	2.10 (u.d.)	1.55 (u.d.)	3.25 (0.88)	2.05 (u.d.)	2.20 (u.d.)	2.90 (u.d.)
Sum	100.1	100.2	100.3	100.4	100.2	100.2	100.2	100.1	100.1	100.1	100.2	100.2	100.1	100.2	100.2	100.2	100.1	100.3	100.2	100.2	99.1	100.1	100.1
Rb (ppm)	145	86	48	78	107	151	72	27	235	67	140	95	127	242	58	138	232	152	171	134	236	174	171
Sr	17	70	22	39	36	25	71	28	37	27	113	125	99	90	100	160	132	103	125	39	218	50	36
Cs	6.21	5.41	1.87	3.69	5.55	5.58	3.78	1.46	16.95	5.14	8.08	6.33	7.84	14.44	3.26	8.51	12.05	10.83	10.22	5.53	20.75	12.63	6.28
Ce	42.49	30.01	32.12	93.68	49.42	63.00	50.84	12.00	115.12	29.63	122.70	61.34	78.35	87.12	58.88	101.28	107.40	31.54	69.60	53.24	91.60	36.27	49.05
Sm	3.16	3.06	2.60	9.39	5.98	6.85	4.70	1.54	8.59	2.68	10.93	4.43	6.74	8.07	5.14	8.08	8.59	3.98	6.33	6.00	6.92	2.91	3.98
Eu	0.570	0.592	0.510	1.520	1.030	1.060	0.878	0.290	1.429	0.480	1.274	0.801	1.259	1.229	0.968	1.359	1.772	0.679	1.090	0.950	1.450	0.502	0.650
Gd	2.71	2.99	2.39	8.89	5.67	5.60	4.52	1.68	6.84	2.71	9.98	4.03	5.53	7.80	4.99	7.56	7.85	4.11	5.47	5.66	6.36	2.80	3.04
Eu/Eu*	0.9	0.9	0.9	0.8	0.8	0.8	0.9	0.8	0.9	0.8	0.6	0.9	0.9	0.7	0.9	0.8	1.0	0.8	0.9	0.7	1.0	0.8	0.9
CIA	70	72	68	63	67	69	62	65	70	69	68	58	64	68	55	66	64	67	62	66	61	70	70
CIA (c)	85	80	85	63	67	74	62	65	78	69	69	58	64	78	55	66	67	67	63	72	63	71	73
Facies	Arg.	Sd.	Arg.	Sd.	Arg.	Arg.	Sd.	Sd.	Arg.	Sd.	Sd.	Sd.	Arg.	Arg.	Sd.	Sd.	Arg.	Arg.	Arg.	Arg.	Arg.	Arg.	Arg.
Labels Fig. 7.3	W28	W27	W26	W25	W24	W23	W17	W16	W15	W14	W13	W12	W11	W10	W9	W8	W7	W6	W5	W4	W3	W2	W1

Sample order is from the upper sequence (left) to the lower sequence (right). (Arg.) Argillite; and (Sd.) sandstone. [CIA(c)] Corrected CIA.

7.12 References

Anderson, H.E., Davis, W.D., 1995. U-Pb geochronology of the Moyie sills, Purcell Supergroup, southeastern British Columbia: implications for the Mesoproterozoic geological history of the Purcell (Belt) basin. Can. J. Earth Sci. 32, 1180-1193.

Anderson, H.E., Goodfellow, W.D., 2000. Geochemistry and isotope chemistry of the Moyie sills: implications for the early tectonic setting of the Mesoproterozoic Purcell basin. In: Lydon, J.W., Höy, T., Slack, J.F., Knapp, M.E., (eds.), The Geological Environment of the Sullivan Deposit, British Columbia. Geol. Assoc. Can. Min. Dep. Div. Spec. Publ. 1, pp. 302-321.

Aspler, L.B., Chiarenzelli, J.R., Cousens, B.L., 2004. Fluvial, lacustrine and volcanic sedimentation in the Angikuni sub-basin, and initiation of ~1.84-1.79 Ga Baker Lake basin, western Churchill Province, Nunavut, Canada. Precambrian Res. 129, 225-250.

Bhat, M.I., Ghosh, S.K., 2001. Geochemistry of the 2.51 Ga old Rampur Group pelites, western Himalayas: implications for their provenance and weathering. Precambrian Res. 108, 1-16.

Chandler, F.W., 2000. The Belt-Purcell Basin as a low-latitude passive rift: implications for the geological environment of Sullivan type deposits. In: Lydon, J.W., Höy, T., Slack, J.F., Knapp, M.E., (eds.), The Geological Environment of the Sullivan Deposit, British Columbia. Geol. Assoc. Can. Min. Dep. Div. Spec. Publ. 1, pp. 82-112.

Condie, K.C., 1993. Chemical composition and evolution of the upper continental crust: contrasting results from surface samples and shales. Chem. Geol. 104, 1-37.

Condie, K.C., 2004. Precambrian superplumes events. In: Eriksson, P.G., Altermann, W., Nelson, D.R., Mueller, W.U., Catuneanu, O., (eds.), The Precambrian: Tempos and Events, Developments in Precambrian Geology 12, Elsevier, Amsterdam, pp. 163-172.

Condie, K.C., Des Marais, D.J., Abbott, D., 2000. Geologic evidence for a mantle superplume event at 1.9 Ga. Geochem. Geophy. Geosys. 1, 2000GC000095.

Condie, K.C., Des Marais, D.J., Abbott, D., 2001. Precambrian superplumes and supercontinents: a record in black shales, carbon isotopes, and paleoclimates? Precambrian Res. 106, 239-260.

Connor, J.J., Reynolds, M.W., Whipple, J.W., 1984. Stratigraphy of the Ravalli Group, Belt basin, Montana and Idaho. In: Hobbs, S.W., (ed.), The Belt Abstracts with Summaries, Belt Symposium II, Montana Bur. Min. Geol., Spec. Publ. 90, pp. 13-15.

Cook, N.D.J., Ashley, P. M., 1992. Metaeveporite sequence, exhalative chemical sediments and associate rocks in the Proterozoic Willyama Supergroup, south Australia: implications for metallogenesis. Precambrian Res. 56, 211-226.

Cullers, R.L., Podkovyrov, V.N., 2002. The source and origin of terrigenous sedimentary rocks in the Mesoproterozoic Ui group, southeastern Russia. Precambrian Res. 117, 157-183.

Duddy, I. R., 1980. Redistribution and fractionation of rare-earth and other elements in a weathering profile. Chem. Geol. 30, 363-381.

Eriksson, P.G., Catuneanu, O., Nelson, D.R., Mueller, W.U., Alterman, W., 2004. Towards a synthesis. In: Eriksson, P.G., Altermann, W., Nelson, D.R., Mueller, W.U., Catuneanu, O., (eds.), The Precambrian: Tempos and Events, Developments in Precambrian Geology 12, Elsevier, Amsterdam, pp. 705-723.

Ernst, R.E., Buchan, K.L., 2002. Maximum size and distribution in time and space of mantle plumes: evidence from large igneous provinces. J. Geodynamics 34, 711-714.

Evans, K.V., Aleinikoff, J.N., Obradovich, J.D., Fanning, C.M., 2000. SHRIMP U-Pb geochronology of volcanic rocks, Belt Supergroup, western Montana: evidence for rapid deposition of sedimentary strata. Can. J. Earth Sci. 37, 1287-1300.

Fan, J., Kerrich, R., 1997. Geochemical characteristics of aluminum depleted and undepleted komatiites and HREE-enriched low-Ti tholeiites, western Abitibi greenstone belt: a heterogeneous mantle plume-convergent margin environment. Geochim. Cosmochim. Acta 61, 4723-4744.

Fayek M., Kyser T.K., 1997. Characterization of multiple fluid-flow events and rare earth-element mobility associated with formation of unconformity-type uranium deposits in the Athabasca Basin, Saskatchewan. Can. Mineral. 35, 627-658.

Fedo, C.M., Nesbitt, H.W., Young, G.M., 1995. Unraveling the effects of potassium metasomatism in sedimentary rocks and paleosols, with implications for paleoweathering conditions and provenance. Geology 23, 921-924.

Folk, R.L., 1968. Petrology of sedimentary rocks. Hemphill's, Austin, U.S.A.

Frimmel, H.E., Jian, S.Y., 2001. Marine evaporites from an oceanic island in the Neoproterozoic Adamastor Ocean. Precambrian Res. 105, 57-71.

Gaillardet, J., Dupré, B., Allègre, C.J, 1999. Geochemistry of large river suspended sediments: silicate weathering or recycling tracer? Geochim. Cosmochim. 63, 4037-4051.

Gao, S., Wedepohl, K.H., 1995. The negative Eu anomaly in Archean sedimentary rocks: implications for decomposition, age and importance of their granitic sources. Earth Planet. Sci. Lett. 133, 81-94.

Godard, E.N.J., 1997. Sediment dispersal pathways in quartzite units of the lower Prichard Formation Pine Creek drainage, Idaho. In: Link, P. K., (ed.), Geologic Guidebook to the Belt-Purcell Supergroup, Glacier National Park and Vicinity, Montana and Adjacent Canada, Field Trip Guidebook for the Belt Symposium III, Belt Association, Pocatello, Idaho, pp. 44-55.

Golani, P.R., Pandit, M.K., Sial, A.N., Fallick, A.E., Ferreira, V.P., Roy, A.B., 2002. B-Na rich Palaeoproterozoic Aravalli metasediments of evaporitic association, NW India: a new repository of gold mineralization. Precambrian Res. 116, 183-198.

González-Álvarez, I., Kerrich, R., *submitted*. Basinal brines and REE mobility in the Belt-Purcell Supergroup, Western North America. G^3.

González-Álvarez, I., Kusiak, M.A., Kerrich, R., *in press*. A trace element and Chemical Th-U total Pb dating study in the lower Belt-Purcell Supergroup, western North America: provenance and diagenetic implications. Chem. Geol.

González-Álvarez, I.J., Kerrich, R., Pratt, B.R., 2003. Geochimistry of the Appekunny and the Grinnell formations: Mesoproterozoic siliciclastic rocks of the Belt-Purcell Supergroup, western USA and Canada. IAS 22nd International Meeting of Sedimentologists, Abstracts book, 68.

Harrison, J.E., 1972. Precambrian Belt Basin of northwestern United States: its geometry, sedimentation, and copper occurrences. Geol. Soc. Am. Bull. 83, 1215-1240.

Hoffman, P.F., 1999. "Snowball earth" theory still stands. Nature 400, 708.

Holland, H.D., 1978. The chemistry of the atmosphere and oceans. Wiley & Sons, New York, U.S.A.

Isley A.E., Abbott D.H., 1999. Plume-related mafic volcanism and the deposition of banded iron formation. J. Geophy. Res. Solid Earth 104, 15461-15477.

Jackson, G.D., and Iannelli, T.R. 1981. Rift-related cyclic sedimentation in the Neohelikian Borden Basin, northern Baffin Island. In: Campbell, F.H.A., (ed.), Proterozoic Basins of Canada. Geol. Surv. Canada Spec. Paper 81, pp. 269–302.

Jahren, A.H., 2002. The geochemical consequences of the mid-Cretaceous superplume. J. Geodynamics 34, 177-197.

Jenner, G.A, Longerich, H.P., Jackson, S.E., Fryer, B.J., 1990. ICP-MS a powerful tool for high precision trace-element analysis in earth sciences: evidence from analysis of selected USGS reference samples, Chem. Geol. 83, 133-148.

Kerrich, R. and González-Álvarez, I.J., 2003. Basinal fluid evolution in the Appekunny-Grinnell Formation, 1.4 Ga Belt Supergroup. Geol. Soc. Am. Ann. Meeting, Programs with Abstracts, 243-3.

Kerr, A.C., 1998. Oceanic plateau formation: a cause of mass extinction and black shale deposition around the Cenomanian-Turonian boundary? J. Geol. Soc. 115, 619-626.

Kleinkopf, M.D., 1997. Interpretation of regional aeromagnetic and gravity anomalies Belt-Purcell terrane and adjacent areas, northern Rocky Mountains United States and Canada. Belt Symposium III. In: Berg, R.B., (ed.), Belt Symposium III, Montana Bureau Min. Geol. Spec. Publ. 112, pp. 210-221.

Krauskopf, K.B., 1982. Introduction to geochemistry. McGraw-Hill, Singapore.

Kyser, K., Hiatt, E., Renac, C., Durocher, K., Holk, G., Deckart, K., 2000. Diagenetic fluids in Paleo- and Mesoproterozoic sedimentary basins and their implications for long protected fluid histories. In: Kyser, K., (ed.), Fluids and Basin Evolution, Min. Assoc. Can., Short Course Series, Kingston, Ontario, 28, pp. 225-262.

Li, C., Peng, P., Sheng, G., Fu, J., Yan, Y., 2003. A molecular an isotopic study of Meso- to Neoproterozoic 1.73-0.85 Ga sediments from the Jixian section, Yanshan Basin, North China. Precambrian Res. 125, 337-356.

Link, P.K., 1997. The Grinnell, Empire and Helena formations along Baring Creek and at Siyeh Pass, Glacier National Park. In: Link, P.K., (ed.), Geologic Guidebook to the Belt-Purcell Supergroup, Glacier National Park and Vicinity, Montana and Adjacent Canada, Field Trip Guidebook for the Belt Symposium III, Belt Association, Pocatello, Idaho, U.S.A., pp. 113-124.

Lydon, J.W., 2000. A synopsis of the understanding of the geological environment of the Sullivan Deposit. In: Lydon, J.W., Höy, T., Slack, J.F., Knapp, M.E., (eds.), The Geological Environment of the Sullivan Deposit, British Columbia. Geol. Assoc. Can. Min. Dep. Div. Spec. Publ. 1, pp. 12-31.

Lydon, J.W., Walker, R., Anderson, H.E., 2000. Lithogeochemistry of the Aldridge Formation and the chemical effects of burial diagenesis. In: Lydon, J.W., Höy, T., Slack, J.F., Knapp, M.E., (eds.), The Geological Environment of the Sullivan Deposit, British Columbia. Geol. Assoc. Can. Min. Dep. Div. Spec. Publ. 1, pp. 137-179.

Maas, R., McCulloch, M.T., 1991. The provenance of Archean clastic metasediments in the Narryer gneiss complex, western Australia: trace element geochemistry, Nd isotopes, and U-Pb ages for detrital zircons: Geochim. Cosmochim. Acta 55, 1915-1932.

Marsh, J., 1991. REE fractionation and Ce anomalies in weathered Karoo dolerite, Chem. Geol. 90, 189-194.

Maxwell, D.T., Hower, J., 1967. High-grade diagenesis and low-grade metamorphism of illite in the Precambrian Belt series. Am. Min. 52, 843-857.

Maynard, J.B., Ritger, S.D., Sutton, S.J., 1991. Chemistry of sands from modern Indus River and the Archean Witwatersrand Basin: implications for the composition of the Archean atmosphere. Geology 19, 265-267.

Mazumder R., Sarkar, S., 2004. Sedimentation history of the Palaeoproterozoic Dhanjori Formation, Singhbhum, eastern India. Precambrian Res. 130, 267-287.

McDaniel, D.K., Hemming, S.R., McLennan, S.M. Hanson, G.N., 1994. Resetting of neodymium isotopes and redistribution of REEs during sedimentary processes: the early Proterozoic Chelmsford Formation, Sudbury Basin, Ontario, Canada, Geochim. Cosmochim. Acta 58, 931-941.

McLennan, S.M., Taylor, S.R., Kroner, A., 1983. Geochemical evolution of Archean shales from South Africa: the Swaziland and Pongola Supergroups. Precambrian Res. 22, 93-124.

McLennan, S.M., Simonetti, A., Goldstein, S.L., 2000. Nd and Pb isotopic evidence for provenance and post-depositional alteration of the Paleoproterozoic Huronian Supergroup, Canada. Precambrian Res. 102, 263-278.

McLennan, S.M., Taylor, S.R., McCulloch, M.T., Maynard, J.B., 1990. Geochemical and Nd-Sr isotopic composition of deep-sea turbidites: crustal evolution and plate tectonic associations. Geochim. Cosmochim. Acta 54, 2015-2050.

McMechan, M.E., 1981. The middle Proterozoic Purcell Supergroup in the southwestern Rocky and south-

eastern Purcell Mountains, British Columbia and the initiation of the Cordilleran miogeocline, southern Canada and adjacent United States. Bull. Can. Petrol. Geol. 29, 583-621.

Moore, D.M., Reynolds, R.C., 1997. X-ray diffraction and the identification and analysis of clay minerals. Oxford University Press, New York, NY, U.S.A.

Nesbitt, H.W., Markovics, G., Price, R.A., 1980. Chemical processes affecting alkalies and alkaline earths during continental weathering. Geochim. Cosmochim. Acta 44, 1659-1666.

Nesbitt, H.W., Young, G.M., 1982. Early Proterozoic climates and plate motions inferred from major element chemistry of lutites. Nature 299, 715-717.

Nesbitt, H.W., Young, G.M., 2004. Ancient climatic and tectonic settings inferred from paleosols developed on igneous rocks. In: Eriksson, P.G., Altermann, W., Nelson, D.R., Mueller, W.U., Catuneanu, O., (eds.), The Precambrian: Tempos and Events, Developments in Precambrian Geology 12, Elsevier, Amsterdam, pp. 482-493.

Ohmoto, H., 2004. Archean atmosphere, hydrosphere and biosphere. In: Eriksson, P.G., Altermann, W., Nelson, D.R., Mueller, W.U., Catuneanu, O., (eds.), The Precambrian: Tempos and Events, Developments in Precambrian Geology 12, Elsevier, Amsterdam, pp. 361-387.

O'Neill, J.M., 1997. Stratigraphic character and structural setting of the Belt Supergroup in the Highland Mountains southwestern Montana. In: Berg, R.B., (ed.), Belt Symposium III, Montana Bureau Min. Geol. Spec. Publ. 112, pp. 12-16.

Peng, Q.M., Palmer, M.R., 1995. The Palaeoproterozoic boron deposits in eastern Liaoning, China: a metamorphosed evaporite. Precambrian Res. 27, 185-197.

Pesonen, L.J., Elming, Elming, S.-A., Mertanen, S., Pisarevsky, S., D'Agrella-Filho, M.S., Meert, J.G., Schmidt, P.W., Abrahamsen, N., Bylund, G., 2003. Paleomagnetic configuration of continents during the Proterozoic. Tectonophysics 375, 289-324.

Potts, P. J., Webb, P.C., Watson, J.S., 1992. Zirconium determination by ED-XRF: a critical evaluation of silicate reference materials as calibration standards, Geostandards Lett. 14, 127-136.

Pratt, B.R., 2001. Oceanography, bathymetry and syndepositional tectonics of a Precambrian intracratonic basin: integrating sediment, storms, earthquakes and tsunamis in the Belt Supergroup (Helena Formation, ca. 1.45 Ga), western North America. Sedim. Geol. 141, 371-394.

Price, R.A., 1964. The Precambrian Purcell system in the Rocky Mountains of southern Alberta and British Columbia. Bull. Can. Petroleum Geol. 12, 399-426.

Price, R.A., Sears, J.W, 2000. A preliminary palinspastic map of the Mesoproterozoic Belt-Purcell Supergroup, Canada and USA: implications for the tectonic setting and structural evolution of the Purcell anticlinorium and the Sullivan deposit. In: Lydon, J.W., Höy, T., Slack, J.F., Knapp, M.E., (eds.), The Geological Environment of the Sullivan Deposit, British Columbia. Geol. Assoc. Can. Min. Dep. Div. Spec. Publ. 1, pp. 61-81.

Rainbird, R.H., 1992. Anatomy of a large-scale braid-plain quartzarenite from the Neoproterozoic Shaler Group, Victoria Island, Northwest Territories, Canada. Geol. Sur. Can. Contrib. 35191, 2537-2550.

Rainbird, R.H., Nesbitt, H.W, Donalson, J.A., 1990. Formation and diagenesis of a sub-Huronian saprolith: comparison with a modern weathering profile. J. Geol. 98, 801-822.

Rainbird, R.H., Heaman, L.M., Young, G.M., 1992. sampling Laurentia: detrital zircon geochronology offers evidence for an extensive Neoproterozoic river system originating from Grenville orogen. Geology, 20, 351-354

Rainbird, R.H., Jefferson, C.W., Young, C.M., 1996. The early Neoproterozoic sedimentary Succession B of northwestern Laurentia: correlations and paleogeograpic significance. Geol. Soc. Am. Bull. 108, 454-470.

Rainbird, R.H., McNicoll, V.J., Thériault, Heaman, L.M., Abbott, J.G., Long, D.G.F., Thorkelson, D.J., 1997. Pan-continental river system draining Grenville orogen recorded by U-Pb and Sm-Nd geochronology of neoproterozoic quartzarenites and mudrocks, northwestern Canada. J. Geol. 105, 1-17.

Rainbird, R.H., Hadlari, T., Aspler, L.B., Donaldson, J.A., LeCheminant, A.N., Peterson, T.D., 2003. Sequence stratigraphy and evolution of the Paleoproterozoic intracontinental Baker Lake and Thelon basins, western Churchill Province, Nunavut, Canada. Precambrian Res. 125, 21-53.

Ramaekers, P., Catuneanu, O., 2004. Development and sequences of the Athabasca basin, early Proterozoic, saskatchewan and Alberta, Canada. In: Eriksson, P.G., Altermann, W., Nelson, D.R., Mueller, W.U., Catuneanu, O., (eds.), The Precambrian: Tempos and Events, Developments in Precambrian Geology 12, Elsevier, Amsterdam, pp. 705-723.

Ray, J.S., Veizer, J., Davis, W.J., 2003. C, O, Sr and Pb isotope systematics of carbonate sequences of the Vindhyan Supergroup, India: age, diagenesis, correlations and implications for global events. Precambrian Res. 121, 103-140.

Rogers, J.J.W., Santosh, M., 2004. Continents and supercontinents. Oxford Universy Press. New York, NY, U. S. A.

Ross, G.M., Villenueve, M.E., 2003. Provenance of the Mesoproterozoic (1.45 Ga) Belt Basin (western North America): another piece in the pre-Rodinia paleogeographic puzzle. Geol. Soc. Am. 115, 1191-1217.

Ross, G.M., Parrish, R.R., Dudás, F.Ö., 1991. Provenance of the Bonner Formation (Belt Supergroup), Montana: insights from U-Pb and Sm-Nd analyses of detrital minerals. Geology 19, 340-343.

Sawyer, E.W., 1986. The influence on source rock type, chemical weathering and sorting on the geochemistry of the clastic sediments from the Quetico metasedimentary belt, Superior Province, Canada. Chem. Geol. 55, 77-95.

Sears, J.W., Chamberlain, K.R., Buckley, S.N., 1998. Structural and U-Pb geochronological evidence for 1.47 Ga rifting in the Belt basin, western Montana. Can. J. Earth Sci. 35, 467-475.

Sears, J.W., Price, R.A., Khudoley, A.K, 2004. Linking the Mesoproterozoic Belt-Purcell Supergroup and Udzha basin across the west Laurentia-Siberia connection. Precambrian Res. 129, 291-308.

Schieber, J.A., 1990. Distribution of REE in the eastern Belt Supergroup (Montana, U.S.A.): implications for stratigraphic correlations and basin evolution. Chem. Geol. 81, 83-98.

Schieber, J.A., 1992. A combined petrographical-geochemical provenance study of the Newland Formation, Mid-Proterozoic of Montana. Geol. Magaz. 129, 223-237.

Schieber, J.A., 1997. Sedimentological, geochemical, and mineralogical features of the Belt Supergroup and their bearing on the lacustrine versus marine debate. In: Link, P.K., (ed.), Geologic Guidebook to the Belt-Purcell Supergroup, Glacier National Park and Vicinity, Montana and Adjacent Canada, Field Trip Guidebook for the Belt Symposium III, Belt Association, Pocatello, Idaho, U.S.A., pp. 177-189.

Slack, J.F., Höy, T., 2000. Geochemistry and provenance of clastic metasedimentary rocks of the Aldridge and Fort Steele formations, Purcell Supergroup, southeastern British Columbia. In: Lydon, J.W., Höy, T., Slack, J.F., Knapp, M.E., (eds.), The Geological Environment of the Sullivan Deposit, British Columbia. Geol. Assoc. Can. Min. Dep. Div. Spec. Publ. 1, pp. 180-201.

Taylor, S.R., McLennan, S.M., 1985. The continental crust: its composition and evolution. Blackwell, Oxford, U.K.

Taylor, S.R., McLennan, S.M., 1995. The geochemical evolution of the continental crust. Rev. Geophy. 33, 241-265.

Tiessen, H., Roberts, T.L., Stewart, J.W.B., 1983. Carbonate analysis in soils and minerals by accid digestion and two-endpoint titration. Comm. Soil Sci. Plant An. 14, 161-164.

Tran, H.T., Ansdell, K., Bethune, K., Watters, B., Ashton, K., 2003. Nd isotope and geochemical constraints on the depositional setting of Paleoproterozoic metasedimentary rocks along the margin of the Archean Hearne craton. Precambrian Res. 123, 1-28.

Veizer, J., Jansen, S.L., 1979. Basement and sedimentary recycle and continental evolution. J. Geol. 87, 341-370.

Veizer, J., Mackenzie, F.T., 2004. Evolution of sedimentary rocks. In: MacKenzie, F.T., (ed.), Sediment, Diagenesis, and Sedimentary Rocks, Treatise on Geochimistry, Holland, H.D., Turekian, K.K., (eds.), Elsevier, Oxford, New York, 7, pp. 369-407.

Wallace, C.A., Harrison, J.E., Lidke, D.J., 1993. Lithofacies of the Helena and Wallace Formations (Belt Supergroup, middle Proterozoic), Montana and Idaho. Belt Symposium III, Informal program and abstracts, Montana, pp. 3.

Whiple, J.W., Connor, J.J., Raup, O.B., McGrimsey, R.G., 1984. Preliminary report on the stratigraphy of the Belt Supergroup, Glacier National Park and adjacent Whitefish Range, Montana. In: McBane, J.D., Garrison, P.B., (eds.), Northwest Montana and Adjacent Canada, Montana Geol. Soc. Guidebook, 1984 Field Conference and Symposium, pp. 33-50.

Whipple, J.W., Binda, P.L., Winston, D., 1997. Geologic guide to Glacier National Park, Montana and areas adjacent to Waterton, Alberta. Belt Symposium III. In: Link, P.K., (ed.), Geologic Guidebook to the Belt-Purcell Supergroup, Glacier National Park and Vicinity, Montana and Adjacent Canada, Field Trip Guidebook for the Belt Symposium III, Belt Association, Pocatello, Idaho, U.S.A., pp. 125-155.

Windley, B.F., 1995. The evolving continents. Wiley and sons, New York, NY, U.S.A.

White, B.G., Winston, D., 1982. The Revett-St. Regis "transition zone" near the Bunker Hill mine, Coeur d'Alene District, Idaho. In: Reid, R.R., Williams, G.A., (eds.), Society of Economic Geologists Coeur d'Alene Field Conference. Idaho Bur. Min. Geol. Bull. 24, pp.16-17.

Winston, D., 1986. Sedimentology of the Ravalli Group, middle Belt carbonate and Missoula Group, middle Proterozoic Belt Supergroup, Montana, Idaho and Washington. In: Roberts, S.M., (ed.), A Guide to Proterozoic Rocks of Western Montana and Adjacent Areas. Montana Bur. Min. Geol. Spec. Publ. 94, pp. 85-124.

Winston, D., 1989. A sedimentary and tectonic interpretation of the Belt. In: Hanshaw, P.M., (ed.), Middle Proterozoic Belt Supergroup, Western Montana, 28th International Geological Congress, Field Trip Guidebook T334. Am. Geophysical Union, pp. 437-469.

Winston, D., 1990. Evidence for intracratonic, fluvial and lacustrine settings of Middle to late Proterozoic basins of western U.S.A. In: Gower, C.F., Rivers, T., Ryan, B., (eds.), Mid-Proterozoic Laurentia-Baltica. Geol. Assoc. Can. Spec. Paper 38, 535-564.

Winston, D., Lyons, T., 1997. Sedimentary cycles in the St. Regis, Empire and Helena formations of the middle Proterozoic Belt Supergroup, northwestern Montana. In: Link, P.K., (ed.), Geological Guidebook to the Belt-Purcell Supergroup, Glacier National Park and Vicinity, Montana and Adjacent Canada, Belt Symposium III, Field Trip guidebook, Belt association, Spokane, pp. 21-51.

Wronkiewicz, D.J., Condie, K.C., 1989. Geochemistry and provenance of sediments from the Pongola Supergroup, South Africa: evidence for a 3.0-Ga-old continental craton. Geochim. Cosmochim. Acta 53, 1537-1549.

Young, G.M., 1999. Some aspects of the geochemistry, provenance and palaeoclimatology of the Torridonian of NW Scotland. J. Geol. Soc. 156, 1097-1111.

Young, G.M., 2004. Earth's two great Precambrian glaciations: aftermath of the "snowball earth" hypothesis. In: Eriksson, P.G., Altermann, W., Nelson, D.R., Mueller, W.U., Catuneanu, O., (eds.), The Precambrian: Tempos and Events, Developments in Precambrian Geology 12, Elsevier, Amsterdam, pp. 440-447.

Xie, Q., J. Jain, M. Sun, R. Kerrich, and J. Fan 1994, ICP-MS analysis of basalt BIR-1 for trace elements, Geostandards Newsletters 18, 53-63.

Zhao, G., Sun, M., Wilde, S.A., and Li, S., 2004. A Paleo-Mesoproterozoic supercontinent: assembly, growth and breakup. Earth Sci. Rev. 67, 91-123.

CHAPTER VIII

Conclusions

(1) Argillites are sharply interbedded with sandstone units in the Appekunny and Grinnell formations of the lower Belt-Purcell Supergroup sequence, at Waterton-Glacier International Peace Park. Both facies have the same geochemical signature, albeit variably depleted by detrital quartz. Their REE, multi-element, Cr-Ni, and Th/Sc-Sc geochemical systematics is consistent with a dominantly post-Archean source area.

The REE and HFSE budget in sandstones is dominated by the clay fraction, and therefore the compositional signature of sandstones and argillites is not diagnostic of a similar or different provenance of the two facies. Sandstone developed in a separate high-energy environment, and argillite and sandstone became interbedded during storms, accounting for the sharp interbedding of the two facies.

(2) Detrital monazite age spectra for argillites and sandstones of the Appekunny Formation are similar, consistent with a common provenance. This resolves uncertainties inherent in trace element data for the two facies, as well as previous zircon data for sandstones alone.

(3) Provenance for the Grinnell and Appekunny sandstones and argillites is interpreted to be from Paleoproterozoic terranes varing in each from ~1800-1600 Ma, including the Penokean, Yavapai, and Mazatzal Provinces located to the east and south of the basin. Minor age grouping at ~1600-1500 in the Appekunny Formation could be the result of sediments from the Priest River Complex in the west and/or an unknown western terrane. Marginal Archean contributions could be from the Wyoming Craton or other Archean terranes in Laurentia to the east.

(4) The Belt-Purcell sequence records three major diagenetic stages displayed in argillites and sandstones: (1) K-addition, having similar REE and multi-element patterns as PA-UCC, albeit at 0.8 to 1.5 times PA-UCC due to less/more SiO_2, weathering; (2) a stage characterized by widespread additions of HREE, HFSE mobility, featuring REE/REE, REE/HFSE or HFSE/HFSE

fractionation; and (3) local dolomitization with REE and HFSE mobility.

Gains and/or losses of Cs, Sb, Co, Cr, V, Mo, and Cu during stages (1) and/or (2), and/or absolute additions of heavy REE are complementary in the dolomitization diagenetic stage, consistent with evolution of the brines to lower pH by reaction with primary carbonate sedimentary rocks. Stage (1) is common in Precambrian siliciclastic sequences, whereas stage (2) of preferential HREE addition is not. Stage (2) is not due to heavy mineral sorting of zircon, provenance or weathering imprints. Stage (1) may have preceded or been coeval with stage (2).

(5) Stages 1 and 2 record mobility of U and Ce, commensurate with oxidizing conditions. Mobility of HREE and HFSE is known only in oxidized alkaline brines. Such brines may have derived via dissolution of evaporites known to be present in the Belt-Purcell Supergroup. Consecuently, REE and HFSE fractionation in argillites and sandstones throughout the Belt-Purcell Supergroup could be interpreted as due to basinal brine events.

(6) Monazites from the Appekunny and Grinnell formations are texturally rounded grains, inclusions in rounded quartz grains, or individual euhedral. The first texture is interpreted as detrital, and compositionally are characterized by ages >~1400 Ma, higher Th_2O, Y, and lower LREE/HREE contents than euhedral individual monazite grains with chemical ages <~1400 Ma that posses opposed compositional characteristics, and viewed as diagenetic.

(7) Chemical ages of diagenetic monazites indicate REE and HFSE mobility in the Belt-Purcell Supergroup at ~1400-300 Ma. Similarly, diagenetic age groupings have been documented in other Laurentian and Australian basins, which can be correlated to large-scale advective flow of basinal brines 100s Ma after deposition. Changes of hydraulic gradient could be connected to tectonics, distal and/or local such as the dispersal of the supercontinent Columbia at ~1500 Ma, the Grenville orogen at ~1300-1100 Ma, and break up of Rodinia starting at ~900 Ma.

(8) Chemical index of alteration for argillites and sandstones, corrected for diagenetic K-addition average at 73 and 66 respectively, relative to a PAAS value of 70. These results, coupled with correlation of CIA with Eu/Eu*, and high K/Cs ratios, and low Sr, Ca, and Na relative to PA-UCC, could be interpreted as the result of a moderate to intense weathered provenance being drained by a Amazon-scale river system on a large landmass. Recycled weathered sediments and/or sedimentary rocks in the catchment may contribute to the measured CIA.

(9) The presence of minor pristine feldspars lowers the CIA values, and may signify that there were minor contributions from minor source proximal to the Belt-Purcell Basin with short-distance transport under the arid to semi-arid climate of the depositional setting.

(10) Moderate weathering of the larger provenance may be associated with elevated levels of atmospheric CO_2 degassed from a mantle plume implicated in the rifting of the supercontinent Columbia at ~1500 Ma. Mantle degassing may also be enhanced as new ocean spreading centres developed.

The three interrelated aspects of this thesis provide an integrated view of the Mesoproterozoic in western Laurentia, albeit with global effects: provenance, weathering intensity, and multiple diagenetic fluid events in the Belt-Purcell Supergroup rocks.

APPENDIX I

Appendix Ia. Geographic coordinates for samples collected at Waterton-Glacier International Peace Park and near areas.

Sample	North	West	Figs. 3.2, 3.3, 3.4
35(2)G1	N49º 00’ 53.2’’	W114º 41’ 25.0’’	G70
35(1)G1	N49º 00’ 53.2’’	W114º 41’ 25.0’’	G69
35G1USO	N49º 00’ 53.2’’	W114º 41’ 25.0’’	G68
34(2)G1	N48º 57’ 39.8’’	W114º 45’ 03.1’’	G67
34(1)G1	N48º 57’ 37.9’’	W114º 45’ 14.1’’	G66
34G1USO	N48º 57’ 17.0’’	W114º 45’ 22.9’’	G65
33(2)G1	N48º 55’ 50.5’’	W114º 45’ 27.7’’	G64
33(1)G1	N48º 55’ 50.5’’	W114º 45’ 27.7’’	G63
33G1USO	N48º 56’ 53.8’’	W114º 45’ 27.4’’	G62
32(2)G1	N48º 58’ 60’’	W114º 46’ 50’’	G61
32(1)G1	N48º 58’ 50’’	W114º 46’ 45’’	G60
32G1USO	N48º 56’ 50.0’’	W114º 45’ 45.0’’	G59
31G1USO	N48º 40’ 18.6’’	W113º 46 05.6’’	G58
31(2)G1	N48º 45’ 39.2’’	W113º 47’ 06.3’’	G57
31(1)G1	N48º 45’ 37.2’’	W113º 47’ 11.4’’	G56
30G1uso	N48º 42’ 16.0’’	W113º 44’ 11.4’’	G55
30(2)G1	N48º 42’ 02.7’’	W113º 44’ 03.3’’	G54
30(1)G1	N48º 41’ 56.3’’	W113º 43’ 58.0’’	G53
28(2)G1	N48º 41’ 51.1’’	W113º 43’ 32.5’’	G52
28G1USO	N48º 41’ 56.5’’	W113º 42’ 18.2’’	G51
28(1)G1	N48º 41’ 41.3’’	W113º 40’ 57.1’’	G50
27(3)G1	N48º 40’ 54.0’’	W113º 38’ 18.3’’	G49
27(2)G1	N48º 40’ 52.1’’	W113º 38’ 18.6’’	G48
27G1USO	N48º 40’ 47.8’’	W113º 38’ 16.4’’	G47
27(1)G1	N48º 40’ 43.9’’	W113º 38’ 18.1’’	G46
26(14)Gl	N49º 00’ 25.2’’	W114º 25’ 26.5’’	G45
26(12)G1	N49º 01’ 30.5’’	W113º 28’ 50.2’’	G44
26(10)G1	N49º 08’ 58.1’’	W114º 02’ 05.1’’	G43
26(9)G1	N49º 08’ 56.6’’	W114º 01’ 56.1’’	G42
26(7)G1	N49º 08’ 57.4’’	W114º 01’ 50.8’’	G41
26(6)G1	N49º 08’ 31.5’’	W114º 01’ 10.4’’	G40
26(5)G1	N49º 08’ 26.3’’	W114º 01’ 11.6’’	G39
26(3)G1	N49º 08’ 19.5’’	W114º 01’ 16.2’’	G38
26(2)G1	N49º 07’ 42.1’’	W114º 01’ 34.5’’	G37

Appendix Ia. (continued)

Sample	North	West	Figs. 3.2, 3.3, 3.4
USO 27	N48º 46’ 50’’	W113º 42’ 20’’	G36
USO 25	N48º 46’ 50’’	W113º 42’ 20’’	G35
USO 24	N48º 46’ 50’’	W113º 42’ 20’’	G34
USO 23	N48º 46’ 50’’	W113º 42’ 20’’	G33
26 Gl Uso	N48º 40’ 31.5’’	W113º 36’ 14.4’’	G32
USO 10	N48º 41’ 30’’	W113º 33’ 50’’	G31
USO 12	N48º 41’ 30’’	W113º 33’ 50’’	G30
USO 10	N48º 41’ 30’’	W113º 33’ 50’’	G29
USO 8	N48º 41’ 30’’	W113º 33’ 50’’	G28
25 Gl Uso	N48º 41’ 09.3’’	W113º 33’ 50.2’’	G27
USO 9	N48º 41’ 30’’	W113º 33’ 50’’	G26
USO 11	N48º 41’ 30’’	W113º 33’ 50’’	G25
USO 7	N48º 41’ 30’’	W113º 33’ 50’’	G24
USO 6	N48º 41’ 30’’	W113º 33’ 50’’	G23
USO 5	N48º 41’ 30’’	W113º 33’ 50’’	G22
USO 4	N48º 41’ 30’’	W113º 33’ 50’’	G21
USO 3	N48º 41’ 30’’	W113º 33’ 50’’	G20
USO 2	N48º 41’ 30’’	W113º 33’ 50’’	G19
USO 1	N48º 41’ 30’’	W113º 33’ 50’’	G18
USO 19	N48º 41’ 30’’	W113º 33’ 50’’	G17
USO 20	N48º 41’ 30’’	W113º 33’ 50’’	G16
USO 26	N48º 41’ 30’’	W113º 33’ 50’’	G15
USO 22	N48º 41’ 30’’	W113º 33’ 50’’	G14
USO 18	N48º 41’ 30’’	W113º 33’ 50’’	G13
USO 17	N48º 41’ 30’’	W113º 33’ 50’’	G12
USO 16	N48º 41’ 30’’	W113º 33’ 50’’	G11
USO 21	N48º 41’ 30’’	W113º 33’ 50’’	G10
USO 15	N48º 41’ 30’’	W113º 33’ 50’’	G9
USO 14	N48º 41’ 30’’	W113º 33’ 50’’	G8
USO 13	N48º 41’ 30’’	W113º 33’ 50’’	G7
24G1USO	N48º 41’ 50.2’’	W113º 31’ 20.5’’	G6
24(2)G1	N48º 41’ 40.7’’	W113º 31’ 27.6’’	G5
24(1)G1	N48º 41’ 57.4’’	W113º 31’ 19.2’’	G4
23G1USO	N49º 02’ 01.6’’	W113º 53’ 40.6’’	G3
23(2)G1	N49º 01’ 59.6’’	W113º 53’ 40.2’’	G2
23(1)G1	N49º 01’ 59.0’’	W113º 53’ 40.2’’	G1
Map datum	WGS 84		

Appendix Ib. Geographic coordinates for samples collected at the Purcell Mountains.

Sample	North	West	Figs. 3.2, 3.3, 3.4
22(1)Pu	N49° 55’ 51.0’’	W115° 47’ 32.1’’	P27
22(2)Pu	N49° 56’ 28.7’’	W115° 47’ 07.3’’	P26
22PuUSO	N49° 56’ 14.5’’	W115° 47’ 03.5’’	P25
21(2)Pu	N49° 09’ 27.8’’	W115° 02’ 29.3’’	P24
21(1)Pu	N49° 09’ 27.8’’	W115° 02’ 29.3’’	P23
21PuUSO	N49° 09’ 27.8’’	W115° 02’ 29.3’’	P22
19(2)Pu	N49° 57’ 13.2’’	W115° 49’ 15.1’’	P21
19(1)Pu	N49° 56’ 05.0’’	W115° 49’ 44.8’’	P20
19PuUSO	N49° 18’ 40.8’’	W115° 03’ 42.5’’	P19
18PuUSO	N49° 01’ 36.0’’	W115° 01’ 09.8’’	P18
18(2)PU	N49° 09’ 52.7’’	W115° 05’ 38.4’’	P17
18(1)Pu	N49° 09’ 46.0’’	W115° 05’ 38.1’’	P16
17(2)Pu	N49° 38’ 54.6’’	W115° 35’ 53.2’’	P15
17(1)Pu	N49° 38’ 53.4’’	W115° 35’ 54.1’’	P14
17PuUSO	N49° 38’ 46.6’’	W115° 35’ 56.8’’	P13
16(5)PU	N49° 38’ 22.1’’	W115° 36’ 02.1’’	P12
16(4)Pu	N49° 38’ 24.3’’	W115° 35’ 59.6’’	P11
16(3)PU	N49° 38’ 23.3’’	W115° 36’ 00.6’’	P10
16(2)PU	N49° 38’ 22.6’’	W115° 36’ 00.9’’	P9
16(1)PU	N49° 38’ 22.4’’	W115° 36’ 01.0’’	P8
16PuUSO	N49° 38’ 22.3’’	W115° 36’ 01.1’’	P7
14(1)Pu	N49° 18’ 37.9’’	W115° 50’ 05.9’’	P6
14PuUSO	N49° 14’ 23.6’’	W115° 51’ 58.5’’	P5
14(2)Pu	N49° 14’ 23.6’’	W115° 51’ 58.5’’	P4
FT(3)PU	N49° 47’ 05.5’’	W115° 40’ 38.5’’	P3
FT(2)Pu	N49° 47’ 05.5’’	W115° 40’ 38.5’’	P2
FT(1)Pu	N49° 47’ 05.5’’	W115° 40’ 38.5’’	P1
Map datum	WGS 84		

Appendix Ic. Geographic coordinates for samples collected at the Whitefish Range.

Sample	North	West	Figures 1.3, 1.4, 1.5
11(2)Wh	N48º 27’ 08.9’’	W115º 46’ 14.5’’	W29
11WhUSO	N48º 27’ 08.9’’	W115º 46’ 14.5’’	W28
11(1)Wh	N48º 26’ 53.9’’	W115º 46’ 49.6’’	W27
10WhUSO	N48º 26’ 46.3’’	W115º 47’ 24.6’’	W26
8(2)Wh	N48º 21’ 33.8’’	W115º 19’ 17.7’’	W25
8 Wh USO	N48º 21’ 33.8’’	W115º 19’ 17.7’’	W24
7 Wh USO	N48º 22’ 47.6’’	W115º 19’ 21.6’’	W23
6(2)Wh	N48º 23’ 52.1’’	W115º 19’ 35.0’’	W22
6(1)Wh	N48º 24’ 16.5’’	W115º 19’ 22.5’’	W21
6 Wh USO	N48º 24’ 42.0’’	W115º 19’ 18.6’’	W20
5(2)Wh	N48º 24’ 34.9’’	W115º 18’ 31.9’’	W19
5 Wh USO	N48º 24’ 34.9’’	W115º 18’ 31.9’’	W18
5(1)Wh	N48º 24’ 24.9’’	W115º 18’ 35.3’’	W17
4(2)Wh	N48º 40’ 30.9’’	W114º 46’ 14.6’’	W16
4(1)Wh	N48º 40’ 30.9’’	W114º 46’ 14.6’’	W15
4WhUSO	N48º 40’ 30.9’’	W114º 46 ’14.6’’	W14
3(8)Wh	N48º 49’ 40’’	W115º 14’ 46’’	W13
3(7)Wh	N48º 49’ 40’’	W115º 14’ 46’’	W12
3(6)Wh	N48º 49’ 40’’	W115º 14’ 46’’	W11
3(5)Wh	N48º 49’ 40’’	W115º 14’ 46’’	W10
3(4)Wh	N48º 49’ 40.4’’	W115º 14’ 46.8’’	W9
3(3)Wh	N48º 49’ 44’’	W115º 16’ 12’’	W8
3(2)Wh	N48º 49’ 44’’	W115º 16’ 12’’	W7
3(1)Wh	N48º 49’ 44’’	W115º 16’ 12’’	W6
3WhUSO	N48º 49’ 44.3’’	W115º 16’ 12.5’’	W5
2WhUSO	N48º 41’ 53.7’’	W115º 18’ 27.4’’	W4
1(2)Wh	N48º 36’ 50.7’’	W115º 15’ 00.9’’	W3
1(1)Wh	N48º 31’ 51.8’’	W115º 14’ 18.4’’	W2
1WhUSO	N48º 35’ 04.6’’	W115º 12’ 26.2’’	W1
Map datum	WGS 84		

APPENDIX II

Appendix IIa. Hand sample description of samples collected at Waterton-Glacier International Peace Park

Formation	Sample	Description	Label
Libby	35(2)G1	Green laminated argillite-sandstone	Gl70
Libby	35(1)G1	Green laminated argillite	Gl69
Libby	35G1USO	Grey argillite	Gl68
McNamara	34(2)G1	Green laminated argillite	Gl67
McNamara	34(1)G1	Green laminated argillite	Gl66
McNamara	34G1USO	White laminated argillite	Gl65
Bonner	33(2)G1	White cross-bedded medium-grained size sandstone	Gl64
Bonner	33(1)G1	Red cross-bedded coarse-grained size sandstone	Gl63
Bonner	33G1USO	Red medium-grained size sandstone	Gl62
Mount. Sh.	32(2)G1	Brown laminated argillite	Gl61
Mount. Sh.	32(1)G1	Brown argillite-mudstone	Gl60
Mount. Sh.	32G1USO	Green laminated argillite	Gl59
Shepard	31G1USO	Green laminated/cross rippled argillite-sandstone	Gl58
Shepard	31(2)G1	Green laminated argillite	Gl57
Shepard	31(1)G1	Green laminated argillite	Gl56
Snowslip	30G1uso	Red laminated argillite	Gl55
Snowslip	30(2)G1	Green laminated-cross-bedded argillite-sandstone	Gl54
Snowslip	30(1)G1	Red laminated argillite	Gl53
Helena	28(2)G1	Grey dolomite-argillite	Gl52
Helena	28G1USO	Grey dolomite-mudstone	Gl51
Helena	28(1)G1	Grey dolomite-argillite	Gl50
Empire	27(3)G1	Green laminated argillite	Gl49
Empire	27(2)G1	Green argillite	Gl48
Empire	27G1USO	Green dolomite	Gl47
Empire	27(1)G1	White medium-grained size cross-bedded sandstone	Gl46
Grinnell	26(14)Gl	Green laminated argillite	Gl45
Grinnell	26(12)G1	Red massive argillite	Gl44
Grinnell	26(10)G1	Red laminated argillite	Gl43
Grinnell	26(9)G1	Red medium-grained size sandstone	Gl42
Grinnell	26(7)G1	Red coarse-grained size sandstone	Gl41
Grinnell	26(6)G1	Red argillite	Gl40
Grinnell	26(5)G1	Red-white coarse-grained size sandstone	Gl39
Grinnell	26(4)G1	Red massive argillite-mudstone	Gl38
Grinnell	26(3)G1	White coarse-grained sandstone	Gl37
Grinnell	26(2)Gl	Red laminated argillite	Gl36
Grinnell	USO 27	Green laminated argillite	Gl35
Grinnell	USO 25	Red argillite-mudstone	Gl34
Grinnell	USO 24	Red laminated argillite	Gl33
Grinnell	USO 23	Green medium-grained size sandstone	Gl32
Appekunny	26 Gl Uso	Red coarse-grained size sandstone	Gl31
Appekunny	USO 10	Green mudstone	Gl30
Appekunny	USO 12	Green laminated argillite	Gl29
Appekunny	USO 8	Green medium-grained size sandstone	Gl28

Formation	Sample	Description	Label
Appekunny	25 Gl Uso	Green laminated argillite	Gl27
Appekunny	USO 9	Green medium-grained size sandstone	Gl26
Appekunny	USO 11	Green laminated argillite	Gl25
Appekunny	USO 7	Green coarse-grained size sandstone	Gl24
Appekunny	USO 6	Green laminated argillite	Gl23
Appekunny	USO 5	Green laminated argillite	Gl22
Appekunny	USO 4	Green laminated argillite	Gl21
Appekunny	USO 3	Green laminated argillite	Gl20
Appekunny	USO 2	Green laminated argillite	Gl19
Appekunny	USO 1	Green laminated argillite	Gl18
Appekunny	USO 19	Green coarse-grained size sandstone	Gl17
Appekunny	USO 20	Green laminated argillite	Gl16
Appekunny	USO 26	Green laminated argillite	Gl15
Appekunny	USO 22	Green medium-grained size sandstone	Gl14
Appekunny	USO 18	Green medium-grained size sandstone	Gl13
Appekunny	USO 17	Green laminated argillite	Gl12
Appekunny	USO 16	Green medium-grained size sandstone	Gl11
Appekunny	USO 21	Green coarse-grained size sandstone	Gl10
Appekunny	USO 15	Green laminated argillite	Gl9
Appekunny	USO 14	Green coarse-grained size sandstone	Gl8
Appekunny	USO 13	Green laminated argillite	Gl7
Altyn	24G1USO	Yellow-white dolomite	Gl6
Altyn	24(2)G1	Yellow-white dolomite-argillite	Gl5
Altyn	24(1)G1	Yellow dolomite	Gl4
Waterton	23G1USO	Yellow-white dolomite	Gl3
Waterton	23(2)G1	Grey dolomite with argillite	Gl2
Waterton	23(1)G1	Yellow-white dolomite-argillite	Gl1

Appendix IIb. Hand sample description of samples collected at the Purcell Mountains.

Formation	Sample	Description	Label
Roosville	22(1)Pu	White argillite	P27
Roosville	22(2)Pu	Green laminated argillite	P26
Roosville	22PuUSO	Grey dolomite	P25
Phillips	21(2)Pu	Red laminated argillite	P24
Phillips	21(1)Pu	Red argillite-mudstone	P23
Phillips	21PuUSO	Red laminated fine-medium-grained size sandstone	P22
Gateway	19(2)Pu	Red laminated fine-medium-grained size sandstone	P21
Gateway	19(1)Pu	Green laminated argillite	P20
Gateway	19PuUSO	Green-yellow laminated argillite	P19
Van Creek	18PuUSO	Green argillite	P18
Van Creek	18(2)PU	Grey medium-grained sandstone	P17
Van Creek	18(1)Pu	Grey argillite-mudstone	P16
Kitchener	17(2)Pu	Gray dolomite-argillite	P15
Kitchener	17(1)Pu	Green medium-coarse-grained size sandstone	P14
Kitchener	17PuUSO	Green argillite-mudstone	P13
Creston	16(5)PU	Green laminated argillite-fine-grained size sandstone	P12
Creston	16(4)Pu	Yellow laminated argillite-fine-grained size sandstone	P11
Creston	16(3)PU	Green laminated argillite-fine-grained size sandstone	P10
Creston	16(2)PU	Green laminated argillite-fine-grained size sandstone	P9
Creston	16(1)PU	Green laminated argillite-fine-grained size sandstone	P8
Creston	16PuUSO	Green laminated argillite	P7
Aldridge	14(1)Pu	Green laminated argillite	P6
Aldridge	14PuUSO	Green fine-medium-grained size sandstone	P4
Aldridge	14(2)Pu	Yellow fine-medium-grained size sandstone	P4
Fort Steele	FT(3)PU	White coarse-grained size sandstone	P3
Fort Steele	FT(2)Pu	White argillite-mudstone	P2
Fort Steele	FT(1)Pu	White argillite-mudstone	P1

Appendix IIc. Hand sample description of samples collected at Whitefish Range.

Formation	Sample	Description	Label
Mount Sh.	11(2)Wh	Green laminated argillite-fine-grained size sandstone	W29
Mount Sh.	11WhUSO	Grey laminated argillite	W28
Mount Sh.	11(1)Wh	Green fine-medium-grained size sandstone	W27
Shepard	10WhUSO	Green laminated argillite	W26
Snowslip	8(2)Wh	Green laminated argillite-fine-grained size sandstone	W25
Snowslip	8 Wh USO	Green laminated argillite-fine-grained size sandstone	W24
Wallace	7 Wh USO	Green laminated argillite-fine-grained size sandstone	W23
Helena	6(2)Wh	Grey dolomitic mudstone	W22
Helena	6(1)Wh	Grey dolomitic mudstone	W21
Helena	6 Wh USO	Grey dolomite-argillite	W20
Empire	5(2)Wh	White laminated argillite	W19
Empire	5 Wh USO	White laminated argillite	W18
Empire	5(1)Wh	Green laminated argillite	W17
Spokane	4(2)Wh	Yellow-red coarse-grained size sandstone	W16
Spokane	4(1)Wh	Red laminated argillite	W15
Spokane	4WhUSO	White-red medium-coarse-grained size sandstone	W14
Burke	3(8)Wh	Gray laminated argillite-fine-grained size sandstone	W13
Burke	3(7)Wh	Gray laminated argillite-fine-grained size sandstone	W12
Burke	3(6)Wh	Yellow laminated argillite-fine-grained size sandstone	W11
Burke	3(5)Wh	Green laminated argillite	W10
Burke	3(4)Wh	Green laminated argillite	W9
Burke	3(3)Wh	Green laminated argillite-fine-grained size sandstone	W8
Burke	3(2)Wh	Grey laminated argillite	W7
Burke	3(1)Wh	Gray laminated argillite	W6
Burke	3WhUSO	Green laminated argillite	W5
Pric.-Burke	2WhUSO	Green laminated argillite-fine-grained size sandstone	W4
Prichard	1(2)Wh	Yellow laminated argillite	W3
Prichard	1(1)Wh	Yellow laminated argillite-fine-grained size sandstone	W2
Prichard	1WhUSO	Grey laminated argillite	W1

APPENDIX III

Appendix IIIa. Major and trace element concentration of the Belt-Purcell Supergroup at Waterton-Glacier International Peace Park.

Formation	Libby	Libby	Libby	McNamara	McNamara	McNamara	Bonner	Bonner	Bonner	Mount. Sh..	Mount. Sh.	Mount. Sh..	Shepard
Sample	35(2)G1	35(1)G1	35G1USO	34(2)G1	34(1)G1	34G1USO	33(2)G1	33(1)G1	33G1USO	32(2)G1	32(1)G1	32G1USO	31G1USO
SiO_2 (wt%)	78.65	70.69	62.00	65.50	65.98	70.60	88.85	82.61	80.70	59.11	50.49	66.70	76.30
TiO_2	0.28	0.37	0.72	0.46	0.57	0.50	0.22	0.21	0.31	0.56	0.62	0.57	0.47
Al_2O_3	7.82	12.29	19.00	12.12	15.01	13.00	5.83	8.35	9.73	11.30	9.81	12.10	9.68
Fe_2O_3	5.81	8.42	6.70	3.14	5.33	2.81	0.69	1.88	1.79	3.66	3.59	3.42	4.11
MnO	0.05	0.05	0.06	0.08	0.04	0.03	0.00	0.00	0.00	0.08	0.13	0.03	0.02
MgO	1.41	2.06	2.03	3.50	3.77	2.91	0.70	1.25	1.26	5.71	7.26	4.38	2.57
CaO	1.23	0.12	0.20	4.75	0.43	1.38	0.12	0.13	0.32	5.50	9.29	2.36	0.58
K_2O	1.35	2.24	4.57	2.60	4.07	3.88	1.70	2.19	2.98	3.41	3.19	3.94	2.83
Na_2O	1.17	1.21	1.48	2.08	1.71	1.61	1.22	1.47	1.36	1.62	1.41	1.39	1.21
P_2O_5	0.02	0.05	0.05	0.08	0.11	0.09	0.01	0.02	0.15	0.17	0.16	0.14	0.09
LOI	2.30	2.55	2.85	5.75	3.00	3.25	0.65	1.30	1.50	9.00	14.25	5.15	2.30
Sum	100.2	100.1	99.7	100.1	100.2	100.3	100.1	99.56	100.2	100.2	100.3	100.4	100.2
Li (ppm)	77	73	60	46	95	59	16	27	18	59	58	79	40
Rb	71	92	227	107	176	132	55	82	102	95	99	134	94
Sr	33	30	83	47	73	39	27	52	25	34	39	37	34
Cs	2	3	15	4	7	5	2	4	4	4	4	5	4
Ba	383	390	849	326	1509	753	419	930	371	318	346	458	482
Y	17.2	24.0	5.3	30.4	32.0	26.9	13.7	11.7	15.1	30.8	33.4	5.1	14.0
Zr	173	219	243	186	232	129	348	158	57	287	430	240	89
Hf	4.48	5.92	7.07	5.49	7.33	5.13	7.94	3.87	5.59	8.15	12.70	7.23	3.37
Nb	6.85	9.43	11.23	12.54	15.21	9.77	2.93	3.11	4.16	13.18	14.25	11.65	6.91
Ta	0.50	0.67	0.91	1.02	1.30	1.02	0.42	0.34	1.19	1.05	1.22	0.91	0.66
Th	7.58	8.45	1.58	12.23	15.15	6.98	4.24	4.06	16.52	12.08	15.01	2.18	4.85
U	2.48	2.51	3.41	3.99	3.96	3.88	1.32	1.50	1.93	1.94	3.32	2.28	2.31
La	23.72	38.79	41.94	32.30	40.50	42.56	11.87	13.29	41.94	40.92	40.47	2.21	13.92
Ce	56.70	88.11	88.75	68.61	86.19	93.80	25.97	29.92	88.75	88.92	87.81	8.06	26.73
Pr	6.64	9.78	10.84	8.11	10.20	11.51	3.41	3.63	10.84	10.70	10.34	0.77	3.32
Nd	24.61	36.19	39.37	29.00	36.87	43.51	13.48	13.34	39.37	38.07	36.94	3.56	13.53
Sm	4.55	6.73	7.87	5.89	7.39	8.60	2.48	2.58	7.87	7.50	7.23	0.88	2.76
Eu	0.74	1.16	1.37	0.93	1.28	1.38	0.56	0.56	1.37	1.22	1.18	0.22	0.46
Gd	4.05	5.62	7.33	5.67	6.91	7.90	2.49	2.10	7.33	6.54	6.65	1.03	2.77
Tb	0.54	0.76	1.07	0.81	0.97	1.04	0.35	0.31	1.07	0.90	0.96	0.19	0.44
Dy	3.21	4.55	6.76	5.06	6.03	6.29	2.36	1.86	6.76	5.44	6.14	1.31	2.74
Ho	0.62	0.84	1.38	1.06	1.21	1.27	0.48	0.38	1.38	1.15	1.23	0.27	0.55
Er	1.82	2.46	4.06	3.17	3.60	3.83	1.40	1.16	4.06	3.31	3.80	0.86	1.52
Tm	0.27	0.36	0.61	0.50	0.55	0.60	0.21	0.17	0.61	0.48	0.56	0.13	0.23
Yb	1.71	2.28	4.04	3.24	3.85	4.02	1.44	1.13	4.04	3.36	3.80	0.90	1.54
Lu	0.24	0.30	0.58	0.50	0.53	0.59	0.21	0.16	0.58	0.45	0.53	0.13	0.21
Sc	10.7	14.7	2.4	15.8	17.9	14.3	2.7	6.1	9.8	15.9	16.0	4.4	10.4
V	46.5	69.9	84.7	41.5	64.3	36.9	13.2	25.1	29.6	35.6	50.8	59.6	58.4
Mo	0.6	0.5	0.8	0.5	0.4	0.5	0.3	0.0	0.0	0.7	0.8	0.2	0.2
Cr	114.6	109.3	123.7	62.1	87.8	53.4	20.2	34.9	32.2	53.8	89.3	100.4	75.1
Co	21.7	20.9	15.2	7.9	12.3	2.3	3.1	8.4	5.0	12.8	17.5	7.1	9.5
Ni	34.3	39.7	23.9	12.7	14.7	10.6	8.2	14.8	8.6	15.7	21.1	18.0	12.2
Cu	37.1	51.1	34.7	3.2	2.9	4.2	2.6	1.9	1.5	8.6	13.6	0.0	1.4
Zn	53.8	53.7	108.1	95.4	123.6	57.7	10.5	19.7	15.2	33.9	36.7	28.9	58.2
Sn	2.2	2.3	4.8	2.8	4.0	4.0	1.0	0.9	1.2	1.6	2.5	2.7	2.1
W	2.1	0.9	3.2	1.6	3.2	2.4	0.1	0.5	0.8	1.0	1.4	1.4	1.8
Pb	8.6	6.5	24.5	5.8	6.0	5.0	4.7	6.4	24.1	19.2	27.8	12.1	4.7
Cd	0.0	0.0	0.1	0.0	0.1	0.0	0.2	0.0	0.0	0.0	0.2	0.0	0.0
Tl	0.3	0.5	1.0	0.7	1.1	0.7	0.3	0.5	1.1	0.4	0.5	0.6	0.5
Ga	13.6	15.1	25.0	15.8	18.6	16.7	5.2	7.9	12.0	7.8	10.2	14.2	11.9
As	11.2	10.5	0.0	0.5	1.1	0.0	0.8	0.6	0.8	4.3	7.1	0.7	0.7
Ag	0.0	0.0	0.1	0.0	0.0	0.0	0.0	0.0	0.0	0.2	0.3	0.0	0.0
Sb	0.7	0.4	0.5	0.7	1.0	0.8	0.2	0.4	0.5	0.7	1.1	0.5	0.5
Labels chapter III	G70	G69	G68	G67	G66	G65	G64	G63	G62	G61	G60	G59	G58

Appendix IIIa (continued).

Formation	Shepard	Shepard	Snowslip	Snowslip	Snowslip	Helena	Helena	Helena	Empire	Empire	Empire	Empire	Grinnell
Sample	31(2)G1	31(1)G1	30G1uso	30(2)G1	30(1)G1	28(2)G1	28G1USO	28(1)G1	27(3)G1	27(2)G1	27G1USO	27(1)G1	26(14)Gl
SiO_2 (wt%)	60.05	62.43	66.50	79.03	62.27	52.94	38.50	36.88	55.99	64.44	28.70	83.25	70.82
TiO_2	0.61	0.60	0.46	0.41	0.59	0.33	0.15	0.24	0.29	0.30	0.15	0.02	0.49
Al_2O_3	15.50	14.57	10.30	8.96	15.22	6.43	2.75	6.49	8.40	8.74	3.12	1.64	12.24
Fe_2O_3	8.95	8.70	3.88	3.94	5.45	1.85	0.97	2.51	2.62	2.41	2.18	0.18	2.57
MnO	0.03	0.03	0.17	0.02	0.08	0.06	0.03	0.03	0.07	0.05	0.21	0.03	0.02
MgO	5.47	5.37	3.37	2.26	3.51	4.30	1.58	4.34	7.55	6.15	14.00	2.69	4.48
CaO	0.23	0.19	3.75	0.13	1.37	15.71	29.80	25.22	8.10	5.16	20.10	4.53	0.61
K_2O	3.75	3.33	3.45	1.81	5.70	1.57	0.59	1.62	3.48	3.38	1.02	1.13	4.58
Na_2O	0.98	1.02	1.04	1.50	0.77	1.20	0.35	0.43	0.44	0.50	0.12	0.09	0.79
P_2O_5	0.14	0.09	0.11	0.04	0.10	0.08	0.03	0.04	0.07	0.07	0.03	0.00	0.10
LOI	4.30	3.85	6.70	1.85	4.40	15.75	24.50	22.40	13.05	8.90	30.70	6.40	3.45
Sum	100.1	100.3	99.9	100.1	99.6	100.3	99.2	100.2	100.2	100.2	100.4	100.3	100.1
Li (ppm)	79	64	32	49	74	51	46	105	75	88	76	9	100
Rb	140	128	135	60	238	47	27	61	88	97	35	20	124
Sr	27	27	63	27	30	65	115	72	40	40	58	41	25
Cs	7	5	6	3	11	2	1	4	4	5	1	0	6
Ba	638	519	1002	279	797	322	88	256	1436	544	210	3223	416
Y	38.1	25.9	21.5	23.1	30.3	19.9	15.3	14.1	21.1	23.0	14.3	5.5	19.7
Zr	177	185	86	343	203	216	53	71	116	190	37	89	141
Hf	5.31	5.56	3.07	9.50	6.09	5.70	1.38	1.91	3.25	5.82	1.05	2.33	4.3
Nb	14.08	15.30	6.22	9.48	16.28	8.41	3.18	5.12	8.52	11.12	3.09	0.85	12.38
Ta	1.09	1.08	0.40	0.79	1.16	0.58	0.18	0.32	0.60	0.79	0.21	0.09	0.84
Th	12.69	12.75	4.79	9.59	12.88	7.45	2.56	4.17	7.47	9.72	2.63	1.53	10.17
U	4.01	3.46	2.64	2.59	3.31	1.63	0.74	1.02	3.22	2.87	1.51	0.48	3.55
La	66.58	38.00	22.16	23.94	42.19	21.83	17.68	15.29	23.11	25.22	9.71	5.48	37.77
Ce	142.57	78.86	46.14	47.46	89.84	49.75	37.44	33.42	47.26	56.00	23.35	9.49	73.91
Pr	16.77	9.42	5.43	5.49	10.16	6.03	4.48	3.85	5.63	6.52	2.81	1.21	8.25
Nd	61.85	34.55	21.69	19.43	36.08	22.94	16.24	14.73	19.59	24.42	10.71	4.96	32.65
Sm	11.81	6.22	4.44	3.79	6.94	4.40	3.46	2.84	4.23	4.67	2.43	1.23	5.79
Eu	2.61	1.35	0.81	0.63	1.32	0.73	0.58	0.54	0.64	0.68	0.45	0.26	0.81
Gd	9.51	5.18	4.36	3.82	6.39	4.11	3.23	2.71	3.92	4.34	2.54	1.40	4.48
Tb	1.22	0.73	0.62	0.62	0.87	0.60	0.43	0.40	0.58	0.66	0.38	0.21	0.61
Dy	7.28	4.58	4.09	4.17	5.36	3.82	2.49	2.31	3.63	4.17	2.28	1.25	3.52
Ho	1.40	1.00	0.84	0.89	1.09	0.76	0.49	0.48	0.75	0.82	0.47	0.20	0.76
Er	4.08	2.98	2.43	2.71	3.23	2.27	1.31	1.44	2.21	2.56	1.33	0.58	2.28
Tm	0.62	0.45	0.34	0.40	0.52	0.34	0.18	0.19	0.35	0.39	0.18	0.08	0.36
Yb	4.08	3.16	2.27	2.72	3.39	2.19	1.27	1.43	2.21	2.67	1.28	0.57	2.42
Lu	0.57	0.43	0.33	0.40	0.46	0.33	0.18	0.18	0.34	0.36	0.17	0.06	0.35
Sc	23.5	20.1	11.8	9.0	22.1	13.0	21.7	21.8	12.5	14.5	17.3	6.4	8.7
V	120.3	113.9	41.2	37.0	68.5	20.7	13.3	36.2	33.1	27.9	16.1	2.3	49.1
Mo	0.5	0.2	0.4	0.6	0.4	0.5	0.2	0.3	0.7	0.8	0.0	0.0	0.3
Cr	137.3	133.3	64.5	71.1	101.9	35.9	13.7	35.8	43.9	43.8	24.9	3.0	6.5
Co	33.1	22.2	10.5	8.0	12.9	4.8	1.9	4.8	6.6	8.9	2.2	0.7	7.1
Ni	36.6	27.0	19.8	16.9	22.5	8.9	8.8	24.8	11.7	11.0	6.2	1.6	13.7
Cu	8.0	3.8	3.0	6.2	1.7	4.8	3.9	9.5	8.6	15.6	2.3	1.9	3.1
Zn	132.0	143.0	34.8	53.8	59.5	39.8	12.1	76.2	27.2	27.5	19.5	2.3	36.8
Sn	3.8	3.6	2.2	1.4	3.5	1.0	0.8	1.3	1.7	2.2	0.8	0.6	3.7
W	1.2	1.3	1.7	1.2	1.9	0.9	0.2	0.7	1.1	0.9	0.5	0.0	1.6
Pb	7.9	10.8	4.9	5.0	9.8	6.9	4.5	5.1	7.8	8.9	2.7	1.8	7.7
Cd	0.1	0.0	0.0	0.1	0.2	0.2	0.0	0.2	0.0	0.0	0.0	0.0	0.0
Tl	0.5	0.6	0.6	0.3	1.1	0.2	0.1	0.2	0.5	0.6	0.1	0.1	0.6
Ga	25.3	22.6	13.5	8.7	18.7	6.8	3.9	10.0	9.9	11.1	4.4	3.6	14.7
As	16.7	6.5	0.0	1.4	2.0	2.2	0.6	2.1	9.6	3.6	1.7	0.0	2.5
Ag	0.0	0.0	0.0	0.0	0.0	0.0	0.0	0.0	0.0	0.0	0.0	0.0	0.0
Sb	0.7	0.8	0.9	0.4	1.5	0.3	0.0	0.4	0.6	0.7	0.4	0.1	1.0
Labels chapter III	G57	G56	G55	G54	G53	G52	G51	G50	G49	G48	G47	G46	G45

Appendix IIIa (continued).

Formation Sample	Grinnell 26(12)G1	Grinnell 26(10)G1	Grinnell 26(9)G1	Grinnell 26(7)G1	Grinnell 26(6)G1	Grinnell 26(5)G1	Grinnell 26(4)G1	Grinnell 26(3)G1	Grinnell 26(2)Gl	Grinnell USO 27	Grinnell USO 25	Grinnell USO 24	Grinnell USO 23
SiO_2	61.23	74.08	99.64	94.62	67.54	97.24	58.63	96.82	65.12	66.70	58.00	65.00	91.20
TiO_2	0.48	0.46	0.04	0.07	0.51	0.04	0.62	0.03	0.45	0.55	0.31	0.61	0.06
Al_2O_3	13.75	12.36	0.21	2.45	14.02	1.22	19.19	1.17	12.50	15.70	10.60	13.70	4.65
Fe_2O_3	3.43	3.02	0.20	0.70	5.18	0.24	6.12	0.21	4.35	4.91	4.61	7.23	0.16
MnO	0.12	0.01	0.00	0.01	0.03	0.00	0.04	0.00	0.18	0.52	0.04	0.08	0.03
MgO	4.67	1.43	0.11	0.40	2.84	0.20	3.44	0.32	4.35	2.74	5.90	4.02	0.13
CaO	2.86	0.09	0.00	0.07	0.39	0.03	0.15	0.15	2.35	0.33	6.29	0.73	0.12
K_2O	6.58	6.73	0.16	1.20	6.55	0.77	7.89	0.57	3.93	5.21	1.99	3.80	1.36
Na_2O	0.36	0.14	0.00	0.00	0.07	0.01	0.28	0.03	0.80	0.74	1.81	1.13	1.73
P_2O_5	0.10	0.06	0.00	0.04	0.14	0.00	0.10	0.02	0.11	0.08	0.10	0.19	0.02
LOI	6.50	1.65	0.15	0.55	2.90	0.25	3.70	0.20	5.70	3.15	10.20	3.55	0.30
Sum	100.0	100.0	100.5	100.1	100.1	100.0	100.1	99.5	99.8	100.6	99.8	100.0	99.7
Li (ppm)	89	40	9	25	74	17	81	18	15	50	64	77	5
Rb	166	158	3	31	166	14	243	17	13	200	73	140	24
Sr	25	17	2	6	20	5	13	114	47	19	50	48	88
Cs	9	10	0	2	11	1	16	1	1	12	4	9	1
Ba	331	358	37	85	380	105	393	6525	2041	492	295	465	4661
Y	33.9	20.1	4.4	9.5	26.5	6.7	32.9	18.8	7.4	30.1	26.1	27.7	6.5
Zr	189	120	10	37	161	27	188	17	19	173	117	202	39
Hf	6.0	4.7	0.2	1.1	5.6	0.7	6.2	0.7	0.6	6.2	3.8	6.6	1.0
Nb	15.28	16.12	0.68	1.58	13.47	0.94	16.89	0.58	0.94	11.63	6.84	12.69	0.87
Ta	1.09	1.28	0.03	0.10	0.92	0.07	1.06	0.04	0.07	1.02	0.57	1.05	0.06
Th	13.68	15.68	1.56	2.05	11.79	1.63	13.97	1.43	1.18	14.35	8.48	11.85	1.11
U	4.45	3.64	0.38	0.67	3.22	0.41	4.67	0.39	0.51	3.90	1.86	4.58	0.48
La	41.92	31.30	3.47	7.67	38.98	5.84	46.65	11.92	4.79	43.39	50.77	34.83	5.73
Ce	84.63	63.88	8.32	17.12	82.16	11.60	100.22	20.89	8.65	90.56	98.62	72.41	6.70
Pr	9.85	7.56	1.01	1.93	9.17	1.35	11.37	2.64	1.08	10.36	11.39	8.51	0.98
Nd	38.77	27.68	3.95	7.94	35.72	5.13	41.56	11.13	4.59	38.58	44.07	33.17	3.54
Sm	7.63	4.68	0.82	1.57	5.84	1.18	7.27	3.00	1.30	7.36	9.33	7.31	0.76
Eu	1.07	0.69	0.14	0.31	0.98	0.22	1.29	0.62	0.25	1.32	1.84	1.33	0.21
Gd	6.30	3.58	0.78	1.75	5.16	1.34	6.81	3.75	1.60	6.94	8.46	6.81	1.07
Tb	1.01	0.58	0.14	0.30	0.77	0.21	0.97	0.59	0.27	0.95	1.06	0.92	0.17
Dy	6.07	3.56	0.77	1.74	4.88	1.29	6.31	3.27	1.38	5.93	5.64	5.51	1.10
Ho	1.26	0.75	0.16	0.35	1.03	0.24	1.29	0.60	0.26	1.20	0.99	1.09	0.21
Er	3.91	2.40	0.40	0.98	2.96	0.65	3.84	1.48	0.65	3.62	2.75	3.24	0.54
Tm	0.62	0.38	0.06	0.13	0.46	0.09	0.60	0.20	0.09	0.54	0.38	0.47	0.08
Yb	4.29	2.69	0.33	0.85	3.10	0.59	4.16	1.15	0.57	3.60	2.60	3.11	0.51
Lu	0.61	0.40	0.06	0.13	0.47	0.07	0.61	0.15	0.08	0.56	0.39	0.49	0.07
Sc	12.4	9.3	0.2	1.8	11.7	0.7	17.5	0.7	0.8	12.5	9.2	11.1	0.7
V	56.1	41.9	1.5	9.1	55.0	3.5	72.5	3.4	6.4	72.7	38.9	69.6	3.0
Mo	0.3	0.3	0.1	0.1	0.3	0.1	0.6	0.6	0.1	0.5	0.7	0.4	0.1
Cr	7.6	6.2	0.7	1.4	10.1	0.8	11.7	0.5	1.0	75.9	103.3	30.0	10.8
Co	8.2	6.0	0.6	1.8	11.5	0.7	12.3	1.4	1.3	6.9	14.8	11.0	5.5
Ni	17.1	11.7	1.3	4.0	21.5	1.9	21.2	2.3	3.1	17.8	17.3	27.4	2.8
Cu	2.9	2.1	3.5	12.9	2.3	1.6	14.0	3.4	1.6	1.8	3.3	3.8	2.6
Zn	72.4	34.7	4.4	11.6	67.3	6.0	70.4	13.2	13.0	50.1	62.7	93.4	11.9
Sn	7.2	6.3	3.7	3.9	6.5	1.2	7.5	1.2	3.5	2.4	3.4	2.5	1.5
W	1.8	1.8	0.1	0.1	1.9	0.1	2.0	0.0	0.1	2.8	3.4	1.7	11.2
Pb	9.2	11.3	2.6	2.9	17.1	2.6	19.6	4.5	6.7	15.2	17.3	14.2	2.9
Cd	0.0	0.0	0.0	0.0	0.0	0.0	0.1	0.0	0.0	0.0	0.0	0.1	0.0
Tl	0.7	0.7	0.0	0.1	0.8	0.1	1.1	0.1	0.1	1.0	0.3	0.7	0.1
Ga	18.6	13.3	0.3	3.0	17.8	1.0	26.4	0.0	0.0	12.1	21.2	16.5	5.6
As	11.4	6.7	1.2	2.8	7.7	3.0	10.2	4.6	2.4	3.5	7.4	4.2	0.9
Ag	0.0	0.0	0.0	0.0	0.0	0.0	0.0	0.0	0.0	0.4	0.3	0.4	0.1
Sb	1.8	1.4	0.1	0.3	2.2	0.2	2.2	0.1	0.2	0.7	1.2	1.0	0.2
Labels chapter III	G44	G43	G42	G41	G40	G39	G38	G37	G36	G35	G34	G33	G32

Appendix IIIa (continued).

Formation Sample	App. 26 Gl Uso	App. USO 10	App. USO 12	App. USO 8	App. 25 Gl Uso	App. USO 9	App. USO 11	App. USO 7	App. USO 6	App. USO 5	App. USO 4	App. USO 3	App. USO 2
SiO_2	96.40	12.70	68.50	92.00	69.50	90.50	61.80	97.50	66.70	68.10	69.50	68.90	73.50
TiO_2	0.09	0.10	0.52	0.04	0.49	0.04	0.43	0.02	0.62	0.59	0.47	0.45	0.44
Al_2O_3	1.12	2.41	13.60	2.14	12.60	3.29	10.80	0.92	16.30	14.80	13.00	12.60	11.60
Fe_2O_3	0.34	1.60	4.73	1.34	3.54	1.38	4.69	0.37	4.37	4.45	3.72	3.62	2.55
MnO	0.02	0.11	0.03	0.05	0.07	0.06	0.19	0.18	0.02	0.06	0.06	0.11	0.04
MgO	0.43	17.40	2.74	1.46	3.70	1.53	5.29	0.09	2.77	2.67	3.94	3.87	2.90
CaO	0.27	25.70	1.15	0.80	1.17	0.55	4.65	0.18	0.26	0.38	0.92	1.47	0.90
K_2O	0.22	0.92	4.53	0.34	3.62	0.69	2.96	0.20	4.92	4.25	3.56	3.51	3.43
Na_2O	0.29	0.06	0.65	0.25	1.44	0.53	0.80	0.26	1.25	1.65	1.47	1.55	1.66
P_2O_5	0.02	0.03	0.12	0.05	0.12	0.08	0.12	0.06	0.09	0.08	0.10	0.09	0.09
LOI	0.85	39.10	3.50	1.65	3.95	1.60	8.55	0.30	2.75	2.60	3.50	3.95	2.90
Sum	100.0	100.1	100.0	100.1	100.2	100.2	100.2	100.0	100.0	99.6	100.2	100.1	100.0
Li (ppm)	13	17	50	24	44	27	48	6	54	48	56	56	45
Rb	7	29	198	13	118	23	115	6	191	162	133	126	120
Sr	10	48	53	34	44	10	51	7	27	32	37	59	53
Cs	1	1	10	0	7	1	5	0	10	7	7	7	6
Ba	243	76	1273	691	721	183	570	170	595	562	544	964	1142
Y	4.5	13.9	26.8	7.1	33.2	9.0	25.9	4.1	36.7	28.7	32.6	31.5	31.6
Zr	14	31	182	43	191	37	156	22	203	236	255	220	289
Hf	0.4	0.9	5.5	1.0	6.4	0.9	4.8	0.7	6.6	7.5	7.7	6.5	8.5
Nb	0.47	2.44	11.85	0.74	9.02	0.70	9.80	0.25	13.58	11.78	10.95	9.29	10.79
Ta	0.04	0.15	0.89	0.06	0.61	0.07	0.73	0.03	1.05	0.91	0.80	0.66	0.74
Th	0.83	2.47	11.83	1.71	10.13	1.79	9.37	1.25	13.31	11.83	9.84	10.23	9.15
U	0.45	0.71	2.90	0.63	2.98	0.56	2.08	0.42	3.37	3.35	2.74	3.16	2.68
La	3.06	14.76	43.96	5.54	28.46	14.08	31.69	3.60	46.13	33.78	32.04	29.20	32.45
Ce	5.61	30.84	85.54	13.61	56.10	30.76	64.01	8.37	100.39	70.32	68.07	61.74	65.36
Pr	0.84	3.81	9.25	1.63	7.47	3.74	7.44	0.98	11.45	8.11	8.15	7.47	8.14
Nd	3.42	14.89	34.59	5.56	30.15	14.40	28.45	3.47	44.97	31.83	32.51	30.48	31.69
Sm	0.87	3.48	7.33	1.27	6.58	2.87	6.41	0.82	9.52	6.89	7.30	6.97	7.03
Eu	0.18	0.78	1.28	0.22	1.16	0.51	1.26	0.16	1.81	1.25	1.37	1.31	1.30
Gd	0.99	3.47	5.99	1.32	6.40	2.43	6.12	0.83	8.99	6.00	6.81	6.59	6.48
Tb	0.14	0.45	0.85	0.23	0.94	0.30	0.84	0.14	1.19	0.84	0.93	0.92	0.91
Dy	0.84	2.63	4.91	1.19	6.27	1.61	4.80	0.82	7.34	5.18	5.86	5.69	5.65
Ho	0.16	0.49	1.00	0.23	1.29	0.30	0.93	0.15	1.41	1.09	1.20	1.14	1.17
Er	0.43	1.30	2.91	0.68	3.98	0.78	2.70	0.41	4.04	3.31	3.66	3.50	3.45
Tm	0.06	0.17	0.47	0.10	0.60	0.11	0.41	0.06	0.60	0.52	0.56	0.53	0.57
Yb	0.37	1.10	3.13	0.62	4.11	0.70	2.57	0.37	3.89	3.60	3.80	3.58	3.59
Lu	0.05	0.17	0.48	0.09	0.60	0.11	0.39	0.06	0.60	0.57	0.61	0.57	0.58
Sc	1.8	6.8	12.0	1.3	15.3	1.4	11.2	0.6	15.2	12.3	10.5	10.1	8.5
V	5.7	15.5	61.4	10.1	32.4	13.2	54.9	2.9	72.4	56.0	41.5	36.6	36.3
Mo	6.5	0.2	0.2	0.1	1.6	0.2	0.2	0.2	0.3	0.3	1.3	0.3	0.5
Cr	12.9	23.5	89.6	14.2	36.9	19.2	69.4	14.0	91.1	63.8	61.2	70.2	78.4
Co	1.4	5.5	11.6	6.2	5.3	5.4	10.4	3.2	11.4	7.3	8.9	10.0	11.3
Ni	45.3	7.2	21.9	6.3	26.0	7.3	23.8	7.7	51.3	19.9	16.1	19.6	15.9
Cu	33.2	3.2	2.7	1.8	8.8	1.3	3.3	6.8	29.2	7.2	38.9	10.7	5.8
Zn	23.4	6.5	58.3	24.0	58.6	28.0	50.1	7.2	58.5	50.4	65.2	72.8	91.0
Sn	2.0	0.8	3.5	2.8	3.1	0.8	2.4	2.9	3.0	2.8	2.5	3.1	3.4
W	0.2	35.6	4.9	11.6	1.0	0.3	1.8	0.2	4.3	1.0	3.6	1.4	5.1
Pb	4.8	2.2	3.4	1.3	3.0	1.3	3.5	2.3	3.6	4.7	15.3	4.0	8.5
Cd	0.0	0.0	0.0	0.0	0.0	0.0	0.0	0.0	0.1	0.0	0.0	0.0	0.1
Tl	0.0	0.1	0.8	0.0	0.5	0.1	0.5	0.0	0.9	0.7	0.5	0.5	0.5
Ga	0.2	3.3	12.7	0.0	17.1	4.3	9.7	1.3	19.4	11.0	13.8	12.7	19.8
As	6.2	1.6	1.5	0.7	1.0	0.6	1.1	1.5	2.1	3.9	0.9	1.4	1.9
Ag	0.1	0.1	0.4	0.1		0.1	0.3	0.1	0.6	0.6	0.6	0.7	0.5
Sb	1.6	0.2	1.0	0.1	0.6	0.2	0.5	0.4	1.0	0.7	0.7	0.7	0.6
Labels chapter III	G31	G30	G29	G28	G27	G26	G25	G24	G23	G22	G21	G20	G19

Appendix IIIa (continued).

Formation	App.	App.	App.	App.	App.	App.	App.	App.	App.	App.	App.	App.	Altyn
Sample	USO 1	USO 19	USO 20	USO 26	USO 22	USO 18	USO 17	USO 16	USO 21	USO 15	USO 14	USO 13	24G1USO
SiO_2	71.60	96.20	75.30	76.70	85.80	90.10	74.60	86.00	98.40	71.60	86.70	69.60	13.20
TiO_2	0.39	0.02	0.29	0.12	0.06	0.03	0.49	0.07	0.02	0.57	0.07	0.49	0.14
Al_2O_3	11.50	1.31	9.57	5.26	6.88	5.34	11.00	7.03	0.55	13.50	5.75	13.40	3.11
Fe_2O_3	3.41	0.27	4.14	1.80	0.72	0.42	4.07	0.87	0.25	2.02	0.64	4.75	1.19
MnO	0.12	0.02	0.04	0.13	0.02	0.01	0.02	0.02	0.02	0.01	0.02	0.07	0.04
MgO	2.17	0.41	4.23	3.54	1.27	0.92	2.78	1.50	0.28	3.16	1.23	2.59	17.80
CaO	2.68	0.40	0.72	3.78	0.53	0.13	0.31	0.11	0.11	0.30	0.80	0.59	25.40
K_2O	2.14	0.63	1.26	0.88	1.48	1.65	3.03	2.54	0.17	5.61	2.32	4.63	0.94
Na_2O	3.07	0.00	1.91	1.60	2.19	1.06	1.40	0.90	0.00	0.47	1.18	0.57	0.32
P_2O_5	0.10	0.03	0.08	0.05	0.03	0.05	0.13	0.02	0.03	0.10	0.03	0.11	0.03
LOI	3.00	0.85	2.70	6.15	1.25	0.65	2.25	1.20	0.30	2.85	1.35	3.10	38.20
Sum	100.1	100.1	100.2	100.0	100.2	100.3	100.0	100.2	100.1	100.1	100.0	99.9	100.4
Li (ppm)	33	9	93	32	21	19	44	23	11	102	29	48	39
Rb	73	14	39	24	38	38	106	62	4	163	44	193	31
Sr	57	21	32	29	28	10	40	19	3	28	28	47	61
Cs	3	0	1	1	1	1	4	1	0	12	1	9	2
Ba	293	754	205	245	331	146	838	365	37	1551	607	1167	87
Y	26.5	2.5	17.6	17.6	2.6	4.9	23.4	5.7	4.2	12.7	3.9	30.4	15.0
Zr	248	12	163	220	43	23	282	52	15	208	37	156	30
Hf	7.3	0.3	4.4	5.2	1.1	0.5	8.2	1.0	0.4	6.1	0.8	5.1	0.84
Nb	9.81	0.30	6.66	2.82	0.85	0.31	11.34	1.04	0.17	11.14	1.57	11.90	1.39
Ta	0.71	0.03	0.49	0.20	0.07	0.04	0.88	0.09	0.01	0.87	0.12	1.00	0.11
Th	9.04	1.07	6.04	2.95	1.40	1.26	10.81	1.50	0.78	11.70	1.43	11.76	2.21
U	2.39	0.35	1.63	0.89	0.35	0.51	2.17	0.54	0.31	2.51	0.44	2.80	1.15
La	28.41	4.63	18.67	11.02	6.83	8.13	38.84	5.84	2.40	32.69	5.31	45.10	17.25
Ce	60.20	5.34	38.48	21.70	10.31	13.53	80.41	8.69	3.80	55.55	8.84	90.93	36.78
Pr	7.38	0.83	4.82	2.72	1.28	2.00	9.23	1.43	0.64	5.78	1.14	10.60	3.82
Nd	29.19	3.10	18.96	11.17	4.58	7.07	34.50	4.87	2.59	19.79	4.23	41.58	14.01
Sm	7.05	0.69	4.12	3.05	0.97	1.36	6.64	0.91	0.69	3.03	0.92	7.97	2.62
Eu	1.21	0.13	0.71	0.73	0.24	0.34	1.11	0.30	0.16	0.55	0.19	1.42	0.48
Gd	6.51	0.65	3.80	3.87	0.80	1.18	5.62	1.02	0.87	2.40	0.79	7.21	2.59
Tb	0.87	0.10	0.55	0.59	0.10	0.16	0.76	0.18	0.15	0.32	0.10	0.98	0.36
Dy	5.02	0.49	3.26	3.67	0.49	0.82	4.47	0.97	0.72	2.07	0.63	5.71	2.12
Ho	1.01	0.09	0.67	0.66	0.10	0.15	0.88	0.19	0.15	0.46	0.13	1.12	0.45
Er	2.91	0.28	1.95	1.74	0.30	0.43	2.63	0.54	0.38	1.56	0.38	3.47	1.25
Tm	0.45	0.04	0.29	0.25	0.04	0.06	0.40	0.08	0.05	0.27	0.05	0.55	0.17
Yb	2.97	0.30	2.01	1.59	0.32	0.42	2.65	0.54	0.30	1.88	0.38	3.41	1.09
Lu	0.47	0.04	0.32	0.25	0.05	0.06	0.42	0.09	0.05	0.31	0.06	0.53	0.14
Sc	8.1	0.8	5.2	3.0	1.7	0.7	7.6	1.4	0.4	10.1	1.7	10.7	12.7
V	31.7	2.1	28.6	10.2	9.4	3.8	36.5	8.3	1.6	49.4	6.6	61.4	14.8
Mo	0.4	0.2	0.3	0.6	0.2	0.2	0.4	0.1	0.2	0.5	0.1	0.4	0.0
Cr	65.7	4.7	32.5	55.4	7.5	3.6	73.5	12.6	4.2	71.6	8.3	79.1	16.3
Co	13.6	3.3	4.4	6.5	3.5	3.2	11.7	3.3	5.6	7.1	4.3	13.8	3.1
Ni	25.4	3.8	12.9	7.6	22.7	2.1	21.0	2.8	1.1	17.2	12.6	23.5	8.9
Cu	20.3	1.8	7.1	3.2	4.1	6.1	2.7	9.5	3.1	13.0	12.4	2.4	3.9
Zn	84.9	6.2	55.1	26.8	43.6	4.2	33.9	14.7	5.2	23.2	6.2	48.3	16.0
Sn	2.2	3.8	2.4	0.5	3.2	0.5	2.2	1.1	0.4	3.0	0.4	2.9	0.6
W	4.2	8.3	0.7	0.3	0.2	0.3	7.0	0.4	15.6	33.2	8.6	1.5	0.0
Pb	12.7	1.0	10.8	8.8	3.2	1.9	4.8	4.3	1.2	16.8	9.0	3.2	4.8
Cd	0.0	0.0	0.0	0.0	0.0	0.0	0.1	0.0	0.0	0.0	0.0	0.0	0.0
Tl	0.3	0.1	0.2	0.1	0.1	0.2	0.4	0.2	0.0	0.6	0.2	0.8	0.2
Ga	13.7	1.7	10.4	3.7	0.0	2.6	11.0	7.6	0.6	7.9	0.0	11.3	4.8
As	4.8	1.7	1.5	4.4	1.1	0.6	2.8	0.6	0.8	3.6	5.7	1.5	2.6
Ag	0.5	0.0	0.3	0.2	0.1	0.0	0.4	0.1	0.0	0.5	0.1	0.4	0.0
Sb	0.6	0.2	0.5	0.2	0.4	0.1	1.4	0.3	0.1	1.5	0.2	1.0	0.3
Labels chapter III	G18	G17	G16	G15	G14	G13	G12	G11	G10	G9	G8	G7	G6

Appendix IIIa (continued).

Formation	Altyn	Altyn	Waterton	Waterton	Waterton
Sample	24(2)G1	24(1)G1	23G1USO	23(2)G1	23(1)G1
SiO_2	36.13	4.05	16.40	25.85	45.63
TiO_2	0.17	0.04	0.19	0.30	0.34
Al_2O_3	5.27	0.56	4.05	6.03	12.32
Fe_2O_3	0.60	0.41	1.37	1.19	1.19
MnO	0.01	0.12	0.02	0.02	0.00
MgO	12.02	0.96	17.10	13.53	8.92
CaO	16.86	51.93	22.80	19.22	8.51
K_2O	2.68	0.08	1.98	4.02	9.33
Na_2O	0.45	0.05	0.11	0.10	0.10
P_2O_5	0.06	0.06	0.03	0.03	0.03
LOI	26.00	41.60	36.10	30.00	13.95
Sum	100.4	99.9	100.1	100.3	100.4
Li (ppm)	74	4	85	43	152
Rb	46	3	40	67	138
Sr	46	347	30	28	20
Cs	3	0	1	2	3
Ba	870	330	108	207	234
Y	13.9	3.8	11.7	12.6	23.5
Zr	134	6	40	61	238
Hf	3.26	0.15	1.14	1.63	7.47
Nb	1.67	0.75	4.36	8.62	17.71
Ta	0.13	0.03	0.24	0.47	1.24
Th	4.31	0.24	3.47	6.02	16.90
U	1.84	1.15	0.65	2.07	4.02
La	13.57	2.21	14.17	13.21	55.52
Ce	27.55	3.42	27.32	25.59	99.92
Pr	3.13	0.40	3.38	3.13	11.05
Nd	11.12	1.52	12.32	11.39	34.75
Sm	2.27	0.24	2.17	2.04	4.34
Eu	0.41	0.06	0.38	0.35	0.52
Gd	2.03	0.26	1.94	1.86	3.32
Tb	0.29	0.04	0.25	0.26	0.52
Dy	1.97	0.27	1.52	1.62	3.77
Ho	0.39	0.06	0.32	0.35	0.89
Er	1.27	0.20	0.92	1.10	2.86
Tm	0.20	0.03	0.14	0.17	0.46
Yb	1.12	0.18	0.84	1.07	3.24
Lu	0.15	0.01	0.11	0.15	0.44
Sc	14.6	6.5	14.5	16.1	12.7
V	21.2	7.0	14.5	26.5	20.9
Mo	0.4	0.5	0.0	0.3	0.2
Cr	22.2	4.8	21.8	30.5	20.6
Co	1.5	1.2	3.2	3.8	3.9
Ni	5.9	10.5	9.6	9.1	9.1
Cu	12.7	2.1	33.0	9.1	3.3
Zn	12.8	7.7	14.3	18.4	14.7
Sn	1.1	0.2	0.9	1.0	3.2
W	0.5	0.0	0.3	0.4	0.6
Pb	4.5	2.3	2.6	15.0	13.3
Cd	0.0	0.0	0.0	0.0	0.1
Tl	0.3	0.1	0.1	0.3	0.3
Ga	4.1	2.5	5.7	7.4	14.3
As	0.0	0.5	0.9	0.6	2.0
Ag	0.1	0.0	0.0	0.0	0.0
Sb	0.3	0.1	0.0	0.1	0.3
Labels chapter III	G5	G4	G3	G2	G1

Sample order is from the upper sequence (left) to the lower sequence (right). (App.) Appekuny.

Appendix IIIb. Major and trace element concentration of the Belt-Purcell Supergroup at the Purcell Mountains.

Formation	Roosville	Roosville	Roosville	Phillips	Phillips	Phillips	Gateway	Gateway	Gateway	Van Creek	Van Creek	Van Creek	Kitchener	Kitchener
Sample	22(1)Pu	22(2)Pu	22PuUSO	21(2)Pu	21(1)Pu	21PuUSO	19(2)Pu	19(1)Pu	19PuUSO	18PuUSO	18(2)PU	18(1)Pu	17(2)Pu	17(1)Pu
SiO_2 (wt%)	68.61	66.19	8.64	71.88	61.02	78.90	71.41	67.53	62.90	68.80	83.00	54.59	46.57	88.99
TiO_2	0.47	0.63	0.08	0.40	0.85	0.46	0.58	0.54	0.52	0.72	0.34	0.58	0.30	0.12
Al_2O_3	13.55	18.27	0.80	11.91	18.82	9.88	16.17	12.30	11.50	15.30	7.81	14.02	6.82	4.60
Fe_2O_3	2.92	3.77	0.85	2.98	6.79	2.95	1.59	4.08	2.90	4.62	2.75	1.83	2.57	1.88
MnO	0.06	0.00	0.10	0.01	0.01	0.00	0.00	0.30	0.05	0.01	0.09	0.01	0.10	0.02
MgO	3.32	1.84	19.00	1.34	2.01	1.18	1.69	4.45	5.23	2.06	1.04	6.31	8.41	1.50
CaO	1.71	0.13	28.40	2.70	0.16	0.44	0.19	1.86	4.39	0.22	0.17	6.11	16.53	0.27
K_2O	3.60	5.34	0.31	3.52	6.08	2.51	5.45	3.29	4.05	4.48	2.15	5.15	1.44	1.44
Na_2O	1.43	0.45	0.03	1.66	1.18	2.04	0.27	0.06	0.38	1.23	1.23	0.67	0.05	0.10
P_2O_5	0.10	0.06	0.03	1.83	0.10	0.03	0.09	0.12	0.09	0.08	0.06	0.11	0.07	0.04
LOI	4.40	3.30	41.90	1.85	3.00	1.75	2.60	5.60	8.30	2.60	1.40	10.70	17.35	1.20
Sum	100.3	100.1	100.1	100.2	100.2	100.2	100.2	100.3	100.3	100.2	100.1	100.3	100.3	100.2
Li (ppm)	50	35	19	34	30	65	30	63	57	69	40	259	65	13
Rb	134	199	18	139	254	72	186	111	131	128	61	206	72	62
Sr	21	7	46	50	21	87	28	21	46	25	21	30	87	9
Cs	3	9	0	6	8	4	5	3	3	9	3	18	4	2
Ba	442	392	50	371	1044	169	513	255	392	575	316	675	169	324
Y	27.1	24.7	7.8	34.3	28.5	16.5	30.4	30.6	21.4	28.0	22.3	31.4	23.9	20.1
Zr	285	189	20	280	217	116	279	423	79	168	187	294	127	62
Hf	8.41	6.36	0.50	8.15	6.67	3.93	8.87	12.86	2.79	5.62	5.21	9.17	3.58	1.80
Nb	13.06	13.37	1.19	9.81	20.45	6.18	15.44	13.91	8.25	10.78	5.32	18.76	8.67	2.46
Ta	1.03	1.24	0.07	0.80	1.54	0.60	1.32	1.13	0.81	0.75	0.57	1.40	0.61	0.20
Th	11.98	15.34	1.02	8.88	16.15	4.89	15.10	13.21	5.66	8.65	6.63	19.25	8.27	3.83
U	3.56	3.05	1.06	6.35	5.29	1.92	4.69	3.30	3.17	3.74	2.17	6.18	1.92	0.94
La	33.29	48.79	7.21	19.75	51.45	23.55	32.04	33.31	37.29	34.11	16.61	46.98	26.54	21.77
Ce	66.09	104.41	16.45	48.79	104.95	44.00	61.01	80.88	57.00	62.00	38.52	101.72	58.69	48.09
Pr	7.77	12.32	1.91	6.37	11.58	5.60	6.83	9.44	8.33	8.09	4.26	11.61	6.86	5.72
Nd	27.52	45.62	7.31	30.82	41.87	22.52	23.82	36.25	32.43	30.63	16.44	40.70	25.60	21.41
Sm	5.40	8.35	1.32	11.26	7.79	4.08	4.50	6.92	5.79	5.68	3.28	7.00	4.88	4.04
Eu	0.84	1.34	0.24	2.96	1.54	0.73	0.73	1.05	1.03	1.09	0.70	0.88	0.76	0.68
Gd	4.90	6.35	1.27	14.44	6.43	3.68	4.43	6.28	4.55	5.24	3.84	5.57	4.60	4.10
Tb	0.74	0.79	0.18	1.75	0.87	0.51	0.68	0.89	0.62	0.77	0.65	0.74	0.67	0.58
Dy	4.66	4.46	1.07	8.19	5.20	3.26	5.03	5.83	4.00	5.34	4.14	5.25	4.07	3.54
Ho	1.06	0.96	0.23	1.28	1.07	0.62	1.10	1.19	0.77	1.14	0.82	1.17	0.84	0.69
Er	3.39	3.08	0.66	3.27	3.46	1.75	3.58	3.84	2.35	3.33	2.50	3.79	2.50	1.99
Tm	0.54	0.51	0.09	0.45	0.55	0.27	0.54	0.61	0.36	0.52	0.36	0.62	0.38	0.27
Yb	3.86	3.57	0.58	3.03	3.74	1.81	3.88	4.08	2.40	3.37	2.56	4.39	2.69	1.62
Lu	0.53	0.52	0.07	0.43	0.53	0.27	0.57	0.61	0.36	0.50	0.35	0.60	0.36	0.21
Sc	14.9	20.6	10.8	12.7	30.0	13.5	14.0	15.2	18.2	21.0	7.3	15.6	14.4	3.5
V	52.0	58.6	9.3	50.3	99.6	27.0	59.6	46.4	65.7	85.3	31.3	46.5	27.0	13.7
Mo	0.8	0.7	0.0	0.4	0.7	0.1	1.7	4.8	0.6	0.4	2.1	1.4	0.1	2.0
Cr	78.1	78.6	10.1	70.6	170.7	49.4	57.2	92.6	77.6	119.7	56.2	50.0	49.4	34.4
Co	7.4	9.7	1.2	14.5	13.5	4.8	13.5	59.3	10.3	14.2	15.8	10.2	4.8	6.1
Ni	10.7	11.1	6.0	18.2	18.1	10.8	14.5	42.9	14.8	20.3	20.2	15.0	10.8	8.5
Cu	0.0	3.7	2.4	1.4	0.0	3.0	24.7	209.6	5.5	11.4	21.9	25.9	3.0	3.6
Zn	10.8	35.9	82.7	17.7	0.0	31.9	11.1	15.7	10.7	47.4	6.9	15.1	31.9	35.9
Sn	3.8	5.0	0.3	2.0	4.0	1.6	5.3	2.9	3.4	3.4	1.7	3.4	1.6	1.1
W	2.0	2.0	0.0	1.1	2.7	1.2	2.6	4.8	1.1	2.5	1.7	2.2	1.2	1.1
Pb	3.7	2.6	27.2	9.0	6.4	4.4	27.1	12.1	7.1	7.4	12.6	33.1	4.4	2.8
Cd	0.2	0.0	0.3	0.0	0.0	0.4	0.0	0.0	0.0	0.3	0.0	0.0	0.4	0.0
Tl	0.6	0.7	0.0	0.7	1.2	0.3	0.8	1.6	0.4	0.5	0.7	1.2	0.3	0.4
Ga	14.9	23.0	1.1	14.7	24.8	8.3	21.1	14.2	14.3	18.2	8.7	16.7	8.3	6.3
As	2.7	6.3	1.2	3.6	0.9	8.1	47.8	6.1	1.7	1.1	5.8	23.7	8.1	0.8
Ag	0.0	0.0	0.0	0.0	0.0	0.0	0.1	0.0	0.0	0.1	0.1	0.0	0.0	0.0
Sb	0.8	1.1	0.4	0.8	1.3	0.3	5.1	2.5	0.8	0.6	1.0	3.6	0.3	0.3
Labels chapter III	P27	P26	P25	P24	P23	P22	P21	P20	P19	P18	P17	P16	P15	P14

Appendix IIIb (continued).

Formation	Kitchener	Creston	Creston	Creston	Creston	Creston	Creston	Aldridge	Aldridge	Aldridge	Fort Steele	Fort Steele	Fort Steele
Sample	17PuUSO	16(5)PU	16(4)Pu	16(3)PU	16(2)PU	16(1)PU	16PuUSO	14(1)Pu	14PuUSO	14(2)Pu	FT(3)PU	FT(2)Pu	FT(1)Pu
SiO_2 (wt%)	50.80	75.52	70.93	73.03	77.71	75.68	62.00	65.09	83.70	79.22	90.06	55.90	59.46
TiO_2	0.25	0.47	0.58	0.50	0.43	0.40	0.49	0.57	0.39	0.44	0.14	0.40	0.96
Al_2O_3	7.74	12.39	14.98	13.32	11.72	10.78	12.80	15.43	8.48	9.68	4.42	10.11	19.69
Fe_2O_3	3.84	2.78	4.13	4.23	3.12	4.46	4.34	8.71	2.13	3.26	1.65	3.46	5.85
MnO	0.11	0.02	0.04	0.05	0.01	0.00	0.10	0.06	0.02	0.04	0.00	0.07	0.02
MgO	9.70	1.85	1.49	1.21	0.67	3.33	7.73	2.23	0.78	1.08	1.66	7.54	4.32
CaO	14.60	0.19	0.22	0.39	0.02	0.07	2.67	0.18	0.14	0.68	0.05	10.87	0.12
K_2O	4.40	2.85	3.89	2.47	3.39	2.59	1.12	3.40	1.98	2.39	0.96	3.71	5.12
Na_2O	1.16	1.89	1.10	2.44	0.76	0.10	3.63	1.08	1.21	1.26	0.07	3.14	0.24
P_2O_5	0.07	0.12	0.05	0.04	0.03	0.04	0.09	0.12	0.03	0.04	0.00	0.08	0.10
LOI	7.35	1.95	2.55	2.30	2.15	2.75	4.30	3.15	1.15	1.80	1.15	4.75	4.05
Sum	100.2	100.1	100.2	100.1	100.1	100.3	99.3	100.2	100.1	100.0	100.2	100.2	100.1
Li (ppm)	0	8	22	20	22	16	40	68	12	29	10	0	19
Rb	50	124	187	120	149	112	58	173	94	122	21	46	116
Sr	65	12	48	116	17	9	91	69	47	110	4	73	9
Cs	0	4	8	7	3	4	4	21	6	8	0	0	1
Ba	1579	349	966	562	544	289	174	648	351	379	108	923	704
Y	12.6	35.2	42.7	65.7	36.0	41.6	22.6	29.3	7.1	23.8	3.8	23.9	30.7
Zr	66	212	341	394	247	239	92	216	53	337	178	120	290
Hf	1.96	6.06	10.14	11.82	7.20	6.81	3.16	6.30	1.72	9.58	4.74	3.74	8.32
Nb	6.08	11.79	19.99	15.82	9.61	7.90	8.59	12.19	6.69	11.42	1.65	11.22	19.19
Ta	0.39	0.89	1.48	1.24	1.14	0.79	0.67	1.13	0.54	1.03	0.22	0.75	1.40
Th	4.40	11.77	17.58	15.61	12.70	10.86	7.26	12.81	4.56	13.26	2.42	8.97	13.42
U	1.65	2.55	4.34	3.75	3.36	2.03	2.75	3.12	2.09	2.58	0.63	2.60	2.25
La	13.94	69.99	57.80	52.33	32.00	41.60	26.37	10.72	3.69	16.41	6.13	28.18	45.70
Ce	28.52	152.68	128.03	117.25	72.24	92.20	50.00	32.09	5.00	36.54	14.12	58.62	97.75
Pr	3.56	17.96	14.88	13.73	8.18	10.85	6.03	3.06	0.88	4.54	1.59	6.77	11.17
Nd	12.98	66.27	54.12	50.32	29.85	39.21	24.50	11.86	3.35	16.01	5.10	25.43	41.20
Sm	2.46	12.67	10.61	10.20	5.80	7.88	4.48	2.67	0.69	3.22	0.96	4.91	7.12
Eu	0.39	2.06	1.56	1.53	1.06	1.54	0.79	0.56	0.12	0.69	0.14	1.00	2.02
Gd	2.20	8.35	9.11	10.64	6.18	7.59	4.45	3.75	0.71	2.98	0.86	4.67	6.54
Tb	0.32	1.02	1.29	1.71	0.94	1.13	0.63	0.70	0.13	0.51	0.12	0.68	0.94
Dy	2.05	6.31	7.88	11.30	6.51	7.23	4.31	5.06	1.03	3.79	0.64	4.11	5.47
Ho	0.44	1.30	1.54	2.37	1.33	1.51	0.86	1.12	0.25	0.91	0.14	0.86	1.15
Er	1.37	3.75	4.72	7.01	3.99	4.54	2.50	3.52	0.91	2.91	0.40	2.65	3.28
Tm	0.21	0.56	0.71	0.98	0.57	0.65	0.36	0.50	0.16	0.46	0.06	0.39	0.46
Yb	1.50	3.73	4.84	6.49	3.98	4.18	2.44	3.57	1.28	3.22	0.45	2.70	3.24
Lu	0.22	0.51	0.68	0.94	0.53	0.58	0.36	0.52	0.22	0.48	0.07	0.37	0.44
Sc	15.9	9.6	14.4	14.0	9.2	10.2	15.2	22.5	10.9	12.5	2.7	15.8	25.7
V	37.4	46.2	36.6	44.8	37.8	37.3	61.3	73.8	28.5	39.0	20.1	52.2	121.2
Mo	0.3	0.3	0.9	0.7	0.8	0.3	8.9	0.7	0.7	0.4	0.0	0.4	0.5
Cr	54.6	66.9	66.9	77.4	57.5	67.1	80.7	162.0	46.5	84.7	39.1	70.9	190.4
Co	8.4	11.1	11.9	10.6	9.8	9.4	14.3	26.5	3.6	11.4	7.1	7.7	21.5
Ni	12.3	14.0	12.7	12.2	13.3	18.7	18.9	38.0	4.9	8.5	10.8	12.3	42.3
Cu	1.7	1.8	12.2	9.1	6.6	16.0	9.1	69.9	9.1	24.9	2.4	1.9	0.0
Zn	73.1	32.9	43.9	84.7	41.2	37.1	109.4	112.3	25.8	26.1	8.3	41.4	0.0
Sn	1.5	2.4	3.3	3.4	4.1	2.3	3.1	3.0	2.5	2.0	0.5	2.0	2.5
W	0.3	1.7	2.5	2.1	2.1	2.0	1.7	1.7	1.3	1.2	0.2	0.4	1.2
Pb	8.9	3.8	5.6	17.7	12.6	2.8	9.4	28.1	10.9	14.1	5.6	2.0	1.6
Cd	0.0	0.0	0.0	0.0	0.0	0.0	0.0	0.4	0.0	0.0	0.0	0.2	0.0
Tl	0.2	0.6	0.9	0.5	0.8	0.5	0.5	1.1	0.5	0.6	0.1	0.1	0.4
Ga	3.6	15.1	18.1	17.1	14.8	14.0	17.0	18.8	9.6	9.7	5.7	6.2	22.2
As	0.0	1.1	2.3	9.9	2.6	1.7	0.5	20.6	0.0	0.9	0.7	1.0	1.0
Ag	0.0	0.0	0.0	0.0	0.0	0.0	0.1	0.0	0.0	0.1	0.0	0.0	0.0
Sb	0.8	0.5	0.8	0.8	1.6	0.6	0.4	1.9	0.2	0.2	0.1	0.6	0.1
Labels chapter III	P13	P12	P11	P10	P9	P8	P7	P6	P5	P4	.P3	P2	P1

Sample order is from the upper sequence (left) to the lower sequence (right).

Appendix IIIc. Major and trace element concentration of the Belt-Purcell Supergroup at Whitefish Range.

Formation	Mount Sh.	Mount Sh.	Mount Sh.	Shepard	Snowslip	Snowslip	Wallace	Helena	Helena	Helena	Empire	Empire	Empire	Spokane
Sample	11(2)Wh	11WhUSO	11(1)Wh	10WhUSO	8(2)Wh	8 Wh USO	7 Wh USO	6(2)Wh	6(1)Wh	6 Wh USO	5(2)Wh	5 Wh USO	5(1)Wh	4(2)Wh
SiO_2 (wt%)	72.29	68.10	78.90	75.30	80.08	74.40	68.30	42.28	41.30	67.31	67.22	64.10	79.93	95.93
TiO_2	0.52	0.60	0.47	0.41	0.51	0.67	0.58	0.20	0.33	0.34	0.43	0.54	0.35	0.07
Al_2O_3	10.18	12.80	8.35	7.27	10.15	12.60	13.80	5.88	8.28	10.06	9.98	11.90	8.95	1.84
Fe_2O_3	3.11	4.37	3.19	4.66	2.62	3.79	3.93	2.56	2.87	2.53	2.97	2.86	2.09	0.65
MnO	0.02	0.00	0.01	0.01	0.02	0.03	0.01	0.08	0.06	0.04	0.09	0.10	0.03	0.01
MgO	3.78	4.09	2.77	3.94	1.11	1.76	4.32	10.57	6.75	4.21	3.67	4.67	0.84	0.38
CaO	1.76	0.93	0.60	2.01	0.18	0.09	0.86	14.52	18.00	5.37	5.81	3.66	1.77	0.09
K_2O	3.95	5.00	3.02	3.06	1.86	2.58	3.65	2.10	2.29	3.11	1.60	2.35	1.85	0.39
Na_2O	0.08	0.11	0.03	0.07	2.22	1.99	1.45	0.69	0.71	1.22	2.22	2.55	2.11	0.30
P_2O_5	0.08	0.12	0.13	0.11	0.05	0.04	0.07	0.04	0.07	0.10	0.09	0.09	0.05	0.04
LOI	4.45	3.80	2.30	3.30	1.45	2.10	3.05	21.25	19.50	5.75	6.00	6.80	2.10	0.35
Sum	100.3	100.1	100.2	100.3	100.4	100.2	100.2	100.2	100.2	100.2	100.2	99.8	100.2	100.1
Li (ppm)	32	47	29	43	49	31	105	59	88	78	44	46	19	20
Rb	109	145	86	48	78	107	151	84	77	133	67	96	72	27
Sr	19	17	70	22	39	36	25	69	105	46	153	80	71	28
Cs	4	6	5	2	4	6	6	5	4	9	4	6	4	1
Ba	331	338	3213	353	226	364	710	420	599	682	854	715	531	92
Y	26.4	14.7	22.3	15.9	45.5	28.2	24.3	17.1	23.2	22.1	27.7	13.1	26.6	8.9
Zr	267	58	662	151	324	99	186	83	89	169	220	114	173	81
Hf	6.94	2.11	16.86	4.06	8.3	3.3	6.9	2.57	2.74	4.83	6.41	3.8	4.44	1.58
Nb	13.65	6.85	12.22	6.28	11.64	10.78	15.93	6.94	9.22	7.71	9.25	12.4	9.46	1.07
Ta	1.03	0.59	0.91	0.45	1.36	0.76	1.33	0.39	0.60	0.62	0.79	0.88	0.66	0.09
Th	11.78	4.8	9.37	4.15	12.55	6.11	10.41	5.18	7.53	9.02	9.65	11.55	6.93	2.32
U	2.97	3.53	1.97	2.27	2.95	3.79	3.44	1.76	2.58	2.73	1.64	2.51	1.29	0.53
La	29.70	25.22	13.07	14.78	41.05	37.84	35.53	10.94	29.00	19.48	25.49	22.60	22.36	7.01
Ce	66.07	42.49	30.01	32.12	93.68	49.42	63.00	23.36	60.85	45.03	57.46	57.00	50.84	12.00
Pr	8.37	5.61	3.97	4.21	11.85	7.48	8.80	3.07	7.27	5.20	6.88	5.97	6.13	1.84
Nd	31.23	21.59	14.82	16.27	45.32	33.32	36.19	11.53	26.04	19.18	25.14	23.60	21.89	6.82
Sm	5.68	3.16	3.06	2.60	9.39	5.98	6.85	2.74	4.91	4.03	5.19	4.67	4.70	1.54
Eu	1.04	0.57	0.59	0.51	1.52	1.03	1.06	0.46	0.78	0.55	0.91	0.84	0.88	0.29
Gd	5.23	2.71	2.99	2.39	8.89	5.67	5.60	3.04	4.33	3.86	4.87	3.99	4.52	1.68
Tb	0.77	0.41	0.49	0.38	1.31	0.84	0.76	0.50	0.62	0.59	0.79	0.51	0.70	0.26
Dy	4.67	2.56	3.56	2.53	8.44	5.39	4.97	2.88	3.84	3.81	4.89	2.90	4.48	1.49
Ho	0.99	0.57	0.75	0.55	1.71	1.13	1.06	0.61	0.78	0.78	0.96	0.53	0.85	0.26
Er	2.88	1.65	2.52	1.58	4.74	3.36	3.51	1.77	2.36	2.43	2.83	1.53	2.55	0.72
Tm	0.44	0.24	0.40	0.25	0.70	0.49	0.58	0.27	0.38	0.40	0.43	0.29	0.40	0.11
Yb	2.88	1.65	2.83	1.68	4.57	3.15	4.15	1.86	2.45	2.60	2.84	2.02	2.66	0.62
Lu	0.41	0.25	0.42	0.24	0.63	0.49	0.68	0.26	0.35	0.40	0.38	0.29	0.37	0.09
Sc	11.9	11.5	8.4	8.3	5.9	18.4	25.3	13.8	15.5	13.0	12.3	10.5	8.6	2.5
V	46.1	65.3	31.1	22.8	38.4	56.0	49.4	21.5	38.9	36.1	33.8	50.2	28.1	10.6
Mo	0.2	0.0	0.2	0.4	1.2	4.3	0.3	0.3	1.0	0.4	0.3	0.4	0.0	0.0
Cr	88.5	92.2	96.7	90.0	62.5	86.9	72.6	37.2	50.8	56.4	71.0	60.7	50.9	15.0
Co	8.0	9.5	14.3	13.9	6.8	3.3	4.8	3.3	6.6	4.4	8.0	8.3	3.4	3.3
Ni	16.9	28.3	19.1	14.8	8.9	6.7	9.1	8.3	19.0	8.9	13.3	13.0	0.0	5.0
Cu	0.0	2.8	0.0	2.5	8.8	5.6	3.9	1.6	29.2	8.0	19.2	2.8	5.0	4.5
Zn	0.9	19.8	23.0	14.3	49.0	38.8	47.4	26.0	51.6	51.4	54.0	53.7	17.8	15.1
Sn	2.3	3.1	1.4	1.1	2.2	2.8	3.4	1.6	2.1	2.3	2.1	2.7	1.9	1.2
W	1.6	2.3	6.2	1.5	2.1	3.0	1.7	0.6	1.4	1.2	1.6	1.8	1.6	0.3
Pb	5.2	5.1	5.1	4.3	133.5	22.2	7.5	6.6	7.4	12.2	8.8	4.4	6.3	4.6
Cd	0.0	0.0	0.3	0.3	0.4	0.0	0.0	0.0	0.2	0.2	0.0	0.0	0.1	0.0
Tl	0.4	0.5	0.3	0.2	0.4	0.5	0.6	0.5	0.4	0.9	0.4	0.5	0.3	0.1
Ga	10.8	16.0	0.0	6.8	12.5	13.7	16.3	6.6	9.7	11.0	12.5	12.6	7.9	2.0
As	1.3	1.2	1.1	2.0	7.0	6.7	1.0	2.6	1.5	9.5	0.8	0.0	1.2	1.0
Ag	0.0	0.0	0.1	0.0	0.0	0.0	0.0	0.0	0.0	0.0	0.0	0.0	0.0	0.0
Sb	1.2	1.8	6.9	0.6	0.6	0.7	0.5	0.3	0.7	0.4	0.6	1.2	0.7	0.2
Labels chapter III	W29	W28	W27	W26	W25	W24	W23	W22	W21	W20	W19	W18	W17	W16

Appendix IIIc (continued).

Formation	Spokane	Spokane	Burke	Burke	Burke	Burke	Burke	Burke	Burke	Burke	Burke	Pric.-Burke	Prichard	Prichard	Prichard
Sample	4(1)Wh	4WhUSO	3(8)Wh	3(7)Wh	3(6)Wh	3(5)Wh	3(4)Wh	3(3)Wh	3(2)Wh	3(1)Wh	3WhUSO	2WhUSO	1(2)Wh	1(1)Wh	1WhUSO
SiO_2 (wt%)	63.28	84.80	77.82	76.88	71.72	63.88	83.61	75.83	63.09	67.01	71.30	70.60	61.75	70.28	65.90
TiO_2	0.64	0.22	0.39	0.40	0.65	0.70	0.29	0.41	0.82	0.56	0.62	0.50	0.64	0.59	0.68
Al_2O_3	17.68	5.58	11.56	11.43	14.75	18.17	8.74	12.17	18.99	15.77	14.20	13.10	18.55	14.98	17.10
Fe_2O_3	6.01	2.01	2.49	3.72	3.84	4.80	1.47	3.41	4.98	4.97	4.36	2.76	5.28	5.07	5.52
MnO	0.03	0.17	0.07	0.08	0.05	0.16	0.03	0.05	0.07	0.07	0.06	0.03	0.07	0.05	0.03
MgO	2.64	1.52	0.93	1.17	0.96	2.35	0.36	0.84	1.12	3.47	1.49	2.89	2.14	1.53	1.76
CaO	0.21	1.24	0.86	1.06	1.00	0.57	0.66	0.99	0.86	1.03	0.78	1.27	1.41	0.24	0.22
K_2O	5.23	1.43	2.99	1.80	3.28	5.12	1.26	2.90	5.31	3.57	3.49	3.89	3.66	3.55	4.30
Na_2O	1.06	0.59	1.37	2.62	1.95	1.25	2.73	1.97	2.14	1.48	2.13	1.62	3.31	1.41	1.49
P_2O_5	0.14	0.05	0.04	0.01	0.07	0.05	0.00	0.10	0.02	0.11	0.03	0.09	0.05	0.06	0.07
LOI	3.00	2.40	1.50	0.90	1.65	2.95	0.90	1.35	2.50	2.10	1.55	3.25	2.05	2.20	2.90
Sum	100.1	100.1	100.2	100.2	100.1	100.2	100.2	100.2	100.1	100.3	100.2	100.2	99.07	100.1	100.1
Li (ppm)	46	22	28	31	34	61	10	29	42	57	38	53	53	52	47
Rb	235	67	140	95	127	242	58	138	232	152	171	134	236	174	171
Sr	37	27	113	125	99	90	100	160	132	103	125	39	218	50	36
Cs	17	5	8	6	8	14	3	9	12	11	10	6	21	13	6
Ba	934	353	670	311	882	1173	293	709	1283	886	716	771	544	620	1098
Y	30.0	14.7	46.9	19.4	25.3	39.2	22.3	37.5	39.5	30.5	27.6	25.6	31.5	21.5	10.2
Zr	240	59	234	130	179	219	137	205	274	222	97	143	185	222	170
Hf	6.74	1.82	6.65	3.08	5.42	6.75	3.35	5.13	8.89	6.13	3.29	4.55	5.49	6.02	5.03
Nb	15.53	3.22	18.50	10.95	12.24	16.80	7.05	13.34	19.41	16.08	9.09	10.09	17.11	17.62	15.5
Ta	1.07	0.24	1.45	0.67	0.96	1.28	0.48	1.00	1.31	1.07	0.56	0.74	1.24	1.26	1.2
Th	14.67	3.14	14.03	8.46	11.22	16.95	7.64	10.44	18.22	9.04	8.9	6.88	13.15	10.14	5.8
U	4.06	1.24	3.77	1.74	3.21	4.52	1.91	3.29	4.04	2.56	3.87	3.91	2.08	1.92	4.00
La	53.77	13.08	52.82	25.29	34.36	36.91	29.36	42.52	46.15	16.15	36.03	31.46	43.07	18.00	22.54
Ce	115.12	29.63	122.70	61.34	78.35	87.12	58.88	101.28	107.40	31.54	69.60	53.24	91.60	36.27	49.05
Pr	13.24	3.33	14.60	6.52	9.26	10.56	7.38	10.91	12.38	4.25	8.00	7.51	10.59	4.37	5.81
Nd	48.05	12.85	53.67	23.62	32.78	38.59	27.10	40.67	44.23	16.21	34.25	30.65	37.98	15.73	23.03
Sm	8.59	2.68	10.93	4.43	6.74	8.07	5.14	8.08	8.59	3.98	6.33	6.00	6.92	2.91	3.98
Eu	1.43	0.48	1.27	0.80	1.26	1.23	0.97	1.36	1.77	0.68	1.09	0.95	1.45	0.50	0.65
Gd	6.84	2.71	9.98	4.03	5.53	7.80	4.99	7.56	7.85	4.11	5.47	5.66	6.36	2.80	3.04
Tb	0.90	0.41	1.48	0.53	0.75	1.21	0.63	1.10	1.17	0.68	0.72	0.74	0.89	0.42	0.38
Dy	5.43	2.71	9.36	3.38	4.85	7.69	3.89	6.79	7.62	4.77	5.25	4.79	5.64	3.07	2.16
Ho	1.12	0.54	1.94	0.70	1.04	1.57	0.80	1.37	1.58	1.08	1.09	0.96	1.20	0.72	0.43
Er	3.57	1.53	5.63	2.14	3.25	4.71	2.32	4.05	4.63	3.49	3.19	2.92	3.45	2.60	1.23
Tm	0.57	0.22	0.85	0.34	0.52	0.70	0.32	0.61	0.70	0.56	0.46	0.44	0.53	0.44	0.19
Yb	3.87	1.42	5.44	2.43	3.41	4.75	2.24	4.02	4.66	3.91	3.07	3.02	3.60	3.36	1.29
Lu	0.60	0.20	0.77	0.37	0.48	0.67	0.35	0.58	0.76	0.58	0.45	0.46	0.58	0.53	0.20
Sc	36.6	8.3	36.5	29.9	31.3	43.8	11.3	27.9	46.8	36.9	17.6	18.5	49.1	33.1	6.6
V	78.5	24.3	33.8	32.2	56.1	86.7	22.9	51.7	70.9	74.9	58.3	36.0	90.4	65.3	98.7
Mo	0.4	0.3	0.3	0.2	0.3	0.6	0.3	0.2	0.5	2.0	0.3	0.6	1.9	0.7	0.7
Cr	112.6	38.9	58.0	69.4	89.4	123.8	34.6	61.4	130.5	120.1	77.8	60.4	119.9	107.3	122.7
Co	14.6	7.0	5.7	10.1	10.1	19.1	6.7	7.8	12.6	14.8	11.1	2.3	11.2	7.1	14.8
Ni	26.6	11.8	6.2	16.0	7.9	31.9	7.0	14.4	17.9	27.7	15.9	7.7	12.8	5.5	27.5
Cu	2.6	1.7	1.1	18.9	9.9	67.5	10.5	5.0	0.0	0.0	12.9	4.0	29.2	17.1	8.3
Zn	87.6	41.2	40.2	74.4	44.6	99.2	25.8	53.2	58.3	83.4	75.6	56.7	105.4	74.4	43.6
Sn	4.3	1.3	3.8	2.7	3.4	4.2	1.6	2.8	4.7	2.9	3.7	3.9	3.5	3.4	3.9
W	2.7	0.5	1.9	1.3	2.7	2.7	1.0	1.9	3.4	2.0	2.3	2.2	2.9	3.1	2.3
Pb	27.0	9.8	22.2	17.4	11.9	22.4	11.4	15.2	19.9	27.7	19.7	4.8	59.8	15.5	8.1
Cd	0.2	0.0	0.0	0.2	0.3	0.0	0.0	0.0	0.1	0.0	0.0	0.3	0.3	0.1	0.5
Tl	1.3	0.2	0.7	0.5	0.6	1.2	0.4	0.7	1.1	0.8	1.0	0.7	1.4	0.8	0.8
Ga	21.6	5.7	14.3	12.1	15.7	26.8	7.6	13.9	20.5	20.1	16.3	14.7	21.7	18.4	17.5
As	1.7	1.2	0.6	0.4	1.6	0.0	1.0	0.5	1.4	1.9	0.6	1.1	0.5	1.9	7.0
Ag	0.0	0.0	0.3	0.0	0.0	0.4	0.0	0.0	0.0	0.1	0.0	0.0	0.2	0.0	0.0
Sb	1.9	0.8	0.7	0.5	0.7	0.5	1.0	0.2	0.6	0.2	1.2	0.7	0.3	0.6	0.9
Labels chapter III	W15	W14	W13	W12	W11	W10	W9	W8	W7	W6	W5	W4	W3	W2	W1

Sample order is from the upper sequence (left) to the lower sequence (right).